frontiers | Research Topics

Endocrine regulation and physiological adaptation of stress response in aquatic organisms

Edited by
Yiming Li, Yi-Feng Li, Marco António Campinho and Juan Fuentes

Published in
Frontiers in Physiology
Frontiers in Marine Science

ISSN 1664-8714
ISBN 978-2-8325-4793-9
DOI 10.3389/978-2-8325-4793-9

About Frontiers

Frontiers is more than just an open access publisher of scholarly articles: it is a pioneering approach to the world of academia, radically improving the way scholarly research is managed. The grand vision of Frontiers is a world where all people have an equal opportunity to seek, share and generate knowledge. Frontiers provides immediate and permanent online open access to all its publications, but this alone is not enough to realize our grand goals.

Frontiers journal series

The Frontiers journal series is a multi-tier and interdisciplinary set of open-access, online journals, promising a paradigm shift from the current review, selection and dissemination processes in academic publishing. All Frontiers journals are driven by researchers for researchers; therefore, they constitute a service to the scholarly community. At the same time, the *Frontiers journal series* operates on a revolutionary invention, the tiered publishing system, initially addressing specific communities of scholars, and gradually climbing up to broader public understanding, thus serving the interests of the lay society, too.

Dedication to quality

Each Frontiers article is a landmark of the highest quality, thanks to genuinely collaborative interactions between authors and review editors, who include some of the world's best academicians. Research must be certified by peers before entering a stream of knowledge that may eventually reach the public - and shape society; therefore, Frontiers only applies the most rigorous and unbiased reviews. Frontiers revolutionizes research publishing by freely delivering the most outstanding research, evaluated with no bias from both the academic and social point of view. By applying the most advanced information technologies, Frontiers is catapulting scholarly publishing into a new generation.

What are Frontiers Research Topics?

Frontiers Research Topics are very popular trademarks of the *Frontiers journals series*: they are collections of at least ten articles, all centered on a particular subject. With their unique mix of varied contributions from Original Research to Review Articles, Frontiers Research Topics unify the most influential researchers, the latest key findings and historical advances in a hot research area.

Find out more on how to host your own Frontiers Research Topic or contribute to one as an author by contacting the Frontiers editorial office: frontiersin.org/about/contact

Endocrine regulation and physiological adaptation of stress response in aquatic organisms

Topic editors

Yiming Li — Fishery Machinery and Instrument Research Institute, China
Yi-Feng Li — Shanghai Ocean University, China
Marco António Campinho — University of Algarve, Portugal
Juan Fuentes — Institute of Marine Sciences of Andalusia, Spanish National Research Council (CSIC), Spain

Citation

Li, Y., Li, Y.-F., Campinho, M. A., Fuentes, J., eds. (2024). *Endocrine regulation and physiological adaptation of stress response in aquatic organisms*. Lausanne: Frontiers Media SA. doi: 10.3389/978-2-8325-4793-9

Table of contents

frontiers | Frontiers in Physiology

TYPE Editorial
PUBLISHED 08 April 2024
DOI 10.3389/fphys.2024.1406986

OPEN ACCESS

EDITED AND REVIEWED BY
Pung Pung Hwang,
Academia Sinica, Taiwan

*CORRESPONDENCE
Yiming Li,
liyiming183@163.com

RECEIVED 26 March 2024
ACCEPTED 28 March 2024
PUBLISHED 08 April 2024

CITATION
Li Y, Li Y-F, Campinho MA and Fuentes J (2024), Editorial: Endocrine regulation and physiological adaptation of stress response in aquatic organisms.
Front. Physiol. 15:1406986.
doi: 10.3389/fphys.2024.1406986

Editorial: Endocrine regulation and physiological adaptation of stress response in aquatic organisms

Yiming Li[1]*, Yi-Feng Li[2,3], Marco António Campinho[4,5] and Juan Fuentes[6]

[1]Fishery Machinery and Instrument Research Institute, Chinese Academy of Fisheries Sciences, Shanghai, China, [2]International Research Centre for Marine Biosciences, Ministry of Science and Technology, Shanghai Ocean University, Shanghai, China, [3]Key Laboratory of Exploration and Utilization of Aquatic Genetic Resources, Ministry of Education, Shanghai Ocean University, Shanghai, China, [4]Algarve Biomedical Centre-Research Institute, Faro, Portugal, [5]Faculty of Medicine and Biomedical Sciences, University of the Algarve, Faro, Portugal, [6]Instituto de Ciencias Marinas de Andalucía (ICMAN), Consejo Superior de Investigaciones Científicas (CSIC), Puerto Real, Spain

KEYWORDS

stress response, aquatic organisms, endocrine regulation, physiological adaptation, homeostasis

Editorial on the Research Topic
Endocrine regulation and physiological adaptation of stress response in aquatic organisms

Organismal growth is a complex, genetically regulated process that integrates various physiological signaling pathways, where endocrine regulation is pivotal. In fully developed animals, endocrine regulation plays a central role in maintaining homeostasis and adapting to changing environmental and biological conditions. In aquatic organisms, environmental stressors such as environmental temperature, hypoxia, salinity changes, and exposure to pollutants can disrupt homeostasis, leading to physiological, molecular, and behavioral responses. Understanding the molecular and cellular mechanisms of endocrine regulation and physiological adaptation in response to environmental stresses is crucial, significantly impacting aquatic ecosystems. The main objective of this Research Topic was to explore and discuss these mechanisms, providing valuable insights into aquatic animal biology and adaptation.

Several studies have provided valuable insights into various fish and mollusk species' physiology and adaptation mechanisms in response to environmental stressors.

Ruiz et al. explored the physiological responses of rainbow trout under repeated hypoxia exposure, revealing resistance patterns to anoxic events.

Ma et al. investigated the utilization of carbohydrates in fish after intraperitoneal injection or oral administration of glucose or fructose, highlighting the effects on blood sugar levels and hypoxia tolerance. In addition, turbot and tiger fish are intolerant to acute hypoxia, and adding glucose or fructose improves hypoxia tolerance in both marine fish species by activating anaerobic glycolysis. The study provides essential scientific information for understanding the mechanism of glucose and fructose utilization in fish and improving hypoxia tolerance.

Cheng et al. delved into the molecular regulation mechanisms of high-temperature environments in paddy field carp (PF-carp), shedding light on biochemical parameters and gene pathways affected by heat stress.

Wang et al. described the transcriptional temperature response on *Bombyx Mori* larva. These results contribute to a further understanding of the mechanism of high-temperature resistance in invertebrates in the context of global warming. Qiu et al. identified that McNrf2 could protect mussels from benzopyrene-induced oxidative stress (Bap) by inhibiting McSLC35E2. They further describe potential *McNrf2* target genes after ChIP-seq, revealing the highly complex regulation responses to oxidative stress in marine invertebrates.

Liu et al. studied the toxic effect of ammonia nitrogen stress on the intestinal tract of banded catfish (*Pelteobagrus fulvidraco*). The findings of this study suggest that ammonia nitrogen stress destroys the intestinal mucosal barrier and induces intestinal inflammation, which provides valuable data for intestinal immunotoxicology studies in aquatic organisms.

Holhorea et al. combined biometric, behavioral, physiological, and external tissue damage scoring systems to understand the endocrine response to different stocking densities. This suggests that the growth-regulatory shift in high-density fish cultures supports active rather than passive behavior, which is thought to be adaptive and can maintain active and synchronized feeding behavior while minimizing the risk of oxidative stress and epidermal skin damage.

Zeng et al. identified the *elovl8* gene from *P. fulvidraco* and analyzed its evolutionary and molecular characteristics and transcriptional changes under different nutritional states. This analysis indicates that *elovl8* is involved in HUFAs biosynthesis in early development.

Impellitteri et al. investigated the response of mediterranean mussel (*Mytilus galloprovincialis*) to chlorpromazine (Cpz). These results indicate that Cpz can cause non-specific biochemical and cellular disorders even at low picomolar concentrations, which is significant for healthy culture and ecotoxicity studies of purple mussels.

Zhang et al. investigated the effects of microplastics on intestinal morphology and inflammatory response of Largemouth bass (*Micropterus salmoides*) (carnivorous fish), grass carp (*Ctenopharyngodon idella*) (herbivorous fish), and swordfish (*Xiphias gladius*) (omnivorous fish) with different feeding methods. Different fish's genetic responses differed according to different sizes and concentrations of microplastic exposure. The reasons for the different effects of microplastics on fish are unknown but may be due to differences in the structure and function of the digestive system. The results of this study provide a theoretical basis for further analysis of the pathological mechanism of fish intestines caused by microplastics.

Liu et al. used golden cuttlefish (*Sepia esculenta*) and ricefield eel (*Monopterus albus*) to explore the effects of polystyrene nanoparticles. Transcriptome analysis showed a wide genetic response. This study not only provides a new reference for understanding the mechanism of acute polystyrene nanoparticles-induced stress response, providing valuable ecotoxicological data for assessing the impact on invertebrate and vertebrate aquatic species.

Chen et al. described NHE and NKA gene families in the cobia fish (*R. canadum*) and their response to salinity changes. The results provide valuable insights into the molecular mechanisms governing ion transport and osmoregulation in *R. canadum*, contributing to developing strategies for enhancing aquaculture practices for this species.

Lin et al. studied the molecular cloning and expression profile of elongation of very long-chain fatty acids protein 6 (elovl6) in mud crabs (*Scylla paramamosain*) with dietary fatty acids, environmental salinity, and starvation stress. The findings of this study help understand the function and regulatory mechanism of fatty acid synthesis in crustaceans.

Liu et al. utilized single-cell transcriptome analysis to investigate the cellular immune response in dark sleeper fish (*Odontobutis potamophila*) infected with a co-pathogenic species *Aeromonas veronii*. The study contributes valuable insights into the immune response mechanisms in teleosts and provides a foundation for further research on cellular immunity in fish species.

The research conducted by Shu et al. investigated the impact of short-term water velocity stimulation on ovarian development in grass carp (*Ctenopharyngodon idellus*). The study provides valuable insights into the ovarian development of grass carp under short-term water velocity stimulation, offering potential regulatory genes and pathways for further ecological regulation strategies.

Zhang et al. explore the role of ionotropic glutamate receptors (iGluRs) in mediating excitatory neurosignals and environmental stress responses in Pacific oysters (*Crassostrea gigas*, Cg). Exposure to five heavy metals triggers a significant upregulation of *CgGRIA4* expression, indicating a robust response to metal stress. This research improves our understanding of iGluRs in metal stress response, signaling pathways, and environmental adaptability, paving the way for future investigations into cellular signaling mechanisms and neurotoxicity.

In conclusion, the diverse studies presented in this Research Topic collectively contribute to understanding physiological adaptations in aquatic organisms under various environmental stressors. From molecular pathways to physiological responses, these investigations offer valuable insights into the mechanisms governing organismal growth, endocrine regulation, and adaptation to environmental challenges in fish and mollusks. By elucidating the intricate interplay between genetics, environment, and physiology, these studies lay a foundation for further research on aquatic organism health and ecosystem sustainability.

Exploring the molecular and cellular mechanisms underlying endocrine regulation and physiological adaptations in response to environmental stresses is essential for safeguarding aquatic ecosystems. Further research should focus on integrating omics approaches, advanced imaging techniques, and environmental monitoring to deepen our understanding of how aquatic organisms cope with changing environmental conditions. By unraveling the complexities of adaptation mechanisms, we can better inform conservation efforts, sustainable aquaculture practices, and environmental management strategies to preserve the health and diversity of aquatic ecosystems for future generations.

Author contributions

YL: Writing–original draft, Writing–review and editing. Y-FL: Writing–original draft, Writing–review and editing. MC:

Writing–original draft, Writing–review and editing. JF: Writing–original draft, Writing–review and editing.

Conflict of interest

The authors declare that the research was conducted in the absence of any commercial or financial relationships that could be construed as a potential conflict of interest.

Publisher's note

frontiers | Frontiers in Physiology

TYPE Original Research
PUBLISHED 10 May 2023
DOI 10.3389/fphys.2023.1189375

OPEN ACCESS

EDITED BY
Yiming Li,
Fishery Machinery and Instrument Research Institute, China

REVIEWED BY
Tianming Wang,
Zhejiang Ocean University, China
Qichen Jiang,
Freshwater Fisheries Research Institute of Jiangsu Province, China
Meihua Fan,
Zhejiang Ocean University, China

*CORRESPONDENCE
Zan Li,
lizanlxm@163.com
Jianmin Yang,
ladderup@126.com
Tingzhu Yuan,
yuantingzhu@sina.com

RECEIVED 19 March 2023
ACCEPTED 28 April 2023
PUBLISHED 10 May 2023

CITATION
Wang Y, Bao X, Wang W, Xu X, Liu X, Li Z, Yang J and Yuan T (2023), Exploration of anti-stress mechanisms in high temperature exposed juvenile golden cuttlefish (*Sepia esculenta*) based on transcriptome profiling.
Front. Physiol. 14:1189375.
doi: 10.3389/fphys.2023.1189375

Exploration of anti-stress mechanisms in high temperature exposed juvenile golden cuttlefish (*Sepia esculenta*) based on transcriptome profiling

Yongjie Wang[1], Xiaokai Bao[1], Weijun Wang[1], Xiaohui Xu[1], Xiumei Liu[2], Zan Li[1]*, Jianmin Yang[1]* and Tingzhu Yuan[1,3]*

[1]School of Agriculture, Ludong University, Yantai, China, [2]College of Life Sciences, Yantai University, Yantai, China, [3]Marine Economy Promotion Center of Changdao County Marine Ecological Civilization Comprehensive Experimental Zone, Yantai, China

Sepia esculenta is a cephalopod widely distributed in the Western Pacific Ocean, and there has been growing research interest due to its high economic and nutritional value. The limited anti-stress capacity of larvae renders challenges for their adaptation to high ambient temperatures. Exposure to high temperatures produces intense stress responses, thereby affecting survival, metabolism, immunity, and other life activities. Notably, the molecular mechanisms by which larval cuttlefish cope with high temperatures are not well understood. As such, in the present study, transcriptome sequencing of *S. esculenta* larvae was performed and 1,927 differentially expressed genes (DEGs) were identified. DEGs were subjected to functional enrichment analyses using the Gene Ontology (GO) and Kyoto Encyclopedia of Genes and Genomes (KEGG) databases. The top 20 terms of biological processes in GO and 20 high-temperature stress-related pathways in KEGG functional enrichment analysis were identified. A protein-protein interaction network was constructed to investigate the interaction between temperature stress-related genes. A total of 30 key genes with a high degree of participation in KEGG signaling pathways or protein-protein interactions were identified and subsequently validated using quantitative RT-PCR. Through a comprehensive analysis of the protein-protein interaction network and KEGG signaling pathway, the functions of three hub genes (HSP90AA1, PSMD6, and PSMA5), which belong to the heat shock protein family and proteasome, were explored. The present results can facilitate further understanding of the mechanism of high temperature resistance in invertebrates and provide a reference for the *S. esculenta* industry in the context of global warming.

KEYWORDS

high-temperature, stress, protein-protein interaction network, *Sepia esculenta*, transcriptome

1 Introduction

The rapid acceleration of global industrialization has resulted in a significant release of carbon dioxide into the atmosphere, which has led to global warming and subsequent oceanic warming (Nick et al., 2013; Al-Ghussain, 2019; Liu et al., 2020). High temperature will have a strong negative impact on the reproduction and development of marine biological physiological functions (Jones et al., 2013; Li et al., 2016). As an example, prolonged exposure of fish (Vargas-Chacoff et al., 2019), shellfish (Li et al., 2016; Martinez et al., 2018), mollusks (Trigg et al., 2020), and other marine animals to high-temperature marine environments will increase the burden of maintaining physiological activities, and while decreasing their ability to cope with other environmental changes, ultimately affecting their healthy growth. Additionally, high seawater temperatures can lead to stress responses in marine organisms (Dalvi et al., 2017; Samaras et al., 2018). For instance, rising seawater temperatures caused by global warming could impair the physiological function of *Crassostrea virginica* by disrupting the pro-oxidation-antioxidant system (Rahman and Rahman, 2021). When *Piscium* are exposed to high temperatures, the catecholaminergic (norepinephrine and dopaminergic) system is altered, which affects the synthesis, release, and metabolism of neurotransmitters (Alfonso et al., 2021).

Sepia esculenta is a commercially significant species belonging to the cuttlefish family, found primarily in the northern seas of China, and possessing high economic value (Guo et al., 2021). In actual aquaculture production, high-temperature seawater will significantly affect the immunity, metabolism, reproduction, and other life activities of *S. esculenta*, which is undoubtedly a significant challenge for *S. esculenta* factory farming (Bian et al., 2018).

In recent years, there has been considerable progress in high-throughput transcriptome sequencing technology, and biological analysis through high-throughput transcriptome sequencing has become more accurate (Morozova et al., 2009; Qian et al., 2014; Bao et al., 2022a; Bao et al., 2022b). To illustrate, through such technology, the expression of heat stress genes in *Pinctada fucata* have been found to be significantly reduced after being stimulated by multiple high temperatures, indicating that *P. fucata* is able to gradually adapt to the impact of high temperatures on their life activities (Li et al., 2016). The larvae possess a relatively weak capacity to endure environmental stress when in their initial phase of growth and development. Thus, elevated seawater temperature significantly impairs the routine life activities of marine larvae (Ginger et al., 2013; Kaplan et al., 2013). In the present study, transcriptome sequencing was performed to explore the mechanism of high-temperature stress in *S. esculenta* larvae.

In the present, high-throughput transcriptome sequencing technology was used to sequence the *S. esculenta* larvae exposed to high temperatures for 0, 4, and 24 h, and the data obtained were mapped to the reference genome of *S. esculenta*. Subsequently, differentially expressed genes (DEGs) were examined using cluster heatmap analysis and subjected to enrichment analyses of GO and KEGG. The protein-protein interaction (PPI) network was constructed by means of the selected DEGs. A combination of the KEGG signaling pathway and the protein-protein interaction network to was innovatively used explore the expression of key genes and families in *S. esculenta* after high-temperature stress. Finally, the expression patterns of key DEGs were verified using quantitative RT-PCR (qRT-PCR). The results provide a reference for further exploration of the temperature stress mechanism of *S. esculenta,* and can be beneficial for the factory farming of *S. esculenta* in terms of facilitating understanding of the negative effects of global warming.

2 Materials and methods

2.1 Experiment materials

In the present experiment, adult *S. esculenta* samples (weight = 351.87 ± 12.68 g, mantle length = 14.82 ± 0.21 mL) were collected from the marine region near Qingdao, and were held for a period of time in the pool for temporary breeding to ensure the adaptation of adults to the environment. An attachment net was placed in the pool to collect eggs. The temperature at the time of temporary breeding was 21.5°C ± 1°C. The eggs are oval, 7 ± 1 mm in diameter and translucent, which were typically collected every day and placed in perforated plastic pots. Pots were placed in another pool with flowing seawater (dissolved oxygen = 5.5 mg/L, pH = 8.2, and salinity = 30.5 ± 0.3) and continuous oxygenation, and the water temperature and other indicators were the same as those of the parent pool.

2.2 Experimental process

In two square 120 L buckets, each bucket was filled with 100 L seawater. The new hatched larvae were transferred to the experimental bucket half an hour after the incubation was completed. The water temperature before the larvae were transferred to the experimental bucket was 21°C ± 1°C. According to prior research, the seawater temperature of the experimental group was set to 28°C, and the temperature of the seawater in the control group was set to 23°C. During the experiment, one hundred larvae of *S. esculenta* were put into each bucket, and samples were taken at 4 and 24 h. Samples at the 0 h time point were obtained individually. All of the samples were stored in cryovials in liquid nitrogen.

2.3 RNA extraction and library construction and sequencing

RNA extraction, library construction, and sequencing were supported by Beijing Novogene Company. RNA was extracted from the whole larvae using standard extraction methods, followed by strict quality control with the Agilent 2100 bioanalyzer of RNA samples (Masotti and Preckel, 2006). The kit used for library construction was NEBNext® Ultra™ Directional RNA Library Prep Kit for Illumina®. When creating the library, nine larvae were collected from each group at every time point, and three samples were pooled randomly together to form a total of three biological replicates (C_0h_1, C_0h_2, C_0h_3, C_4h_1, C_4h_2, C_4h_3, C_24h_1, C_24h_2, C_24h_3, T_4h_1, T_4h_2, T_4h_3, T_24h_1, T_24h_2, and T_24h_3). *S. esculenta* larvae were sequenced using Illumina NovaSeq 6000 (Illumina, United States).

TABLE 1 List of primers used for quantitative RT-PCR validation.

Gene name	Forward primer (5′-3′)	TM (°C)	Reverse primer (5′-3′)	TM (°C)	Amplicon length (bp)
COL12A1	CGCAGTCCTTGAGAACATAG	60	CGTTGTAGTCGTCGTTGTAG	60	157
COL15A1	GTCATCCAGTTGGGTGTTAG	60	CAGTGTCCGAGCAGATTATAC	60	149
COL6A3	ACGGCAGAACGAACAATC	60	CACCTTTCATGTCCACTACTC	60	108
COL6A5	AGAGCGCAACCATTCATC	60	GAATAGACGTCTCGACAAGC	60	102
COL6A6	GCAGTTCTGATCTCGTCTTT	60	GGTGACTTCCTTGATGTCTG	60	101
DNAJA1	GCTGGTGAAGGAGATCAATG	60	GATCATCACCCTGTCGTTTG	61	100
DNAJC10	CATCAGCTCCTTGGGTAATC	60	GCTTCCAACATTCACCAAAC	60	110
HSP90AA1	CAACACCCTGACCCTTATTG	60	CCACAAGGTAAGCCGAATAG	60	176
HSPA8	CCTTCTCCTCTTGGATGTTG	60	GCTTGGTAGGAATGGTTGT	60	101
HYOU1	GGAAGTCTTTCAGCTCCTTG	60	GCACGGACACCTTTGTATT	60	103
ODC1	ACATGGGAGCCTACACTT	60	CACCACACAACGGGATTT	60	116
PIK3R1	CAGTTTGTAGTCGGGAAAGAG	60	TAAAGCAGCCAGCCAATC	60	104
PIK3R4	CTTCCAACTGCCTACCTTTC	60	CGAGTGCTTATTCGGTCATAC	60	103
PSMA2	GCTACTGCAATGGGTAAGAA	60	ACTCTCCTTCAGGGTTAAGA	60	117
PSMA4	CCTCGGATGGTGTTCTCTTA	61	CAACACTGCAAGCCATATCA	61	114
PSMA5	CTCACCAGAAGGCAGATTG	60	CAACACGACACCCTCATTT	60	100
PSMA6	CACTTGGGTGCTGTATGATT	60	CAGCAGCAGTGGCTTTAT	60	108
PSMA8	GCAAAGACTGTTCGTGAGTA	60	CCAGATTGGACCACTTCTAAC	60	113
PSMB2	CATGGCTATGGTGCCTATTT	60	CATGGAAGGAGGGAAGATTG	60	145
PSMB5	CCCACGCTTATGGTGTATTG	61	CATCTCTGTGTGTTGCATGA	60	105
PSMB6	TCAGAGTAGCAGCCCATATC	61	CCTGTCCTCCTCTGTGTTTA	61	105
PSMC3	CTCAGGACCAAGAAGAAGAAG	60	CCAATGACAGGCAGGAAATA	60	115
PSMD1	CTGCCCAGCAAGACATATT	60	CCAGCATTACAAGACCCATAG	60	102
PSMD12	CCAGGAGGCTTGTTCTTATG	60	GTGTAAGCCGAGCTCTTTC	60	125
PSMD2	CCCAGCCAAGGCTTTATT	60	TCTGTTGGAACCAGCATAAG	60	103
PSMD3	ATTGTCGCCAAGGCTATTC	60	GGCTCTCTGGTTGAGTAAATG	60	107
PSMD6	AGTCTTACCGAAGCCTTACT	60	GCGTCCAGCAGCAATAAA	61	101
PSMD7	GGTTTGTGGAGTACTACTTG	60	GTCCAGAAACCACACAGATT	60	112
PSMD8	AAGCAGAGCCATCGAAAC	60	CGGGCAGATTATCCTTGTAG	60	153
SUGT1	GAGAAGGCAATCGTGGATAC	60	GGGCGTCTTGGTAATTCTT	60	112

2.4 Gene function annotation and screening of DEGs

In the present study, the structure and function of unigenes were annotated into several databases, including NR, SwissProt, KEGG, GO, Interpro, and PFAM. DEGs were screened out using the DESeq2 package for R as a negative binomial distribution model. First of all, data were imported for building the dds model, and then the DESeq function was used to estimate the dispersion of the samples. Afterwards the difference in gene expressions was analyzed by this package. DEGs with |Log2 Fold Change| ≥ 0 (Love et al., 2014) and *p*-value ≤0.05 were screened out.

2.5 Enrichment analyses

DAVID v6.8 (Jiao et al., 2012) was used for GO and KEGG enrichment analyses. DEGs were enriched into GO terms and KEGG signaling pathways to understand the response mechanism of *S. esculenta* after high-temperature exposure.

TABLE 2 RNA-Seq data.

Sample	Raw reads	Clean reads	Clean reads Q30 (%)	Clean reads Q20 (%)	Total mapping	Mapping rate (%)
C_0h_1	44,822,088	44,401,358	93.02	97.42	38,945,045	87.71
C_0h_2	46,604,268	46,067,346	92.97	97.39	40,192,257	87.25
C_0h_3	42,199,716	41,745,596	92.31	97.08	35,955,570	86.13
C_4h_1	42,594,570	42,050,900	93.35	97.56	37,123,254	88.28
C_4h_2	45,122,216	44,583,624	92.89	97.37	39,143,445	87.80
C_4h_3	43,910,186	43,339,204	93.00	97.44	37,996,122	87.67
C_24h_1	44,237,100	43,609,904	93.06	97.45	38,548,116	88.39
C_24h_2	45,963,126	45,180,404	93.07	97.49	39,479,438	87.38
C_24h_3	45,268,732	44,022,418	93.27	97.58	38,685,844	87.88
T_4h_1	44,626,628	44,162,538	93.06	97.48	38,927,372	88.15
T_4h_2	42,318,638	41,872,474	93.24	97.53	36,828,643	87.95
T_4h_3	40,793,398	40,357,954	92.99	97.40	35,682,178	88.41
T_24h_1	41,849,070	41,155,332	93.09	97.43	36,127,995	87.78
T_24h_2	45,764,258	44,923,156	93.11	97.48	39,397,933	87.70
T_24h_3	46,116,390	45,123,238	93.10	97.47	39,109,229	86.67

2.6 Protein-protein interaction network

STRING v11.5 (Szklarczyk et al., 2019) was used to construct a PPI network. Genes that play significant roles in response to high-temperature stress in *S. esculenta* larvae were then selected based on the number of PPI and KEGG signaling pathways.

2.7 Quantitative RT-PCR validation

Primer Premier 5.0 (Ren et al., 2004) was used to design gene-specific primers (Table 1). In addition, qRT-PCR was performed to validate 30 genes that exhibit significant involvement in response to high-temperature stress in *S. esculenta*. The *β-actin* gene was used as a reference gene for qRT-PCR.

3 Results

3.1 Sequencing results and quality

High-throughput sequencing technology was used to sequence the samples of *S. esculenta* larvae. On average, 87.68% of the high-quality reads were able to be aligned to the reference genome, and the percentage of high-quality reads with a Q30 score was 93.04% (Table 2). Such data indicate that the sequencing quality of all samples was adequate for subsequent analysis.

3.2 Gene function annotation

A total of 32,138 genes were annotated to different databases, and most genes were annotated to the NR database, reaching 73.67% (Table 3). At the same time, a large number of genes were annotated in the SwissProt and KEGG databases.

TABLE 3 Gene function annotations.

	Number of genes	Percentage (%)
Annotated in NR	23,677	73.67
Annotated in SwissProt	19,757	61.48
Annotated in KEGG	16,509	51.37
Annotated in GO	1,788	5.56
Annotated in Interpro	9,032	28.10
Annotated in PFAM	6,879	21.40
Total unigenes	32,138	100.00

3.3 Differential gene expression analysis

3.3.1 Volcano plot of DEGs

The volcano plot shows that 991 DEGs were identified, of which 498 DEGs were upregulated and 493 were downregulated in the 4 h exposure sample. In the 24 h exposure sample, 1,064 DEGs were identified among which, 470 DEGs were upregulated, and 594 DEGs were downregulated (Figure 1).

3.3.2 Venn diagram analysis of DEGs

A total of 1,927 genes were differentially expressed, of which 128 genes were co-expressed at both 4 and 24 h (Figure 2).

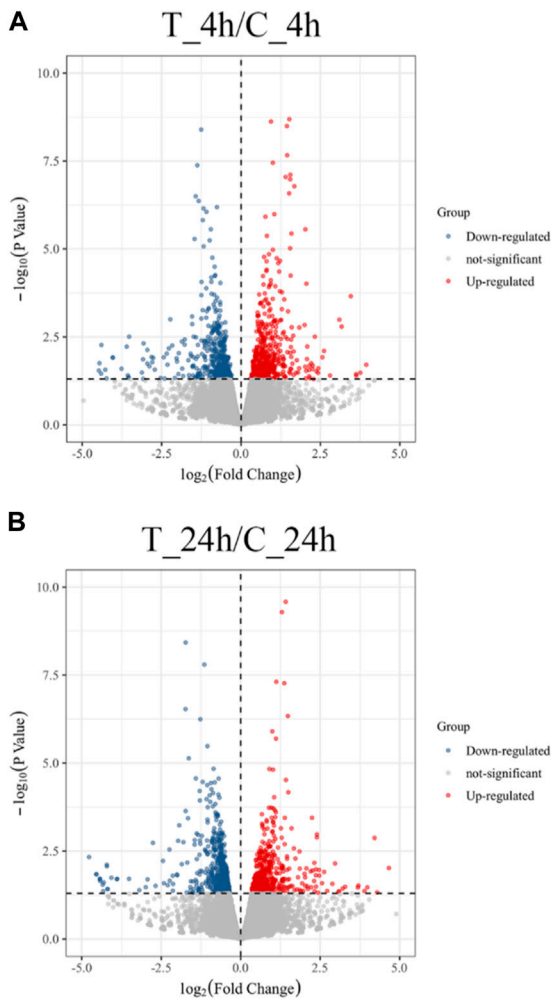

FIGURE 1
Volcano plot of the distribution expression of DEGs. **(A)** DEGs expression distributions between T_4h/C_4h. Red dots represent upregulated DEGs; blue dots are downregulated DEGs; grey dots indicate non-significantly genes. **(B)** DEGs expression distributions between T_24h/C_24h. Each dot represents a gene.

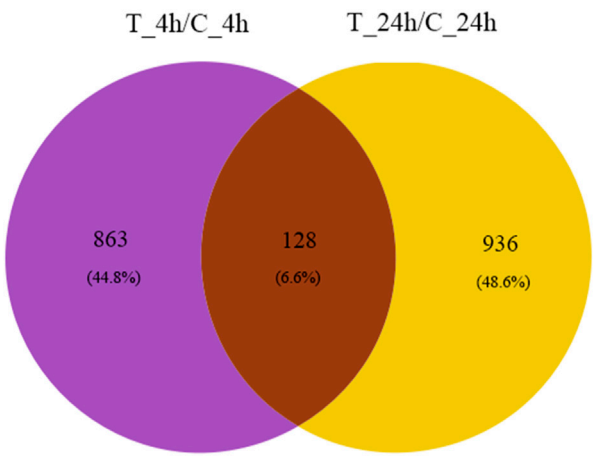

FIGURE 2
Venn diagram of DEGs. The purple and yellow regions represent the number of genes significantly expressed at 4 and 24 h after exposure, respectively. The number of genes co-expressed at 4 and 24 h is represented by brown areas.

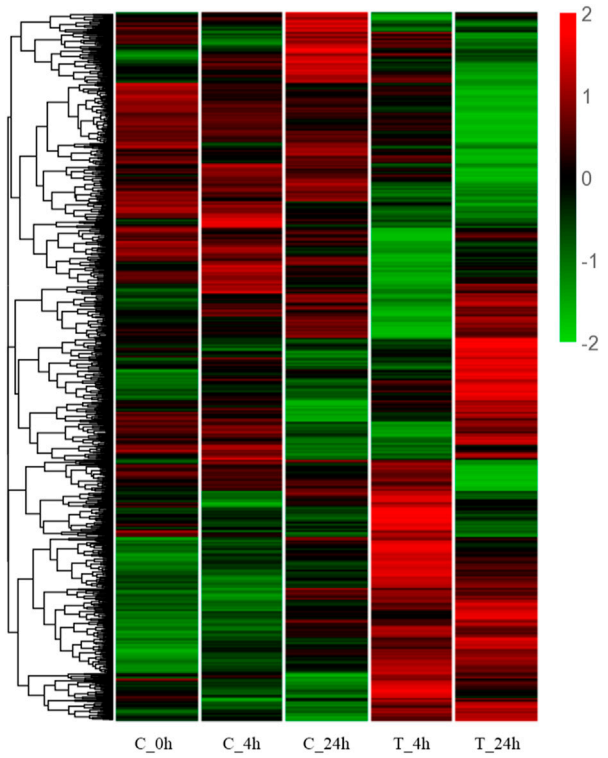

FIGURE 3
Hierarchical clustering heatmap of DEGs. The Y-axis represents each gene, and the X-axis represents the different treatment groups. Colors ranging from green to red indicating low to high expression levels.

3.3.3 Cluster heatmap analysis

The cluster heatmap (Figure 3) shows that the blank control group (C_0h), the 4 h control group (C_4h), and the 24 h control group (C_24h) had basically the same expression pattern. Compared with the 4 h control group (C_4h), the gene expression patterns in the 4 h experimental group (T_4h) were significantly different. A different trend was observed in the two groups (C_24h) (T_24h) at 24 h.

3.4 Functional enrichment analyses of GO and KEGG

Through GO functional enrichment analysis, DEGs were enriched into three categories: biological process, cellular component, and molecular function. The top 20 terms of the biological process and the top 10 terms of the cellular component and molecular function were selected (p-value ≤ 0.05) (Figure 4). A large number of the top 20 terms in the biological process were associated with high-temperature stress.

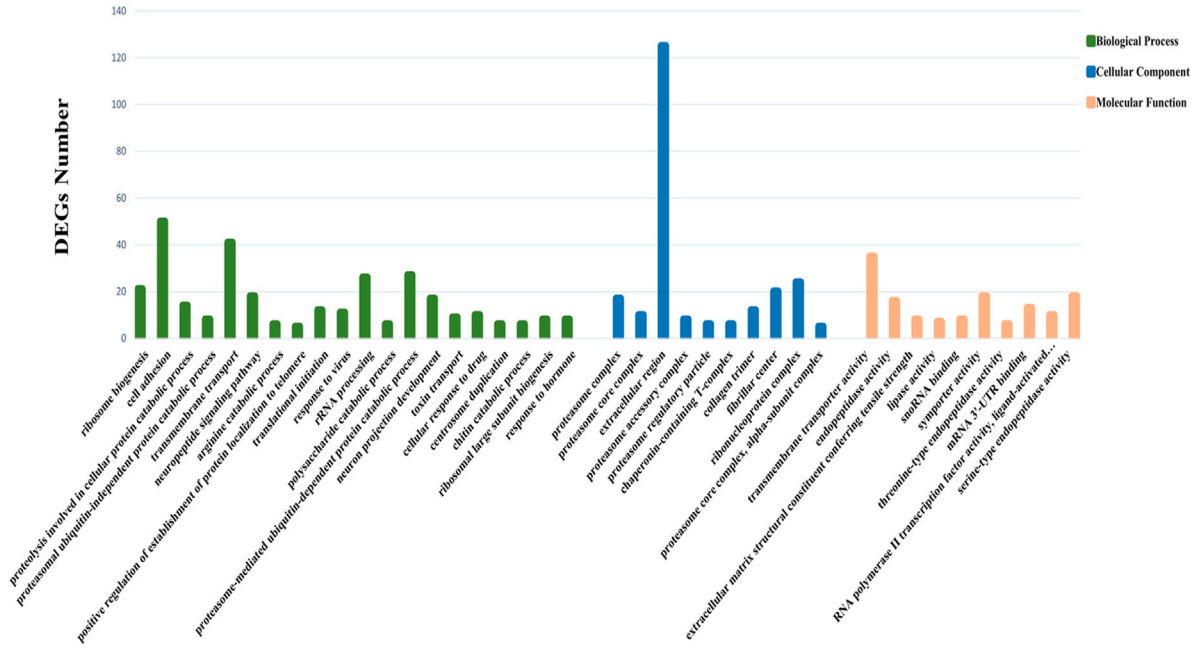

FIGURE 4
GO enrichment analysis of DEGs. The Y-axis represents the number of DEGs enriched to this term; the X-axis stands for the specific terms based on GO.

The KEGG enrichment analysis results indicate that a large number of DEGs were enriched in multiple level-2 KEGG signaling pathways (Figure 5). Further, 20 level-3 KEGG signaling pathways were significantly enriched after exposure to high temperatures (Table 4).

Among the 20 significantly enriched KEGG signaling pathways after high-temperature exposure, a total of 97 DEGs were enriched. Such genes that are involved in multiple high-temperature stress-related signaling pathways may be a significant factor in the process of resisting high-temperature stress in *S. esculenta*.

3.5 Construction of protein-protein interaction network

In the present study, 97 DEGs (Supplementary Table S1) enriched in the KEGG pathways identified after high-temperature exposure were used to construct a PPI network (Figure 6), thereby facilitating identification of key genes after high-temperature exposure.

Table 5 shows the network parameters. The average node degree was 6.96, the clustering coefficient was 0.574 and the PPI enrichment *p*-value was 1.0E-16. The parameters indicate significant interactions between the above DEGs.

3.6 Selection of key high temperature stress response genes

After exposing *S. esculenta* larvae to high temperature, there was a significant level of interaction observed among the DEGs. The number of protein interactions was used as the main reference factor, combined with the number of KEGG signaling pathway participation to select the key genes. Finally, 30 key genes were identified. Table 6 displays the 30 identified key DEGs, along with their corresponding numbers of PPI and KEGG signaling pathways.

The 30 key DEGs could be further divided into five categories based on their families and functions, including the PI3K-Akt signaling pathway, heat shock protein family, proteasome family, collagen family, and other genes regulating high temperature stress.

3.7 Validation of key DEGs using quantitative RT-PCR

The accuracy of the expression of 30 key genes was verified using qRT-PCR. The expression patterns of genes obtained from qRT-PCR were consistent with those obtained from RNA-Seq analysis, suggesting that the RNA-Seq results are reliable (Figure 7).

4 Discussion

4.1 Expression and functional enrichment analysis of DEGs

In the present study, 1,927 DEGs that play significant roles in the resistance to high-temperature stress in the *S. esculenta* were screened. Volcano plot analysis showed that more genes appeared differentially expressed as the duration of high-temperature exposure increased. Cluster heatmap analysis showed that a large number of DEGs showed different expression patterns at 4 h (T_4h) and 24 h (T_24h). A total of 1,927 DEGs were used for GO and KEGG functional enrichment analysis. The majority of the top 20 terms identified in the

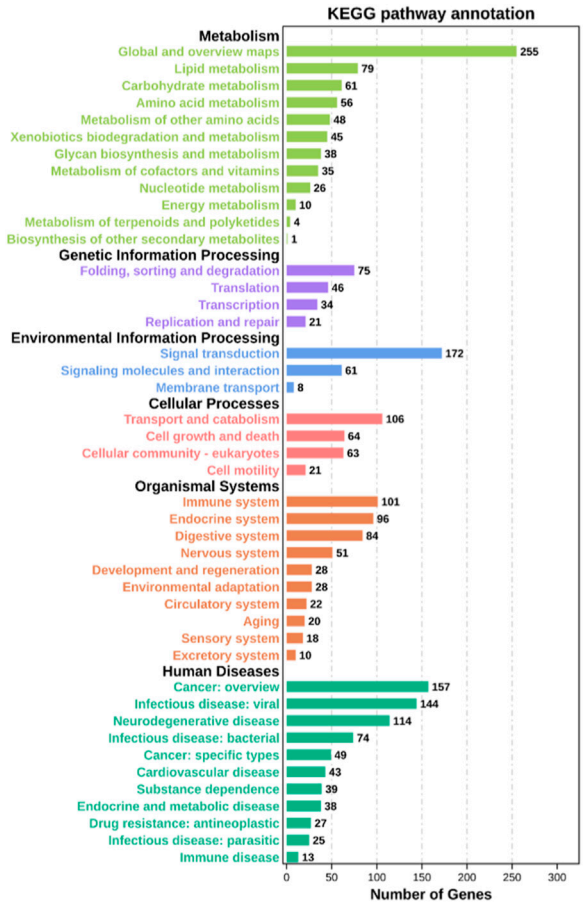

FIGURE 5
Level-2 KEGG signaling pathway annotation. The Y-axis indicates level-2 KEGG classes; the X-axis represents the corresponding number of DEGs.

TABLE 4 Twenty significantly enriched KEGG signaling pathways related to high temperature exposure.

Pathway	Number of DEGs
Antigen processing and presentation	4
Apelin signaling pathway	9
Arginine and proline metabolism	6
Arginine biosynthesis	3
ECM-receptor interaction	7
FoxO signaling pathway	5
MAPK signaling pathway	6
Neurotrophin signaling pathway	3
NOD-like receptor signaling pathway	6
PI3K-Akt signaling pathway	8
Proteasome	16
Protein digestion and absorption	9
Protein processing in endoplasmic reticulum	9
Ras signaling pathway	3
Relaxin signaling pathway	3
Retinol metabolism	3
Ribosome biogenesis in eukaryotes	5
RNA degradation	6
Steroid hormone biosynthesis	4
Transcriptional misregulation in cancer	11

cluster of biological processes, as revealed by the GO enrichment analysis, were associated with the response to high-temperature stress. The significantly enriched transmembrane transport identified through GO enrichment analysis could enhance material exchange between organelles and effectively alleviate cell stimulation (Schendzielorz et al., 2018; Jones et al., 2019; Zhong and Zhao, 2019; Ming et al., 2020). Proteasome ubiquitination, a process that helps to remove damaged proteins to reduce cell damage caused by external stimulus, was downregulated at 24 h (Shringarpure et al., 2001; Myers et al., 2018). The described biological processes may be significant factors in larval stress following high temperature exposure. In addition, among the 20 significantly enriched KEGG signaling pathways, the PI3K-Akt signaling pathway and MAPK signaling pathway play a crucial role in mollusk immunity (Song et al., 2005; Kharchenko et al., 2010; Vergadi et al., 2017; Wang et al., 2019; Qiao et al., 2021; Bao et al., 2022a). The immune response of *S. esculenta* larvae might be activated to protect against the injury caused by high temperature exposure. The results of GO and KEGG functional enrichment analyses show that the larvae of *S. esculenta* might have an intense stress response after being stimulated by high-temperature seawater. The analysis of GO terms and KEGG pathways can facilitate comprehensive understanding of the response mechanisms of *S. esculenta* larvae to temperature stress, which is beneficial for actual artificial breeding.

4.2 Analysis of PPI network

The growth and development of organisms, and metabolism, immunity, and other physiological functions are inseparable from the participation of proteins, which are the basis of all life activities (Ahmad et al., 2021; Chandhini et al., 2021; Li et al., 2021). The analysis of the interaction between proteins facilitates further understanding of the resisting mechanism of high-temperature stress in *S. esculenta* larvae. In the present study, a PPI network was constructed using 97 high-temperature stress-related DEGs in 20 significantly enriched KEGG signaling pathways. The results of the network show that there were strong interactions between proteins. For instance, HSP90AA1 (Heat shock protein 90 alpha family class A member 1), PSMD6 (Proteasome 26S subunit, non-ATPase 6), PSMA5 (Proteasome 20S subunit alpha 5), and ODC1 (Ornithine decarboxylase 1) interacted with over 20 proteins. Therefore, the suggestion of the present authors is that the aforementioned proteins may play central roles in the mechanism of high-temperature stress in *S. esculenta* larvae. Further investigation is necessary to elucidate the mechanism of action of the identified key genes involved in the response to high-temperature stress in *S. esculenta* larvae.

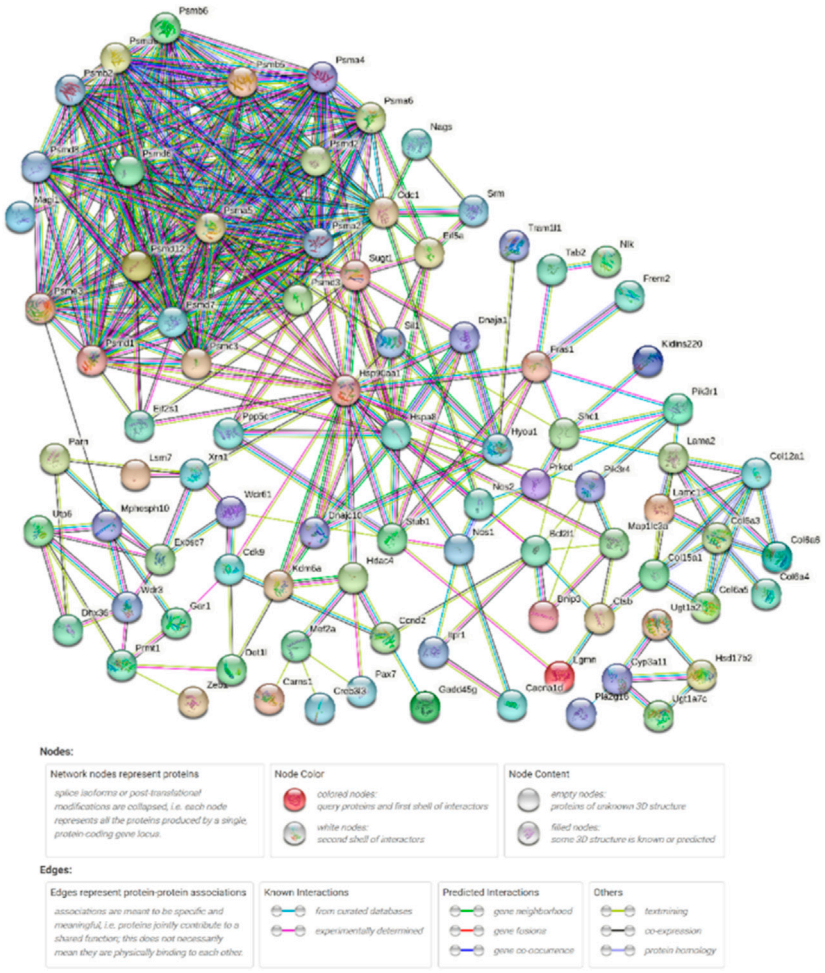

FIGURE 6
High-temperature stress-related PPI network. Network nodes represent proteins. Legends represent relationships between nodes.

TABLE 5 Statistics of temperature stress response-related PPI network parameters.

Network stats	
Number of nodes	92
Number of edges	320
Average node degree	6.96
Clustering coefficient	0.574
Expected number of edges	115
PPI enrichment *p*-value	1.0E-16

4.3 Analysis of critical pathways and families

In the present study, transcriptome sequencing technology was used to analyze the stress reaction of *S. esculenta* larvae in high-temperature seawater, and the results can facilitate further understanding of to further understand the stress mechanism of high-temperature resistance in larvae. Finally, 30 key genes with a high number of interactions or a high number of KEGG signaling pathway involvement were identified.

4.3.1 PI3K-Akt signaling pathway regulates immune defense

The PI3K-Akt signaling pathway plays a central role in immune regulation by controlling the proliferation, differentiation, and migration of immune cells (Song et al., 2005; Vergadi et al., 2017; Bao et al., 2022a). Previous studies have shown that the PI3K-Akt signaling pathway in mollusks is involved in and regulates immune processes (Canesi et al., 2002; Fukao and Koyasu, 2003; Troutman et al., 2012). For example, the PI3K-Akt signaling pathway can regulate phagocytosis during the immune response elicited by organismal stimulation. Further, the pathway can induce an immune defense response and control the apoptosis and growth of immune cells following environmental stimulation (Sun et al., 2016; Yu et al., 2019; Wang et al., 2020). In the present study, two genes including PIK3R1 (Phosphoinositide-3-kinase regulatory subunit 1) and PIK3R4 (Phosphoinositide-3-kinase regulatory subunit 4) were identified. As previously reported, environmental stimuli can down-regulate the expression of

TABLE 6 Thirty key DEGs and their corresponding number of PPI and KEGG signaling pathways.

Gene name	Number of protein-protein interaction	Number of KEGG signaling pathway
COL12A1	6	1
COL15A1	6	1
COL6A3	7	3
COL6A5	3	3
COL6A6	3	3
DNAJA1	5	1
DNAJC10	5	1
HSP90AA1	26	1
HSPA8	14	2
HYOU1	7	1
ODC1	21	1
PIK3R1	5	1
PIK3R4	5	1
PSMA2	19	1
PSMA4	18	1
PSMA5	21	1
PSMA6	19	1
PSMA8	17	1
PSMB2	17	1
PSMB5	17	1
PSMB6	17	1
PSMC3	18	1
PSMD1	20	1
PSMD12	20	1
PSMD2	18	1
PSMD3	19	1
PSMD6	21	1
PSMD7	18	1
PSMD8	17	1
SUGT1	11	1

PIK3R1, which in turn activates the mitochondrial apoptosis and death receptor pathways (Yin et al., 2020). PIK3R4 expression promotes the formation of autolysosomes for protein degradation (Gámez-Díaz et al., 2022). The results suggest that the PI3K-Akt signaling pathway may play a significant role in the resistance of *S. esculenta* larvae to high-temperature stress. We speculated that the PI3K-Akt signaling pathway may induce the activation of immune signaling factors to induce immune defense in larvae when stimulated by high temperature. At the same time, the expressions levels of PIK3R1 and PIK3R4 enriched in this pathway were significantly downregulated, which may also induce the apoptotic pathway to alleviate the damage of high-temperature exposure.

4.3.2 Heat shock protein repair damage

Heat shock proteins are a class of chaperone proteins that is widely present in various organisms and is expressed in large quantities in response to high temperature stimulation (Brokordt et al., 2009; Zuehlke et al., 2015; Wu et al., 2017). The main function of heat shock proteins is to assist in the refolding of misfolded proteins, as well as to remove damaged amino acid chains that cannot be properly folded and to degrade damaged proteins. Such

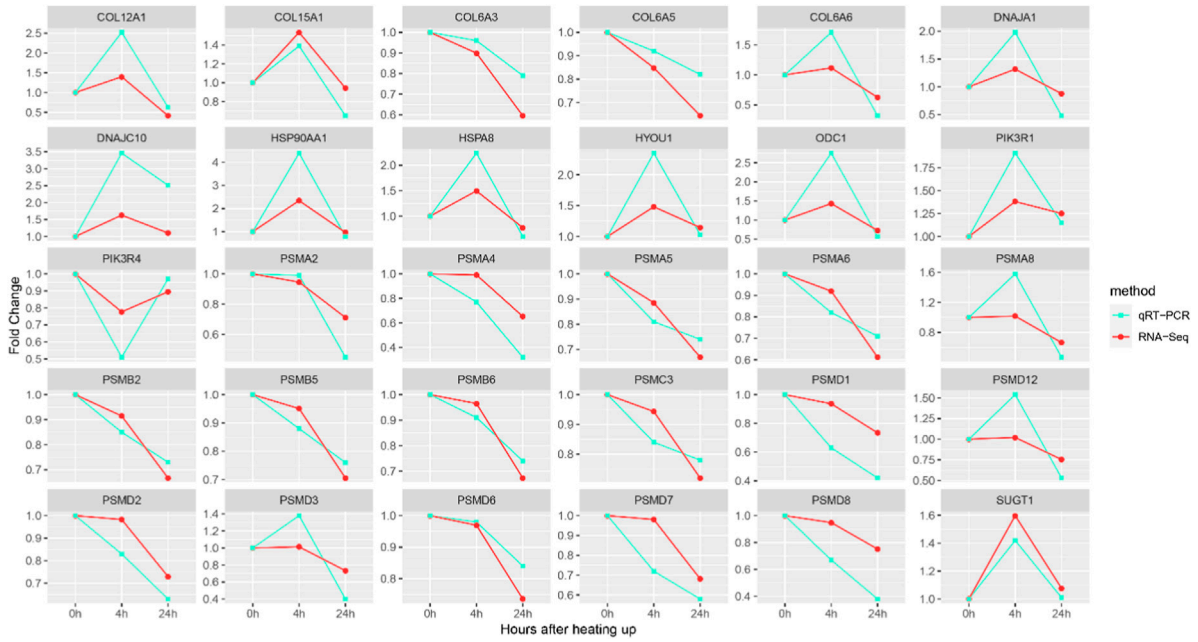

FIGURE 7
qRT-PCR and RNA-Seq results of key DEGs. The Y-axis represents the fold change and the X-axis represents the time of high temperature exposure.

actions contribute to maintaining protein homeostasis within organisms (Sghaier et al., 2004; Brun et al., 2008; Kumar et al., 2022). At the same time, HSPs can also improve the resistance to stress in the organism. Previous studies have indicated that the energy metabolism and antioxidant capacity of *Ruditapes philippinarum* can be improved after a brief high-temperature treatment (Zhang et al., 2023). In the present study, HSP90AA1, HSPA8 [Heat shock protein family A (HSP70) member 8], DNAJC10 [DNAJ heat shock protein family (HSP40) member C10], and DNAJA1 [DNAJ heat shock protein family (HSP40) member A1] in the HSPs family had strong interactions with other proteins, and were significantly upregulated in 4 h after high-temperature stress. HSP90AA1 had the highest number of PPI. Previous studies have linked HSP90AA1 to protein trafficking, transcriptional regulation of gene expression, and epigenetic processes (Csermely et al., 1998; Wegele et al., 2004). HSP90AA1 is sensitive to temperature and can respond quickly to high-temperature stimulation, being a soluble protein of the HSPs family, which mainly exists in the cytoplasm (Pearl and Prodromou, 2006; Swirplies et al., 2019). Similar to the functions of other HSPs family genes, HSP90AA1 can bind to hydrophobic fragments of the proteasome, thereby facilitating generation and removal of damaged proteins (Kuckelkorn et al., 2000; Gouy and Delmotte, 2008; Hayashi and Kamikawa, 2011; Reeg et al., 2016). However, differing from other chaperone proteins, HSP90AA1 has a high binding specificity (Lawless et al., 2013). HSPA8, with the participation of ATP, binds to the hydrophobic fragment of the newly generated protein to help the protein fold correctly (Stricher et al., 2013). Deletion of the gene causes selective tissue deformities during embryonic development (Wang et al., 2022). DNAJC10 and DNAJA1 belong to small molecule HSPs (HSP40s), which can bind to HSP70s through the J domain to enhance the interactions

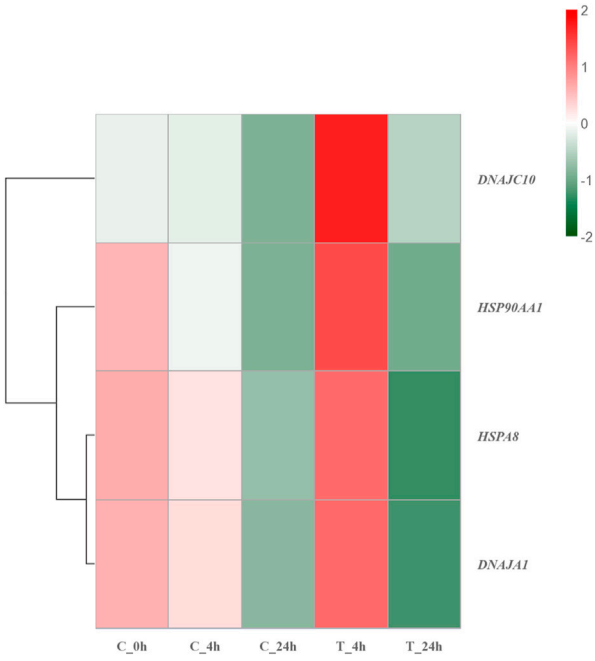

FIGURE 8
Hierarchical clustering heatmap of HSP family genes. Colors ranging from green to red indicating low to high expression levels.

between HSP70s and substrates (Qiu et al., 2006; Liu et al., 2020). HSP40s are involved in immune defense when the organism is stimulated (Yan et al., 2021). Figure 8 shows that the genes of HSPs were significantly upregulated after 4 h of exposure to

high temperature, while the genes of the HSPs were significantly downregulated after 24 h of exposure. Such findings could be attributed to prolonged exposure to high temperatures causing damage to the larval stress resistance system, leading to inadequate expression of HSPs. Based on the described results, macromolecular HSPs, HSP90AA1 and HSPA8, may protect against protein damage caused by high temperatures by binding to newly generated proteins to help them fold correctly. Small molecule HSPs, DNAJC10 and DNAJA1, may combine with HSP70s to help the protein fold correctly and improve the heat resistance of the organism. At the same time, the anti-stress mechanism of *S. esculenta* larvae was activated by HSPs families to alleviate the damage caused by high temperature stimulation. Extended exposure to high temperature can surpass the threshold of the anti-stress system, resulting in a decrease or impairment of the system.

4.3.3 Proteasome function is disrupted

The proteasome is a large cylindrical protein complex that primarily degrades unwanted or damaged proteins by cleaving peptide bonds (Morozov et al., 2019; Račková and Csekes, 2020). Such function is the primary mechanism through which cells regulate the concentrations of specific proteins and remove misfolded proteins (Shin et al., 2020; Wang et al., 2020). The components of the proteasome family include 20s core particles, 19s regulatory particles, and 11s regulatory particles (Raynes et al., 2016). Previous studies have reported significant upregulation of genes encoding proteasome and antioxidant enzymes in *Chlamys opercularis* when exposed to the toxin domoic acid (Ventoso et al., 2019). Similarly, genes involved in the ubiquitin-proteasome pathway were found to be significantly upregulated after *R. philippinarum* infection with *Vibrio anguillarum* (Lin et al., 2022). Among the identified key DEGs in the present study, PSMCs and PSMDs belong to the 26s proteasome, which consists of a 20s core granule and two 19s regulatory granules. PSMD6, a member of the 26S proteasome, had the highest number of PPI within the top three. During the degradation of proteins damaged by high-temperature stimulation by the 26S proteasome, the small molecule protein ubiquitin is required to covalently link the degraded proteins in a process called ubiquitination (Saeki, 2017; Shin et al., 2020). The ubiquitinated protein is then recognized by the 19S regulatory particles, which requires the participation of ATP, and the degradation of the protein is conducted by the β subunit in the 20S core particle (Saeki, 2017; Shin et al., 2020; Bhat et al., 2022). When the high-temperature stress response occurs, heat shock proteins are abundantly expressed. HSPs can bind to the hydrophobic regions of misfolded proteins to guide the conjugation of ubiquitin to misfolded proteins and improve the degradation efficiency of proteasomes (Kuckelkorn et al., 2000; Reeg et al., 2016). The PSMAs and PSMBs identified in the genes belong to the 20S proteasome, which contains only one 20S core particle. PSMA5 belongs to the category of 20S proteasome and is one of the top three genes in the number of PPI. The 20S complex can also act alone to degrade damaged proteins when the organism is acutely stimulated (Shringarpure et al., 2001; Myers et al., 2018; Abi Habib et al., 2020; Sahu et al., 2021). The proteasome plays a central role in removing erroneous proteins and maintaining cell stability in *S. esculenta* larvae when stimulated by high temperatures. In contrast

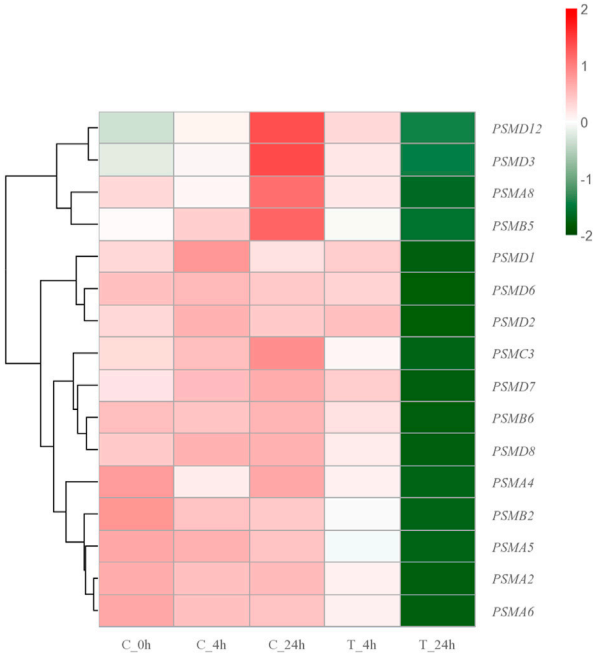

FIGURE 9
Hierarchical clustering heatmap of proteasome family genes. The colors ranging from green to red indicate low to high expression levels.

to the expression trend of HSPs family genes, genes of the proteasome family were consistently downregulated with increasing exposure time after high-temperature exposure (Figure 9). In consideration of the fact that the main function of proteasomes is to degrade erroneous proteins, we hypothesized that proteasomes should operate at normal temperature rather than excessive temperature (28°C). Exposure to high temperatures can lead to a malfunction of the proteasome-ubiquitin system. Meanwhile, prolonged exposure to high-temperature can cause more serious damage to the anti-stress system of *S. esculenta* larvae, which in turn leads to the reduction of gene expression.

4.3.4 Collagen involved in tissue repair

Collagen is a structural protein containing a triple helical domain that plays a central role in maintaining cellular organization (Ricard-Blum and Ruggiero, 2005; Ricard-Blum, 2011). Collagen also has other vital roles, such as being involved in cell adhesion, chemotaxis and migration, as well as regulating wound healing and tissue remodeling (Brown and Timpl, 1995; Myllyharju and Kivirikko, 2004). Previous research has suggested that HSPs play a role in regulating collagen synthesis induced by transforming growth factor-β, possibly through modulation of Smad 2/3 phosphorylation (Lee et al., 2016). Additionally, HSPs have the ability to bind to newly synthesized collagen and assist in proper folding, resulting in the formation of a stable triple helix structure (Nagata, 1996; Mala and Rose, 2010). In the present study, the associated genes enriched to encode the proteasome included COL6A3 (Collagen type VI alpha 3 chain), COL12A1 (Collagen type XII alpha 1 chain), COL15A1 (Collagen type XV alpha 1 chain),

COL6A5 (Collagen type VI alpha 5 chain), and COL6A6 (Collagen type VI alpha 6 chain). The expression levels of such genes were significantly upregulated after 4 and 24 h of exposure. The results suggest that collagen is a significant factor in the resistance of *S. esculenta* larvae to high temperature stress. It is hypothesized that collagen is involved in tissue repair and facilitate repair and regeneration of cells after high temperature stress.

4.4 Other high-temperature stress related DEGs

ODC1, SUGT1 (SGT1 homolog, MIS12 kinetochore complex assembly cochaperone), and HYOU1 (Hypoxia upregulated 1) were also identified as genes that have significant roles in the stress resistance mechanism of *S. esculenta* larvae after high-temperature exposure. The significant downregulation of ODC1 can mitigate the apoptosis and damage resulting from exposure to high temperatures in the organism (Jeffries et al., 2012; Jiang et al., 2018). Additionally, SUGT1 can activate the NOD-like receptor family to eliminate damaged proteins, thereby counteracting the negative impacts of high-temperature stress (da Silva Correia et al., 2007; Hong and Hahn, 2016). The expression product of the HYOU1 gene can activate the PI3K-AKT signaling pathway to promote cell growth and migration (Li et al., 2019; Wang et al., 2022). Such genes were all significantly downregulated, indicating that excessive temperature would destroy the anti-stress system of *S. esculenta* larvae and reduce the expression of proteins.

5 Conclusion

In the present study, transcriptome sequencing technology was used to preliminarily analyze the mechanism of high-temperature stress in *S. esculenta* larvae. Through the analysis of functional enrichment and protein-protein interaction networks, a significant number of DEGs that play crucial roles in response to stress were identified. The expression trends of key genes in the heat shock protein family and proteasome family indicated that prolonged high-temperature exposure would disrupt the larval stress system. In conclusion, high-temperature exposure could significantly affect the *S. esculenta* larvae stress system, and even prolonged high temperature could cause severe damage to the stress system. The obtained results offer valuable insights to investigate the mechanism underlying the stress response of cephalopods upon exposure to high temperatures.

Data availability statement

The datasets presented in this study can be found in online repositories. The names of the repository/repositories and accession number(s) can be found below: https://www.ncbi.nlm.nih.gov/bioproject/PRJNA947123.

Ethics statement

The animal study was reviewed and approved by the protocols of the Institutional Animal Care and Use Committee of the Ludong University (protocol number LDU-IRB20210308NXY) and the China Government Principles for the Utilization and Care of Invertebrate Animals Used in Testing, Research, and Training (State Science and Technology Commission of the People's Republic of China for No. 2, 31 October 1988. http://www.gov.cn/gongbao/content/2011/content_1860757.htm).

Author contributions

ZL and JY designed and supervised the study. YW, XB, TY, WW, XX, and XL prepared the samples. YW, XB, XX, and XL analyzed all sequencing data. YW wrote the manuscript. All authors listed have made a substantial, direct, and intellectual contribution to the work and approved it for publication.

Funding

This research was supported by the earmarked fund for CARS-49, and the Natural Science Foundation of Shandong Province (No. ZR2019BC052).

Conflict of interest

The authors declare that the research was conducted in the absence of any commercial or financial relationships that could be construed as a potential conflict of interest.

Publisher's note

Supplementary material

The Supplementary Material for this article can be found online at: https://www.frontiersin.org/articles/10.3389/fphys.2023.1189375/full#supplementary-material

References

Abi Habib, J., De Plaen, E., Stroobant, V., Zivkovic, D., Bousquet, M. P., Guillaume, B., et al. (2020). Efficiency of the four proteasome subtypes to degrade ubiquitinated or oxidized proteins. *Sci. Rep.* 10 (1), 15765. doi:10.1038/s41598-020-71550-5

Ahmad, I., Ahmed, I., Fatma, S., and Peres, H. (2021). Role of branched-chain amino acids on growth, physiology and metabolism of different fish species: A review. *Aquacult. Nutr.* 27, 1270–1289. doi:10.1111/anu.13267

Al-Ghussain, L. (2019). Global warming: Review on driving forces and mitigation. *Environ. Prog. Sustain. Energy.* 38, 13–21. doi:10.1002/ep.13041

Alfonso, S., Gesto, M., and Sadoul, B. (2021). Temperature increase and its effects on fish stress physiology in the context of global warming. *J. Fish. Biol.* 98 (6), 1496–1508. doi:10.1111/jfb.14599

Bao, X., Wang, W., Chen, X., Feng, Y., Xu, X., Sun, G., et al. (2022a). Exploration of immune response mechanisms in cadmium and copper co-exposed juvenile golden cuttlefish (*Sepia esculenta*) based on transcriptome profiling. *Front. Immunol.* 13, 963931. doi:10.3389/fimmu.2022.963931

Bao, X., Wang, W., Yuan, T., Li, Y., Chen, X., Liu, X., et al. (2022b). Transcriptome profiling based on larvae at different time points after hatching provides a core set of gene resource for understanding the immune response mechanisms of the egg-protecting behavior against *Vibrio anguillarum* infection in *Amphioctopus fangsiao*. *Fish. Shellfish Immunol.* 124, 430–441. doi:10.1016/j.fsi.2022.04.030

Bhat, S. A., Vasi, Z., Adhikari, R., Gudur, A., Ali, A., Jiang, L., et al. (2022). Ubiquitin proteasome system in immune regulation and therapeutics. *Curr. Opin. Pharmacol.* 67, 102310. doi:10.1016/j.coph.2022.102310

Bian, L., Liu, C., Chen, S., Zhao, F., Ge, J., and Tan, J. (2018). Transcriptome analysis of gene expression patterns during embryonic development in golden cuttlefish (*Sepia esculenta*). *Genes Genomics* 40 (3), 253–263. doi:10.1007/s13258-017-0588-6

Brokordt, K., Leiva, N., Jeno, K., Martínez, G., and Winkler, F. (2009). Effect of allozyme heterozygosity on basal and induced levels of heat shock protein (Hsp70), in juvenile *Concholepas concholepas* (Mollusca). *J. Exp. Mar. Biol. Ecol.* 370 (1-2), 18–26. doi:10.1016/j.jembe.2008.11.007

Brown, J. C., and Timpl, R. (1995). The collagen superfamily. *Int. Arch. Allergy Immunol.* 107 (4), 484–490. doi:10.1159/000237090

Brun, N. T., Bricelj, V. M., MacRae, T. H., and Ross, N. W. (2008). Heat shock protein responses in thermally stressed bay scallops, *Argopecten irradians*, and sea scallops, *Placopecten magellanicus*. *J. Exp. Mar. Biol. Ecol.* 358 (2), 151–162. doi:10.1016/j.jembe.2008.02.006

Canesi, L., Gallo, G., Gavioli, M., and Pruzzo, C. (2002). Bacteria-hemocyte interactions and phagocytosis in marine bivalves. *Microsc. Res. Tech.* 57 (6), 469–476. doi:10.1002/jemt.10100

Chandhini, S., Trumboo, B., Jose, S., Varghese, T., Rajesh, M., and Kumar, V. J. R. (2021). Insulin-like growth factor signalling and its significance as a biomarker in fish and shellfish research. *Fish. Physiol. Biochem.* 47 (4), 1011–1031. doi:10.1007/s10695-021-00961-6

Csermely, P., Schnaider, T., Soti, C., Prohászka, Z., and Nardai, G. (1998). The 90-kDa molecular chaperone family: Structure, function, and clinical applications. A comprehensive review. *Pharmacol. Ther.* 79 (2), 129–168. doi:10.1016/s0163-7258(98)00013-8

da Silva Correia, J., Miranda, Y., Leonard, N., and Ulevitch, R. (2007). SGT1 is essential for Nod1 activation. *Proc. Natl. Acad. Sci. U. S. A.* 104 (16), 6764–6769. doi:10.1073/pnas.0610926104

Dalvi, R. S., Das, T., Debnath, D., Yengkokpam, S., Baruah, K., Tiwari, L. R., et al. (2017). Metabolic and cellular stress responses of catfish, *Horabagrus brachysoma* (Gunther) acclimated to increasing temperatures. *J. Therm. Biol.* 65, 32–40. doi:10.1016/j.jtherbio.2017.02.003

Fukao, T., and Koyasu, S. (2003). PI3K and negative regulation of TLR signaling. *Trends Immunol.* 24 (7), 358–363. doi:10.1016/s1471-4906(03)00139-x

Gámez-Díaz, L., Ligeon, L., Sindram, E., Deau, M., Sanchez-Martin, P., Nestel, S., et al. (2022). LRBA balances antigen presentation and T-cell responses by facilitating autophagy through the binding to PIK3R4 and FYCO1. Biorxiv. doi:10.1101/2022.10.17.512524

Ginger, K. W., Vera, C. B., R, D., Dennis, C. K., Adela, L. J., Yu, Z., et al. (2013). Larval and post-larval stages of Pacific oyster (*Crassostrea gigas*) are resistant to elevated CO2. *PLoS One* 8 (5), e64147. doi:10.1371/journal.pone.0064147

Gouy, M., and Delmotte, S. (2008). Remote access to ACNUC nucleotide and protein sequence databases at PBIL. *Biochimie* 90 (4), 555–562. doi:10.1016/j.biochi.2007.07.003

Guo, H., Zhang, D., Wang, L., Li, W., He, P., Näslund, J., et al. (2021). Sperm competition in golden cuttlefish *Sepia esculenta*: The impact of mating order and male size. *Aquaculture* 530, 735929. doi:10.1016/j.aquaculture.2020.735929

Hayashi, K., and Kamikawa, Y. (2011). HSP90 is crucial for regulation of LAT expression in activated T cells. *Mol. Immunol.* 48 (6-7), 941–946. doi:10.1016/j.molimm.2010.12.014

Hong, T. J., and Hahn, J. S. (2016). Application of SGT1-Hsp90 chaperone complex for soluble expression of NOD1 LRR domain in *E. coli*. *Biochem. Biophys. Res. Commun.* 478 (4), 1647–1652. doi:10.1016/j.bbrc.2016.08.174

Jeffries, K. M., Hinch, S. G., Sierocinski, T., Clark, T. D., Eliason, E. J., Donaldson, M. R., et al. (2012). Consequences of high temperatures and premature mortality on the transcriptome and blood physiology of wild adult sockeye salmon (*Oncorhynchus nerka*). *Ecol. Evol.* 2 (7), 1747–1764. doi:10.1002/ece3.274

Jiang, F., Gao, Y., Dong, C., and Xiong, S. (2018). ODC1 inhibits the inflammatory response and ROS-induced apoptosis in macrophages. *Biochem. Biophys. Res. Commun.* 504 (4), 734–741. doi:10.1016/j.bbrc.2018.09.023

Jiao, X., Sherman, B. T., Huang da, W., Stephens, R., Baseler, M. W., Lane, H. C., et al. (2012). DAVID-WS: A stateful web service to facilitate gene/protein list analysis. *Bioinformatics* 28 (13), 1805–1806. doi:10.1093/bioinformatics/bts251

Jones, H. R., Johnson, K. M., and Kelly, M. W. (2019). Synergistic effects of temperature and salinity on the gene expression and physiology of *Crassostrea virginica*. *Integr. Comp. Biol.* 59 (2), 306–319. doi:10.1093/icb/icz035

Jones, M. C., Dye, S. R., Fernandes, J. A., Frölicher, T. L., Pinnegar, J. K., Warren, R., et al. (2013). Predicting the impact of climate change on threatened species in UK waters. *PLoS One* 8 (1), e54216. doi:10.1371/journal.pone.0054216

Kaplan, M. B., Mooney, T. A., McCorkle, D. C., and Cohen, A. L. (2013). Adverse effects of ocean acidification on early development of squid (*Doryteuthis pealeii*). *PLoS One* 8 (5), e63714. doi:10.1371/journal.pone.0063714

Kharchenko, O. A., Grinkevich, V. V., Vorobiova, O. V., and Grinkevich, L. N. (2010). Learning-induced lateralized activation of the MAPK/ERK cascade in identified neurons of the food-aversion network in the mollusk *Helix lucorum*. *Neurobiol. Learn. Mem.* 94 (2), 158–166. doi:10.1016/j.nlm.2010.05.002

Kuckelkorn, U., Knuehl, C., Boes-Fabian, B., Drung, I., and Kloetzel, P. M. (2000). The effect of heat shock on 20S/26S proteasomes. *Biol. Chem.* 381 (9-10), 1017–1023. doi:10.1515/BC.2000.125

Kumar, V., Roy, S., Behera, B. K., and Das, B. K. (2022). Heat shock proteins (hsps) in cellular homeostasis: A promising tool for health management in Crustacean aquaculture. *Life (Basel).* 12 (11), 1777. doi:10.3390/life12111777

Lawless, N., Blacklock, K., Berrigan, E., and Verkhivker, G. (2013). Structural bioinformatics and protein docking analysis of the molecular chaperone-kinase interactions: Towards allosteric inhibition of protein kinases by targeting the hsp90-cdc37 chaperone machinery. *Pharm. (Basel)* 6 (11), 1407–1428. doi:10.3390/ph6111407

Lee, S. B., Lim, A. R., Rah, D. K., Kim, K. S., and Min, H. J. (2016). Modulation of heat shock protein 90 affects TGF-β-induced collagen synthesis in human dermal fibroblast cells. *Tissue Cell* 48 (6), 616–623. doi:10.1016/j.tice.2016.09.002

Li, S., Liu, C., Huang, J., Liu, Y., Zhang, S., Zheng, G., et al. (2016). Transcriptome and biomineralization responses of the pearl oyster *Pinctada fucata* to elevated CO2 and temperature. *Sci. Rep.* 6, 18943. doi:10.1038/srep18943

Li, X., Zhang, N. X., Ye, H. Y., Song, P. P., Chang, W., Chen, L., et al. (2019). HYOU1 promotes cell growth and metastasis via activating PI3K/AKT signaling in epithelial ovarian cancer and predicts poor prognosis. *Eur. Rev. Med. Pharmacol. Sci.* 23 (10), 4126–4135. doi:10.26355/eurrev_201901_17914

Li, Z., Bao, X., Liu, X., Li, Y., Cui, M., Liu, X., et al. (2021). Transcriptome profiling based on protein-protein interaction networks provides a set of core genes for understanding the immune response mechanisms of the egg-protecting behavior in *Octopus ocellatus*. *Fish. Shellfish Immunol.* 117, 113–123. doi:10.1016/j.fsi.2021.07.020

Lin, Z., Nie, H., Zhang, Y., Yin, Z., and Yan, X. (2022). Genome-wide identification and analysis of HECT E3 ubiquitin ligase gene family in *Ruditapes philippinarum* and their involvement in the response to heat stress and *Vibrio anguillarum* infection. *Comp. Biochem. Physiol. Part D. Genomics Proteomics.* 43, 101012. doi:10.1016/j.cbd.2022.101012

Liu, L., Lin, L., Ma, Z., Wang, G., and Wu, M. (2020). iTRAQ-based quantitative proteomic analysis of *Sargassum fusiformein* response to high temperature stress. *Aquacult. Res.* 52 (1), 185–195. doi:10.1111/are.14880

Liu, Q., Liang, C., and Zhou, L. (2020). Structural and functional analysis of the Hsp70/Hsp40 chaperone system. *Protein Sci.* 29 (2), 378–390. doi:10.1002/pro.3725

Love, M. I., Huber, W., and Anders, S. (2014). Moderated estimation of fold change and dispersion for RNA-seq data with DESeq2. *Genome Biol.* 15 (12), 550. doi:10.1186/s13059-014-0550-8

Mala, J. G., and Rose, C. (2010). Interactions of heat shock protein 47 with collagen and the stress response: An unconventional chaperone model? *Life Sci.* 87 (19-22), 579–586. doi:10.1016/j.lfs.2010.09.024

Martinez, M., Mangano, M. C., Maricchiolo, G., Genovese, L., Mazzola, A., and Sarà, G. (2018). Measuring the effects of temperature rise on Mediterranean shellfish aquaculture. *Ecol. Indic.* 88, 71–78. doi:10.1016/j.ecolind.2018.01.002

Masotti, A., and Preckel, T. (2006). Analysis of small RNAs with the agilent 2100 bioanalyzer. *Nat. Methods.* 3, 658. doi:10.1038/nmeth908

Ming, Z., Pang, Y., and Liu, J. (2020). Mechanical deformation mediated transmembrane transport. *Macromol. Rapid Commun.* 41 (2), e1900518. doi:10.1002/marc.201900518

Morozov, A. V., Burov, A. V., Astakhova, T. M., Spasskaya, D. S., Margulis, B. A., and Karpov, V. L. (2019). Dynamics of the functional activity and expression of proteasome subunits during cellular adaptation to heat shock. *Mol. Biol. Mosk.* 53 (4), 638–647. doi:10.1134/S0026898419040086

Morozova, O., Hirst, M., and Marra, M. A. (2009). Applications of new sequencing technologies for transcriptome analysis. *Annu. Rev. Genomics Hum. Genet.* 10, 135–151. doi:10.1146/annurev-genom-082908-145957

Myers, N., Olender, T., Savidor, A., Levin, Y., Reuven, N., and Shaul, Y. (2018). The disordered landscape of the 20S proteasome substrates reveals tight association with phase separated granules. *Proteomics* 18 (21-22), e1800076. doi:10.1002/pmic.201800076

Myllyharju, J., and Kivirikko, K. I. (2004). Collagens, modifying enzymes and their mutations in humans, flies and worms. *Trends Genet.* 20 (1), 33–43. doi:10.1016/j.tig.2003.11.004

Nagata, K. (1996). Hsp47: A collagen-specific molecular chaperone. *Trends biochem. Sci.* 21 (1), 22–26. doi:10.1016/0968-0004(96)80881-4

Nick, F. M., Vieli, A., Andersen, M. L., Joughin, I., Payne, A., Edwards, T. L., et al. (2013). Future sea-level rise from Greenland's main outlet glaciers in a warming climate. *Nature* 497 (7448), 235–238. doi:10.1038/nature12068

Pearl, L. H., and Prodromou, C. (2006). Structure and mechanism of the Hsp90 molecular chaperone machinery. *Annu. Rev. Biochem.* 75, 271–294. doi:10.1146/annurev.biochem.75.103004.142738

Qian, X., Ba, Y., Zhuang, Q., and Zhong, G. (2014). RNA-Seq technology and its application in fish transcriptomics. *OMICS* 18 (2), 98–110. doi:10.1089/omi.2013.0110

Qiao, Y., Yan, W., He, J., Liu, X., Zhang, Q., and Wang, X. (2021). Identification, evolution and expression analyses of mapk gene family in Japanese flounder (*Paralichthys olivaceus*) provide insight into its divergent functions on biotic and abiotic stresses response. *Aquat. Toxicol.* 241, 106005. doi:10.1016/j.aquatox.2021.106005

Qiu, X. B., Shao, Y. M., Miao, S., and Wang, L. (2006). The diversity of the DnaJ/Hsp40 family, the crucial partners for Hsp70 chaperones. *Cell Mol. Life Sci.* 63 (22), 2560–2570. doi:10.1007/s00018-006-6192-6

Račková, L., and Csekes, E. (2020). Proteasome biology: Chemistry and bioengineering insights. *Polym. (Basel)* 12 (12), 2909. doi:10.3390/polym12122909

Rahman, M. S., and Rahman, M. S. (2021). Effects of elevated temperature on prooxidant-antioxidant homeostasis and redox status in the American oyster: Signaling pathways of cellular apoptosis during heat stress. *Environ. Res.* 196, 110428. doi:10.1016/j.envres.2020.110428

Raynes, R., Pomatto, L. C., and Davies, K. J. (2016). Degradation of oxidized proteins by the proteasome: Distinguishing between the 20S, 26S, and immunoproteasome proteolytic pathways. *Mol. Asp. Med.* 50, 41–55. doi:10.1016/j.mam.2016.05.001

Reeg, S., Jung, T., Castro, J. P., Davies, K. J. A., Henze, A., and Grune, T. (2016). The molecular chaperone Hsp70 promotes the proteolytic removal of oxidatively damaged proteins by the proteasome. *Free Radic. Biol. Med.* 99, 153–166. doi:10.1016/j.freeradbiomed.2016.08.002

Ren, L., Zhu, B., Zhang, Y., Wang, H., Li, C., Su, Y., et al. (2004). The research of applying primer premier 5.0 to design PCR primer. *J. Jinzhou. Med. Coll.* 25 (6), 43–46. doi:10.3969/j.issn.1674-0424.2004.06.015

Ricard-Blum, S., and Ruggiero, F. (2005). The collagen superfamily: From the extracellular matrix to the cell membrane. *Pathol. Biol. Paris.* 53 (7), 430–442. doi:10.1016/j.patbio.2004.12.024

Ricard-Blum, S. (2011). The collagen family. *Cold Spring Harb. Perspect. Biol.* 3 (1), a004978. doi:10.1101/cshperspect.a004978

Saeki, Y. (2017). Ubiquitin recognition by the proteasome. *J. Biochem.* 161 (2), 113–124. doi:10.1093/jb/mvw091

Sahu, I., Mali, S. M., Sulkshane, P., Xu, C., Rozenberg, A., Morag, R., et al. (2021). The 20S as a stand-alone proteasome in cells can degrade the ubiquitin tag. *Nat. Commun.* 12 (1), 6173. doi:10.1038/s41467-021-26427-0

Samaras, A., Papandroulakis, N., Lika, K., and Pavlidis, M. (2018). Water temperature modifies the acute stress response of European sea bass, *Dicentrarchus labrax* L. (1758). *J. Therm. Biol.* 78, 84–91. doi:10.1016/j.jtherbio.2018.09.006

Schendzielorz, A. B., Bragoszewski, P., Naumenko, N., Gomkale, R., Schulz, C., Guiard, B., et al. (2018). Motor recruitment to the TIM23 channel's lateral gate restricts polypeptide release into the inner membrane. *Nat. Commun.* 9 (1), 4028. doi:10.1038/s41467-018-06492-8

Sghaier, H., Le Ai, T. H., Horiike, T., and Shinozawa, T. (2004). Molecular chaperones: Proposal of a systematic computer-oriented nomenclature and construction of a centralized database. *Silico. Biol.* 4 (3), 311–322.

Shin, J. Y., Muniyappan, S., Tran, N. N., Park, H., Lee, S. B., and Lee, B. H. (2020). Deubiquitination reactions on the proteasome for proteasome versatility. *Int. J. Mol. Sci.* 21 (15), 5312. doi:10.3390/ijms21155312

Shringarpure, R., Grune, T., and Davies, K. J. (2001). Protein oxidation and 20S proteasome-dependent proteolysis in mammalian cells. *Cell Mol. Life Sci.* 58 (10), 1442–1450. doi:10.1007/PL00000787

Song, G., Ouyang, G., and Bao, S. (2005). The activation of Akt/PKB signaling pathway and cell survival. *J. Cell. Mol. Med.* 9 (1), 59–71. doi:10.1111/j.1582-4934.2005.tb00337.x

Stricher, F., Macri, C., Ruff, M., and Muller, S. (2013). HSPA8/HSC70 chaperone protein: Structure, function, and chemical targeting. *Autophagy* 9 (12), 1937–1954. doi:10.4161/auto.26448

Sun, Y., Zhang, X., Wang, G., Lin, S., Zeng, X., Wang, Y., et al. (2016). PI3K-AKT signaling pathway is involved in hypoxia/thermal-induced immunosuppression of small abalone *Haliotis diversicolor*. *Fish. Shellfish Immunol.* 59, 492–508. doi:10.1016/j.fsi.2016.11.011

Swirplies, F., Wuertz, S., Baßmann, B., Orban, A., Schäfer, N., Brunner, R. M., et al. (2019). Identification of molecular stress indicators in pikeperch *Sander lucioperca* correlating with rising water temperatures. *Aquaculture* 501, 260–271. doi:10.1016/j.aquaculture.2018.11.043

Szklarczyk, D., Gable, A. L., Lyon, D., Junge, A., Wyder, S., Huerta-Cepas, J., et al. (2019). STRING v11: Protein-protein association networks with increased coverage, supporting functional discovery in genome-wide experimental datasets. *Nucleic Acids Res.* 47 (D1), D607–D613. doi:10.1093/nar/gky1131

Trigg, S. A., Mitchell, K. R., Thompson, R. E., Eudeline, B., Vadopalas, B., Timmins-Schiffman, E. B., et al. (2020). Temporal proteomic profiling reveals insight into critical developmental processes and temperature-influenced physiological response differences in a bivalve mollusc. *Bmc. Genomics.* 21 (1), 723. doi:10.1186/s12864-020-07127-3

Troutman, T. D., Bazan, J. F., and Pasare, C. (2012). Toll-like receptors, signaling adapters and regulation of the pro-inflammatory response by PI3K. *Cell Cycle* 11 (19), 3559–3567. doi:10.4161/cc.21572

Vargas-Chacoff, L., Muñoz, J. L. P., Ocampo, D., Paschke, K., and Navarro, J. M. (2019). The effect of alterations in salinity and temperature on neuroendocrine responses of the Antarctic fish *Harpagifer antarcticus*. *Comp. Biochem. Physiol. A. Mol. Integr. Physiol.* 235, 131–137. doi:10.1016/j.cbpa.2019.05.029

Ventoso, P., Pazos, A. J., Pérez-Parallé, M. L., Blanco, J., Triviño, J. C., and Sánchez, J. L. (2019). RNA-seq transcriptome profiling of the queen scallop (*Aequipecten opercularis*) digestive gland after exposure to domoic acid-producing *pseudo-nitzschia*. *Toxins (Basel).* 11 (2), 97. doi:10.3390/toxins11020097

Vergadi, E., Ieronymaki, E., Lyroni, K., Vaporidi, K., and Tsatsanis, C. (2017). Akt signaling pathway in macrophage activation and M1/M2 polarization. *J. Immunol.* 198 (3), 1006–1014. doi:10.4049/jimmunol.1601515

Wang, C., Zhang, X., Wang, X., Zhai, Y., Li, M., Pan, J., et al. (2022). Genetic deletion of hspa8 leads to selective tissue malformations in zebrafish embryonic development. *J. Cell Sci.* 135 (21), jcs259734. doi:10.1242/jcs.259734

Wang, H., Pan, L., Xu, R., Si, L., and Zhang, X. (2019). The molecular mechanism of Nrf2-Keap1 signaling pathway in the antioxidant defense response induced by BaP in the scallop *Chlamys farreri*. *Fish. Shellfish Immunol.* 92, 489–499. doi:10.1016/j.fsi.2019.06.006

Wang, W., Jiang, X., Xia, F., Chen, X., Li, G., Liu, L., et al. (2022). HYOU1 promotes cell proliferation, migration, and invasion via the PI3K/AKT/FOXO1 feedback loop in bladder cancer. *Mol. Biol. Rep.* 50, 453–464. doi:10.1007/s11033-022-07978-x

Wang, X., Meul, T., and Meiners, S. (2020). Exploring the proteasome system: A novel concept of proteasome inhibition and regulation. *Pharmacol. Ther.* 211, 107526. doi:10.1016/j.pharmthera.2020.107526

Wang, Y., Zhou, S., Liu, T., Chen, M., and Zhang, X. (2020). De novo transcriptome analysis of stressed blood clam (*Anadara broughtonii*) and identification of genes associated with hemoglobin. *Genes Genomics* 42 (2), 189–202. doi:10.1007/s13258-019-00887-7

Wegele, H., Müller, L., and Buchner, J. (2004). Hsp70 and Hsp90-a relay team for protein folding. *Rev. Physiol. Biochem. Pharmacol.* 151, 1–44. doi:10.1007/s10254-003-0021-1

Wu, J., Liu, T., Rios, Z., Mei, Q., Lin, X., and Cao, S. (2017). Heat shock proteins and cancer. *Trends Pharmacol. Sci.* 38 (3), 226–256. doi:10.1016/j.tips.2016.11.009

Yan, W., Qiao, Y., Qu, J., Liu, X., Zhang, Q., and Wang, X. (2021). The hsp40 gene family in Japanese flounder: Identification, phylogenetic relationships, molecular evolution analysis, and expression patterns. *Front. Mar. Sci.* 7. doi:10.3389/fmars.2020.596534

Yin, K., Cui, Y., Sun, T., Qi, X., Zhang, Y., and Lin, H. (2020). Antagonistic effect of selenium on lead-induced neutrophil apoptosis in chickens via miR-16-5p targeting of PiK3R1 and IGF1R. *Chemosphere* 246, 125794. doi:10.1016/j.chemosphere.2019.125794

Yu, J., Wang, H., Yue, X., and Liu, B. (2019). Dynamic immune and metabolism response of clam *Meretrix petechialis* to *Vibrio challenge* revealed by a time series of transcriptome analysis. *Fish. Shellfish Immunol.* 94, 17–26. doi:10.1016/j.fsi.2019.08.057

Zhang, Y., Nie, H., and Yan, X. (2023). Metabolomic analysis provides new insights into the heat-hardening response of Manila clam (*Ruditapes philippinarum*) to high temperature stress. *Sci. Total Environ.* 857 (2), 159430. doi:10.1016/j.scitotenv.2022.159430

Zhong, J., and Zhao, X. (2019). Transcriptomic analysis of viable but non-culturable *Escherichia coli* O157:H7 formation induced by low temperature. *Microorganisms* 7 (12), 634. doi:10.3390/microorganisms7120634

Zuehlke, A. D., Beebe, K., Neckers, L., and Prince, T. (2015). Regulation and function of the human HSP90AA1 gene. *Gene* 570 (1), 8–16. doi:10.1016/j.gene.2015.06.018

frontiers | Frontiers in Physiology

TYPE Original Research
PUBLISHED 18 May 2023
DOI 10.3389/fphys.2023.1201914

OPEN ACCESS

EDITED BY
Yi-Feng Li,
Shanghai Ocean University, China

REVIEWED BY
Peng Liu,
University of South China, China
Xiang-Fei Li,
Nanjing Agricultural University, China

*CORRESPONDENCE
Qichen Jiang,
qichenjiang@live.cn
Xiaojun Zhang,
zxj9307@163.com

†These authors share first authorship

RECEIVED 07 April 2023
ACCEPTED 02 May 2023
PUBLISHED 18 May 2023

CITATION
Liu G, Zhu C, Gao X, Zheng Y, Zhu X, Jiang H, Wei W, Jiang Q and Zhang X (2023), Single-cell transcriptome analysis reveals a cellular immune response in freshwater dark sleeper (*Odontobutis potamophila*) after infection with *Aeromonas veronii*.
Front. Physiol. 14:1201914.
doi: 10.3389/fphys.2023.1201914

Single-cell transcriptome analysis reveals a cellular immune response in freshwater dark sleeper (*Odontobutis potamophila*) after infection with *Aeromonas veronii*

Guoxing Liu[1,2,3†], Chenxi Zhu[2†], Xiaojian Gao[1], You Zheng[2,3], Xinhai Zhu[1], Hucheng Jiang[2,3], Wanhong Wei[1], Qichen Jiang[1,2,3*] and Xiaojun Zhang[1*]

[1]College of Animal Science and Technology, Yangzhou University, Yangzhou, China, [2]Freshwater Fisheries Research Institute of Jiangsu Province, Nanjing, China, [3]Low-temperature Germplasm Bank of Important Economic Fish (Freshwater Fisheries Research Institute of Jiangsu Province) of Jiangsu Provincial Science and Technology Resources (Agricultural Germplasm Resources) Coordination Service Platform, Nanjing, China

The bacterium *Aeromonas veronii* is a co-pathogenic species that can negatively impact the health of both humans and aquatic animals. In this study, we used single-cell transcriptome analysis (scRNA-seq) to investigate the effects of infection with *A. veronii* on head kidney cells and the regulation of gene expression in the dark sleeper (*Odontobutis potamophila*). scRNA-seq was used to assess the effects of infection with *A. veronii* in *O. potamophila* B cells, endothelial cells, macrophages, and granulocytes, and differential enrichment analysis of gene expression in B cells and granulocytes was performed. The analyses revealed a significant increase in neutrophils and decrease in eosinophils in granulocytes infected with *A. veronii*. Activation of neutrophils enhanced ribosome biogenesis by up-regulating the expression of *RPS12* and *RPL12* to fight against invading pathogens. Crucial pro-inflammatory mediators *IL1B, IGHV1-4*, and the major histocompatibility class II genes *MHC2A* and *MHC2DAB*, which are involved in virulence processes, were upregulated, suggesting that *A. veronii* activates an immune response that presents antigens and activates immunoglobulin receptors in B cells. These cellular immune responses triggered by infection with *A. veronii* enriched the available scRNA-seq data for teleosts, and these results are important for understanding the evolution of cellular immune defense and functional differentiation of head kidney cells.

KEYWORDS

***Aeromonas* veronii, ScRNA-seq, Odontobutis potamophila, immune response, granulocytes, B cell**

1 Introduction

Aeromonas veronii is a globally distributed pathogenic bacterium that can cause various diseases and affect the healthy growth of aquatic organisms such as fish, shrimp, and shellfish, resulting in huge losses to the aquaculture industry (Hickman-Brenner et al., 1987). *A. veronii* is widely dispersed in rivers, lakes, ponds, and seas and has a high degree of

environmental adaptability. It is a typical human-animal-aquatic pathogen that may be isolated from water sources, soil, and the bodies of both humans and animals (Wu et al., 2007).

The dark sleeper (*Odontobutis potamophila*) is a freshwater fish popular in China (Iwata et al., 1985). It has high meat content, tasty flavor, high nutritional value, and excellent health benefits (Zhu et al., 2022). However, in May 2021, *O. potamophila* in a fish farm in Changshu, Jiangsu Province, China, experienced an illness, with skin ulcers as one of the primary symptoms. *Aeromonas veronii* was later shown to be the primary pathogen in the sick fish. Studies have shown that *A. veronii* can cause hemorrhagic septicemia in carp (*Carassius gibelio*) (Sun et al., 2016), tilapia (*Oreochromis niloticus*) (Dong et al., 2017), bass (*L. maculatus*) (Wang et al., 2021), and channel catfish (*Ictalurus punctatus*) (Hoai et al., 2019), mainly manifesting as hemorrhage and congestion of the body surface and organs to varying degrees (Yu et al., 2010). In a prior study of the pathogenicity and histopathology of *A. veronii* in *O. potamophila*, we discovered that *A. veronii* triggered innate immunity and led to mass mortality of the hosts (Liu et al., 2022). Acute mortality of the catfish *Ictalurus lunetas* also occurred after infection by *A. veronii* (Zhang et al., 2016). In *Lateolabrax maculatus*, *A. veronii* infection rapidly activated the chemokine signal pathway and stimulated an acute inflammatory response (Wang et al., 2022).

Molecular understanding of fish immunology is growing, but *in vitro* and *in vivo* research on fish immune activity is still in its infancy. Currently, data on markers for specific fish cell populations and cell subpopulation determinants are limited (Huang et al., 2021), which is an ongoing issue for fish immunologists. However, several cutting-edge methods, including single-cell RNA sequencing (scRNA-seq), are now being used to investigate the cellular immunological functions of teleost fish.

In the present study, we performed scRNA-seq on head kidney cells of *O. potamophila* to characterize the functional heterogeneity of cells. We identified genetic markers for each cell cluster and analyzed their main functions, thereby filling a gap in the taxonomic identification of *O. potamophila* cells. We also comprehensively analyzed the cellular immune response and gene expression profile under the influence of *A. veronii* infection, which is important for a better understanding of the immune response of *O. potamophila* to pathogens.

2 Materials and methods

2.1 Experimental fish and *A. Veronii* strains

Healthy *O. potamophila* (15 ± 1.5 g) were provided by Yangzhong Base of the Freshwater Fisheries Research Institute of Jiangsu Province, China. *Aeromonas veronii* stl3-1 was isolated from diseased *O. potamophila* (see (Liu et al., 2022) for specific information about the diseased strain). *Aeromonas veronii* stl3-1 was inoculated in a common broth medium, incubated at 28°C and 1,180 g on a shaker for 18 h, centrifuged at 5,000 *g* for 10 min, and the supernatant was discarded. The bacteria in the pellet were resuspended in sterile phosphate-buffered saline at pH 7.4, and the concentration was adjusted to 1.8×10^6 CFU/mL.

2.2 Artificial infection experiment

After 1 week of acclimation, healthy *O. potamophila* were divided into an infected group (TAV) and an uninfected control group (CK). Three replicates, each containing 20 fishes, were set up for each group. Each fish in the infected group was injected intraperitoneally with 100 μL (1.8×10^6 CFU/mL) of *A. veronii* stl3-1 suspension. The fish in the control group were injected with sterile phosphate buffered saline (pH 7.4) in the same manner and at the same dose. Fish were sacrificed, and head kidney tissues from the infected and control groups were taken 24 h after injection. To avoid small sample size and individual differences, three head kidney tissues from each biological replicate were mixed to generate a sample).

2.3 Ethical statement

All treatments of fish in this study were strictly in accordance with the guidelines of Animal Experiment Ethics Committee of Yangzhou University. The protocol was approved by Animal Experiment Ethics Committee of Yangzhou University (permit number: 201802003).

2.3 Cell range analysis and quality control based on full-length transcriptome data

We compared full-length transcripts produced by triple sequencing splicing and performed data quality statistics on the raw data using the 10 × single-cell transcriptome quality control analysis program Cell Ranger (V6.1.2) (Melsted et al., 2021). Single-cell cDNA libraries were sequenced using the double-end sequencing mode of the Illumina HiSeq 4000 sequencing platform. The program locates cell-specific barcode sequence markers in the sequence and unique molecular identifier markers for various mRNA molecules inside each cell to quantify the high-throughput single-cell transcriptome.

2.4 Dimensionality reduction and cluster analysis

The filtered data were normalized before analysis by dividing the count value by 10,000 to obtain the log value. We selected the top 2000 highly variable genes for subsequent descending and clustering analysis. Principal component analysis was used for dimensionality reduction, and then Uniform Manifold Approximation and Projection (UMAP) and t-Distributed Stochastic Neighbor Embedding (tSNE) were used for secondary dimensionality reduction and visualization. After the clustering results were obtained, differential gene analysis was performed on different clusters (i.e., screening for marker genes). Marker gene screening criteria were $|\log FC| > 0.25$ and $p < 0.01$. The top 20 highly variable genes were used for the heatmap display which was used to help identify core marker genes. Cells in different clusters of samples from different tissue sources were counted. Barplots were used to display the results and help identify the differential clusters. The Chi-square test was performed for cells in the different grouping of clusters.

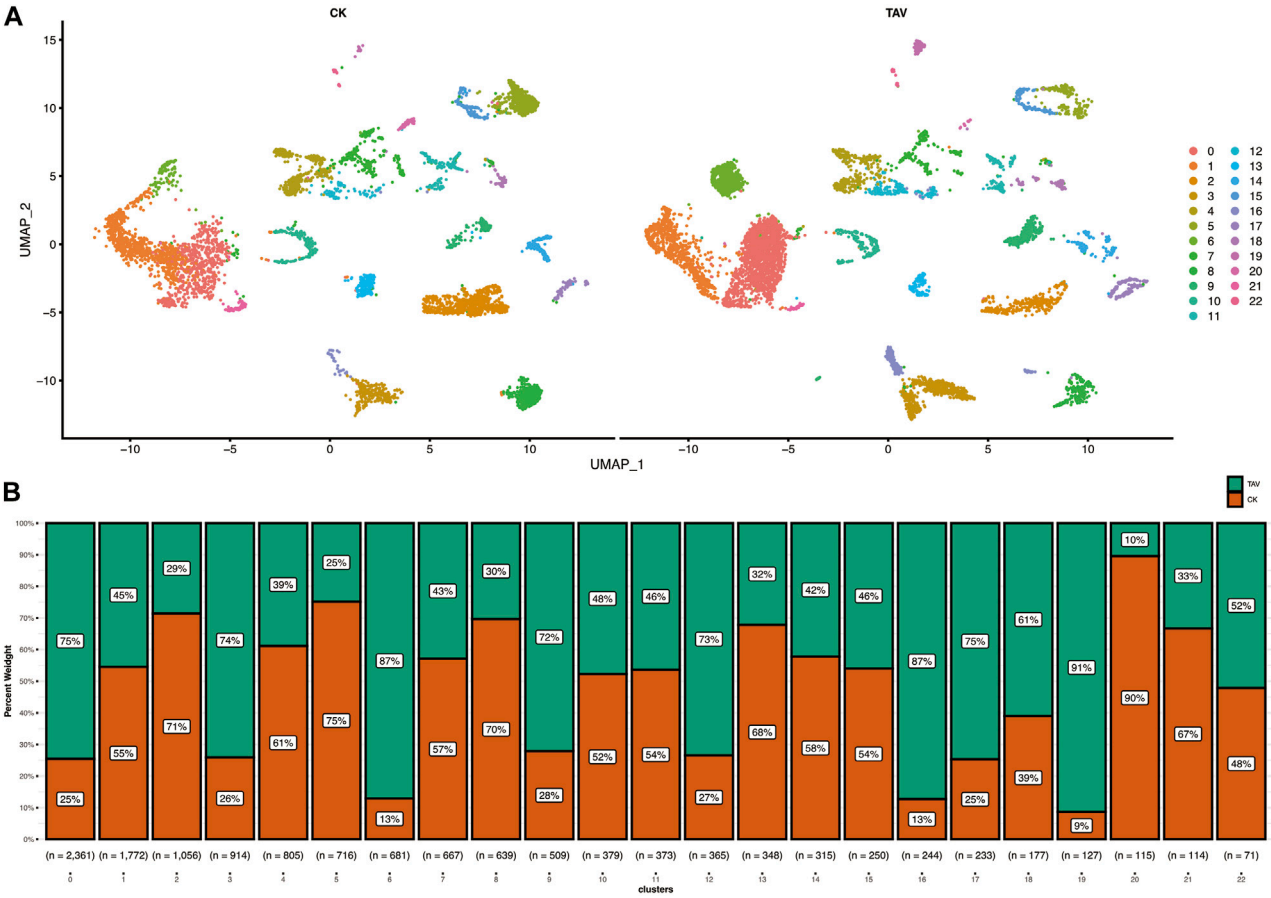

FIGURE 1
(A) Twenty-two cell clusters with uniform flow shape approximation and projection (UMAP) space were identified and displayed. **(B)** Statistical histogram showing the number of cells in each cluster for the TAV and CK groups.

2.5 Cell subpopulation identification

Since *O. potamophila* were not single-cell annotated, we first compared the transcripts to the NCBI nr library, Swissprot database, Kyoto Encyclopedia of Genes and Genomes (KEGG) database, Ensembl zebrafish database, and Ensembl tilapia database using NCBI-blast-2.5.0, with a threshold of 1e-05. We used the orthology module in Ensembl biomart to obtain the human homologs of genes annotated to zebrafish. In this project, marker genes were compiled, and a featurePlot was plotted to visualize gene expression distribution and identify clusters. The heatmap clearly shows the expression of known marker genes in different clusters. After the annotation was completed, the cell types obtained from the annotation were mapped to UMAP and tSNE maps.

2.6 Differential and functional enrichment analysis

For each cluster, genes with expression that differed between sample sources were analyzed, and the threshold for TAV vs. CK differential gene screening was $|\log2(FC)| > 0.25$ and $p < 0.05$. The differential genes of each cluster of each sample were subjected to KEGG (Kyoto Encyclopedia of Genes and Genomes) and GO (Gene Ontology) enrichment analysis. GO enrichment analysis is an international standardized transcriptional function classification system that provides a set of dynamically updated standard taxonomic names to adequately describe the properties of transcripts and transcript products in organisms (Falcon and Gentleman, 2007). GO function analysis provides taxonomic annotation of differentially expressed transcripts as well as a significant enrichment analysis of differentially expressed transcripts (Kanehisa and Goto, 2000).

2.7 Granulocyte cell and B cell subpopulation analysis

2.7.1 Subtype analysis

Granulocyte cells and B cells were analyzed in further detail. The subpopulations of cells were separated out and then re-dimensioned, clustered, and annotated. After the annotation was completed, the annotated types were mapped to the UMAP and tSNE maps.

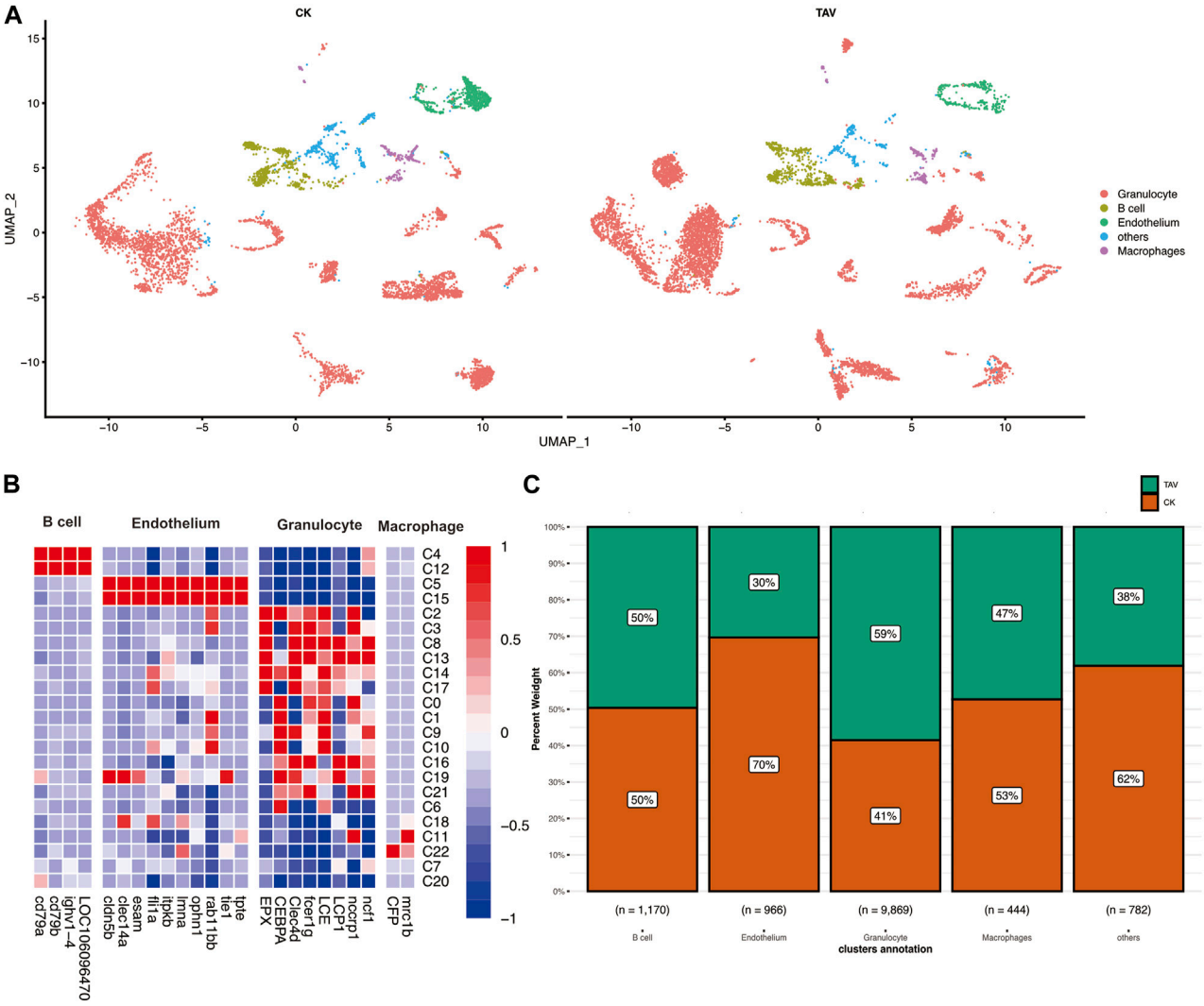

FIGURE 2
(A) UMAP plot showing identification of putative cell types based on the expression of marker genes in mammals and fish. **(B)** Heatmap of putative marker genes in B cells, endothelial cells, macrophages, and granulocytes in cell clusters, with the expression levels of genes in different cells indicated by different colors. The redder the color, the higher the expression level, and the more purple the color, the lower the expression level. **(C)** Histogram showing the number of cells per cell type for B cells, endothelial cells, macrophages, and granulocytes.

3 Results

3.1 Dimensionality reduction and clustering results

Cell viability was confirmed to be approximately 98% by microscopic examination. The total number of cells measured in the total sample was 13,382, with 7174 cells detected in the TAV group and 6208 cells detected in the CK group. After quality control and mapping using Cell Ranger software, the 13,382 cells had a total read length of 589,228,107 bp with an average read length of 44,031 bp per cell acquisition (Figure 1). In total, 23 cell clusters (clusters 0–22) were characterized (Figure 1A). The percentage of each cell cluster in the TAV and CK groups is shown in Figure 1B.

3.2 Cell subpopulation identification results

Twenty-three cell clusters (clusters 0–22) were characterized (Figure 2A). Each cell subset-specific gene is shown in the heatmap, and the 23 cell clusters were grouped into B cells, granulocytes, endothelial cells, and macrophages (Figure 2B). In the TAV group, 5774 cells from cell clusters 0, 1, 2, 3, 6, 8, 9, 10, 13, 14, 16, 17, 18, 19, and 21; and 4095 cells from the CK group were classified as granulocytes. In the CK group, 589 cells in cell clusters 4 and 12 and 581 cells from the TAV group were classified as B cells. In the CK group, 234 cells from clusters 11 and 22, and 210 cells from the TAV group, were classified as macrophages. The remaining 484 cells in the CK group and 298 cells in the TAV group were not identified but were found in clusters 7 and 20. These results show a relatively large difference

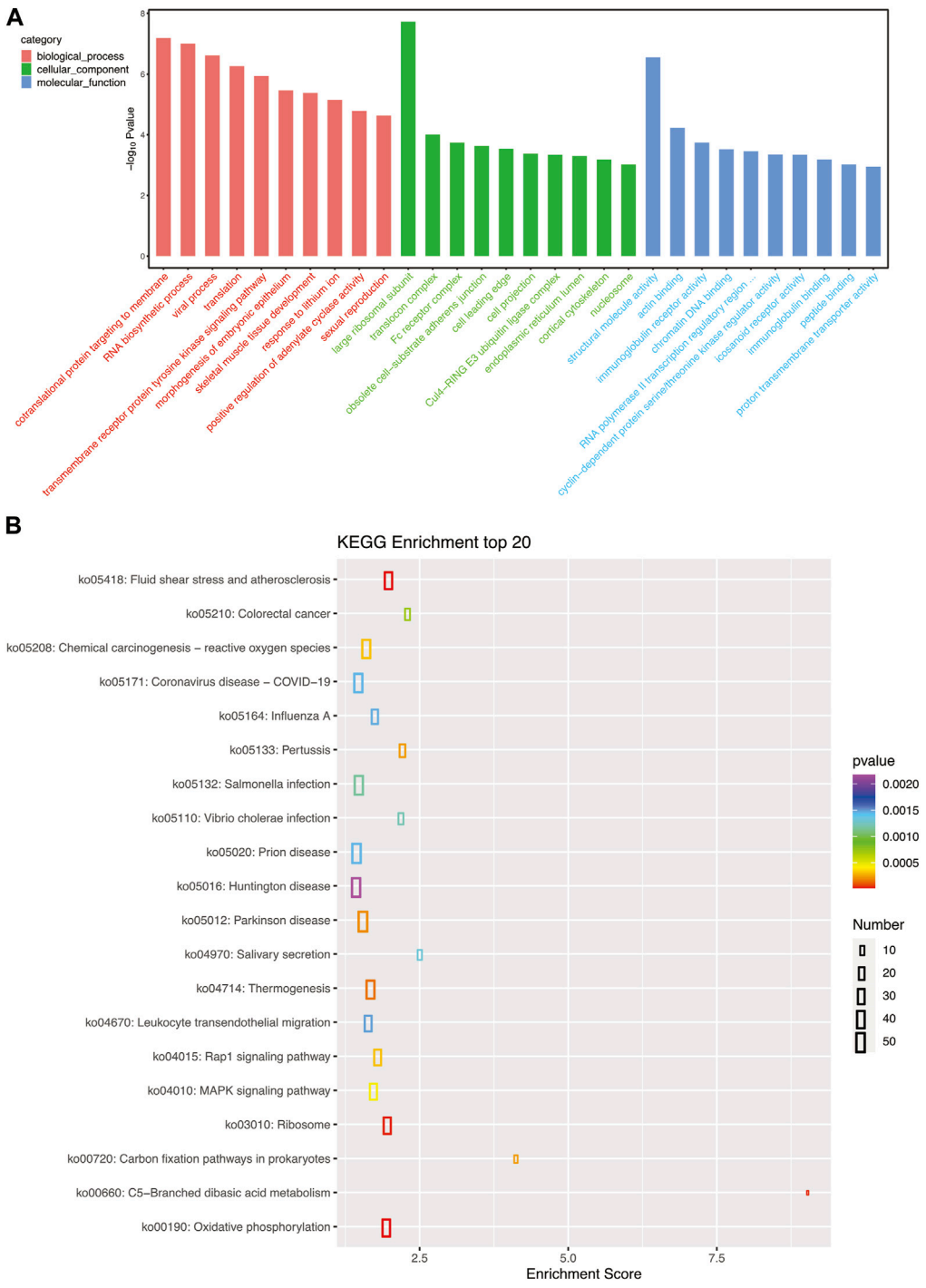

FIGURE 3
(A) GO pathways enriched for each granulocyte subset gene; the top 10 most important GO pathways enriched in cellular processes, molecular functions, and cellular components are shown. **(B)** The top 20 most important KEGG pathways enriched for each granulocyte subset gene.

between granulocyte and endothelial cell numbers between the TAV and CK groups. Granulocytes as a whole were more abundant in the TAV group, whereas endothelial cells as were less abundant in the TAV group, compared to the CK group (Figure 2C).

3.3 Granulocyte subpopulation analysis results

To examine the biological functions of DEGs, GO and KEGG pathway analysis was performed on all DEGs. GO annotations of

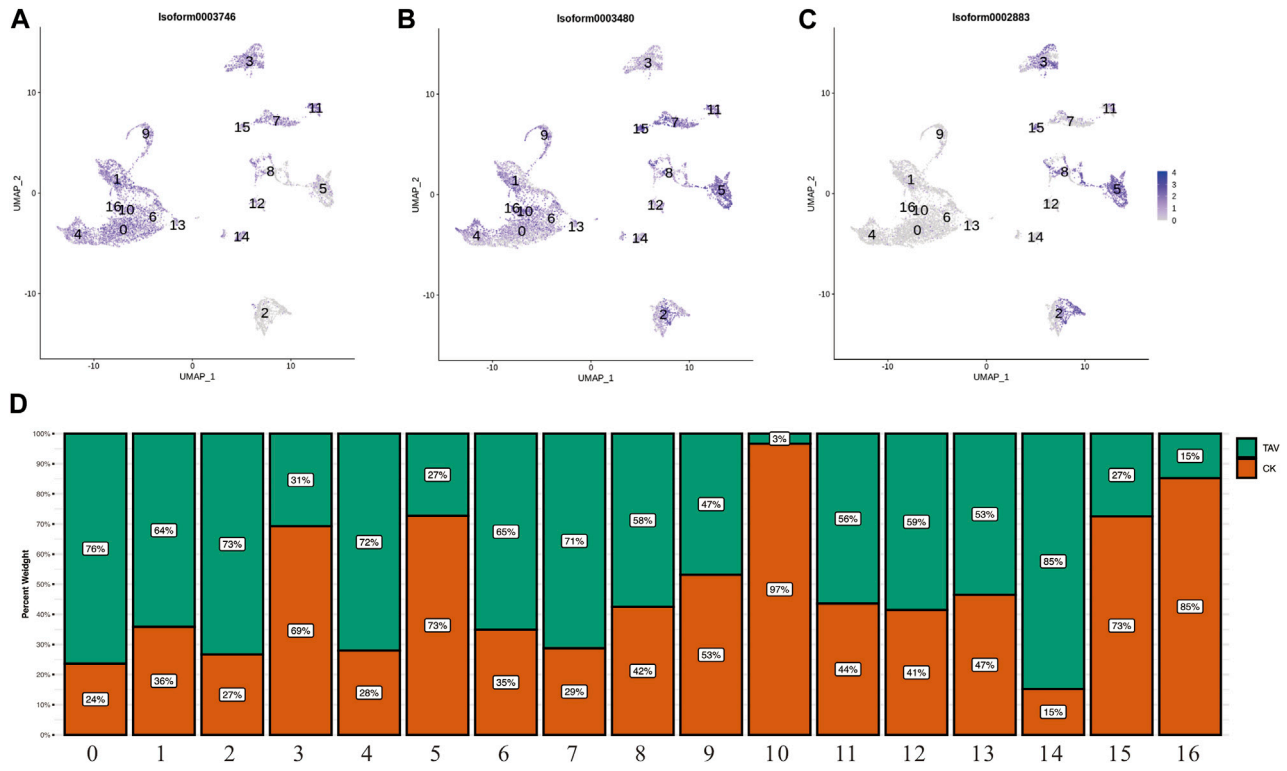

FIGURE 4
(A) UMAP plots of the neutrophil marker gene CEBPA (Isoform0003746). **(B)** UMAP plots of the neutrophil marker gene ncf1 (Isoform0003480). **(C)** UMAP plots of the eosinophil marker gene EPX (Isoform0002883). **(D)** Histogram showing the number of cells per cell cluster in granulocytes.

these genes were classified into three categories based on their functions and pathways: biological processes, cellular components, and molecular functions. Large ribosomal subunit in cellular components and structural molecular activity in molecular functions were the significantly influenced functions (Figure 3A). KEGG pathway analysis also demonstrated the influence of *A. veronii* on related pathways (Figure 3B). Pathways significantly affected by the bacterium were ribosome (ko03010), fluid shear stress and atherosclerosis (ko05418), and oxidative phosphorylation (ko00190).

Neutrophil marker genes CEBPA (Isoform0003746), ncf1 (Isoform0003480), EPX (Isoform0002883) were observed in UMAP (Figures 4A–C). Neutrophils were present in the cell clusters 1, 4, 6, 9, 10, 13, 14, and 16; and eosinophils were present in cluster 5 (Figure 4). Relative to the control (TAV), neutrophil number was significantly higher and eosinophil number was significantly lower in the granulocytes in the CK group (Figure 4D).

3.4 Results of B cell subpopulation analysis

As shown in Figure 5A, the biological processes in the GO pathway that were significantly affected by bacterial infection were RNA biosynthesis process, viral process, and T helper cell differentiation. In the cellular components category, the ribosomal small subunit and ribosomal large subunit were the significantly affected functions. The structural molecular activity in the molecular functions category was the significantly affected function, which is consistent with the affected pathways identified in granulocytes. The KEGG pathway analysis showed that bacterial infection significantly affected immune relative pathway such as graft-versus-host disease (ko05332), viral myocarditis (ko05416), and inflammatory bowel disease (ko05321) pathways (Figure 5B).

The UMAP of B cell marker genes *cd79a* (Isoform0023335), *cd79b* (Isoform0022658), and *ighv1–4* (Isoform0016838) were obtained based on relevant literature and transcriptome data (Figures 6A–C). Cell clusters 0, 1, 2, 3, and 4 could not be identified based on the available B cell marker genes. The number of cells in clusters 1 and 4 in B cells was significantly higher in the TAV group compared to the CK group (Figure 6D).

4 Discussion

Research on markers of teleost cell populations and cell subpopulation determinants is still relatively sparse. However, several cutting-edge methods, including scRNA-seq, are now being used to study the cellular immunological functions of fish. In this study, we used scRNA-seq to investigate the effects of infection with *A. veronii* on the head kidney cells of *O. potamophila* and on the regulation of gene expression.

In this study, cells from *O. potamophila* were categorized into B cells, endothelium cells, macrophages, and granulocytes based on the

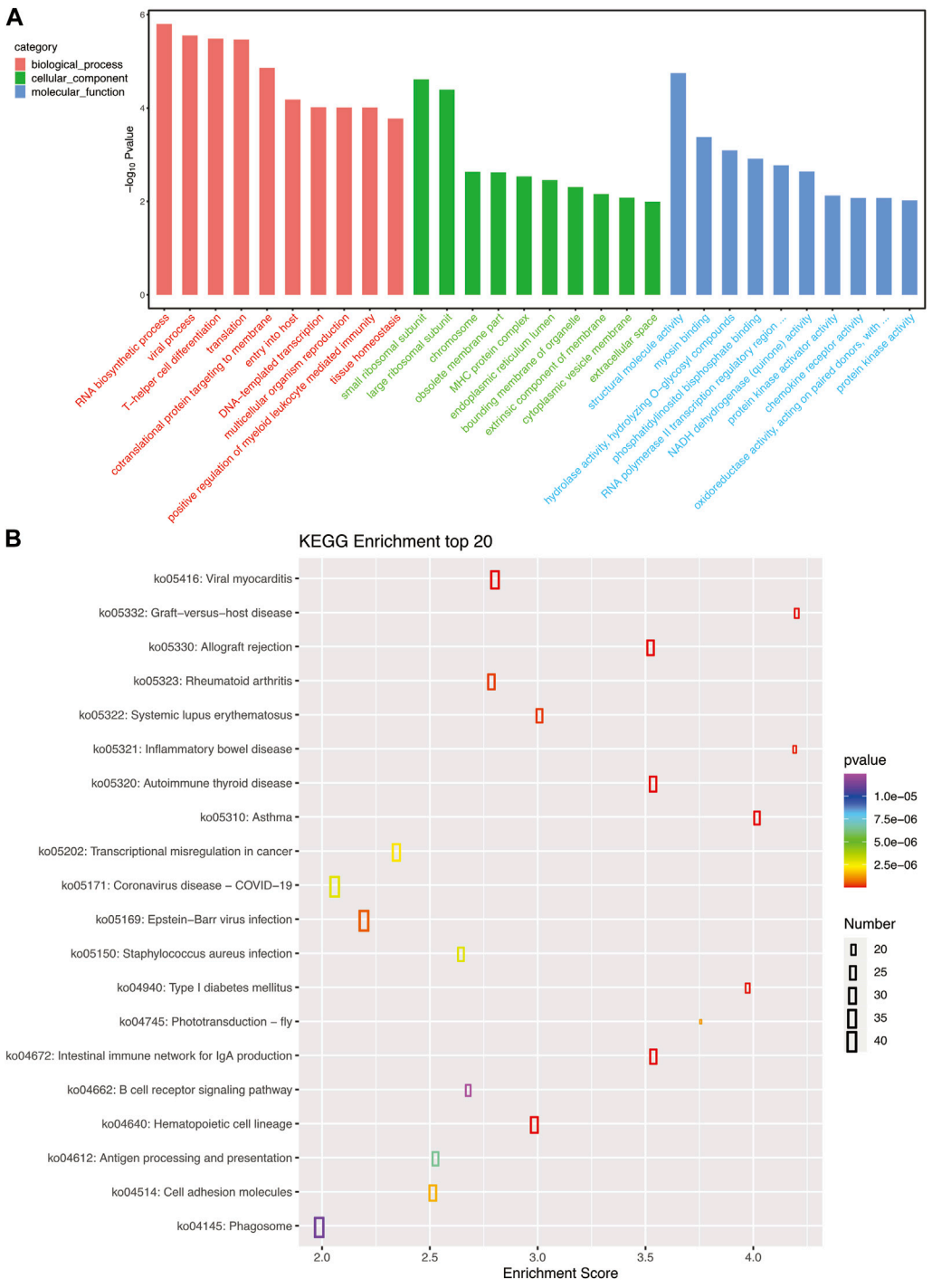

FIGURE 5
(A) GO pathways enriched for each B cell subset gene; the top 10 most important GO pathways enriched in cellular processes, molecular functions, and cellular components are shown. **(B)** The top 20 most important KEGG pathways enriched for each B cell subset gene.

expression patterns of marker genes. However, we were unable to identify the full range of cellular subpopulations based on known marker genes. The differentiation or polarization of these immune cells (e.g., macrophages can polarize into M1 or M2 macrophages) is triggered by corresponding cytokines and transcription factors in response to stress and immune and inflammatory responses (Uribe et al., 2011). Not all cell subtypes were present in the kidneys of *O. potamophila* and other single-cell sequencing studies of cells isolated from fish kidney tissue did not find rag1 gene expressing cells (i.e., these fish lack mature T cells), which may explain the inability to identify these cell subtypes (Wang et al., 1996; Moore et al., 2016). However, the cell clusters obtained in this study will provide useful information for further research of the inflammatory response of *O. potamophila*. We used UMAP analysis to visualize transcriptional differences between B cell

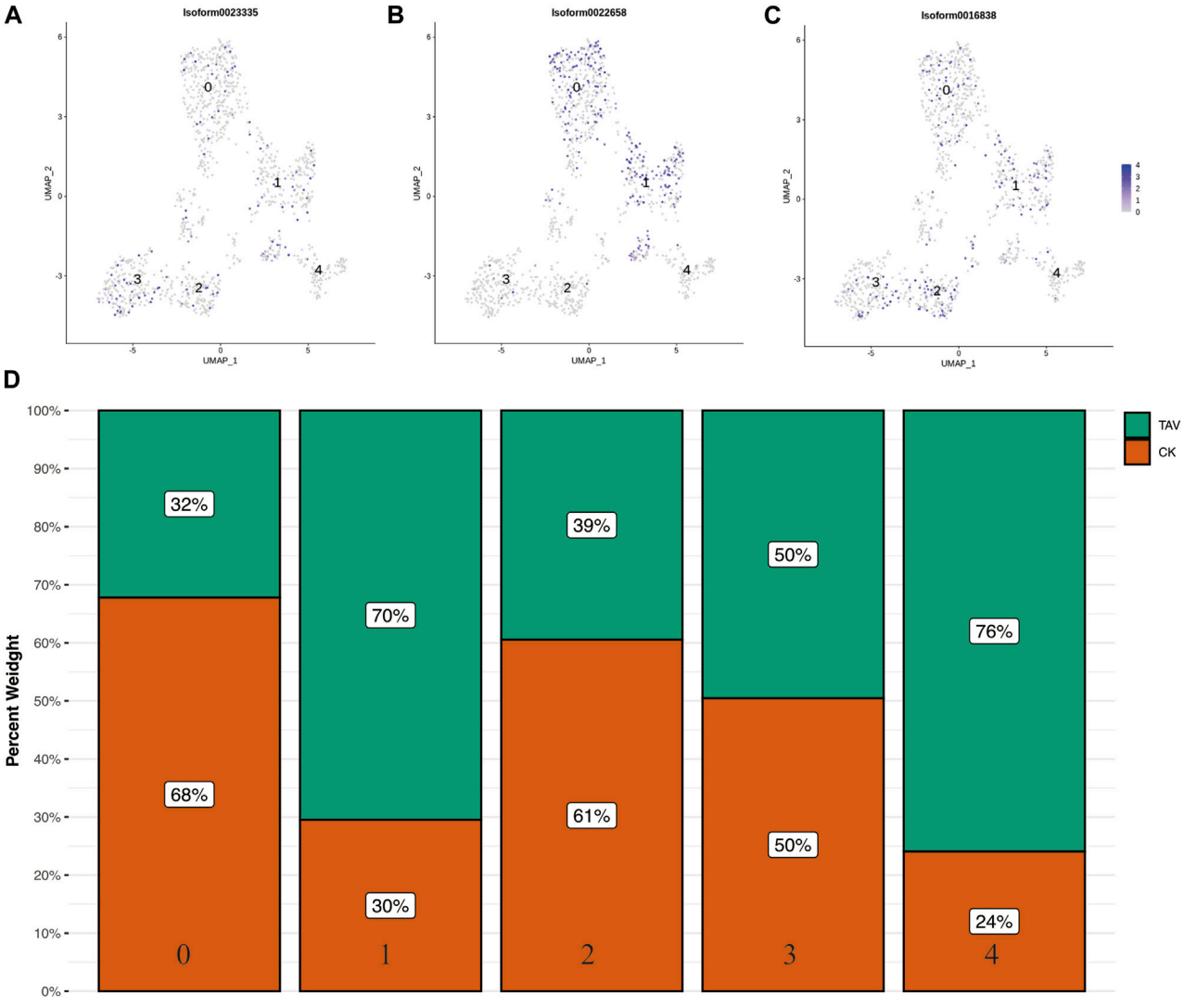

FIGURE 6
UMAP plots of B cell universal marker gene **(A)** *cd79a* (Isoform0023335), **(B)** *cd79b* (Isoform0022658), and **(C)** *ighv1-4* (Isoform0016838). **(D)** Histograms of the number of cells per cell cluster type in B cells.

subpopulations, but the results showed that marker genes were not significantly different among different subpopulations of B cells (Figures 6A–C). This result likely reflects the widespread and unpredictable heterogeneity in the expression of these marker genes across cells.

In granulocyte clusters, eosinophil protein X (*EPX*) is a specific marker gene for eosinophils (Wechsler et al., 2021) and CLECSF8 (*CLEC4D*) (Wilson et al., 2015), CCAAT/enhancer-binding protein-alpha (*CEBPA*), and ecnccrp-1 (*NCCRP1*) (Ishimoto et al., 2004) are neutrophil-specific marker genes. Members of the Cebp family are well-known key regulators involved in neutrophil development, and *CEBPA* plays a key role in the proliferation of mitotic neutrophil progenitor cells (Zhang et al., 1997; Xie et al., 2020). Granulocytes are known to contain neutrophils, eosinophils, basophils, and mast cells (Ainsworth, 1992). Our results showed that neutrophil numbers in granulocytes increased significantly after fish were infected with *A. veronii*, whereas eosinophil numbers decreased. Neutrophils migrate from the circulation to infected tissues in response to inflammatory stimuli and protect the host by phagocytosing, killing, and digesting bacterial and fungal pathogens (Newburger, 2006; Amulic et al., 2012). Significant enrichment of ribosomal biogenesis was detected by GO analysis, indicated that genes related to structural molecular activity and large ribosomal subunit were affected by bacterial infection. The protein components, also known as ribosomal proteins (rps), play a critical role in ribosome and protein synthesis, and several perform important extra-ribosomal functions and are involved in DNA repair, transcriptional regulation, and apoptosis (Chang et al., 2015). Expression of RPS12 and RPL12 were upregulated after infection with *A. veronii*, which indicated more protein synthesis in cells (Supplementary material S1). This results in a highly functional cell population, with neutrophils activated to increase ribosomal protein levels to fight against invading pathogens (Schneider et al., 2014).

Fish B cells are functioning antibody-secreting cells that generate particular antibodies in response to external invader antigens, and they are crucial for adaptive immunity (Parra et al., 2013). Unlike mammals, there are no specific antibodies that can be used to accurately distinguish the developmental/differentiation status of fish B cells, which hinders studies of their function. In the present study, clusters of cells expressing cd79a (Minegishi et al., 1999), cd79b (Niu et al., 2020), and ighv1-4 (Tang et al., 2017) were identified as B cell populations. *CD79b* and *CD79a* are genes that encode the B cell receptor accessory proteins B29 and mb1 (Huse et al., 2022). The IGHV1-4 expression product, immunoglobulin M (IgM) is thought to be a ubiquitous vertebrate immunoglobulin that innately recognizes and binds a variety of antigens (Dooley and Flajnik, 2005). IgM has been used as a marker of mature B cells in trout and grouper (Zhang et al., 2010; Castro et al., 2014). IgM+ B cells have a strong phagocytic capacity and are able to kill microorganisms that are phagocytosed by the cells (Li et al., 2006). Subsequent studies have shown that rainbow trout IgT + B cells also contain subpopulations with phagocytic and bactericidal capabilities (Zhang et al., 2010). Other teleost species, including catfish, cod, and Atlantic salmon, contain phagocytic B cells and feature adaptive immune responses to characteristic pathogens (Øverland et al., 2010).

GO enrichment analysis of DEGs in B cells from fish infected with *A. veronii*, RNA biosynthesis process, viral process, and T helper cell differentiation significant changes. Expression of crucial pro-inflammatory mediators such as *IL1B* and *IGHV1-4*, which are involved in virulence processes, was upregulated (Supplementary material S1), suggesting that *A. veronii* activates immunoglobulin receptors. Major histocompatibility complex (MHC) class II genes *MHC2A* and *MHC2DAB* were also upregulated after infection with *A. veronii*. Antigen-presenting cells are key regulators of immunity, and the expression of MHCII molecules is restricted to some of them, including B cells (Watts, 1997). B cells utilize the specialized MHCII antigen presentation pathway to process B cell receptor-bound and internalized protein antigens and then present selected peptides in complex with MHCII to $CD4^+$ T cells. The immune response of B cells of *O. potamophila* stimulated by *A. veronii* was similar to that of mammalian B-1 B cells, with IgT^+ and IgM^+ head kidney B cells proliferating rapidly and secreting IgT and IgM, respectively, in response to pathogenic stimulation (Zhang et al., 2010).

5 Conclusion

In this study, we used the expression of marker genes to group *O. potamophila* cells into B cells, endothelial cells, macrophages, and granulocytes, and we performed differential enrichment analysis of gene expression in B cells and granulocytes of fish infected with *A. veronii*. The combined analysis revealed a significant increase in neutrophils and decrease in eosinophils in granulocytes of fish infected with *A. veronii*. Activation of neutrophils enhanced ribosome biogenesis by up-regulating the expression of *RPS12* and *RPL12* to fight against invading pathogens. Crucial pro-inflammatory mediators such as *IL1B, IGHV1–4*, and MHC class II genes *MHC2A* and *MHC2DAB*, which are involved in virulence processes, were upregulated, suggesting that *A. veronii* activates an immune response that presents antigens and activates immunoglobulin receptors in B cells. These cellular immune responses identified by single-cell sequencing increase our knowledge about teleost species and lay the foundation for subsequent cellular immune studies.

Data availability statement

The datasets presented in this study can be found in online repositories. The names of the repository/repositories is NCBI and accession number(s) is GSE229275.

Author contributions

GL and CZ designed and supervised the study. XG, YZ, XHZ, and HJ prepared the samples. WW, GL and CZ analyzed all sequencing data. QJ and XJZ provided financial support. GL and CZ wrote the manuscript. All authors have read and approved the final manuscript. All authors listed have made a substantial, direct, and intellectual contribution to the work and approved it for publication.

Funding

This work was supported by the earmarked fund for Jiangsu Agricultural Industry Technology System (JATS (2022) 415; JATS (2022) 417) and the Agricultural Major New Variety Creation Project in Jiangsu province (PZCZ201743).

Conflict of interest

The authors declare that the research was conducted in the absence of any commercial or financial relationships that could be construed as a potential conflict of interest.

Publisher's note

Supplementary material

The Supplementary Material for this article can be found online at: https://www.frontiersin.org/articles/10.3389/fphys.2023.1201914/full#supplementary-material

References

Ainsworth, A. J. (1992). Fish granulocytes: Morphology, distribution, and function. *Annu. Rev. fish Dis.* 2, 123–148. doi:10.1016/0959-8030(92)90060-b

Amulic, B., Cazalet, C., Hayes, G. L., Metzler, K. D., and Zychlinsky, A. (2012). Neutrophil function: From mechanisms to disease. *Annu. Rev. Immunol.* 30, 459–489. doi:10.1146/annurev-immunol-020711-074942

Castro, R., Bromage, E., Abós, B., Pignatelli, J., Granja, A. G., Luque, A., et al. (2014). CCR7 is mainly expressed in teleost gills, where it defines an IgD+ IgM− B lymphocyte subset. *J. Immunol.* 192 (3), 1257–1266. doi:10.4049/jimmunol.1302471

Chang, K.-C., Wen, J.-D., and Yang, L.-W. (2015). Functional importance of mobile ribosomal proteins. *BioMed Res. Int.* 2015, 539238. doi:10.1155/2015/539238

Dong, H., Techatanakitarnan, C., Jindakittikul, P., Thaiprayoon, A., Taengphu, S., Charoensapsri, W., et al. (2017). Aeromonas jandaei and Aeromonas veronii caused disease and mortality in Nile tilapia, *Oreochromis niloticus* (L). *J. Fish Dis.* 40 (10), 1395–1403. doi:10.1111/jfd.12617

Dooley, H., and Flajnik, M. F. (2005). Shark immunity bites back: Affinity maturation and memory response in the nurse shark, *Ginglymostoma cirratum*. *Eur. J. Immunol.* 35 (3), 936–945. doi:10.1002/eji.200425760

Falcon, S., and Gentleman, R. (2007). Using GOstats to test gene lists for GO term association. *Bioinformatics* 23 (2), 257–258. doi:10.1093/bioinformatics/btl567

Hickman-Brenner, F., MacDonald, K., Steigerwalt, A., Fanning, G., Brenner, D. J., and Farmer, J., 3rd (1987). Aeromonas veronii, a new ornithine decarboxylase-positive species that may cause diarrhea. *J. Clin. Microbiol.* 25 (5), 900–906. doi:10.1128/JCM.25.5.900-906.1987

Hoai, T. D., Trang, T. T., Van Tuyen, N., Giang, N. T. H., and Van Van, K. (2019). Aeromonas veronii caused disease and mortality in channel catfish in Vietnam. *Aquaculture* 513, 734425. doi:10.1016/j.aquaculture.2019.734425

Huang, L., Qiao, Y., Xu, W., Gong, L., He, R., Qi, W., et al. (2021). Full-length transcriptome: A reliable alternative for single-cell RNA-seq analysis in the spleen of teleost without reference genome. *Front. Immunol.* 12, 737332. doi:10.3389/fimmu.2021.737332

Huse, K., Bai, B., Hilden, V. I., Bollum, L. K., Våtsveen, T. K., Munthe, L. A., et al. (2022). Mechanism of CD79A and CD79B support for IgM+ B cell fitness through B cell receptor surface expression. *J. Immunol.* 209 (10), 2042–2053. (Baltimore, Md.: 1950). doi:10.4049/jimmunol.2200144

Ishimoto, Y., Savan, R., Endo, M., and Sakai, M. (2004). Non-specific cytotoxic cell receptor (NCCRP)-1 type gene in tilapia (*Oreochromis niloticus*): Its cloning and analysis. *Fish Shellfish Immunol.* 16 (2), 163–172. doi:10.1016/S1050-4648(03)00059-7

Iwata, A., Jeon, S.-R., Mizuno, N., and Choi, K.-C. (1985). A revision of the eleotrid goby genus Odontobutis in Japan, Korea and China. *Jpn. J. Ichthyology* 31 (4), 373–388.

Kanehisa, M., and Goto, S. (2000). Kegg: Kyoto encyclopedia of genes and genomes. *Nucleic acids Res.* 28 (1), 27–30. doi:10.1093/nar/28.1.27

Li, J., Barreda, D. R., Zhang, Y.-A., Boshra, H., Gelman, A. E., LaPatra, S., et al. (2006). B lymphocytes from early vertebrates have potent phagocytic and microbicidal abilities. *Nat. Immunol.* 7 (10), 1116–1124. doi:10.1038/ni1389

Liu, G., Li, J., Jiang, Z., Zhu, X., Gao, X., Jiang, Q., et al. (2022). Pathogenicity of Aeromonas veronii causing mass mortalities of Odontobutis potamophila and its induced host immune response. *Fish Shellfish Immunol.* 125, 180–189. doi:10.1016/j.fsi.2022.05.009

Melsted, P., Booeshaghi, A. S., Liu, L., Gao, F., Lu, L., Min, K. H., et al. (2021). Modular, efficient and constant-memory single-cell RNA-seq preprocessing. *Nat. Biotechnol.* 39 (7), 813–818. doi:10.1038/s41587-021-00870-2

Minegishi, Y., Coustan-Smith, E., Rapalus, L., Ersoy, F., Campana, D., and Conley, M. E. (1999). Mutations in Igalpha (CD79a) result in a complete block in B-cell development. *J. Clin. investigation* 104 (8), 1115–1121. doi:10.1172/JCI7696

Moore, F. E., Garcia, E. G., Lobbardi, R., Jain, E., Tang, Q., Moore, J. C., et al. (2016). Single-cell transcriptional analysis of normal, aberrant, and malignant hematopoiesis in zebrafish. *J. Exp. Med.* 213 (6), 979–992. doi:10.1084/jem.20152013

Newburger, P. E. (2006). Disorders of neutrophil number and function. *ASH Educ. Program Book* 2006 (1), 104–110. doi:10.1182/asheducation-2006.1.104

Niu, J., Huang, Y., Liu, X., Zhang, Z., Tang, J., Wang, B., et al. (2020). Single-cell RNA-seq reveals different subsets of non-specific cytotoxic cells in teleost. *Genomics* 112 (6), 5170–5179. doi:10.1016/j.ygeno.2020.09.031

Øverland, H. S., Pettersen, E. F., Rønneseth, A., and Wergeland, H. I. (2010). Phagocytosis by B-cells and neutrophils in Atlantic salmon (*Salmo salar* L) and Atlantic cod (*Gadus morhua* L). *Fish shellfish Immunol.* 28 (1), 193–204. doi:10.1016/j.fsi.2009.10.021

Parra, D., Takizawa, F., and Sunyer, J. O. (2013). Evolution of B cell immunity. *Annu. Rev. animal Biosci.* 1, 65–97. doi:10.1146/annurev-animal-031412-103651

Schneider, W. M., Chevillotte, M. D., and Rice, C. M. (2014). Interferon-stimulated genes: A complex web of host defenses. *Annu. Rev. Immunol.* 32, 513–545. doi:10.1146/annurev-immunol-032713-120231

Sun, J., Zhang, X., Gao, X., Jiang, Q., Wen, Y., and Lin, L. (2016). Characterization of virulence properties of Aeromonas veronii isolated from diseased Gibel Carp (*Carassius gibelio*). *Int. J. Mol. Sci.* 17 (4), 496. doi:10.3390/ijms17040496

Tang, Q., Iyer, S., Lobbardi, R., Moore, J. C., Chen, H., Lareau, C., et al. (2017). Dissecting hematopoietic and renal cell heterogeneity in adult zebrafish at single-cell resolution using RNA sequencing. *J. Exp. Med.* 214 (10), 2875–2887. doi:10.1084/jem.20170976

Uribe, C., Folch, H., Enríquez, R., and Moran, G. (2011). Innate and adaptive immunity in teleost fish: A review. *Veterinarni Med.* 56 (10), 486–503. doi:10.17221/3294-vetmed

Wang, B., Holländer, G. A., Nichoglannopoulou, A., Simpson, S. J., Orange, J. S., Gutierrez-Ramos, J.-C., et al. (1996). Natural killer cell development is blocked in the context of aberrant T lymphocyte ontogeny. *Int. Immunol.* 8 (6), 939–949. doi:10.1093/intimm/8.6.939

Wang, B., Hu, J., Feng, J., Zhang, Y., Sun, Y., Jiang, B., et al. (2022). Acute septicemia and immune response of spotted sea bass (Lateolabrax maculatus) to Aeromonas veronii infection. *Fish Shellfish Immunol.* 124, 47–55. doi:10.1016/j.fsi.2022.03.030

Wang, B., Mao, C., Feng, J., Li, Y., Hu, J., Jiang, B., et al. (2021). A first report of Aeromonas veronii infection of the sea bass, Lateolabrax maculatus in China. *Front. Veterinary Sci.* 7, 600587. doi:10.3389/fvets.2020.600587

Watts, C. (1997). Capture and processing of exogenous antigens for presentation on MHC molecules. *Annu. Rev. Immunol.* 15 (1), 821–850. doi:10.1146/annurev.immunol.15.1.821

Wechsler, M. E., Munitz, A., Ackerman, S. J., Drake, M. G., Jackson, D. J., Wardlaw, A. J., et al. (2021). Eosinophils in health and disease: A state-of-the-art review. *Mayo Clin. Proc.* 96, 2694–2707. Elsevier. doi:10.1016/j.mayocp.2021.04.025

Wilson, G. J., Marakalala, M. J., Hoving, J. C., Van Laarhoven, A., Drummond, R. A., Kerscher, B., et al. (2015). The C-type lectin receptor CLECSF8/CLEC4D is a key component of anti-mycobacterial immunity. *Cell host microbe* 17 (2), 252–259. doi:10.1016/j.chom.2015.01.004

Wu, C.-J., Wu, J.-J., Yan, J.-J., Lee, H.-C., Lee, N.-Y., Chang, C.-M., et al. (2007). Clinical significance and distribution of putative virulence markers of 116 consecutive clinical Aeromonas isolates in southern Taiwan. *J. Infect.* 54 (2), 151–158. doi:10.1016/j.jinf.2006.04.002

Xie, X., Shi, Q., Wu, P., Zhang, X., Luo, H. R., Su, J., et al. (2020). Single-cell transcriptome profiling reveals neutrophil heterogeneity in homeostasis and infection. *Nat. Immunol.* 21, 1119–1133. doi:10.1038/s41590-020-0736-z

Yu, J.-H., Han, J.-J., Kim, H.-J., Kang, S.-G., and Park, S.-W. (2010). First report of Aeromonas veronii infection in farmed Israeli carp *Cyprinus carpio* in Korea. *J. fish pathology* 23 (2), 165–176.

Zhang, D. E., Zhang, P., Wang, N. D., Hetherington, C. J., Darlington, G. J., and Tenen, D. G. (1997). Absence of granulocyte colony-stimulating factor signaling and neutrophil development in CCAAT enhancer binding protein alpha-deficient mice. *Proc. Natl. Acad. Sci. U. S. A.* 94 (2), 569–574. doi:10.1073/pnas.94.2.569

Zhang, D., Xu, D.-H., Shoemaker, C., and Yao, Y. G. (2016). Integrative analyses of leprosy susceptibility genes indicate a common autoimmune profile. *Aquac. Rep.* 3, 18–27. doi:10.1016/j.jdermsci.2016.01.001

Zhang, Y.-A., Salinas, I., Li, J., Parra, D., Bjork, S., Xu, Z., et al. (2010). IgT, a primitive immunoglobulin class specialized in mucosal immunity. *Nat. Immunol.* 11 (9), 827–835. doi:10.1038/ni.1913

Zhu, C., Liu, G., Gu, X., Yin, J., Xia, A., Han, M., et al. (2022). Effect of quercetin on muscle growth and antioxidant status of the dark sleeper Odontobutis potamophila. *Front. Genet.* 13, 938526. doi:10.3389/fgene.2022.938526

frontiers | Frontiers in Physiology

TYPE Original Research
PUBLISHED 12 July 2023
DOI 10.3389/fphys.2023.1221205

OPEN ACCESS

EDITED BY
Yiming Li,
Fishery Machinery and Instrument Research Institute, China

REVIEWED BY
Xuexi Wang,
Fujian Agriculture and Forestry University, China
Jiamin Li,
Ocean University of China, China

*CORRESPONDENCE
Weiqing Huang,
393634584@qq.com
Shaojiang Ruan,
1519402065@qq.com
Kunhuang Han,
153827825@qq.com

RECEIVED 12 May 2023
ACCEPTED 28 June 2023
PUBLISHED 12 July 2023

CITATION
Lin Z, Wu Z, Huang C, Lin H, Zhang M, Chen M, Han K, Huang W and Ruan S (2023), Cloning and expression characterization of elongation of very long-chain fatty acids protein 6 (*elovl6*) with dietary fatty acids, ambient salinity and starvation stress in *Scylla paramamosain*. *Front. Physiol.* 14:1221205. doi: 10.3389/fphys.2023.1221205

Cloning and expression characterization of elongation of very long-chain fatty acids protein 6 (*elovl6*) with dietary fatty acids, ambient salinity and starvation stress in *Scylla paramamosain*

Zhideng Lin[1,2], Zhouyu Wu[1], Chaoyang Huang[1], Huangbin Lin[1], Mingyao Zhang[1], Mingfeng Chen[1], Kunhuang Han[1,2]*, Weiqing Huang[1,2]* and Shaojiang Ruan[1,2]*

[1]College of Life Science, Ningde Normal University, Ningde, China, [2]Engineering Research Center of Mindong Aquatic Product Deep-Processing, Ningde Normal University, Ningde, China

Introduction: Elongation of very long-chain fatty acids protein 6 (ELOVL6) played crucial roles in regulating energy expenditure and fatty acid metabolism. Many studies have performed to investigate the physiological roles and regulatory mechanisms of *elovl6* in fish and animals, while few studies were reported in crustaceans.

Methods: Here we reported on the molecular cloning, tissue distribution and expression profiles in response to dietary fatty acids, ambient salinity and starvation stress in *Scylla paramamosain* by using rapid amplification of cDNA ends (RACE) and quantitative real-time PCR.

Results: Three *elovl6* isoforms (named *elovl6a, elovl6b* and *elovl6c*) were isolated from *S. paramamosain* in the present study. The complete sequence of *elovl6a* was 1345 bp, the full-length sequence of *elovl6b* was 1419 bp, and the obtained *elovl6c* sequence was 1375 bp in full length. The *elovl6a, elovl6b* and *elovl6c* encoded 287, 329 and 301 amino acids respectively, and exhibited the typical structural features of ELOVL protein family members. Phylogenetic analysis showed that the ELOVL6a from *S. paramamosain* clustered most closely to ELOVL6 from *Portunus trituberculatus* and *Eriocheir sinensis*, while the ELOVL6b and ELOVL6c from *S. paramamosain* gathered alone into a single branch. Quantitative real-time PCR exhibited that the relatively abundant expression of *elovl6b* was observed in intestine and stomach, and the *elovl6a* and *elovl6c* were highly expressed in hepatopancreas. In addition, studies found that replacing fish oil with soybean oil could significantly increase the transcriptional levels of three *elovl6* in hepatopancreas of *S. paramamosain*, and the expression of *elovl6a* and *elovl6c* in hepatopancreas were more sensitive to dietary fatty acids than the *elovl6b*. Compared with the normal sea water group (27‰), the expression of sterol-regulatory element binding protein1c *(srebp-1), elovl6a, elovl6b* and *elovl6c* were upregulated in the low salinity groups, particularly in 7‰. On the contrary, the starvation stress suppressed the expression of *srebp-1, elovl6a, elovl6b* and *elovl6c*.

Discussion: These results may contribute to understand the functions of *elovl6* in fatty acid synthesis and regulatory mechanisms in crustaceans.

KEYWORDS

ELOVL6, fatty acids, salinity stress, starvation stress, *Scylla paramamosain*

1 Introduction

The synthesis of long chain fatty acids (LCFAs) *de novo* was accomplished by elongation and desaturation steps (Green et al., 2010; Xie et al., 2021). As rate-limiting enzymes, elongation of very long-chain fatty acids proteins (ELOVL) were responsible for catalyzing the elongation step, which can elongate two carbons to pre-existing fatty acyl chains (Green et al., 2010; Guillou et al., 2010). The ELOVL family was divided into seven members in mammals based on different catalytic substrates and sequence characterization (Jakobsson et al., 2006). Generally, ELOVL5, ELOVL4 and ELOVL2 were inclined to elongate polyunsaturated fatty acids (PUFA), while ELOVL7, ELOVL6, ELOVL3 and ELOVL1 preferred to catalyze monounsaturated fatty acids (MUFA) and saturated fatty acids (SFA) (Castro et al., 2016). As a final elongase participated in LCFAs *de novo*, the ELOVL6 was first reported in mice, which showed the functions of elongating palmitoleic acid (C16:1n-7) and palmitate (C16:0) to vaccenci acid (C18:1n-7) and stearate (C18:0) respectively (Moon et al., 2001; Matsuzaka et al., 2002; Shi et al., 2017). Recently, numerous studies have been investigated to determine the physiological roles and regulatory mechanisms of *elovl6* in mammals (Matsuzaka et al., 2007; Saito et al., 2011; Tan et al., 2015; Bae et al., 2016; Su et al., 2018). By contrast, the roles of *elovl6* in aquatic animals was still unclear, which only reported in *Larimichthys crocea* (Li et al., 2019), *Misgurnus anguillicaudatus* (Chen et al., 2018), *Oncorhynchus mykiss* (Li et al., 2020) and *Eriocheir sinensis* (Shi et al., 2016).

The *elovl6* is mainly expressed in lipogenic tissues and is closely associated with metabolic diseases (like atherogenesis, insulin resistance and hepatic inflammation) and energy balance (Matsuzaka et al., 2007; Matsuzaka and Shimano, 2009; Takashi et al., 2012; Motoko et al., 2015; Tan et al., 2015; Zhao et al., 2017; Nakamura et al., 2018; Su et al., 2018). Previous studies have shown that the expression of *elovl6* was sensitive to nutrients (Matsuzaka et al., 2002; Leroux et al., 2016; Shi et al., 2016; Li et al., 2019), environmental factors (Tan et al., 2015; Chen et al., 2018) and hormonal (Matsuzaka et al., 2007; Matsuzaka and Shimno, 2009; Sun et al., 2013; Li et al., 2020). In mammals, transcription of *elovl6* was regulated by the transcription factors such as carbohydrate response element binding protein (CHREB), sterol-regulatory element binding protein-1c (SREBP-1C) and liver X receptor α (LXR α), and the transcriptional level was intimately related to dietary lipid addition (Matsuzaka et al., 2002; Kumadaki et al., 2008; Ducheix et al., 2011; Sun et al., 2013; Bae et al., 2016). Likewise, both *in vivo* and *in vitro* demonstrated that dietary fatty acids could markedly affect the *elovl6* expression through regulating related transcription factors for *L. crocea* and *O. mykiss* (Li et al., 2019; 2020). Besides, the *elovl6* plays a vital role in keeping fatty acids and energy balances in dealing with cold stress (Tan et al., 2015; Chen et al., 2018). Studies have found that the transcriptional level of *elovl6* was significantly increased in brown adipose tissue under the cold stress, and *elovl6*$^{-/-}$ mice showed lower heat-producing capability in brown adipose tissue (Tan et al., 2015). Similar result was also observed in *M. anguillicaudatus*, which found that the *elovl6* expression could be induced by the cold stress for producing fatty acids to maintain proper membrane fluidity (Chen et al., 2018). In addition to temperature stress, aquatic animals also often need face salinity and starvation stress. In aquatic animals, supply of energy is crucial for coping with salinity and starvation stress, as well as maintenance of suitable cell membrane fluidity is also important adaptive way during osmoregulation. However, to the best our knowledge, the roles of *elovl6* in the face of salinity and starvation stress are still poorly understood.

The mud crab, *Scylla paramamosain*, is a kind of important marine crustacean species (Ye et al., 2010). Because of high nutritional value, unique flavor, high output and high economic value, the mud crab has been widely cultured in the coastal areas of southern China with a yield of around 152,065 tons in 2021 (China Fishery Statistical Yearbook, 2022). The present study aimed to determine the molecular features of three *elovl6* and their expression profiles in reaction to ambient salinity, dietary fatty acids and starvation. These results may be beneficial for further understanding the functions of *elovl6* in fatty acid synthesis and regulatory mechanism in crustaceans.

2 Materials and methods

2.1 Nutrition experiment

Six isonitrogenous (45% crude protein) and isolipidic (9.5% crude lipid) experimental diets were prepared by substituting fish oil with 0% (FO group), 20% (SO-20 group), 40% (SO-40 group), 60% (SO-60 group), 80% (SO-80 group) and 100% (SO-100 group) soybean oil. The dietary protein sources were provided with casein and white fishmeal, and lipid sources were supplied by soybean oil, cholesterol, phospholipids and fish oil. The specific feed formula, diet making process, experimental design, experimental condition and sample collection have been described in our previous studies (Lin et al., 2017; Lin et al., 2018).

2.2 Salinity stress experiment

The 21-day salinity stress experiment was conducted in culture system of Ningde Normal University. The salinity was set as 27‰, 22‰, 17‰, 12‰ and 7‰. The crabs used in the present study were bought from a local crab farm in Sandu bay (Ningde, Fujian, China), and the crabs were temporarily cultured for adapting to the experimental environment and diets. Subsequently, ninety healthy crabs (initial average weight: 62.90 ± 1.98 g) with intact limbs were assigned to fifteen polypropylene buckets (Zhongkehai, Qingdao, China). There were five groups, each with three replicates, and each replicate with six crabs. The crabs were fed commercial diets twice daily (8:30 and 18:00) to apparent satiation during experiment. Feces and residual diets were removed once a day. During the salinity stress experiment, water quality

parameters were as follows: the temperature ranged from 19.1°C to 22.4°C, oxygen concentration more than 5.0 mg L^{-1} and ammonia nitrogen lower than 0.05 mg L^{-1}. At the end of the trial, the crabs were dissected to obtain the hepatopancreas and muscle samples after being starved for 24 h. Then, the samples were immediately frozen in liquid nitrogen and stored at −80°C for further treatment.

2.3 Starvation stress experiment

The crabs (64.51 ± 0.83 g) used in the present study were purchased from Sandu bay (Ningde, Fujian, China), and 4-week starvation stress experiment was performed in culture system of Ningde Normal University. The starvation stress experiment contained two treatments: starvation group (SG) and feeding group (FG). Thirty-six vigorous crabs were randomly divided into six polypropylene buckets after being temporarily reared for acclimatization. Each treatment has three replicates, and each replicate has six crabs. During the starvation stress experiment, the crabs in feeding group was fed twice daily (8:30 and 18:00) to apparent satiation with a local bivalve mollusc (*Sinonovacula constrzcta*), and starvation group was not fed any food. Uneaten feeds and feces were cleared once daily, and 30% water from each tank was exchanged per day. During the experiment, dissolved oxygen of water was more than 7.0 mg L^{-1}, water temperature ranged from 15.3°C to 20.3°C and ammonia nitrogen was lower than 0.05 mg L^{-1}. The hepatopancreas and muscle samples were collected and immediately frozen in liquid nitrogen after the experiment completed. Subsequently, the samples above were stored at −80°C for further analysis.

2.4 RNA isolation, first-strand cDNA synthesis and full-length cDNA cloning

Total RNA was extracted from the fresh hepatopancreas using Trizol reagent (Invitrogen, United States) according to the manufacturer's instructions. After determining the quality and concentration of total RNA, SMARTer™ RACE cDNA Amplification kit (Clontech, United States) was used to produce the first-strand cDNA based on specification. The cDNA samples were kept in −20°C as subsequent cloning templates.

Three partial cDNA sequences of *elovl6s*, named *elovl6a*, *elovl6b* and *elovl6c*, were obtained from our previous transcriptome sequencing. Related primers were designed according to the sequences above, and the primers have been shown in Table 1. 5′ and 3′ rapid amplification of cDNA ends (RACE) methods were applied to clone the 5′ untranslated region (UTR) and 3′ UTR of three *elovl6s* using touch-down PCR (first round PCR) and nested PCR (second round PCR) strategies. The primers of elovl6a 3-1, elovl6a 5-1, elovl6b 3-1, elovl6b 5-1, elovl6c 3-1 and elovl6c 5-1 were applied to touch-down PCR, and the primers of elovl6a 3-2, elovl6a 5-2, elovl6b 3-2, elovl6b 5-2, elovl6c 3-2 and elovl6c 5-2 were used to nested PCR. The amplification program and reaction system of touch-down PCR and nested PCR have been shown in our previous studies (Lin et al., 2017; Lin et al., 2018). Target band was purified with SanPrep Column DNA Gel Extraction Kit (Sangon Biotech, Shanghai, China.), and then cloned into pMD 19-T simple vector (Takara, Dalian, China). The sequence information of positive clones was determined by sequencing with a commercial company (BGI, Shenzhen, China).

2.5 Sequence and phylogenetic analysis

Homology searches were performed with BLAST at the National Center for Biotechnology Information (http://www.ncbi.nlm.nih.gov/). The multiple alignments were created using the DNAMAN software. Transmembrane structure was predicted utilizing the TMHMM 2.0 (https://services.healthtech.dtu.dk/services/TMHMM-2.0/). The phylogenetic analysis based on the amino acid sequences was constructed by the Neighbour-Joining algorithm with the software MEGA version 7.0.

2.6 Quantitative real-time PCR

Six mud crabs (average weight: 103.60 ± 6.20 g) were used to investigate the *elovl6a, elovl6b* and *elovl6c* expression levels in different tissues (epidermis, gill, hepatopancreas, cranial ganglia, eyestalk, thoracic ganglia, stomach, intestine, muscle and heart) by using quantitative real-time PCR. Likewise, quantitative real-time PCR was also applied to detect the *elovl6a*, *elovl6b* and *elovl6c* mRNA levels in response to dietary fatty acids, salinity stress and starvation stress. The *β-actin* gene from *S. paramamosain* was selected as reference for internal standardization. Primers used in quantitative real-time PCR were given in Table 1. The amplification program and reaction system of quantitative real-time PCR have been described in our previous studies used for determining tissue distribution as well as *elovl6a*, *elovl6b* and *elovl6c* expression levels in response to dietary fatty acids (Lin et al., 2017; Lin et al., 2018). In addition, as for salinity and starvation stress experiment, the total RNA of muscle and hepatopancreas was isolated by using TRNzol universal Reagent (Tiangen, Beijing, China). The single-strand cDNA was synthesized using PrimeScript® RT reagent Kit with gDNA Eraser with 1 μg of total RNA, and the obtained cDNA was diluted by 4 times using ultra-pure water for further analysis. Five different thinned cDNA samples were used to determine the standard curves. The amplification efficiency of primers used in the present study was between 95% and 105% by counting with formula $E = 10^{(-1/\text{Slope})}-1$. Quantitative real-time PCR was performed in a total volume of 20 μL including 10 μL 2 × ChamQ universal SYBR qPCR Master Mix (Q711–02/03, Vazyme Biotech Co., Ltd., Nanjing, China), 1.0 μL of the diluted cDNA template, 0.4 μL of each primer (10 μM) and 8.2 μL of sterile distilled H_2O. The program of quantitative real-time PCR was 95°C for 30 s, followed by 40 cycles of 95°C for 10 s and 60°C for 30 s, and then a dissociation curve (95°C for 15 s, 60°C for 60 s and 95°C for 15 s) was performed to identify unicity of PCR product. The relative mRNA expression levels were calculated by $2^{-\Delta\Delta Ct}$ method (Livak and Schmittgen, 2001).

2.7 Statistical analysis

Results were shown in the form of means ± SEM (standard error of the mean). After checking homogeneity and normality,

TABLE 1 Names and sequences of primers used in the present study.

Primer	Sequence (5′-3′)	Objective
Oligo-	AAGCAGTGGTATCAACGCAGAGTACXXXXX	First-Strand cDNA Synthesis
UPM (long)	CTAATACGACTCACTATAGGGCAAGCAGTGGTATCAACGCAGAGT	RACE-PCR
UPM (short)	CTAATACGACTCACTATAGGGC	RACE-PCR
NUP	AAGCAGTGGTATCAACGCAGAGT	RACE-PCR
M13F	CGCCAGGGTTTTCCCAGTCACGAC	PCR screening
M13R	AGCGGATAACAATTTCACACAGGA	PCR screening
β-actin R	GCGGCAGTGGTCATCTCCT	qRT-PCR
Srebp-1 F	GCTTCAAGGGATGAGGTTTGC	qRT-PCR
Srebp-1 R	GGATCTTCTGAGGTCCTGAGGTACT	qRT-PCR
β-actin F	GCCCTTCCTCACGCTATCCT	qRT-PCR
For elovl6a clone and qRT-PCR		
elovl6a 3–1	AGTACCGCCCTCGATTTGAGCTCCG	3′RACE
elovl6a 3–2	GGACCCAGTTTCCTTGACAACCGTGT	3′RACE
elovl6a 5–1	CCACCCACACGGTTGTCAAGGAAACT	5′RACE
elovl6a 5–2	TCGAGGGCGGTACTGCATGTAAAGTTG	5′RACE
Q-elovl6a F	TCACTCCTCAAAAAACCACGC	qRT-PCR
Q-elovl6a R	GCTGACACACGACACGCTCAA	qRT-PCR
For elovl6b clone and qRT-PCR		
elovl6b 3–1	CGTTACCTCCACCAACTTCACCTACCG	3′RACE
elovl6b 3–2	GCCTTACGCACCACGCCTGAAATG	3′RACE
elovl6b 5–1	CAGCATTTCAGGCGTGGTGCGTAAG	5′RACE
elovl6b 5–2	TCGGCGGGAGTGTCAGGTCGTAG	5′RACE
Q-elovl6b F	TTCACCTACCGCTACACCTTCA	qRT-PCR
Q-elovl6b R	ACTTGGGTCGCTTTTCCATCAC	qRT-PCR
For elovl6c clone and qRT-PCR		
elovl6c 3–1	CTACATGGTGGGCGCCTACATGGC	3′RACE
elovl6c 3–2	TGTTCACGTTGAGCAAGGTGCCAGA	3′RACE
elovl6c 5–1	TGGCACCTTGCTCAACGTGAACATC	5′RACE
elovl6c 5–2	GGTCAAAAGCAGGTCGGGTCTCCA	5′RACE
Q-elovl6c F	TCTACGGCGGAAACTGGGTG	qRT-PCR
Q-elovl6c R	TGCTTGCGGAGGTCAAAAGC	qRT-PCR

X, undisclosed base in the proprietary SMARTer, oligo sequence.

one-way analysis of variance (ANOVA) followed by Duncan's multiple comparison test was used to determine the differences of tissue distribution, nutrition experiment and salinity stress experiment. In addition, independent-samples *t*-test was applied to analyze differences in starvation stress experiment. All statistical analysis was carried out by SPSS 20.0 (SPSS, Chicago, IL, United States), and *p* values less than 0.05 was considered to be statistically significant.

3 Results

3.1 cDNA cloning and sequence analysis

The full-length cDNA sequences of *elovl6a*, *elovl6b* and *elovl6c* were obtained by overlapping the corresponding expressed sequence tags (ESTs) with the amplified fragments using the RACE technology. The sequences of *elovl6a*, *elovl6b* and *elovl6c* were

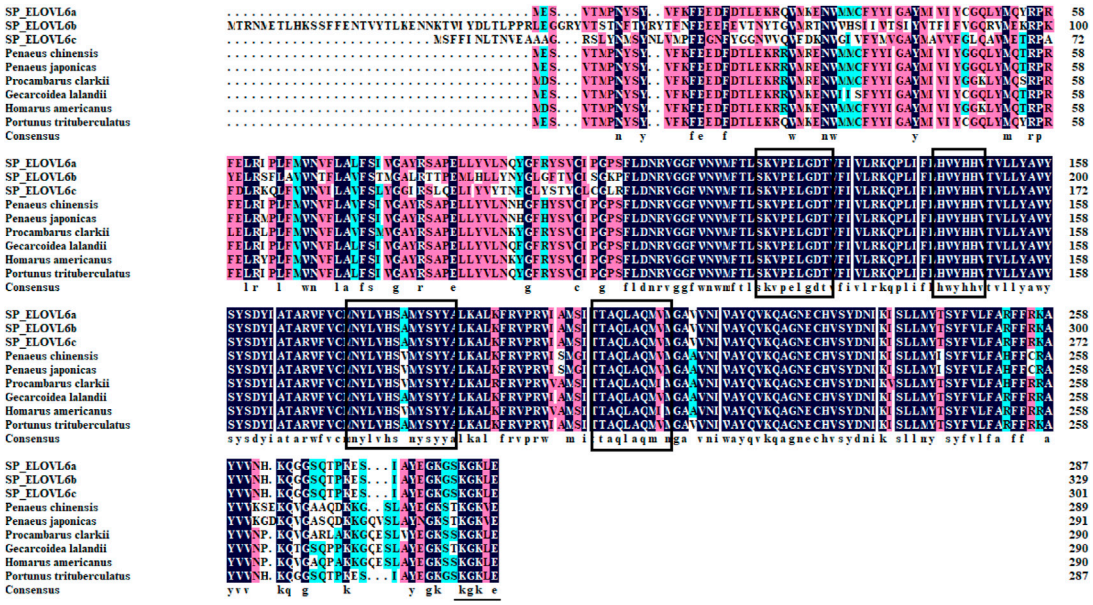

FIGURE 1
Multiple alignments of the ELOVL6 amino acid sequences between *Scylla paramamosain* and other crustaceans. The threshold for similarity shading was set at 50%. Identical residues are shaded black. Amino acid residues that are conserved in at least 75% and 50% of sequences are shaded in pink and cyan, respectively. The motifs highly conserved are boxed among elongases, and the endoplasmic reticulum retention signal is underlined. SP_ELOVL6a: *Scylla paramamosain* ELOVL6a; SP_ELOVL6b: *Scylla paramamosain* ELOVL6b; SP_ELOVL6c: *Scylla paramamosain* ELOVL6c. *Procambarus clarkii* (XP_045621678), *Homarus americanus* (XP_042209792), *Penaeus japonicas* (XP_042885566), *Portunus trituberculatus* (XP_045136269), *Penaeus chinensis* (XP_047487575) and *Gecarcoidea lalandii* (QKG32709).

submitted to GenBank getting the accession numbers MF784574, OQ863017 and OQ863018 respectively. The complete sequence of *elovl6a* was 1345 bp containing a 5′-UTR of 176 bp, a 3′-UTR of 305 bp with a poly A tail and an open reading frame (ORF) of 864 bp encoding a putative protein of 287 amino acids, and the full-length sequence of *elovl6b* was 1419 bp and consists of a 990 bp ORF from 126 bp to 1115 bp encoding a putative protein of 329 amino acids, 125 bp of 5′-UTR and 304 bp of 3′-UTR with a poly A tail. In addition, the obtained *elovl6c* sequence was 1375 bp in full length with 167 bp of 5′-UTR and 302 bp of 3′-UTR including poly A tail, which contained an ORF of 906 bp encoding a putative protein of 301 amino acids. All the ELOVL6s possessed the endoplasmic reticulum retention signal (KXKXX) and membrane-spanning domains (Supplemented Fig. s1-3). Multiple alignments of ELOVL6a, ELOVL6b and ELOVL6c indicated that the predicted amino acid sequences contained characteristic conserved motifs of the microsomal ELOVL family, like HXXHH (histidine box), KXXEXXDT, NXXXHXXMYXYY and TXXQXXQ (Figure 1).

3.2 Homology and phylogenetic analysis

The results of phylogenetic tree showed that the three mud crab ELOVL6 gathered together with their corresponding orthologues, and separated with the ELOVL1, ELOVL2, ELOVL3, ELOVL4, ELOVL5 and ELOVL7. The mud crab ELOVL6a clustered most closely to ELOVL6 from *Portunus trituberculatus*, and further clustered with *E. sinensis*. In addition, the mud crab ELOVL6b and ELOVL6c gathered alone into a single branch and then clustered with other ELOVL6 from crustaceans (Figure 2).

3.3 Tissue distribution

Quantitative real-time PCR was used to analyze mRNA levels of *elovl6a*, *elovl6b* and *elovl6c* in the tissues of healthy crabs, including thoracic ganglia, stomach, heart, gill, epidermis, hepatopancreas, intestine, muscle, eyestalk and cranial ganglia. As illustrated in Figure 3, *elovl6a*, *elovl6b* and *elovl6c* could be detected in all the examined tissues, but existed obvious differences in expression levels. The relatively abundant expression of *elovl6a* was observed in hepatopancreas and stomach, moderate expression in intestine and cranial ganglia and low expression in epidermis, gill, heart, eyestalk, muscle and thoracic ganglia. The *elovl6c* was expressed at significantly higher levels in hepatopancreas and stomach compared to other tissues ($p < 0.05$). By contrast, the *elovl6b* was mainly expressed in the stomach, followed by the intestine and hepatopancreas.

3.4 Transcriptional levels of *elovl6a*, *elovl6b* and *elovl6c* in response to dietary fatty acids

The mRNA levels of *elovl6s* in hepatopancreas were observably influenced by the dietary fatty acids ($p < 0.05$). The crabs fed SO-60, SO-80 and SO-100 diets showed markedly higher *elovl6a* mRNA

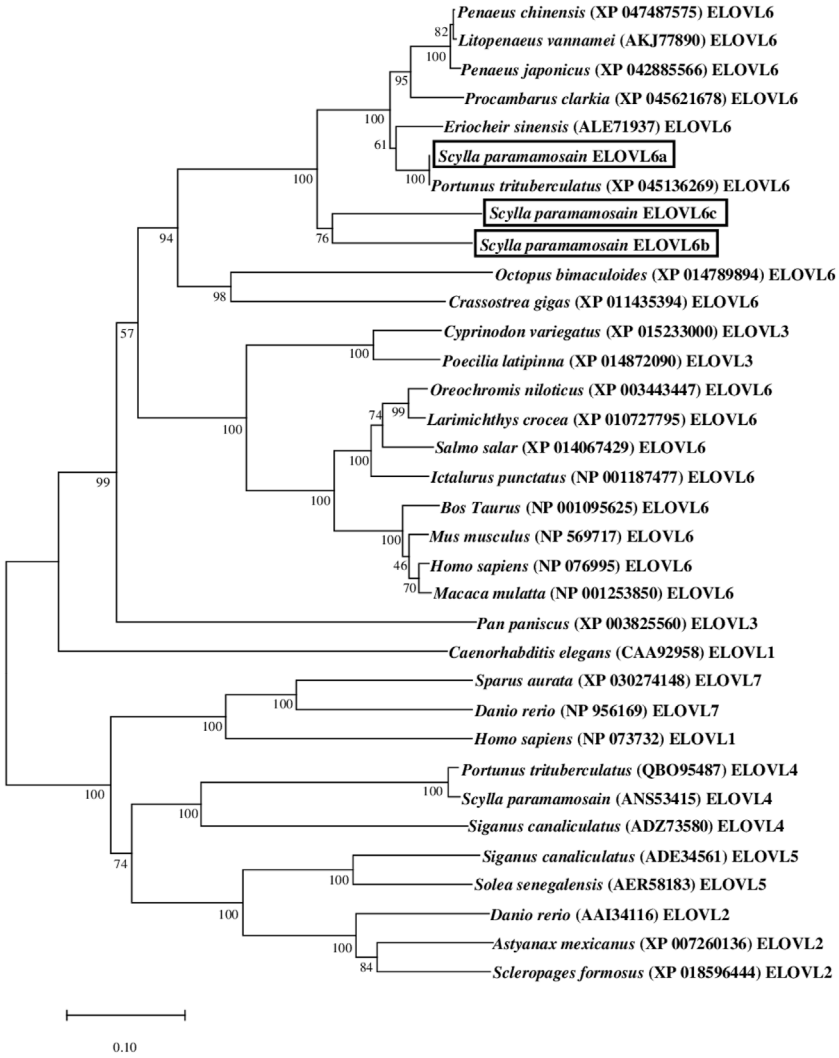

FIGURE 2
Phylogenetic analysis between the amino acid sequences of *Scylla paramamosain* ELOVL6 and 31 available ELOVL sequences. The tree was constructed using the neighbor joining method with MEGA 7.0. The horizontal branch length is proportional to amino acid substitution rate per site. Numbers represent the frequencies with which the tree topology presented was replicated after 1000 bootstrap iterations.

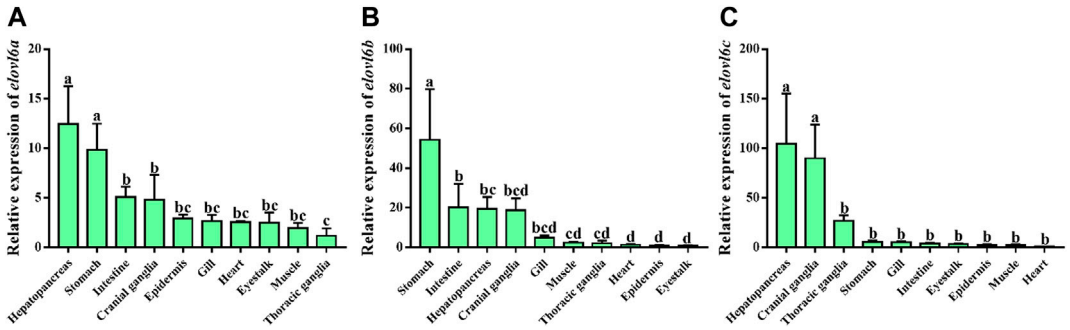

FIGURE 3
Relative mRNA levels of *elovl6* in different tissues of *Scylla paramamosain*. Vertical bars represented mean ± SEM (n = 6) for each tissue. Letters show significant differences ($p < 0.05$) among tissues as determined by one-way ANOVA followed by Duncan's multiple comparison test.

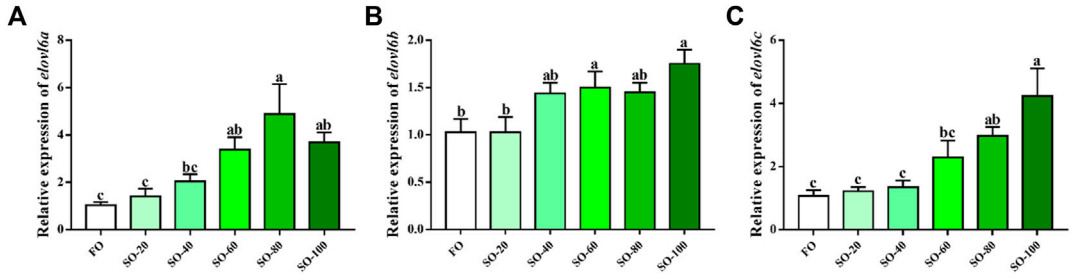

FIGURE 4
Relative expression levels of *elovl6* in hepatopancreas of *Scylla paramamosain* fed six experimental diets. Bars with different superscripts are significantly different ($p < 0.05$, one-way ANOVA and Duncan's multiple comparison test). FO means that fish oil is the only dietary lipid source, numerical values after SO refer to the percentage of dietary fish oil replaced by soybean oil.

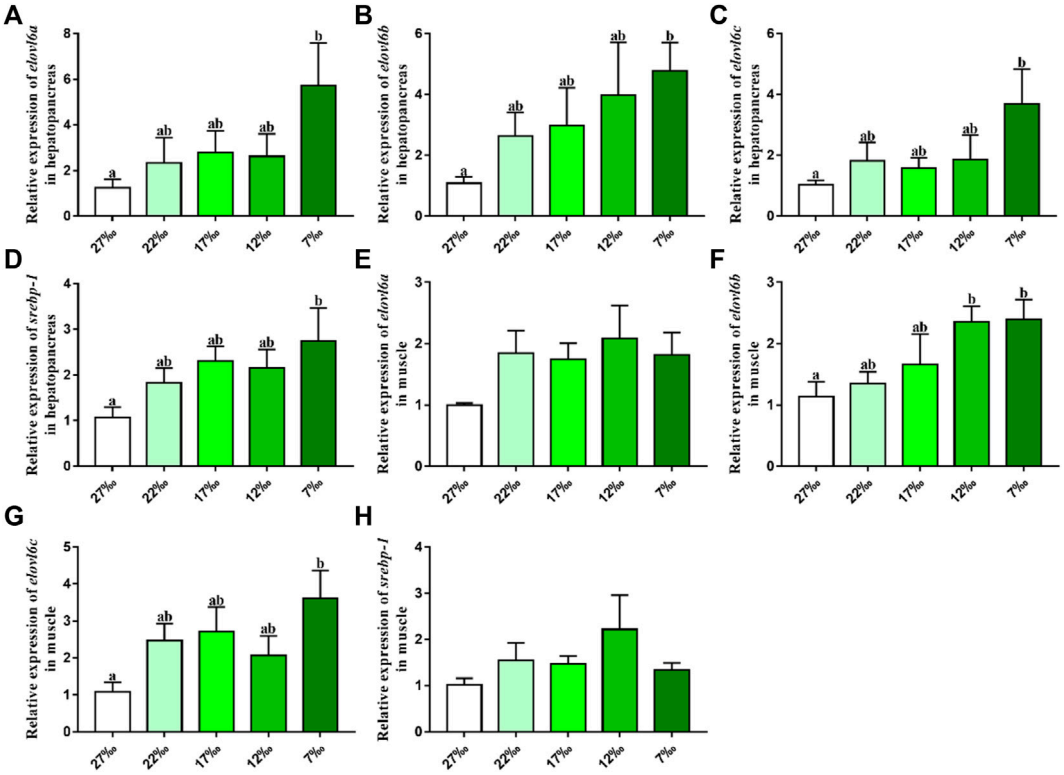

FIGURE 5
Relative expression levels of *elovl6* and *srebp-1* in hepatopancreas and muscle of *Scylla paramamosain* in response to salinity stress. Bars with different superscripts are significantly different ($p < 0.05$, one-way ANOVA and Duncan's multiple comparison test). Numerical values refer to seawater salinity.

levels than those fed FO and SO-20 diets ($p < 0.05$). There was no significant difference between the FO and SO-20 groups in the *elovl6a* expression ($p > 0.05$). The mRNA levels of *elovl6b* in the SO-60 and SO-100 groups were dramatically upregulated when compared with the FO group. ($p < 0.05$). Although no significant differences were detected among the FO, SO-40 and SO-80 groups, the SO-40 and SO-80 groups had the higher *elovl6b* mRNA levels than the FO group ($p > 0.05$). In addition, the *elovl6c* transcriptional levels showed increasing tendency with the increased replacement of dietary fish oil by soybean oil, and the SO-80 and SO-100 groups exhibited significantly higher *elovl6c* transcriptional levels than the FO group ($p < 0.05$) (Figure 4).

3.5 Transcriptional levels of *elovl6a*, *elovl6b*, *elovl6c* and *srebp-1* in response to ambient salinity

The effects of ambient salinity on the mRNA levels of *elovl6a*, *elovl6b*, *elovl6c* and *srebp-1* in hepatopancreas and

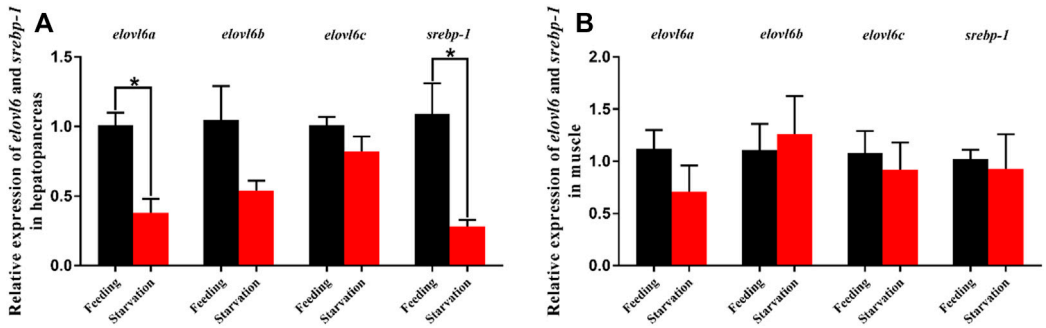

FIGURE 6
Relative expression levels of *elovl6* and *srebp-1* in hepatopancreas and muscle of *Scylla paramamosain* in response to starvation stress. * indicates significant difference between feeding group and starvation group ($p < 0.05$, independent-samples *t*-test).

muscle are presented in Figure 5. Compared with the 27‰ salinity group, the mRNA levels of *elovl6a*, *elovl6b*, *elovl6c* and *srebp-1* in hepatopancreas were upregulated in the 22‰, 17‰, 12‰ and 7‰ salinity groups, and the 7‰ salinity group showed a significant difference with the 27‰ salinity group ($p < 0.05$). There were no significant differences in *elovl6a* and *srebp-1* expression of muscle, although the 22‰, 17‰, 12‰ and 7‰ salinity groups had the higher levels than the 27‰ salinity group ($p > 0.05$). The *elovl6b* and *elovl6c* transcriptional levels in the 27‰ salinity group were also lower than the 22‰, 17‰, 12‰ and 7‰ salinity groups. In addition, the *elovl6c* mRNA levels in 7‰ salinity group and *elovl6b* transcriptional levels in 7‰ and 12‰ salinity groups exhibited markedly higher values than the 27‰ salinity group ($p < 0.05$).

3.6 Transcriptional levels of *elovl6a*, *elovl6b*, *elovl6c* and *srebp-1* in response to starvation stress

The effects of starvation stress on the mRNA levels of *elovl6a*, *elovl6b*, *elovl6c* and *srebp-1* in hepatopancreas and muscle are shown in Figure 6. Compared with the feeding group, the *elovl6a*, *elovl6b*, *elovl6c* and *srebp-1* transcriptional levels in hepatopancreas were downregulated in the starvation group. The *elovl6a* and *srebp-1* expression levels in hepatopancreas of starvation group were dramatically lower than the feeding group ($p < 0.01$). Additionally, no significant differences in *elovl6a*, *elovl6b*, *elovl6c* and *srebp-1* expression levels of muscle were observed between the starvation group and feeding group ($p > 0.05$).

4 Discussion

As a final elongase participated in LCFAs *de novo* in conjunction with fatty acid synthase and stearoyl-CoA desaturase, the ELOVL6 was located in endoplasmic reticulum, which possessed the ability to elongate C16:1n-7 and C16:0 to C18:1n-7 and C18:0 respectively (Green et al., 2010; Shi et al., 2017). Previous studies have exhibited that the ELOVL6 was closely related to metabolic diseases and energy balance in mammal and fish (Takashi et al., 2012; Motoko et al., 2015; Tan et al., 2015; Zhao et al., 2017; Chen et al., 2018; Nakamura et al., 2018; Su et al., 2018), while few studies were reported in crustaceans. In the present study, three *elovl6* isoforms were isolated from the *S. paramamosain*, and the deduced amino acids have the typical structural features of ELOVL protein family members (Tocher, 2015), such as conserved motifs (KXXEXXDT, NXXXHXXMYXYY and TXXQXXQ), histidine box (HXXHH) and transmembrane regions. The phylogenetic analysis showed that the *S. paramamosain* ELOVL6 gathered together with their orthologues from crustaceans and separated with the ELOVL1, ELOVL2, ELOVL3, ELOVL4, ELOVL5 and ELOVL7, which further supported that the isolated genes were *elovl6*. The ELOVL6a from *S. paramamosain* clustered most closely to ELOVL6 from *P. trituberculatus* and *E. sinensis*, which indicated that they have an intimate relationship. In addition, the ELOVL6b and ELOVL6c from *S. paramamosain* gathered alone into a single branch, suggesting ELOVL6b and ELOVL6c have a closer genetic relationship than ELOVL6a and ELOVL6 from other crustaceans.

Studies in mice have indicated that the *elovl6* was mainly expressed in liver and brain (Moon et al., 2001; Matsuzaka et al., 2002; Bae et al., 2016). Similar results were also observed in *L. crocea* and *O. mykiss*, which found that the high expression of *elovl6* was detected in the liver, brain and eye (Li et al., 2019; Li et al., 2020). By contrast, three *elovl6* isoforms from *M. anguillicaudatus* exhibited different expression patterns, and muscle and ovary were the main expression sites (Chen et al., 2018). The results of present study showed that the highest expression levels of the *elovl6a* and *elovl6c* from *S. paramamosain* were the hepatopancreas. This result was consistent with a past study of Shi et al. (2016), who detected that *elovl6* was highly expressed in hepatopancreas of *E. sinensis*. Normally, the hepatopancreas is considered as a main lipid metabolism and storage organ akin to liver of vertebrates (Wen et al., 2001; Tian et al., 2023). The results above may indicate that the *elovl6a* and *elovl6c* mainly acted in the hepatopancreas in *S. paramamosain*. In addition, digestive organs are now regarded as an important site of fatty acid metabolism, at least in salmonids (Bell et al., 2003). The present study also found that the relatively abundant expression of *elovl6b* was

observed in intestine and stomach, and the *elovl6a* also had high expression levels, suggesting *elovl6a* and *elovl6b* may plays an important role in fatty acid synthesis of these tissues in *S. paramamosain*.

Previous studies have demonstrated that the expression of *elovl6* could markedly affect by dietary fatty acids (Matsuzaka et al., 2002; Leroux et al., 2016; Shi et al., 2016; Li et al., 2019; Li et al., 2020). In mice, compared with fat-free diet, the diets added with eicosapentaenoic acid or linoleates significantly suppressed the *elovl6* expression, and the reduction was more obvious in fish oil rich in docosahexaenoic acid and eicosapentaenoic acid (Matsuzaka et al., 2002). In addition, studies found that *O. mykiss* fed diets containing fish oil exhibited higher the transcriptional level of *elovl6* in liver than those fed diets with soybean oil or linseed oil (Li et al., 2019). On the contrary, results from *L. crocea* have exhibited that the mRNA levels of *elovl6* in liver were observably upregulated in the soybean oil, linseed oil, or palm oil groups when compared with the fish oil group. Besides, hepatocytes from *L. crocea* treated with linoleic acid, α-linolenic acid or palmitic acid also obtained similar results above, and this increase may be regulated by related transcription factors like hepatocyte nuclear factor 1α (HNF1α) and retinoid X receptor α (RXRα) (Li et al., 2020). Likewise, the present study also found that replacing fish oil with soybean oil could significantly increase the transcriptional levels of three *elovl6* in hepatopancreas of *S. paramamosain*. This result was consistent with a study from *E. sinensis*, which observed that soybean oil group had markedly higher expression of *elovl6* than the fish oil group (Shi et al., 2016). Our past study has detected that compared with fish oil, soybean oil markedly upregulated the *srebp-1* expression, and the SREBP-1, as a transcription factor, can activate target gene expression like *elovl6* (Hao et al., 2018). Thus, we speculated that soybean oil rich in linoleic acid promoted the *elovl6* expression possibly through activating *srebp-1* expression in the present study. Additionally, the expression of *elovl6a* and *elovl6c* in hepatopancreas were more sensitive to dietary fatty acids than the *elovl6b* probably because these two genes are mainly expressed in hepatopancreas.

Besides, the expression of *elovl6* could also markedly affect by the environmental factors. Previous studies have proved that the *elovl6* plays a crucial role in regulating energy expenditure and fatty acid metabolism in adaptation to cold stress (Tan et al., 2015; Chen et al., 2018). In mice, the transcriptional level of *elovl6* was markedly upregulated in brown adipose tissue under the cold stress, and *elovl6*$^{-/-}$ mice exhibited lower heat-producing capability in brown adipose tissue (Tan et al., 2015). Consistently, Chen et al. (2018) found that the expression of three *elovl6* isoforms from *M. anguillicaudatus* could be induced by the cold stress for keeping energy balances and producing fatty acids to maintain proper membrane fluidity. In addition to temperature stress, aquatic animals often require cope with stresses of salinity changes and food scarcity. To the best our knowledge, the present study was the first time to investigate the *elovl6* expression in respond to salinity and starvation stress. The results showed that compared with the normal sea water group (27‰), the expression of *srebp-1*, *elovl6a*, *elovl6b* and *elovl6c* were upregulated in the low salinity groups, particularly in 7‰, suggesting that three *elovl6* may play a crucial role in salinity adaptation for *S. paramamosain*. The possible reason for this result above was that the expression of transcription factors, SREBP-1, could be activated by low salinity, which further promoted the expression of downstream target gene (*elovl6*) for synthesizing suitable fatty acids to maintain membrane fluidity. In addition, the starvation group exhibited lower expression of *srebp-1*, *elovl6a*, *elovl6b* and *elovl6c* than the feeding group. It could be speculated that more fatty acids are preferentially used for providing energy rather than synthesis when food is scarce, therefore three *elovl6* showed lower expression levels. Furthermore, the hepatopancreas was more sensitive to starvation stress than the muscle, and this was related to the hepatopancreas as a center of lipid metabolism.

In conclusion, the three *elovl6* cDNA sequences of *S. paramamosain* were isolated in the present study, and the deduced amino acids exhibited the typical structural features of ELOVL protein family members. The results of tissue distribution indicated that the *elovl6a* and *elovl6c* highly expressed in the hepatopancreas, while the relatively abundant expression of *elovl6b* was observed in intestine and stomach. In addition, the dietary fatty acids and ambient salinity significantly increases the transcriptional levels of three *elovl6*, and starvation stress could inhibit three *elovl6* expression. These results may contribute to understand functions of *elovl6* in fatty acid synthesis and regulatory mechanisms in crustaceans.

Data availability statement

The datasets presented in this study can be found in online repositories. The sequences of elovl6a, elovl6b and elovl6c were submitted to GenBank (https://www.ncbi.nlm.nih.gov/) with the accession numbers MF784574, OQ863017 and OQ863018, respectively.

Ethics statement

The protocols of using animals in this study were approved by the Committee on the Ethics of Animal Experiments of Ningde Normal University.

Author contributions

ZL, WH, KH, and SR conceived this research and designed the experiments; ZL wrote and revised the manuscript; ZL, ZW, CH, HL, MZ, and MC performed experiments. All authors contributed to the article and approved the submitted version.

Funding

This study was aid financially by the Natural Science Foundation of Fujian Province, China (Grant number 2022J05273) and Scientific Research Foundation of Ningde Normal University (Grant number 2022Y04).

Conflict of interest

The authors declare that the research was conducted in the absence of any commercial or financial relationships that could be construed as a potential conflict of interest.

Publisher's note

All claims expressed in this article are solely those of the authors and do not necessarily represent those of their affiliated organizations, or those of the publisher, the editors and the reviewers. Any product that may be evaluated in this article, or claim that may be made by its manufacturer, is not guaranteed or endorsed by the publisher.

Supplementary material

The supplementary material for this article can be found online at: https://www.frontiersin.org/articles/10.3389/fphys.2023.1221205/full#supplementary-material

References

Bae, J. S., Oh, A. R., Lee, H. J., Ahn, Y. H., and Cha, J. Y. (2016). Hepatic Elovl6 gene expression is regulated by the synergistic action of ChREBP and SREBP-1c. *Biochem. Bioph Res. Co.* 478, 1060–1066. doi:10.1016/j.bbrc.2016.08.061

Bell, M. V., Dick, J. R., and Porter, A. E. (2003). Pyloric ceca are significant sites of newly synthesized 22:6n-3 in rainbow trout (*Oncorhynchus mykiss*). *Lipids* 38, 39–44. doi:10.1007/s11745-003-1029-5

Castro, L. F., Tocher, D. R., and Monroig, O. (2016). Long-chain polyunsaturated fatty acid biosynthesis in chordates: Insights into the evolution of Fads and Elovl gene repertoire. *Prog. Lipid Res.* 62, 25–40. doi:10.1016/j.plipres.2016.01.001

Chen, J., Cui, Y., Yan, J., Jiang, J., Cao, X., and Gao, J. (2018). Molecular characterization of elongase of very long-chain fatty acids 6 (elovl6) genes in *Misgurnus anguillicaudatus* and their potential roles in adaptation to cold temperature. *Gene* 666, 134–144. doi:10.1016/j.gene.2018.05.019

China Fishery Statistical Yearbook (2022). *China Fishery statistical Yearbook*. Beijing, China: China Agriculture Press, 28.

Ducheix, S., Lobaccaro, J. M., Martin, P. G., and Guillou, H. (2011). Liver X receptor: An oxysterol sensor and a major player in the control of lipogenesis. *Chem. Phys. Lipids* 164, 500–514. doi:10.1016/j.chemphyslip.2011.06.004

Green, C. D., Ozguden-Akkoc, C. G., Wang, Y., Jump, D. B., and Olson, L. K. (2010). Role of fatty acid elongases in determination of de novo synthesized monounsaturated fatty acid species. *J. Lipid Res.* 51, 1871–1877. doi:10.1194/jlr.M004747

Guillou, H., Zadravec, D., Martin, P. G., and Jacobsson, A. (2010). The key roles of elongases and desaturases in mammalian fatty acid metabolism: Insights from transgenic mice. *Prog. Lipid Res.* 49, 186–199. doi:10.1016/j.plipres.2009.12.002

Hao, M., Lin, Z., Rong, H., Zhu, D., and Wen, X. (2018). Sterol regulatory element binding protein-1: Molecular cloning, tissue distribution and gene expression level in response to nutritional regulation in mud crab, *Scylla paramamosain*. *Biochem. Bioph Res. Co.* 505, 705–711. doi:10.1016/j.bbrc.2018.09.154

Jakobsson, A., Westerberg, R., and Jacobsson, A. (2006). Fatty acid elongases in mammals: Their regulation and roles in metabolism. *Prog. Lipid Res.* 45, 237–249. doi:10.1016/j.plipres.2006.01.004

Kumadaki, S., Matsuzaka, T., Kato, T., Yahagi, N., Yamamoto, T., Okada, S., et al. (2008). Mouse Elovl6 promoter is an SREBP target. *Biochem. Bioph Res. Co.* 368, 261–266. doi:10.1016/j.bbrc.2008.01.075

Leroux, C., Bernard, L., Faulconnier, Y., Rouel, J., de la Foye, A., Domagalski, J., et al. (2016). Bovine mammary nutrigenomics and changes in the milk composition due to rapeseed or sunflower oil supplementation of high-forage or high-concentrate diets. *J. Nutr. Nutr.* 9, 65–82. doi:10.1159/000445996

Li, Y., Pang, Y., Xiang, X., Du, J., Mai, K., and Ai, Q. (2019). Molecular cloning, characterization, and nutritional regulation of Elovl6 in large yellow croaker (*Larimichthys crocea*). *Int. J. Mol. Sci.* 20, 1801. doi:10.3390/ijms20071801

Li, Y., Pang, Y., Zhao, Z., Xiang, X., Mai, K., and Ai, Q. (2020). Molecular Characterization, nutritional and insulin regulation of Elovl6 in rainbow trout (*Oncorhynchus mykiss*). *Biomolecules* 10 (2), 264. doi:10.3390/biom10020264

Lin, Z., Hao, M., Huang, Y., Zou, W., Rong, H., and Wen, X. (2018). Cloning, tissue distribution and nutritional regulation of a fatty acyl Elovl4-like elongase in mud crab, *Scylla paramamosain* (Estampador, 1949). *Comp. Biochem. Phys. B* 217, 70–78. doi:10.1016/j.cbpb.2017.12.010

Lin, Z., Hao, M., Zhu, D., Li, S., and Wen, X. (2017). Molecular cloning, mRNA expression and nutritional regulation of a delta6 fatty acyl desaturase-like gene of mud crab, *Scylla paramamosain*. *Comp. Biochem. Phys. B* 208, 29–37. doi:10.1016/j.cbpb.2017.03.004

Livak, K. J., and Schmittgen, T. D. (2001). Analysis of relative gene expression data using real-time quantitative PCR and the 2(-Delta Delta C(T)) Method. *Methods* 25, 402–408. doi:10.1006/meth.2001.1262

Matsuzaka, T., and Shimano, H. (2009). Elovl6: A new player in fatty acid metabolism and insulin sensitivity. *J. Mol. Med.* 87, 379–384. doi:10.1007/s00109-009-0449-0

Matsuzaka, T., Shimano, H., Yahagi, N., Kato, T., Atsumi, A., Yamamoto, T., et al. (2007). Crucial role of a long-chain fatty acid elongase, Elovl6, in obesity-induced insulin resistance. *Nat. Med.* 13, 1193–1202. doi:10.1038/nm1662

Matsuzaka, T., Shimano, H., Yahagi, N., Yoshikawa, T., Amemiya-Kudo, M., Hasty, A. H., et al. (2002). Cloning and characterization of a mammalian fatty acyl-CoA elongase as a lipogenic enzyme regulated by SREBPs. *J. Lipid Res.* 43, 911–920. doi:10.1016/s0022-2275(20)30465-x

Moon, Y. A., Shah, N. A., Mohapatra, S., Warrington, J. A., and Horton, J. D. (2001). Identification of a mammalian long chain fatty acyl elongase regulated by sterol regulatory element-binding proteins. *J. Biol. Chem.* 276, 45358–45366. doi:10.1074/jbc.M108413200

Motoko, K., Takashi, M., Rie, M., Ryo, S., Naoko, K., Hikari, T., et al. (2015). Absence of Elovl6 attenuates steatohepatitis but promotes gallstone formation in a lithogenic diet-fed Ldlr(-/-) mouse model. *Sci. Rep-UK* 5, 17604. doi:10.1038/srep17604

Nakamura, Y., Matsuzaka, T., Tahara-Hanaoka, S., Shibuya, K., Shimano, H., Nakahashi-Oda, C., et al. (2018). Elovl6 regulates mechanical damage-induced keratinocyte death and skin inflammation. *Cell Death Dis.* 9, 1181. doi:10.1038/s41419-018-1226-1

Saito, R., Matsuzaka, T., Karasawa, T., Sekiya, M., Okada, N., Igarashi, M., et al. (2011). Macrophage Elovl6 deficiency ameliorates foam cell formation and reduces atherosclerosis in low-density lipoprotein receptor-deficient mice. *Arter. Throm Vas* 31, 1973–1979. doi:10.1161/ATVBAHA.110.221663

Shi, H. B., Wu, M., Zhu, J. J., Zhang, C. H., Yao, D. W., Luo, J., et al. (2017). Fatty acid elongase 6 plays a role in the synthesis of long-chain fatty acids in goat mammary epithelial cells. *J. Dairy Sci.* 100, 4987–4995. doi:10.3168/jds.2016-12159

Shi, Q. Y., Yang, Z. G., Yao, Q. Q., Cheng, Y. X., Yang, Q., and Wei, B. H. (2016). Full-length cDNA cloning of Elovl6 and its tentative study in Chinese mitten crab (*Eriocheir sinensis*). *J. Fish. China.* 40, 844–855. doi:10.11964/jfc.2015121019

Su, Y. C., Feng, Y. H., Wu, H. T., Huang, Y. S., Tung, C. L., Wu, P., et al. (2018). Elovl6 is a negative clinical predictor for liver cancer and knockdown of Elovl6 reduces murine liver cancer progression. *Sci. Rep-UK* 8, 6586. doi:10.1038/s41598-018-24633-3

Sun, H., Jiang, T., Wang, S., He, B., Zhang, Y., Piao, D., et al. (2013). The effect of LXRα, ChREBP and Elovl6 in liver and white adipose tissue on medium- and long-chain fatty acid diet-induced insulin resistance. *Diabetes Res. Clin. P. R.* 102, 183–192. doi:10.1016/j.diabres.2013.10.010

Takashi, M., Ayaka, A., Rie, M., Tang, N., Haruna, S., Noriko, S. K., et al. (2012). Elovl6 promotes nonalcoholic steatohepatitis. *Hepatology* 56, 2199–2208. doi:10.1002/hep.25932

Tan, C. Y., Virtue, S., Bidault, G., Dale, M., Hagen, R., Griffin, J. L., et al. (2015). Brown adipose tissue thermogenic capacity is regulated by Elovl6. *Cell Rep.* 13, 2039–2047. doi:10.1016/j.celrep.2015.11.004

Tian, J., Yang, Y., Du, X., Xu, W., Zhu, B., Huang, Y., et al. (2023). Effects of dietary soluble β-1, 3-glucan on the growth performance, antioxidant status, and immune response of the river prawn (*Macrobrachium nipponense*). *Fish. Shellfish Immun.* 138, 108848. doi:10.1016/j.fsi.2023.108848

Tocher, D. R. (2015). Omega-3 long-chain polyunsaturated fatty acids and aquaculture in perspective. *Aquaculture* 449, 94–107. doi:10.1016/j.aquaculture.2015.01.010

Wen, X. B., Chen, L. Q., Ai, C. X., Zhou, Z., and Jiang, H. B. (2001). Variation in lipid composition of Chinese mitten-handed crab, *Eriocheir sinensis* during ovarian maturation. *Comp. Biochem. Phys. B* 130 (1), 95–104. doi:10.1016/s1096-4959(01)00411-0

Xie, D., Chen, C., Dong, Y., You, C., Wang, S., Monroig, O., et al. (2021). Regulation of long-chain polyunsaturated fatty acid biosynthesis in teleost fish. *Prog. Lipid Res.* 82, 101095. doi:10.1016/j.plipres.2021.101095

Ye, H., Tao, Y., Wang, G., Lin, Q., Chen, X., and Li, S. (2010). Experimental nursery culture of the mud crab *Scylla paramamosain* (Estampador) in China. *Aquacult Int.* 19, 313–321. doi:10.1007/s10499-010-9399-3

Zhao, H., Matsuzaka, T., Nakano, Y., Motomura, K., Tang, N., Yokoo, T., et al. (2017). Elovl6 deficiency improves glycemic control in diabetic db/db mice by expanding β-cell mass and increasing insulin secretory capacity. *Diabetes* 66 (7), 1833–1846. doi:10.2337/db16-1277

frontiers | Frontiers in Marine Science

TYPE Original Research
PUBLISHED 21 July 2023
DOI 10.3389/fmars.2023.1228933

OPEN ACCESS

EDITED BY
Yi-Feng Li,
Shanghai Ocean University, China

REVIEWED BY
Sang Yoon Lee,
Cellqua., Inc, Republic of Korea
Chunyan Zhao,
Qingdao Agricultural University, China

*CORRESPONDENCE
Zhongliang Wang
zhongliangwang@vip.163.com

RECEIVED 25 May 2023
ACCEPTED 05 July 2023
PUBLISHED 21 July 2023

CITATION
Chen Z, Huang B, Yan Z, Hong Y, Zhao M, Jin M, Zheng A and Wang Z (2023) Genome–wide expression profile analysis of the NHE and NKA gene family in *Rachycentron canadum* (Linnaeus, 1766) and its response to salinity adaptation. *Front. Mar. Sci.* 10:1228933. doi: 10.3389/fmars.2023.1228933

Genome–wide expression profile analysis of the NHE and NKA gene family in *Rachycentron canadum* (Linnaeus, 1766) and its response to salinity adaptation

Zongfa Chen[1], Baosong Huang[2], Ziqi Yan[1], Yujie Hong[1], Mingming Zhao[1], Minxuan Jin[1], Anna Zheng[1] and Zhongliang Wang[1]*

[1]College of Fisheies, Guangdong Qcean University, Zhanjiang, China, [2]Agricultural Service Center, Agricultural and Rural Bureau of Sanjiao Town, Zhongshan, China

NHE and NKA are important regulators of ion transport in fish and play a pivotal role in maintaining osmotic balance and adapting to salinity changes. However, no systematic identification and functional analysis has been conducted for NHEs and NKAs in the cobia (*Rachycentron canadum*), a commercially important worldwide flatfish. Herein,12 NHE genes were found to be distributed on 10 chromosomes and 12 NKA genes were found to be distributed on 9 chromosomes were identified in the *R. canadum* at the genome-wide level. Histopathological examination of the gills demonstrated the response of gill lamellae and chloride cells to salinity, while the microstructure of the intestine and kidney exhibited changes associated with salinity. The findings show that members of the NHE and NKA gene families are widely distributed in gill, brain, and heart tissues. Specifically, NHE genes exhibited high expression levels in the gill, somatic kidney, and brain, whereas NKA genes displayed prominent expression in the gill, brain, and heart. Moreover, salinity adaptation experiments were conducted to examine the response of NHE and NKA genes. In the intestine, *NHE1* expression was significantly upregulated following both high and low salt stimulation, while the somatic kidney exhibited a proportional response to changes in salinity. Notably, a significant downward trend in *NHE2c* expression was observed in the gill, intestine, and somatic kidney with increasing salinity. Following low-salt acclimation, *NKAα1b* and *NKAβ3a* were significantly down-regulated in the gill, whereas *NKAα3a* and *NKAβ3a* displayed significant up-regulation and down-regulation in the intestine, respectively. In the somatic kidney, *NKAα1b*, *NKAα3a*, and *NKAβ3a* were significantly up-regulated. During high-salt acclimation, the expression patterns of *NKAα1b* and *NKAβ3a* in the gill were consistent with those observed during low-salt acclimation, while *NKAα3a* and *NKAβ1b* exhibited significant upregulation. Our findings underscore the high conservation of NHE and NKA gene family members in *R. canadum* and highlight tissue-

specific expression patterns and their responses to salinity changes. These results provide valuable insights into the molecular mechanisms governing ion transport and osmoregulation in *R. canadum*, contributing to the development of novel strategies for enhancing aquaculture practices of this species.

KEYWORDS

***Rachycentron canadum*, salinity adaptation, NHE, NKA, histopathology, RNA-seq, qRT-PCR**

1 Introduction

The cobia, *Rachycentron canadum*, is a euryhaline teleost known for its ability to tolerate a wide range of salinity levels, ranging from 22.5 to 44.5 ‰, and it exhibits excellent growth performance (Shaffer and Nakamura, 1989; Smith, 1995). In addition to its fast growth rate, *R. canadum* is a carnivorous fish species highly valued for its delicious meat, nutritional content, and robust resistance. As a result, *R. canadum* has become an important mariculture species in the southeast coast of China (Zhou et al., 2006; Chen et al., 2009). However, the culture of *R. canadum* in seawater nets is vulnerable to extreme weather conditions such as typhoons, heavy rains, and cold fronts. The churning of upwelling and surface seawater can lead to significant fluctuations in seawater salinity and temperature, which have a significant impact on the growth and survival of teleost (Benetti et al., 2021). Salinity is one of the key environmental factors that affect the growth and reproduction of fish (Zhang et al., 2017). Teleost can be classified into euryhaline and non-euryhaline species based on their salinity tolerance. Euryhaline teleost often have well-developed mechanisms of osmoregulation that activate osmoregulatory cells, ion channels, enzymes, and hormones in response to salinity stress, allowing them to survive and thrive in a wide range of salinity levels (Fiol and Kültz, 2007; Holmes et al., 2022). Therefore, studying the salinity adaptation mechanisms of euryhaline teleost can provide a theoretical basis for understanding how they maintain organismal homeostasis in different salinity environments.

Euryhaline teleosts are able to adapt to various salinity levels by regulating ion transport, neuroendocrine function, and energy metabolism through osmoregulatory organs such as the gills, intestines, and kidneys (Yamaguchi et al., 2018). At the molecular level, specific genes have been identified as playing a role in regulating salinity adaptation. These genes include ion transporters such as the sodium potassium pump (NKA), Na^+/K^+/$2Cl^-$ cotransporter 1 (*NKCC1*), Na^+/H^+ exchanger 3 (*NHE3*), Na^+/Cl^- cotransporters (NCC), and cystic fibrosis transmembrane conductance regulator (CFTR) (Marshall, 2011; Hwang et al., 2018). In addition, endocrine hormone genes such as growth hormone (GH), hydrocortisone (COR), prolactin (PRL), and insulin-like growth factor-1 (IGF-1) have also been implicated in the regulation of osmolarity (Jia and Lu, 2016).

NHE proteins are widely distributed ion transporter protein, that play a crucial role in regulating Na^+ and H^+ concentration gradients, which is important for physiological processes (Orlowski and Grinstein, 2004). Members of the *NHE* gene family are involved in a range of cellular processes, including intracellular acid-base homeostasis, cell volume regulation, and Na^+ reabsorption in the kidney and gastrointestine (Counillon and Pouysségur, 2000). In studies on osmolarity in fish, *NHE1*, *NHE2*, and *NHE3* are commonly considered as main candidate genes of the NHE family, with research primarily focused on exploring their relationship with dynamic pH balance, osmolarity homeostasis, and ammonia excretion activity (Edwards et al., 2005).

During salinity acclimation, euryhaline teleosts maintain intracellular homeostasis through the action of ion transport proteins and channels mediated by Na^+/K^+-ATPase (NKA) in the gills (Upling, 2020). NKA is a transmembrane protein composed of α and β subunits that are widely distributed in the gill filaments and body kidneys of fish (Han et al., 2022). It mainly relies on the energy generated by ATP hydrolysis to regulate ion concentration homeostasis in the body, achieve active transmembrane transport of Na^+ and K^+, maintain cellular ion homeostasis, and can be used as an important indicator of osmotic pressure regulation in fish (Jiang et al., 2022). In addition, a study on the salinity experiments of migratory Arctic charr(*Salvelinus alpinus*) suggested that inefficient regulation of osmolality may be due to the failure of *NKAα1b* expression (Bystriansky et al., 2007). NKA activity is closely related to environmental salinity (Yang et al., 2022). Generally, in teleost, NKA activity is positively correlated with increasing salinity. For instance, juvenile Turbot(*Scophthalmus maximus*) showed that gill filament NKA activity and plasma osmolality were highest at a salinity of 33.5 ‰ and lowest at 15 ‰ (Imsland et al., 2003). In *Gadus morhua*, *NKAα* expression in gill filaments and body kidneys significantly decreased in hypoosmotic acclimation experiments, while showing an increasing trend in hypertonic water bodies (Larsen et al., 2012). Furthermore, (Shi et al., 2017) investigated the effect of salinity gradient on *Epinephelus moara* and found that NKA activity initially increased and then decreased in all treatment groups (except the 9‰ group) with a sudden decrease in salinity, while the 9‰ group always showed a decrease in NKA enzyme activity, suggesting that very low salinity leads to a decrease in NKA activity, impaired ion transport efficiency in the gills, and prevents excessive ion loss. The pattern of changes in NKA enzyme activity in the gill filaments and liver of juvenile *Amphiprion clarkii* was consistent, with a constant increase within 24 h of low salt stress and a return to

normal or slightly below normal enzyme activity at 48 h and 96 h (Hu et al., 2016). In a seawater desalination experiment with *Lateolabrax japonicus*, gill tissue NKA enzyme activity initially decreased and then increased, following a "U" shape. During the desalination adaptation phase, the activity gradually recovered and stabilized but remained lower than the control group (salinity 30), with a significant difference between the two groups (Zhang et al., 2018). However, the change pattern of NKA activity in teleost was inconsistent, affected by the intensity of salinity adaptation and could be divided into two contradictory types: positive and negative correlation of salinity change. The former, such as *A. clarkii*, *Oreochromis mossambicus*, and *E. moara*, and the latter, such as *Cleisthenes herzensteini* and *Sparus macrocephlus*, may be related to the strength of osmotic stress tolerance of the species (Lin et al., 2006). Additionally, it has been suggested that NKA activity reaches a minimum when the salinity of the water column reaches the isotonic point in fish (Wang et al., 2011). Differences in osmoregulatory capacity and regulation in different fish species, changes in NKA activity involving individual development (adults vs. juveniles) and salinity adaptation patterns (acute vs. chronic, long-term vs. short-term), are closely related to species evolution.

In this study, we conducted a comprehensive analysis of the NHE and NKA gene families in *R. canadum* to investigate their roles in osmoregulation. Our objectives included identifying and characterizing the members of these gene families using genomic data. We examined the conserved structures of the genes, established an evolutionary tree for the species, and performed transcriptome sequencing to explore the expression patterns of the NHE and NKA gene families in *R. canadum* under various salinity conditions. This research provides valuable insights into the involvement of these gene families in osmoregulation and contributes to our understanding of how *R. canadum* adapts to different salinity environments.

2 Materials and methods

2.1 Experimental fish and sampling

The fish used for the experiment were the juvenile fish artificially hatched and cultured by our group. The fish were temporarily kept in a bucket of 1.5 cubic meters of water in a salinity of 28-30‰, a water temperature of 26-28 °C, and a DO of not less than 6 mg·L^{-1}. 180 fish of uniform size, healthy and vigorous with no damage on the body surface were selected for the salinity adaptation experiment after one week of temporary rearing, and the initial weight of the fish was 9.74 ± 0.85 g. The fish were divided into 10‰ salinity group, 30‰ salinity group and 35‰ salinity group with three biological replicates in each group. The fish were cultured in 9 buckets of 500 L size for 4 weeks, with 20 fish randomly placed in each bucket. The culture water salinity was adjusted downward by 4‰/d using fully aerated dechlorinated fresh water or upward by 4‰/d using sea crystals until the salinity of the experimental group reached the preset salinity and then the experiment was officially started. During the culture period, the water was fed twice daily with 6% body weight of commercial compound feed (46% crude protein and 8% crude lipid) without interruption of aeration and the water exchange rate was 30%.

Two sampling were conducted. In the first sampling, five *R. canadum* were randomly selected after seven days of culture, and eight tissues, including gill, intestine, body kidney, brain, stomach, muscle, spleen, and heart, were collected after anesthesia with eugenol (200 mg/L) for tissue distribution assay. In the second sampling, after four weeks of culture, five fish were randomly selected from each barrel, with a total of 15 fish. Among them,6 fish were anesthetized and three tissues of gill, intestine, and body kidney were taken for phenotypic analysis and qPCR detection, and 9 fish were mixed for transcriptome sequencing. All molecular samples were snap frozen in liquid nitrogen and stored at -80 °C after collection.

2.2 HE staining

The fresh tissue was fixed using paraformaldehyde (4%) for 24 h. Afterwards, the tissue was orderly dehydrated using gradient alcohol, and the wax-soaked tissue was embedded in the embedding machine. And further the tissue was cut into slices with its thickness 4 μm, and the paraffin sections were dewaxed and further washed by distilled water. Lastly, the nucleus and cytoplasm were stained by hematoxylin and eosin, respectively.

2.3 Identification of NHE and NKA gene family members in *R. canadum*

For the complete identification of NHE and NKA gene family members in *R. canadum*, this study was based on the whole genome data of *R. canadum* (PRJNA634421) obtained in our laboratory and the NCBI public database, blast identification of NHE and NKA gene family members, recorded as the first round of screening results. The NHE and NKA gene family features were obtained from the Pfam database (http://pfam.xfam.org/) as PF00999 (Sodium/hydrogen exchanger family), PF00287 (Sodium/potassium ATPase beta chain), and PF00690 (Cation transporter/ATPase, N-terminus), respectively. The Hidden Markov Models (HMM) were used to obtain the features of the gene family. The HMMER 3.0 software was used to retrieve the whole-genome data, and the results of the second round of screening were tallied. Integrate the results, delete the mutilated or duplicate sequences and upload to SMART website and NCBI database for duplicate checks. The naming of NHE and NKA gene family members was based on reference comparisons and NCBI search results.

2.4 Structural analysis and genomic localization of the NHE and NKA gene families in *R. canadum*

In order to further investigate the NHE and NKA gene family members, we conducted several analyses. Firstly, we determined the intron and exon length information, as well as the genomic localization, based on the genome annotation file gff. Additionally,

we predicted the molecular weight (MW) and isoelectric point (PI) of the family members using the ExPasy website (http://web.expasy.org/). Moreover, we employed the MEME (Bailey et al., 2015) website (http://meme-suite.org/) to predict amino acid conserved motifs. Furthermore, we predicted the protein structural domains of NHE and NKA gene family members using the SMATR website. Finally, we utilized the TBtools software to map the NHE and NKA gene family structures and genomic localization.

2.5 Evolutionary analysis of the NHE and NKA gene families in *R. canadum*

The NHE and NKA family members from *Homo sapiens*, *Mus musculus*, zebrafish (*Danio rerio*), *S. maximus*, Rainbow Trout (*Oncorhynchus mykiss*), and *L. japonicus* were retrieved from the NCBI database. These sequences served as references for multiple amino acid sequence comparisons and homology analyses, which were performed using ClustalX1.83. The resulting phylogenetic tree was constructed by applying the neighbor-joining method (NJ) through MEGA-X (Kumar et al., 2016) software.

2.6 RNA-seq of NHE and NKA gene families in *R. canadum*

To investigate the impact of different salinity acclimation conditions on the expression patterns of NHE and NKA, RNA was extracted from the gills, intestine, and body kidney of *R. canadum* following 4 weeks of culture in salinities of 10‰, 30‰, and 35‰. RNA from nine fish in each salinity group was pooled to obtain one sample, and Illumina Hiseq^{TM}2000 was used to sequence the transcriptome. The raw mRNA sequencing data has been deposited in the NCBI Sequence Read Archive (SRA) under the accession number SRP202920 (published by our research groups) (Cao et al., 2020).

The raw mRNA sequencing data was processed using fastp (Chen et al., 2018) to remove low-quality data, and the remaining clean reads were mapped to the *R. canadum* genome (PRJNA634421) using HISAT2 software (Kim et al., 2015). StringTie software (Pertea et al., 2015) was then used to assemble the mapped reads. The expression of all genes in each sample (FPKM and reads count) was then calculated using RSEM (Li and Dewey, 2011), and the read count was normalized and analyzed for differentially expressed genes using edgeR (Robinson et al., 2010) ($P<0.05$ for significantly differentially expressed genes, FDR<0.05 and $|\log2FC|> 1$ for highly significant differentially expressed genes).The resulting expression data ($\log_2^{FPKM}$) were utilized to generate a gene expression heat map using TBtools, and correlation analysis was performed.

2.7 Analysis of qPCR expression of NHE and NKA genes in *R. canadum*

Gene-specific primers were designed based on the cDNA sequences for NHE and NKA gene family members, resulting in the amplification of fragments ranging from 100-230 bp (Table 1). β-actin was chosen as the reference gene. qRT-PCR was performed using a Roche Light Cycler^{TM} 96 real-time PCR machine and SYBR$^{®}$Select Master Mix. The expression levels of the three genes in 9 tissues and the expression levels of the genes in osmoregulatory organs such as gills, intestines, and kidneys after salinity adaptation were determined.

The amplification program consisted of an initial denaturation step at 95°C for 10 min followed by 40 cycles of denaturation at 95° C for 10 s, annealing at 60°C for 20 s, and extension at 72°C for 20 s. To minimize errors, three different *R. canadum* individuals were sampled for each salt treatment, and qPCR was repeated three times for each individual. The expression levels of *NHE1*, *NHE2a*, *NHE2c*, *NHE5*, *NKAα1b*, *NKAα3a*, *NKAβ1b*, and *NKAβ3a* genes were analyzed using the $2^{-\Delta\Delta Ct}$ method, and one-way ANOVA (LSD, Duncan) was performed using SPSS22.0 software.

3 Results

3.1 Analysis of organizational structure of *R. canadum* after salinity adaptation

After 30 days of domestication in low salinity water (10 ppt), the length (width) of gill filaments and gill lamellae of *R. canadum* increased significantly. The spacing between gill lamellae decreased, and the cells of gill lamellae were rounded and full. The number of chloride-secreting cells on gill filaments and gill lamellae decreased significantly. In the high salinity group (35 ppt), the number of chloride-secreting cells on gill filaments and gill lamellae increased slightly but not significantly. The width of gill filaments, gill lamellae, and cartilage tissues decreased significantly, and the spacing of gill lamellae increased (Figure 1A).

The microstructure of the intestine of juvenile *R. canadum* in the control group (30 ppt) showed that the single layer of columnar epithelium on the intestinal villi of juvenile *R. canadum* in the low salinity group became thicker, and the number of cupped cells decreased significantly. The size of the cupped cells did not change significantly. In the high-salinity group, the cytosol of the cup-shaped cells was enlarged, and the thickness of the unilamellar columnar epithelium and the number of cup-shaped cells on the intestinal villi did not change significantly (Figure 1B).

In the low salinity group, the tubular diameter of all levels of renal tubules of *R. canadum* increased, and the glomerulus was enlarged, full, and filled. The lumen of its capsule was small. In the high salinity group, the glomerulus atrophied, the lumen of the glomerular capsule increased, and the tubular diameter of all levels of renal tubules decreased slightly (Figure 1C).

3.2 Identification of NHE and NKA gene family members in *R. canadum*

In this study, the NHE and NKA families were characterized using genome–wide data and an HMM model. The analysis identified a total of 12 NHE family members and 12 NKA family

10.3389/fmars.2023.1228933

TABLE 1 Primers for qPCR of gene families.

Primer	Purpose	Sequence(5′-3′)	Length	GC%	Amplicon size
qNHE1-F	qRT-PCR	CCTGGGCACGATCCTGATGTTT	22	54.55	119
qNHE1-R	qRT-PCR	GTCCGTTGAGGTCTGATGGGTT	22	54.55	
qNHE2a-F	qRT-PCR	GCCATTGTTACCTGTGCCCT	20	55.00	168
qNHE2a-R	qRT-PCR	GTTCCACTCGTGCTCTGTTGTTA	23	47.83	
qNHE2b-F	qRT-PCR	CGCAGCAACACCAGCATCCAGTA	23	56.52	187
qNHE2b-R	qRT-PCR	CCACAGCCGTCAGCAACAGAACAC	24	58.33	
qNHE2c-F	qRT-PCR	TCCTCGACAGCGGCTACTTCAT	22	54.55	193
qNHE2c-R	qRT-PCR	ATGATGGCAGCGAACAGCAAGT	22	50.00	
qNHE3 -F	qRT-PCR	GTAGCCGTCATCGCCGTGT	19	63.16	100
q NHE3 -R	qRT-PCR	GCACCACTGTCACACCATCGT	21	57.14	
qNHE5-F	qRT-PCR	TTGCTCTGGTGGTGCTGCTG	20	60.00	166
qNHE5-R	qRT-PCR	ATGGTCGGCTTCCTGCTGGT	20	60.00	
qNHE6a-F	qRT-PCR	TGGACCTGTACGCTCTGCTGTT	22	54.55	101
qNHE6a-R	qRT-PCR	GTTGTCTCCTTCTGGCTGGTATGC	24	54.17	
qNHE6b-F	qRT-PCR	TGGATGGGTCACAGAGAAGGAACA	24	50.00	141
qNHE6b-R	qRT-PCR	CACAACAAGCAGGCAGAGTAGCA	23	52.17	
qNHE7-F	qRT-PCR	CTACCGAGAAGGAGGCAGAGGAA	23	56.52	167
qNHE7-R	qRT-PCR	ACCCACCAGCAAACCGTAAATCAT	24	45.83	
qNHE8-F	qRT-PCR	GAGATGACGACGGAGGAGAGGTGAA	25	56.00	171
qNHE8-R	qRT-PCR	CAGCAGGTGTTGTAGAGTGGATGGT	25	52.00	
qNHE9-F	qRT-PCR	ACTCTGCTGCTGGTCTGCTTCA	22	54.55	153
qNHE9-R	qRT-PCR	TGTTGTGTCCTGCCTCCCTGTA	22	54.55	
qNHEβ-F	qRT-PCR	TCCGCTGAGGTCTTCCATCTGT	22	54.55	141
qNHEβ-R	qRT-PCR	GCTCACGCTGCTCCACATCTTC	22	64.02	
qNKAα1a-F	qRT-PCR	GCTGTCATCTTCCTCATCGGTATCA	25	48.00	123
qNKAα1a-R	qRT-PCR	GTTCTTCACCAGGCAGTTCTTCTTG	25	48.00	
qNKAα1b-F	qRT-PCR	TCGTCATCATCACTGGTTGCTTCTC	25	48.00	177
qNKAα1b-R	qRT-PCR	TGTCTCCACCTTTCACCTCCACTAA	25	48.00	
qNKAα2-F	qRT-PCR	GCATACACACTAACCAGCAACATCC	25	48.00	152
qNKAα2-R	qRT-PCR	GCCGCCTCGTAAGCCAATGA	20	60.00	
qNKAα3a-F	qRT-PCR	GGTGATGGTGTGAACGACTCTCC	23	56.62	149
qNKAα3a-R	qRT-PCR	CCTTCTTCTACTCCTGTGACGATGG	25	52.00	
qNKAα3b-F	qRT-PCR	TCTCAGGCTCCGATGTGTCCAA	22	54.55	196
qNKAα3b-R	qRT-PCR	GGCAGAGGAATGTTGACGATGATGA	25	48.00	
qNKAβ1a-F	qRT-PCR	ACGTGATATTCTACGGATGCTTGG	24	45.83	101
qNKAβ1a-R	qRT-PCR	GACTCTGTCCTGATAGGTGGGTTT	24	50.00	
qNKAβ1b-F	qRT-PCR	GTCTGACACACACCCCACGCT	21	61.99	140
qNKAβ1b-R	qRT-PCR	CTTCATCTGGTCCCTCTGGTTCTC	24	54.17	
qNKAβ2a-F	qRT-PCR	TGTGGAGCCAAGAGTTACAAAGTG	24	45.83	123

(Continued)

TABLE 1 Continued

Primer	Purpose	Sequence(5′-3′)	Length	GC%	Amplicon size
qNKAβ2a-R	qRT-PCR	GCCGTAGTATGGGTAGTACATGAGAT	26	46.15	
qNKAβ2b-F	qRT-PCR	ACTTCAAGCAGGATGACAGCG	21	52.38	206
qNKAβ2b-R	qRT-PCR	ACCACAGGTGACATACGGAGC	21	57.14	
qNKAβ3a-F	qRT-PCR	CGTCTGAAGGTCGGCTGGATAA	22	54.55	136
qNKAβ3a-R	qRT-PCR	CACTCCACCGTCTGCTCAATGT	22	54.55	
qNKAβ3b-F	qRT-PCR	TGTTGCTGCTCACTCTGGATG	21	52.38	192
qNKAβ3b-R	qRT-PCR	CCTCGTTCTTCTCCTGCTCTGTATC	25	52.00	
qNKAβ4-F	qRT-PCR	ATGACATCGCCTTTAACGCCTCTG	24	50.00	181
qNKAβ4-R	qRT-PCR	AACTGACACGCTTTCCGCTCTG	22	54.55	
β-actin-F	qRT-PCR	AGGGAAATTGTGCGTGAC	18	50.00	114
β-actin-R	qRT-PCR	AGGCAGCTCGTAGCTCTT	18	55.56	

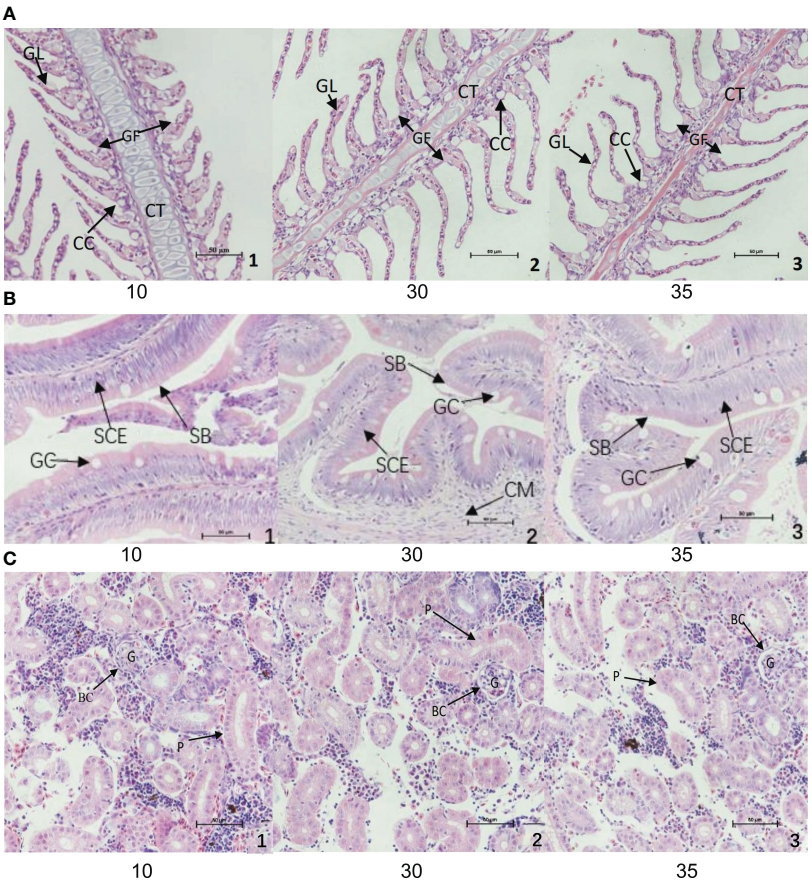

FIGURE 1
Structural changes of gill **(A)**, intestine **(B)** and body kidney **(C)** of juvenile of *R. canadum*. 10, salinity 10 ‰; 30, salinity 30 ‰; 35, salinity 35 ‰. GF, gill filaments; GL, gill small pieces; CC, chlorinated cells; CT, cartilage tissue; SCE, monolayer columnar epithelium; SB, striatum; GC, goblet cells; CM, ring muscle; G, glomerulus; BC, renal capsule; P, renal tubule.

members, including both single-copy and multi-copy genes. Specifically, *NHE2* and *NHE6* were found to be multi-copy genes, while *NKA1*, *NKA3*, and *NKAβ1~3* were also identified as multi-copy genes. The coding sequence (CDS) of NHE genes ranged from 1818 to 2940 bp in length, with amino acid sizes ranging from 606 to 980 aa. The PI ranged from 5.5 to 9.45, and the Mw ranged from 67.04 kD to 107.53 kD. Similarly, the CDS of NKA genes ranged from 837 to 3099 bp in length, with amino acid sizes ranging from 279 to 1033 aa. The PI ranged from 5.01 to 8.09, and the Mw ranged from 32.67 kD to 113.47 kD (Table 2).

3.3 Structural analysis and genomic localization of the NHE and NKA gene families in *R. canadum*

The NHE family members of *R. canadum* had 2 to 16 Coding DNA Sequence (CDS), with *NHE3*, *NHE7*, *NHE8*, and *NHE9* having 16 CDS, and *NHEβ* having the least number of CDS with only 2, which might be attributed to genome assembly issues. In contrast, *NHE1* had the highest number of CDS with 15 (Figure 2A). The number of CDS of NKA family members ranged from 5 to 23, with *NKAα* members and *NKAβ* members showing polarized CDS numbers, where none of the former had less than 21 and all of the latter had less than 10 CDS, implying a correlation between CDS numbers and subtype classification (Figure 2B).

The present study aimed to analyze the motif composition of NHE and NKA genes in *R. canadum* using the MEME website. The results showed that both gene families contained 10 motifs arranged in an organized and regular manner. Most motifs of NHE genes were associated with Na^+/H^+ exchanger structural domains, except for motif4, while all motifs identified in NKA were associated with Cation transporter/ATPase and Hydrolase structural domains. Further analysis revealed that NHE motif1 and motif4 were mainly identified in *NHE1~5*, and motif 8 appeared only twice in *NHE8* and once in all other members. In contrast, motif4 appeared in the anterior segment of the *NHE9* sequence. Furthermore, *NHEβ* lacked motif7 and had more motif10 compared to *NHE1* (Figure 3A). Concerning the NKA gene family, motif10 was found only in the *NKAβ* isoform, while the remaining nine motifs were ordered in the *NKAα* isoform (Figure 3B). The only difference was that motif4 was missing in *NKAα1b*.

The domain information of NHE and NKA genes in *R. canadum* was predicted using the SMART website, which revealed that NHE genes contained CPA1 and NHE structural domains (Figure 3C), and NKA genes contained NKA and CPA-N/C structural domains (Figure 3D).

Genomic localization shows that members of the NHE and NKA gene families of *R. canadum* localize to 10 and 9 superscaffolds, respectively (Figure 4). Specifically, *NHE2b* and *NHE6a* were present simultaneously on superscaffold16 and superscaffold3, respectively, while the remaining eight members of NHE family were distributed randomly on a single superscaffold (Figure 4A). Similarly, 2-3 members of NKA family (*NKAβ1b*, *NKAα1b*, and *NKAα1a*; *NKAα2* and *NKAβ3*) were simultaneously present on superscaffold24 and superscaffold14, respectively. In contrast, the remaining eight members of NKA family were randomly distributed on a single superscaffold (Figure 4B). Moreover, the multi-copy members of NHE family, *NHE2a-c*, were localized to the 9th, 3rd, and 24th superscaffold, respectively, whereas *NHE6a* and *NHE6b* were localized to the 3rd and 12th superscaffold, respectively (Figure 4A) multi-copy. Additionally, the multi-copy members of NKA family, *NKAβ1-3* and *NKAα3a* and *NKAα3b*, were identified in the 7th, 24th, 23rd, 12th, 5th, and 14th superscaffold, respectively, and *NKAα1a* and NKAα1b were localized in both superscaffold 24 (Figure 4B).

TABLE 2 Sequence characteristic of *NHE* and *NKA* gene families.

Gene	PI	Mw/Da	CDS/bp	Length/aa	Location	Accession numbers
NHE1	8.3	89.77	2436	812	Superscaffold 4	OR095067
NHE2a	9.45	98.21	2622	874	Superscaffold 9	OR095068
NHE2b	9.15	75.12	2004	668	Superscaffold 3	OR095069
NHE2c	8.2	94.10	2514	838	Superscaffold 24	OR095070
NHE3	5.95	100.84	2718	906	Superscaffold 16	OR095071
NHE5	8.32	107.53	2940	980	Superscaffold 1	OR095072
NHE6a	5.61	77.32	2079	693	Superscaffold 3	OR095073
NHE6b	6.29	77.73	2118	706	Superscaffold 12	OR095074
NHE7	5.96	77.28	2091	697	Superscaffold 7	OR095075
NHE8	5.72	72.70	1950	650	Superscaffold 6	OR095076
NHE9	5.5	67.04	1818	606	Superscaffold 20	OR095077
NHEβ	8.75	84.83	2295	765	Superscaffold 16	OR095078
NKAα1a	5.23	112.50	3075	1024	Superscaffold 7	OR095079
NKAα1b	5.19	113.47	3099	1033	Superscaffold 24	OR095080
NKAα2	5.3	111.36	3033	1011	Superscaffold 14	OR095081
NKAα3a	5.27	112.73	3069	1023	Superscaffold 5	OR095082
NKAα3b	5.25	111.30	3033	1011	Superscaffold 4	OR095083
NKAβ1a	8.02	34.85	906	302	Superscaffold 24	OR095084
NKAβ1b	6.24	34.42	906	302	Superscaffold 24	OR095085
NKAβ2a	8.09	34.21	894	298	Superscaffold 23	OR095086
NKAβ2b	6.84	35.37	918	306	Superscaffold 12	OR095087
NKAβ3a	5.01	38.73	996	332	Superscaffold 16	OR095088
NKAβ3b	7.51	32.67	837	279	Superscaffold 14	OR095089
NKAβ4	7.61	39.36	1029	343	Superscaffold 3	OR095090

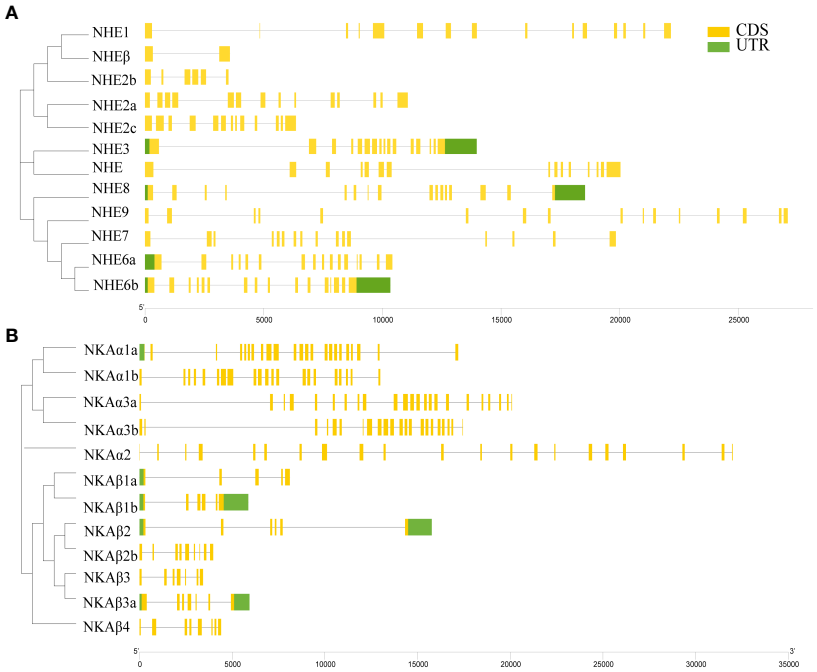

FIGURE 2
Gene structure of NHE **(A)** and NKA **(B)** gene families.

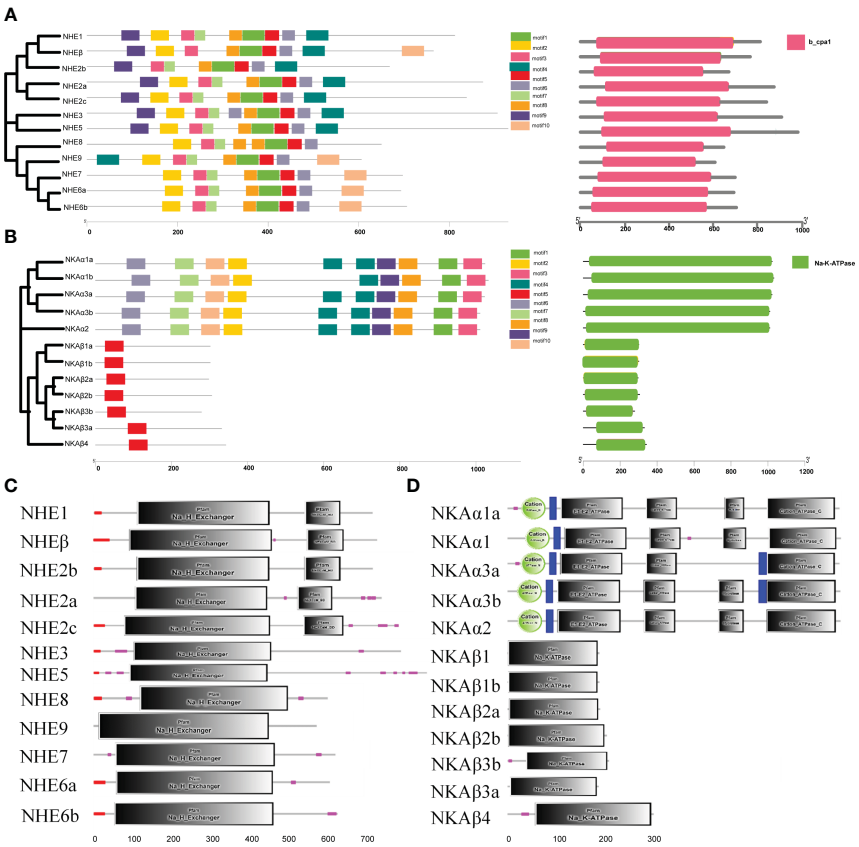

FIGURE 3
Motif of NHE **(A)** and NKA **(B)** gene families and domain of *NHE* **(C)** and *NKA* **(D)** gene families.

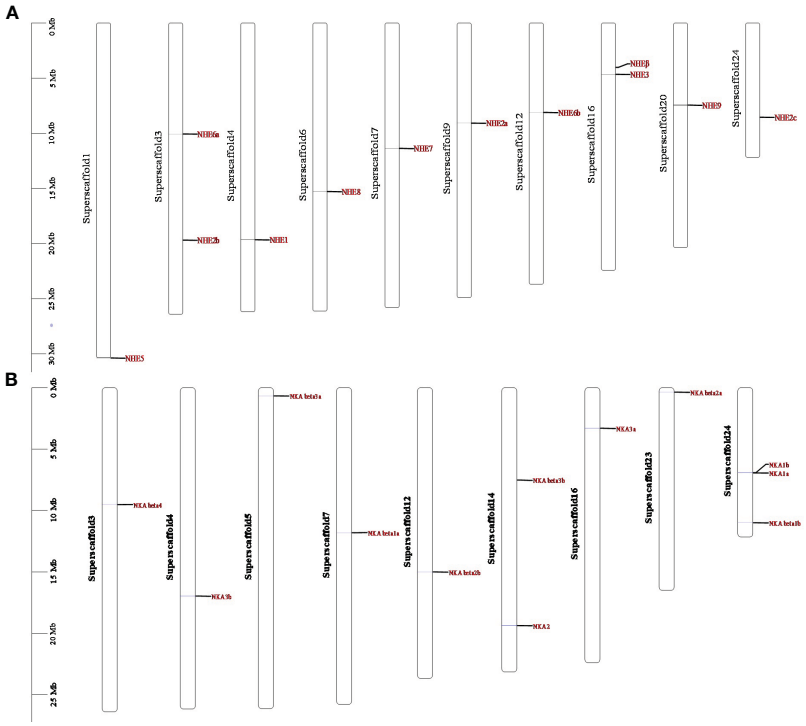

FIGURE 4
Genomic mapping of NHE **(A)** and NKA **(B)** gene families.

3.4 Phylogenetic analysis of the NHE and NKA gene families in *R. canadum*

The NHE and NKA gene family members of six species, including *Homo sapiens*, *Mus musculus*, *D. rerio*, *S. maximus*, *O. mykiss*, and *Lateolabrax maculatus*, were used as references to construct a phylogenetic evolutionary tree, which further verified the accuracy of the annotation of the NHE and NKA genes of *R. canadum* and revealed the variation of these genes during species evolution (Figure 5). The analysis indicated that *NHE1~9* of *R. canadum* were most closely related to teleost and furthest from mammals. *NHE1* and *NHEβ* were clustered into a single clade with teleost such as *D. rerio* and *S. maximus*, respectively, before merging into one clade; *NHE3* and *NHE5* of *R. canadum* were merged into one clade, while *H. sapiens* and *M. musculus* were separate clades. The multi-copy genes *NHE2a~c* were clustered with other species and re-clustered with mammalian *NHE4*, respectively; *NHE6a* and *NHE6b* were alone, and their closest relatives were *L. japonicus*, *S. maximus*, *D. rerio* and *O. mykiss* (Figure 5A). Additionally, the *NKAα* subtype gene and *NKAβ* subtype gene of *R. canadum* were separately divided into the same branch with other species and were most closely located with teleost. Among them, *NKAα4* of *H. sapiens* and *M. musculus* were separately merged with *NKAβ1a* of *R. canadum*. Moreover, *NKAα1a~b* and *NKAα2* of *R. canadum* were closest together and merged into one branch, and *NKAα1* and *NKAα2* of *H. sapiens* and *M. musculus* were independently into one branch (Figure 5B).

3.5 Analysis of the expression patterns of NHE and NKA gene families in *R. canadum*

To investigate the expression patterns of the NHE and NKA gene families in various tissues of *R. canadum* under normal seawater salinity, qRT-PCR was used to determine the gene expression abundance in nine different tissues. The results demonstrated that the NHE and NKA family members of *R. canadum* were widely expressed in all tissues, including the gill, brain, heart, intestine, kidney, liver, spleen, stomach and muscle (Figure 6). Specifically, the tissues with high expression of NHE were the gill, somatic kidney, and brain, while NKA was highly expressed in the gill, brain, and heart.

Of the single-copy genes, *NHE1* and *NHE3* showed similar expression patterns and were mainly concentrated in the gill and somatic kidney. On the other hand, *NHE5* and *NHE7* were highly expressed in the liver and brain, respectively. The highest expression signals of multi-copy genes *NHE2a* and *NHE2b* were detected in the brain and muscle, respectively, while the highest expression tissues were the gill and liver for *NHE6a*, and the somatic kidney and brain for *NHE6b* multi-copy. Furthermore, *NHEβ* and *NHE1* expression patterns were inconsistent, with high expression detected only in the brain and trace expression in other tissues (Figure 6A).

The NKA family members *NKAα1a*, *NKAβ1b*, *NKAβ2a*, and *NKAβ3a* were highly expressed in osmolarity-regulating organs, such as the gill, intestine, and somatic kidney, respectively. Among

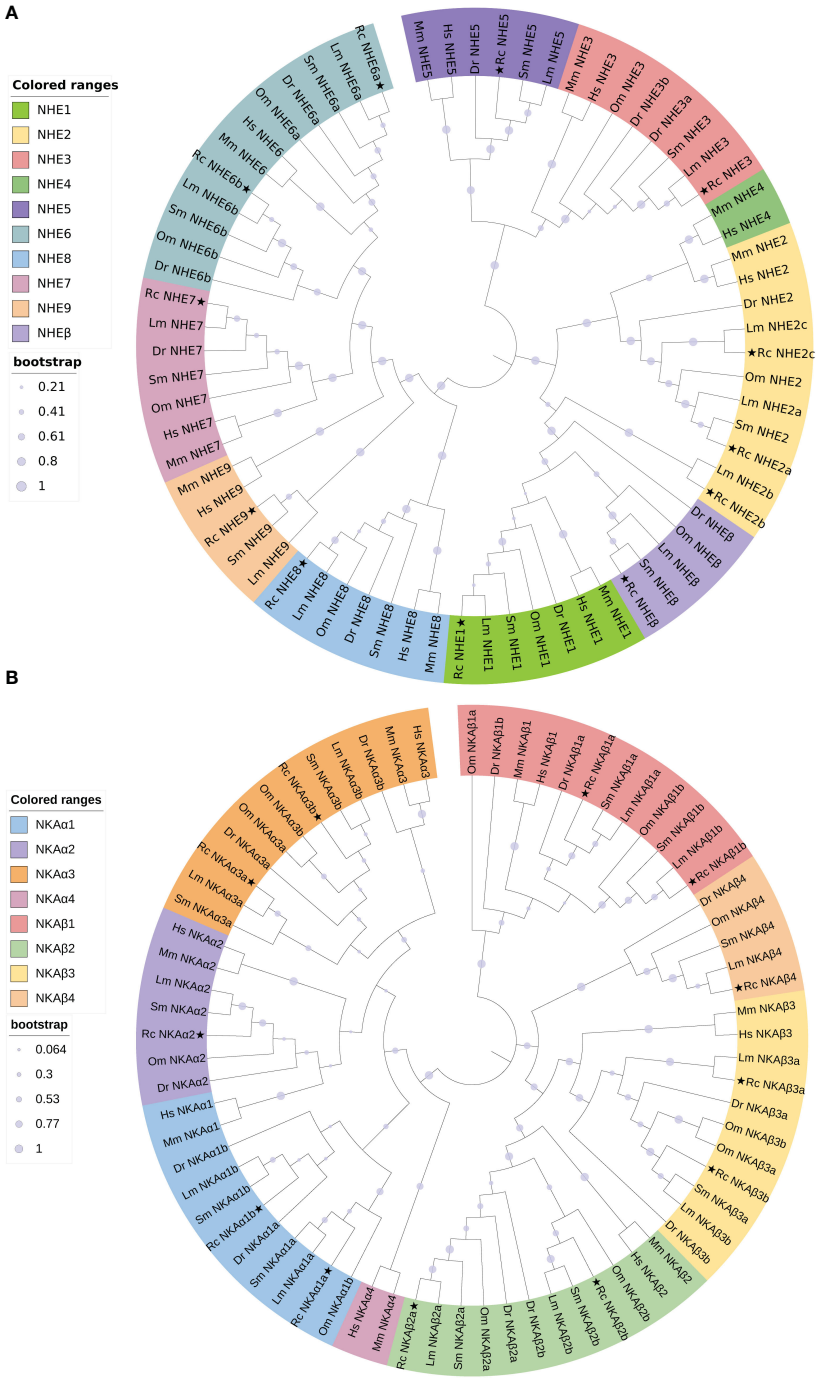

FIGURE 5
Phylogenetic analysis trees of *R. canadum* NHE **(A)** and NKA **(B)** gene families. Rc, *R. canadum*; Dr, *D. rerio*; Sm, *S. maximus*; Lm, *L. maculatus*; Hs, *H. sapiens*; Mm, *M. musculus*.

them, *NKAα1a* was the most highly expressed in the gill. *NKAα2* was expressed only in the brain and muscle, while *NKAβ4* was highly expressed in the brain, with lower expression levels in other tissues. Most of the multi-copy genes (*NKAα1b*, *NKAα3a*, *NKAα3b*, *NKAβ1a*, *NKAβ2a*, *NKAβ2b*, *NKAβ3a*, and *NKAβ3b*) were highly expressed in brain tissues, with *NKAα1b* only detected as a fluorescent signal in brain tissues, not consistent with *NKAα1a*. *NKAα3a* and *NKAα3b* showed similar expression patterns, with high expression in the brain, heart, somatic kidney, and gill in descending order. *NKAβ1a* was highly expressed in several tissues, mainly in the brain, stomach, and muscle, while *NKAβ1b* was highly expressed mainly in the somatic kidney. *NKAβ2a* was highly expressed in the gill, intestine, brain, stomach, and muscle, while *NKAβ2b* was hardly expressed except in the brain and muscle. The expression pattern difference of *NKAβ3a-NKAβ3b* was similar to that of *NKAβ2a-NKAβ2b*. Additionally, fluorescent signals of other

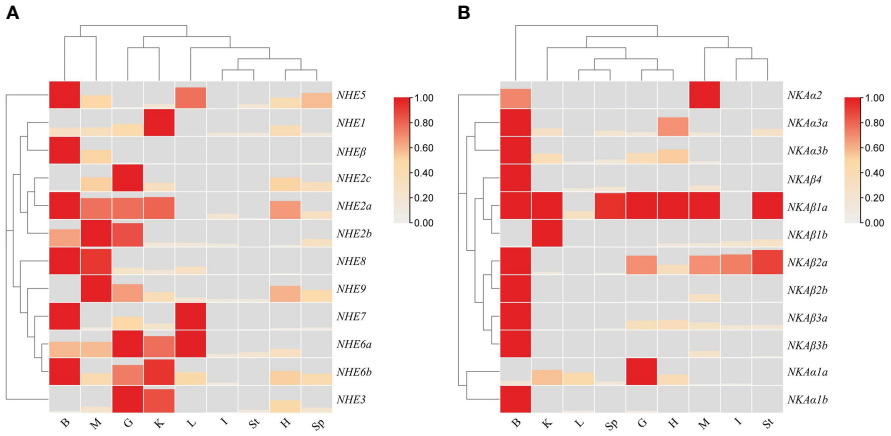

FIGURE 6
Heat map of tissue expression of NHEs **(A)** and NKAs **(B)** in *R. canadum*. G, gill; I:intestine; K,Kidney; L, Liver; H, Heart; B, Brain; Sp, Spleen; St, Stomach; M, Muscle.

members were less frequently detected in the liver, spleen, and stomach, except for *NKAα1a*, *NKAβ1a*, and *NKAβ2a*, which showed expression (Figure 6B).

3.6 Transcriptome analysis of the NHE and NKA gene families in *R. canadum*

The effects of salinity acclimation on the expression patterns of NHE and NKA gene families in different tissues of *R. canadum* was investigated using a reference transcriptome sequencing approach and validated by qRT-PCR. The results demonstrated that the expression patterns of NHE and NKA genes were influenced by salinity and exhibited tissue-specific characteristics (Figure 7). In gill tissues, the expression of *NHE3* was significantly down-regulated under salinity 10 and 35 acclimation conditions compared to the control group acclimated at salinity 30. Additionally, *NHE6b* and *NHE8* were significantly down-regulated under salinity 35 acclimation conditions, while *NHE2a* was significantly down-regulated under salinity 10 acclimation conditions. However, the experimental group exhibited significant upregulation in *NHE2c* expression, and *NHE7* showed significant upregulation under salinity 35 acclimation conditions. In intestinal tissues, the expression levels of NHE genes were significantly increased under experimental conditions (salinity 10 and 35) compared to the salinity 30 control. Specifically, *NHE7* was significantly upregulated under both low (10) and high (35) salinity acclimation conditions, while *NHE1* and *NHE6a-b* were only significantly upregulated under salinity 35 acclimation conditions. *NHE9* exhibited significant upregulation under salinity 10 acclimation conditions. In kidney tissues, *NHE3* expression increased with higher salinity and showed highly significant upregulation at salinity 35, along with significant downregulation at salinity 10 compared to the salinity 30 control. *NHE6a* exhibited significant upregulation at salinity 35, whereas *NHE2a* showed significant downregulation at salinity 10. *NHE5* and *NHEβ* expression levels remained relatively stable across all three salinity acclimation conditions in all tissues, while *NHE2b* and *NHE5* expression levels were comparatively low under all conditions (Figure 7A).

In gill tissues, *NKAα3a*, *NKAα3b*, and *NKAβ1a* expression levels were significantly upregulated under salinity acclimation conditions of 10 and 35, with *NKAα3a* displaying particularly highly significant upregulation at salinity 10 compared to the control group at salinity 30. Conversely, *NKAα1b* expression was significantly downregulated at both salinities 10 and 35. In gill, intestinal, and kidney tissues, the expression levels of *NKAα1a* and *NKAβ1b* showed significant increases with increasing salinity. In intestinal tissues, *NKAβ2a* and *NKAβ4* expression levels were significantly upregulated at salinity acclimation condition of 10, and exhibited highly significant upregulation at salinity acclimation condition of 35. Additionally, *NKAα1b*, *NKAα3b*, *NKAβ1a*, and *NKAβ3a* were significantly upregulated at salinity acclimation condition of 35 compared to the control. In kidney tissues, *NKAβ1a* expression was significantly downregulated at salinity 35, while *NKAα3b* showed significant upregulation at salinity 10 compared to the control group. However, the expression levels of *NKAα2*, *NKAα3a*, and *NKAβ2b* were relatively low under all conditions (Figure 7B). The qRT-PCR validation and RNA-seq were in general agreement in terms of the fold change in differential expression (Figure 7C). In the linear regression analysis of trend changes, $R^2 = 0.8959$ (Figure 7D). The results indicate that the gene expression analysis based on RNA-Seq data is reliable.

3.7 Salinity-adapted qPCR expression analysis of the NHE and NKA gene families of *R. canadum*

To investigate the differences in the expression patterns of some members of the NHE and NKA gene families of *R. canadum* under salinity acclimation, qPCR was performed on *R. canadum* acclimated to salinities of 10‰, 30‰ and 35‰ for 4 weeks in this study. The results showed that the relative expression of *NHE1*

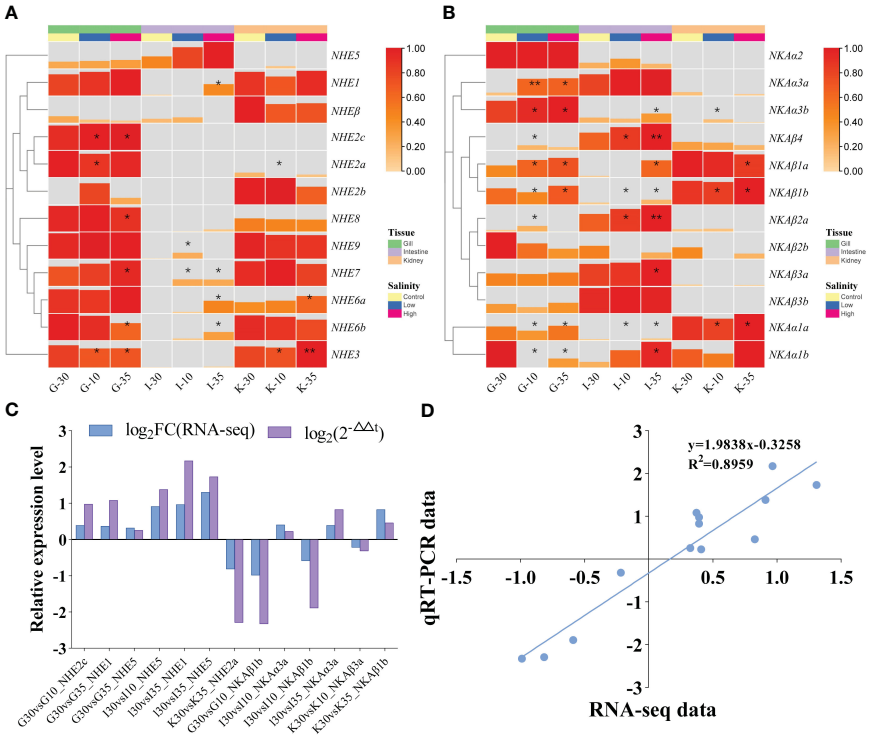

FIGURE 7
Transcriptome expression patterns of NHEs **(A)** and NKAs **(B)** of *R. canadum* under different salinity acclimation. Relative expression level **(C)** and linear regression **(D)** of RNA-Seq and qRT-PCR data that are expressed as a $\log_2$ fold change. 10, salinity 10 ‰; 30, salinity 30 ‰; 35, salinity 35 ‰; G, gill; I, intestine; K, kidney.

was significantly up-regulated in the intestine and down-regulated in the kidney after increasing or decreasing salinity, while the expression was not significantly increased in the gills after decreasing salinity (Figure 8A). In addition, *NHE2a* expression in the gill did not change significantly in low-salt acclimation, while it was significantly down-regulated in high-salt acclimation (Figure 8B). *NHE2c* was significantly down-regulated in gill, intestine and somatic kidney with increasing salinity (Figure 8C), and *NHE5* was also significantly down-regulated in somatic kidney. In addition, the expression pattern of *NHE5* in both gill and intestine was significantly different in a "U" pattern (Figure 8D).

Following low-salt acclimation, significant down-regulation of *NKAα1b* and *NKAβ3a* was observed in the gills of *R. canadum* (Figures 8E, H), while *NKAα3a* and *NKAβ1b* did not exhibit significant changes (Figures 8F, G). In the intestine, *NKAα1b* and *NKAβ1b* did not exhibit significant changes (Figures 8E, G), whereas *NKAα3a* and *NKAβ3a* were significantly up-regulated and down-regulated, respectively (Figures 8F, H). In the somatic kidney, *NKAα1b*, *NKAα3a*, and *NKAβ3a* showed significant up-regulation (Figures 8E, F, H), while *NKAβ1b* did not change significantly (Figure 8G). Upon high-salt acclimation, the expression of *NKAα1b* and *NKAβ3a* in the gills remained consistent with low-salt acclimation (Figures 8E, H), while *NKAα3a* and *NKAβ1b* exhibited significant up-regulation (Figures 8F, G). In the intestine, the expression levels of *NKAα1b*, *NKAα3a*, and *NKAβ1b* were significantly increased (Figures 8E, F, G), while *NKAβ3a* expression levels were significantly decreased (Figure 8H). The expression pattern of *NKAα3a* and *NKAβ3a* in the somatic kidney was consistent with low-salt adaptation (Figures 8F, H), while *NKAα1b* and *NKAβ1b* expression were unaffected by salinity (Figures 8E, G).

4 Discussions

The process of salinity adaptation in fish can be divided into two stages: passive adaptation to the external environment and active osmoregulation (Li et al., 2022). The key to salinity adaptation in fish is ion transport, and this regulation is primarily performed by osmoregulatory organs such as the gills, kidneys, and intestines (Whittamore, 2012; Dawood et al., 2021; Ali et al., 2022). The gills are the major organ of osmoregulation in fish and play an important role in maintaining the balance between the internal and external environment of the fish, which is closely related to the ion transport gene sodium/potassium pump (NKA) on the cell membrane (Dawood et al., 2021). In this study, the gill filaments and gill lamellae of juvenile *R. canadum* in the low salinity group were more round and full, and wider than those in the control group. On *L. japonicus*, *Acipenser schrenckii* and *Gymnocypris przewalskii*, gill tissues underwent similar adaptive changes in order to maintain osmoregulatory homeostasis (Hou et al., 2006; Wang and Hu, 2009; Huang et al., 2022). This is because the gill filaments and gill lamellae of juvenile fish living in a desalinated environment tend to change to wider and longer to facilitate sufficient contact with the water column

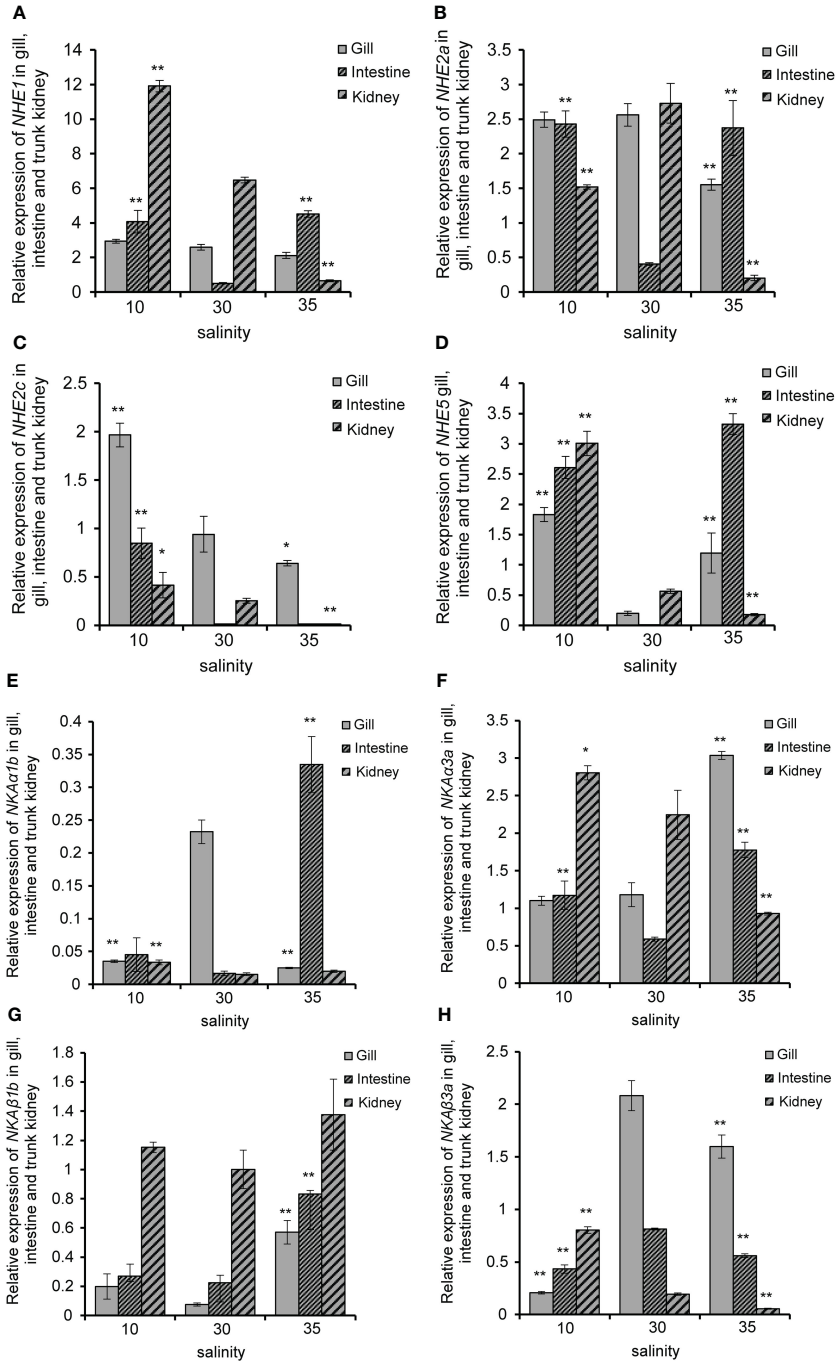

FIGURE 8
Relative expression of *R. canadum NHE1* **(A)**, *NHE2a* **(B)**, *NHE2* **(C)**, *NHE5* **(D)**, *NKAα1b* **(E)**, *NKAα3a* **(F)**, *NKAβ1b* **(G)** *and NKAβ3a* **(H)** in different tissue after salinity adaption. 10, salinity 10 ‰; 30, salinity 30 ‰; 35, salinity 35 ‰. * and* * indicated that the expression of each gene was significantly different from that of the control group, and the significance levels were $P < 0.05,0.01$, respectively.

and thus take up inorganic ions in the water to adapt to the hypotonic environment (Yu et al., 2012; Li et al., 2014). Conversely, gill filament cells shrank, and gill lamellae spacing increased at high salinity. These changes increased water and oxygen exchange between the fish and the external environment, which promoted better survival of fish under high salinity conditions (Yang et al., 2014). In this experiment, the number of chloride-secreting cells in *R. canadum* decreased at low salinity and increased at high salinity. Chloride-secreting cells are important regulatory cells that adapt to different salinities in euryhaline fish, and they have abundant Na^+/K^+-ATPase on the microtubule system in their cytoplasm (Sakamoto et al., 2001). During salinity changes, chloride-secreting cells secrete Cl^- in hypotonic regulation and absorb Na^+ and Cl^- in hypertonic regulation to regulate osmotic pressure homeostasis (Foskett et al., 1983; Marshall, 2011). This shows that the gills of *R. canadum* have certain adaptability when the external salinity changes.

The intestine of fish plays a smaller role in osmoregulation, but it has slao been shown that the intestinal epithelial cell membrane can be involved in active transmembrane transport of Na^+, K^+ and Cl^- inside and outside the cell through ion channel transporter proteins, combined with passive transport of water to maintain osmotic pressure homeostasis in the body (Li et al., 2011). In our study, we observed changes in the intestinal villi structure of juvenile *R. canadum* in the low salinity group, where the monolayer columnar epithelium of intestinal villi became thicker. These results are consistent with the speculation of Sun et al. (2016). who hypothesized that low salinity has a detrimental effect on the intestine of *Takifugu rubripes*. We also observed changes in cupped cells, which secrete mucus to lubricate the epithelial surface and remove waste (Kibenge and Strange, 2021). The number of cupped cells decreased at low salinity, while the cytosol of cupped cells became larger at high salinity. Further research is necessary to determine whether these changes in cupped cells are related to salinity adaptation in juvenile *R. canadum*. The kidney is another important organ in the regulation of osmotic pressure in fish, as the glomerulus filters blood cells and macromolecular proteins from the blood, and the renal tubules reabsorb water, glucose and amino acids (Smith, 1932; Gonzalez, 2012). In this study, the tubular diameter of all levels of renal tubules in the low-salinity group became larger, the glomeruli were expanded, full and filled, and the gap in the inner wall of the renal capsule was reduced; in the high-salinity group, the glomeruli were atrophied and the gap in the inner wall of the renal capsule was increased. This structural change was beneficial to the filtration and reabsorption of nutrients in the blood of juvenile *R. canadum*.

Changes in water salinity have a significant impact on the osmotic pressure of fish organisms, and fish have developed various mechanisms to counteract the negative effects of salinity by activating activities such as their own water-salt regulation (Gonzalez, 2012). Sodium hydrogen exchanger (NHE) is a class of ion channel proteins present in most species, involved in the intracellular and extracellular transport of Na^+ and H^+ ions, and plays a critical role in cellular acid-base homeostasis, cell volume regulation, and osmotic pressure regulatory networks in fish, such as Na+ reabsorption in the kidney, stomach, and intestine (Edwards et al., 2005). *NHE3*, one of the NHE family members, also forms an ion regulatory network in teleost with NKA, *NKCC1*, NCC, and CFTR, which together maintain salt secretion and ion transport of Na^+, K^+, and Cl^- in and out of the membrane (Marshall, 2011). Current studies in fish osmoregulation have focused on *NHE2* and *NHE3*. For example, Yan et al. (2007) reported that *D. rerio* treated with soft water had increased expression of *DrNHE2* and *DrNHE3* genes in the gills and were enriched in mitochondrion-rich cells (MRCs). The gill of *LjNHE3* expression level of *L. japonicus* was upregulated after low salt stress (Inokuchi et al., 2017). The number of *NHE* family members varies somewhat among species; for instance, *NHEβ4* is identified in mammals such as *H. sapiens* and *M. musculus*, but not in teleost such as *D. rerio*, *Oryzias latipes*, and *Dicentrarchus labrax* (Tine et al., 2014). Sodium/potassium-transporting ATPase (NKA), the main active pump in the gill, is responsible for Na^+ ion transport as well as NHE, except that it empowers the ion transport system of multiple osmolarity-regulated epithelial cells by hydrolyzing ATP (Lin et al., 2003). It is now known that in teleosts, NKA exists in both α and β subunits and is classified as such (Zhang et al., 2019). Among them, the former is responsible for adenosine triphosphatase catalysis and Na^+ and K^+ transport activities, while the latter is mainly responsible for auxiliary α-subunit folding (Sundh et al., 2014). A variety of *NKAα* isoforms are expressed in fish osmoregulatory organs, and their expression levels are positively or negatively correlated with salinity changes, indicating that different NKA isoforms are involved in osmoregulatory processes and have different roles (Yang et al., 2016; Hu et al., 2017).Further studies on the NHE and NKA gene families may provide insights into the potential functions of the remaining members and enhance our understanding of osmoregulation in fish.

A total of 12 NHE genes and 12 NKA genes were identified in *R. canadum*. These genes were found to be distributed randomly on 10 and 9 superscaffolds, respectively, which is consistent with the findings reported by Zhang et al. (2019). The gene sequences of NHE and NKA gene family members were compared with those of *O. mykiss*, *L. japonicus* and *S. maximus* to name them and analyze the conserved motifs and structural domain characteristics (Berthelot et al., 2014; Figueras et al., 2016; Gao et al., 2022). The results revealed that the motifs and domains of the NHE genes were concentrated in the Na^+/H^+ exchanger domains, which the identification of the NKA also showed that they closely association with Cation transporter/ATPase and Hydrolase domains, and the motifs and domains of different members were arranged in different patterns. This indicates that the sequence characteristics of NHE and NKA members are closely related to their taxonomy and functions. In other teleost fishes, *NHE4* is commonly missing and *NHEβ* is only found in teleost fishes (Kasahara et al., 2007; Howe et al., 2013; Tine et al., 2014). In this study, *NHE4* was lost but *NHEβ* was identified by phylogenetic analysis. The results shown that NHE and NKA genes were the closest to teleosts in taxonomic status and the farthest from mammals, indicating that the protein sequences of the two family members were highly conserved in species evolution. The results of qRT-PCR showed that NHE and NKA family members were widely distributed in nine tissues such as heart, liver and spleen, and the expression patterns of NHE multi-copy gene members were different, such as *NHE2a* and *NHE2b* high expression tissues. However, the expression patterns of NKA multi-copy gene members are partially similar, all of which are highly expressed in brain tissue, but *NKAβ1a* and *NKAβ1b* are highly expressed in stomach, muscle and body kidney, respectively. There are significant differences between the two, indicating that multi-copy genes are functionally different.

The expression patterns of NHE and NKA gene families in *R. canadum* differed significantly in different salinities. Significant up-regulation of gill *NHE2c* and *NHE5* expression in *R. canadum* occurred after low-salt acclimation, while no significant changes were found in *NHE2a*, and similar results were found in *L. maculatus*, suggesting that *NHE2c* and *NHE5* may play an important role in the gill tissue of *R. canadum* in low-salt acclimation (Zhang et al., 2019). Studies have reported that *NHE1* expression trends in *S. maximus* gill, intestine and somatic kidney

were negatively correlated with salinity changes and showed low salt adaptation (Zhang et al., 2020). In the present study, significant upregulation of *NHE1* in the intestine and somatic kidney of *R. canadum* was similarly identified during hyposalinity acclimation, suggesting that *NHE1* can be involved in hyposalinity acclimation in *R. canadum* through the intestine and somatic kidney. Meanwhile, the expression of *NHE1* and *NHE2a* increased in gill with decreasing salinity, but the degree of difference was not significant, and a significant down-regulation was observed in high-salt acclimation. It is speculated that the reduced expression of *NHE1* and *NHE2a* in high salt is to reduce the ion transport efficiency of gill epithelial cells and prevent the decrease of osmotic pressure *in vivo*.

Few studies related to *NKAα3a* have been reported, and it has been suggested that its role in osmolarity regulation is relatively weak compared to *NKAα1a* (Nilsen et al., 2007). In the present study, the expression of *NKAα3a* and *NKAβ1b* in the gills of *R. canadum* decreased significantly with increasing salinity. Similar results could be found in *O. mossambicus* (Feng et al., 2002). As multi-copy genes, *NKAα1a* and *NKAα1b* are often compared together. In the present study, *NKAα1b* was found to be significantly downregulated in both high and low salt suits, in contrast to *NKAα1a* expression pattern. *NKAα1b* was similarly found to be strongly affected by salinity in *O. mossambicus* and *Galaxias rostratus*, similar to *NKAα1a*, further suggesting that *NKAα1* isoforms appear to differ in function (Tipsmark et al., 2011; Urbina et al., 2013). In addition, two *NKAα* isoforms (*NKAα1a* and *NKAα3b*) were highly expressed in the gills after high salt domestication in *L. maculatus*, indicating the importance of *NKAα* isoform genes in the salt stress response of fish (Zhang et al., 2019).

5 Conclusion

In the present study,12 NHE genes and 12 NKA genes were systematically identified from *R. canadum* genome. These genes were found to be distributed across 10 and 9 superscaffolds. NHE and NKA members of *R. canadum* are closest in taxonomic position to teleosts and furthest from mammals, indicating that the protein sequences of both family members are highly conserved in species evolution. The histology of the gills, intestine and kidneys exhibited changes associated with salinity adaptation. Different expression patterns of *R. canadum* NHE genes and NKA genes were displayed in multiple tissues. At the same time, transcriptome sequencing and qPCR results showed that there were differences in the expression patterns of NHE and NKA gene families under different salinities, which provided research data for the osmotic pressure regulation mechanism of *R. canadum*.

Data availability statement

The datasets presented in this study can be found in online repositories. The names of the repository/repositories and accession number(s) can be found below: https://www.ncbi.nlm.nih.gov/, SRP202920 https://www.ncbi.nlm.nih.gov/, PRJNA634421.

Ethics statement

The animal study was reviewed and approved by Institutional Animal Care and Use Committee (IACUC), Fisheries College, Guangdong Ocean University.

Author contributions

ZW, ZC, and BH contributed to conception and design of the study. ZW organized the database. BH performed the statistical analysis. ZC wrote the first draft of the manuscript. ZY, MZ, MJ, and AZ wrote sections of the manuscript. All authors contributed to manuscript revision, read, and approved the submitted version.

Funding

Guangdong University Innovation Team Project (2021KCXTD026, 2022KCXTD013).

Acknowledgments

We are grateful to Guangzhou Genedenovo Biotechnology Co., Ltd for assisting in sequencing and bioinformatics analysis.

Conflict of interest

The authors declare that the research was conducted in the absence of any commercial or financial relationships that could be construed as a potential conflict of interest.

Publisher's note

Supplementary material

The Supplementary Material for this article can be found online at: https://www.frontiersin.org/articles/10.3389/fmars.2023.1228933/full#supplementary-material

References

Ali, A., Azom, M. G., Sarker, B. S., Rani, H., Alam, M. S., and Islam, M. S. (2022). Repercussion of salinity on hematological parameters and tissue morphology of gill and kidney at early life of tilapia. *Aquaculture Fisheries*. doi: 10.1016/j.aaf.2022.04.006

Bailey, T. L., Johnson, J., Grant, C. E., and Noble, W. S. (2015). The MEME suite. *Nucleic Acids Res.* 43, W39–W49. doi: 10.1093/nar/gkv416

Benetti, D. D., Suarez, J., Camperio, J., Hoenig, R. H., Tudela, C. E., Daugherty, Z., et al. (2021). A review on cobia, *Rachycentron canadum*, aquaculture. *J. World Aquaculture Soc.* 52, 691–709. doi: 10.1111/jwas.12810

Berthelot, C., Brunet, F., Chalopin, D., Juanchich, A., Bernard, M., Noël, B., et al. (2014). The rainbow trout genome provides novel insights into evolution after whole-genome duplication in vertebrates. *Nat. Commun.* 5, 3657. doi: 10.1038/ncomms4657

Bystriansky, J. S., Frick, N. T., Richards, J. G., Schulte, P. M., and Ballantyne, J. S. (2007). Failure to up-regulate gill Na+, K+-ATPase α-subunit isoform α1b may limit seawater tolerance of land-locked Arctic char (*Salvelinus alpinus*). *Comp. Biochem. Physiol. Part A: Mol. Integr. Physiol.* 148, 332–338. doi: 10.1016/j.cbpa.2007.05.007

Cao, D. Y., Li, J. F., Huang, B. S., Zhang, J. D., Pan, C. H., Huang, J. S., et al. (2020). RNA-seq analysis reveals divergent adaptive response to hyper- and hypo-salinity in cobia, *Rachycentron canadum*. *Fish Physiol. Biochem.* 46, 1713–1727. doi: 10.1007/s10695-020-00823-7

Chen, G., Wang, Z. L., Wu, Z. H., and Gu, B. H. (2009). Effects of salinity on growth and energy budget of juvenile cobia, r*achycentron canadum*. *J. World Aquaculture Soc.* 40, 374–382. doi: 10.1111/j.1749-7345.2009.00257.x

Chen, S., Zhou, Y., Chen, Y., and Gu, J. (2018). fastp: an ultra-fast all-in-one FASTQ preprocessor. *Bioinformatics* 34, i884–i890. doi: 10.1093/bioinformatics/bty560

Counillon, L., and Pouysségur, J. (2000). The expanding family of eucaryotic Na^+/H^+ exchangers. *J. Biol. Chem.* 275, 1–4. doi: 10.1074/jbc.275.1.1

Dawood, M. A.O., Noreldin, A. E., and Sewilam, H. (2021). Long term salinity disrupts the hepatic function, intestinal health, and gills antioxidative status in Nile tilapia stressed with hypoxia. *Ecotox Environ. Safe* 220, 112412. doi: 10.1016/j.ecoenv.2021.112412

Edwards, S. L., Wall, B. P., Morrison-Shetlar, A., Sligh, S., Weakley, J. C., and Claiborne, J. B. (2005). The effect of environmental hypercapnia and salinity on the expression of NHE-like isoforms in the gills of a euryhaline fish (*Fundulus heteroclitus*). *J. Exp. Zoology Part A: Comp. Exp. Biol.* 303, 464–475. doi: 10.1002/jez.a.175

Feng, S. H., Leu, J. H., Yang, C. H., Fang, M. J., Huang, C. J., and Hwang, P. P. (2002). Gene expression of na^+-k^+-atpase a1 and a3 subunits in gills of the teleost *Oreochromis mossambicus*, adapted to different environmental salinities. *Mar. Biotechnol.* 4, 379–391. doi: 10.1007/s10126-002-0006-0

Figueras, A., Robledo, D., Corvelo, A., Hermida, M., Pereiro, P., Rubiolo, J. A., et al. (2016). Whole genome sequencing of turbot (*Scophthalmus maximus*; Pleuronectiformes): a fish adapted to demersal life. *DNA Res.* 23, 181–192. doi: 10.1093/dnares/dsw007

Fiol, D. F., and Kültz, D. (2007). Osmotic stress sensing and signaling in fishes. *FEBS J.* 274, 5790–5798. doi: 10.1111/j.1742-4658.2007.06099.x

Foskett, J. K., Bern, H. A., Machen, T. E., and Conner, M. (1983). Chloride cells and the hormonal control of teleost fish osmoregulation. *J. Exp. Biol.* 106, 255–281. doi: 10.1242/jeb.106.1.255

Gao, J., Nie, Z. J., Xu, G. C., and Xu, P. (2022). Genome-wide identification of the NHE gene family in Coilia nasus and its response to salinity challenge and ammonia stress. *BMC Genomics* 23, 1–14. doi: 10.1186/s12864-022-08761-9

Gonzalez, R. J. (2012). The physiology of hyper-salinity tolerance in teleost fish: a review. *J. Comp. Physiol. B* 182, 321–329. doi: 10.1007/s00360-011-0624-9

Han, K., Zhou, L., Zeng, X., Zhang, Z., Zou, P., Huang, W., et al. (2022). Effects of low-salinity acclimation on the Na+/K+ ATPase activity and expression of osmoregulatory-related genes in large yellow croaker (*Larimichthys crocea*). *Aquaculture Rep.* 26, 101326. doi: 10.1016/j.aqrep.2022.101326

Holmes, B. J., Williams, S. M., Barnett, A., Awruch, C. A., Currey-Randall, L. M., Ferreira, L. C., et al. (2022). "Research methods for marine and estuarine fishes," in *Wildlife Research in Australia: Practical and Applied Methods* (Australia: Csiro Publishing), 257–286.

Hou, J. L., Chen, L. Q., Zhuang, P., Zhang, L. Z., Tian, H. J., Wang, W., et al. (2006). Structural changes of chloride cells in gills epithelia of juvenile *Acipenser schrenckii* acclimated to various salinities. *J. Fisheries China* 30, 316–322. doi: 10.1360/aps050066

Howe, K., Clark, M. D., Torroja, C. F., Torrance, J., Berthelot, C., Muffato, M., et al. (2013). The zebrafish reference genome sequence and its relationship to the human genome. *Nature* 496, 498–503. doi: 10.1038/nature12111

Hu, Y. C., Chu, K. F., Yang, W. K., and Lee, T. H. (2017). Na^+, K^+-ATPase β1 subunit associates with α1 subunit modulating a "higher-NKA-in-hyposmotic media" response in gills of euryhaline milkfish, Chanos chanos. *J. Comp. Physiol. B* 187, 995–1007. doi: 10.1007/s00360-017-1066-9

Hu, J., Ye, L., Wu, K. C., and Wang, Y. (2016). Effect of acute salinity stress on serum cortisol and activity of Na^+-K^+-ATPase of juvinile *Amphiprion clarkii*. *South. Aquat. Sci. China* 12, 116–120. doi: 10.3969/j.issn.2095-0780.2016.02.017

Huang, S., Li, C. Z., Li, Z. X., Duanzhi, D., Liu, Y. H., Ran, F. X., et al. (2022). Short-term exposure to 5‰ and 15‰ salinity causes the dynamic changes of the NKA gene, enzyme activities and morphological characteristics in fish tissues of *Gymnocypris przewalskii*. *Aquac Res.* 53, 6389–6398. doi: 10.1111/are.16112

Hwang, J., Kim, S., Seo, Y., Lee, K., Park, C., Choi, Y., et al. (2018). Mechanisms of salinity control in sea bass. *Biotechnol. Bioproc E* 23, 271–277. doi: 10.1007/s12257-018-0049-3

Imsland, A. K., Gunnarsson, S., Foss, A., and Stefansson, S. O. (2003). Gill Na^+, K^+-ATPase activity, plasma chloride and osmolality in juvenile turbot (*Scophthalmus maximus*) reared at different temperatures and salinities. *Aquaculture* 218, 671–683. doi: 10.1016/S0044-8486(02)00423-4

Inokuchi, M., Nakamura, M., Miyanishi, H., Hiroi, J., and Kaneko, T. (2017). Functional classification of gill ionocytes and spatiotemporal changes in their distribution after transfer from seawater to fresh water in Japanese seabass. *J. Exp. Biol.* 220, 4720–4732. doi: 10.1242/jeb.167320

Jia, Q., and Lu, W. (2016). Effects of low salinity stress on plasma osmolality, Cortisol, prolactin and growth hormone of Japanese flounder, *Paralichthys olivaceus*. *J. Shanghai Ocean Univ.* 25, 71–77.

Jiang, Y. H., Yuan, C., Qi, M., Liu, Q. G., and Hu, Z. J. (2022). The effect of salinity stress on enzyme activities, histology, and transcriptome of silver carp (*Hypophthalmichthys molitrix*). *Biology* 11, 1580. doi: 10.3390/biology11111580

Kasahara, M., Naruse, K., Sasaki, S., Nakatani, Y., Qu, W., Ahsan, B., et al. (2007). The medaka draft genome and insights into vertebrate genome evolution. *Nature* 447, 714–719. doi: 10.1038/nature05846

Kibenge, F. S., and Strange, R. J. (2021). "Introduction to the anatomy and physiology of the major aquatic animal species in aquaculture," in *Aquaculture Pharmacology* (Netherlands: Elsevier), 1–111.

Kim, D., Langmead, B., and Salzberg, S. L. (2015). HISAT: a fast spliced aligner with low memory requirements. *Nat. Methods* 12, 357–360. doi: 10.1038/nmeth.3317

Kumar, S., Stecher, G., and Tamura, K. (2016). MEGA7: molecular evolutionary genetics analysis version 7.0 for bigger datasets. *Mol. Biol. Evol.* 33, 1870–1874. doi: 10.1093/molbev/msw054

Larsen, P. F., Nielsen, E. E., Meier, K., Olsvik, P. A., Hansen, M. M., and Loeschcke, V. (2012). Differences in salinity tolerance and gene expression between two populations of Atlantic cod (*Gadus morhua*) in response to salinity stress. *Biochem. Genet.* 50, 454–466. doi: 10.1007/s10528-011-9490-0

Li, B., and Dewey, C. N. (2011). RSEM: accurate transcript quantification from RNA-Seq data with or without a reference genome. *BMC Bioinf.* 12, 1–16. doi: 10.1186/1471-2105-12-323

Li, L., Jiang, M., Wang, Y., Wu, Q., Niu, J., and Shen, X. (2014). Effects of low salinity stress on Na+-K+-ATPase activities, expression of Na+-K+-ATPase β-subunit mRNA and microscopical structure in gill filaments of juvenile Mugil cephalus. *J. Zhejiang Univ. (Agriculture Life Sciences)* 40, 223–230. doi: 10.3785/j.issn.1008-9209.2013.09.031

Li, X. J., Shen, Y. D., Bao, Y. G., Wu, Z. X., Yang, B. Q., Jiao, L. F., et al. (2022). Physiological responses and adaptive strategies to acute low-salinity environmental stress of the euryhaline marine fish black seabream (*Acanthopagrus schlegelii*). *Aquat. Toxicol.* 554, 738117. doi: 10.1016/j.aquaculture.2022.738117

Li, H. Y., Zhu, J. Q., Chen, F., and Ding, L. F. (2011). Themorphology of the digestive tract of *Centropristis striata*. *J. Biol. China* 28, 31–34+46. doi: 10.3969/j.issn.2095-1736.2011.04.031

Lin, Y. M., Chen, C. N., and Lee, T. H. (2003). The expression of gill Na, K-ATPase in milkfish, *Chanos chanos*, acclimated to seawater, brackish water and fresh water. *Comp. Biochem. Physiol. Part A: Mol. Integr. Physiol.* 135, 489–497. doi: 10.1016/S1095-6433(03)00136-3

Lin, Y. M., Chen, C. N., Yoshinaga, T., Tsai, S. C., Shen, I. D., and Lee, T. H. (2006). Short-term effects of hyposmotic shock on Na^+/K^+-ATPase expression in gills of the euryhaline milkfish, *Chanos chanos*. *Comp. Biochem. Physiol. Part A: Mol. Integr. Physiol.* 143, 406–415. doi: 10.1016/j.cbpa.2005.12.031

Marshall, W. S. (2011). Mechanosensitive signalling in fish gill and other ion transporting epithelia. *Acta Physiologica* 202, 487–499. doi: 10.1111/j.1748-1716.2010.02189.x

Nilsen, T. O., Ebbesson, L. O., Madsen, S. S., McCormick, S. D., Andersson, E., Björnsson, B. T., et al. (2007). Differential expression of gill Na^+, K^+-ATPaseα-and β-subunits, Na^+, K^+, $2Cl^-$cotransporter and CFTR anion channel in juvenile anadromous and landlocked Atlantic salmon *Salmo salar*. *J. Exp. Biol.* 210, 2885–2896. doi: 10.1242/jeb.002873

Orlowski, J., and Grinstein, S. (2004). Diversity of the mammalian sodium/proton exchanger SLC9 gene family. *Pflügers Archiv* 447, 549–565. doi: 10.1007/s00424-003-1110-3

Pertea, M., Pertea, G. M., Antonescu, C. M., Chang, T.-C., Mendell, J. T., and Salzberg, S. L. (2015). StringTie enables improved reconstruction of a transcriptome from RNA-seq reads. *Nat. Biotechnol.* 33, 290–295. doi: 10.1038/nbt.3122

Robinson, M. D., McCarthy, D. J., and Smyth, G. K. (2010). edgeR: a Bioconductor package for differential expression analysis of digital gene expression data. *bioinformatics* 26, 139–140. doi: 10.1093/bioinformatics/btp616

Sakamoto, T., Uchida, K., and Yokota, S. (2001). Regulation of the ion-transporting mitochondrion-rich cell during adaptation of teleost fishes to different salinities. *Zoological Sci.* 18, 1163–1174. doi: 10.2108/zsj.18.1163

Shaffer, R. V., and Nakamura, E. L. (1989). *Synopsis of biological data on the cobia Rachycentron canadum (Pisces: Rachycentridae)*. USA: NOAA/National Marine Fisheries Service. Available at: http://hdl.handle.net/1834/20527.

Shi, Z. H., Liao, Y. L., Wang, X. S., Zhang, C. J., Peng, S. M., and Gao, Q. X. (2017). Impact of the abrupt salinity decrease on ion-regulation enzyme activity in the gill and serum osmolality from *Epinehelus moara*. *J. Saf. Environ. China* 17, 1210–1214. doi: 10.13637/j.issn.1009-6094.2017.03.074

Smith, H. W. (1932). Water regulation and its evolution in the fishes. *Q. Rev. Biol.* 7, 1–26. doi: 10.1086/394393

Smith, J. W. (1995). Life history of cobia, Rachycentron canadum (Osteichthyes: Rachycentridae), in North Carolina waters. *Brimleyana* 23, 1–23.

Sun, M. L., Jiang, J. L., Wang, L. P., Chen, F., Han, Y. Z., Jiang, Z. Q., et al. (2016). Structural Changes in Gill, Kidney and Intestine of Juvenile *Takifugu rubripes* under Low Salinity Treatment. *J. Guangdong Ocean Univ. China* 36, 38–43. doi: 10.3969/j.issn.1673-9159.2016.06.007

Sundh, H., Nilsen, T. O., Lindström, J., Hasselberg-Frank, L., Stefansson, S. O., McCormick, S. D., et al. (2014). Development of intestinal ion-transporting mechanisms during smoltification and seawater acclimation in Atlantic salmon *Salmo salar*. *J. Fish Biol.* 85, 1227–1252. doi: 10.1111/jfb.12531

Tine, M., Kuhl, H., Gagnaire, P.-A., Louro, B., Desmarais, E., Martins, R. S., et al. (2014). European sea bass genome and its variation provide insights into adaptation to euryhalinity and speciation. *Nat. Commun.* 5, 5770. doi: 10.1038/ncomms6770

Tipsmark, C. K., Breves, J. P., Seale, A. P., Lerner, D. T., Hirano, T., and Grau, E. G. (2011). Switching of Na^+, K^+-ATPase isoforms by salinity and prolactin in the gill of a cichlid fish. *J. Endocrinol.* 209, 237. doi: 10.1530/JOE-10-0495

Upling, J. Y. (2020). A review on the activity of Na^+/K^+-ATPase in branchial ionocytes and its role in salinity adaptation among diadromous species. *World J. Advanced Res. Rev.* 6, 201–211. doi: 10.30574/wjarr.2020.6.2.0158

Urbina, M. A., Schulte, P. M., Bystriansky, J. S., and Glover, C. N. (2013). Differential expression of Na^+, K^+-ATPase α-1 isoforms during seawater acclimation in the amphidromous galaxiid fish *Galaxias maculatus*. *J. Comp. Physiol. B* 183, 345–357. doi: 10.1007/s00360-012-0719-y

Wang, Y., and Hu, X. C. (2009). Microscopical observation on the gill structure of juvenile *Lateolabrax japonicus* under different salinities. *Mar. Sci.* 33, 138–142. doi: 10.1016/j.elecom.2008.10.019

Wang, S. J., Zhang, H. F., Zhao, J., Yang, Y. Q., and Yang, S. S. (2011). Effects of different salinities on growth and physiology of orange-spotted grouper, *epinephelus coioides*. *J. Guangdong Ocean Univ. China* 31, 39–44. doi: 10.3969/j.issn.1673-9159.2011.06.006

Whittamore, J. M. (2012). Osmoregulation and epithelial water transport: lessons from the intestine of marine teleost fish. *J. Comp. Physiol. B* 182, 1–39. doi: 10.1007/s00360-011-0601-3

Yamaguchi, Y., Breves, J. P., Haws, M. C., Lerner, D. T., Grau, E. G., and Seale, A. P. (2018). Acute salinity tolerance and the control of two prolactins and their receptors in the Nile tilapia (*Oreochromis niloticus*) and Mozambique tilapia (*O. mossambicus*): a comparative study. *Gen. Comp. Endocrinol.* 257, 168–176. doi: 10.1016/j.ygcen.2017.06.018

Yan, J. J., Chou, M. Y., Kaneko, T., and Hwang, P. P. (2007). Gene expression of Na^+/H^+ exchanger in zebrafish H^+-ATPase-rich cells during acclimation to low-Na^+ and acidic environments. *Am. J. Physiology-Cell Physiol.* 293, C1814–C1823. doi: 10.1152/ajpcell.00358.2007

Yang, W. K., Chung, C. H., Cheng, H. C., Tang, C. H., and Lee, T. H. (2016). Different expression patterns of renal Na^+/K^+-ATPase α-isoform-like proteins between tilapia and milkfish following salinity challenges. *Comp. Biochem. Physiol. Part B: Biochem. Mol. Biol.* 202, 23–30. doi: 10.1016/j.cbpb.2016.07.008

Yang, J., Xu, W., Geng, L. W., Guan, H. H., Dang, Y. F., and Jiang, H. F. (2014). Effects of salinity on survival,gill and kidney tissue in juveniles of 5 species. *Freshw. Fisheries China* 44, 7–12. doi: 10.13721/j.cnki.dsyy.2014.04.002

Yang, J. R., Yang, J. L., Chen, M. Q., Fu, Z., Sun, J., Yu, G., et al. (2022). Physical responses of Pinctada fucata to salinity stress. *Front. Mar. Sci.* 8. doi: 10.3389/fmars.2021.792179

Yu, N., Li, J., Ou, Y. J., Wang, Y. C., and Su, H. (2012). Structural changes in gill and kidney of juvenile grey mullet under different salinity. *Ecol. Sci. China* 31, 424–428.

Zhang, J. S., Liu, Z. F., Ma, A. J., Cui, W. X., and Qu, J. B. (2020). Response of aquaporin (AQP1, AQP3) and ion channel protein (CFTR, NHE1) of turbot (*Scophthalmus maximus*) to low-salinity stress. *Prog. IN FISHERY Sci. OF China* 41, 41–49. doi: 10.19663/j.issn2095-9869.20190410003

Zhang, X. Y., Wen, H. S., Qi, X., Zhang, K. Q., Liu, Y., Fan, H. Y., et al. (2019). Na+-K+-ATPase and nka genes in spotted sea bass (*Lateolabrax maculatus*) and their involvement in salinity adaptation. *Comp. Biochem. Physiol. Part A: Mol. Integr. Physiol.* 235, 69–81. doi: 10.1016/j.cbpa.2019.05.017

Zhang, X. Y., Wen, H. S., Wang, H. L., Ren, Y. Y., Zhao, J., and Li, Y. (2017). RNA-Seq analysis of salinity stress–responsive transcriptome in the liver of spotted sea bass (*Lateolabrax maculatus*). *PloS One* 12, e0173238. doi: 10.1371/journal.pone.0173238

Zhang, X. Y., Wen, H. S., Zhang, K. Q., Liu, Y., Fang, X., and Li, Y. (2018). Analysis of the isotonic point and effects of seawater desalination on the Na^+/K^+ /Cl concentration, Na^+-K^+ -ATPase activity and relative gene expressions in *Lateolabrax maculatus*. *J. Fisheries China* 42, 1199–1208. doi: 10.11964/jfc.20170410780

Zhou, Q. C., Wu, Z. H., Tan, B. P., Chi, S. Y., and Yang, Q. H. (2006). Optimal dietary methionine requirement for juvenile cobia (*Rachycentron canadum*). *Aquaculture* 258, 551–557. doi: 10.1016/j.aquaculture.2006.03.035

frontiers | Frontiers in Physiology

TYPE Original Research
PUBLISHED 04 August 2023
DOI 10.3389/fphys.2023.1256005

OPEN ACCESS

EDITED BY
Yiming Li,
Fishery Machinery and Instrument Research Institute, China

REVIEWED BY
Jinran Wu,
Australian Catholic University, Australia
Zhenlu Wang,
Guizhou University, China

*CORRESPONDENCE
Junjie Zhu,
Zhjj@zjhu.edu.cn

RECEIVED 10 July 2023
ACCEPTED 20 July 2023
PUBLISHED 04 August 2023

CITATION
Zhang C, Wang F, Wang Q, Zou J and Zhu J (2023), Species-specific effects of microplastics on juvenile fishes.
Front. Physiol. 14:1256005.
doi: 10.3389/fphys.2023.1256005

Species-specific effects of microplastics on juvenile fishes

Chaonan Zhang[1,2,3], Fei Wang[2], Qiujie Wang[3], Jixing Zou[3] and Junjie Zhu[2]*

[1]Department of Environmental Science, Zhejiang University, Hangzhou, China, [2]National-Local Joint Engineering Laboratory of Aquatic Animal Genetic Breeding and Nutrition, Zhejiang Provincial Key Laboratory of Aquatic Resources Conservation and Development, College of Life Science, Huzhou University, Huzhou, China, [3]Joint Laboratory of Guangdong Province and Hong Kong Region on Marine Bioresource Conservation and Exploitation, College of Marine Sciences, South China Agricultural University, Guangzhou, China

Microplastics contamination have been extensively reported in aquatic ecosystem and organisms. It is wildly acknowledged that the ingestion, accumulation and elimination of microplastics in fishes are species-specific, which mainly depending on the feeding behavior. This study aimed to investigate the effects of microplastics on the morphology and inflammatory response in intestines of fishes with different feeding types. Largemouth bass (carnivorous fish), grass carp (herbivorous fish) and Jian carp (omnivorous fish) were used as organism model. The contributing concentration and size of microplastics were explored as well as the response time and legacy effect in fishes. Two different sizes of polystyrene microplastics (80 nm and 8 μm) were set at three concentrations. And samples were analyzed at different exposure times and depuration times. Histological analysis indicated that multiple abnormalities in intestines were presented in three species fishes after acute exposure microplastics. The mRNA abundance of immune-related genes in the intestine tissues of fishes were significantly fluctuant. There were differential expressions of genes coping with differential sizes and concentrations of microplastics exposure in different fishes. The reason for the difference effects of microplastics on fishes was still unclear but could be due to the difference in the structure and function of the digestive system. These results provided a theoretical basis to further analysis of the mechanism of fish intestinal pathology caused by microplastics.

KEYWORDS

microplastics, species-specific, juvenile fish, gene expression, intestinal morphology

1 Introduction

Plastics have been remarkable materials in peoples' daily life due to its versatile, durable, and incredibly adaptable. Plastics production reached 390 million tonnes in 2021 worldwide with approximately 9% increasing rate every year and China contributed to 32% of world's plastics production (Plastics Europe, 2022). In the meanwhile, the global total of plastic waste reached 380 Tg in 2018 with an exponential growth every year (Rai et al., 2021). Once entering the environment, plastic would degrade or fragment into microplastics through UV radiation, mechanical transformation or biological degradation by microorganisms (Cole et al., 2011; Alimi et al., 2018). Microplastics are defined as small plastic pieces or fibers smaller than 5 mm (NOAA, 2015). They come in many forms, not only secondary sources, but also primary sources, such as microbeads in personal care products (McDevitt et al., 2017). Microplastics contamination have been extensively reported in marine, freshwater

and terrestrial ecosystems (Wang et al., 2020a; Peng et al., 2020; Xu et al., 2020), thus identified as one of the top 10 emerging global environmental problems by the United Nations Environment Program.

Adverse effects of microplastics on fishes have been found in many literatures (Jacob et al., 2020; Anna et al., 2021; Mallik et al., 2021). Due to the attractive color, buoyancy, and food-like properties, fish are particularly prone to ingesting microplastics (Garrido Gamarro et al., 2020). The ingestion of microplastics by fish can cause a variety of consequences: 1) microplastics can lead to physical damage and histopathological alterations (Peda et al., 2016; Jabeen et al., 2018; Ahrendt et al., 2020); 2) microplastics can cause impairments in oxidative, and disorders of inflammatory balance and intestinal microflora (Gu et al., 2020; Huang et al., 2020; Iheanacho and Odo, 2020); 3) microplastics can also lead to fish behavior changes (Brun et al., 2019; Guimarães et al., 2021; Rios-Fuster et al., 2021; Shi et al., 2021); 4) microplastics can act as carriers to intensify further adverse effects of other pollutants on fish (Banaee et al., 2019; Zhang et al., 2019; Li et al., 2023a).

It is wildly acknowledged that the ingestion, accumulation and elimination of microplastics in fishes are species-specific (Mizraji et al., 2017; Xu and Li, 2021). The field investigation found microplastic amounts in filter-feeding and omnivorous fish were higher than that of carnivorous species (Wang et al., 2020b). The laboratory experiment proved that microplastics ingestion in fish larvae was influenced by feeding type of fish, and omnivores fish were less able to eliminate microplastics than filter-feeding fish (Zhang et al., 2021). However, the physiological effects of micro-nano plastics on juvenile fish with different feeding habits have not been reported.

In this study, species-specific effects of microplastics on three commercial fish species with different feeding types were investigated. Largemouth bass, *Micropterus salmoides* is a typical freshwater carnivorous fish species and widely farmed in China due to its strong adaptability, fast growth, delicious taste, and high economic value (Wang et al., 2020c). Grass carp (*Ctenopharyngodon idella*), a herbivorous fish species, is one of the most important freshwater cultivars in China, which annual production exceeded 5.53 million tons in 2019 (China Fishery Statistical Yearbook, 2020). Jian carp (*Cyprinus carpio* var. Jian) is an omnivorous freshwater fish species with an annual production of 24.2 million tons worldwide (Lin et al., 2019; Li et al., 2023b). This study aimed to reveal the effects of microplastics on the morphology and inflammatory response in intestines of fishes with different feeding types. To achieve this goal, histopathological sections were examined, and immune-related genes profiles were used to study the changes in the intestinal tissue of three fishes after microplastics exposure. These results would provide a theoretical basis to further analysis of the mechanism of fish intestinal pathology caused by microplastics.

2 Material and method

2.1 Materials

Polystyrene microplastics with diameters of 80 nm and 8 μm were purchased from Dae Technology Company (Tianjin, China). Largemouth bass, grass carp and Jian carp were bought from a livestock farm in Shunde City (Guangdong, China). Largemouth bass was (5.23 ± 0.62) cm in length and (2.97 ± 0.64) g in weight. Grass carp was (5.81 ± 0.50) cm in length and (3.82 ± 0.91) g in weight. Jian carp was (3.46 ± 0.16) cm in length and (0.93 ± 0.19) g in weight. Fish were acclimatized at 25.2 ± 1.5 °C in culture water (pH 7.1 ± 0.4; dissolved oxygen 6.4 ± 0.5 mg/L) with a 12 h light/dark cycle. Before the experiment, fish were acclimated in 100 L glass tanks for 5 d and were fed with 5.0% body weight fodder (Haid Group, Guangdong, China) twice daily.

2.2 Experimental design

Two different sizes of fluorescent microplastics (80 nm and 8 μm) were set at four concentrations for grass carp and Jian carp: 0, 0.02 mg/L, 0.2 mg/L and 2 mg/L. Based on the previous findings (Zhang et al., 2021), carnivorous fish seemed to be more tolerant to microplastics than other fishes. So, the higher microplastics exposure concentrations (0.05 mg/L, 0.5 mg/L and 5 mg/L) for largemouth bass were set. The concentrations of exposure for MPs were selected based on the other studies (Ding et al., 2018; Li et al., 2020; Zhang et al., 2021). The microplastics with nanometer particle size (80 nm) and micron particle size (8 μm) were compared.

In the exposure experiment, tanks (20 cm × 15 cm × 15 cm) were filled with 2 L of culture water and eight fish. A total of twenty-four tanks were set for each fish species, including control group and replicate group. Each species of fish was tested separately. Three replicate tanks were used for 24 h and 48 h sampling times. After 48 h exposure, the surviving fish were moved to an aquarium with clean water containing no microplastics for 48 h. No feeding was done during exposure and depuration. At 24 and 48 h after exposure and clearance, two fish were dissected from each tank and the intestines were removed for subsequent analysis. This study was carried out in strict accordance with the recommendations in the Guide for the Care and Use of Laboratory Animals of the National Institutes of Health. All surgery was performed under anesthesia, and all efforts were made to minimize suffering.

2.3 Histopathological analysis

A total of 24 fish from the control and experimental groups were anesthetized on ice and intestines were dissected. Intestinal tissue fixed in general-purpose tissue fixator (Servicebio, Wuhan, China), embedded in paraffin wax, sectioned at 4 μm thickness, and stained with hematoxylin-eosin (H&E). Tissue slices were examined and photographed by a microscopy (Nikon, Tokyo, Japan) with the Mshot Image Analysis System.

2.4 RNA extraction and cDNA synthesis

The experimental methods of RNA extraction and cDNA synthesis are presented in Supplementary Text S1. The cDNA was stored at −80°C until further analysis.

10.3389/fphys.2023.1256005

TABLE 1 List of gene primers used for qPCR.

Fish	Genes	Sequence, forward/reverse (5′–3′)
Largemouth bass	β-*actin*	F: ATCGCCGCACTGGTTGTTGAC
		R: CCTGTTGGCTTTGGGGTTC
	IL-8	F: GAGCCATTTTTCCTGGTGACT
		R: TCCTCATTGGTGCTGAAAGATC
	Caspase 3	F: GCTTCATTCGTCTGTGTTC
		R: CGAAAAAGTGATGTGAGGTA
Grass carp	β-*actin*	F: GGCTGTGCTGTCCCTGTA
		R: TTATTGTGGTTACGCTGGA
	*IL-1*β	F: AGAGTTTGGTGAAGAAGAGG
		R: TTATTGTGGTTACGCTGGA
	IL-8	F: ATGAGTCTTAGAGGTCTGGGT
		R: ACAGTGAGGGCTAGGAGGG
	*TGF-*β*1*	F: TTGGGACTTGTGCTCTAT
		R: AGTTCTGCTGGGATGTTT
	*TNF-*α	F: CGCTGCTGTCTGCTTCAC
		R: CCTGGTCCTGGTTCACTC
Jian carp	*18S*	F: CTGAGAAACGGCTACCATTC
		R: GCCTCGAAAGAGACCTGTATTG
	*IL-1*β	F: GAGTGAACTGCACCAAACAAC
		R: GTCGGCACTGTCAGAGTAAAT
	IL-10	F: CTCCGTTCTGCATACAGAGAAA
		R: TCATGACGTGACAGCCATAAG
	*TGF-*β	F: ACGTTTCCAGATGGTTCAGAG
		R: GCCACTTTCTTTGTTTGGGAATA
	TLR-2	F: GTGCTCCTGTGAGTTTGTATCT
		R: TGGAGTGTCGCACACATAATAG

2.5 Immune and enzyme-related gene expression

The SYBR green real-time PCR assay was performed on the CFX Connect TM Real-Time System (BIO-RAD, Hercules, CA, USA) using the SYBR® Green Premix Pro Taq HS qPCR kit (Accurate Biotechnology Co., Ltd., Hunan, China) following the manufacturer's approach. Specific primer sequences are listed in Table 1. Details of the PCR program are presented in Supplementary Text S2. Expression levels of target genes were normalized to the internal reference, and the data were calculated as the fold change in comparison to the control group.

2.6 Statistical analysis

All data were quantified as the mean ± standard error (S.E) and performed by one-way ANOVA using SPSS 17.0 and Excel 2016. Statistical significance between the control and the experimental groups was conducted by the Duncan's multiple range test. A value of $p < 0.05$ was set with statistical significance.

3 Results

3.1 Intestinal morphology

After HE staining, intestinal histomorphology of three fishes were examined using a light microscope. Histopathological sections showed that the intestinal folds of largemouth bass juvenile were in disorder and shortened, infiltrated cells, especially when fish were exposure in higher concentration microplastics of micron scale (Figure 1). In the intestine of grass carp juvenile, there was no difference between the control and the treatments for vacuolization, goblet cell hyperplasia or villus shortening (Supplementary Figure S1). After combing all the scored histopathology features together, there was no significant difference in the intestinal muscular thickness and intestinal villi length between the groups ($p > 0.05$) (Supplementary Figure S2). Juvenile Jian carp showed multiple abnormal intestines after microplastics exposure (Supplementary Figure S3). The intestinal folds in the experimental group were not full or regular. However, no significant difference was found in the muscle thickness or villi length in Jian carp either ($p > 0.05$). Histopathological data of Jian carp are listed in Supplementary Table S1.

3.2 Transcriptional responses of target genes

After 8 μm microplastics exposure 48 h, the expression levels of the immune-related gene (*IL-8*) were significantly upregulated in the intestines of largemouth bass juvenile ($p < 0.05$) (Figure 2C). 80 nm microplastics caused upregulation of *IL-8* in 48 h depuration after exposure 48 h (Figure 2A). Whereas the situation of high concentration exposure was different with mid and low concentration exposure (Figures 2A, C). Expression of *Caspase 3* gene in the intestines of fish exposed 80 nm microplastics 48 h and cleaned 8 μm microplastics 48 h were significantly lower than that in the intestines of fish in the control group ($p < 0.01$) (Figures 2B, D).

The effects of microplastics on the expression of levels of immune-related genes in intestine tissues of grass carp are shown in Figure 3. The relative expression levels of *IL-1β*, *IL-8*, *TGF-β1* and *TNF-α* were all observably upregulated ($p < 0.01$) when exposure 80 nm microplastics at low concentration (20 μg/L) in the start of 24 h. *TGF-β1* and *TNF-α* expression level when exposure 80 nm microplastics 24 h at middle and high concentration (200 μg/L and 2000 μg/L) were significantly upregulated, rather than *IL-1β* and *IL-8* expression level. However, there was different gene expression pattern when exposure 8 μm microplastics.

The mRNA expression levels of *IL-1β*, *IL-10*, *TGF-β* and *TLR-2* in intestines of Jian carp juvenile exposed to microplastics of 80 nm and 8 μm are shown in Figure 4. The upregulation of pro-inflammatory cytokines, such as *IL-1β* and *TLR-2*, or/and downregulation of anti-inflammatory cytokines including *TGF-β1* and *IL-10* could cause inflammation in fish. Noteworthily, Jian carp

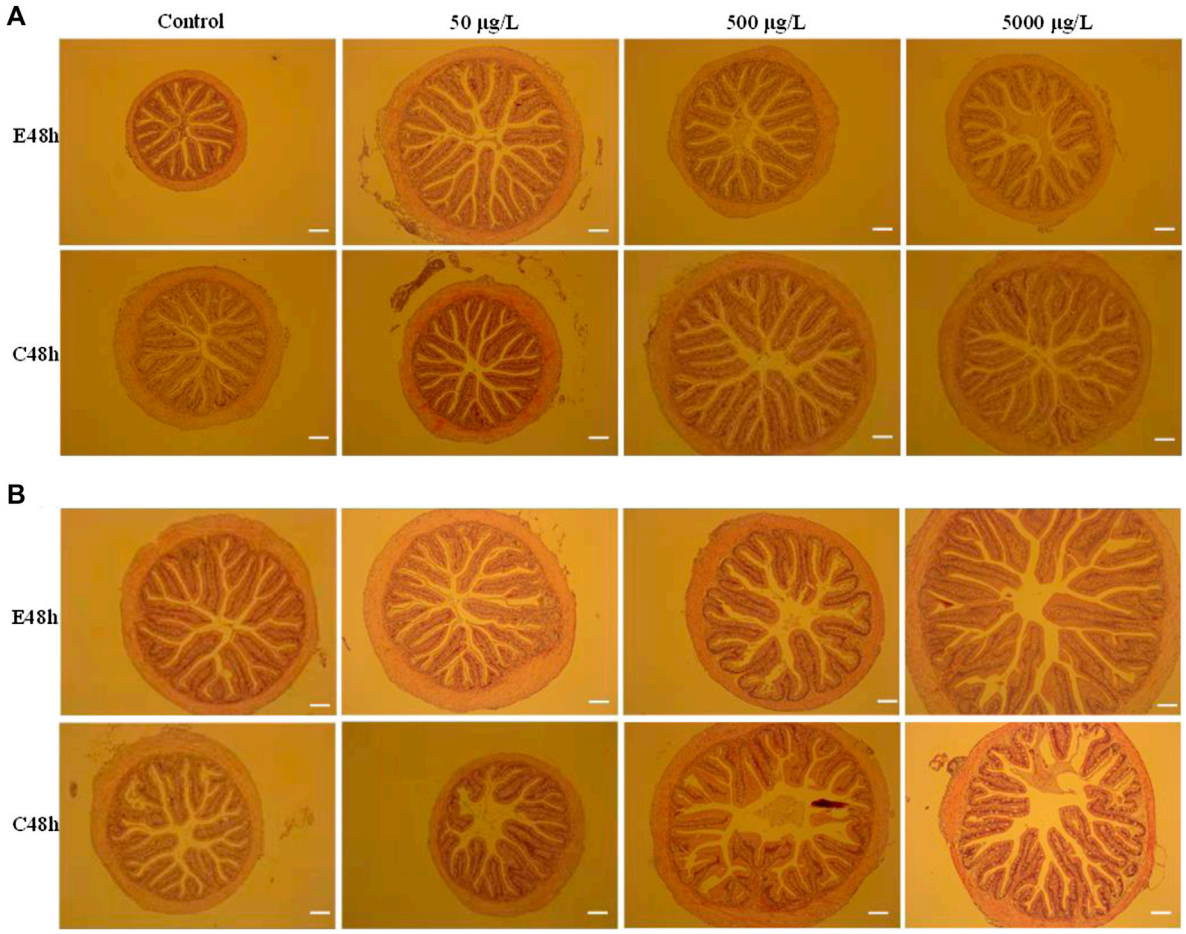

FIGURE 1
Histopathological analysis of intestines of largemouth bass juvenile exposed to polystyrene microspheres of 80 nm **(A)** and 8 μm **(B)** after exposure 48 h and clean 48 h. Exposure concentration and time were shown in the picture. Scale bar = 20 μm.

cured better in 8 μm microplastics treatment than in 80 nm microplastics treatment.

4 Discussion

4.1 Effects of microplastics on intestinal morphology of fish

The intestinal morphological effects of microplastics with a dose-dependent way have been explored in various fishes. Over secretion of goblet cells was found in juvenile guppy (*Poecilia reticulata*) after exposing microplastics with 32–40 μm diameter, and the higher concentration of microplastics, the more goblet cells secreted (Huang et al., 2020). However, the loss of villus and crypt cells was significantly increased due to microplastic physical abrasion in the intestine of juvenile intertidal fish (*Girella laevifrons*), and leukocyte infiltration and hyperemia exposure in the high concentration group were more serious than those in the low concentration group (Ahrendt et al., 2020). In the European sea bass (*Dicentrarchus labrax* L.), intestinal tissues were altered after fish were fed with polyvinyl chloride (PVC) pellets for 90 days (Peda et al., 2016). Another morphometric analyses of sea bass fed polyethylene (PE) microplastics in the diets for 21 days showed a significant reduction in the amounts of goblet cells as well as a decrease in villus height (Espinosa et al., 2019). Histological analysis indicated that multiple abnormalities in intestines are presented in three species fishes after acute exposure microplastics in this study.

As we all known, intestine is vital for the digestion and absorption of nutrients, and intestinal morphology characters, such as muscular layer thickness, villi length, and the number of goblet cells indicate intestine health in fish. To some extent, abnormal in the intestinal sections is an immune response to external stimulus. On one hand, pathological changes of intestinal tract might be the result of microplastics intrusion. On the other hand, it is crucial to determine whether this intrusion outpaces the organism's ability to repair itself. From histopathological analysis of intestines of largemouth bass juvenile exposed to 8 nm and 8 μm microspheres after exposure 48 h and clean 48 h (Figure 1), we found microplastics of lager size and higher concentration cause more serious damage, and the damage seems to be irreversible. Obviously, this change makes fish more sensitive to infection by pathogens. Compared with the intestinal slices of grass carp and Jian carp, Jian carp with smaller

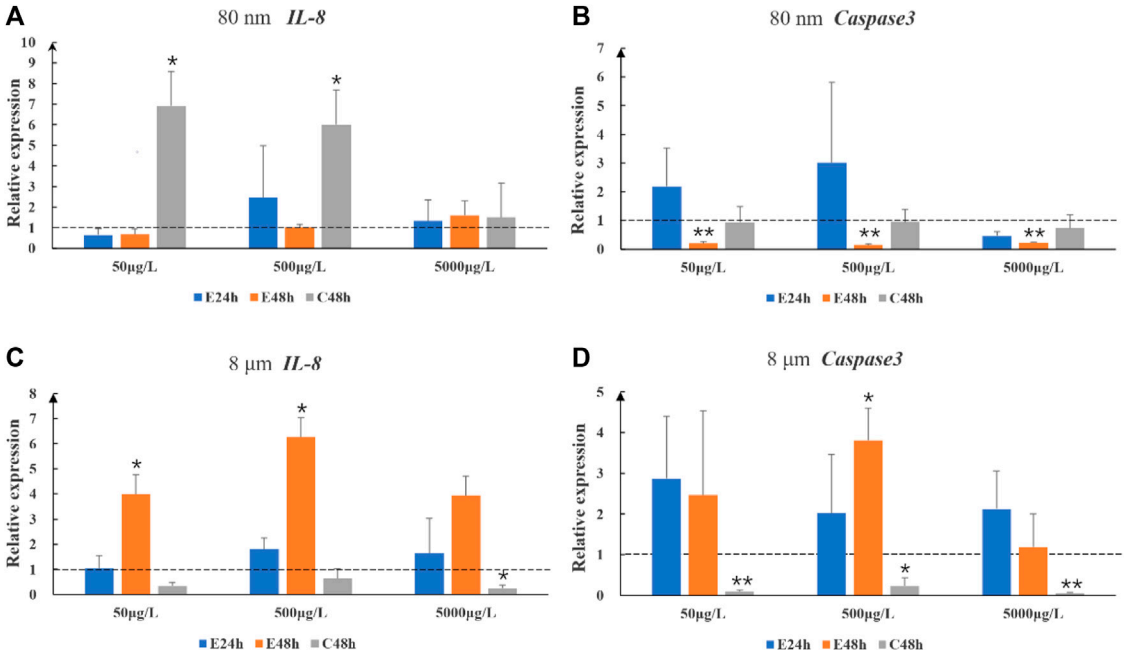

FIGURE 2
The relative gene expression levels (fold change) of *IL-8* **(A,C)** and *Caspase 3* **(B,D)** in intestines of largemouth bass juvenile exposed to microplastics. Data are expressed as mean ± standard deviation. Significant differences from control are shown (*$p < 0.05$; **$p < 0.01$).

intestinal diameter and less perfect villus structure was more seriously damaged by microplastic invasion.

4.2 Effects of microplastics on immune-related genes expression of fish

Many animal studies have indicated that exposure to microplastics impairs oxidative and inflammatory bowel balance (Choi et al., 2018; Ding et al., 2018). Especially, microplastics cause intestinal inflammation, manifested by a significant increase in *IL-1α* levels in the intestine (Hirt and Body-Malapel, 2020). The immune function of organs is highly correlated with the inflammatory response, which is generally considered to be a typical defense response that protects the host from pathogens (Zhong et al., 2020). Cytokines mediate the inflammatory response in fish, which are mainly divided into pro-inflammatory factors (e.g., *TNF-α*, *IL-1β* and *IL-10*) and anti-inflammatory factors (e.g., *IL-10* and *TGF-β*). For example, interleukin is a typical class of cytokines which is mainly involved in regulating all kinds of lymphocytes in the immune system. Tumor necrosis factor α (*TNF-α*), as pleiotropic proinflammatory and potent regulatory cytokines, can regulate cell proliferation, apoptosis or differentiation in the immune system (Cao et al., 2020). Toll-like receptors (*TLRs*), as a crucial innate receptor, can identify pathogen-associated molecular patterns (PAMPs) of invading microorganisms and induce downstream *NF-κB* activation and the production of *TNF-α*, *IL-10* and other cytokines (Meng et al., 2021).

Previous research in adult male zebrafish (*Danio rerio*) showed that exposure to 1,000 μg/L of 0.5 μm microplastics for 14 days significantly upregulated the transcription levels of *IL-1α*, *IL-1β*, and *Ifn* in the intestine (Jin et al., 2018). In the present study, microplastics exposure significantly induced or restrained the mRNA expression of immune-related genes in the intestine tissues of fishes. There were differential expressions of genes coping with differential sizes and concentrations of microplastics in different fishes. Similarly, in other species, such as rats (Wei et al., 2021) and prawn (Li et al., 2023a/b), the mRNA abundance of immune-related genes was increased with microplastics exposure.

4.3 Response time and legacy effect of microplastics with different concentration and size

In terms of damage to intestinal morphology, acute exposure did not cause significant damage at the size and concentration of microplastics exposed in this paper. From the perspective of gene expression level, when exposed to nanoscale microplastics at low concentration, fish can promote self-repair through the upregulation of some inflammatory factors. For micron-scale microplastics, we hypothesized that part of microplastics could be removed by fish excretion after ingestion. Therefore, there was no significant difference in gene expression between the experimental fish and the control group during the recovery period. The effects of microplastics on juvenile fishes are species-specific, the specific mechanism needs to be further studied.

Although time had no significant effect on intestinal morphology, we hypothesized that it was related to exposure

10.3389/fphys.2023.1256005

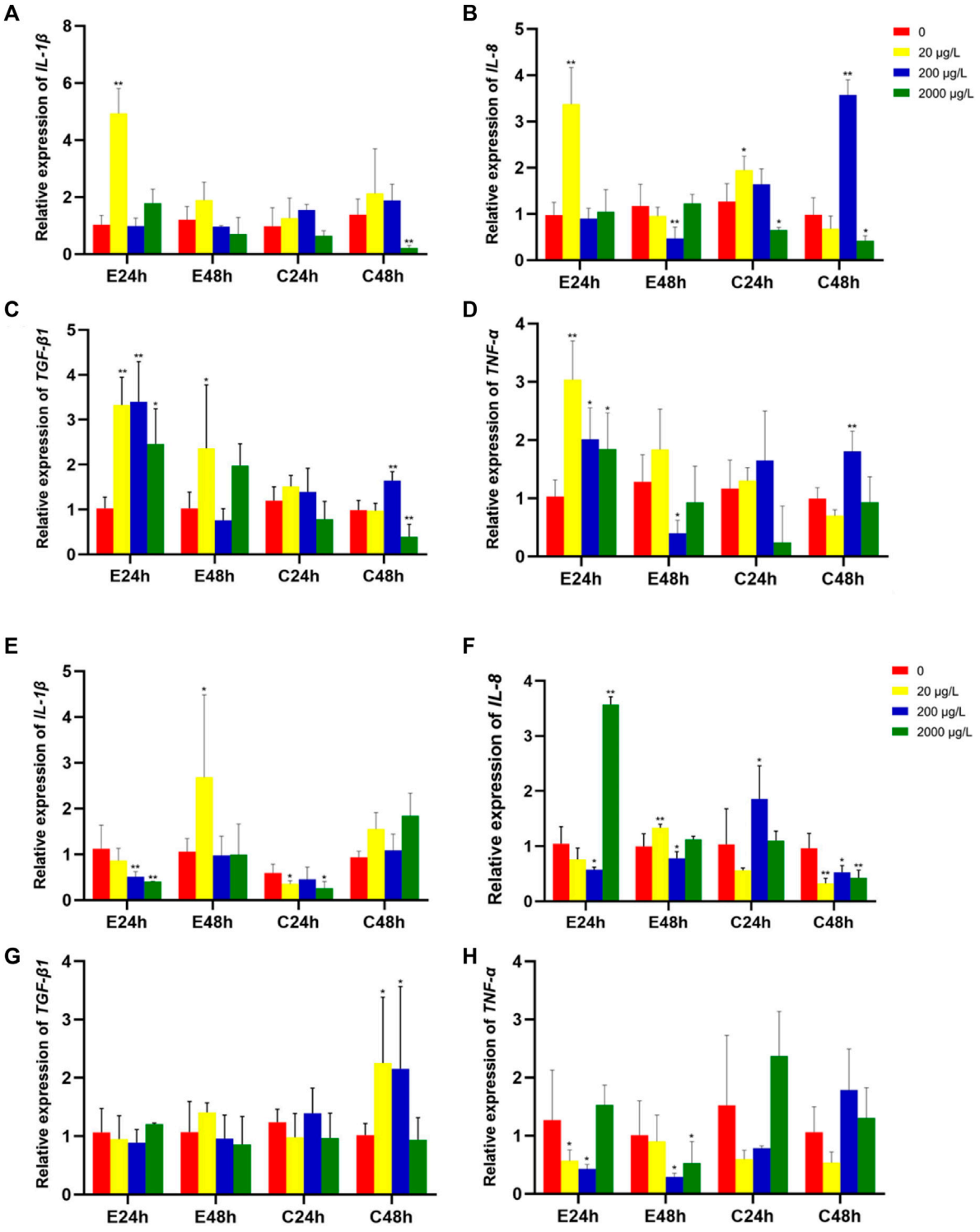

FIGURE 3
The relative gene expression levels (fold change) in intestines of grass carp juvenile exposed to microplastics of 80 nm **(A–D)** and 8 μm **(E–H)**. Data are expressed as mean ± standard deviation. Significant differences from control are shown (*$p < 0.05$; **$p < 0.01$).

conditions. Thankfully, even when exposed to extremely high concentration (mg/L) of microplastics, there is no immediate visible damage to the intestinal morphology of fish. Response time and recovery time of gene expression was species-specific. Grass carp has the longest intestinal tract, followed by Jian carp, and largemouth bass has the shortest intestinal tract, which is related to

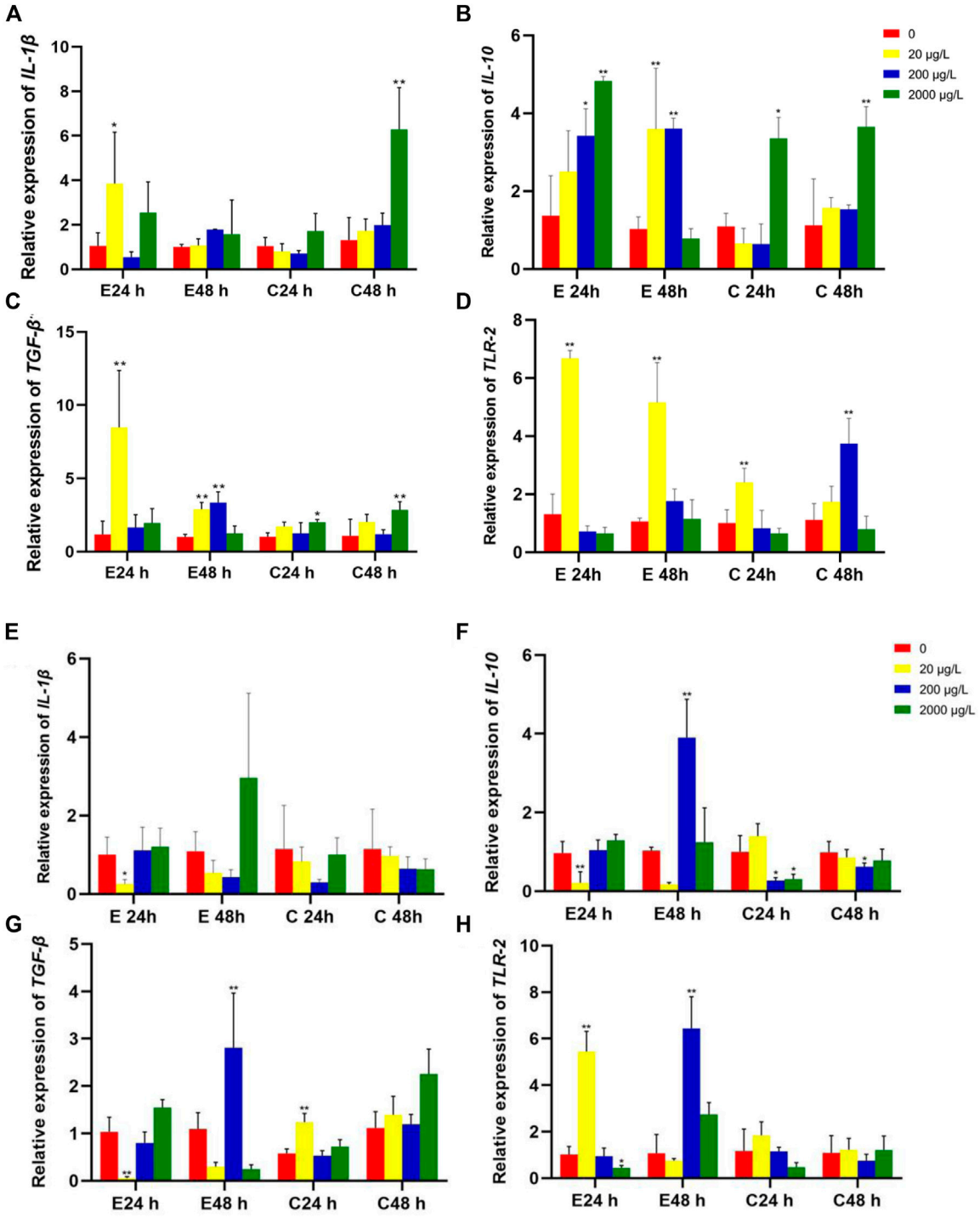

FIGURE 4
The relative gene expression levels (fold change) in intestines of Jian carp juvenile exposed to microplastics of 80 nm **(A–D)** and 8 μm **(E–H)**. Data are expressed as mean ± standard deviation. Significant differences from control are shown (*$p < 0.05$; **$p < 0.01$).

their feeding habits. We hypothesize that the lag time of microplastics in fish intestine is related to the length of the intestine. A methodology to assess how effective Mediterranean fish species, that are known to have ingested marine plastic, were considered gut length as well, which showed fish with smaller gut length is more representative (Bray et al., 2019).

5 Conclusion

In this study, species-specific effects of microplastics on three fishes with different feeding types were investigated. The contributing concentration and size of microplastics, as well as the response time and legacy effect in fishes were also explored. Two different sizes of

fluorescent microplastics (80 nm and 8 μm) were set at four concentrations. Multiple abnormalities in intestines were presented in three species fishes, and there were differential expressions of genes coping with differential sizes and concentrations of microplastics exposure in different fishes. The results of this study would be beneficial for extrapolating microplastics contamination risks to commercial fishes. The reason for the difference effects of microplastics on fishes was still unclear but could be due to the difference in the structure and function of the digestive system. This study will provide a valuable steppingstone for future research, where we hope to address the microplastics research gap between various fish species.

Data availability statement

The original contributions presented in the study are included in the article/Supplementary Materials, further inquiries can be directed to the corresponding author.

Ethics statement

The animal study was reviewed and approved by Animal Ethics and Welfare Committee, South China Agricultural University.

Author contributions

CZ: Data curation, Investigation, Methodology, Project administration, Validation, Writing–original draft, Writing–review and editing. FW: Conceptualization, Supervision, Validation, Visualization, Writing–original draft. QW: Conceptualization, Data curation, Formal Analysis, Software, Writing–original draft. JiZ: Methodology, Project administration, Resources, Validation, Writing–review and editing. JuZ: Funding acquisition, Project administration, Validation, Visualization, Writing–review and editing.

Funding

The author(s) declare financial support was received for the research, authorship, and/or publication of this article. This study was funded by Key Research and Development Program of Zhejiang Province (2019C02082) and Science and Technology Project of Zhejiang Province (2021YSZX007 and 2021C02069-2-02).

Acknowledgments

We thank the editor and reviewers for their constructive and insightful feedback, which improved the manuscript.

Conflict of interest

The authors declare that the research was conducted in the absence of any commercial or financial relationships that could be construed as a potential conflict of interest.

Publisher's note

Supplementary material

The Supplementary Material for this article can be found online at: https://www.frontiersin.org/articles/10.3389/fphys.2023.1256005/full#supplementary-material

References

Ahrendt, C., Perez-Venegas, D. J., Urbina, M., Gonzalez, C., Echeveste, P., Aldana, M., et al. (2020). Microplastic ingestion cause intestinal lesions in the intertidal fish Girella laevifrons. *Mar. Pollut. Bull.* 151, 110795. doi:10.1016/j.marpolbul.2019.110795

Alimi, O. S., Farner Budarz, J., Hernandez, L. M., and Tufenkji, N. (2018). Microplastics and nanoplastics in aquatic environments: Aggregation, deposition, and enhanced contaminant transport. *Environ. Sci. Technol.* 52, 1704–1724. doi:10.1021/acs.est.7b05559

Anna, K., Krause, S., Lynch, I., GregorySmith, H. S., and Nel, H. (2021). Nano and microplastic interactions with freshwater biota – current knowledge, challenges and future solutions. *Environ. Int.* 152, 106504. doi:10.1016/j.envint.2021.106504

Banaee, M., Soltanian, S., Sureda, A., Gholamhosseini, A., Haghi, B. N., Akhlaghi, M., et al. (2019). Evaluation of single and combined effects of cadmium and micro-plastic particles on biochemical and immunological parameters of common carp (*Cyprinus carpio*). *Chemosphere* 236, 124335. doi:10.1016/j.chemosphere.2019.07.066

Bray, L., Digka, N., Tsangaris, C., Camedda, A., Gambaiani, D., de Lucia, G. A., et al. (2019). Determining suitable fish to monitor plastic ingestion trends in the Mediterranean Sea. *Environ. Pollut.* 247, 1071–1077. doi:10.1016/j.envpol.2019.01.100

Brun, N. R., van Hage, P., Hunting, E. R., Haramis, A. G., Vink, S. C., Vijver, M. G., et al. (2019). Polystyrene nanoplastics disrupt glucose metabolism and cortisol levels with a possible link to behavioural changes in larval zebrafish. *Commun. Biol.* 2, 382. doi:10.1038/s42003-019-0629-6

Cao, S., Xiong, D., Luo, W., Tang, J., Qu, F., Zhou, Y., et al. (2020). Effects of dietary soy isoflavones on growth, antioxidant status, immune response and resistance of juvenile grass carp (*Ctenopharyngodon idella*) to Aeromonas hydrophila challenge. *Aquac. Res.* 51, 2472–2482. doi:10.1111/are.14590

Choi, J. S., Jung, Y., Hong, N., Hong, S. H., and Park, J. (2018). Toxicological effects of irregularly shaped and spherical microplastics in a marine teleost, the sheepshead minnow (*Cyprinodon variegatus*). *Mar. Pollut. Bull.* 129, 231–234. doi:10.7181/acfs.2018.02033

Cole, M., Lindeque, P., Halsband, C., and Galloway, T. S. (2011). Microplastics as contaminants in the marine environment: A review. *Mar. Pollut. Bull.* 62, 2588–2597. doi:10.1016/j.marpolbul.2011.09.025

Ding, J., Zhang, S., Razanajatovo, R. M., Zou, H., and Zhu, W. (2018). Accumulation, tissue distribution, and biochemical effects of polystyrene microplastics in the freshwater fish red tilapia (*Oreochromis niloticus*). *Environ. Pollut.* 238, 1–9. doi:10.1016/j.envpol.2018.03.001

Espinosa, C., Esteban, M. Á., and Cuesta, A. (2019). Dietary administration of PVC and PE microplastics produces histological damage, oxidative stress and immunoregulation in European sea bass (*Dicentrarchus labrax* L). *Fish. Shellfish Immun.* 95, 574–583. doi:10.1016/j.fsi.2019.10.072

Garrido Gamarro, E., Ryder, J., Elvevoll, E. O., and Olsen, R. L. (2020). Microplastics in fish and shellfish - a threat to seafood safety? *J. Aquat. Food Prod. Trans.* 29, 417–425. doi:10.1080/10498850.2020.1739793

Gu, H., Wang, S., Wang, X., Yu, X., Hu, M., Huang, W., et al. (2020). Nanoplastics impair the intestinal health of the juvenile large yellow croaker *Larimichthys crocea*. *J. Hazard. Mat.* 397, 122773. doi:10.1016/j.jhazmat.2020.122773

Guimarães, A. T. B., Estrela, F. N., Rodrigues, A. S. D. L., Chagas, T. Q., Pereira, P. S., Silva, F. G., et al. (2021). Nanopolystyrene particles at environmentally relevant concentrations causes behavioral and biochemical changes in juvenile grass carp (*Ctenopharyngodon idella*). *J. Hazard. Mat.* 403, 123864. doi:10.1016/j.jhazmat.2020.123864

Hirt, N., and Body-Malapel, M. (2020). Immunotoxicity and intestinal effects of nano- and microplastics: A review of the literature. *Part. Fibre Toxicol.* 17, 57. doi:10.1186/s12989-020-00387-7

Huang, J. N., Wen, B., Zhu, J. G., Zhang, Y. S., Gao, J. Z., and Chen, Z. Z. (2020). Exposure to microplastics impairs digestive performance, stimulates immune response and induces microbiota dysbiosis in the gut of juvenile guppy (*Poecilia reticulata*). *Sci. Total Environ.* 733, 138929. doi:10.1016/j.scitotenv.2020.138929

Iheanacho, S. C., and Odo, G. E. (2020). Dietary exposure to polyvinyl chloride microparticles induced oxidative stress and hepatic damage in *Clarias gariepinus* (Burchell, 1822). *Environ. Sci. Pollut. Res. Int.* 27, 21159–21173. doi:10.1007/s11356-020-08611-9

Jabeen, K., Li, B., Chen, Q., Su, L., Wu, C., Hollert, H., et al. (2018). Effects of virgin microplastics on goldfish (*Carassius auratus*). *Chemosphere* 213, 323–332. doi:10.1016/j.chemosphere.2018.09.031

Jacob, H., Besson, M., Swarzenski, P. W., Lecchini, D., and Metian, M. (2020). Effects of virgin micro- and nanoplastics on fish: Trends, meta-analysis, and perspectives. *Environ. Sci. Technol.* 54, 4733–4745. doi:10.1021/acs.est.9b05995

Jin, Y., Xia, J., Pan, Z., Yang, J., Wang, W., and Fu, Z. (2018). Polystyrene microplastics induce microbiota dysbiosis and inflammation in the gut of adult zebrafish. *Environ. Pollut.* 235, 322–329. doi:10.1016/j.envpol.2017.12.088

Li, Y., Du, X., Li, W., Jiang, Q., Ye, Y., Yang, Y., et al. (2023a). Two genes related to apoptosis in the hepatopancreas of juvenile prawn, Macrobrachium nipponense: Molecular characterization and transcriptional response to nanoplastic exposure. *Sci. Total Environ.* 877, 162863. doi:10.1016/j.scitotenv.2023.162863

Li, Y., Liu, Z., Li, M., Jiang, Q., Wu, D., Huang, Y., et al. (2020). Effects of nanoplastics on antioxidant and immune enzyme activities and related gene expression in juvenile Macrobrachium nipponense. *J. Hazard. Mat.* 398, 122990. doi:10.1016/j.jhazmat.2020.122990

Li, Y., Ye, Y., Na, R., Jiang, Q., Liu, X., Zhao, Y., et al. (2023b). Polystyrene nanoplastics decrease nutrient accumulation, disturb sex hormones, and inhibit reproductive development in juvenile Macrobrachium nipponense. *Sci. Total Environ.* 891, 164481. doi:10.1016/j.scitotenv.2023.164481

Lin, Y., Zeng, D., He, P., Wei, P., Hui, W., Wu, T., et al. (2019). mRNA and microRNA transcriptomics analyses in intermuscular bones of two carp species, rice flower carp (*Cyprinus carpio* var. Quanzhounensis) and Jian carp (*Cyprinus carpio* var. Jian). *Comp. Biochem. Physiol. Part D. Genomics Proteomics* 30, 71–80. doi:10.1016/j.cbd.2019.01.013

Mallik, A., Martin Xavier, K. A., Naidu, B. C., and Nayak, B. B. (2021). Ecotoxicological and physiological risks of microplastics on fish and their possible mitigation measures. *Sci. Total Environ.* 779, 146433. doi:10.1016/j.scitotenv.2021.146433

McDevitt, J. P., Criddle, C. S., Morse, M., Hale, R. C., Bott, C. B., and Rochman, C. M. (2017). Addressing the issue of microplastics in the wake of the microbead-free waters act—a new standard can facilitate improved policy. *Environ. Sci. Technol.* 51, 6611–6617. doi:10.1021/acs.est.6b05812

Meng, X., Wu, S., Hu, W., Zhu, Z., Yang, G., Zhang, Y., et al. (2021). Clostridium butyricum improves immune responses and remodels the intestinal microbiota of common carp (*Cyprinus carpio* L). *Aquaculture* 530, 735753. doi:10.1016/j.aquaculture.2020.735753

Mizraji, R., Ahrendt, C., Perez-Venegas, D., Vargas, J., Pulgar, J., Aldana, M., et al. (2017). Is the feeding type related with the content of microplastics in intertidal fish gut? *Mar. Pollut. Bull.* 116, 498–500. doi:10.1016/j.marpolbul.2017.01.008

NOAA (2015). National oceanic and atmospheric administration. Microplastics Available at: https://marinedebris.noaa.gov/sites/default/files/MicroplasticsOnePager_0.pdf.

Peda, C., Caccamo, L., Fossi, M. C., Gai, F., Andaloro, F., Genovese, L., et al. (2016). Intestinal alterations in European sea bass *Dicentrarchus labrax* (Linnaeus, 1758) exposed to microplastics: Preliminary results. *Environ. Pollut.* 212, 251–256. doi:10.1016/j.envpol.2016.01.083

Peng, L., Fu, D., Qi, H., Lan, C. Q., Yu, H., and Ge, C. (2020). Micro- and nano-plastics in marine environment: Source, distribution and threats — a review. *Sci. Total Environ.* 698, 134254. doi:10.1016/j.scitotenv.2019.134254

Plastics Europe (2022). Plastics - the facts 2021: An analysis of European plastics production, demand and waste data. Available at: https://plasticseurope.org/knowledge-hub/plastics-the-facts-2022/.

Rai, P. K., Lee, J., Brown, R. J. C., and Kim, K. (2021). Environmental fate, ecotoxicity biomarkers, and potential health effects of micro- and nano-scale plastic contamination. *J. Hazard. Mat.* 403, 123910. doi:10.1016/j.jhazmat.2020.123910

Rios-Fuster, B., Arechavala-Lopez, P., García-Marcos, K., Alomar, C., Compa, M., Álvarez, E., et al. (2021). Experimental evidence of physiological and behavioral effects of microplastic ingestion in *Sparus aurata*. *Aquat. Toxicol.* 231, 105737. doi:10.1016/j.aquatox.2020.105737

Shi, W., Sun, S., Han, Y., Tang, Y., Zhou, W., Du, X., et al. (2021). Microplastics impair olfactory-mediated behaviors of goldfish *Carassius auratus*. *J. Hazard. Mat.* 409, 125016. doi:10.1016/j.jhazmat.2020.125016

Wang, S., Ge, J., Yu, X., and Li, H. (2020a). Environmental fate and impacts of microplastics in soil ecosystems: Progress and perspective. *Sci. Total Environ.* 708, 134841. doi:10.1016/j.scitotenv.2019.134841

Wang, S., Ni, J., Nie, Z., Gao, J., Sun, Y., Shao, N., et al. (2020c). Effects of stocking density on growth, serum parameters, antioxidant status, liver and intestine histology and gene expression of largemouth bass (*Micropterus salmoides*) farmed in the in-pond raceway system. *Aquac. Res.* 51, 5228–5240. doi:10.1111/are.14862

Wang, S., Zhang, C., Pan, Z., Sun, D., Zhou, A., Xie, S., et al. (2020b). Microplastics in wild freshwater fish of different feeding habits from Beijiang and Pearl River Delta regions, south China. *Chemosphere* 258, 127345. doi:10.1016/j.chemosphere.2020.127345

Wei, J., Wang, X., Liu, Q., Zhou, N., Zhu, S., Li, Z., et al. (2021). The impact of polystyrene microplastics on cardiomyocytes pyroptosis through NLRP3/Caspase-1 signaling pathway and oxidative stress in Wistar rats. *Environ. Toxicol.* 36, 935–944. doi:10.1002/tox.23095

Xu, J., and Li, D. (2021). Feeding behavior responses of a juvenile hybrid grouper, *Epinephelus fuscoguttatus*♀ × *E. lanceolatus*♂, to microplastics. *Environ. Pollut.* 268, 115648. doi:10.1016/j.envpol.2020.115648

Xu, S., Ma, J., Ji, R., Pan, K., and Miao, A. (2020). Microplastics in aquatic environments: Occurrence, accumulation, and biological effects. *Sci. Total Environ.* 703, 134699. doi:10.1016/j.scitotenv.2019.134699

Zhang, C., Wang, J., Zhou, A., Ye, Q., Feng, Y., Wang, Z., et al. (2021). Species-specific effect of microplastics on fish embryos and observation of toxicity kinetics in larvae. *J. Hazard. Mat.* 403, 123948. doi:10.1016/j.jhazmat.2020.123948

Zhang, S., Ding, J., Razanajatovo, R. M., Jiang, H., Zou, H., and Zhu, W. (2019). Interactive effects of polystyrene microplastics and roxithromycin on bioaccumulation and biochemical status in the freshwater fish red tilapia (*Oreochromis niloticus*). *Sci. Total Environ.* 648, 1431–1439. doi:10.1016/j.scitotenv.2018.08.266

Zhong, J., Wu, P., Feng, L., Jiang, W., Liu, Y., Kuang, S., et al. (2020). Dietary phytic acid weakened the antimicrobial activity and aggravated the inflammatory status of head kidney, spleen and skin in on-growing grass carp (*Ctenopharyngodon idella*). *Fish. Shellfish Immun.* 103, 256–265. doi:10.1016/j.fsi.2020.05.037

frontiers | Frontiers in Physiology

TYPE Original Research
PUBLISHED 08 August 2023
DOI 10.3389/fphys.2023.1250513

OPEN ACCESS

EDITED BY
Yiming Li,
Fishery Machinery and Instrument Research Institute, China

REVIEWED BY
Weiwei Wang,
Ocean University of China, China
Qiang Ma,
Chinese Academy of Fishery Sciences (CAFS), China
Qichen Jiang,
Freshwater Fisheries Research Institute of Jiangsu Province, China

*CORRESPONDENCE
Zan Li,
lizanlxm@163.com

RECEIVED 30 June 2023
ACCEPTED 01 August 2023
PUBLISHED 08 August 2023

CITATION
Liu X, Yang J and Li Z (2023), Transcriptomic analysis of oxidative stress mechanisms induced by acute nanoplastic exposure in *Sepia esculenta* larvae.
Front. Physiol. 14:1250513.
doi: 10.3389/fphys.2023.1250513

Transcriptomic analysis of oxidative stress mechanisms induced by acute nanoplastic exposure in *Sepia esculenta* larvae

Xiumei Liu[1], Jianmin Yang[2] and Zan Li[2]*

[1]College of Life Sciences, Yantai University, Yantai, China, [2]School of Agriculture, Ludong University, Yantai, China

Nanoplastics (NPs), as a new type of pollutant with a size small than 1 μm, are ubiquitous and harmful to organisms. There has been an increasing amount of research concerning the effects of NPs on organisms over recent years, especially on aquatic animals. However, there is a limited study on the impact of NPs on mollusk cephalopods. In this research, *Sepia esculenta*, belonging to Cephalopoda, Coleoidea, Sepioidea, was selected to explore the effects caused by NPs exposure. The *S. esculenta* larvae were exposed to polystyrene NPs (PS-NPs) with diameter 50 nm (100 mg/L) for 4 h. The detection of oxidative stress biomarkers displayed an obvious increase in SOD (superoxide dismutase) activity and MDA (malondialdehyde) level. Then, RNA-Seq was performed to explore the oxidative stress response at mRNA level. The transcriptome analysis demonstrated that the expression of 2,570 genes was affected by PS-NPs. Besides, the signaling pathways of ribosome, ribosome biogenesis in eukaryotes, proteasome, and MAPK were enriched. This study not only provides novel references for understanding the mechanisms of oxidative stress response induced by NPs, but also reminds us to follow with interest the influence of acute exposure to NPs.

KEYWORDS

nanoplastics, oxidative stress, ribosome, proteasome, MAPK signaling pathway

1 Introduction

Plastics have been used heavily due to their incredible versatility, which have had a huge impact on society and environment (Porta, 2021). The growth rate of this material production is astonishing, with a production of approximately 390 million metric tons in 2021 (Statista Research Department, 2023). At present, the plastic industry has become one of the world's largest manufacturing industries. It is estimated that plastic production will increase by more than twice the current production by 2100 (Stegmann et al., 2022). However, most of the plastic currently produced is disposable, resulting in a large amount of waste plastics. Due to the high price of recycled plastics, the vast majority of waste plastics are traditional plastics that are difficult to biodegrade. In addition, improper handling methods have led to the accumulation of most waste plastics in the environment (Geyer et al., 2017). This has made plastic pollution a significant concern for people. The common waste plastics are thermoplastics used for packaging, for instance, polystyrene (PS), polyvinyl chloride (PVC), and polyethylene (PE) (Narancic and O'Connor, 2019). Plastic pieces in the environment constantly break down through biological, chemical, and physical

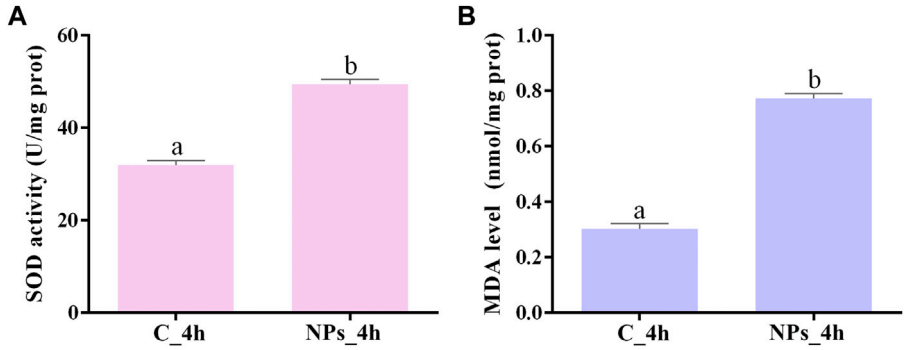

FIGURE 1
The detection results of SOD activity **(A)** and MDA level **(B)**. The different lowercase letters above the column stand for significant difference between groups ($p < 0.05$).

processes, ultimately decomposing into nanoscopic fragments, known as nanoplastics (NPs, <1 μm) (Gigault et al., 2018; Ferreira et al., 2019). According to ATSDR reports, PS and PVC are common NPs (Kumar et al., 2022).

NPs are widely distributed in various ecosystems, causing certain damage to organisms and even posing a threat to human health. Ingestion of aquatic organisms contaminated with NPs is one of the main routes of NPs exposure to humans (Leslie et al., 2022). Molluscs are one of the main aquatic foods that provide abundant nutrients for humans. However, NPs can lead to toxicity on mollusks just like other animals (Ferreira et al., 2019). First of all, NPs can reduce the successfully fertilization rate of gametes and increase the malformation rate of embryo-larval development (Tallec et al., 2018; Rist et al., 2019). Through multiple methods, such as determination of i-Ca and transcriptome analysis, the researchers found that NPs led to the growth inhibition of *Tetrahymena thermophile* by affecting Ca signaling, and phosphatidylinositol signaling (Wu et al., 2021). Transcriptome analysis results displayed that NPs hindered the reproduction and population growth of *Brachionus plicatilis* by causing metabolic abnormalities and oxidative stress (Shin and Jeong, 2022). In addition, it was found that NPs not only triggered the apoptosis in different tissues of *Corbicula fluminea*, but also induced intestinal epithelial inflammatory response (Li et al., 2021). Through multi-omics and histopathological analysis, it was found that NPs induced intestinal epithelial damage, intestinal microbial community changes, and abnormal metabolism of carbohydrates and arachidonic acid in *Eisenia fetida* (Tang et al., 2023). In the intestine of *Apostichopus japonicas* and *Procambarus clarkii*, the changes in microbial community caused by NPs exposure might be related to oxidative stress (Han et al., 2022; Zhao et al., 2023). Oxidative stress is the common response caused by NPs in mollusks, such as *Mytilus* spp. (Cole et al., 2020), *C. fluminea* (Li et al., 2020), *Mytilus galloprovincialis* (Wang et al., 2023), *Crassostrea virginica* (Lebordais et al., 2021), and *Monodonta labio* (Li and Han, 2022). Besides, NPs were also found to trigger oxidative stress in *Procambarus clarkia*, *Daphnia pulex* and *Ciona robusta* via transcriptome analysis (Liu et al., 2021a; Capanni et al., 2021; Eliso et al., 2023).

Cephalopoda, as the third-largest and most advanced class of Mollusca, cannot only provide high-quality proteins for humans, but also have scientific research value. Currently, there is no evidence to suggest that NPs have been detected in cephalopods. However, microplastics (MPs, 1 μm–5 mm) have been detected in wild cephalopods *Sepia officinalis* (Oliveira et al., 2020), *Octopus vulgaris* (Pedà et al., 2022), *Octopus variabilis* (Gong et al., 2021), *Amphioctopus fangsiao* (Yu et al., 2022a), *Dosidicus gigas*, *Abralia veranyi* and *Vampyroteuthis infernalis* (Ferreira et al., 2022). Given that the size of NPs are smaller than MPs, NPs are more easily ingested and difficult to detect. Therefore, NPs may have an impact on cephalopods. However, the toxic molecular mechanisms of oxidative stress caused by NPs to cephalopods are still unexplored.

The golden cuttlefish *Sepia esculenta*, one of the important economic cephalopod species, is distributed mainly in the seas of Russia, China, Singapore, South of Korea, Japan and Philippins (Wang and Zheng, 2017). The *S. esculenta* generally live in the coastal environment that is easily contaminated by plastics (Pedrotti et al., 2016). In this paper, we chose *S. esculenta* larvae to explore the effect of acute NPs exposure on cephalopods. The changes of SOD and MDA enzyme activities revealed that NPs caused oxidative stress to *S. esculenta* larvae. Twenty key genes involved in responding to NPs exposure were obtained by analyzing the transcriptome profiles of *S. esculenta* larvae exposed to NPs for 4 h. The results provide a reference for analyzing organism's toxic mechanism caused by NPs.

2 Materials and methods

2.1 *S. esculenta* larvae collection and exposure study

The sexual maturity *S. esculenta* were collected in Qingdao sea area, China, and temporarily raised until laying eggs. The eggs were collected and placed in a breeding pool with flowing seawater and continuously oxygenated during hatching. The eggs hatched after a month and were divided into two groups of 50 individuals in each group. Larvae of control group (C) grew in normal seawater, and exposed group (NPs) larvae grew in

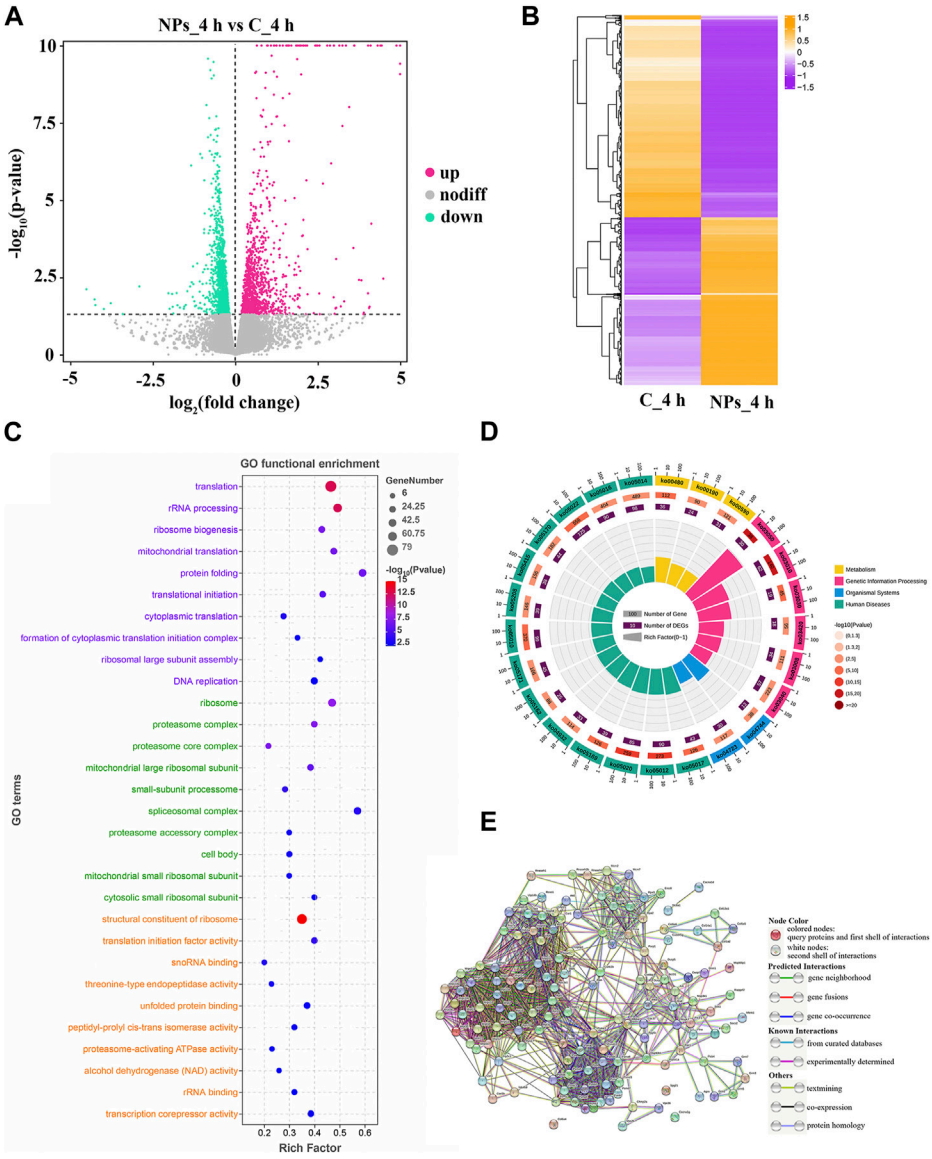

FIGURE 2
(A) Expression of DEGs between C_4h and NPs_4h. Upregulated genes are depicted as rose dots, downregulated genes as medium spring green dots, and non-regulated genes as grey dots. **(B)** Clustering of DEG expression profiles. Each row represents the expression levels of a DEG in each group, while each column represents the overall expression patterns of all DEGs in a group. **(C)** Top 10 significant GO terms. The vertical axis represents GO terms categorized into Biological Process (BP, lavender), Cellular Component (CC, light green), and Molecular Function (MF, orange-yellow). The horizontal axis stands for the rich factor. **(D)** Top 25 level-2 KEGG signaling pathways results. **(E)** PPI network. The circles represent proteins, and the connections between them indicate their interactions, with different connection modes indicating various interaction types.

seawater with NPs (100 mg/L). Then, the above larvae were collected at 0 h (C_0 h) and 4 h (C_4 h and NPs_4 h) respectively. The collected larvae were stored in liquid nitrogen for future use.

2.2 Assay of oxidative stress

The activity of SOD were measured by Total Superoxide Dismutase (T-SOD) assay kit (Hydroxylamine method) purchased from Nanjing Jiancheng Bioengineering Institute. In addition, the MDA levels were detected using Malondialdehyde (MDA) assay kit (TBA method) according to the instructions. Eight replicates were set in each group (C_4h and NPs_4h), and the measured tissue fluid was obtained by grinding 8 randomly selected whole larvae.

The calculation formula for SOD activity is as follows:

$$A = \frac{\text{OD value (contrast tube} - \text{testing tube)}}{\text{OD value of contrast tube}} \div 50\% \times \frac{V1}{V2} \div C$$

Notes: A, total SOD activity (U/mg prot); V1, total volume of reaction solution (mL); V2, volume of sampling amount (mL); C, protein concentration of testing sample (mg prot/mL).

The calculation formula for MDA level is as follows:

TABLE 1 Significant level-3 KEGG signaling pathways enrichment analysis results.

Pathways	Number of DEGs
Apoptosis	4
Chemical carcinogenesis - reactive oxygen species	6
DNA replication	12
ECM-receptor interaction	4
Endocytosis	5
Growth hormone synthesis, secretion and action	4
MAPK signaling pathway	18
Nucleotide excision repair	9
Phospholipase D signaling pathway	9
PI3K-Akt signaling pathway	5
Proteasome	21
Protein digestion and absorption	6
Ribosome	32
Ribosome biogenesis in eukaryotes	23

$$L = \frac{\text{OD value (testing tube} - \text{contrast tube)}}{\text{OD value (standard tube} - \text{blank tube)}} \times C1 \div C2$$

Notes: L, MDA level (nmol/mg prot); C1, concentration of standard substance (10 nmol/mL); C2, protein concentration of testing sample (mg prot/mL).

2.3 RNA extraction and sequencing

We used the TRI Reagent method (Rio et al., 2010) with the manufacturer's protocol to extract total RNA and identified the integrity using Agilent 2100 bioanalyzer (Sodowich et al., 2007). Nine larvae were randomly selected for RNA extraction from groups C_0h, C_4h, and NPs_4h, respectively. Then, the RNA of 9 larvae with equal molar masses in each group was mixed into 3 replicates for subsequent sequencing. Using NEBNext® Ultra™ RNA Library Prep Kit for Illumina® to construct the transcriptome library (Parkhomchuk et al., 2009). Raw reads were sequenced by Illumina NovaSeq 6000 (Illumina, United States), whose SRA accession number were SRR23936172, SRR23936173, SRR23936174, SRR23936175, SRR23936181, SRR23936182, SRR25114243, SRR25114244 and SRR25114245. Removing low quality reads from raw reads to obtain clean reads. The obtained clean reads were mapped to the reference genome (unpublished) using HISAT2.

2.4 DEG identification

In this study, the DESeq2 software of R was used as a model to screen differentially expressed genes (DEGs). First, the data were involved in constructing the ddsmodel, after which the dispersion of the samples was estimated using the DESeq function, and finally the differences in gene expression were analyzed. DEGs with p-value ≤0.05 to compare groups C_4h and NPs_4h were screened out (Love et al., 2014).

2.5 Functional enrichment analyses and network construction

The functional enrichment analysis was performed on DEGs. To ascertain the GO terms and the distribution of DEGs, GO analyses were deployed on the union set distinguished at two distinct time points. Additionally, Gene Set Enrichment Analysis was employed to identify immune-related pathways and genes through the KEGG pathway analysis, thus elucidating the functions of DEGs. Enrichment analyses of GO and KEGG were executed using the DAVID database (https://david.ncifcrf.gov/) 2021 (Jiao et al., 2012). The construction of a protein-protein interaction (PPI) network can offer insights into the correlations amongst oxidative stress pathways, thereby simplifying the identification of pivotal genes. In this study, we leveraged the STRING database (https://cn.string-db.org) to construct a robust PPI network (Szklarczyk et al., 2019).

2.6 Quantitative RT-PCR assay

The accuracy of RNA-Seq was verified via qRT-PCR. In this study, 30 hub genes were pinpointed for validation via qRT-PCR. Utilizing Primer Premier 5.0 software, gene primer sequences were formulated based on the spliced transcriptome. The primers related information used in the qRT-PCR is shown in Supplementary Table S1. The gene of *β-actin* is used as housekeeper gene for qRT-PCR due to its evident stability within this experiment. The fluorescence quantification methods implemented were adapted from Liu et al.'s work (Liu et al., 2017).

3 Result

3.1 Detection of oxidative stress biomarkers

As shown in Figure 1A, the activity of SOD was higher in the *S. esculenta* larvae exposed to PS-NPs than that in control group (p-value = 3.1E-5). The results of RNA-Seq data analysis showed that the transcript levels of SOD were also increased in *S. esculenta* larvae exposed to PS-NPs (Supplementary Table S2). Besides, the level of MDA in *S. esculenta* larvae whole body was increased after PS-NPs exposure (p-value = 6.0E-6) (Figure 1B).

3.2 Sequencing and analysis of transcriptome

The changes of physiological biomarkers pointed out that the acute exposure of PS-NPs induced oxidative stress in *S. esculenta* larvae. To explore the molecular mechanisms involved, transcriptome sequencing projects were performed. The average of 45,989,845 raw reads per sample were sequenced. Subsequently,

TABLE 2 Statistics of key genes.

Gene name (abbreviation)	Gene name (official full name)	Number of KEGG signaling pathways	Number of protein–protein interactions
RPS5	ribosomal protein S5	1	48
RPS9	ribosomal protein S9	1	45
MRPL4	mitochondrial ribosomal protein L4	1	44
MRPS11	mitochondrial ribosomal protein S11	1	44
NHP2L1	small nuclear ribonucleoprotein 13	1	42
RPL5	ribosomal protein L5	1	42
RPL9	ribosomal protein L9	1	40
RPS20	ribosomal protein S20	1	39
MRPL1	mitochondrial ribosomal protein L1	1	38
RPS3A1	ribosomal protein S3A1	1	37
MRPL15	mitochondrial ribosomal protein L15	1	36
MRPL3	mitochondrial ribosomal protein L3	1	36
RPL13A	ribosomal protein L13A	1	36
MRPS14	mitochondrial ribosomal protein S14	1	35
NFKBIA	NFKB inhibitor alpha	1	32
RPL10	ribosomal protein L10	1	32
PSMA2	proteasome 20S subunit alpha 2	1	31
PSMA3	proteasome 20S subunit alpha 3	1	31
MRPS10	mitochondrial ribosomal protein S10	1	30
PSMA6	proteasome 20S subunit alpha 6	1	30
RPL19	ribosomal protein L19	1	30
MRPL12	mitochondrial ribosomal protein L12	1	29
GTPBP4	GTP binding protein 4	1	28
NMD3	NMD3 ribosome export adaptor	1	28
MRPL17	mitochondrial ribosomal protein L17	1	27
PSMA8	proteasome 20S subunit alpha 8	1	27
MRPL19	mitochondrial ribosomal protein L19	1	26
MRPL23	mitochondrial ribosomal protein L23	1	26
MRPL32	mitochondrial ribosomal protein L32	1	26
PSMA5	proteasome 20S subunit alpha 5	1	26

after filtering, an average of 44,771,357 clean reads were generated for each sample. The average of Q20 and Q30 were 96.91% and 92.00%, respectively. And the average of GC content in clean reads was 40.24% (Supplementary Table S3). These results suggested a high quality of sequencing.

As the results of differential expression analysis, there were a total of 2570 DEGs (1,166 up- and 1,404 downregulated) at 4 h after PS-NPs exposure (Figure 2A). DEGs expression distribution of all groups was shown in the heatmap, which displayed an obvious difference in the expression pattern of DEGs between the PS-NPs exposure group and non-exposed groups (Figure 2B).

To investigate the function of DEGs, GO and KEGG enrichment analysis were conducted. As shown in Figure 2C, 145 significant GO terms were enriched, and translation, structural constituent of ribosome, and other terms are important for mediating oxidative stress. Based on level-2 KEGG enrichment analysis results, these DEGs were participating in multiple signaling pathways (Figure 2D). The enrichment of 14 KEGG signaling pathways (level-3), such as Ribosome, Proteasome, and MAPK signaling pathway, suggested that PS-NPs exposure have affected multiple biological processes in *S. esculenta* larvae (Table 1).

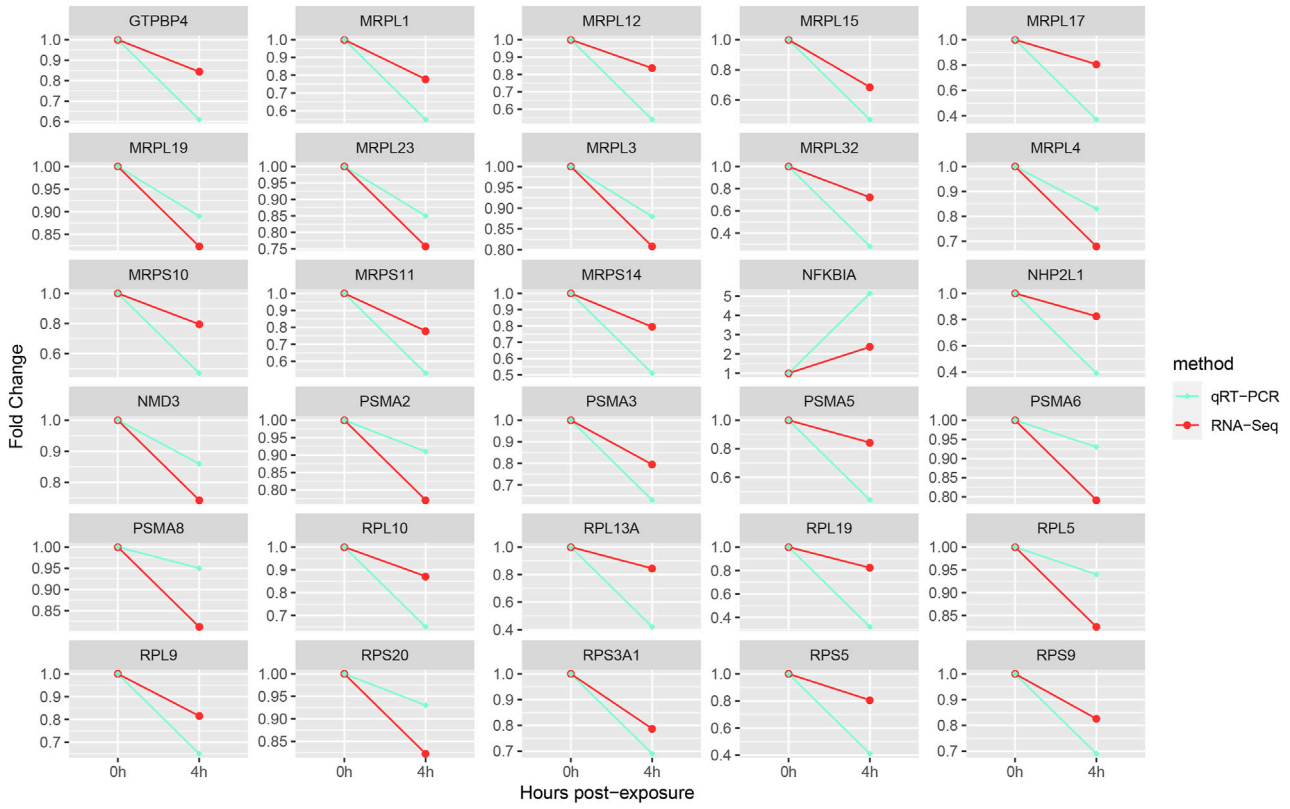

FIGURE 3
Gene expression verification.

Subsequently, 139 DEGs involved in KEGG signaling pathways of Table 1 were used to construct the PPI network to scan hub genes regulating multiple biological processes affected (Figure 2E). The relevant parameters of PPI network are displayed in Supplementary Table S4. Considering the numbers of involved in KEGG signaling pathway and protein interaction, 30 key DEGs were obtained, for instance, RPS5, RPS9 and MRPL4 (Table 2).

3.3 Validation of key DEGs

The key DEGs were chosen for quantitative RT-PCR. The results showed the trend of qRT-PCR was consistent with that of RNA-Seq, which suggested that results of transcriptome profile were reliable and accurate (Figure 3).

4 Discussion

In recent years, NPs have received increasing attentions as emerging pollutants. Researchers have conducted *in vitro* experiments on various cell types, as well as *in vivo* experiments on model and non-model animals, to study and reveal the toxic effects of NPs (Schröter and Ventura, 2022). However, it is still essential to discuss the toxic effects of NPs in more species. Molluscs, such as bivalves and gastropods, are an important branch in the study of aquatic non-model organisms (Sendra et al., 2021). To enrich the research scope of the effect of NPs on organisms, we selected the *S. esculenta* larvae of Cephalopoda Octopus in Mollusca as the research object. The larvae used in our study have similar size, whose total length is 10.8 ± 0.2 mm and weight is 63.2 ± 8.4 mg. In addition, among various types of waste plastics, PS was chosen because of their higher abundance than others in the coastal sea waters, which also posed a threat to the growth of *S. esculenta* larvae (Pedrotti et al., 2016). Moreover, the smaller the size of the NPs, the easier it is to enter into biological body, even cells. The 50-nm-diameter PS-NPs have been confirmed to cross the intestinal barrier of *Dicentrarchus labrax* after 15 min of exposure (Vagner et al., 2022). Alvarez-Román et al. found that carboxylated PS-NPs (20 nm) could across skin barrier of porcine ear in 2 h (Alvarez-Román et al., 2004). For analyzing the impact of PS-NPs on *S. esculenta* larvae in a short period of time, we selected high concentrations of beads with a diameter of 50 nm. Although the effects of PS-NPs were caused by high concentration, the results can still serve as a reference for further research.

4.1 Physiological response

Oxidative stress and even oxidative damage are common in various organisms exposed to NPs, such as mammalian cells, *Danio rerio*, *D. pulex*, and *M. galloprovincialis* (Sarasamma et al., 2020; Liu et al., 2021a; Banerjee and Shelver, 2021; Gonçalves et al., 2022). The occurrence of oxidative stress is triggered by high doses of reactive

oxygen species (ROS, like superoxide anion). The removal of ROS in aerobic organisms relies on antioxidant systems. SOD, an important member of the antioxidant enzyme system, has the ability of catalyzing the disproportionation of superoxide anion to hydrogen peroxide, and is used as a biomarker for oxidative stress (Fukai and Ushio-Fukai, 2011). Studies have shown that NPs can enter cells through internalization pathways, causing raise of ROS production and SOD activity, and even directly binding to SOD to alter its activity (Schröter and Ventura, 2022; Wang et al., 2022). In addition, the increase of ROS production could lead to lipid peroxidation. The metabolomics analysis results confirmed that the metabolism of membrane lipids in *Sinonovacula constricta* was affected by acute exposure to PS-NPs (Jiang and Zhang, 2021). MDA, a biomarker of oxidative stress, is an important membrane lipid peroxidation product and can also intensify membrane damage (Sillero-Ríos et al., 2018). After exposure of PS-NPs, SOD activity significantly enhanced, indicating an increase in ROS production. This result is consistent with the improvement of SOD activity in the *Ietalurus punetaus* larvae and in the gills and digestive glands of *Mytilus* spp. caused by acute exposure to NPs (Cole et al., 2020; Jiang et al., 2022). Moreover, the improvement of MDA level suggested the occurrence of membrane lipid oxidation. Research has found that SOD activity and MDA levels also increased in intestine of *A. fangsiao* after exposure to high concentrations of MPs (Zheng et al., 2022). These results indicated that acute exposure to high concentration of PS-NPs can disrupt the redox balance and cause oxidative stress response, which reminded us the hazards of acute exposure to high concentrations of NPs.

4.2 mRNA level response

Transcriptome analysis is widely used in the study of molecular level in biology along with the development of sequencing technologies. In recent years, transcriptome analysis has gradually been applied in the toxicology research of NPs on aquatic organisms, such as *B. plicatilis*, *D. pulex*, *Isognomon alatus*, *Mytilus coruscus*, *Cherax quadricarinatus*, *C. robusta*, *D. rerio*, *Oreochromis mossambicus*, *I. punetaus* (Liu et al., 2021a; Pang et al., 2021; Arini et al., 2022; Yu et al., 2022b; Cheng et al., 2022; Jiang et al., 2022; Shin and Jeong, 2022; Eliso et al., 2023; Qi et al., 2023). To research the effect of NPs on the molecular level of *S. esculenta* larvae, we applied RNA-Seq technology in this research.

4.2.1 Translation related signaling pathways and genes

Oxidative stress can influence various biological processes, such as protein synthesis. Proteomic analysis showed that exposure to NPs had an impact on the expression of *D. pulex* proteins (Liu et al., 2021b). The ribosomes, which is composed of ribosomal proteins and ribosomal RNA (rRNA), play a crucial role in cellular protein synthesis. Therefore, the ribosome biogenesis is crucial during the growth and development of organisms. Meanwhile, the ribosome biogenesis, as the most costly cellular process, must be heavily regulated and respond rapidly to stress (such as oxidative stress) or environmental cues (Piazzi et al., 2019). KEGG enrichment analysis of DEGs indicated significant enrichment of Ribosome and Ribosome biogenesis in eukaryotes signaling pathways (Table 1), which is similar to the results of KEGG enrichment analysis in *B. plicatilis* (Shin and Jeong, 2022). This indicates that the ribosome biogenesis of *S. esculenta* larvae did respond to oxidative stress caused by PS-NPs exposure. The eukaryotic ribosome is composed of a large subunit (consisting of 47 Rpls and rRNA of 25S, 5.8S and 5S) and a small subunit (comprising 33 Rpses and 18S rRNA) (Baßler and Hurt, 2019). As shown in Table 2, multiple key genes encoding ribosomal proteins (including *RPL5*, *RPL9*, *RPL10*, *RPL19*, *RPS5*, *RPS9*, *RPS 20* and *RPS3A1*) and mitochondrial ribosomal proteins (containing *MRPL4*, *MRPS11*, *MRPL1*, *MRPL15*, *MRPL3*, *MRPS14*, *MRPS10*, *MRPL12*, *MRPL17*, *MRPL19*, *MRPL23* and *MRPL32*) were screened. In addition, the expression of the above genes was reduced (Figure 2). This suggests that *S. esculenta* larvae respond with oxidative stress induced by PS-NPs exposure by reducing ribosome biogenesis to avoid excessive energy consumption.

4.2.2 Proteasome signaling pathway

Oxidative stress can caused protein oxidation, resulting in protein structure damage. Besides, NPs were reported to interact with proteins to change or even damage protein structures (Hollóczki and Gehrke, 2019; Jiang et al., 2022). To maintain cellular functions, the changed or damaged proteins need to be repaired or removal. The physiological process of protein degradation that consumes vast amounts of energy is mostly regulated by ubiquitin-proteasome system in eukaryotes (Budenholzer et al., 2017). The proteasome is distributed extensively in the cytoplasm and nucleus and is responsible for eliminating damaged proteins (Breusing and Grune, 2008). In *I. punetaus* exposed to PS-NPs, transcriptomic and metabolomics analysis results showed that the response of proteasomes was induced and the contents of energy metabolites were reduced (Jiang et al., 2022). In this study, proteasome signaling pathway was also enriched (Table 1). While the key genes related to proteasome synthesis were downregulated (Figure 3), which indicated that the process of protein degradation was inhibited by reducing the number of proteasome. Additionally, studies have demonstrated that the protein degradation of proteasome mediated decreased at high level of oxidative stress (Breusing and Grune, 2008). These indicate that *S. esculenta* larvae suppress protein degradation process and retain energy by reducing proteasome number to cope with PS-NPs exposure and strong oxidative stress caused.

4.2.3 MAPK signaling pathway

The MAPK signaling pathway plays a critical role in mediating cell functions, for instance, adaptation to various stress. Researches have demonstrated that the MAPK signaling pathway was activated by oxidative stress to trigger inflammation, apoptosis, autophagy, etc (Kim and Choi, 2015). PS-NPs were shown to induce oxidative stress and activate the MAPK signaling pathway in *Monopterus albus* and *Mus musculus* spleen (Tang et al., 2022; Zhu et al., 2023). ROS are considered an important physiological modulator of MAPK signaling pathway. A study found that PS-NPs exposure induced an increase in ROS and activated the expression of genes in the antioxidant system mediated by MAPK-HIF-1/NFκB signaling pathway in *D. pulex* (Liu et al., 2020). In addition, the research showed that NPs exposure caused the activation of components of p38 MAPK signaling pathway in *M. galloprovincialis* hemocytes (Canesi et al., 2016). In *Caenorhabditis elegans*, p38 MAPK signaling pathway was reported to be activated and mediated the protective

response to NPs (Qu et al., 2019). And the modulation of genes involved in the MAPK signaling pathway by NPs has been reported in *Paracentrotus lividus* (Della Torre et al., 2014). In the KEGG enrichment analysis results of this study, MAPK signaling pathway was also obtained (Table 1), implying that this signaling pathway played a role in the adaptation to oxidative stress induce by PS-NPs in *S. esculenta* larvae.

5 Conclusion

Oxidative stress is a common biological response caused by NPs exposure. In this study, even acute exposure of *S. esculenta* larvae to high concentration PS-NPs could lead to oxidative stress response. In addition, transcriptome analysis showed that translation related ribosome and ribosome biogenesis signaling pathway, protein degradation related proteasome pathway, and adapting to stress related MAPK signaling pathway were obtained. These results provide new references to understand the mechanisms of oxidative stress response induced by NPs.

Data availability statement

The datasets presented in this study can be found in online repositories. The names of the repository/repositories and accession number(s) can be found below: https://www.ncbi.nlm.nih.gov/bioproject/PRJNA947123.

Ethics statement

The animal study was approved by the Institutional Animal Care and Use Committee of the Ludong University (protocol number LDU-IRB20210308NXY). The study was conducted in accordance with the local legislation and institutional requirements.

Author contributions

XL: concentration, methodology, and writing-original draft. JY: funding acquisition, resources, and supervision. ZL: concentration, methodology, and writing-review and editing. All authors contributed to the article and approved the submitted version.

Funding

This research was funded by the Ministry of Agriculture of the People's Republic of China (CARS-49).

Conflict of interest

The authors declare that the research was conducted in the absence of any commercial or financial relationships that could be construed as a potential conflict of interest.

Publisher's note

All claims expressed in this article are solely those of the authors and do not necessarily represent those of their affiliated organizations, or those of the publisher, the editors and the reviewers. Any product that may be evaluated in this article, or claim that may be made by its manufacturer, is not guaranteed or endorsed by the publisher.

Supplementary material

The Supplementary Material for this article can be found online at: https://www.frontiersin.org/articles/10.3389/fphys.2023.1250513/full#supplementary-material

References

Alvarez-Román, R., Naik, A., Kalia, Y. N., Guy, R. H., and Fessi, H. (2004). Skin penetration and distribution of polymeric nanoparticles. *J. Control Release* 99, 53–62. doi:10.1016/j.jconrel.2004.06.015

Arini, A., Gigault, J., Venel, Z., Bertucci, A., and Baudrimont, M. (2022). The underestimated toxic effects of nanoplastics coming from marine sources: A demonstration on oysters (Isognomon alatus). *Chemosphere* 295, 133824. doi:10.1016/j.chemosphere.2022.133824

Banerjee, A., and Shelver, W. L. (2021). Micro- and nanoplastic induced cellular toxicity in mammals: A review. *Sci. Total Environ.* 755, 142518. doi:10.1016/j.scitotenv.2020.142518

Baßler, J., and Hurt, E. (2019). Eukaryotic ribosome assembly. *Annu. Rev. Biochem.* 88, 281–306. doi:10.1146/annurev-biochem-013118-110817

Breusing, N., and Grune, T. (2008). Regulation of proteasome-mediated protein degradation during oxidative stress and aging. *Biol. Chem.* 389, 203–209. doi:10.1515/BC.2008.029

Budenholzer, L., Cheng, C. L., Li, Y., and Hochstrasser, M. (2017). Proteasome structure and assembly. *J. Mol. Biol.* 429, 3500–3524. doi:10.1016/j.jmb.2017.05.027

Canesi, L., Ciacci, C., Fabbri, R., Balbi, T., Salis, A., Damonte, G., et al. (2016). Interactions of cationic polystyrene nanoparticles with marine bivalve hemocytes in a physiological environment: Role of soluble hemolymph proteins. *Environ. Res.* 150, 73–81. doi:10.1016/j.envres.2016.05.045

Capanni, F., Greco, S., Tomasi, N., Giulianini, P. G., and Manfrin, C. (2021). Orally administered nano-polystyrene caused vitellogenin alteration and oxidative stress in the red swamp crayfish (*Procambarus clarkii*). *Sci. Total Environ.* 791, 147984. doi:10.1016/j.scitotenv.2021.147984

Cheng, H., Dai, Y., Ruan, X., Duan, X., Zhang, C., Li, L., et al. (2022). Effects of nanoplastic exposure on the immunity and metabolism of red crayfish (Cherax quadricarinatus) based on high-throughput sequencing. *Ecotoxicol. Environ. Saf.* 245, 114114. doi:10.1016/j.ecoenv.2022.114114

Cole, M., Liddle, C., Consolandi, G., Drago, C., Hird, C., Lindeque, P. K., et al. (2020). Microplastics, microfibres and nanoplastics cause variable sub-lethal responses in mussels (Mytilus spp). *Mar. Pollut. Bull.* 160, 111552. doi:10.1016/j.marpolbul.2020.111552

Della Torre, C., Bergami, E., Salvati, A., Faleri, C., Cirino, P., Dawson, K. A., et al. (2014). Accumulation and embryotoxicity of polystyrene nanoparticles at early stage of development of sea urchin embryos *Paracentrotus lividus*. *Environ. Sci. Technol.* 48, 12302–12311. doi:10.1021/es502569w

Eliso, M. C., Bergami, E., Bonciani, L., Riccio, R., Belli, G., Belli, M., et al. (2023). Application of transcriptome profiling to inquire into the mechanism of nanoplastics toxicity during Ciona robusta embryogenesis. *Environ. Pollut.* 318, 120892. doi:10.1016/j.envpol.2022.120892

Ferreira, G. V. B., Justino, A. K. S., Eduardo, L. N., Lenoble, V., Fauvelle, V., Schmidt, N., et al. (2022). Plastic in the inferno: Microplastic contamination in deep-sea cephalopods (Vampyroteuthis infernalis and Abralia veranyi) from the southwestern Atlantic. *Mar. Pollut. Bull.* 174, 113309. doi:10.1016/j.marpolbul.2021.113309

Ferreira, I., Venâncio, C., Lopes, I., and Oliveira, M. (2019). Nanoplastics and marine organisms: What has been studied? *Environ. Toxicol. Pharmacol.* 67, 1–7. doi:10.1016/j.etap.2019.01.006

Fukai, T., and Ushio-Fukai, M. (2011). Superoxide dismutases: Role in redox signaling, vascular function, and diseases. *Antioxid. Redox Signal* 15, 1583–1606. doi:10.1089/ars.2011.3999

Geyer, R., Jambeck, J. R., and Law, K. L. (2017). Production, use, and fate of all plastics ever made. *Sci. Adv.* 3, e1700782. doi:10.1126/sciadv.1700782

Gigault, J., Halle, A. T., Baudrimont, M., Pascal, P. Y., Gauffre, F., Phi, T. L., et al. (2018). Current opinion: What is a nanoplastic? *Environ. Pollut.* 235, 1030–1034. doi:10.1016/j.envpol.2018.01.024

Gonçalves, J. M., Sousa, V. S., Teixeira, M. R., and Bebianno, M. J. (2022). Chronic toxicity of polystyrene nanoparticles in the marine mussel *Mytilus galloprovincialis*. *Chemosphere* 287, 132356. doi:10.1016/j.chemosphere.2021.132356

Gong, Y., Wang, Y., Chen, L., Li, Y., Chen, X., and Liu, B. (2021). Microplastics in different tissues of a pelagic squid (Dosidicus gigas) in the northern Humboldt Current ecosystem. *Mar. Pollut. Bull.* 169, 112509. doi:10.1016/j.marpolbul.2021.112509

Han, M., Gao, T., Liu, G., Zhu, C., Zhang, T., Sun, M., et al. (2022). The effect of a polystyrene nanoplastic on the intestinal microbes and oxidative stress defense of the freshwater crayfish, *Procambarus clarkii*. *Sci. Total Environ.* 833, 155722. doi:10.1016/j.scitotenv.2022.155722

Hollóczki, O., and Gehrke, S. (2019). Nanoplastics can change the secondary structure of proteins. *Sci. Rep.* 9, 16013. doi:10.1038/s41598-019-52495-w

Jiang, Q., Chen, X., Jiang, H., Wang, M., Zhang, T., and Zhang, W. (2022). Effects of acute exposure to polystyrene nanoplastics on the channel catfish larvae: Insights from energy metabolism and transcriptomic analysis. *Front. Physiol.* 13, 923278. doi:10.3389/fphys.2022.923278

Jiang, Q., and Zhang, W. (2021). Gradual effects of gradient concentrations of polystyrene nanoplastics on metabolic processes of the razor clams. *Environ. Pollut.* 287, 117631. doi:10.1016/j.envpol.2021.117631

Jiao, X., Sherman, B. T., Huang, W., Stephens, R., Baseler, M. W., Lane, H. C., et al. (2012). DAVID-WS: A stateful web service to facilitate gene/protein list analysis. *Bioinformatics* 28, 1805–1806. doi:10.1093/bioinformatics/bts251

Kim, E. K., and Choi, E. J. (2015). Compromised MAPK signaling in human diseases: An update. *Arch. Toxicol.* 89, 867–882. doi:10.1007/s00204-015-1472-2

Kumar, R., Manna, C., Padha, S., Verma, A., Sharma, P., Dhar, A., et al. (2022). Micro(nano)plastics pollution and human health: How plastics can induce carcinogenesis to humans? *Chemosphere* 298, 134267. doi:10.1016/j.chemosphere.2022.134267

Lebordais, M., Gutierrez-Villagomez, J. M., Gigault, J., Baudrimont, M., and Langlois, V. S. (2021). Molecular impacts of dietary exposure to nanoplastics combined with arsenic in Canadian oysters (*Crassostrea virginica*) and bioaccumulation comparison with Caribbean oysters (Isognomon alatus). *Chemosphere* 277, 130331. doi:10.1016/j.chemosphere.2021.130331

Leslie, H. A., van Velzen, M. J. M., Brandsma, S. H., Vethaak, A. D., Garcia-Vallejo, J. J., and Lamoree, M. H. (2022). Discovery and quantification of plastic particle pollution in human blood. *Environ. Int.* 163, 107199. doi:10.1016/j.envint.2022.107199

Li, Z., Feng, C., Pang, W., Tian, C., and Zhao, Y. (2021). Nanoplastic-induced genotoxicity and intestinal damage in freshwater benthic clams (Corbicula fluminea): Comparison with microplastics. *ACS Nano* 15, 9469–9481. doi:10.1021/acsnano.1c02407

Li, Z., Feng, C., Wu, Y., and Guo, X. (2020). Impacts of nanoplastics on bivalve: Fluorescence tracing of organ accumulation, oxidative stress and damage. *J. Hazard Mater* 392, 122418. doi:10.1016/j.jhazmat.2020.122418

Li, Z., and Han, Z. (2022). Transcriptional response of short-term nanoplastic exposure in Monodonta labio. *Mar. Pollut. Bull.* 182, 114005. doi:10.1016/j.marpolbul.2022.114005

Liu, X., Li, Z., Wu, W., Liu, Y., Liu, J., He, Y., et al. (2017). Sequencing-based network analysis provides a core set of gene resource for understanding kidney immune response against Edwardsiella tarda infection in Japanese flounder. *Fish. Shellfish Immunol.* 67, 643–654. doi:10.1016/j.fsi.2017.06.051

Liu, Z., Huang, Y., Jiao, Y., Chen, Q., Wu, D., Yu, P., et al. (2020). Polystyrene nanoplastic induces ROS production and affects the MAPK-HIF-1/NFkB-mediated antioxidant system in *Daphnia pulex*. *Aquat. Toxicol.* 220, 105420. doi:10.1016/j.aquatox.2020.105420

Liu, Z., Li, Y., Pérez, E., Jiang, Q., Chen, Q., Jiao, Y., et al. (2021a). Polystyrene nanoplastic induces oxidative stress, immune defense, and glycometabolism change in *Daphnia pulex*: Application of transcriptome profiling in risk assessment of nanoplastics. *J. Hazard Mater* 402, 123778. doi:10.1016/j.jhazmat.2020.123778

Liu, Z., Li, Y., Sepúlveda, M. S., Jiang, Q., Jiao, Y., Chen, Q., et al. (2021b). Development of an adverse outcome pathway for nanoplastic toxicity in *Daphnia pulex* using proteomics. *Sci. Total Environ.* 766, 144249. doi:10.1016/j.scitotenv.2020.144249

Love, M. I., Huber, W., and Anders, S. (2014). Moderated estimation of fold change and dispersion for RNA-seq data with DESeq2. *Genome Biol.* 15, 550. doi:10.1186/s13059-014-0550-8

Narancic, T., and O'Connor, K. E. (2019). Plastic waste as a global challenge: Are biodegradable plastics the answer to the plastic waste problem? *Microbiol. Read.* 165, 129–137. doi:10.1099/mic.0.000749

Oliveira, A. R., Sardinha-Silva, A., Andrews, P. L. R., Green, D., Cooke, G. M., Hall, S., et al. (2020). Microplastics presence in cultured and wild-caught cuttlefish, Sepia officinalis. *Mar. Pollut. Bull.* 160, 111553. doi:10.1016/j.marpolbul.2020.111553

Pang, M., Wang, Y., Tang, Y., Dai, J., Tong, J., and Jin, G. (2021). Transcriptome sequencing and metabolite analysis reveal the toxic effects of nanoplastics on tilapia after exposure to polystyrene. *Environ. Pollut.* 277, 116860. doi:10.1016/j.envpol.2021.116860

Parkhomchuk, D., Borodina, T., Amstislavskiy, V., Banaru, M., Hallen, L., Krobitsch, S., et al. (2009). Transcriptome analysis by strand-specific sequencing of complementary DNA. *Nucleic Acids Res.* 37, e123. doi:10.1093/nar/gkp596

Pedà, C., Longo, F., Berti, C., Laface, F., De Domenico, F., Consoli, P., et al. (2022). The waste collector: Information from a pilot study on the interaction between the common octopus (*Octopus vulgaris*, cuvier, 1797) and marine litter in bottom traps fishing and first evidence of plastic ingestion. *Mar. Pollut. Bull.* 174, 113185. doi:10.1016/j.marpolbul.2021.113185

Pedrotti, M. L., Petit, S., Elineau, A., Bruzaud, S., Crebassa, J. C., Dumontet, B., et al. (2016). Changes in the floating plastic pollution of the mediterranean sea in relation to the distance to land. *PLoS One* 11, e0161581. doi:10.1371/journal.pone.0161581

Piazzi, M., Bavelloni, A., Gallo, A., Faenza, I., and Blalock, W. L. (2019). Signal transduction in ribosome biogenesis: A recipe to avoid disaster. *Int. J. Mol. Sci.* 20, 2718. doi:10.3390/ijms20112718

Porta, R. (2021). Anthropocene, the plastic age and future perspectives. *FEBS Open Bio* 11, 948–953. doi:10.1002/2211-5463.13122

Qi, P., Qiu, L., Feng, D., Gu, Z., Guo, B., and Yan, X. (2023). Distinguish the toxic differentiations between acute exposure of micro- and nano-plastics on bivalves: An integrated study based on transcriptomic sequencing. *Aquat. Toxicol.* 254, 106367. doi:10.1016/j.aquatox.2022.106367

Qu, M., Liu, Y., Xu, K., and Wang, D. (2019). Activation of p38 MAPK signaling-mediated endoplasmic reticulum unfolded protein response by nanopolystyrene particles. *Adv. Biosyst.* 3, e1800325. doi:10.1002/adbi.201800325

Rio, D. C., Ares, M., Jr, Hannon, G. J., and Nilsen, T. W. (2010). Purification of RNA using TRIzol (TRI reagent). *Cold Spring Harb. Protoc.* 2010, prot5439. doi:10.1101/pdb.prot5439

Rist, S., Baun, A., Almeda, R., and Hartmann, N. B. (2019). Ingestion and effects of micro- and nanoplastics in blue mussel (*Mytilus edulis*) larvae. *Mar. Pollut. Bull.* 140, 423–430. doi:10.1016/j.marpolbul.2019.01.069

Sarasamma, S., Audira, G., Siregar, P., Malhotra, N., Lai, Y. H., Liang, S. T., et al. (2020). Nanoplastics cause neurobehavioral impairments, reproductive and oxidative damages, and biomarker responses in zebrafish: Throwing up alarms of wide spread health risk of exposure. *Int. J. Mol. Sci.* 21, 1410. doi:10.3390/ijms21041410

Schröter, L., and Ventura, N. (2022). Nanoplastic toxicity: Insights and challenges from experimental model systems. *Small* 18, e2201680. doi:10.1002/smll.202201680

Sendra, M., Sparaventi, E., Novoa, B., and Figueras, A. (2021). An overview of the internalization and effects of microplastics and nanoplastics as pollutants of emerging concern in bivalves. *Sci. Total Environ.* 753, 142024. doi:10.1016/j.scitotenv.2020.142024

Shin, H., and Jeong, C. B. (2022). Metabolism deficiency and oxidative stress induced by plastic particles in the rotifer *Brachionus plicatilis*: Common and distinct phenotypic and transcriptomic responses to nano- and microplastics. *Mar. Pollut. Bull.* 182, 113981. doi:10.1016/j.marpolbul.2022.113981

Sillero-Ríos, J., Sureda, A., Capó, X., Oliver-Codorniú, M., and Arechavala-Lopez, P. (2018). Biomarkers of physiological responses of *Octopus vulgaris* to different coastal environments in the western Mediterranean Sea. *Mar. Pollut. Bull.* 128, 240–247. doi:10.1016/j.marpolbul.2018.01.032

Sodowich, B. I., Fadl, I., and Burns, C. (2007). Method validation of *in vitro* RNA transcript analysis on the Agilent 2100 Bioanalyzer. *Electrophoresis* 28, 2368–2378. doi:10.1002/elps.200600673

Statista Research Department (2023). *Global plastic production (1950–2021)*. Available at: https://www.statista.com/statistics/282732/global-production-of-plastics-since-1950 (Accessed March 24, 2023).

Stegmann, P., Daioglou, V., Londo, M., van Vuuren, D. P., and Junginger, M. (2022). Plastic futures and their CO_2 emissions. *Nature* 612, 272–276. doi:10.1038/s41586-022-05422-5

Szklarczyk, D., Gable, A. L., Lyon, D., Junge, A., Wyder, S., Huerta-Cepas, J., et al. (2019). STRING v11: Protein-protein association networks with increased coverage, supporting functional discovery in genome-wide experimental datasets. *Nucleic Acids Res.* 47, D607–D613. doi:10.1093/nar/gky1131

Tallec, K., Huvet, A., Di Poi, C., González-Fernández, C., Lambert, C., Petton, B., et al. (2018). Nanoplastics impaired oyster free living stages, gametes and embryos. *Environ. Pollut.* 242, 1226–1235. doi:10.1016/j.envpol.2018.08.020

Tang, R., Zhu, D., Luo, Y., He, D., Zhang, H., El-Naggar, A., et al. (2023). Nanoplastics induce molecular toxicity in earthworm: Integrated multi-omics, morphological, and intestinal microorganism analyses. *J. Hazard Mater* 442, 130034. doi:10.1016/j.jhazmat.2022.130034

Tang, X., Fan, X., Xu, T., He, Y., Chi, Q., Li, Z., et al. (2022). Polystyrene nanoplastics exacerbated lipopolysaccharide-induced necroptosis and inflammation via the ROS/MAPK pathway in mice spleen. *Environ. Toxicol.* 37, 2552–2565. doi:10.1002/tox.23618

Vagner, M., Boudry, G., Courcot, L., Vincent, D., Dehaut, A., Duflos, G., et al. (2022). Experimental evidence that polystyrene nanoplastics cross the intestinal barrier of European seabass. *Environ. Int.* 166, 107340. doi:10.1016/j.envint.2022.107340

Wang, J. H., and Zheng, X. D. (2017). Comparison of the genetic relationship between nine Cephalopod species based on cluster analysis of karyotype evolutionary distance. *Comp. Cytogenet* 11, 477–494. doi:10.3897/CompCytogen.v11i3.12752

Wang, X., Zhang, Q., Zhang, T., Shao, S., Wang, Q., Dong, Z., et al. (2023). Evaluation of antioxidant capacity and digestive enzyme activities in *Mytilus galloprovincialis* exposed to nanoplastics under different patterns of hypoxia. *Mar. Environ. Res.* 183, 105849. doi:10.1016/j.marenvres.2022.105849

Wang, Y., Shi, H., Li, T., Yu, L., Qi, Y., Tian, G., et al. (2022). Size-dependent effects of nanoplastics on structure and function of superoxide dismutase. *Chemosphere* 309, 136768. doi:10.1016/j.chemosphere.2022.136768

Wu, C., Guo, W. B., Liu, Y. Y., Yang, L., and Miao, A. J. (2021). Perturbation of calcium homeostasis and multixenobiotic resistance by nanoplastics in the ciliate Tetrahymena thermophila. *J. Hazard Mater* 403, 123923. doi:10.1016/j.jhazmat.2020.123923

Yu, J., Chen, L., Gu, W., Liu, S., and Wu, B. (2022b). Heterogeneity effects of nanoplastics and lead on zebrafish intestinal cells identified by single-cell sequencing. *Chemosphere* 289, 133133. doi:10.1016/j.chemosphere.2021.133133

Yu, J., Huang, W., Wang, Y., Wang, Y., Cao, L., Yang, Z., et al. (2022a). Microplastic pollution in the environment and organisms of Xiangshan Bay, East China Sea: An area of intensive mariculture. *Water Res.* 212, 118117. doi:10.1016/j.watres.2022.118117

Zhao, Z., Wang, X., Jiang, J., Dong, Y., Pan, Y., Guan, X., et al. (2023). Adverse effects of polystyrene nanoplastics on sea cucumber Apostichopus japonicus and their association with gut microbiota dysbiosis. *Chemosphere* 330, 138568. doi:10.1016/j.chemosphere.2023.138568

Zheng, J., Li, C., and Zheng, X. (2022). Toxic effects of polystyrene microplastics on the intestine of Amphioctopus fangsiao (Mollusca: Cephalopoda): From physiological responses to underlying molecular mechanisms. *Chemosphere* 308, 136362. doi:10.1016/j.chemosphere.2022.136362

Zhu, C., Zhou, W., Han, M., Yang, Y., Li, Y., Jiang, Q., et al. (2023). Dietary polystyrene nanoplastics exposure alters hepatic glycolipid metabolism, triggering inflammatory responses and apoptosis in *Monopterus albus*. *Sci. Total Environ.* 891, 164460. doi:10.1016/j.scitotenv.2023.164460

frontiers | Frontiers in Physiology

TYPE Original Research
PUBLISHED 31 August 2023
DOI 10.3389/fphys.2023.1248999

OPEN ACCESS

EDITED BY
Yi-Feng Li,
Shanghai Ocean University, China

REVIEWED BY
Chunyan Zhao,
Qingdao Agricultural University, China
Yao Zheng,
Chinese Academy of Fishery Sciences, China

*CORRESPONDENCE
Tingting Shu,
18778004858@163.com
Jing Yang,
yang_jing7@ctg.com.cn

RECEIVED 28 June 2023
ACCEPTED 14 August 2023
PUBLISHED 31 August 2023

CITATION
Shu T, Chen Y, Xiao K, Huang H, Jia J, Yu Z, Jiang W and Yang J (2023), Effects of short-term water velocity stimulation on the biochemical and transcriptional responses of grass carp (*Ctenopharyngodon idellus*). *Front. Physiol.* 14:1248999. doi: 10.3389/fphys.2023.1248999

Effects of short-term water velocity stimulation on the biochemical and transcriptional responses of grass carp (*Ctenopharyngodon idellus*)

Tingting Shu[1,2]*, Yan Chen[1,2,3], Kan Xiao[1,2], Hongtao Huang[1,2], Jingyi Jia[4], Zhaoxi Yu[1,2], Wei Jiang[1,2] and Jing Yang[1,2]*

[1]Chinese Sturgeon Research Institute, China Three Gorges Corporation, Yichang, China, [2]Hubei Key Laboratory of Three Gorges Project for Conservation of Fishes, Yichang, China, [3]State Key Laboratory for Cellular Stress Biology, Innovation Centre for Cell Signaling Network, School of Life Sciences, Xiamen University, Xiamen, China, [4]Institute of Hydrobiology, Chinese Academy of Sciences, Wuhan, China

Since 2011, ecological operation trials of the Three Gorges Reservoir (TGR) have been continuously conducted to improve the spawning quantity of the four major Chinese carp species below the Gezhouba Dam. In particular, exploring the effects of short-term water velocity stimulation on ovarian development in grass carp (*Ctenopharyngodon idellus*) is essential to understand the response of natural reproduction to ecological flows. We performed ovary histology analysis and biochemical assays among individuals with or without stimulation by running water. Although there were no obvious effects on the ovarian development characteristics of grass carp under short-term water velocity stimulation, estradiol, progesterone, follicle-stimulating hormone (FSH), and triiodothyronine (T3) concentrations were elevated. Then, we further explored the ovarian development of grass carp under short-term water velocity stimulation by RNA sequencing of ovarian tissues. In total, 221 and 741 genes were up- or downregulated under short-term water velocity stimulation, respectively, compared to the control group. The majority of differentially expressed genes (DEGs) were enriched in pathways including ABC transporters, cytokine-cytokine receptor interaction, ECM-receptor interaction, and steroid hormone biosynthesis. Important genes including *gpr4*, *vtg1*, *C-type lectin*, *hsd17b1*, *cyp19a1a*, *cyp17a1*, and *rdh12* that are involved in ovarian development were regulated. Our results provide new insights and reveal potential regulatory genes and pathways involved in the ovarian development of grass carp under short-term water velocity stimulation, which may be beneficial when devising further ecological regulation strategies.

KEYWORDS

grass carp, water velocity, ovary, hormones, transcriptome

Introduction

Construction of hydraulic engineering not only significantly alters the natural hydrologic regime and water quality in the upstream and downstream of the dam (Poff and Schmidt, 2016; Chen et al., 2020), but also has undesirable ecological effects on aquatic species (Stone, 2016), and finally reduces the aquatic biodiversity (Liu et al., 2021). As the most severely

affected biota at the top of the aquatic food chain, fish are often chosen as indicator species for determining the health status of the riverine ecosystems (Gao et al., 2009; She et al., 2023). Dam operations affect the spawning activity of native fish species and thus threaten aquatic populations and communities (Barbarossa et al., 2020; Mouchlianitis et al., 2021), and have been reported on rivers all over the world, such as the Madeira River, the Snake River, and the Colorado River in foreign basins (Finch et al., 2015; Cella-Ribeiro et al., 2017; McClure et al., 2020), as well as the Yangtze River, the Jinsha River, the Pearl River, the Han River, the Gan River, and the Lancang-Mekong River in domestic basins (Zhang C. et al., 2019; Zhang P. et al., 2019).

Fish reproduction is likely triggered by a variety of environmental factors, including flow velocity, water temperature, photoperiod, and dissolved oxygen (King et al., 2016; Buddendorf et al., 2017; Fellman et al., 2019). These environmental factors have a complex impact on fish spawning behaviors and gonadal development through adjusting the biological process of hormone synthesis and secretion. Among these environmental factors, water flow velocity is a key environmental factor that affects spawning and fertilization for fishes delivering drifting eggs (Lechner et al., 2014). Moreover, water flow velocity plays a crucial role in determining nutrient retention and oxygen delivery during fish spawning (McDonnell, 2000). Additionally, water flow velocity also affects gonadal development. Stimulated by water flows, fish generate impulses into the hypothalamus through sensory organs, and stimulate gonadotropin-releasing hormone (GnRH) release that direct acts on GnRH nerve terminals (Liu et al., 2021). Besides, the weakening of the water flow stimulus will lead to a decline in gonadal development among fish, resulting in a reduction of spawning quantity in watersheds, and potentially causing long-term cumulative differences in the population structure of fish stocks (Zhang W. et al., 2019).

The four major Chinese carp species, including grass carp (*Ctenopharyngodon idellus*), silver carp (*Hypophthalmichthys molitrix*), bighead carp (*Hypophthalmichthys nobilis*), and black carp (*Mylopharyngodon piceus*), play important roles in Chinese aquaculture and capture fisheries (Cao et al., 2015). A spawning site from Yichang to Chenglingji, situated at the middle reaches of the Yangtze River, is one of the most important natural reproduction zones of these Chinese carps, which accounting for 42.7% of the total spawning capacity along the river (Guo et al., 2011; Li et al., 2013a). However, in recent decades, due to the remarkable changes in hydrological conditions caused by the impoundment of the Three Gorges Reservoir (TGR), spawning behaviors and sexual maturation process of the four carp species have been severely hindered (Chen et al., 2021). In 2003, the number of fish eggs and larvae was only 10% of that in 2002, when the TGR began operation (Xie and Chen, 2001; Li et al., 2013b). Previous studies showed that water flow velocity suitable for grass carp spawning and sexual maturation mainly ranged from 0.33 to 1.50 m/s (Lin et al., 2022). Thus, providing essential ecological flows is widely recognized as an effective means of maintaining ecological integrity and restoring habitats for the spawning of major fish species in rivers (Stamou et al., 2018; Yang et al., 2019). However, the physiological mechanism of the response of natural reproduction to ecological flows is still unclear.

In this study, we used sexually mature female grass carp to conduct laboratory experiments to explore the effect of flow velocity on gonadal development in fish. The objective of the present study was to understand how flow velocity affect the gonadal development of grass carp. Specifically, we sought to a) explore the effect of short-term flow velocity on biochemical response, and b) analyze the possible regulatory mechanism of short-term flow velocity on the gonadal development of female grass carp. Our findings will provide a scientific basis for riverine ecosystem protection of the Yangtze River.

Materials and methods

Fish

Sexually mature females (n = 30, body length of 70.56 ± 3.13 cm, body weight of 5.16 ± 0.85 kg) and males (n = 30, body length of 68.40 ± 3.03 cm, body weight of 4.45 ± 0.70 kg) of grass carp were collected from Tengda Ecological Agriculture Development Co., Ltd. in Zhijiang City, Hubei Province, China. The grass carps were domesticated in Chinese Sturgeon Research Institute for 2 weeks, kept in a recirculating aquaculture system under controlled temperature conditions (21°C ± 0.5°C) with constant aeration, and fed in excess duckweed twice a day prior to the experimental trials.

Experimental design

The experiment was performed in 20,000 L PVC circular tanks. Sixty grass carps were randomly divided into three groups with 10 females and 10 males, including the water velocity stimulation group, the hormone injection group, and the control group, labelled ZS, JS, and NS, respectively. Previous studies showed that suitable water flow velocity for grass carp spawning and sexual maturation mainly ranged from 0.33 to 1.50 m/s. However, even though ecological flows are provided, water mobility will weaken significantly in the middle and lower reaches of the Yangtze River. It was found that the flow velocity is rarely exceeding 0.5 m/s from April to June (Zhou et al., 2009; Wang et al., 2016; Liu et al., 2021). In some reservoir areas, the flow velocity cannot even reach 0.2 m/s (Xu et al., 2017). Therefore, we set a water velocity of 0.5 m/s in the ZS group. In the JS group, the females were injected with 2 mg/kg domperidone and 2.5 μg/kg LHRH-A2, at the base of the pectoral fin.

After 3 h, females were selected for sampling, including blood and ovaries. To avoid catching stress, fish were anesthetized by immersion with benzocaine (200 mg/L) (Geraylou et al., 2012; Wang et al., 2015), and then killed by a sharp blow to the head based on a previously described procedure (Hultmann et al., 2012). Blood samples were collected quickly from the caudal vein of each fish, then centrifuged at 3,000 g for 15 min at 4°C. The obtained serum samples were then transferred to −80°C for storage until enzyme linked immunosorbent assay (ELISA). Ovary tissues were also collected, and some of them were quickly fixed in 4% paraformaldehyde (PFA) in phosphate-buffered saline (PBS) at room temperature for 24 h for histological sections, and other ovaries were rapidly frozen in liquid nitrogen, then stored at −80°C until ELISA and RNA extraction.

Histological analyses (hematoxylin and eosin (H&E) staining)

The fixed ovaries were dehydrated in graded ethanol solutions, and infiltrated with xylene. The sectioning and staining procedures were performed as described in a previous study (Lau et al., 2016). Briefly, the samples were embedded and processed for paraffin sectioning using a Leica RM2235 microtome (Leica Biosystems, Germany). Paraffin sections of 5 μm in thickness were mounted on slides, deparaffinized, rehydrated, and washed with ultrapure water. After staining with H&E, dehydrated, and mounted, the sections were observed and imaged by a Nikon Eclipse Ni-U microscope (Nikon, Japan). Scale bars are provided in the lower right corner of each image.

Hormones measurement using ELISA

The concentrations of testosterone, estradiol, progesterone, and 17α,20β-dihydroxy-4-pregnen-3-one (DHP), as well as triiodothyronine (T3), thyroxine (T4), follicle-stimulating hormone (FSH), and luteinizing hormone (LH) in serum and ovaries were measured using commercial ELISA kits (mlbio, Shanghai). Briefly, 300 μL of serum was diluted to 500 μL with PBS, while 0.1 g ovary samples were isolated and homogenized in 1 mL PBS in a TGrinder H24R Tissue Homogenizer (TIANGEN, China). Following homogenization, the hormones were extracted with an organic solvent four times according to the manufacturer's instructions. The layers were allowed to separate by vortex and centrifugation. Then the organic phase was transferred to a fresh tube and evaporated by heating to 30°C under a gentle stream of nitrogen. Finally, the extracts were dissolved in 200 μL ELISA buffer and the hormone concentrations were measured according to the manufacturer's instructions.

Transcriptome analyses

The ovary samples from grass carp were isolated and homogenized in a TGrinder H24R Tissue Homogenizer (TIANGEN, China), and total RNA was extracted by TRIzol reagent (Ambion, America) following the manufacturer's instructions. RNA concentration was determined using NanoDrop One (Thermo Scientific, America), and the integrity and quality were assessed by RNA denaturing gel electrophoresis. High-quality RNA samples were selected for library construction. Using an Illumina NovaSeq 6000 system, RNA-Seq reads were generated by sequencing. Fastp (version 0.19.7) was used to generate clean reads. Then *de novo* assembly of clean reads was conducted with Trinity software (v2.6.6) and all assembled full-length sequences were named unigenes. All the unigenes were predicted and used for Blastx search and annotation against the NR, NT, KOG, SwissProt, PFAM, KEGG, and GO databases. After assembly, gene expression abundance was calculated using the Fragments Per Kilobase of transcript per Million mapped reads (FPKM) values. Differential expression analysis was performed using the DESeq2 package (v1.20.0) with a log2 fold change (FC) of 1.5 and a p-value cutoff of 0.05 ($|\log2FC| \geq 1.5$, $p < 0.05$). GO function enrichment analysis and KEGG pathway enrichment analysis of differential gene sets were implemented using the Bioconductor R package clusterProfiler (v 3.18.1).

Quantitative real-time PCR (qRT-PCR)

Independent RNA samples were extracted and used for cDNA synthesis for qRT-PCR to confirm the transcriptome results. RNA template with a content of 1.5 μg was used for reverse transcription to synthesize cDNA using the EasyScript® One-Step gDNA Removal and cDNA Synthesis SuperMix kit (TransGen Biotech, Beijing) according to the manufacturer's guidelines. All primers were designed using Primer-BLAST in the National Center for Biotechnology Information (NCBI), and the sequences are listed in Table 1. The primers for qRT-PCR were validated by agarose gel electrophoresis and DNA sequencing of PCR products. For amplification, the TransStart® Tip Green qPCR SuperMix (TransGen Biotech, Beijing) and StepOnePlus™ real-time system (ABI, America) were used. All mRNA levels were calculated as the fold expression relative to the housekeeping gene, *β-actin*, *ef1a*, and *gapdh* and expressed as a fold change compared to the control group. Each sample was run in triplicate repeats and data analysis was performed using the ΔΔCt method (Schmittgen and Livak, 2008).

Statistical analysis

Statistical analysis was performed with GraphPad Prism 8.0 software (GraphPad software, America). All results were presented as mean ± standard deviation (SD) in each experimental group. Differences were determined using one-way ANOVA followed by Fisher's least significant difference (LSD) test for multiple comparisons. For all statistical comparisons, $p < 0.05$ was considered statistically significant.

Results

Histopathology of ovary

To determine the maturation level of grass carp gonads, we examined dissected ovaries by histological sections with H&E staining. Well-differentiated ovaries were observed in all groups, occupied by many full-grown follicles with normal reproductive characteristics (Figure 1). After short-term water velocity stimulation and the hormone injection, respectively, the development characteristics were similar to those of the control group. Specifically, the yolk filled the ovaries. Oocytes were easily identified by their large spherical nucleoli, each of which contained numerous nucleoli and a large cytoplasmic region bordered by a visible cell membrane. Each oocyte was a different size and was surrounded by a thin follicular cell layer. Most follicular cells contained ovoid nuclei and were stained with black, indicating that the fish used was in the pre-spawning period. No substantial effect was observed in the histological sections of the JS and ZS groups when compared to the NS group.

10.3389/fphys.2023.1248999

TABLE 1 Primer Sequences Used for qRT-PCR Analysis.

Gene	Direction[a]	Primer sequences (5′to 3′)	Primer length (bp[b])	Amplicon length (bp)
cyp17a1	F	TGAGGAACACAAGGTGACCTACAG	24	109
	R	GACATCACGAGTGCTGCTG	19	
hsd17b1	F	GGCACCATCCGCACCA	16	111
	R	CTCGTTGAATGGCAAACCCT	20	
slc12a2	F	GTTGCTGAAGACCTCCGTCA	20	208
	R	TATCAAGTCCCTCTCGCAGT	20	
vtg1	F	GTGATGCACCTGCCCAGATTG	21	159
	R	CCTTGAACTGAGACCAGATAGCCTC	25	
β-*actin*	F	TGGACTCTGGTGATGGTGTGAC	22	247
	R	GAGGAAGAAGAGGCAGCGGTTC	22	
ef1a	F	AAAATTGGCGGTATTGGAAC	20	274
	R	TGATGACCTGGGCAGTGAA	19	
gapdh	F	CACCCATGGCAAGTACAAGG	20	151
	R	GACACCGGTAGACTCCACAA	20	

[a]F, forward; R, reverse.
[b]base pairs.

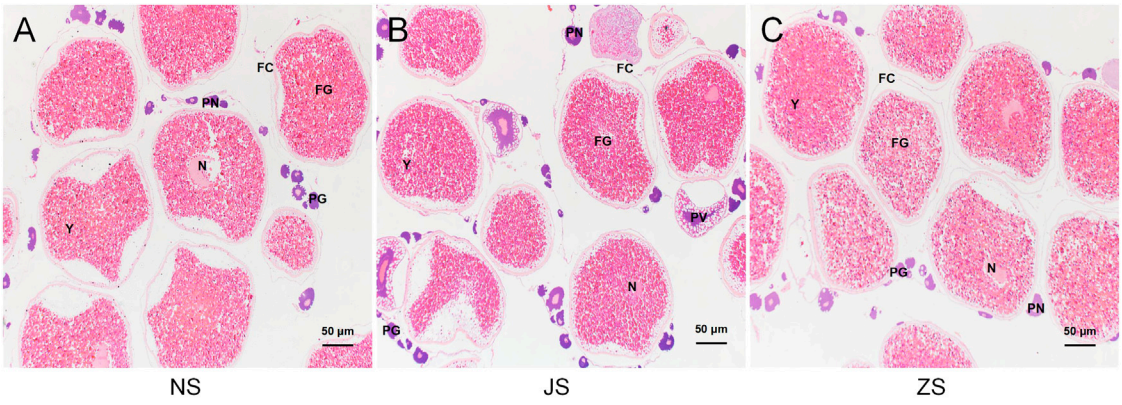

FIGURE 1
Histological sections of the ovarian status of grass carp. **(A)** NS group. **(B)** JS group. **(C)** ZS group. PG, primary growth follicle; PN, perinucleolar follicle; PV, previtellogenic follicle; FG, full-grown follicle; N, nucleus; Y, yolks; FC, follicle cells.

Measurement of hormone concentrations

The concentrations of several important sex steroids were measured in female grass carp. Serum and ovary testosterone concentrations did not differ among the three groups (Figures 2A,E). Serum and ovary estradiol, progesterone, as well as DHP concentrations were significantly higher in the JS group than those in the NS group (Figures 2B–D,F–H). However, only ovary estradiol and progesterone concentrations in the ZS group were significantly elevated (Figures 2F,G). Serum estradiol, progesterone, and DHP concentrations, as well as ovary DHP concentration in the ZS group were slightly increased, although there were not statistically significant (Figures 2B–D,H).

Meanwhile, we examined serum and ovary gonadotropins, FSH and LH, in female grass carp. Both serum and ovary FSH and LH concentrations in the JS group were significantly increased compared to the NS group (Figures 3A,B,E,F). However, only enhanced serum and ovary FSH concentrations were observed in the ZS group (Figures 3A,E). LH concentrations were also compared, but did not show any significant differences. (Figures 3B,F).

Serum and ovary T3 and T4 concentrations were also evaluated in female grass carp. We observed that serum and ovary

10.3389/fphys.2023.1248999

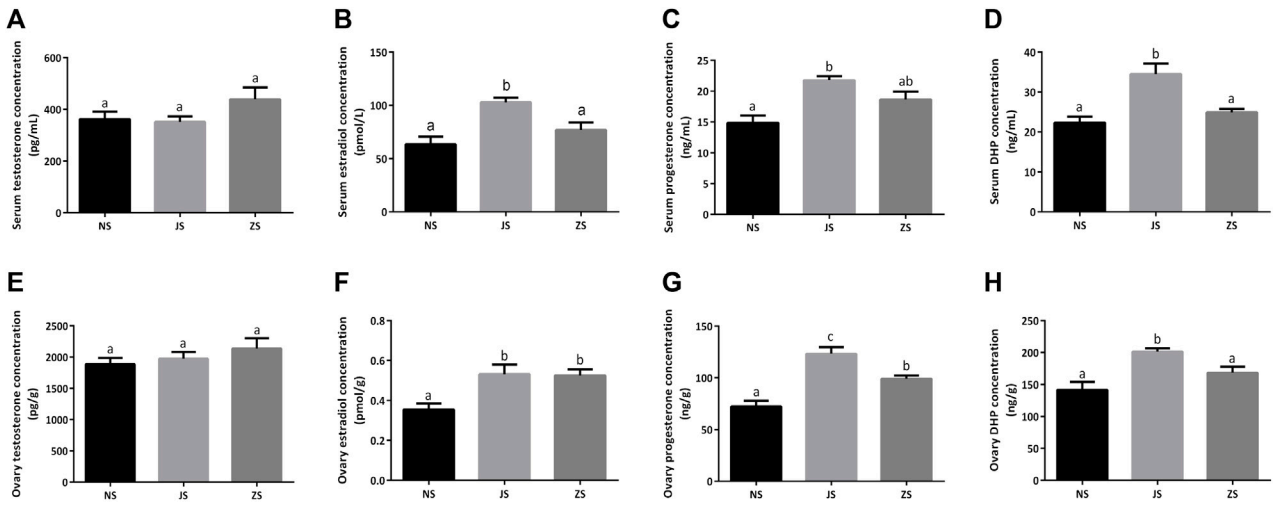

FIGURE 2
The sex steroid hormones measurements. Serum concentrations of testosterone **(A)**, estradiol **(B)**, progesterone **(C)**, and DHP **(D)** in the NS, JS, and ZS groups. Ovary concentrations of testosterone **(E)**, estradiol **(F)**, progesterone **(G)**, and DHP **(H)** in the NS, JS, and ZS groups. The letters in the bar charts represent significant differences.

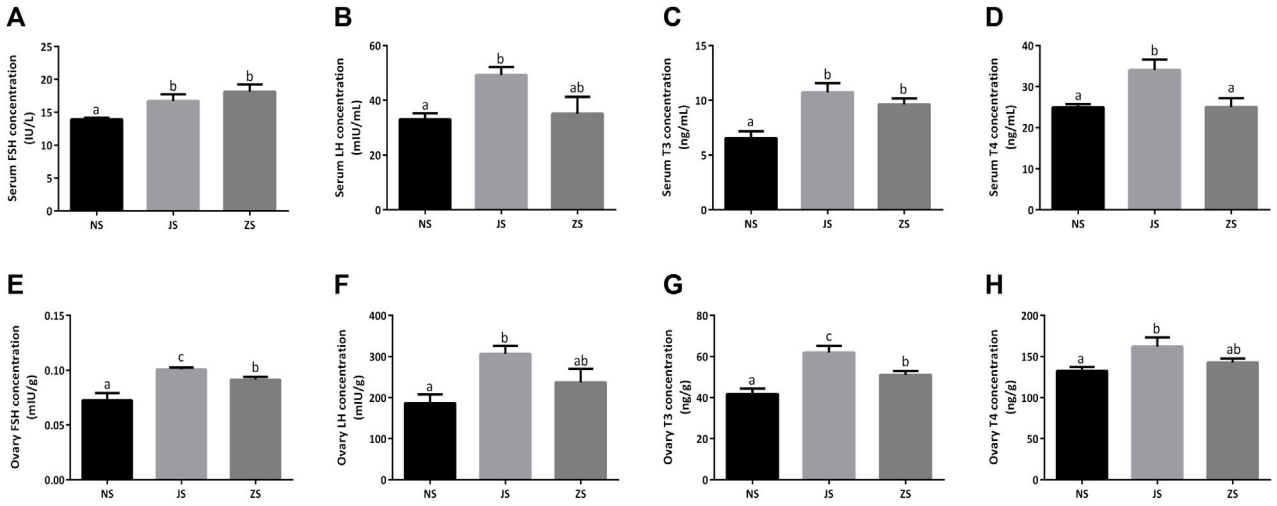

FIGURE 3
The gonadotropins and thyroid hormones measurements. Serum concentrations of FSH **(A)**, LH **(B)**, T3 **(C)**, and T4 **(D)** in the NS, JS, and ZS groups. Ovary concentrations of FSH **(E)**, LH **(F)**, T3 **(G)**, and T4 **(H)** in the NS, JS, and ZS groups. The letters in the bar charts represent significant differences.

T3 concentrations in the JS and ZS groups were significantly higher than that in the NS group while elevated serum and ovary T4 concentrations were only observed in the JS group (Figures 3C,D,G,H).

Overview of RNA-Seq

To identify the underlying molecular signaling pathways of short-term water velocity stimulation on the ovary transcriptional profile in grass carp, nine mRNA libraries were constructed and sequenced from NS, JS, and ZS ovary tissues using the Illumina NovaSeq 6000 system. All datasets from the Illumina sequencing platform are available in the NCBI Short Read Archive (SRA) database with the accession number (PRJNA977722). The main sequencing characteristics are listed in Table 2. A total length of 206,508,378 bp raw reads were obtained from the nine samples, and an average length of 21,593,012 bp clean reads were obtained from each sample after strict filtering. The Q20, Q30, and mapping rates for each group were within 96.90%–97.31%, 92.29%–93.18%, and 83.94%–85.97%, respectively, indicating that sequencing quality was

TABLE 2 Basic information of mRNA sequencing data of all samples in this study.

Sample	Raw reads	Clean reads	Q20 (%)	Q30 (%)	GC content (%)	Mapping ratio (%)
JS1	23,250,235	21,795,802	97.15	92.88	43.70	84.65
JS2	22,783,142	21,723,825	97.18	92.90	46.41	85.28
JS3	22,340,031	21,024,203	97.27	92.97	45.99	85.66
NS1	23,968,696	22,360,102	97.20	92.87	46.84	85.79
NS2	23,074,431	21,666,859	97.31	93.18	47.96	85.97
NS3	23,007,719	21,557,974	97.07	92.71	44.24	83.94
ZS1	23,045,475	21,720,377	97.04	92.62	45.22	84.70
ZS2	22,332,042	21,181,680	96.90	92.29	44.39	85.70
ZS3	22,706,607	21,306,290	97.19	92.91	45.47	84.48

TABLE 3 The statistics of annotation.

	Total unigenes	NR	NT	KOG	SwissProt	PFAM	GO	KEGG
Number of Unigenes	37,976	24,104	34,400	9,022	20,054	17,969	17,966	13,402
Percentage (%)	100	63.47	90.58	23.75	52.8	47.31	47.3	35.29

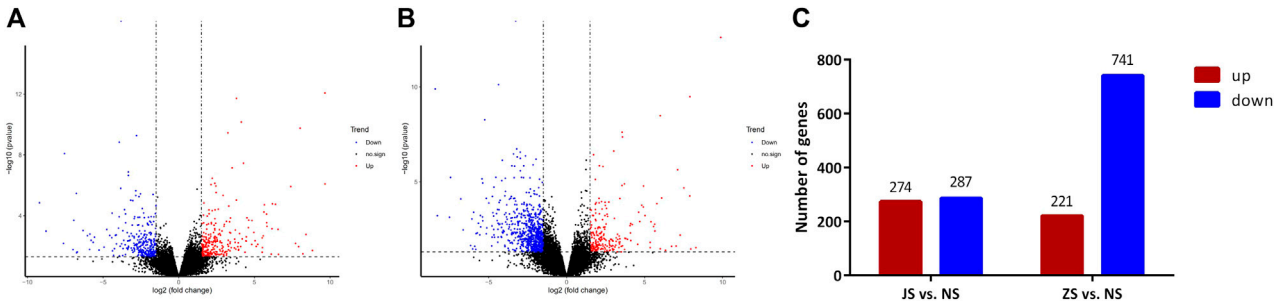

FIGURE 4
Volcano diagram of differential expression genes and numbers of DEGs in each comparison. **(A)** Volcano diagram of differential expression genes in JS vs. NS group. **(B)** Volcano diagram of differential expression genes in ZS vs. NS group. Significantly upregulated and downregulated genes are indicated in red and blue, respectively, and those not significantly different are in black. **(C)** The number of differentially expressed genes between different groups.

acceptable for further analysis. Totally, 37,976 unigenes were acquired from *de novo* assembly. All unigenes were annotated by seven databases, including NR, NT, KOG, SwissProt, PFAM, KEGG, and GO databases (Table 3).

Differentially expressed genes (DEGs) and pathway analysis

RNA sequencing analysis showed that the transcriptome profiles of JS and ZS groups were distinct from the NS group. Out of 21,248 annotated genes, we identified 561 differentially regulated genes between the JS and NS groups. Among the 561 regulated genes, 287 genes were highly expressed in the NS group while 274 genes were upregulated in the JS group (Figures 4A,C). Compared with expression levels in the NS group, 962 genes were differentially expressed in the ZS group, of which 221 and 741 were up- or downregulated in the ovary of treated fish (Figures 4B,C). Genes including *G protein-coupled receptor 4* (*gpr4*), *caspase a* (*caspa*), *solute carrier family 12, member 2* (*slc12a2*), *sterile alpha motif domain containing 9 like* (*samd9l*), *SRY-box transcription factor 4* (*sox4*), *forkhead box B1* (*foxb1*), *collagen type IV alpha 1 chain* (*col4a1*), *early growth response 1* (*egr1*), *vitellogenin 1* (*vtg1*), and *cytochrome P450 family 17, subfamily A member 1* (*cyp17a1*) were significantly regulated (Table 4). These results suggest that short-term water velocity stimulation had a significant effect on transcription in the ovary.

We evaluated DEGs between the NS and JS groups, as well as the NS and ZS groups by GO and KEGG functional enrichment analyses. GO analysis revealed that genes from different signaling networks were significantly affected in the JS and ZS groups compared to the NS group. The important gene ontology

TABLE 4 Some significantly regulated genes.

Gene	Log2 fold change	
	JS vs. NS	ZS vs. NS
gpr4	8.02	7.91
caspa	5.83	5.41
samd9l	3.53	3.58
slc12a2	2.03	2.02
sox4	1.88	1.84
foxb1	−6.94	−4.4
col4a1	−4.56	−5.4
egr1	−2.91	−3.51
vtg1	−2.91	−2.87
cyp17a1	−2.11	−2.05

upregulated in the JS and ZS groups included signaling receptor activator activity (*cxcl11.6*, *slc12a2*, *abcg5*), signaling receptor binding (*cxcl11.6*, *slc12a2*, *abcg5*), transmembrane signaling receptor activity (*gpr4*, *or131-2*, *tas1r1*, *cd84*), and nucleoside binding (*rab9a*, *rab1a*, *abcc2*) (Figures 5A,B, Supplemental Table S1, S2). Significantly downregulated gene ontology in the JS and ZS groups contained tetrapyrrole binding (*ba1*, *lama1*, *cyp17a1*, *cyp19a1a*), cell wall macromolecule metabolic process (*col4a1*, *pc*), DNA polymerase activity (*pol*, *znf180*), and ubiquitin-like protein transferase activity (*znf180*, *znf333*, *birc6*, *ercc6*, *rnf114*) (Figures 5C,D, Supplemental Table S1, S2).

By comparing the DEGs to the KEGG pathway enrichment database, potential functions of the significant DEGs were analyzed to further understand the ovarian development of grass carp under short-term water velocity stimulation. For short-term water velocity stimulation treatment, 30 KEGG pathways (7 upregulated and 23 downregulated pathways) were significantly enriched in the ZS group (Figures 6B,D). Besides, compared with the NS group, 37 KEGG pathways (11 upregulated and 26 downregulated

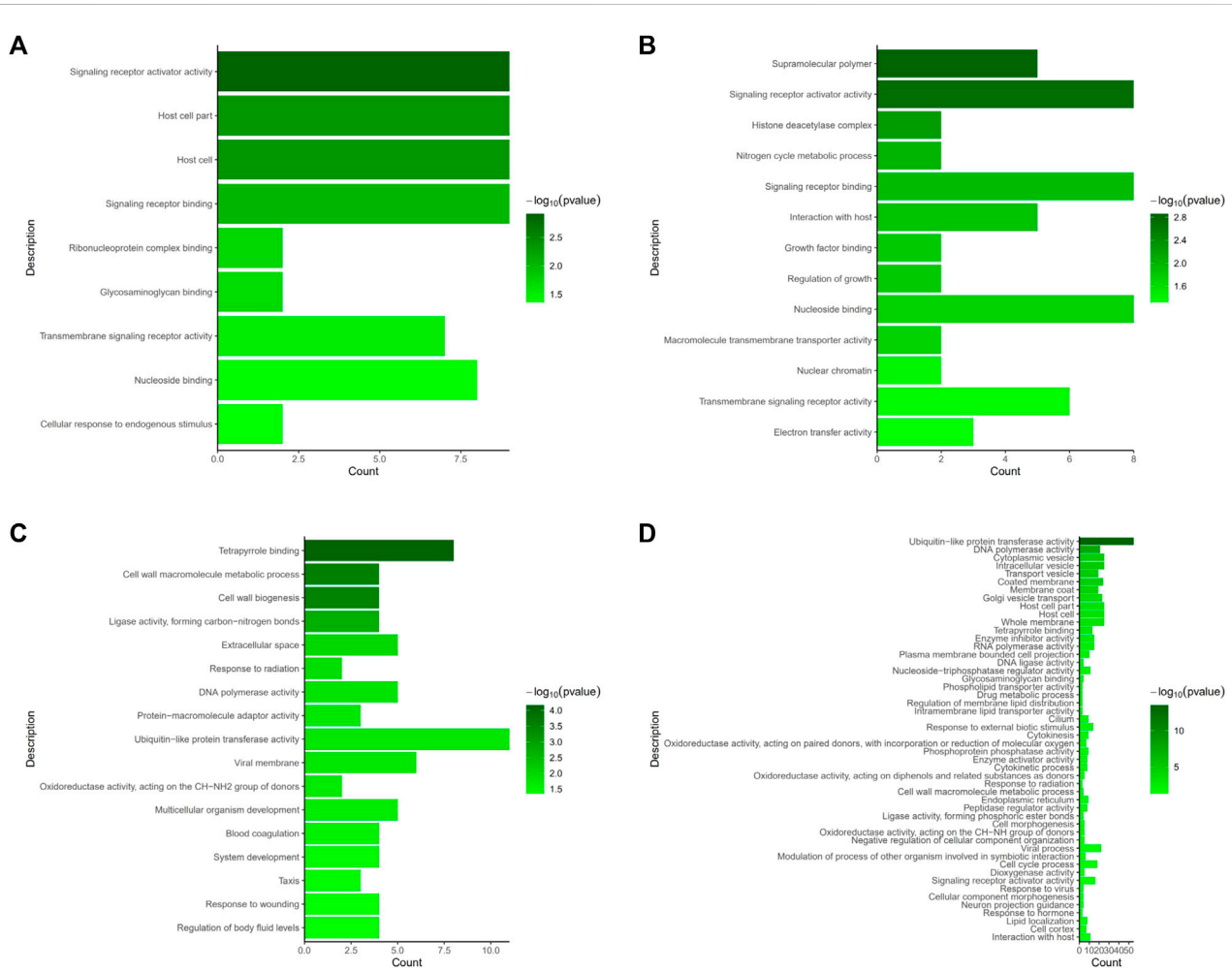

FIGURE 5
GO terms enrichment analysis of the differentially expressed genes. **(A)** Upregulated GO terms in JS vs. NS group. **(B)** Upregulated GO terms in ZS vs. NS group. **(C)** Downregulated GO terms in JS vs. NS group. **(D)** Downregulated GO terms in ZS vs. NS group.

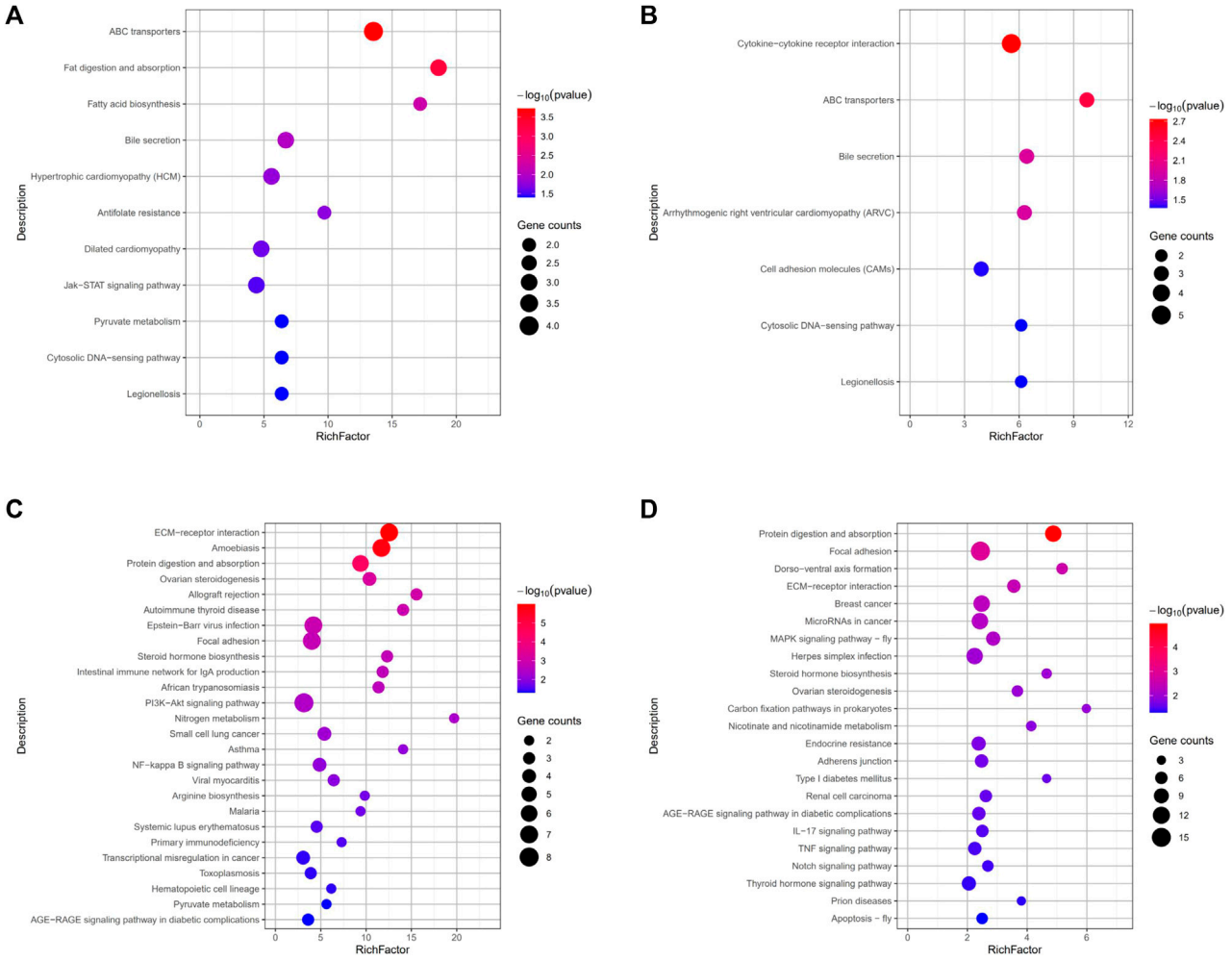

FIGURE 6
KEGG pathways enrichment analysis of the differentially expressed genes. **(A)** Upregulated pathways in JS vs. NS group. **(B)** Upregulated pathways in ZS vs. NS group. **(C)** Downregulated pathways in JS vs. NS group. **(D)** Downregulated pathways in ZS vs. NS group.

pathways) were significantly enriched in the JS group (Figures 6A,C). The KEGG enrichment analysis showed that genes involved in different pathways, such as ABC transporters (*abcc2*, *abcg5*), bile secretion (*abcc2*, *abcg5*), cytosolic DNA-sensing pathway (*caspa*, *cxcl11.6*), legionellosis (*caspa*, *rab1a*), ECM-receptor interaction (*lama1*, *col1a1*, *col4a1*, *col6a2*, *col1a2*, *col6a1*), protein digestion and absorption (*mme*, *col1a1*, *col4a1*, *col6a2*, *col1a2*, *col6a1*), ovarian steroidogenesis (*cyp17a1*, *cyp19a1a*, *hsd17b1*), focal adhesion (*lama1*, *col1a1*, *col4a1*, *col6a2*, *col1a2*, *col6a1*), steroid hormone biosynthesis (*cyp17a1*, *cyp19a1a*, *hsd17b1*), and AGE-RAGE signaling pathway in diabetic complications (*col1a1*, *col4a1*, *col1a2*) were differentially regulated in the JS and ZS groups (Figures 6A–D; Supplemental Table S3, S4).

RNA sequencing data confirmation

Four DEGs (*cyp17a1*, *hsd17b1*, *slc12a2*, and *vtg1*) were randomly selected to further validate the reliability of DEGs identified by RNA-Seq. The qRT-PCR results were consistent with those of RNA-Seq (Figure 7; Supplemental Figure S1, S2), indicating that the RNA-Seq data was accurate.

Discussion

Because of the influence of large reservoirs distributed in the Yangtze River, the flow regime has been severely altered and flow velocity in the middle and lower river reaches is rarely exceeding 0.5 m/s from April to June (Zhou et al., 2009; Wang et al., 2016; Liu et al., 2021). In some reservoir areas, the flow velocity cannot even reach 0.2 m/s (Xu et al., 2017). To explore the effect of flow velocity on the ovarian development of female grass carp, we evaluated ovarian histology, hormone concentrations, and transcription levels of genes related to the ovaries. Our results revealed that even if ovarian development characteristics were not affected by short-term water velocity stimulation, the concentrations of sex steroids, gonadotropins, and thyroid hormones, as well as the

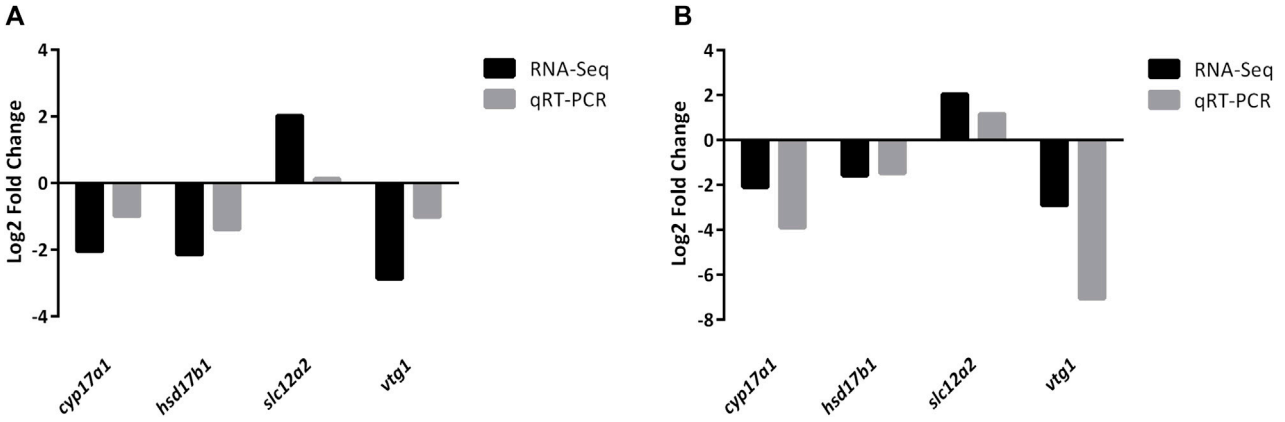

FIGURE 7
Validation of randomly selected four DEGs of RNA-Seq results using qRT-PCR analysis. All mRNA levels were calculated as the fold expression relative to the housekeeping gene *β-actin*. **(A)** Relative fold change of DEGs between qRT-PCR and RNA-Seq results in JS vs. NS group. **(B)** Relative fold change of DEGs between qRT-PCR and RNA-Seq results in ZS vs. NS group. Relative expression levels from the RNA-Seq results were calculated as log2FC values.

transcriptional levels were significantly altered in female grass carp. These findings provide fundamental knowledge for technical support for ecological protection and restoration of hydraulic engineering.

Normal oocyte development and maturation are critical for successful reproduction in fish (Nakayama et al., 2004). However, no spawning activity was observed in the ZS group at a velocity of 0.5 m/s. Previous studies have shown that the required flow velocity for spawning differs greatly among different fish species. The determined triggering velocity of female silver carp was about 1.0 m/s in flume experiments (Chen et al., 2021), and female Atlantic salmon (*Salmo salar*)) constructs spawning redds in areas with an averaged flow velocity of 0.53 m/s (Beland et al., 1982). Generally, for the four major Chinese carp species, the velocity during the spawning period was 0.6–1.3 m/s, and the most appropriate velocity was 0.9–1.0 m/s (Dai et al., 2022).

The hypothalamus-pituitary-gonad (HPG) axis is responsible for fundamental regulation of all developmental stages of ovarian follicles, including progression to maturation or follicular atresia. And the pituitary gonadotropins, FSH and LH, which subsequently act on the ovary and regulate ovarian follicular development, maturity, steroidogenesis, and growth factor production, are the key players in the HPG axis (Patino et al., 2001; Nagahama and Yamashita, 2008; Zhang D. et al., 2022). In this study, we used serum and ovary testosterone, estradiol, progesterone, and DHP, as well as FSH, LH, T3 and T4 levels to represent gonadal development (Gadekar, 2014; Tucker et al., 2020), and measured these levels using ELISA. Normal reproductive functions in female fish are attributed to the sex steroid hormones, which mainly include testosterone, estradiol, progesterone, and DHP. By triggering germinal vesicle breakdown during final oocyte maturation, testosterone may contribute to oocyte growth and development (So et al., 1985). Moreover, testosterone is also involved in female steroidogenesis and acts as a substrate for aromatase during estradiol synthesis, which concentration is not stable in female fish (Barannikova et al., 2004). Estradiol is a crucial sex steroid hormone, and plays a significant role in stimulating the liver to produce the yolk precursor protein, vitellogenin, which is subsequently incorporated into the developing oocyte (Barannikova et al., 2004). Estradiol levels increase dramatically in the oocytes during vitellogenesis and decrease when vitellogenesis is complete (Amiri et al., 1996; Barannikova, 1999). Progesterone is a vital steroidogenic mediator for oocyte growth and maturation in female fish (Al-Hasawi, 2022). Our study showed that ovary estradiol and progesterone concentrations were all upregulated in the ZS and JS groups compared to the NS group (Figures 2F,G), indicating a positive effect of flow stimulation on fish gonad development. DHP acts as the most potent maturation-inducing steroid (MIS) in stimulating final oocyte maturation in fish (Amiri et al., 1999). In our study, serum and ovary DHP concentration in the ZS group was slightly increased (Figures 2D,H), although this was not statistically significant. Pituitary gonadotropins, FSH and LH, are major regulators of steroidogenesis by the ovary, resulting in the synthesis of sex steroid hormones that play critical roles in the orderly progression of growth and development of ovarian follicles (Harding et al., 2023). It is well known that thyroid hormones, T3 and T4, play a dominant role in oocyte development and final maturation and are well established in fish (Weber et al., 1992). We found that serum and ovary FSH and T3 concentrations in the ZS group were significantly elevated, as well as in the JS group (Figures 3A,C,E,G). However, no significant changes in LH and T4 levels were observed in the ZS group (Figures 3B,D,F,H). The underlying mechanism is unknown and requires further exploration. However, these data still show that short-term water velocity stimulation has an important influence on the ovarian development in female grass carp.

To understand the impact of short-term water velocity stimulation on gene expression of selected endocrine pathways and explore their underlying molecular mechanisms in fish, ovary samples from the NS, JS, and ZS groups were analyzed. Transcriptomic analysis of ovaries from the NS, JS, and ZS groups provided evidence that the water flow velocity is important for regulating genes from different signaling pathways. G protein-coupled receptors (GPRs), the largest membrane receptor

family in eukaryotes, play a pivotal role in regulating various essential physiological and biochemical processes, including sexual maturation and reproduction (Flaherty et al., 2008; Nguyen et al., 2018). Ovarian development and maturation are controlled by many important factors, such as hormones and their receptors, which predominantly bind and activate GPRs on the cell surface, thereby initiating multiple downstream cascades (Zhang X. et al., 2022). We showed that *gpr4* was significantly upregulated in the ZS group, suggesting that it may regulate the ovarian development of grass carp under short-term water velocity stimulation. In fish oocytes, lectin may prevent polyspermy fertilization and participate in the formation of fertilization shell through binding with glycoproteins. Furthermore, lectin and vitellin are closely bound to ovomucin to form the basic structure of the vitellin outer membrane (Kido et al., 1992). In our study, the expression of *C-type lectin* was upregulated in the ZS group, suggesting that lectin affects ovarian development in grass carp under short-term water velocity stimulation.

Vitellogenin 1 (Vtg1) which plays a very important role in oocytes development was downregulated in the ZS group (Table 4). A large proportion of energy-related biomolecules from the liver, such as vitellogenin and lipids, are absorbed and utilized by the reproductive system (Della Torre et al., 2014; Zhang D. et al., 2022). In the turbot (*Scophthalmus maximus*), Xue et al. found that the ovary displayed a higher estradiol level and lower *vtg* expression, indicating that some other factors limit high *vtg* expression (Xue et al., 2018). Similar to the results of the present experiment, previous work in conger eel (*Conger myriaster*) also reported that flowing water could inhibit the gene expression of liver *vtg* and reduce VTG synthesis in the liver, which may promote lipid accumulation (Liu et al., 2022). In our study, flowing water stimulation may inhibit yolk accumulation during the ovarian development of grass carp. Retinol and its derivatives are known to play important roles in female reproductive processes, including follicular development, ovarian steroidogenesis, and oocyte maturation (Wang et al., 2022). Retinol dehydrogenase 12 (*rdh12*), a novel member of the microsomal short-chain dehydrogenase/reductase protein superfamily, has been identified as a key component in steroid metabolism (Keller and Adamski, 2007). In our results, *rdh12* expression was also decreased in the ZS group. Researchers have identified several genes that encode crucial enzymes in the steroidogenesis pathway, including *cyp19a1a*, *cyp17a1*, and *hsd17b1*, which could synthesize estradiol and progesterone, and play an important role in ovarian development and reproduction in fish (Fang et al., 2019; Li et al., 2021). Transcriptomic analysis showed that *cyp19a1a*, *cyp17a1*, and *hsd17b1* were also downregulated in the ZS group compared to the NS group. It has been proven that *cyp19a1a*, *cyp17a1*, and *hsd17b1* mRNAs showed a significant decrease when oocytes matured. Moreover, gene set enrichment analysis (GSEA) showed that the steroid hormone biosynthesis pathway was downregulated and that *cyp19a1a*, *cyp17a1*, and *hsd17b1* were core genes in this pathway (Dong et al., 2021). These findings revealed that these genes and this pathway play key roles in oocyte maturation. As previously described in ovoviviparous black rockfish (*Sebastes schlegeli*), the transcription level of *cyp19a1a* in ovary declined when the ovary developed from vitellogenic stage to ovulation stage during the reproductive cycle (Wen et al., 2014). A decreased *cyp19a1a* expression was also reported in amago salmon (*Oncorhynchus rhodurus*), rainbow trout (*Oncorhynchus mykiss*), and spotted scat (*Scatophagus argus*) during final maturation (Young et al., 1983; Gohin et al., 2011; Liu et al., 2015). In Japanese eel (*Anguilla japonica*), the expression of related transcripts *hsd17b1* and *cyp19a1a* declined at the migratory nucleus stage (Lai et al., 2022). These suggest that they can promote gonadal maturation in grass carp.

Utilizing KEGG pathway enrichment, the main biochemical metabolism and signal transduction pathways involved in genes can be identified. Generally, follicle development strongly depends on communication between germ cells and surrounding somatic cells through cytokine-cytokine receptor interaction, such as Kit and KitL (Matzuk et al., 2002; Saatcioglu et al., 2016). We observed a great number of genes in cytokine-cytokine receptor interaction obviously upregulated in ovaries of the ZS group (Figure 6B; Supplemental Table S4), indicating that the normal conservation between germ cells and somatic cells was already activated. Pathway analysis results indicated that 7 genes, including *lama1*, *col1a1*, *col1a2*, *col4a1*, *col6a1*, *col6a2*, and *col6a3*, enriched in ECM-receptor interaction were down regulated under short-term water velocity stimulation (Figure 6D; Supplemental Table S4). The pathways associated with ECM-receptor interaction play crucial roles in various biological processes, including cell migration, proliferation, follicle growth, and oocyte maturation (Berkholtz et al., 2006; Reing et al., 2009; Deng et al., 2022). Therefore, we speculate that these genes might have significant implications in the transition from the follicular development stage to the oocyte maturation stage. However, the specific mechanism remains unknown, and the functions of these genes in the reproductive cycle require further study.

Conclusion

We investigated the ovarian development of grass carp under short-term water velocity stimulation by histology analysis, biochemical assays, and RNA-Seq technology. Although there was no obvious effect on the ovarian development characteristics of grass carp under short-term water velocity stimulation, estradiol, progesterone, FSH, and T3 concentrations were elevated. Totally, 962 DEGs with 741 downregulated genes and 221 upregulated genes were identified in transcriptome data. The key genes identified were enriched in ABC transporters, cytokine-cytokine receptor interaction, ECM-receptor interaction, and steroid hormone biosynthesis, which play an essential role in the response of the ovaries in grass carp to short-term water velocity stimulation. This study provides new insights into the ovarian development of grass carp under short-term water velocity stimulation. However, these transcriptomic data are still preliminary, and the function of the DEGs in reproductive cycle of fish species requires further investigation.

Data availability statement

The datasets presented in this study can be found in online repositories. The names of the repository/repositories and accession

number(s) can be found below: https://www.ncbi.nlm.nih.gov/, PRJNA977722.

Ethics statement

The animal study was approved by Animal ethics committee of Institute of Hydrobiology, Chinese Academy of Sciences. The study was conducted in accordance with the local legislation and institutional requirements.

Author contributions

TS conducted most of the experiments for this work. YC, KX, and HH provided help with fish rearing and sampling. JJ, ZY, and WJ gave valuable suggestion and discussion, TS and JY performed training and provided insights for this work. TS wrote the paper and prepared all of the figures. All authors contributed to the article and approved the submitted version.

Funding

This study received funding from Hubei Provincial Natural Science Foundation of China (2022CFB738), and Director's Fund of the Hubei Key Laboratory of Three Gorges Project for Conservation of Fishes, China Three Gorges Corporation (25901-2022-27). The funders were not involved in the study design, collection, analysis, interpretation of data, the writing of this article or the decision to submit it for publication.

Acknowledgments

We would like to thank Xin Zhu, Binzhong Wang, Dezhi Zhang, and Wei Wang from Chinese Sturgeon Research Institute, China Three Gorges Corporation for the support of the culture system in this research work.

Conflict of interest

TS, YC, KX, HH, ZY, WJ, and JY are employed by China Three Gorges Corporation.

The remaining author declares that the research was conducted in the absence of any commercial or financial relationships that could be construed as a potential conflict of interest.

Publisher's note

Supplementary material

The Supplementary Material for this article can be found online at: https://www.frontiersin.org/articles/10.3389/fphys.2023.1248999/full#supplementary-material

References

Al-Hasawi, Z. M. M. (2022). Adverse impacts of toxic metal pollutants on sex steroid hormones of Siganus rivulatus (teleostei: siganidae) from the red sea. *Fishes* 7 (6), 367. doi:10.3390/fishes7060367

Amiri, B. M., Maebayashi, M., Adachi, S., Moberg, G. P., Doroshov, S. I., and Yamauchi, K. (1999). *In vitro* steroidogenesis by testicular fragments and ovarian follicles in a hybrid sturgeon, Bester. *Fish Physiology Biochem.* 21 (1), 1–14. doi:10.1023/a:1007706128184

Amiri, B. M., Maebayashi, M., Hara, A., Adachi, S., and Yamauchi, K. (1996). Ovarian development and serum sex steroid and vitellogenin profiles in the female cultured sturgeon hybrid, the bester. *J. fish Biol.* 48, 1164–1178. doi:10.1111/j.1095-8649.1996.tb01812.x

Barannikova, I. A., Bayunova, L. V., and Semenkova, T. B. (2004). Serum levels of testosterone, 11-ketotestosterone and oestradiol-17beta in three species of sturgeon during gonadal development and final maturation induced by hormonal treatment. *J. Fish Biol.* 64 (5), 1330–1338. doi:10.1111/j.0022-1112.2004.00395.x

Barannikova, I. A. (1999). Sex steroids in the serum of Caspian sturgeons and their specific cytosol binding in brain and gonads during the migratory cycle. *J. Appl. Ichthyology-Zeitschrift Fur Angewandte Ichthyologie* 15 (4-5), 193–195. doi:10.1111/j.1439-0426.1999.tb00232.x

Barbarossa, V., Schmitt, R. J. P., Huijbregts, M. A. J., Zarfl, C., King, H., and Schipper, A. M. (2020). Impacts of current and future large dams on the geographic range connectivity of freshwater fish worldwide. *Proc. Natl. Acad. Sci. U. S. A.* 117 (7), 3648–3655. doi:10.1073/pnas.1912776117

Beland, K. F., Jordan, R. M., and Meister, A. L. (1982). Water depth and velocity preferences of spawning Atlantic salmon in Maine rivers. *North Am. J. Fish. Manag.* 2(1), 11–13.

Berkholtz, C. B., Shea, L. D., and Woodruff, T. K. (2006). Extracellular matrix functions in follicle maturation. *Seminars Reproductive Med.* 24 (4), 262–269. doi:10.1055/s-2006-948555

Buddendorf, W. B., Malcolm, I. A., Geris, J., Fabris, L., Millidine, K. J., Wilkinson, M. E., et al. (2017). Spatio-temporal effects of river regulation on habitat quality for Atlantic salmon fry. *Ecol. Indic.* 83, 292–302. doi:10.1016/j.ecolind.2017.08.006

Cao, L., Naylor, R., Henriksson, P., Leadbitter, D., Metian, M., Troell, M., et al. (2015). Global food supply. China's aquaculture and the world's wild fisheries. *Science* 347 (6218), 133–135. doi:10.1126/science.1260149

Cella-Ribeiro, A., da Costa Doria, C. R., Dutka-Gianelli, J., Alves, H., and Torrente-Vilara, G. (2017). Temporal fish community responses to two cascade run-of-river dams in the Madeira River, Amazon basin. *Ecohydrology* 10 (8), e1889. doi:10.1002/eco.1889

Chen, Q., Shi, W., Huisman, J., Maberly, S. C., Zhang, J., Yu, J., et al. (2020). Hydropower reservoirs on the upper Mekong River modify nutrient bioavailability downstream. *Natl. Sci. Rev.* 7 (9), 1449–1457. doi:10.1093/nsr/nwaa026

Chen, Q., Zhang, J., Chen, Y., Mo, K., Wang, J., Tang, L., et al. (2021). Inducing flow velocities to manage fish reproduction in regulated rivers. *Engineering* 7 (2), 178–186. doi:10.1016/j.eng.2020.06.013

Dai, L. Q., Wang, Y., Dai, H. C., Li, W., Zheng, T. G., and Zhang, Q. S. (2022). Assessment of environmental flow requirements for four major Chinese carps in the lower reaches of the Jinsha River, southwest China. *Front. Ecol. Evol.* 10. doi:10.3389/fevo.2022.810889

Della Torre, S., Benedusi, V., Fontana, R., and Maggi, A. (2014). Energy metabolism and fertility-a balance preserved for female health. *Nat. Rev. Endocrinol.* 10 (1), 13–23. doi:10.1038/nrendo.2013.203

Deng, H., Sun, A., and Yang, S. (2022). A characterization and comparative analysis of ovary transcriptome in locally adopted xiangxi and angus cattle. *Pak. J. Agric. Sci.* 59 (2), 341–347. doi:10.21162/pakjas/22.765

Dong, Y., Lyu, L., Zhang, D., Li, J., Wen, H., and Shi, B. (2021). Integrated lncRNA and mRNA transcriptome analyses in the ovary of Cynoglossus semilaevis reveal genes and pathways potentially involved in reproduction. *Front. Genet.* 12, 671729. doi:10.3389/fgene.2021.671729

Fang, D.-A., Yang, X.-j., Feng, X., Zhou, Y.-F., Xu, D.-P., Zhang, M.-Y., et al. (2019). FoxL2 combined with Cyp19a1a regulate the spawning upstream migration in Coilia nasus. *Gene* 710, 307–315. doi:10.1016/j.gene.2019.05.037

Fellman, J. B., Hood, E., Nagorski, S., Hudson, J., and Pyare, S. (2019). Interactive physical and biotic factors control dissolved oxygen in salmon spawning streams in coastal Alaska. *Aquat. Sci.* 81 (1), 2. doi:10.1007/s00027-018-0597-9

Finch, C., Pine, W., III, and Limburg, K. (2015). Do hydropeaking flows alter juvenile fish growth rates? A test with juvenile humpback chub in the Colorado river river. *River Res. Appl.* 31 (2), 156–164. doi:10.1002/rra.2725

Flaherty, P., Radhakrishnan, M. L., Dinh, T., Rebres, R. A., Roach, T. I., Jordan, M. I., et al. (2008). A dual receptor crosstalk model of G-protein-coupled signal transduction. *Plos Comput. Biol.* 4 (9), e1000185. doi:10.1371/journal.pcbi.1000185

Gadekar, G. P. (2014). Studies on the seasonal histomorphological changes in the ovary of Indian major carp, Labeo Rohita (HAM). *Bioscan* 9 (3), 1037–1042.

Gao, X., Zhao, S., Zhang, C., and XiangyangTu (2009). Index system and method for assessing the health status of river. *J. Hydraulic Eng.* 40 (8), 962–968. doi:10.3321/j.issn:0559-9350.2009.08.010

Geraylou, Z., Souffreau, C., Rurangwa, E., D'Hondt, S., Callewaert, L., Courtin, C. M., et al. (2012). Effects of arabinoxylan-oligosaccharides (AXOS) on juvenile Siberian sturgeon (*Acipenser baerii*) performance, immune responses and gastrointestinal microbial community. *Fish Shellfish Immunol.* 33 (4), 718–724. doi:10.1016/j.fsi.2012.06.010

Gohin, M., Bodinier, P., Fostier, A., Chesnel, F., and Bobe, J. (2011). Aromatase is expressed and active in the rainbow trout oocyte during final oocyte maturation. *Mol. Reproduction Dev.* 78 (7), 510–518. doi:10.1002/mrd.21335

Guo, W., Wang, H., Xu, J., Xia, Z., Ma, X. H., Wang, Y. C., et al. (2011). Gender-specific interactions between alcohol metabolism genes and severity of quantitative alcohol-related-traits in a Tibetan population. *J. Hydroelectr. Eng.* 30(3), 22–25. doi:10.1016/j.neulet.2011.03.020

Harding, L., Schultz, I. R., Young, G., and Swanson, P. (2023). Salmonid pituitary cells as a test system for identifying endocrine disrupting compounds. *Environ. Toxicol. Chem.* 42, 1730–1742. doi:10.1002/etc.5644

Hultmann, L., Phu, T. M., Tobiassen, T., Aas-Hansen, O., and Rustad, T. (2012). Effects of pre-slaughter stress on proteolytic enzyme activities and muscle quality of farmed Atlantic cod (*Gadus morhua*). *Food Chem.* 134 (3), 1399–1408. doi:10.1016/j.foodchem.2012.03.038

Keller, B., and Adamski, J. (2007). RDH12, a retinol dehydrogenase causing Leber's congenital amaurosis, is also involved in steroid metabolism. *J. Steroid Biochem. Mol. Biol.* 104 (3-5), 190–194. doi:10.1016/j.jsbmb.2007.03.015

Kido, S., Morimoto, A., Kim, F., and Doi, Y. K. (1992). Isolation of a novel protein from the outer layer of the vitelline membrane. *Biochem. J.* 286, 17–22. doi:10.1042/bj2860017

King, A. J., Gwinn, D. C., Tonkin, Z., Mahoney, J., Raymond, S., and Beesley, L. (2016). Using abiotic drivers of fish spawning to inform environmental flow management. *J. Appl. Ecol.* 53 (1), 34–43. doi:10.1111/1365-2664.12542

Lai, X. J., Peng, S., and Wang, Y. L. (2022). Dynamic transcriptome analysis of ovarian follicles in artificial maturing Japanese eel (Anguilla japonica). *Theriogenology* 180, 176–188. doi:10.1016/j.theriogenology.2021.12.031

Lau, E. S.-W., Zhang, Z., Qin, M., and Ge, W. (2016). Knockout of zebrafish ovarian aromatase gene (cyp19a1a) by TALEN and CRISPR/Cas9 leads to all-male offspring due to failed ovarian differentiation. *Sci. Rep.* 6, 37357. doi:10.1038/srep37357

Lechner, A., Keckeis, H., Schludermann, E., Humphries, P., McCasker, N., and Tritthart, M. (2014). Hydraulic forces impact larval fish drift in the free flowing section of a large European river. *Ecohydrology* 7 (2), 648–658. doi:10.1002/eco.1386

Li, J., Xia, Z., Dai, H., Yin, W., Zhang, F., Liu, M. F., et al. (2013a). Immunosuppression and the infection caused by gut mucosal barrier dysfunction in patients with early severe acute pancreatitis. *J. Hydraulic Eng.* 44 (8), 892–900. doi:10.2741/4150

Li, J., Xia, Z., Wang, Y., Zhang, W., Duan, M. H., Liu, Y. T., et al. (2013b). Pulmonary hypertension in POEMS syndrome. *Ecohydrology* 6 (3), 393–398. doi:10.3324/haematol.2012.073031

Li, Z., Ren, X., Guo, Y., Ru, X., Tian, C., Shi, H., et al. (2021). Identification and ovarian developmental regulation of Insulin-like growth factor 3 in spotted scat (*Scatophagus argus*). *Aquac. Rep.* 21, 100866. doi:10.1016/j.aqrep.2021.100866

Lin, J., Li, Y., Liu, Y., Peng, Q., Zhang, D., and Jin, T. (2022). Recent progress in ecological operation and adaptive management for stimulating fish natural spawning. *J. Hydraulic Eng.* 53 (4), 483–495. doi:10.13243/j.cnki.slxb.20210774

Liu, H., Mu, X., Gui, L., Su, M., Li, H., Zhang, G., et al. (2015). Characterization and gonadal expression of FOXL2 relative to Cyp19a genes in spotted scat *Scatophagus argus*. *Gene* 561 (1), 6–14. doi:10.1016/j.gene.2014.12.060

Liu, H., Yin, X. A., Qiu, X., Qin, J., Yang, W., and Zhang, J. (2021). Coupled influence of flow velocity and water temperature on grass carp swimming behaviour and gonad development. *Hydrol. Process.* 35 (4). doi:10.1002/hyp.14052

Liu, R. C., Li, K., Wang, G. X., Jiang, Z. X., Ba, X. B., and Liu, L. P. (2022). Effect of swimming on the induction of vitellogenin in Conger eel (*Conger myriaster*). *Front. Mar. Sci.* 9. doi:10.3389/fmars.2022.887074

Matzuk, M. M., Burns, K. H., Viveiros, M. M., and Eppig, J. J. (2002). Intercellular communication in the mammalian ovary: oocytes carry the conversation. *Science* 296 (5576), 2178–2180. doi:10.1126/science.1071965

McClure, C., Quist, M. C., Kozfkay, J. R., Peterson, M. P., and Schill, D. J. (2020). Movement dynamics of smallmouth bass in a large western river system. *North Am. J. Fish. Manag.* 40 (1), 154–162. doi:10.1002/nafm.10389

McDonnell, R. A. (2000). Hierarchical modelling of the environmental impacts of river impoundment based on a GIS. *Hydrol. Process.* 14 (11-12), 2123–2142. doi:10.1002/1099-1085(20000815/30)14:11/12<2123:Aid-hyp59>3.0.Co;2-z

Mouchlianitis, F. A., Bobori, D., Tsakoumis, E., Sapounidis, A., Kritikaki, E., and Ganias, K. (2021). Does fragmented river connectivity alter the reproductive behavior of the potamodromous fish Alburnus vistonicus? *Hydrobiologia* 848 (17), 4029–4044. doi:10.1007/s10750-021-04621-x

Nagahama, Y., and Yamashita, M. (2008). Regulation of oocyte maturation in fish. *Dev. Growth and Differ.* 50, S195–S219. doi:10.1111/j.1440-169X.2008.01019.x

Nakayama, K., Oshima, Y., Yamaguchi, T., Tsuruda, Y., Kang, I. J., Kobayashi, M., et al. (2004). Fertilization success and sexual behavior in male medaka, *Oryzias latipes*, exposed to tributyltin. *Chemosphere* 55 (10), 1331–1337. doi:10.1016/j.chemosphere.2003.11.050

Nguyen, T. V., Rotllant, G. E., Cummins, S. F., Elizur, A., and Ventura, T. (2018). Insights into sexual maturation and reproduction in the Norway lobster (*Nephrops norvegicus*) via *in silico* prediction and characterization of neuropeptides and G protein-coupled receptors. *Front. Endocrinol.* 9, 430. doi:10.3389/fendo.2018.00430

Patino, R., Yoshizaki, G., Thomas, P., and Kagawa, H. (2001). Gonadotropic control of ovarian follicle maturation: the two-stage concept and its mechanisms. *Comp. Biochem. Physiology B-Biochemistry Mol. Biol.* 129 (2-3), 427–439. doi:10.1016/s1096-4959(01)00344-x

Poff, N. L., and Schmidt, J. C. (2016). How dams can go with the flow. *Science* 353 (6304), 1099–1100. doi:10.1126/science.aah4926

Reing, J. E., Zhang, L., Myers-Irvin, J., Cordero, K. E., Freytes, D. O., Heber-Katz, E., et al. (2009). Degradation products of extracellular matrix affect cell migration and proliferation. *Tissue Eng. Part A* 15 (3), 605–614. doi:10.1089/ten.tea.2007.0425

Saatcioglu, H. D., Cuevas, I., and Castrillon, D. H. (2016). Control of oocyte reawakening by kit. *Plos Genet.* 12 (8), e1006215. doi:10.1371/journal.pgen.1006215

Schmittgen, T. D., and Livak, K. J. (2008). Analyzing real-time PCR data by the comparative CT method. *Nat. Protoc.* 3, 1101–1108. doi:10.1038/nprot.2008.73

She, Z., Tang, Y., Chen, L., Nong, X., and Li, X. (2023). Determination of suitable ecological flow regimes for spawning of four major Chinese carps: a case study of the hongshui river, China. *Ecol. Inf.* 76, 102061. doi:10.1016/j.ecoinf.2023.102061

So, Y. P., Idler, D. R., Truscott, B., and Walsh, J. M. (1985). Progestogens, androgens and their glucuronides in the terminal stages of oocyte maturation in landlocked Atlantic salmon. *J. steroid Biochem. Mol. Biol.* 23 (5-), 583–591. part-P1). doi:10.1016/0022-4731(85)90008-1

Stamou, A., Polydera, A., Papadonikolaki, G., Martinez-Capel, F., Munoz-Mas, R., Papadaki, C., et al. (2018). Determination of environmental flows in rivers using an integrated hydrological-hydrodynamic-habitat modelling approach. *J. Environ. Manag.* 209, 273–285. doi:10.1016/j.jenvman.2017.12.038

Stone, R. (2016). Dam-building threatens Mekong fisheries. *Science* 354 (6316), 1084–1085. doi:10.1126/science.354.6316.1084

Tucker, E. K., Zurliene, M. E., Suski, C. D., and Nowak, R. A. (2020). Gonad development and reproductive hormones of invasive silver carp (*Hypophthalmichthys molitrix*) in the Illinois River. *Biol. Reproduction* 102 (3), 647–659. doi:10.1093/biolre/ioz207

Wang, B., Liu, Y., Feng, L., Jiang, W.-D., Kuang, S.-Y., Jiang, J., et al. (2015). Effects of dietary arginine supplementation on growth performance, flesh quality, muscle antioxidant capacity and antioxidant-related signalling molecule expression in young grass carp (Ctenopharyngodon idella). *Food Chem.* 167, 91–99. doi:10.1016/j.foodchem.2014.06.091

Wang, J., Li, J., Ge, Q., Li, W., and Li, J. (2022). Full-length transcriptome sequencing and comparative transcriptomic analysis provide insights into the ovarian maturation of exopalaemon carinicauda. *Front. Mar. Sci.* 9. doi:10.3389/fmars.2022.906730

Wang, Y., Rhoads, B. L., and Wang, D. (2016). Assessment of the flow regime alterations in the middle reach of the Yangtze River associated with dam construction: potential ecological implications. *Hydrol. Process.* 30 (21), 3949–3966. doi:10.1002/hyp.10921

Weber, G. M., Okimoto, D. K., Richman, N. H., and Grau, E. G. (1992). Patterns of thyroxine and triiodothyronine in serum and follicle-bound oocytes of the tilapia, *Oreochromis mossambicus*, during oogenesis. *General Comp. Endocrinol.* 85 (3), 392–404. doi:10.1016/0016-6480(92)90084-w

Wen, H. S., Mu, W. J., Yang, Y. P., Shi, D., He, F., and Li, J. F. (2014). Molecular physiology mechanism of cytochrome P450 aromatase-regulating gonad development in ovoviviparous black rockfish (Sebastes schlegeli). *Aquac. Res.* 45 (10), 1685–1696. doi:10.1111/are.12114

Xie, P., and Chen, Y. Y. (2001). Invasive carp in China's plateau lakes. *Science* 294 (5544), 999–1000. doi:10.1126/science.294.5544.999c

Xu, Z., Yin, X., Sun, T., Cai, Y., Ding, Y., Yang, W., et al. (2017). Labyrinths in large reservoirs: an invisible barrier to fish migration and the solution through reservoir operation. *Water Resour. Res.* 53 (1), 817–831. doi:10.1002/2016wr019485

Xue, R., Wang, X., Xu, S., Liu, Y., Feng, C., Zhao, C., et al. (2018). Expression profile and localization of vitellogenin mRNA and protein during ovarian development in

turbot (*Scophthalmus maximus*). *Comp. Biochem. Physiology B-Biochemistry Mol. Biol.* 226, 53–63. doi:10.1016/j.cbpb.2018.08.002

Yang, Z., Hu, P., Wang, J., Zhao, Y., and Zhang, W. (2019). Ecological flow process acknowledging different spawning patterns in the Songhua River. *Ecol. Eng.* 132, 56–64. doi:10.1016/j.ecoleng.2018.12.034

Young, G., Kagawa, H., and Nagahama, Y. (1983). Evidence for a decrease in aromatase activity in the ovarian granulosa cells of amago salmon (Oncorhynchus rhodurus) associated with final oocyte maturation. *Biol. Reproduction* 29 (2), 310–315. doi:10.1095/biolreprod29.2.310

Zhang, C., Ding, C. Z., Ding, L. Y., Chen, L. Q., Hu, J. M., Tao, J., et al. (2019a). Ratcheting behavior of intervertebral discs under cyclic compression: experiment and prediction. *Rev. Fish Biol. Fish.* 29 (4), 895–902. doi:10.1111/os.12530

Zhang, D., Shi, B., Shao, P., Shao, C., Wang, C., Li, J., et al. (2022a). The identification of miRNAs that regulate ovarian maturation in Cynoglossus semilaevis. *Aquaculture* 555, 738250. doi:10.1016/j.aquaculture.2022.738250

Zhang, P., Qiao, Y., Schineider, M., Chang, J. B., Mutzner, R., Fluixa-Sanmartin, J., et al. (2019b). Using a hierarchical model framework to assess climate change and hydropower operation impacts on the habitat of an imperiled fish in the Jinsha River, China. *Sci. Total Environ.* 646, 1624–1638. doi:10.1016/j.scitotenv.2018.07.318

Zhang, W., Peng, H., Jia, Y., Ni, G., Yang, Z., and Zeng, Q. (2019c). Investigating the simultaneous ecological operation of dam gates to meet the water flow requirements of fish spawning migration. *Pol. J. Environ. Stud.* 28 (3), 1967–1980. doi:10.15244/pjoes/89983

Zhang, X., Wang, J., Wang, C., Li, W., Ge, Q., Qin, Z., et al. (2022b). Effects of long-term high carbonate alkalinity stress on the ovarian development in exopalaemon carinicauda. *Water* 14 (22), 3690. doi:10.3390/w14223690

Zhou, G., Wang, H., Shao, X., and Jia, D. (2009). Numerical model for sediment transport and bed degradation in the Yangtze River channel downstream of three Gorges reservoir. *J. Hydraulic Eng.* 135 (9), 729–740. doi:10.1061/(asce)0733-9429(2009)135:9(729)

frontiers | Frontiers in Physiology

TYPE Original Research
PUBLISHED 13 September 2023
DOI 10.3389/fphys.2023.1267953

OPEN ACCESS

EDITED BY
Yiming Li,
Fishery Machinery and Instrument Research Institute, China

REVIEWED BY
Daniel Carneiro Moreira,
University of Brasilia, Brazil
Paula Mariela González,
University of Buenos Aires, Argentina

*CORRESPONDENCE
Caterina Faggio,
cfaggio@unime.it

RECEIVED 27 July 2023
ACCEPTED 31 August 2023
PUBLISHED 13 September 2023

CITATION
Impellitteri F, Yunko K, Martyniuk V, Khoma V, Piccione G, Stoliar O and Faggio C (2023), Cellular and oxidative stress responses of *Mytilus galloprovincialis* to chlorpromazine: implications of an antipsychotic drug exposure study.
Front. Physiol. 14:1267953.
doi: 10.3389/fphys.2023.1267953

Cellular and oxidative stress responses of *Mytilus galloprovincialis* to chlorpromazine: implications of an antipsychotic drug exposure study

Federica Impellitteri [1], Kateryna Yunko [2], Viktoria Martyniuk [2], Vira Khoma [3], Giuseppe Piccione [1], Oksana Stoliar [2,4] and Caterina Faggio [4]*

[1]Department of Veterinary Sciences, University of Messina, Messina, Italy, [2]Ternopil Volodymyr Hnatiuk National Pedagogical University, Ternopil, Ukraine, [3]Ternopil Scientific Research Forensic Center of the Ministry of Internal Affairs of Ukraine, Ternopil, Ukraine, [4]Department of Chemical, Biological, Pharmaceutical and Environmental Sciences, University of Messina, Messina, Italy

Introduction: Bivalve molluscs like *Mytilus galloprovincialis* are valuable bioindicators due to their filter-feeding lifestyle, wide distribution, and ability to concentrate xenobiotics. Studying the effects of pharmaceuticals on these molluscs is crucial given their presence in surface waters. This study investigated the response of *M. galloprovincialis* to chlorpromazine (Cpz), an antipsychotic with antiviral activity against influenza, HIV, and coronaviruses in human cells.

Methods: In this study, we examined the 14-day impact of chlorpromazine (Cpz) on the model species *M. galloprovincialis* at two concentrations (Cpz 1: 12 ng $^{L-1}$ or 37 pM; Cpz 2: 12 µg $^{L-1}$ or 37 nM). To ensure controlled exposure, a stock solution of Cpz was prepared and introduced into the tanks to match the intended concentrations. Seawater and stock solutions were refreshed every 48 h. The primary focus of this study centered on evaluating cell viability, cell volume regulation, and oxidative stress indicators.

Results: Although cell volume regulation, as assessed by decreasing regulatory volume Regulation volume decrease, did not show statistically significant changes during the experiment, digestive cell viability, on the other hand, showed a significant decrease ($p < 0.01$) in the Cpz 2 group, suggesting effects on the general health and survival of these cells. Biochemically, in both Cpz 1 and Cpz 2, superoxide dismutase activity increased, while catalase (CAT) decreased, causing an elevated lipid peroxidation thiobarbituric acid-reactive substances and protein carbonyls, particularly in the Cpz 2 group. The level of reduced glutathione (GSH) increased in both exposures, whereas the level of GSSG increased only in the Cpz 1 group. Consequently, the GSH/GSSG ratio was elevated in the Cpz 2 group only.

Discussion: A comparison of the magnitudes of anti- and pro-oxidative manifestations indicated a pro-oxidative shift in both exposures. These findings show that Cpz induces non-specific symptoms of biochemical and cellular disturbances in *M. galloprovincialis* even at the low picomolar concentration.

KEYWORDS

pharmaceuticals, bivalve mollusc, ecotoxicity, cell volume regulation, oxidative stress, antioxidants

1 Introduction

Bivalve molluscs like *Mytilus galloprovincialis* are valuable bioindicators due to their filter-feeding lifestyle, wide distribution, and ability to concentrate xenobiotics (Pain-Devin et al., 2014; Freitas et al., 2020; Pagano et al., 2020; Curpan et al., 2022). Particularly, their validity to reflect the impact of micropollutants, like pharmaceuticals, has been proven in recent years (Faggio et al., 2018; Piedade et al., 2020; Martyniuk et al., 2022a; Martyniuk et al., 2022b; Martyniuk et al., 2023; Chahouri et al., 2023; Impellitteri et al., 2023a; Impellitteri et al., 2023b). The pharmaceuticals represent a comparatively novel group of micropollutants of increasing concern given their widely discharged into water bodies on a continual basis (Bottoni et al., 2010; Fabbri and Franzellitti, 2016; Turani et al., 2019; Martyniuk et al., 2023; Porretti et al., 2022). They fall into the water along with the insufficiently purified sewage from water treatment plants and directly from households in rural areas, which often lack wastewater treatment facilities (Burgos-Aceves et al., 2018; Burgos-Aceves et al., 2021). Among the most expected pharmaceuticals of emerging concern that leaked into the surface waters, antipsychotic drugs attract special attention (Escudero et al., 2021; Moreira et al., 2022; Sehonova et al., 2017). They are increasingly used to treat a wide range of diseases. Currently, about 100 million people worldwide are affected by neurological disorders and represent 20% of the global burden of disease (Aleya and Uddin, 2020). Antipsychotics have a complex pharmacological profile, acting on multiple receptors common for different phyla, which are often referred to as 'dirty drugs' (Escudero et al., 2021). Therefore, their effects as water contaminants are particularly complicated to indicate and predict. This statement is completely related to chlorpromazine (Cpz), a member of the phenothiazine family of drugs. Its discovery 70 years ago marked the beginning of the application of the heterogeneous class of antipsychotics in medicine. Cpz is listed in the World Health Organization (WHO) Model Lists of Essential Medicines lists as one of five major medicines used in psychotic disorders for curing schizophrenia and schizophrenia-like psychoses (Dudley et al., 2017). With respect to the assessment of schizophrenia as a serious mental illness affecting around 1% of the adult population worldwide, and recommended dosage of Cpz in the range being 400–800 mg/day, the potential input of this drug into surface water can be significant.

Data concerning the concentrations of Cpz in surface waters are scarce. In the influents of municipal wastewater treatment plants in Beijing, China, the concentration of Cpz reached levels of 5–364 ng L^{-1} (Yuan et al., 2013). However, some local water sources were reported to contain much higher Cpz concentrations. For example, Cpz was found among 15 particularly hazardous chemicals present at high concentrations (mg L^{-1}) in hospital wastewater (Frédéric and Yves, 2014). The persistence of Cpz in river water and strong adsorption on sediments have also been reported (Jiménez et al., 2016). Moreover, its presence in the water is expected to increase due to the development of new directions of Cpz applications in medicine. Its interference with topoisomerase action, similar to several anti-cancer drugs, has attracted attention to its potential as an anti-cancer agent (Darkin et al., 1984), and recent studies have confirmed its impact on the cell cycle in the oncogenesis (Lee et al., 2015; Xu et al., 2022). Another novel direction for Cpz utilization in medicine is associated with its antiviral activity against SARS-CoV-2 achieved through a membrane destabilizing effect (Stip et al., 2020).

These prospects increase the likelihood of Cpz entering surface waters and underscore the urgency of understanding its effects on aquatic habitats. The current body of research in this area is still limited, contradictory, and primarily focused on physiological indices. A high toxic pressure of Cpz has been confirmed in fish plasma models, with a concentration of 36 ng L^{-1} corresponding to critical environmental concentrations (CEC) (Sanderson et al., 2004). In the larvae of *Mytilus galloprovincialis*, Cpz inhibited metamorphosis by 50% (IC_{50}) at a concentration of 1.6×10^{-6} M (Yang et al., 2011). Nonetheless, in the rotifer *Brachionus calyciflorus*, known for its higher sensitivity to drugs compared to other invertebrates, exposure to Cpz significantly decreased life expectancy at hatching, the net reproduction rate, generation time, population growth rate, and dopamine concentration. This effect was observed at relatively high concentrations of 0.8, 1.2, 1.6, 2.0, 2.4, 2.8, and 3.2 mg/L (in acute exposure), as well as at concentrations of 0.125, 0.25, and 0.5 mg/L over a 7-day period (Feng et al., 2022). Biochemical responses to Cpz, particularly oxidative stress manifestations, are reported mainly in fish and in acute exposures to high (hundreds of μg and mg per L) concentrations (Li et al., 2008; Atama et al., 2022). To the best of our knowledge, biochemical responses of bivalve molluscs to Cpz in low (56 nM) concentrations were studied only in our previous works (Khoma et al., 2020; Khoma et al., 2022).

Based on this limited information concerning the effects of Cpz on aquatic animals and its complex pharmacological profile (Escudero et al., 2021), we expected that the common manifestations of cellular and biochemical stress responses can reflect the severity of the Cpz impact. Thus, the focus of this study was to indicate the effect of the Cpz on the marine mussel *Mytilus galloprovincialis* in the sub-chronic exposure. To reflect the effect of Cpz, we studied cell viability, cell volume regulation, and oxidative stress indexes. Among the markers of exposure, we selected the oxidative stress response because prolonged or high-dose treatment with pharmaceuticals causes as a side effect reactive oxygen species (ROS) generation. This is confirmed by a large body of data concerning the activities of antioxidant enzymes in exposed marine species (see the review of Fabbri and Franzellitti, 2016). For this study, we selected the first-line defense antioxidant enzymes superoxide dismutase (SOD) and catalase, and non-enzymatic antioxidant and most abundant low-weight intracellular thiol glutathione that directly reacts with ROS and other reactive species, and most approved indexes of the oxidative injury of lipids and proteins (Lushchak, 2012; Ighodaro and Akinloye, 2017; Lushchak and Storey, 2021). Two concentrations of Cpz

were selected for this study. The low concentration corresponded to the level detected in sewage treatment plant effluents (Baresel et al., 2015) and fell within the limits reported for surface waters (Yuan et al., 2013). This concentration was also compared with the critical environmental concentration estimated in the freshwater invertebrate *Gammarus pulex* and the human therapeutic plasma concentration of 36 ng L^{-1} (Miller et al., 2019). The high concentration corresponded to levels approximately equal to 1/100 of the EC50 value (1.805 mg L^{-1}) for *Daphnia magna* (Oliveira et al., 2015). Additionally, it was equivalent to the concentration of Cpz applied in our previous study to the freshwater bivalve mollusc *Unio tumidus* (18.0 µg L^{-1} for 14 days), which induced oxidative stress in this species (Khoma et al., 2020; Khoma et al., 2022).

2 Materials and methods

2.1 Experimental design

During the experiment, 200 bivalve molluscs of *Mytilus galloprovincialis* were collected and purchased from a commercial farm at "Faro Lake" by the "FARAU SRL Company, Frutti di Mare" in Messina, Italy. The specimens were divided into four groups (two replicates of 25 animals per group) and acclimatised for about 2 weeks in eight aquariums with 25 L of water each, equipped with oxygen aerators. Prior to commencing the main study, preliminary stability tests with Cpz were conducted in our experimental conditions. These tests involved analyzing the Cpz concentration at regular intervals over a period of 2 days within the tanks, ensuring that any potential degradation or decline was carefully monitored. Two Cpz concentrations (Cpz 1: 12 ng L^{-1}; Cpz 2: 12 µg L^{-1}) were administered to mussels for 14 days. Untreated molluscs (C-group) were also examined after the same period. Every 2 days, the tank's water was changed, and the chemicals were also prepared and refilled at the same time. The molluscs were fed with filtered lake water that had been enriched with nutrients and was given by the same company that provided animals during the experiment (salinity: 3.4% ± 0.02%, pH: 7.6 ± 0.01, T: 16.77°C ± 0.09°C). The experimental room had a light mode of 12:12 light-dark and was 18°C. After every water exchange, the salinity, pH, and temperature of the water were checked and matched the same standards as initially. After exposure, the molluscs were immediately anesthetized on ice and dissected.

2.2 Haemolymph collection

To perform cell viability tests on hemolymph, approximately 1 mL of hemolymph was extracted from the anterior adductor muscle of each mussel using a 1 mL plastic syringe equipped with a 23-gauge needle, following the established protocol described in the literature (Impellitteri et al., 2022; Pagano et al., 2022; Tresnakova et al., 2023b).

2.3 Cell viability of digestive gland cells and haemocytes

The present study investigated the effects of Cpz on cell viability by analyzing both haemolymph and digestive glands collected from pooled mussels (*Mytilus galloprovincialis*). The DG cells were isolated following a series of steps. Initially, the digestive glands were obtained from randomly selected animals in the aquarium. The glands were then mechanically minced and washed with a calcium and magnesium-free solution (CMFS; 1,100 mOsm; pH 7.3). Subsequently, the resulting mixture was transferred to a tube containing 6 mL of dissociating solution (0.01% collagenase) in CMSF and stirred slowly for 60 min at 18°C. The suspension was then filtered and centrifuged (500 rpm/10 min/4°C). After removing the supernatant, the cells were resuspended twice with saline. The samples were returned to the thermostatic bath at 18°C for another hour and then analysed using the staining techniques outlined below. Two distinct colorimetric assays, the Trypan Blue (TB) exclusion method and Neutral Red (NR) retention assay, were employed for this purpose. In the TB exclusion method, cells were stained with Trypan blue, which selectively enters non-viable cells with compromised membranes. Viable cells, in contrast, prevent the uptake of Trypan blue dye. The percentage of unstained cells in the cell suspension was used as an indicator of cell viability and helped assess the extent of cellular damage caused by Cpz. The neutral red retention assay (NR) was conducted to further assess lysosomal membrane stability. Following a 15-min incubation period, living cells exhibited the ability to absorb and bind the neutral red dye within their lysosomes. The extent of dye retention provided valuable insights into the stability of the lysosomal membrane, crucial for understanding the impact of Cpz on cellular structures. Cell viability was assessed according to the following formula:

$$cell\ viability\ (\%) = \frac{number\ of\ viable\ cells}{total\ number\ of\ cells} \times 100$$

This assay is based on the work of Torre et al. (2013) and has been widely used to study the effects of various substances on living cells, including recently (Porretti et al., 2023).

2.4 Regulation of volume decrease (RVD) evaluation

To evaluate the RVD assay in the digestive gland (DG) cells of *Mytilus galloprovincialis*, we adopted the methodology outlined by Pagano et al. (2016) and Impellitteri et al. (2023b). In particular, the procedures for isolating digestive gland cells and preparing samples for the RVD technique remain consistent with those outlined in section 2.3. Cell samples from DG were placed on a slide and observed under a light microscope (Carl Zeiss Axioskop 20, Wetzlar, Germany), connected to a Canon 550D camera. Three photos were taken sequentially after a gentle isotonic solution wash. Then, the sample was gently washed with a hypotonic solution (800 mOsm) before capturing images. The images were captured every minute for the first 10 minutes and then every 5 minutes for the subsequent 25 minutes. ImageJ software was used to compare the cell area of the exposed cells with that of the control group. In each experimental group, images were taken of 15 cells to ensure reliable measurements for the comparison.

2.5 Biomarkers of oxidative stress

For the biochemical analysis, the samples of digestive gland tissues in single-use aliquots were prepared individually from eight mussels in each experimental assay. Homogenates 10% w/v in 0.1 M

phosphate buffer, pH 7.4, containing 100 mM KCl and 1 mM EDTA, as well as 0.1 mM phenylmethylsulfonyl fluoride (PMSF) for proteolysis inhibition were utilized. Applied assays are described in detail in the Supplements (Martyniuk et al., 2022a; Martyniuk et al., 2022b).

For the enzyme assays, homogenates were centrifuged at 6,000 x *g* for 10 min. The resulting supernatants were kept at −40°C for measurements. The protein concentration in the supernatant (soluble protein) was measured according to the method of Lowry et al. (1951), using bovine serum albumin as the protein standard. The absorbance values were measured on a spectrophotometer UV/Vis ULAB 102UV (China).

Superoxide dismutase (SOD, EC 1.15.1.1) activity was measured according to the non-enzymatic assay based on aerobic reduction of nitro-blue tetrazolium (NBT) in the presence of phenazine methosulphate and NADH (Fried, 1975). The reduction of NBT was registered at 560 nm. The results were expressed as SOD units per mg of soluble protein (one unit of SOD is defined as the amount of enzyme that causes 50% inhibition of NBT reduction).

Catalase (CAT, EC 1.11.1.6) activity was measured by monitoring the decomposition of H_2O_2 according to Aebi (1974). The reaction was measured at 240 nm (ε = 0.04 mM^{-1} cm^{-1}) and expressed as μmol min^{-1}·mg^{-1} soluble protein.

Total glutathione (reduced plus oxidized, GSH plus GSSG, correspondingly) concentration was quantified in the protein-free extract of 10% w/v homogenate by the glutathione reductase recycling assay (Griffith, 1980) using 5,5′-dithio-bis(2-nitrobenzoic acid) DTNB for thiols quantification. To obtain the extract, 20% sulfosalicylic acid was added to homogenate in the proportion 1:3 and mix was centrifuged (12,000×*g*, 4 °C). Standards were prepared from GSH, and concentrations were expressed as μmol per g wet weight. To estimate the GSSG (in GSH-Eq) level, the protein free sample was treated with 2-vinylpyridine prior to the assay. The concentration of GSH was calculated as the difference between the total glutathione and GSSG concentrations. The redox-index of glutathione (RI GSH) as the ratio of concentrations GSH/GSSG was calculated.

The products of lipid peroxidation (LPO) were determined in the 10% w/v homogenate as the production of thiobarbituric acid-reactive substances (TBARS) after the sedimentation of proteins in sulfosalicylic acid (Ohkawa et al., 1979). The absorbance of the chromogen was determined at 532 nm (ε = 1.56 × 10^5 M^{-1} cm^{-1}). Concentrations were expressed as nmol·g^{-1} fresh weight (FW).

Protein carbonyls (PC) as an index of protein oxidation were analyzed in the sediments of proteins from digestive gland tissue in sulfosalicylic acid with 2.4-dinitrophenylhydrazine (DNPH) (Reznick and Packer, 1994). PC concentrations were calculated from the absorbance at 370 nm using a molar absorption coefficient of 22.000 M^{-1} cm^{-1} and expressed as μmol PC·g^{-1} FW.

2.6 Statistical analysis

The one-way ANOVA and Tukey's *post hoc* test were used to compare the viability of digestive gland and haemocyte cells. Results for RVD tests were obtained by employing one-way ANOVA and Tukey's *post hoc* multiple comparison tests. The significance of the *p*-value was established as $p < 0.05$. The results were expressed as mean ± standard error. For all biochemical traits, the sample size was six from six individuals. Data were tested for normality and homogeneity of variance by using the Shapiro-Wilk test and Levene's tests, respectively. Whenever possible, data were normalized by Box-Cox common transforming method. One-way ANOVA was used to test the effect of treatments, followed by *post hoc* procedures. Pearson correlation analysis was performed to analyze the strength and direction of the linear relationship between two continuous variables. The correlation was significant at $p < 0.05$ level. For the data that were not normally distributed, non-parametric tests (Kruskall–Wallis ANOVA and Mann–Whitney U-test) were performed. Normalized, Box-Cox transformed data were subjected to the principal component analysis (PCA) to assess the relations between measured parameters utilizing the rotation method Varimax with Kaiser Normalization, and Canonical discriminant analysis was utilized for the separation of the exposed groups. The IBM SPSS Statistics version 24 software for Windows was used for calculations.

The calculation of the balance between the levels of antioxidants and prooxidative manifestations (an index of Antioxidant/Pro-oxidant Balance, APB) was accomplished. It was defined as the shift of the equilibrium between antioxidant (SOD, CAT, GSH) and pro-oxidative manifestation (TBARS, Protein carbonyls, GSSG) values. Mean values in each group were utilized for this calculation and marked as Mi for exposed groups and Mc for control group. Each index in the exposed groups was standardized as a rate of deviation from control value A = 100*(Mi-Mc)/Mc. The integrative index APB was calculated as the ratio (SOD+CAT+GSH)/(TBARS+PC+GSSG) in the relative units assuming that the mean value of APB in the control group equalled 1.0 (Khoma et al., 2020).

3 Results

3.1 Cell viability of digestive gland cells and haemocytes

After 14 days of exposure, the viability of digestive gland cells remained high across all conditions tested, with a percentage of cells found alive above 90%. However, significant differences were observed between the groups (Table 1). The group exposed to the higher concentration (Cpz 2) exhibited significantly lower viability ("**" $p < 0.01$) compared to the control group (C) and to the lower concentration (Cpz 1; "aa" $p < 0.01$). This observation was consistent in both the NR and TB tests.

On the other hand, following the same exposure period, hemolymph cells from all tested conditions, displayed high lysosomal membrane stability, with over 90% cell viability. This trend was consistent across the groups and was also reflected in the Trypan Blue exclusion method (Table 2).

3.2 Regulation of volume decrease (RVD) evaluation

M. galloprovincialis is an osmoconform organism, which translates into the ability of the cells of the digestive gland to

TABLE 1 Percentage of the digestive cells' viability in *Mytilus galloprovincialis* after 14 days of exposure to chlorpromazine (Cpz). The tests conducted were Trypan Blue (TB) exclusion method and Neutral Red (NR) retention assay. Values are presented as mean ± SE (n = 12).

Method	Sampling time	Tested group		
		Control (0 mg/L)	Cpz 1 (12 ng L^{-1})	Cpz 2 (12 µg L^{-1})
TB	14 Days	99% ± 1	98% ± 0.6	95% ± 2.2**aa
NR	14 Days	99% ± 0.1	98% ± 0.2	94% ± 0.7**aa

One-way ANOVA, was used to assert the difference between the control group and for comparing the treats to each other. The * represents the differences compared to the control group: *$p < 0.05$, **$p < 0.01$. The letter "a" represents the differences in the treated groups; Cpz 2 was compared to Cpz 1: "a" < 0.05, "aa" < 0.01.

TABLE 2 Percentage of the haemocytes' viability in *Mytilus galloprovincialis* after 14 days of exposure to chlorpromazine (Cpz). The tests conducted were Trypan Blue (TB) exclusion method and Neutral Red (NR) retention assay. Values are presented as mean ± SE (n = 12).

Method	Sampling time	Tested group		
		Control (0 mg/L)	Cpz 1 (12 ng L)	Cpz 2 (12 µg L)
TB	14 Days	98% ± 0.5	98% ± 0.4	97% ± 0.6
NR	14 Days	98% ± 0.2	98% ± 0.3	96% ± 0.8

One-way ANOVA, was used to assert the difference between the control group and for comparing the treats to each other. The * represents the differences compared to the control group: *$p < 0.05$, **$p < 0.01$. The letter "a" represents the differences in the treated groups; Cpz 2 was compared to Cpz 1: "a" < 0.05, "aa" < 0.01.

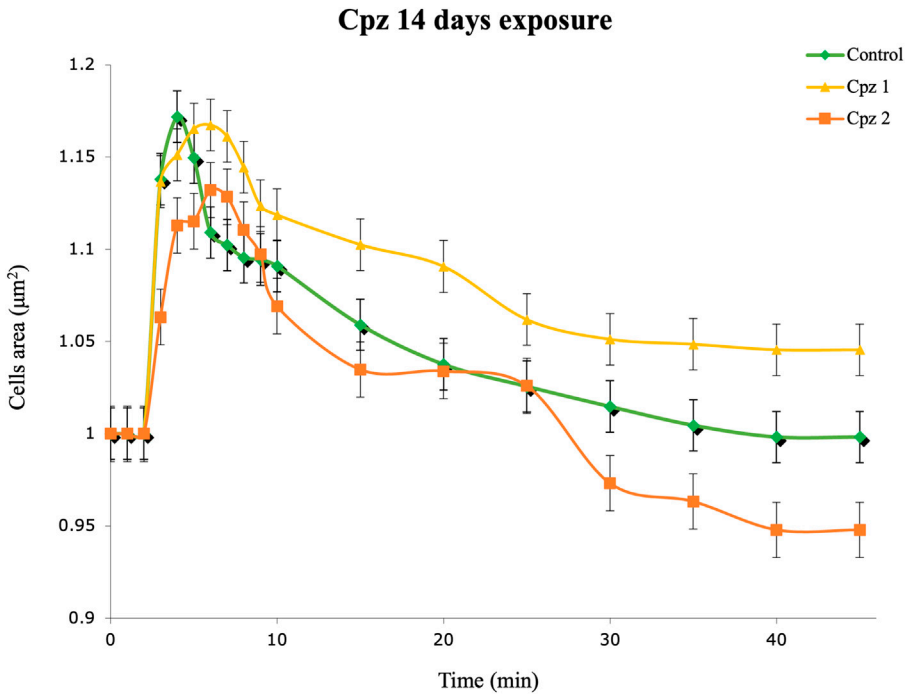

FIGURE 1
Regulation volume decrease (RVD) of digestive gland cells of *Mytilus galloprovincialis* after 14 days of exposure to Chlorpromazine (Cpz). Rhombuses (◆) represent control (0 mg L^{-1}); triangles (▲) represent the Cpz 1 group (12 ng $L^{-1}$of Cpz); squares (■) represent the Cpz 2 group (12 µg $L^{-1}$of Cpz). Data are presented as mean ± SE (n = 12).

regulate their volume in the presence of a hypotonic solution. This regulatory mechanism results in swelling and subsequent gradual restoration of their original volumetric dimensions over time. Consequently, under physiological conditions, when exposed to a hypotonic environment, digestive gland cells swell and then gradually return to their original volume, demonstrating their ability to maintain cellular homeostasis.

Our statistical analysis revealed no statistically significant differences in the results of the Cpz exposure experiments compared to the control group. However, upon closer

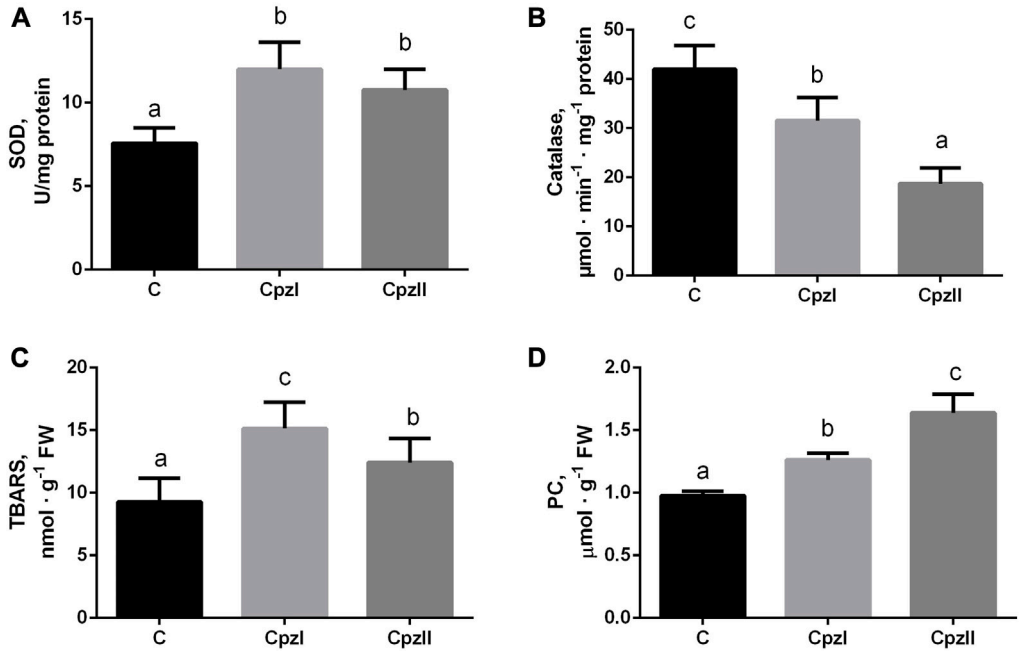

FIGURE 2
The antioxidant enzyme activities and manifestations of oxidative lesions in the digestive gland of bivalve molluscs *Mytilus galloprovincialis* following exposure to two concentrations of chlorpromazine (Cpz) for 14 days: **(A)**, superoxide dismutase; **(B)**, catalase; **(C)**, TBARS; **(D)**, Protein carbonyls. Groups: C - control group, Cpz 1–12 ng $L^{-1}$of Cpz; Cpz 2–12 μg $L^{-1}$of Cpz. Different letters above the columns indicate significant differences between groups, $M \pm SD$, $N = 8$, $p < 0.05$. Data were analyzed by using SPSS Statistics for Windows, Version 24.

examination of the data, subtle variations can still be observed between the tested and control groups. In the Cpz 1 group, we observed a trend whereby DG cells appeared to have difficulty returning to their initial volume, resulting in prolonged swelling (Figure 1). Furthermore, DG cells exposed to the highest concentration of Cpz showed unusual contraction patterns.

3.3 Oxidative stress indexes

The evaluation of the antioxidant manifestations detected opposite trends for each studied enzyme in both exposed groups (Figures 2A, B). The SOD activity increased, and catalase, particularly in Cpz 2 group, - decreased. This misbalance in the antioxidant activities was accompanied by the elevation of TBARS and protein carbonyls levels (Figures 2C, D).

3.3.1 Exposed versus control

The concentration of GSH increased similarly in both exposures to Cpz, whereas the level of GSSG increased only by the low Cpz concentration, and, consequently, RI GSH increased compared to control under the effect of CpzII only (Figures 3A–C).

The mean value of antioxidant/pro-oxidant manifestations (APB) in the control group was taken as 1.0. The calculations of its shift in the exposures indicated that in both exposed groups, despite the individual indexes had different concentration-dependent deviations (Figure 3D), APB decreased against control almost equally (by 52.8% and 50.8% in the Cpz 1 and Cpz 2 groups correspondingly).

4 Discussion

To obtain a complete understanding of the health status of the model organism, we conducted cell tests on both haemolymph and digestive gland cells. With regard to haemolymphatic cells, they represent the first line of defence against pathogens and xenobiotics and can be considered suitable biomarkers for monitoring the effects of environmental stress (Multisanti et al., 2023). Hemocytes can recognize and eliminate pathogens and xenobiotics through phagocytosis and the secretion of antimicrobial peptides, various humoral factors, and reactive oxygen intermediates (Impellitteri et al., 2022). By evaluating the viability of hemocytes, we gained valuable insights into the overall health status of our model organism. The viability of hemocytes is indicative of their capacity to respond to stressors and maintain their functional integrity in the presence of environmental challenges. The digestive gland (DG) of *M. galloprovincialis* assumes a crucial function in digesting nutrients vital for the organism's survival. Moreover, the DG serves as a critical detoxification centre. Nevertheless, owing to its vulnerability to the buildup of pollutants, this organ can become a central target for environmental stressors. By assessing the viability of haemocytes together with that of digestive gland cells, we can understand how Cpz may influence the body's immune defence and detoxification capabilities. NR uptake is a valuable indicator for assessing the stability of lysosomal membranes in bivalve cells. Lysosomes play a crucial role as cytoplasmic organelles, harbouring several hydrolytic enzymes with optimal activity at acidic pH levels. Their ability to degrade a wide range of biological molecules is crucial for cell health.

10.3389/fphys.2023.1267953

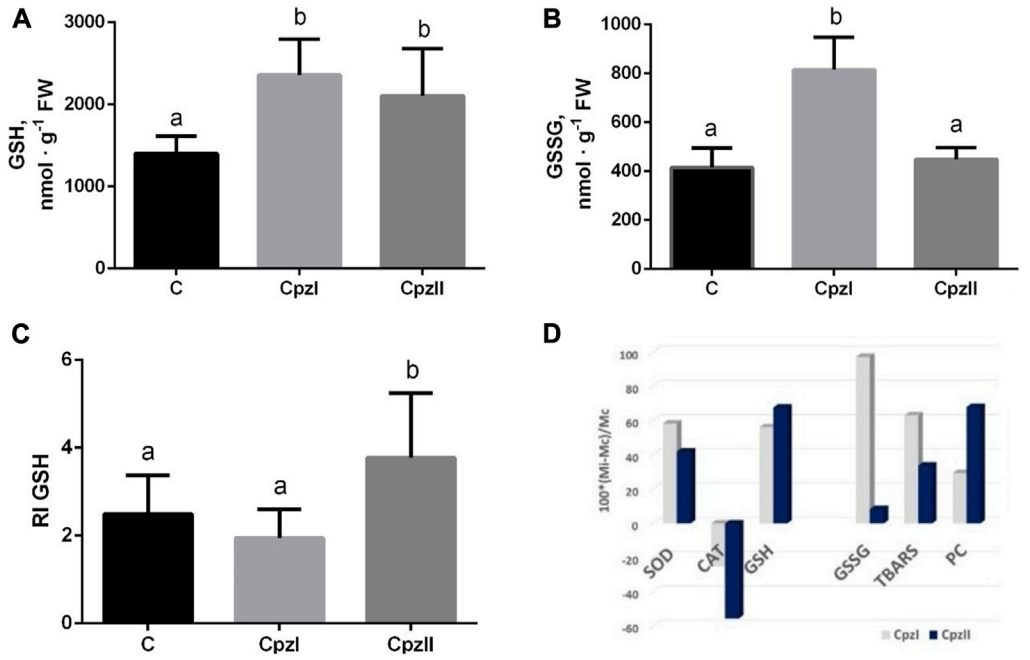

FIGURE 3
The concentrations of GSH **(A)**, GSSG **(B)**, redox index of glutathione **(C)**, and relative changes of each analyzed oxidative stress index **(D)** in the digestive gland of bivalve molluscs *Mytilus galloprovincialis* following exposure to two concentrations of chlorpromazine (Cpz) for 14 days. Groups: C - control group, Cpz 1–12 ng $L^{-1}$of Cpz; Cpz 2–12 μg $L^{-1}$of Cpz. Different letters above the columns indicate significant differences between groups, $M \pm SD$, $N = 8$, $p < 0.05$. Data were analyzed by using SPSS Statistics for Windows, Version 24.

It is particularly noteworthy that lysosomes act as specific targets for the toxic effects of many contaminants, accumulating pollutants and becoming sensitive indicators of cellular health. In mussels, the lysosomal vacuolar system is particularly important (Moore et al., 2004). Digestive gland cells, enriched with lysosomes, are a key interface between the organism and its environment, facilitating intracellular digestion. In addition, the small granulocytes of the haemolymph, also rich in lysosomes, contribute to digestion processes and innate immune response mechanisms (Martínez-Gómez et al., 2015). Efficient regulation of this process could contribute significantly to the ability of some organisms to adapt and survive in stressful and polluted habitats.

The trypan blue exclusion test allowed us to ascertain the number of viable cells in a cell suspension. In our results, only digestive gland cells showed substantial significance ($p \leq 0.01$) in the Cpz 2 group compared to the control group, in both the NR and TB tests. The observed decline in cell viability suggests potential damage to the cell membrane. These findings align with similar studies reported in the literature (e.g., Pagano et al., 2022; Impellitteri et al., 2023a; Tresnakova et al., 2023a; Impellitteri et al., 2023b; Tresnakova et al., 2023b).

However, it is crucial to note that although the integrity of the cell membrane may remain intact, such as in haemolymph cells, the overall viability of the cell, including its growth and functionality, may still be affected.

While our viability tests indicated potential detrimental effects of Cpz on DG cells, the examination of these cells' ability to regain their original volume when exposed to a hypotonic solution, as demonstrated by the RVD assay, did not reveal statistically significant differences among the treatment groups compared to the control group. Cells of osmoconform organisms can sense and respond to osmotic changes in their environment by adjusting volume (Tresnakova et al., 2023a; Impellitteri et al., 2023b; Tresnakova et al., 2023b). The RVD evaluation can detect changes in this process caused by pollutants, offering an accurate approach to evaluating cellular harm. In the Cpz 1 group, we noted a pattern in which DG cells seemed to struggle to revert to their original volume, leading to a prolonged state of swelling. Conversely, DG cells exposed to the highest Cpz concentration displayed atypical shrinkage patterns. It is crucial to emphasize that while these observations may appear notable in the graphical representation (Figure 1), they did not reach statistical significance in our analysis. We acknowledge that the absence of statistical significance indicates that these differences could be attributed to chance variation rather than true effects of Cpz exposure.

The response of oxidative stress is a common biological phenomenon that is caused by external or internal adverse effects in organisms, including bivalve molluscs (Fabbri and Franzellitti, 2016; Moreira et al., 2016; Paital et al., 2016; Gnatyshyna et al., 2020; Matozzo et al., 2020). However, the manifestations of oxidative stress differ depending on the severity of the impact (Lushchak, 2011; Moreira et al., 2016). In the present study, despite it was indicated the increase in both antioxidative (SOD, GSH) and oxidative (TBARS, PC, GSSG) manifestations (Figure 3D), the general direction of their imbalance was pro-oxidative. The catalase activity was the most vulnerable target of the pharmaceutical Cpz. Its decrease in both exposures seems to be

the crucial event in the prooxidative shift that allows transient accumulation of hydrogen peroxide H_2O_2 and hydroxyl radical OH·, the reactive intermediates of the activity of SOD, resulting in greater oxidative lesions (Ransy et al., 2020; Alam et al., 2022). This manifestation is consistent with other results concerning the impaired antioxidant capacity in bivalve molluscs. For example, in the 15-day exposure of *M. galloprovincialis* to mixtures of non-steroidal inflammatory drugs ibuprofen and diclofenac and selective serotonin reuptake inhibitor fluoxetine without or along with the addition of copper, a catalase gene expression was downregulated. In the cladoceran species *Daphnia* magna, exposure to 1.0 μg of Cpz L^{-1} also caused a decrease in catalase activity, as the most prominent sign of oxidative stress (Oliveira et al., 2015).

Among indexes of oxidative stress, GSSG has shown the most selective concentration-depending response. The balanced increase of GSH and GSSG levels in the Cpz 1 group can be explained by the activation of glutathione peroxidase-related way of the destruction of H_2O_2 coupled with the oxidation of the GSH (Manduzio et al., 2005). Under exposure to higher Cpz concentration, the utilization of GSH seems to be reduced, which, in turn, leads to the elevated redox balance modulating cellular metabolism (Xiao and Loscalzo, 2020; Martyniuk et al., 2022b).

Importantly, the indicated features of the oxidative changes in the present study are similar to that reported early for the freshwater bivalve mollusc *Unio tumidus* subjected to Cpz in the concentration of 18.0 μg L^{-1} for 14 days (Khoma et al., 2020; Khoma et al., 2022). In particular, there were confirmed the responses of catalase, TBARS and GSH, and the total balance of antioxidants versus prooxidative changes (APB).

Phenothiazine and its derivatives including Cpz have been known for many years as potent antioxidants, based on its reducing activity via the formation of radical cation, in the interaction, for example, with the thiyl radical derived from GSH (Tamba and O`Neill, 1991). Nevertheless, the studies on vertebrates inform about its antioxidant or prooxidant effects. In fish *Carassius auratus*, acute toxicity of Cpz indicated as the median lethal concentration (LC_{50}) in 24, 48 and 96 has 1.11, 0.43 and 0.32 mg L^{-1} correspondingly, was accompanied with the oxidative manifestations different depending on the time of exposure (Li et al., 2008).

Some signs of Cpz pro-oxidative effects were confirmed in the erythrocytes from human blood treated with Cpz in concentrations observed *in vivo* at therapeutic doses (1–100 μM) for 2 hours (Ficarra et al., 2016). However, unlike our finding for molluscs, these authors had shown almost twice reduce in GSH/GSSG ratio. In the brain of rats, the chronic intraperitoneal administration of Cpz (5 and 10 mg kg^{-1}) induced the antioxidant enzyme SOD, but did not affect catalase, and inhibited lipid peroxidation (Roy et al., 1984).

Hence, our results confirm that the impact on the antioxidant-pro-oxidant balance is the intrinsic feature of Cpz toxicity. According to the intensity-based classifications of oxidative stress strong oxidative stress (Lushchak and Storey, 2021), or "oxidative distress" (Sies, 2017) was caused even by low pM and nM concentrations of Cpz, which induced the increase of the level of ROS-modified molecules and disturbed activities of antioxidant enzymes, and consequently, it has been implicated in the cellular injury.

Bivalve molluscs represent vulnerable to the oxidative impact of Cpz model organisms. The deleterious physiological effects of Cpz detected in the present study, obviously are the consequences of the biochemical changes caused by Cpz. Therefore, aiming to create a realistic view of the Cpz ecotoxicity on aquatic habitats it is crucially important to study its effect in prolonged exposures with a focus on the antioxidant capacity as the most probable target of this reductive active compound.

5 Conclusion

Based on our findings, it has been observed that Cpz (Chlorpromazine), even at low nanomolar concentrations, induces non-specific symptoms of biochemical and physiological disturbances in *M. galloprovincialis*, a species of marine mussel. These disturbances manifest in various ways and appear to affect the vitality of cells, leading to an imbalance in oxidative stress with a pro-oxidative shift. The impact of Cpz in *M. galloprovincialis* suggests that this substance can have detrimental effects on the mussels even at very low concentrations. In light of our findings, it is essential to consider the implications of potential environmental exposure to Cpz, as marine organisms such as mussels often come into contact with diverse pollutants and pharmaceuticals that enter aquatic environments. Further research and monitoring may be necessary to better understand the extent of Cpz's effects on marine ecosystems and to assess potential risks to aquatic organisms like *M. galloprovincialis*. Understanding these impacts can aid in developing appropriate measures to protect aquatic environments and the organisms living within them.

Data availability statement

The original contributions presented in the study are included in the article/Supplementary Material, further inquiries can be directed to the corresponding author.

Ethics statement

Ethical approval was not required for the study involving animals in accordance with the local legislation and institutional requirements because this is not applicable, because they are invertebrates and the legislation do not require ethical approval.

Author contributions

FI: Formal Analysis, Methodology, Writing–review and editing. KY: Investigation, Software, Validation, Visualization, Writing–original draft. VM: Investigation, Validation, Visualization, Writing–original draft. VK: Investigation, Validation, Visualization, Writing–original draft. GP: Supervision, Validation, Writing–review and editing. OS: Conceptualization, Data curation, Project administration, Writing–original draft, Writing–review and editing. CF: Project administration, Supervision, Writing–original draft, Writing–review and editing.

Funding

The author(s) declare financial support was received for the research, authorship, and/or publication of this article. This work has been partially granted to Oksana Stoliar by the University of Messina, Italy (Award of Visiting Professor in the academic year 2022/2023).

Conflict of interest

The authors declare that the research was conducted in the absence of any commercial or financial relationships that could be construed as a potential conflict of interest.

The author(s) declared that they were an editorial board member of Frontiers, at the time of submission. This had no impact on the peer review process and the final decision.

Publisher's note

References

Aebi, H. (1974). "Catalase," in *Methods of enzymatic analysis* (London: Academic Press), 671–684.

Alam, M. R., Ehiguese, F. O., Vitale, D., and Martín-Díaz, M. L. (2022). Oxidative stress response to hydrogen peroxide exposure of *Mytilus galloprovincialis* and *Ruditapes philippinarum:* reduced embryogenesis success and altered biochemical response of sentinel marine bivalve species. *Environ. Chem. Ecotoxicol.* 4, 97–105. doi:10.1016/j.enceco.2022.01.002

Aleya, L., and Uddin, M. S. (2020). Environmental pollutants and the risk of neurological disorders. *Environ. Sci. Pollut. Res. Int.* 27, 44657–44658. doi:10.1007/s11356-020-11272-3

Atama, C. I., Nnaji, E. C., Christian Ezeoyili, I., Udeani, F. O., Onovo, C. J., Ike Ossai, N., et al. (2022). Neuromodulatory and oxidative stress evaluations in African catfish *Clarias gariepinus* exposed to antipsychotic drug chlorpromazine. *Drug Chem. Toxicol.* 45, 1318–1324. doi:10.1080/01480545.2020.1822391

Baresel, C., Palm Cousins, A., Hörsing, M., Ek, M., Ejhed, H., Allard, A. S., et al. (2015). *Pharmaceutical residues and other emerging substances in the effluent of sewage treatment plants*. IVL Swedish Environmental Research Institute. Report B, 2226.

Bottoni, P., Caroli, S., and Barra Caracciolo, A. (2010). Pharmaceuticals as priority water contaminants. *Toxicol. Environ. Chem.* 92, 549–565. doi:10.1080/02772241003614320

Burgos-Aceves, M. A., Abo-Al-Ela, H. G., and Faggio, C. (2021). Impact of phthalates and bisphenols plasticizers on haemocyte immune function of aquatic invertebrates: A review on physiological, biochemical, and genomic aspects. *J. Hazard. Mat.* 419, 126426. doi:10.1016/j.jhazmat.2021.126426

Burgos-Aceves, M. A., Cohen, A., Paolella, G., Lepretti, M., Smith, Y., Faggio, C., et al. (2018). Modulation of mitochondrial functions by xenobiotic-induced microRNA: from environmental sentinel organisms to mammals. *Sci. Total Env.* 645, 79–88. doi:10.1016/j.scitotenv.2018.07.109

Chahouri, A., Yacoubi, B., Moukrim, A., and Banaoui, A. (2023). Bivalve molluscs as bioindicators of multiple stressors in the marine environment: recent advances. *Cont. Shelf Res.* 264, 105056. doi:10.1016/j.csr.2023.105056

Curpan, A. S., Impellitteri, F., Plavan, G., Ciobica, A., and Faggio, C. (2022). Review: *mytilus galloprovincialis*: an essential, low-cost model organism for the impact of xenobiotics on oxidative stress and public health. *Comp. Biochem. Physiol. C Toxicol. Pharmacol.* 256, 109302. doi:10.1016/j.cbpc.2022.109302

Darkin, S., McQuillan, J., and Ralph, R. K. (1984). Chlorpromazine: a potential anticancer agent? *Biochem. Biophys. Res. Commun.* 125, 184–191. doi:10.1016/s0006-291x(84)80352-6

Dudley, K., Liu, X., and De Haan, S. (2017). Chlorpromazine dose for people with schizophrenia. *Cochrane Database Syst. Rev.* 4, CD007778. doi:10.1002/14651858.CD007778.pub2

Escudero, J., Muñoz, J. L., Morera-Herreras, T., Hernandez, R., Medrano, J., Domingo-Echaburu, S., et al. (2021). Antipsychotics as environmental pollutants: an underrated threat? *Sci. Total Environ.* 769, 144634. doi:10.1016/j.scitotenv.2020.144634

Fabbri, E., and Franzellitti, S. (2016). Human pharmaceuticals in the marine environment: focus on exposure and biological effects in animal species. *Environ. Toxicol. Chem.* 35, 799–812. doi:10.1002/etc.3131

Faggio, C., Tsarpali, V., and Dailianis, S. (2018). Mussel digestive gland as a model tissue for assessing xenobiotics: an overview. *Sci. Total Environ.* 636, 220–229. doi:10.1016/j.scitotenv.2018.04.264

Feng, S., Zhang, Y., Gao, F., Li, M., Zhu, L., Wen, H., et al. (2022). Inhibitory effects of antipsychotic chlorpromazine on the survival, reproduction and population growth other than neurotransmitters of zooplankton in light of global warming. *Int. J. Environ. Res. Public Health.* 19, 16167. doi:10.3390/ijerph192316167

Ficarra, S., Russo, A., Barreca, D., Giunta, E., Galtieri, A., and Tellone, E. (2016). Short-Term effects of chlorpromazine on oxidative stress in erythrocyte functionality: activation of metabolism and membrane perturbation. *Oxid. Med. Cell Longev.* 2016, 2394130. doi:10.1155/2016/2394130

Frédéric, O., and Yves, P. (2014). Pharmaceuticals in hospital wastewater: their ecotoxicity and contribution to the environmental hazard of the effluent. *Chemosphere* 115, 31–39. doi:10.1016/j.chemosphere.2014.01.016

Freitas, R., Silvestro, S., Coppola, F., Costa, S., Meucci, V., Battaglia, F., et al. (2020). Toxic impacts induced by Sodium lauryl sulfate in *Mytilus galloprovincialis*. *Comp. Biochem. Physiol. A Mol. Integr. Physiol.* 242, 110656. doi:10.1016/j.cbpa.2020.110656

Fried, R. (1975). Enzymatic and non-enzymatic assay of superoxide dismutase. *Biochimie* 57, 657–660. doi:10.1016/s0300-9084(75)80147-7

Gnatyshyna, L., Khoma, V., Mishchuk, O., Martinyuk, V., Spriņģe, G., and Stoliar, O. (2020). Multi-marker study of the responses of the *Unio tumidus* from the areas of small and micro hydropower plants at the Dniester River Basin, Ukraine. *Environ. Sci. Pollut. Res. Int.* 27, 11038–11049. doi:10.1007/s11356-020-07698-4

Griffith, O. W. (1980). Determination of glutathione and glutathione disulfide using glutathione reductase and 2-vinylpyridine. *Anal. Biochem.* 106, 207–212. doi:10.1016/0003-2697(80)90139-6

Ighodaro, O. M., and Akinloye, O. A. (2017). First line defence antioxidants-superoxide dismutase (SOD), catalase (CAT) and glutathione peroxidase (GPX): their fundamental role in the entire antioxidant defence grid. *Alexandria J. Med.* 54, 287–293. doi:10.1016/j.ajme.2017.09.001

Impellitteri, F., Curpăn, A. S., Plăvan, G., Ciobica, A., and Faggio, C. (2022). Hemocytes: A useful tool for assessing the toxicity of microplastics, heavy metals, and pesticides on aquatic invertebrates. *Int. J. Environ. Res. Public Health.* 19, 16830. doi:10.3390/ijerph192416830

Impellitteri, F., Multisanti, C. R., Rusanova, P., Piccione, G., Falco, F., and Faggio, C. (2023a). Exploring the impact of contaminants of emerging concern on fish and invertebrates Physiology in the mediterranean sea. *Biology* 12, 767. doi:10.3390/biology12060767

Impellitteri, F., Yunko, K., Martyniuk, V., Matskiv, T., Lechachenko, S., Khoma, V., et al. (2023b). Physiological and biochemical responses to caffeine and microplastics in *Mytilus galloprovincialis*. *Sci. Total Environ.* 890, 164075. doi:10.1016/j.scitotenv.2023.164075

Khoma, V., Gnatyshyna, L., Martinyuk, V., Mackiv, T., Yunko, K., Formanchuk, R., et al. (2020). Combined exposures to low Roundup concentration induce thiolome response in bivalve mollusk. *Sci. Issues TNPU. Ser. Biol.* 80, 72–78. doi:10.25128/2078-2357.20.3-4.9

Khoma, V., Martinyuk, V., Matskiv, T., Gnatyshyna, L., Baranovsky, V., Gladiuk, M., et al. (2022). Environmental concentrations of Roundup in combination with chlorpromazine or heating causes biochemical disturbances in the bivalve mollusc *Unio tumidus*. *Environ. Sci. Pollut. Res. Int.* 29, 14131–14142. doi:10.1007/s11356-021-16775-1

Lee, W. Y., Lee, W. T., Cheng, C. H., Chen, K. C., Chou, C. M., Chung, C. H., et al. (2015). Repositioning antipsychotic chlorpromazine for treating colorectal cancer by inhibiting sirtuin 1. *Oncotarget* 6, 27580–27595. doi:10.18632/oncotarget.4768

Li, T., Zhou, Q., Zhang, N., and Luo, Y. (2008). Toxic effects of chlorpromazine on *Carassius auratus* and its oxidative stress. *J. Environ. Sci. Health B.* 43, 638–643. doi:10.1080/03601230802352674

Lowry, O. H., Rosebrough, N. J., Farr, A. L., and Randall, R. J. (1951). Protein measurement with the Folin phenol reagent. *J. Biol. Chem.* 193, 265–275. doi:10.1016/S0021-9258(19)52451-6

Lushchak, V. I. (2011). Environmentally induced oxidative stress in aquatic animals. *Aquat. Toxicol.* 101, 13–30. doi:10.1016/j.aquatox.2010.10.006

Lushchak, V. I. (2012). Glutathione homeostasis and functions: potential targets for medical interventions. *J. Amino Acids* 2012, 736837. doi:10.1155/2012/736837

Lushchak, V. I., and Storey, K. B. (2021). Oxidative stress concept updated: definitions, classifications, and regulatory pathways implicated. *EXCLI J.* 20, 956–967. doi:10.17179/excli2021-3596

Manduzio, H., Rocher, B., Durand, F., Galap, C., and Leboulenger, F. (2005). The point about oxidative stress in molluscs. *Inf. Syst. J.* 2.

Martínez-Gómez, C., Bignell, J. P., and Lowe, D. (2015). Lysosomal membrane stability in mussels. *ICES Tech. Mar. Environ. Sci.* 56, 1–46.

Martyniuk, V., Gylytė, B., Matskiv, T., Khoma, V., Tulaidan, H., Gnatyshyna, L., et al. (2022a). Stress responses of bivalve mollusc *Unio tumidus* from two areas to ibuprofen, microplastic and their mixture. *Ecotoxicology* 31, 1369–1381. doi:10.1007/s10646-022-02594-8

Martyniuk, V., Khoma, V., Matskiv, T., Baranovsky, V., Orlova-Hudim, K., Gylytė, B., et al. (2022b). Indication of the impact of environmental stress on the responses of the bivalve mollusk *Unio tumidus* to ibuprofen and microplastics based on biomarkers of reductive stress and apoptosis. *Comp. Biochem. Physiol. C Toxicol. Pharmacol.* 261, 109425. doi:10.1016/j.cbpc.2022.109425

Martyniuk, V., Khoma, V., Matskiv, T., Yunko, K., Gnatyshyna, L., Stoliar, O., et al. (2023). Combined effect of microplastic, salinomycin and heating on *Unio tumidus*. *Environ. Toxicol. Pharmacol.* 98, 104068. doi:10.1016/j.etap.2023.104068

Matozzo, V., Fabrello, J., and Marin, M. G. (2020). The effects of glyphosate and its commercial formulations to marine invertebrates: a review. *J. Mar. Sci. Eng.* 8, 399. doi:10.3390/jmse8060399

Miller, T. H., Ng, K. T., Bury, S. T., Bury, S. E., Bury, N. R., and Barron, L. P. (2019). Biomonitoring of pesticides, pharmaceuticals and illicit drugs in a freshwater invertebrate to estimate toxic or effect pressure. *Environ. Int.* 129, 595–606. doi:10.1016/j.envint.2019.04.038

Moore, M. N., Lowe, D., and Köhler, A. (2004). Biological effects of contaminants: measurement of lysosomal membrane stability. *ICES Tech. Mar. Environ. Sci.* 36, 1–31. doi:10.17895/ices.pub.5060

Moreira, D. C., Venancio, L. P. R., Sabino, M. A. C. T., and Hermes-Lima, M. (2016). How widespread is preparation for oxidative stress in the animal kingdom? *Comp. Biochem. Physiol. A Mol. Integr. Physiol.* 200, 64–78. doi:10.1016/j.cbpa.2016.01.023

Moreira, D. G., Aires, A., de Lourdes Pereira, M., and Oliveira, M. (2022). Levels and effects of antidepressant drugs to aquatic organisms. *Comp. Biochem. Physiol. C Toxicol. Pharmacol.* 256, 109322. doi:10.1016/j.cbpc.2022.109322

Multisanti, C. R., Riolo, K., Impellitteri, F., Chebbi, I., Faggio, C., and Giannetto, A. (2023). Short-term *in vitro* exposure of *Pinctada imbricata's* haemocytes to quaternium-15: exploring physiological and cellular responses. *Environ. Toxicol. Pharmacol.* 101, 104198. doi:10.1016/j.etap.2023.104198

Ohkawa, H., Ohishi, N., and Yagi, K. (1979). Assay for lipid peroxides in animal tissues by thiobarbituric acid reaction. *Anal. Biochem.* 95, 351–358. doi:10.1016/0003-2697(79)90738-3

Oliveira, L. L., Antunes, S. C., Gonçalves, F., Rocha, O., and Nunes, B. (2015). Evaluation of ecotoxicological effects of drugs on *Daphnia magna* using different enzymatic biomarkers. *Ecotoxicol. Environ. Saf.* 119, 123–131. doi:10.1016/j.ecoenv.2015.04.028

Pagano, M., Capillo, G., Sanfilippo, M., Palato, S., Trischitta, F., Manganaro, A., et al. (2016). Evaluation of functionality and biological responses of *Mytilus galloprovincialis* after exposure to quaternium-15 (methenamine 3-chloroallylochloride). *Molecules* 21, 144. doi:10.3390/molecules21020144

Pagano, M., Savoca, S., Impellitteri, F., Albano, M., Capillo, G., and Faggio, C. (2022). Toxicological evaluation of acetylsalicylic acid in non-target organisms: chronic exposure on *Mytilus galloprovincialis* (lamarck, 1819). *Front. Physiol.* 13, 920952. doi:10.3389/fphys.2022.920952

Pagano, M., Stara, A., Aliko, V., and Faggio, C. (2020). Impact of neonicotinoids to aquatic invertebrates—*in vitro* studies on *Mytilus galloprovincialis*: A review. *J. Mar. Sci. Eng.* 8, 801. doi:10.3390/jmse8100801

Pain-Devin, S., Cossu-Leguille, C., Geffard, A., Giambérini, L., Jouenne, T., Minguez, L., et al. (2014). Towards a better understanding of biomarker response in field survey: a case study in eight populations of zebra mussels. *Aquat. Toxicol.* 155, 52–61. doi:10.1016/j.aquatox.2014.06.008

Paital, B., Panda, S. K., Hati, A. K., Mohanty, B., Mohapatra, M. K., Kanungo, S., et al. (2016). Longevity of animals under reactive oxygen species stress and disease susceptibility due to global warming. *World J. Biol. Chem.* 7, 110–127. doi:10.4331/wjbc.v7.i1.110

Piedade, F., Bio, S., and Nunes, B. (2020). Effects of common pharmaceutical drugs (paracetamol and acetylsalicylic acid) short term exposure on biomarkers of the mussel Mytilus spp. *Environ. Toxicol. Pharmacol.* 73, 103276. doi:10.1016/j.etap.2019.103276

Porretti, M., Arrigo, F., Di Bella, G., and Faggio, C. (2022). Impact of pharmaceutical products on zebrafish: an effective tool to assess aquatic pollution. *Comp. Biochem. Physiol. C Toxicol. Pharmacol.* 261, 109439. doi:10.1016/j.cbpc.2022.109439

Porretti, M., Impellitteri, F., Caferro, A., Albergamo, A., Litrenta, F., Filice, M., et al. (2023). Assessment of the effects of non-phthalate plasticizer DEHT on the bivalve molluscs *Mytilus galloprovincialis*. *Chemosphere* 336, 139273. doi:10.1016/j.chemosphere.2023.139273

Ransy, C., Vaz, C., Lombès, A., and Bouillaud, F. (2020). Use of H2O2 to cause oxidative stress, the catalase issue. *Int. J. Mol. Sci.* 21, 9149. doi:10.3390/ijms21239149

Reznick, A. Z., and Packer, L. (1994). Oxidative damage to proteins: spectrophotometric method for carbonyl assay. *Methods Enzymol.* 233, 357–363. doi:10.1016/s0076-6879(94)33041-7

Roy, D., Pathak, D. N., and Singh, R. (1984). Effects of chlorpromazine on the activities of antioxidant enzymes and lipid peroxidation in the various regions of aging rat brain. *J. Neurochem.* 42, 628–633. doi:10.1111/j.1471-4159.1984.tb02728.x

Sanderson, H., Johnson, D. J., Reitsm, T., Brain, R. A., Wilson, C. J., and Solo, K. R. (2004). Ranking and prioritization of environmental risks of pharmaceuticals in surface waters. *Regul. Toxicol. Pharmacol.* 39 (2), 158–183. doi:10.1016/j.yrtph.2003.12.006

Sehonova, P., Plhalova, L., Blahova, J., Doubkova, V., Marsalek, P., Prokes, M., et al. (2017). Effects of selected tricyclic antidepressants on early-life stages of common carp (*Cyprinus carpio*). *Chemosphere* 185, 1072–1080. doi:10.1016/j.chemosphere.2017.07.092

Sies, H. (2017). Hydrogen peroxide as a central redox signaling molecule in physiological oxidative stress: oxidative eustress. *Redox Biol.* 11, 613–619. doi:10.1016/j.redox.2016.12.035

Stip, E., Rizvi, T. A., Mustafa, F., Javaid, S., Aburuz, S., Ahmed, N. N., et al. (2020). The large action of chlorpromazine: translational and transdisciplinary considerations in the face of COVID-19. *Front. Pharmacol.* 11, 577678. doi:10.3389/fphar.2020.577678

Tamba, M., and O'Neill, P. (1991). Redox reactions of thiol free radicals with the antioxidants ascorbate and chlorpromazine: role in radioprotection. *J. Chem. Soc. Perkin. Trans.* 2, 1681–1685. doi:10.1039/P29910001681

Torre, A., Trischitta, F., and Faggio, C. (2013). Effect of CdCl2 on regulatory volume decrease (RVD) in *Mytilus galloprovincialis* digestive cells. *Toxicol. Vitro* 27, 1260–1266. doi:10.1016/j.tiv.2013.02.017

Tresnakova, N., Famulari, S., Zicarelli, G., Impellitteri, F., Pagano, M., Presti, G., et al. (2023a). Multi-characteristic toxicity of enantioselective chiral fungicide tebuconazole to a model organism mediterranean mussel *Mytilus galloprovincialis* lamarck, 1819 (bivalve: *mytilidae*). *Sci. Total Environ.* 862, 160874. doi:10.1016/j.scitotenv.2022.160874

Tresnakova, N., Impellitteri, F., Famulari, S., Porretti, M., Filice, M., Caferro, A., et al. (2023b). Fitness assessment of *Mytilus galloprovincialis* Lamarck, 1819 after exposure to herbicide metabolite propachlor ESA. *Environ. Pollut.* 331, 121878. doi:10.1016/j.envpol.2023.121878

Turani, B., Aliko, V., and Faggio, C. (2019). Amphibian embryos as an alternative model to study the pharmaceutical toxicity of cyclophosphamide and ibuprofen. *J. Biol. Res.* 92, 72–76. doi:10.4081/jbr.2019.8370

Xiao, W., and Loscalzo, J. (2020). Metabolic responses to reductive stress. *Antioxid. Redox Signal.* 32, 1330–1347. doi:10.1089/ars.2019.7803

Xu, F., Xi, H., Liao, M., Zhang, Y., Ma, H., Wu, M., et al. (2022). Repurposed antipsychotic chlorpromazine inhibits colorectal cancer and pulmonary metastasis by inducing G2/M cell cycle arrest, apoptosis, and autophagy. *Cancer Chemother. Pharmacol.* 89, 331–346. doi:10.1007/s00280-021-04386-z

Yang, J. L., Li, Y. F., Bao, W. Y., Satuito, C. G., and Kitamura, H. (2011). Larval metamorphosis of the mussel *Mytilus galloprovincialis* Lamarck, 1819 in response to neurotransmitter blockers and tetraethylammonium. *Biofouling* 27, 193–199. doi:10.1080/08927014.2011.553717

Yuan, S., Jiang, X., Xia, X., Zhang, H., and Zheng, S. (2013). Detection, occurrence and fate of 22 psychiatric pharmaceuticals in psychiatric hospital and municipal wastewater treatment plants in Beijing, China. *Chemosphere* 90, 2520–2525. doi:10.1016/j.chemosphere.2012.10.089

frontiers | Frontiers in Physiology

TYPE Original Research
PUBLISHED 19 September 2023
DOI 10.3389/fphys.2023.1279051

OPEN ACCESS

EDITED BY
Yiming Li,
Fishery Machinery and Instrument Research Institute, China

REVIEWED BY
Hong Meiling,
Hainan Normal University, China
Huan Wang,
Ningbo University, China

*CORRESPONDENCE
Yongqiang Deng,
dyqhxl@126.com

†These authors have contributed equally to this work

RECEIVED 17 August 2023
ACCEPTED 04 September 2023
PUBLISHED 19 September 2023

CITATION
Liu S, Luo L, Zuo F, Huang X, Zhong L, Liu S, Geng Y, Ou Y, Chen D, Cai W and Deng Y (2023), Ammonia nitrogen stress damages the intestinal mucosal barrier of yellow catfish (*Pelteobagrus fulvidraco*) and induces intestinal inflammation. *Front. Physiol.* 14:1279051. doi: 10.3389/fphys.2023.1279051

Ammonia nitrogen stress damages the intestinal mucosal barrier of yellow catfish (*Pelteobagrus fulvidraco*) and induces intestinal inflammation

Senyue Liu[1,2†], Lin Luo[2†], Fengyuan Zuo[2†], Xiaoli Huang[2], Liang Zhong[2,3], Sha Liu[2], Yi Geng[4], Yangping Ou[4], Defang Chen[4], Wenlong Cai[3] and Yongqiang Deng[1*]

[1]Fisheries Research Institute, Sichuan Academy of Agricultural Sciences, Chengdu, Sichuan, China, [2]Department of Aquaculture, College of Animal Science & Technology, Sichuan Agricultural University, Chengdu, Sichuan, China, [3]State Key Lab of Marine Pollution, Department of Infectious Diseases and Public Health, Jockey Club College of Veterinary Medicine and Life Sciences, City University of Hong Kong, Hong Kong, Hong Kong SAR, China, [4]Department of Basic Veterinary, College of Veterinary Medicine, Sichuan Agricultural University, Chengdu, Sichuan, China

Nitrogen from ammonia is one of the most common pollutants toxics to aquatic species in aquatic environment. The intestinal mucosa is one of the key mucosal defenses of aquatic species, and the accumulation of ammonia nitrogen in water environment will cause irreversible damage to intestinal function. In this study, histology, immunohistochemistry, ultrastructural pathology, enzyme activity analysis and qRT-PCR were performed to reveal the toxic effect of ammonia nitrogen stress on the intestine of *Pelteobagrus fulvidraco*. According to histological findings, ammonia nitrogen stress caused structural damage to the intestine and reduced the number of mucous cells. Enzyme activity analysis revealed that the activity of bactericidal substances (Lysozyme, alkaline phosphatase, and ACP) had decreased. The ultrastructure revealed sparse and shortened microvilli as well as badly degraded tight junctions. Immunohistochemistry for ZO-1 demonstrated an impaired intestinal mucosal barrier. Furthermore, qRT-PCR revealed that tight junction related genes (*ZO-1, Occludin, Claudin-1*) were downregulated, while the pore-forming protein *Claudin-2* was upregulated. Furthermore, as ammonia nitrogen concentration grew, so did the positive signal of Zap-70 (T/NK cell) and the expression of inflammation-related genes (*TNF*, *IL-1β*, *IL-8*, *IL-10)*. In light of the above findings, we conclude that ammonia nitrogen stress damages intestinal mucosal barrier of *Pelteobagrus fulvidraco* and induces intestinal inflammation.

KEYWORDS

ammonia nitrogen, mucosal immune, mucosal barrier damage, intestinal inflammation, *Pelteobagrus fulvidraco*

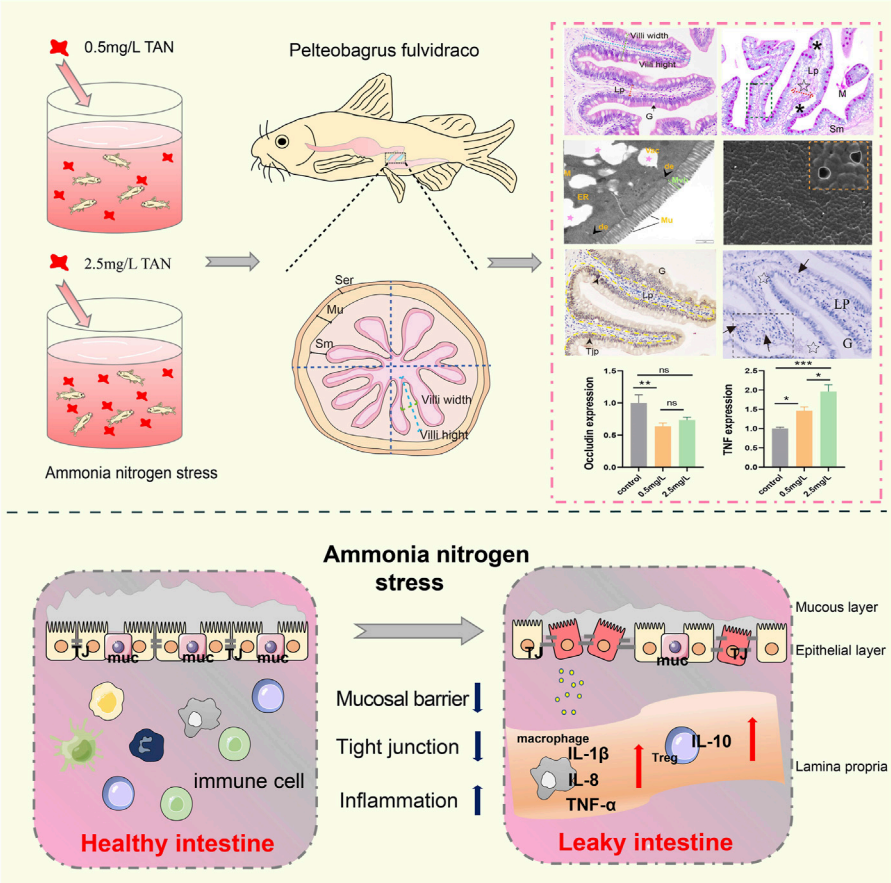

GRAPHICAL ABSTRACT

1 Introduction

Nitrogen sources derived from ammonia have been utilized to assess water quality in the aquaculture industry, and it is regarded as a long-term contaminant in the aquatic environment (Zhang et al., 2021). In aquaculture water environment, ammonia nitrogen exists in the form of non-ionic ammonia (NH_3) and ionic ammonia (NH_4^+) which converts to each other and maintains dynamic balance under specified pH, temperature, and salinity parameters (Kleinhenz et al., 2018; Hongxing et al., 2021). However, due to aquatic creatures' exceptional sensitivity to ammonia nitrogen, excessive quantities of ammonia nitrogen can be hazardous to them, with NH3 being the primary source of ammonia toxicity (Kathyayani et al., 2019; Zhang et al., 2020). At specific water temperatures and pH levels, NH_3 diffuses through biological cell membranes more easily than NH_4^+, leading to metabolic alterations, oxidative stress, inflammation and disease (Lu et al., 2022).

Intestine, one of the body's first lines of defense, is the main route for many aquatic animals to absorb environmental pollutants (Pustiglione Marinsek et al., 2018). The variety of intestinal microbiota, tissue structure, and physiological function will alter in response to changes in the aqueous environment, and can be utilized as a reflection of environmental pollution. Therefore, intestine is a vital organ for assessing water environmental pollutants (Gonçalves et al., 2020; Zhang et al., 2020). Intestinal mucosal is critical in maintaining homeostasis. In general, intestinal mucosal barrier system can be divided into biological barrier, chemical barrier and mechanical barrier. Biological barrier refers to the parasitic bacteria residing in the intestine with colonizing resistance to foreign strains (Bischoff et al., 2014). Chemical barrier includes mucins, defencins, lysozyme, alkaline phosphatase and other bacteriostatic substances (Ghosh et al., 2021), which are not only beneficial to prevent microbial invasion, but also play a coordinating role in the immune defense process (Wu et al., 2019). The mechanical barrier is composed primarily of intestinal epidermal cells and intercellular junction components including attachment junctions (AJ), tight junctions (TJ), and desmosome. They play vital roles in maintaining intestinal epidermal permeability and preventing intestinal lumen substances from entering the intestine (Camilleri et al., 2012). Numerous studies have shown that ammonia nitrogen accumulation in aquatic environments can irreversibly damage the normal structure and barrier function of intestine (Wood et al., 2019; Qian et al., 2021; Wang et al., 2021).

Yellow catfish (*Pelteobagrus fulvidraco*) is an essential component of China's freshwater ecosystem and a significant economic species, with a total output of 560,000 t in 2020 (Administration, 2021). As a representative of benthic animals in aquatic ecosystems, yellow catfish can be utilized to evaluate the bioaccumulation rate of contaminants in water, providing a suitable

model for environmental monitoring (Chen et al., 2012; Kim et al., 2012). However, with the rapid development of high-density intensive farming, ammonia nitrogen accumulation has become a universal problem for ecology and aquaculture, leading to environmental pollution (Li et al., 2020). For example, diseases increased during the breeding of yellow catfish due to increasing ammonia stress, resulting in a mortality rate of over 70% and massive economic losses (Chen et al., 2016). Although many studies on the toxic effects of ammonia nitrogen on aquatic animals have been undertaken, few studies have focused on the impact of ammonia stress on intestinal histology in fish. In addition, how ammonia nitrogen affects the intestinal mucosal barrier of yellow catfish and its related mechanisms remain unclear. Therefore, it is particularly important to elucidate the toxic effect of ammonia nitrogen on the intestine of yellow catfish, which can not only help to assess the potential risks of ammonia nitrogen stress on aquatic animals, but also provide insights for management strategies and intervention targets for ammonia nitrogen-induced stress.

2 Materials and methods

2.1 Experimental fish

Yellow catfish (53.67 ± 4.90g) used in this study were obtained from a fish farm in Chengdu (Sichuan province, China), with no superficial injuries. Five fish were randomly selected for examination, no bacteria or parasites were found. These fish were kept in a circular tank (600 L water volume) with constant aeration for 1 week at 23°C–24°C. Floating commercial feed was provided satiably twice a day (8 a.m. and 6 p.m.), with one third of the water was changed daily. The approximate composition of commercial feed is as follows: 40% crude protein, 5% crude fat, 8.1% ± 0.3% crude fibr and 16% crude ash. Feeding was ceased 1 day before ammonia nitrogen exposure.

2.2 Ammonia nitrogen exposure experiment and sample collection

Fish were equally divided into three groups: control group (total ammonia nitrogen (TA-N) 0 mg/L), 0.5 mg/L group (TA-N 0.5 mg/L, common stressful and toxic concentration exceeding the standard in modern fisheries), and 2.5 mg/L group (TA-N 2.5 mg/L, 10% 96-h LC_{50}). They were kept in three circular tanks, and were continuously aerated. Then, based on previous research (Liu, 2022; Zhong, 2022), a 28-day stress experiment was conducted. Briefly, the TA-N concentration in water was determined using the Nessler reagent-colorimetry method (SI Appendix) (Kołacińska and Koncki, 2014). By adding 10 mg/L ammonium chloride solution as needed, the expected ammonia nitrogen concentration was achieved. The fish were fed with commercial feed in a satiated manner. To reduce the impact of exogenous nitrogen, the unconsumed feed was removed after half an hour of feeding. To reduce the impact of nitrogen in the excrement, water was changed in a 1/3 ratio at 9:00 a.m. every day to remove excrement from the water. To ensure ammonia nitrogen concentration stability, water TA-N concentration was measured twice a day (9 a.m. and 21 p.m.), and immediately adjusted to the specified experimental level. During the experimental period, the water temperature was 23°C–24°C, the dissolved oxygen was 8.0 - 8.9 mg/L, the pH was 6.5-7.1, and the actual ammonia nitrogen concentration is shown in Supplementary Table S1.

After 28 days of ammonia nitrogen exposure, fish were anesthetized with buffered MS222 (250 mg/L; Aladdin, China), and posterior intestine tissue samples were immediately collected for downstream analysis.

2.3 Histology, AB-PAS, and immunohistochemical studies

2.3.1 Hematoxylin-eosin staining

Eighteen intestine samples (6 samples per group) were obtained for histopathological analysis. Briefly, the posterior intestines were removed with sterile forceps, immediately prefixed in 4% paraformaldehyde for 24 h, rinsed in running tap water for 24 h, and then routine dehydration and paraffin embedding were performed. Subsequently, the tissues were sliced with a thickness of 5 μm (Lycra, Germany), and stained with classical hematoxylin and eosin (H & E). Photographs were taken under an optical microscope (Nikon Eclipse E200, Japan). Each tissue section was divided into 4 areas (Figure 1D), and a single intestinal villus was randomly selected from each area. ImageJ was used for morphological measurements (including villi height, villi width, submucosal thickness and lamina propria width), and pathological changes of intestinal tissues (including edema of submucosa, thickening of the lamina propria, villi swelling, lamina propria hemorrhage, infiltration of lymphocytes, cell death, disorder of cell arrangement, and damaged striate border) were analyzed by pathological score. The severity of the lesions is indicated by a score (S) ranging from 1 to 7 (Barišić et al., 2018): (1) unaltered; (3) mild; (5) moderate; and (7) severe.

2.3.2 Alcian blue and periodic acid–schiff staining

The above paraffin sections of intestinal samples were dewaxed in xylene, hydrated, and stained for 20 min with Alcian blue solution (pH 2.5). Later, the samples were oxidized in Periodic acid (5 g/L) for 5 min, rinsed with distilled water for 10 min, and immersed in Schiff's reagent for 20 min under dark conditions before being washed with distilled water. Finally, the samples were stained with Hematoxylin for 2 min before being sealed with neutral gum. Nikon Eclipse E200 (Japan) was used to evaluate tissue slides. Each tissue section was divided into 4 areas (Figure 1D), and a single intestinal villus was randomly selected from each area. The thickness of the epithelial layer and the number of mucus cells of a single villus were measured and recorded.

2.3.3 Immunohistochemical studies

The above paraffin sections were dewaxed to water and then placed in a repair box containing citric acid antigen repair buffer (pH 6.0). Then, the slices were placed in 3% hydrogen peroxide solution for 25 min before being rinsed three times in PBS (pH 7.4) for 5 min each to block endogenous peroxidase. Afterward, the tissues were evenly covered with 3% BSA (Thermo Fisher, United States) and sealed at room temperature for 30min. The primary antibodies Zap-70 Rabbit

10.3389/fphys.2023.1279051

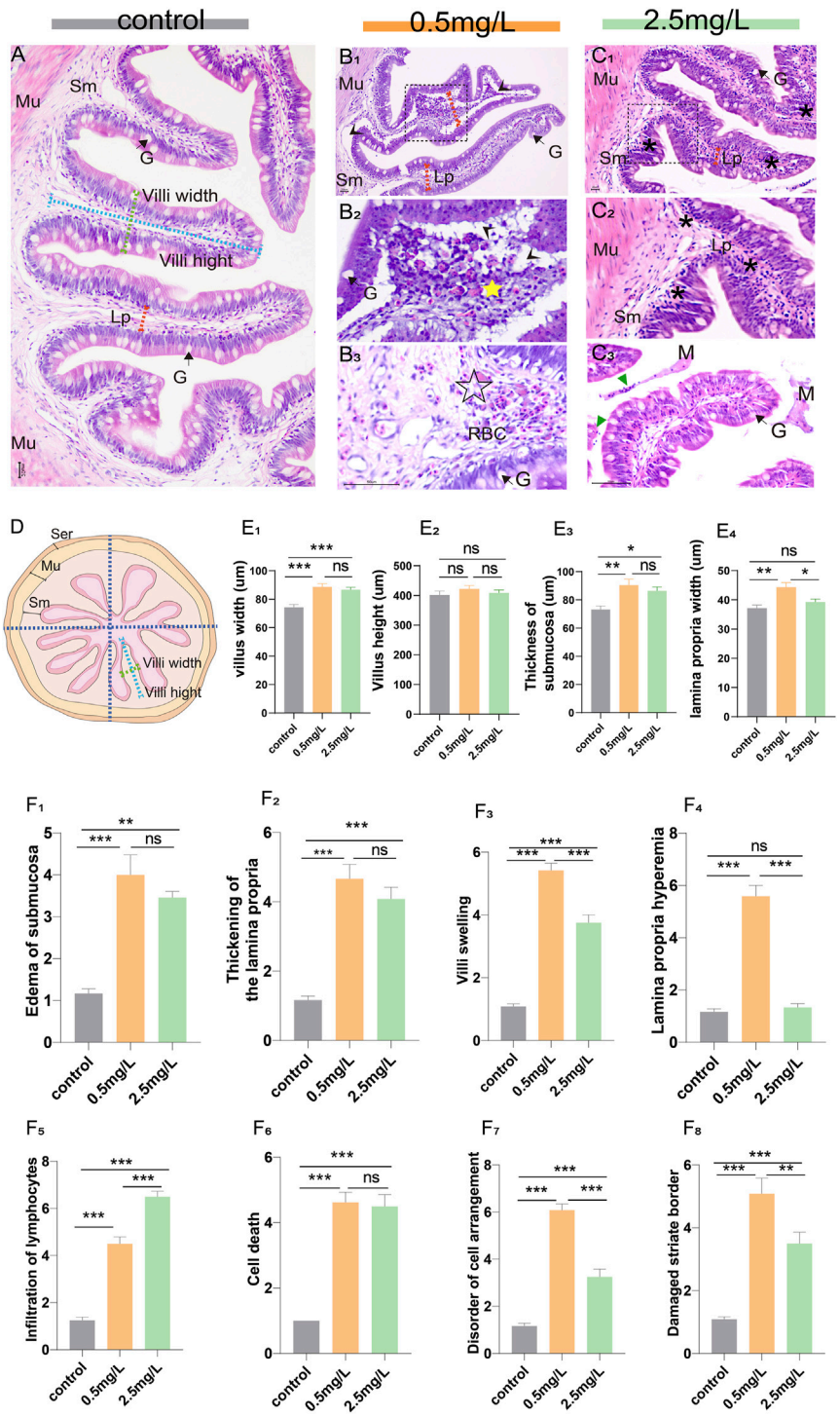

FIGURE 1
Histopathological observation of intestine of yellow catfish. **(A)** Intestine of the control group, the villi were regular in shape, the dashed blue line, dashed green line, and dashed red arrows represent villi height, villi width, and lamina propria width, respectively. **(B_1-B_3)** Intestine of the 0.5 mg/L group: **(B_1)**, the intestinal villi were severely vacuolated (arrowhead), and the thickness of lamina propria increased (dashed red arrows). **(B_2)**, Local zoom of Fig **(B_1)**, showing disorder of cell arrangement (yellow star), lamina propria edema and vacuolation (arrowhead). **(B_3)**, The lamina propria showed marked hyperemia (☆) with numerous red blood cells. **(C_1-C_3)** Intestine of the 2.5 mg/L group: **(C_1)**, the villi were swollen with marked inflammatory cell infiltration (*). **(C_2)**, Local zoom of Fig **(C_1)**. **(C_3)**, there were necrotic and exfoliated intestinal epithelial cells and inflammatory cells (green triangle) in the intestinal lumen, along with some mucous. **(D)** Schematic of the transverse section of the intestine, which is divided into 4 areas, the dashed blue line, dashed green line, and dashed red arrows represent villi height, villi width, and lamina propria width, respectively. **(E_1–E_4)** Morphological measurements of villi width, villi height, thickness of submucosa, and lamina propria width, respectively. **(F_1–F_8)** The histopathological scores for edema of submucosa, thickening of the lamina propria, villi swelling, lamina propria hemorrhage, infiltration of lymphocytes, cell death, disorder of cell arrangement, and damaged striate border, respectively. Sm, submucosa; Mu, muscularis; G, goblet cell; Lp, lamina propria; M, mucosa; RBC, red blood cell. *, **, ***, and ns representing $p < 0.05$, 0.01, 0.001, and nonsignificant, respectively. ($n = 6$).

monoclonal antibody (99f2, CST, Massachusetts, United States) and ZO-1 Rabbit polyclonal antibody (GB111402, Servicebio, China) were added and incubated overnight in a wet box at 4 °C. After washing, tissues were covered with Goat Anti-Rabbit IgG (H&L) Alexa Flour 488secondary antibody (Thermo Fisher, United States), and incubated at room temperature for 50min. Following PBS washing, sections were immersed in diaminobenzidine hydrochloride (DAB) and re-stained with hematoxylin. The sections were observed under Nikon Eclipse E200 (Japan). Each tissue section was divided into 4 areas (Figure 1D), and a single intestinal villus was randomly selected from each area. ImageJ was used to assess mean optical density (IOD SUM/area), and IHC Profiler was used to assess immunohistochemistry score (IHC score) (Varghese et al., 2014). The following are the scoring criteria: (3) strongly positive; (2) positively; (1) moderately positive; and (0) negatively.

2.4 Transmission electron microscopy (TEM)

Eighteen intestine samples (6 samples per group) were selected for transmission electron microscopy (TEM) analysis. The samples were fixed in 2.5% glutaraldehyde for 24 h at 4°C before being washed with PBS (pH 7.2). They were then fixed with 1% osmic acid, washed with PBS, dehydrated with continuous acetone, embedded, sliced, and stained with uranium acetate and lead citrate. Micrographs were taken with TEM (Hitachi H-7500, Japan) operating at 80 kV. The length of microvilli and the diameter of mucinous granules were measured and recorded using ImageJ software. The ultrastructural pathological changes of intestinal tissue were evaluated, including necrosis, tight junctions fuzzy, vacuolization, mitochondrial cristae contraction and swelling, endoplasmic reticulum swelling, mitochondrial necrosis, mitochondrial myelinoid lesions, autophagy and apoptosis. The samples were assessed using a scoring system (Zhang et al., 2011) ranging from 1 to 7, depending on the severity of the lesions: (1) unaltered; (3) mild; (5) moderate; and (7) severe.

2.5 Scanning electron microscopy (SEM)

SEM analysis was performed on eighteen intestine samples (6 samples per group). The intestines were cut into 5-mm size pieces, washed in 1% S-carboxymethyl-L-cysteine for 30s to remove mucus before being stored in 2.5% glutaraldehyde sodium bicarbonate buffer (0.1 M pH 7.2). Subsequently, the samples were dehydrated in ascending series of ethanol before being dried with liquid CO_2 in a critical point dryer (HCP-02 Hitachi). The samples were scanned at 20 kV with a FEI Inspect S50 SEM (FEI, United States). The density of microvilli on the surface of intestinal cells (0.25 μm^2 region) was assessed using SEM images (magnification 30,000).

2.6 Biochemical analysis

Eighteen intestine samples (6 samples per group) were selected for biochemical analysis. After homogenizing the samples with ice-cold physiological saline (1:19, wt/vol), they were centrifuged at 8,000 rpm for 15 min. The Lysozyme (LZM), alkaline phosphatase (AKP) and acid phosphatase (ACP) activities of tissue supernatant were examined with lysozyme assay kit (A050-1-1), alkaline phosphatase assay kit (A059-2-2) and acid phosphatase assay kit (A060-2-1) respectively, following the manufacturer's instructions (Jian Cheng Bioengineering Institute, Nanjing, China).

2.7 Total RNA extraction and cDNA synthesis

Nine intestine samples (3 samples per group) were randomly selected for extraction of RNAs using TRIzol reagent (Invitrogen, United States) according to the manufacturer's instructions. Subsequently, the concentration and purit of RNA as well as the RIN value were determined using a Nanodrop 2000 spectrophotometer (Thermo Scientific, United States), a 1.2% (w/v) agarose gel electrophoresis, and an Agilent 2,100, respectively. To remove gDNA, an equal amount of total RNA (1g) was incubated with RNase-Free ddH20 and gDNase Mix. Using the Superscript first strand synthesis system (Abm, Canada), reverse transcription was performed in a 20 μL reaction volume containing 10 μL of the RNA template, 4 μL of the 5 x RO-Easy™ Mix and 6 μL of RNase-Free ddH_20.

2.8 Quantitative real-time PCR (qRT-PCR) analysis

Quantitative real-time PCR (qRT-PCR) was performed to analyze the expression of immune-related genes (*IL-1β, IL-10, IL-8, TNF-α*) and tight junctions-related genes (*ZO-1, Occludin, Claudin-1, Claudin-2*). The *β-actin* gene of yellow catfish was employed as an internal reference to normalize gene expression levels (Zhou et al., 2021). qRT-PCR was performed in a total volume of 10 μL containing 5 μL of TB Green™ Premix Ex Taq™ II, 0.2 μL of Rox, 1 μL of cDNA, 0.8 μL of each primer (specific primers outlined in Supplementary Table S2) and 2 μL of double distilled water. The reaction conditions used were as follows: 95°C for 3 min, followed by 39 cycles of 95°C for 10 s, 57°C for 20 s and 72°C for 20 s, with the dissolution curve increasing from 0.5°C to 95°C every 5 s, and the gene expression was estimated by the $2^{-\Delta\Delta CT}$ method (Livak and Schmittgen, 2001).

2.9 Statistical analyses

In this study, all data were presented as mean ± SD (standard deviation). SPSS 27.0 software (IBM Corp., Chicago, United States) was used to assess the statistical differences. GraphPad Prism (United States) and Adobe Illustrator (United States) software were used to create the charts. After normality test, the one-way ANOVA analysis was used to evaluate the significant difference. (*, **, ***, and ns representing $p <$ 0.05, 0.01, 0.001, and nonsignificant, respectively.)

3 Results

3.1 Histopathological observation

The structure of the intestinal wall can be divided into four layers based on histological observation: the mucosal layer, the

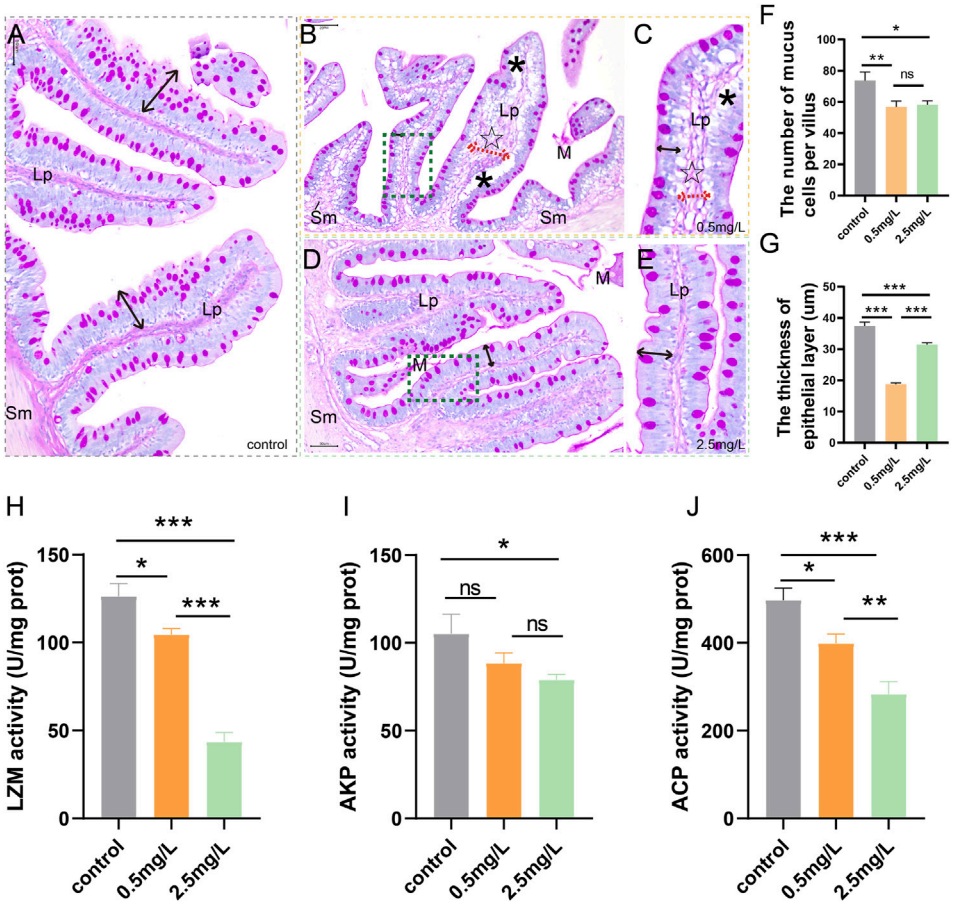

FIGURE 2
AB-PAS staining results and activity of bacteriostatic substances of intestine after ammonia nitrogen exposure **(A)** The control group showed abundant mucus cells and thick epithelial layer (black double-headed arrow). **(B)** The intestine of 0.5 mg/L group, showed vacuolation (*), sparse mucous cells, and thickened lamina propria (dashed red arrows, ☆). **(C)** Local zoom of Fig B, significantly reduced epithelial layer thickness (black double-headed arrow). **(D)** The intestine of 2.5 mg/L group, showed decreased mucous cells, and moderately decreased epithelial layer thickness (black double-headed arrow). **(E)** Local zoom of Fig **(D)** **(F)** Mucous cell count in intestine tissue. **(G)** Statistical analysis of epithelial layer thickness. **(H–J)** Activities of LZM, AKP and ACP, respectively. Sm, submucosa; Lp, lamina propria; M, mucosa.*, **, ***, and ns representing $p < 0.05$, 0.01, 0.001, and nonsignificant, respectively. ($n = 6$).

submucosal layer, the muscular layer, and the serosal layer. In the control group (Figure 1A), the villi were nicely organized and the epithelial cells were intact. However, the intestinal lesions in the two-ammonia nitrogen-exposed groups were distinct. In the 0.5 mg/L group (Figure 1B), there was intestinal villus edema (Figure $1B_2$, E_1), marked submucosal dilatation (Figure $1E_3$), lamina propria thickening (Figure $1B_1$, E_4) and severe hyperemia (Figure $1B_3$). Interestingly, in the 2.5 mg/L group, the cell composition was relatively uniform, and the most noticeable histopathological change was inflammatory cell infiltration (Figure 1C). In brief, exposure to different concentrations of ammonia nitrogen resulted in disparate types of lesions in the intestine of yellow catfish (Figures 1F; Supplementary Figure S1). Low concentrations (0.5 mg/L) mainly caused reversible changes such as lamina propria hemorrhage, vacuolation and edema, while high concentrations (2.5 mg/L) mainly led to inflammation.

3.2 Ammonia nitrogen exposure leads to defects in the intestinal mucosal chemical barrier

To investigate whether ammonia nitrogen exposure may damage the chemical barrier of intestinal mucosa, AB-PAS staining and enzyme activity analysis were performed. According to the AB-PAS staining results, in the control group (Figure 2A), the epithelial layer was relatively thick and the mucus cells were evenly distributed on the mucosal surface. In the low concentration (0.5 mg/L) group (Figures 2B, C), mucous cells were sparsely distributed and decreased in number, and the thickness of epithelial layer was markedly reduced. Compared with the control group, the number of mucous cells in the high ammonia nitrogen concentration (2.5 mg/L) group was also decreased (Figures 2D, E), and the thickness of epithelial layer was moderately reduced. In brief, after ammonia nitrogen exposure,

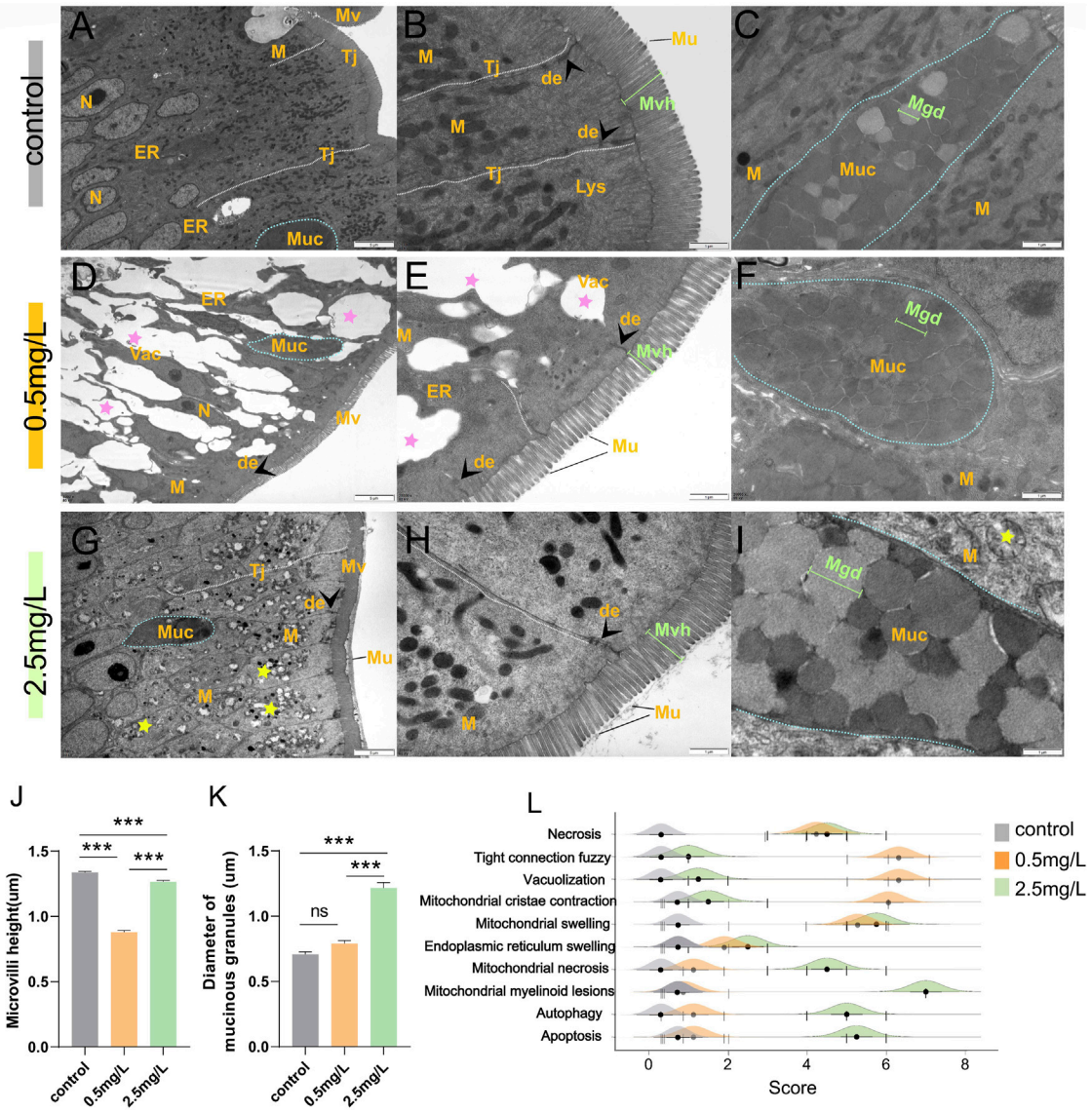

FIGURE 3
Transmission electron microscope observation of intestine after ammonia nitrogen exposure. **(A–C)** TEM results of intestine in control group: **(A)** Tight junctions were intact (white dotted line), organelles were abundant, and cell morphology was regular; **(B)** Tight junctions were complete (white dashed line) with visible desmosomes (arrowhead), microvilli were dense and long in height; **(C)** Mucus cells (blue dotted line) contained abundant mucus particles. **(D–F)** TEM results of intestine in 0.5 mg/L group: **(D)** The tight junctions were blurred and showing obvious vacuolation (pink star), and few organelles; **(E)** Some tight junctions (white dashed line) disappeared; the microvilli were sparse with significantly reduced height; **(F)** Mucus cells (blue dotted line) contained dark mucus granules. **(G–I)** TEM results of intestine in 2.5 mg/L group: **(G)** The tight junctions (white dotted line) were relatively intact, but a large number of mitochondria showed internal vacuolation, membrane damage, and myelinoid lesions (yellow star); **(H)** The microvilli were slightly sparse and shortened; **(I)** Mucus cells (blue dotted line) contained dark and pale mucus granules. **(J)** Statistical analysis of microvilli height. **(K)** Statistical analysis the diameter of mucinous granules. **(L)** Intestinal ultrastructural pathological scores of the three groups. N, nucleus; M, mitochondria; ER, endoplasmic reticulum; Tj, tight junctions; Mv, microvilli; Muc, mucus cells; de, desmosomes; Lys, lysosomes; Mvh, microvilli height; Mgd, mucinous granules diameter.*, **, ***, and ns representing $p < 0.05$, 0.01, 0.001, and nonsignificant, respectively. ($n = 6$).

the number of mucus cells (Figure 2F) and the thickness of epithelial layer (Figure 2G) decreased, especially in low concentration group.

According to the results of enzyme activity analysis, the activities of LZM (Figure 2H), AKP (Figure 2I) and ACP (Figure 2J) in the intestine tissues decreased gradually with increasing ammonia nitrogen concentration, indicating that ammonia nitrogen significantly inhibited the activity of intestinal bacteriostatic substances and damaged the chemical barrier of mucosa.

3.3 Ammonia nitrogen exposure leads to defects in the intestinal mucosal physical barrier

To investigate the effect of ammonia nitrogen exposure on ultrastructural structure and physical barrier, transmission electron microscopy (TEM) and scanning electron microscopy (SEM) were performed. According to the TEM results, in the

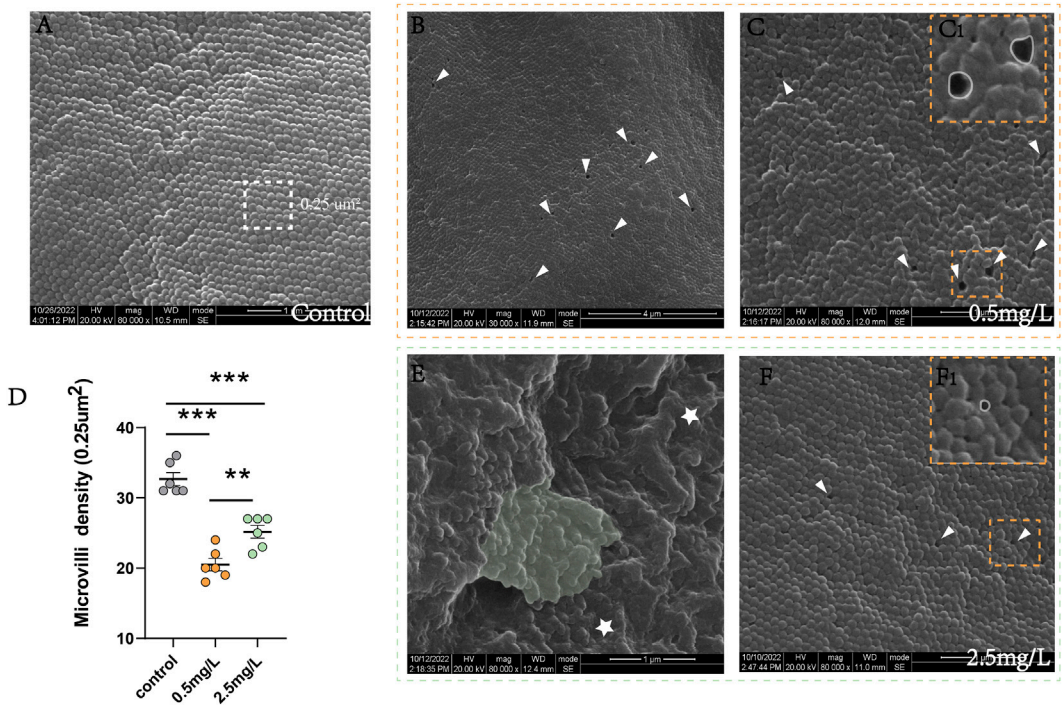

FIGURE 4
Scanning electron microscope observation of intestine after ammonia nitrogen exposure **(A)** The microvilli in control group were compact and neatly arranged. **(B–C)** The microvilli in 0.5 mg/L group: **(B)** The microvilli showed extensive cavities (white triangle); **(C)** The microvilli were slightly swollen with cavities (white triangle); (C_1) Local zoom of Fig C, the diameter of the cavity was long (white circle). **(D)** Statistical analysis of microvilli density (0.25 um^2). **(E–F)** The microvilli in 2.5 mg/L group: **(E)** The microvilli were obviously swollen (star) and adhered to each other (green background); **(F)** Occasionally small cavities (white triangle) were seen between the microvilli; (F_1) Local zoom of Fig F, the diameter of the cavity diameter was shorter (white circle). *, **, ***, and ns representing $p < 0.05$, 0.01, 0.001, and nonsignificant, respectively. ($n = 6$).

control group (Figures 3A–C), the free surface of intestinal mucosal epithelium was densely arranged with tidy microvilli (Figure 3A). At the free end of epithelial cells, there were abundant cell-cell junction complexes, including tight junctions and desmosomes, as well as a large number of mitochondria with extremely high electron density (Figure 3B). In the 0.5 mg/L group (Figures 3D–F), the intestinal epithelium was severely vacuolated (Figure 3D), and the tight junctions were blurred (Supplementary Figure S1C) or even broken (Supplementary Figure S1D). In addition, the microvilli were sparsely arranged with significantly shortened height (Figure 3E). Interestingly, in the 2.5 mg/L group (Figures 3G–I), the tight junctions of the intestinal epithelium were relatively complete, the microvilli were arranged neatly, and the height was slightly shortened (Figure 3H). The main characteristics were diffused mitochondria vacuolation (Figure 3G) and significant increase in the diameter of mucous particles (Figures 3I, K). In addition, a variety of pathological changes (Figures 3L; Supplementary Figure S2) including necrosis, mitochondrial cristae contraction, mitochondrial swelling, endoplasmic reticulum swelling, mitochondrial necrosis, autophagy and apoptosis were also discovered. In brief, exposure to ammonia nitrogen severely damaged intestinal epithelium, resulting in shortened microvilli height (Figure 3J) and enlarged mucous particle diameter (Figure 3K).

The results of SEM showed that the intestinal microvilli of the control group (Figure 4A) were neat and compact, while samples in the ammonia nitrogen-exposed group showed obvious pathological changes and severe physical damage to the epithelial barrier. Under low concentration of ammonia stress (Figures 4B, C), the microvilli density decreased sharply (Figure 4D), and considerable number of cavities could be visible (Figure 4C). Under high concentration stress (Figures 4E, F), the microvilli swelled and attached to each other (Figure 4E), with occasional cavities (Figure 4F). And the microvilli density was significantly lower than that of control group, but higher than that of 0.5 mg/L ammonia-exposed group (Figure 4D).

3.4 Ammonia nitrogen exposure breaks the tight junctions between intestinal mucosal epithelial cells

To investigate whether ammonia nitrogen exposure could cause damage to the tight junctions between intestinal mucosal epithelial cells, immunohistochemical analysis and qRT-PCR were conducted. In the control group (Figure 5A), the mucosal barrier was intact and ZO-1 protein was evenly distributed in the intestinal mucosa. However, the two-ammonia nitrogen-exposed groups showed different degrees of ZO-1 signal attenuation. In the low concentration group (Figures 5B,C), the positive signal of ZO-1 decreased sharply, and some mucosal barriers were broken. In the high concentration group (Figures 5D,E), the positive signal of ZO-1 decreased moderately, but the mucosal barrier was relatively intact. Statistical analysis of mean

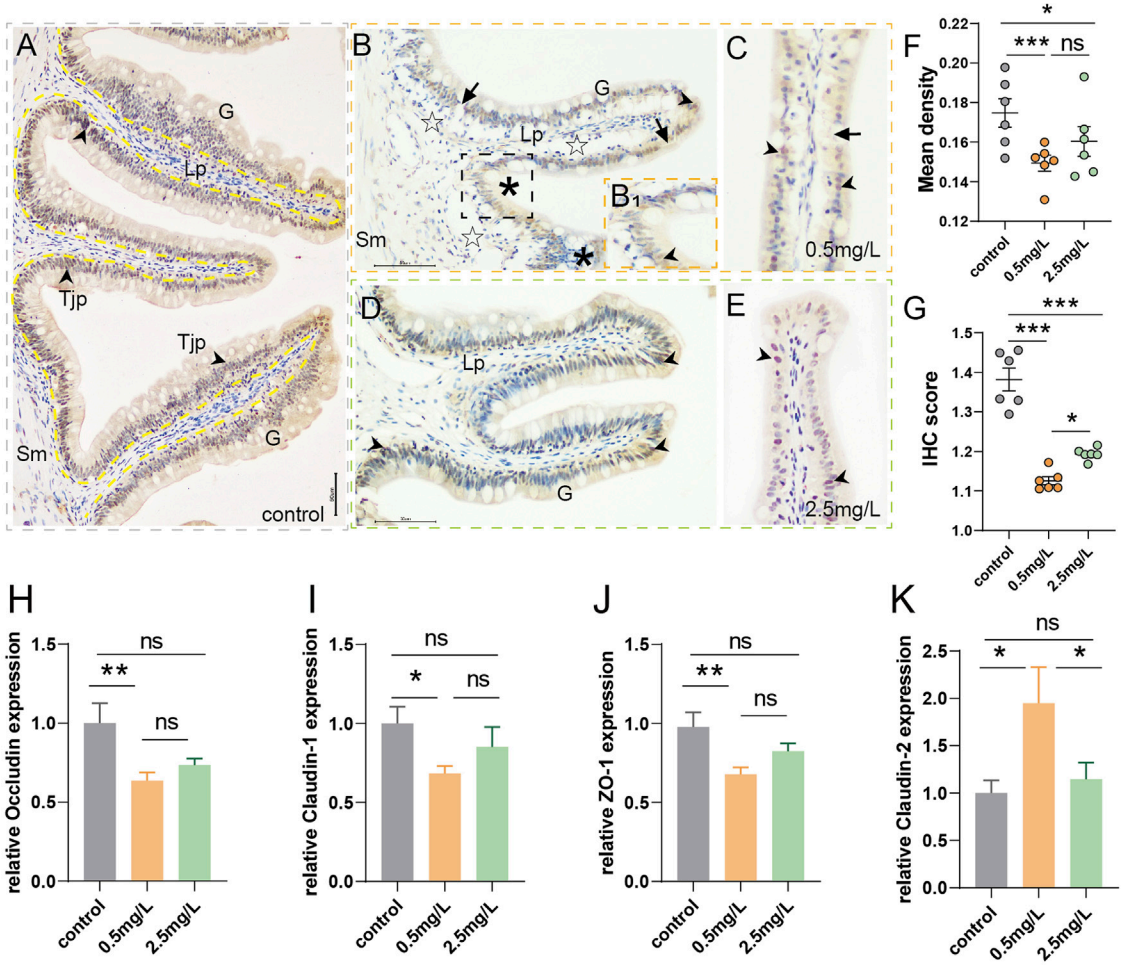

FIGURE 5
Immunohistochemical observation of ZO-1 (brown) and tight junction-related gene expression **(A)** Immunohistochemical analysis of control group, showed abundant ZO-1$^+$ cells (arrowhead) with intact and thick mucosal barrier (yellow dotted line, black arrow). **(B, C)** Immunohistochemical analysis of 0.5 mg/L group: **(B)** Showed obvious vacuolation (☆), a small number of ZO-1$^+$ cells (arrowhead), and gaps in mucosal barrier (arrows); B_1, Local zoom of Fig B, some tight junction proteins migrated up to the surface of goblet cells (*); **(C)** Showed incomplete mucosal barrier (arrows) and sparse tight junction proteins (arrowhead). **(D, E)** Immunohistochemical analysis of 2.5 mg/L group: **(D)** Showed moderate number of ZO-1$^+$ cells (arrowhead), **(E)** Showed relatively complete mucosal barrier (arrows). **(F)** Statistical analysis of mean optical density. **(G)** Statistical analysis of IHC score. (n = 6) **(H–K)** *Occludin* expression, *Claudin-1* expression, *ZO-1*expression, *Claudin-2* expression, respectively. (n = 3) Sm, submucosa; G, goblet cell; Lp, lamina propria; Tjp, tight junction protein. *, **, ***, and ns representing $p < 0.05$, 0.01, 0.001, and nonsignificant, respectively.

density (Figure 5F) and IHC (immunohistochemical) scores (Figure 5G), showed that ZO-1 signal was strongest in the control group, followed by the 2.5 mg/L group and the 0.5 mg/L group.

In addition, genes associated with the promotion of tight junctions (*Occludin, Claudin-1, ZO-1*) (Figures 5H–J) decreased significantly in the 0.5 mg/L group compared to the control group, and also showed a downward but not significant trend in the 2.5 mg/L group. There was no significant difference between the two-ammonia nitrogen-exposed groups. As for *Claudin-2* (Figure 5K), a pore-forming protein that inhibits tight junctions and promotes cell permeability, showed the opposite trend. These findings corroborated immunohistochemistry findings, indicating that ammonia nitrogen exposure (especially at low concentrations) damaged the chemical barrier of intestinal mucosa, affected the formation of tight junctions between cells, and enhanced the paracellular permeability, which might lead to impairment of the intestinal mucosa's defensive barrier function and induce inflammation.

3.5 Ammonia nitrogen exposure induces severe inflammation

To investigate whether ammonia nitrogen stress could cause intestinal inflammation, immunohistochemical studies and qRT-PCR were conducted. In the three groups (Figures 6A–C), T/NK cells, positive signals of Zap-70 (Lee et al., 2021), were mainly distributed in the gut-associated lymphoid tissue (GALT) of lamina propria. In the control group (Figure 6A), the positive signal was infrequent. In the 0.5 mg/L group (Figure 6B), a moderate number of T/NK cells were scattered in lamina propria, while a large number of T/NK cells gathered in the 2.5 mg/L group (Figure 6C). The statistical results of the mean optical density (Figure 6D) and IHC score (Immunohistochemistry score) (Figure 6E) were comparable with the preceding results, indicating that a large number of

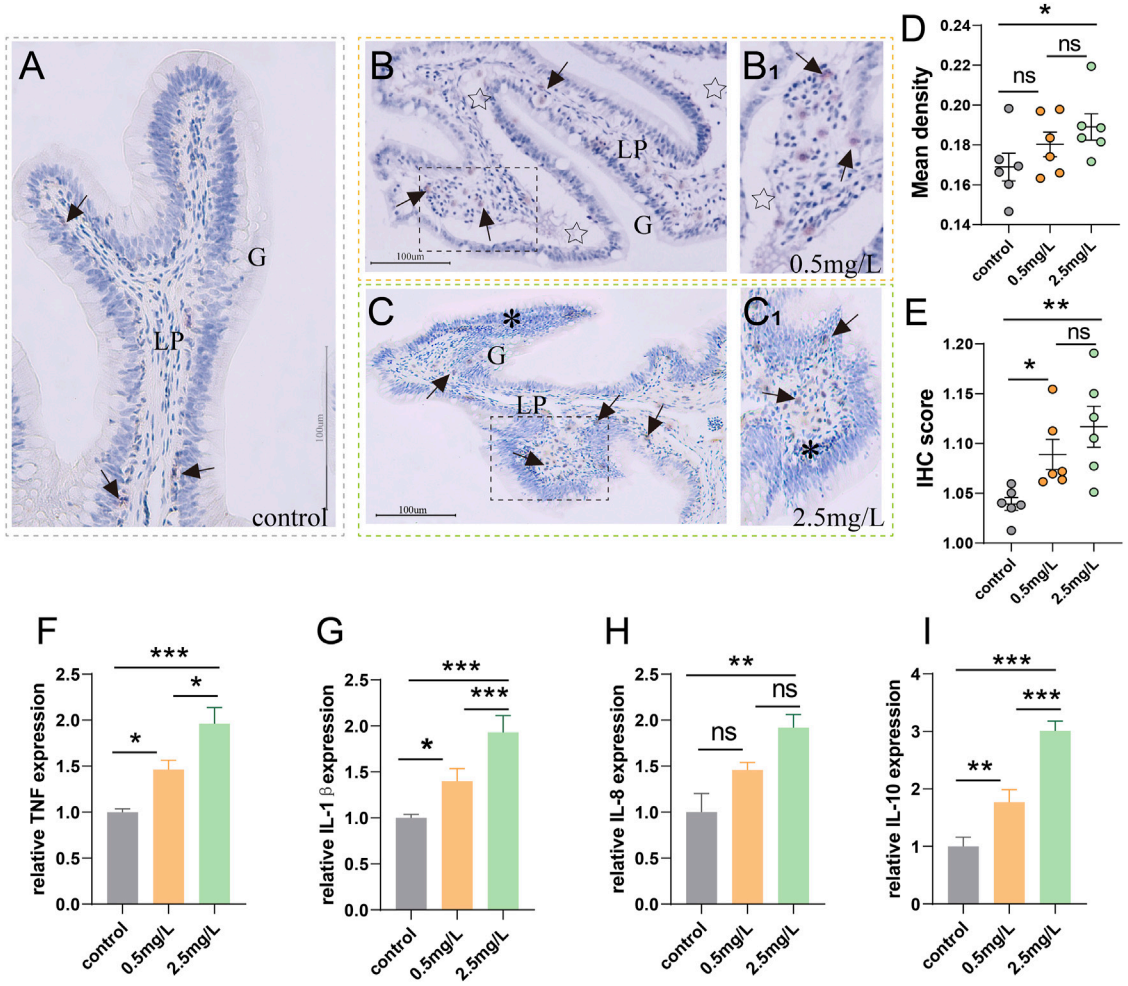

FIGURE 6
Immunohistochemical observation of Zap-70 (brown) and inflammation-related gene expression **(A)** Immunohistochemical analysis of control group, a few Zap-70$^+$ cells (arrows) appeared. **(B)** Immunohistochemical analysis of 0.5 mg/L group, severe tissue vacuolation (star) accompanied by a moderate number of Zap-70$^+$ cells (arrows). (B_1) Local zoom of Fig **(B)**. **(C)** Immunohistochemical analysis of 2.5 mg/L group, showed abundant Zap-70$^+$ cells (arrows) and marked lymphocytic infiltration (*). (C_1) Local zoom of Fig **(C)** **(D)** Statistical analysis of mean optical density. **(E)** Statistical analysis of IHC score. (n = 6) **(F–I)** *TNF-α* expression, *IL-1β* expression, *IL-8* expression, *IL-10* expression, respectively. (n = 3) Lp, lamina propria. *, **, ***, and ns representing $p < 0.05$, 0.01, 0.001, and nonsignificant, respectively.

lymphocyte aggregation was induced by ammonia nitrogen stress.

According to the results of gene expression, as ammonia nitrogen concentration increased, the expressions of key inflammatory biomarkers (Figures 6F–I) such as *TNF-α*, *IL-1β*, *IL-8* and *IL-10* increased significantly, especially in the 2.5 mg/L group. In light of the aforementioned findings, it is possible that ammonia nitrogen stress triggered severe inflammatory response.

4 Discussion

The health of aquatic organisms is positively correlated with water quality and environment (Zimmerli et al., 2007). Since fish are directly exposed to the water, their homeostasis mechanisms are highly dependent on the existing conditions of the surrounding water environment, therefore, even minor changes in water quality can result in a variety of biological responses in fish. Pollution-induced histopathological changes not only reflect the specific effects of pollutants on aquatic organisms, but can also be detected before irreversible effects occur (Wester and Canton, 1991). Therefore, histological methods are considered as sensitive and early warning signals for pollution, and have the advantages of being used to assess potential risks to species survival and environmental protection. Numerous studies have reported that ammonia nitrogen stress has a degenerative effect on fish intestinal tissue. Cao (ShenpingCao et al., 2021) reported that under 50 mg/L ammonia nitrogen stress, the intestinal villi of grass carp swelled substantially and expanded in width. Zhang *et al.* (Zhang et al., 2021) reported that ammonia nitrogen exposure not only caused intestinal inflammation in *Corbicula fluminea*, but also led to changes in the physical structure of intestine, including vacuolation and villi defect. Consistently, similar results were found in this study. After ammonia nitrogen stress, obvious histopathological damage such

as vacuolation, intestinal villi swelling, thickening of submucosa and lamina propria, and lamina propria hemorrhage were observed under light microscope. In addition, we also observed significant ultrastructural damage, including autophagy, apoptosis, necrosis, mitochondrial myelination death, and endoplasmic reticulum swelling. These results indicate that ammonia nitrogen stress can seriously damage the intestine of yellow catfish, resulting in severe histopathological changes.

The intestinal epithelium acts as a barrier against the spread of pathogens, toxins, and allergens from the lumen to the mucosal tissues, with mucin and antibacterial compounds serving as the primary components of the intestinal chemical barrier (Peterson and Artis, 2014). Mucus cells secrete mucin, which constitutes the main skeleton structure of the mucus layer and plays an important role in mucosal immunity (Kruatrachue et al., 2003). Therefore, an increase in the number of mucus cells usually leads to increased mucus secretion, which contributes to diluting and detoxifying toxic compounds (Andreozzi et al., 1994). Antibacterial compounds such as ACP, AKP, and LZM are beneficial for local LPS detoxification, and have anti-inflammatory effects (Omonijo et al., 2019). Chen *et al.* (Chen et al., 2011) reported the negative effect of ammonia nitrogen on intestinal chemical barrier of tilapia, and they found the enzyme activities of SOD, LZM, AKP and C3 were significantly reduced after exposure. In this study, after ammonia nitrogen stress, the number of mucus cells and the enzyme activity of antibacterial substances (LZM, AKP, and ACP) were substantially decreased in the intestine of yellow catfish, indicating the degradation of intestinal mucosal chemical barrier.

Tight junctions, including claudin family proteins, occludin, and ZO-1, are beneficial to maintain the physical integrity of the intestinal epidermal barrier. Disruption or defects in the intestinal barrier integrity may cause microbial imbalances and other harmful substances to cross the epithelial barrier, leading to activation of immune cells and intestinal inflammation (Kabat et al., 2014; Suzuki, 2020). Khan *et al.* (Khan et al., 2021) reported that ammonia nitrogen exposure caused significant downregulation of *claudin* and *occludin* in *Mauremys sinensis*. Similarly, Ding *et al.* (Ding et al., 2021) found that ammonia nitrogen stress resulted in sparse and shortened intestinal villi, downregulation of tight junction genes, and increased cell permeability in *Trachemys scripta elegans*. In this study, compared with the control group, the intestinal villi of yellow catfish in the ammonia nitrogen exposure group were sparse and shorter, the cavities between the microvilli were obvious and the tight junctions were blurred. The gene expression of tight sealing proteins (*Occludin*, *Claudin-1* and *ZO-1*) was upregulated, while the gene expression of pore-forming protein (*Claudin-2*) was downregulated. These results indicate that ammonia nitrogen stress damages the integrity of intestinal mucosal physical barrier, enhances paracellular permeability, and may induce inflammation.

Inflammation is not only a universal defense response to stress, but also an indispensable part for tissue repair (Lv et al., 2017). External stimulation can induce cytokine maturation and participate in the regulation of inflammatory response. Numerous studies have shown that the expression level of cytokines can be considered as effective biomarkers of aquatic organisms' inflammatory responses (Zhang et al., 2015; Jin et al., 2017). IL-1β, IL-8 and TNF-α are the major pro-inflammatory factors, which play significant roles in the development of inflammatory and autoimmune diseases (Weber et al., 2010). Previous study found that ammonia nitrogen stress caused apoptosis and increased expression of *TNF*, *IL-1β* and *IL-8* in *Pelteobagrus fulvidraco* (Li et al., 2020). This study likewise yielded similar results. With the increase of ammonia nitrogen level, the expression levels of *TNF-α*, *IL-1β* and *IL-8* increased, and the tissue sections exhibited obvious inflammatory cell infiltration. Furthermore, Zap-70 immunohistochemistry indicated that ammonia nitrogen stress induced recruitment of T/NK cells to the site of inflammation. Taken together, these findings demonstrate that ammonia nitrogen stress induces a strong inflammatory response in the intestine of yellow catfish.

An interesting finding in this study was that, the low concentration group (0.5 mg/L) had more severe damage to the intestinal physical barrier than the high concentration group (2.5 mg/L), including lower expression of tight junction related genes, sparser and shorter microvilli, and more blurred mucosal barrier. However, the high concentration group (2.5 mg/L) showed a trend of mucosal barrier repair. In fact, a growing number of studies have shown that certain inflammatory cytokines contribute to barrier protection. Although IL-17A is known to be an inflammatory cytokine, but it also protects the mucosal barrier by affecting *Occludin* expression (Lee et al., 2015). Shih *et al.* (Dudakov et al., 2015) revealed that following gastrointestinal infection, *IL-22* was upregulated, promoting tissue regeneration, barrier formation, and antibacterial defense. Jarry *et al.* (Jarry et al., 2008) revealed that IL-10 could provide barrier protection and participate in epithelial repair induced by intestinal inflammation. Therefore, highly regulated spatiotemporal interactions between mucosal cytokines (including pro-inflammatory and anti-inflammatory factors) may benefit epithelial barrier repair. In this study, the expression level of pro-inflammatory factors (*IL-1β, IL-8, TNF-α*) rose with the increase of ammonia nitrogen concentration, and the expression level of tight junction related genes (*Occludin*, *Claudin-1*, *ZO-1*) decreased first and then increased. Moreover, the high ammonia concentration group also had the highest expression of anti-inflammatory factor *IL-10*. Considering the above points, we believe that at the sampling time point, fish in the high concentration group were in the later stages of inflammation resolution and tissue repair period, whereas fish in the low concentration group were still in the major inflammatory stage.

Under natural conditions, TAN and pNH_3 levels in intestinal chyme are very high (Bucking and Wood, 2012), exceeding the water ammonia levels considered toxic to fish (Randall and Tsui, 2002). However, the intestine can still maintain homeostasis and normal morphological structure, implying that the intestinal epithelium should be well adapted to deal with high ammonia levels at the enteric surface. Interestingly, our work suggests that ammonia nitrogen has a significant toxic effect on the intestine of yellow catfish. Whether this effect is direct or indirect, and whether it is mediated by blood ammonia or cortisol, remains unclear and needs further investigation.

5 Conclusion

In this study, we systematically evaluated the pathological changes after ammonia nitrogen challenge in yellow catfish after

an ammonia nitrogen challenge at the histological, molecular, and ultrastructural levels, as well as the inflammation-related immune response. In conclusion, this investigation demonstrates that ammonia nitrogen stress can damage the intestinal mucosal barrier of yellow catfish and induce intestinal inflammation.

Data availability statement

The datasets presented in this study can be found in online repositories. The names of the repository/repositories and accession number(s) can be found in the article/Supplementary Material.

Author contributions

SeL: Formal analysis, Investigation, Methodology, Writing–original draft, Writing–review and editing. LL: Project administration, Investigation. FZ: Project administration, Investigation. XH: Conceptualization, Data curation. LZ: Supervision. ShL: Validation. YG: Resources, Software. DC: Resources, Software. YO: Validation, Visualization. WC: Investigation, Data curation. YD: Methodology, Writing–review and editing.

Funding

The authors declare financial support was received for the research, authorship, and/or publication of this article. This work was supported by Fisheries Research Institute ,Sichuan Academy of Agricultural Sciences (2021YFYZ0015), Sichuan Science and Technology Program (2021JDRC0125), Sichuan Science and Technology Key Research and Development Program (2022YFS0478) and Sichuan International Science and Technology Innovation Cooperation Foundation (2020YFH0156).

Acknowledgments

We would like to thank Service Bio (Wuhan, Hubei province) for Zap-70 (99F2-Cell Signaling) Rabbit mAb antibody, as well as Lilai Bio (Chengdu, Sichuan province) for Transmission electron microscopy assay. In addition, we would like to thank “Sichuan Science and Technology Program”, “Sichuan Science and Technology Key Research and Development Program”, and “Sichuan International Science and Technology Innovation Cooperation Foundation” for supporting this study.

Conflict of interest

The authors declare that the research was conducted in the absence of any commercial or financial relationships that could be construed as a potential conflict of interest.

Publisher’s note

All claims expressed in this article are solely those of the authors and do not necessarily represent those of their affiliated organizations, or those of the publisher, the editors and the reviewers. Any product that may be evaluated in this article, or claim that may be made by its manufacturer, is not guaranteed or endorsed by the publisher.

Supplementary material

The Supplementary Material for this article can be found online at: https://www.frontiersin.org/articles/10.3389/fphys.2023.1279051/full#supplementary-material

References

Administration, M. o. A. F. (2021). *Statistics of China Fishery yearbook*. Beijing: China Agriculture Press.

Andreozzi, G., Antonucci, R., Affatato, C., Gargiulo, G., and Battaglini, P. (1994). The effect of cadmium on the intestine of *Carassius auratus*. *Anat. Histol. Embryol.* 23 (2), 102–111. doi:10.1111/j.1439-0264.1994.tb00242.x

Barišić, J., Filipović Marijić, V., Mijošek, T., Čož-Rakovac, R., Dragun, Z., Krasnići, N., et al. (2018). Evaluation of architectural and histopathological biomarkers in the intestine of brown trout (*Salmo trutta* Linnaeus, 1758) challenged with environmental pollution. *Sci. Total Environ.* 642, 656–664. doi:10.1016/j.scitotenv.2018.06.045

Bischoff, S. C., Barbara, G., Buurman, W., Ockhuizen, T., Schulzke, J. D., Serino, M., et al. (2014). Intestinal permeability--a new target for disease prevention and therapy. *BMC Gastroenterol.* 14, 189. doi:10.1186/s12876-014-0189-7

Bucking, C., and Wood, C. M. (2012). Digestion of a single meal affects gene expression of ion and ammonia transporters and glutamine synthetase activity in the gastrointestinal tract of freshwater rainbow trout. *J. Comp. Physiol. B* 182 (3), 341–350. doi:10.1007/s00360-011-0622-y

Camilleri, M., Madsen, K., Spiller, R., Greenwood-Van Meerveld, B., and Verne, G. N. (2012). Intestinal barrier function in health and gastrointestinal disease. *Neurogastroenterol. Motil.* 24 (6), 503–512. doi:10.1111/j.1365-2982.2012.01921.x

Chen, J., Zang, X., Gengdong, H. U., Jianhong, Q. U., and Fan, L. (2011). The immune response of GIFT *Oreochromis niloticus* and its susceptibility to Streptococcus iniae under stress in different ammonia. *Ecol. Environ. Sci.* doi:10.1016/S1671-2927(11)60313-1

Chen, Q. L., Luo, Z., Zheng, J. L., Li, X. D., Liu, C. X., Zhao, Y. H., et al. (2012). Protective effects of calcium on copper toxicity in *Pelteobagrus fulvidraco*: copper accumulation, enzymatic activities, histology. *Ecotoxicol. Environ. Saf.* 76 (2), 126–134. doi:10.1016/j.ecoenv.2011.10.007

Chen, Q., Zhao, H., Huang, Y., Cao, J., Wang, G., Sun, Y., et al. (2016). Effects of dietary arginine levels on growth performance, body composition, serum biochemical indices and resistance ability against ammonia-nitrogen stress in juvenile yellow catfish (*Pelteobagrus fulvidraco*). *Anim. Nutr.* 2 (3), 204–210. doi:10.1016/j.aninu.2016.07.001

Ding, L., Huang, Z., Lu, Y., Liang, L., Li, N., Xu, Z., et al. (2021). Toxic effects of ammonia on intestinal health and microbiota in red-eared slider (*Trachemys scripta* elegans). *Chemosphere* 280, 130630. doi:10.1016/j.chemosphere.2021.130630

Dudakov, J. A., Hanash, A. M., and van den Brink, M. R. (2015). Interleukin-22: immunobiology and pathology. *Annu. Rev. Immunol.* 33, 747–785. doi:10.1146/annurev-immunol-032414-112123

Ghosh, S. S., Wang, J., Yannie, P. J., Cooper, R. C., Sandhu, Y. K., Kakiyama, G., et al. (2021). Over-expression of intestinal alkaline phosphatase attenuates atherosclerosis. *Circ. Res.* 128 (11), 1646–1659. doi:10.1161/circresaha.120.317144

Gonçalves, A. R. N., Marinsek, G. P., de Souza Abessa, D. M., and de Britto Mari, R. (2020). Adaptative responses of myenteric neurons of Sphoeroides testudineus to environmental pollution. *Neurotoxicology* 76, 84–92. doi:10.1016/j.neuro.2019.10.008

Hongxing, G., Xiafei, L., Jialing, L., Zhenquan, C., Luoyu, G., Lei, L., et al. (2021). Effects of acute ammonia exposure on antioxidant and detoxification metabolism in clam Cyclina sinensis. *Ecotoxicol. Environ. Saf.* 211, 111895. doi:10.1016/j.ecoenv.2021.111895

Jarry, A., Bossard, C., Bou-Hanna, C., Masson, D., Espaze, E., Denis, M. G., et al. (2008). Mucosal IL-10 and TGF-beta play crucial roles in preventing LPS-driven, IFN-gamma-mediated epithelial damage in human colon explants. *J. Clin. Invest.* 118 (3), 1132–1142. doi:10.1172/jci32140

Jin, Y., Wu, S., Zeng, Z., and Fu, Z. (2017). Effects of environmental pollutants on gut microbiota. *Environ. Pollut.* 222, 1–9. doi:10.1016/j.envpol.2016.11.045

Kabat, A. M., Srinivasan, N., and Maloy, K. J. (2014). Modulation of immune development and function by intestinal microbiota. *Trends Immunol.* 35 (11), 507–517. doi:10.1016/j.it.2014.07.010

Kathyayani, S. A., Poornima, M., Sukumaran, S., Nagavel, A., and Muralidhar, M. (2019). Effect of ammonia stress on immune variables of Pacific white shrimp Penaeus vannamei under varying levels of pH and susceptibility to white spot syndrome virus. *Ecotoxicol. Environ. Saf.* 184, 109626. doi:10.1016/j.ecoenv.2019.109626

Khan, I., Huang, Z., Liang, L., Li, N., Ali, Z., Ding, L., et al. (2021). Ammonia stress influences intestinal histomorphology, immune status and microbiota of Chinese striped-neck turtle (Mauremys sinensis). *Ecotoxicol. Environ. Saf.* 222, 112471. doi:10.1016/j.ecoenv.2021.112471

Kim, J. H., Rhee, J. S., Dahms, H. U., Lee, Y. M., Han, K. N., and Lee, J. S. (2012). The yellow catfish, *Pelteobagrus fulvidraco* (siluriformes) metallothionein cDNA: molecular cloning and transcript expression level in response to exposure to the heavy metals Cd, Cu, and Zn. *Fish. Physiol. Biochem.* 38 (5), 1331–1342. doi:10.1007/s10695-012-9621-5

Kleinhenz, L. S., Trenfield, M. A., Mooney, T. J., Humphrey, C. L., van Dam, R. A., Nugegoda, D., et al. (2018). Acute ammonia toxicity to the larvae (glochidia) of the tropical Australian freshwater mussel Velesunio spp. Using a modified toxicity test protocol. *Environ. Toxicol. Chem.* 37 (8), 2175–2187. doi:10.1002/etc.4175

Kołacińska, K., and Koncki, R. (2014). A novel optoelectronic detector and improved flow analysis procedure for ammonia determination with Nessler's reagent. *Anal. Sci.* 30 (10), 1019–1022. doi:10.2116/analsci.30.1019

Kruatrachue, M., Rangsayatorn, N., Pokethitiyook, P., Upatham, E. S., and Singhakaew, S. (2003). Histopathological changes in the gastrointestinal tract of fish, Puntius gonionotus, fed on dietary cadmium. *Bull. Environ. Contam. Toxicol.* 71 (3), 561–569. doi:10.1007/s00128-003-8795-z

Lee, J. S., Tato, C. M., Joyce-Shaikh, B., Gulen, M. F., Cayatte, C., Chen, Y., et al. (2015). Interleukin-23-Independent IL-17 production regulates intestinal epithelial permeability. *Immunity* 43 (4), 727–738. doi:10.1016/j.immuni.2015.09.003

Lee, P. T., Yamamoto, F. Y., Low, C. F., Loh, J. Y., and Chong, C. M. (2021). Gut immune system and the implications of oral-administered immunoprophylaxis in finfish aquaculture. *Front. Immunol.* 12, 773193. doi:10.3389/fimmu.2021.773193

Li, M., Zhang, M., Qian, Y., Shi, G., and Wang, R. (2020). Ammonia toxicity in the yellow catfish (*Pelteobagrus fulvidraco*): the mechanistic insight from physiological detoxification to poisoning. *Fish. Shellfish Immunol.* 102, 195–202. doi:10.1016/j.fsi.2020.04.042

Liu, S. (2022). *Effects of ammonia nitrogen stress on gill respiration and immune function of yellow catfish (*Pelteobagrus fulvidraco*) and its mechanism*. Cheng du: Sichuan Agricultural University.

Livak, K. J., and Schmittgen, T. D. (2001). Analysis of relative gene expression data using real-time quantitative PCR and the 2(-Delta Delta C(T)) Method. *Methods* 25 (4), 402–408. doi:10.1006/meth.2001.1262

Lu, J., Yao, T., Shi, S., and Ye, L. (2022). Effects of acute ammonia nitrogen exposure on metabolic and immunological responses in the Hong Kong oyster Crassostrea hongkongensis. *Ecotoxicol. Environ. Saf.* 237, 113518. doi:10.1016/j.ecoenv.2022.113518

Lv, Z., Wei, Z., Zhang, Z., Li, C., Shao, Y., Zhang, W., et al. (2017). Characterization of NLRP3-like gene from Apostichopus japonicus provides new evidence on inflammation response in invertebrates. *Fish. Shellfish Immunol.* 68, 114–123. doi:10.1016/j.fsi.2017.07.024

Omonijo, F. A., Liu, S., Hui, Q., Zhang, H., Lahaye, L., Bodin, J. C., et al. (2019). Thymol improves barrier function and attenuates inflammatory responses in porcine intestinal epithelial cells during lipopolysaccharide (LPS)-Induced inflammation. *J. Agric. Food Chem.* 67 (2), 615–624. doi:10.1021/acs.jafc.8b05480

Peterson, L. W., and Artis, D. (2014). Intestinal epithelial cells: regulators of barrier function and immune homeostasis. *Nat. Rev. Immunol.* 14 (3), 141–153. doi:10.1038/nri3608

Pustiglione Marinsek, G., Moledo de Souza Abessa, D., Gusso-Choueri, P. K., Brasil Choueri, R., Nascimento Gonçalves, A. R., D'Angelo Barroso, B. V., et al. (2018). Enteric nervous system analyses: new biomarkers for environmental quality assessment. *Mar. Pollut. Bull.* 137, 711–722. doi:10.1016/j.marpolbul.2018.11.015

Qian, L., Miao, L., Abba, B. S. A., Lin, Y., Jiang, W., Chen, S., et al. (2021). Molecular characterization and expression of sirtuin 2, sirtuin 3, and sirtuin 5 in the Wuchang bream (*Megalobrama amblycephala*) in response to acute temperature and ammonia nitrogen stress. *Comp. Biochem. Physiol. B Biochem. Mol. Biol.* 252, 110520. doi:10.1016/j.cbpb.2020.110520

Randall, D. J., and Tsui, T. K. (2002). Ammonia toxicity in fish. *Mar. Pollut. Bull.* 45 (1-12), 17–23. doi:10.1016/s0025-326x(02)00227-8

ShenpingCao, D., Zhao, D., Huang, R., Xiao, Y., Xu, W., Liu, X., et al. (2021). The influence of acute ammonia stress on intestinal oxidative stress, histology, digestive enzymatic activities and PepT1 activity of grass carp (Ctenopharyngodon idella). *Aquac. Rep.* 20, 100722. doi:10.1016/j.aqrep.2021.100722

Suzuki, T. (2020). Regulation of the intestinal barrier by nutrients: the role of tight junctions. *Anim. Sci. J.* 91 (1), e13357. doi:10.1111/asj.13357

Varghese, F., Bukhari, A. B., Malhotra, R., De, A., and IHC Profiler (2014). IHC profiler: an open source plugin for the quantitative evaluation and automated scoring of immunohistochemistry images of human tissue samples. *PLoS One* 9 (5), e96801. doi:10.1371/journal.pone.0096801

Wang, S., Li, X., Zhang, M., Jiang, H., Wang, R., Qian, Y., et al. (2021). Ammonia stress disrupts intestinal microbial community and amino acid metabolism of juvenile yellow catfish (*Pelteobagrus fulvidraco*). *Ecotoxicol. Environ. Saf.* 227, 112932. doi:10.1016/j.ecoenv.2021.112932

Weber, A., Wasiliew, P., and Kracht, M. (2010). Interleukin-1beta (IL-1beta) processing pathway. *Sci. Signal* 3 (105), cm2. doi:10.1126/scisignal.3105cm2

Wester, P. W., and Canton, J. H. (1991). The usefulness of histopathology in aquatic toxicity studies. *Comp. Biochem. Physiol. C Comp. Pharmacol. Toxicol.* 100 (1-2), 115–117. doi:10.1016/0742-8413(91)90135-g

Wood, C. M., Liew, H. J., De Boeck, G., Hoogenboom, J. L., and Anderson, W. G. (2019). Nitrogen handling in the elasmobranch gut: A role for microbial urease. *J. Exp. Biol.* 222, jeb194787. doi:10.1242/jeb.194787

Wu, Y., Tang, L., Wang, B., Sun, Q., Zhao, P., and Li, W. (2019). The role of autophagy in maintaining intestinal mucosal barrier. *J. Cell Physiol.* 234 (11), 19406–19419. doi:10.1002/jcp.28722

Zhang, S., Jin, Y., Zeng, Z., Liu, Z., and Fu, Z. (2015). Subchronic exposure of mice to cadmium perturbs their hepatic energy metabolism and gut microbiome. *Chem. Res. Toxicol.* 28 (10), 2000–2009. doi:10.1021/acs.chemrestox.5b00237

Zhang, S., Lü, B., Chao, G. Q., Chen, F. M., Chen, M. Y., and Chen, H. Q. (2011). The effects of milk and milk products on non-steroidal anti-inflammatory drug induced intestinal damage in rats. *Zhonghua Nei Ke Za Zhi* 50 (9), 771–775. doi:10.1038/cdd.2010.68

Zhang, T., Yan, Z., Zheng, X., Wang, S., Fan, J., and Liu, Z. (2020). Effects of acute ammonia toxicity on oxidative stress, DNA damage and apoptosis in digestive gland and gill of Asian clam (Corbicula fluminea). *Fish. Shellfish Immunol.* 99, 514–525. doi:10.1016/j.fsi.2020.02.046

Zhang, T., Zhang, Y., Xu, J., Yan, Z., Sun, Q., Huang, Y., et al. (2021). Toxic effects of ammonia on the intestine of the Asian clam (Corbicula fluminea). *Environ. Pollut.* 287, 117617. doi:10.1016/j.envpol.2021.117617

Zhong, L. (2022). *Effects of ammonia nitrogen stress on gill excretion and osmotic pressure regulation of yellow catfish (*Pelteobagrus fulvidraco*)*. Cheng du: Sichuan Agricultural University.

Zhou, X., Zhang, G. R., Ji, W., Shi, Z. C., Ma, X. F., Luo, Z. L., et al. (2021). Expression and function analysis of interleukin-17a/F1, 2, and 3 genes in yellow catfish (*Pelteobagrus fulvidraco*): distinct bioactivity of recombinant IL-17a/F1, 2, and 3. *Front. Immunol.* 12, 626895. doi:10.3389/fimmu.2021.626895

Zimmerli, S., Bernet, D., Burkhardt-Holm, P., Schmidt-Posthaus, H., Vonlanthen, P., Wahli, T., et al. (2007). Assessment of fish health status in four Swiss rivers showing a decline of brown trout catches. *Aquat. Sci.* 69 (1), 11–25. doi:10.1007/s00027-006-0844-3

frontiers | Frontiers in Marine Science

TYPE Original Research
PUBLISHED 21 September 2023
DOI 10.3389/fmars.2023.1270776

OPEN ACCESS

EDITED BY
Yiming Li,
Fishery Machinery and Instrument Research Institute, China

REVIEWED BY
Zhendong Qin,
Zhongkai University of Agriculture and Engineering, China
Xiaochen Yuan,
Anhui Agricultural University, China

*CORRESPONDENCE
Wei Hu
huwei19872006@163.com
Han-Wen Yuan
hanwen_yuan@126.com
Zheng-Yong Wen
zhengyong_wen@126.com

†These authors have contributed equally to this work

RECEIVED 01 August 2023
ACCEPTED 29 August 2023
PUBLISHED 21 September 2023

CITATION
Zeng W-H, Wei X-Y, Qin W, Qin C-J, Shi Q, Guo S-T, Prathomya P, Zhang S-Y, Fu P, Hu W, Yuan H-W and Wen Z-Y (2023) Molecular characterization, spatiotemporal expression patterns of fatty acid elongase (*elovl8*) gene, and its transcription changes in response to different diet stimuli in yellow catfish (*Pelteobagrus fulvidraco*). *Front. Mar. Sci.* 10:1270776. doi: 10.3389/fmars.2023.1270776

Molecular characterization, spatiotemporal expression patterns of fatty acid elongase (*elovl8*) gene, and its transcription changes in response to different diet stimuli in yellow catfish (*Pelteobagrus fulvidraco*)

Wan-Hong Zeng[1,2†], Xiu-Ying Wei[2†], Wei Qin[2], Chuan-Jie Qin[2], Qiong Shi[2,3,4], Sheng-Tao Guo[5], Panita Prathomya[6], Shi-Yong Zhang[7], Peng Fu[8], Wei Hu[1*], Han-Wen Yuan[1*] and Zheng-Yong Wen[1,2,3*]

[1]School of Animal Science, Yangtze University, Jingzhou, China, [2]Key Laboratory of Sichuan Province for Fishes Conservation and Utilization in the Upper Reaches of the Yangtze River, Neijiang Normal University, Neijiang, China, [3]Shenzhen Key Lab of Marine Genomics, Guangdong Provincial Key Lab of Molecular Breeding in Marine Economic Animals, BGI Academy of Marine Sciences, BGI Marine, BGI, Shenzhen, China, [4]Laboratory of Aquatic Genomics, College of Life Sciences and Oceanography, Shenzhen University, Shenzhen, China, [5]Key Laboratory of Bio-Resources and Eco-Environment of Ministry of Education, College of Life Sciences, Sichuan University, Chengdu, China, [6]Department of Animal and Aquatic Sciences, Faculty of Agriculture, Chiang Mai University, Chiang Mai, Thailand, [7]Freshwater Fisheries Research Institute of Jiangsu Province, Nanjing, China, [8]Chongqing Fisheries Science Research Institute, Chongqing, China

Elongase of very long-chain fatty acid 8 (Elovl8) is a new member identified in the Elovl family that is involved in the synthesis of highly unsaturated fatty acids (HUFAs). However, the evolutionary and physiological roles of this enzyme are still largely unknown. In the present study, the *elovl8* gene was identified and characterized from yellow catfish *Pelteobagrus fulvidraco*, and then its evolutionary and molecular characteristics as well as transcriptional changes in response to various nutritional status were determined. Results showed that the open reading frame (ORF) of *elovl8* was 795 bp in length, encoding a protein of 264 amino acids. Multiple sequences alignment showed that the yellow catfish Elovl8 was highly conserved with other homologs in teleosts, sharing similar structural characteristics (including six conserved transmembrane α-helical domains, four conserved elongase motifs, and three highly conserved cysteine residues). Meanwhile, comparisons of genetic synteny confirmed that the *elovl8* gene identified from the yellow catfish was the homolog of *elovl8b* in other teleosts, and thus, the *elovl8a* gene was lost in the genome of the yellow catfish. Gene structure analysis revealed that the *elovl8b* gene contained eight exons and seven introns, which was highly conserved in teleosts, implying the functional conservation among various fish species. Tissue distribution analysis detected by

real-time quantitative PCR (RT-qPCR) showed that the *elovl8* gene was extensively expressed in all detected tissues except eyes, with high expression levels in the intestine and liver. Temporal expression analysis revealed that the expression level of *elovl8* was stably expressed in the early 12 h after fertilization, and then dramatically decreased at 24, 48, 72, and 96 h after fertilization, implying that *elovl8* is required for HUFA biosynthesis in the early development stages. Functional experiments showed that the expression of the *elovl8* gene was stimulated after feeding with egg yolk but was not obviously affected after feeding with halogenated worms, indicating that diets full of HUFAs can inhibit the expression of *elovl8* in yellow catfish. Our findings will help us to better understand the evolutionary and functional characteristics of *elovl8* in teleosts, and lay a solid basis for investigating the regulation mechanism of HUFA biosynthesis.

KEYWORDS

yellow catfish, *elovl8*, gene cloning, gene expression, HUFA biosynthesis

Introduction

Highly unsaturated fatty acids (HUFAs) are a series of straight-chain fatty acids with three or more double bonds and 20 or more carbon atoms, which play important roles in maintaining cell membrane fluidity, regulating fat metabolism, enhancing immunity, and reducing inflammation (Zhang et al., 2019; Ri et al., 2022). Notably, eicosapentaenoic acid (EPA, 20:5n-3) and docosahexaenoic acid (DHA, 22:6n-3) are the most prominent HUFAs that play critical roles involved in promoting growth and development, and preventing cardiovascular and neurodevelopmental disorders (De Giuseppe et al., 2014; Zárate et al., 2017).

Usually, vertebrates possess the ability to biosynthesize HUFAs by using essential polyunsaturated fatty acids as precursors with two critical rate-limiting enzymes including elongases of very long chain fatty acids (Elovls) and fatty acid desaturases (Fads) (Oboh et al., 2017). The former can elongate the carbon chain of polyunsaturated fatty acids while the latter can introduce a double bond at a specific position on the carbon chain to produce desaturation (Nakamura and Nara, 2004; Guillou et al., 2010). In teleosts, it is commonly accepted that freshwater and migratory fishes have obvious capacity to biosynthesize HUFAs while seawater fishes usually have lower or no capacity to achieve this goal because they are surrounded by an environment with abundant HUFAs in diets (Li et al., 2010; Jaya-Ram et al., 2011). Meanwhile, it seems that food habitats also have effects on the HUFA biosynthesis in teleosts. For example, herbivorous or omnivorous freshwater fishes such as grass carp (Du et al., 2006) and zebrafish (Ishak et al., 2008) are proved to have the ability to synthesize arachidonic acid (AA), EPA, and DHA with linoleic acid (LA) and linolenic acid (LNA) as precursors. Differently, carnivorous fishes such as groupers (Li et al., 2016) and gilthead seabream (Ganga et al., 2005) lack this kind of capacity or have a weak capacity, and thus higher levels of dietary HUFAs are required to meet their requirements for growth, development, and reproduction. However, more studies are still required to investigate the exact mechanisms involved in HUFA biosynthesis in teleosts.

Thus far, seven members named ELOVL1–ELOVL7 in the ELOVL family were identified in mammals, and these members showed different substrate specificities for various fatty acid substrates (Jakobsson et al., 2006; Ohno et al., 2010). Overall, ELOVL1, ELOVL3, ELOVL6, and ELOVL7 primarily extend saturated fatty acids as well as monounsaturated fatty acids; ELOVL2, ELOVL4, and ELOVL5 mainly catalyze the elongation reactions of polyunsaturated fatty acids, while Elovl4 prolongs both very-long-chain saturated fatty acids and very-long-chain polyunsaturated fatty acids (Agbaga et al., 2008; Guillou et al., 2010). Recently, a novel teleost-specific member of the Elovl family, named Elovl8, had been identified in a marine rabbitfish (*Siganus canaliculatus*) (Li et al., 2020). Genetic synteny and gene phylogeny revealed that this new member commonly contains two isoforms, and it seemed that the *elovl8a* gene has been lost in some fish genomes (Li et al., 2020). Further functional experiments indicated that Elovl8b but not Elovl8a possesses the capacity to biosynthesize HUFAs (Li et al., 2020). Consistently, a single *elovl8b* gene was identified in hybrid grouper (*Epinephelus fuscoguttatus* ♀ × *Epinephelus lanceolatus* ♂), and functional experiments revealed that diets full of HUFAs can inhibit *elovl8b* transcription in liver, suggesting that a negative feedback regulation of the HUFA synthetic pathway existed (Wu et al., 2022). However, the evolutionary and functional characteristics of this new member are still largely unclear, and much more studies are required to illustrate these issues.

Yellow catfish (*Pelteobagrus fulvidraco*) belongs to family Bagridae, order Siluriformes, and is an omnivorous freshwater fish that is widely cultured in China due to its rapid growth, good taste, and valuable nutrition values (Guo et al., 2023; Wei et al.,

2023). Thus far, two key genes involved in HUFA biosynthesis including *fad2* and *elovl5* have been identified in yellow catfish (Song et al., 2015; Qin et al., 2017), but their exact roles have not been well investigated. In the present study, we identified a teleost-specific *elovl8* gene from yellow catfish, and then its evolutionary and molecular characteristics, spatiotemporal expression patterns, and functional traits were determined for the first time. Our findings will provide not only a novel insight into mechanisms involved in HUFA biosynthesis in yellow catfish, but also valuable data for better understanding the evolutionary and functional traits of *elovl8* in teleosts.

Materials and methods

Fish sampling

Yellow catfish (weight = 32.6 ± 3.1 g) used in this study were purchased from a fishery farm in Sichuan province of China, and fishes were transported to the laboratory and temporarily reared in 1 m × 1 m × 1 m net boxes set up in a 16-m^2 microfluidic pond. Fishes were reared for 2 weeks in a natural light condition (12 L/12 D), and water temperature was maintained at 24–26°C. Fishes were fed with commercial feed (approximately 3%–4% of body weight) at 19:00 every day as described in our previous studies (Da et al., 2022). Experimental fishes showed normal feeding and activity during the accumulation period. After that, five fishes were randomly selected and used for tissue distribution studies. Fishes were anesthetized with MS-222 before decapitated, and then tissues including adipose, brain, barbel, eye, gill, gonad, heart, intestine, kidney, liver, muscle, spleen, and stomach were collected. Tissue samples were immediately frozen in liquid nitrogen, and subsequently stored at −80°C until further utilization.

Meanwhile, fertilized eggs of yellow catfish used in this study were obtained by artificial breeding in our laboratory. During incubation, the development status of yellow catfish embryos was observed with a microscope, and five embryos and larvae were respectively sampled at each time point including 0 h, 3 h, 6 h, 12 h, 24 h, 36 h, 48 h, 72 h, and 96 h after fertilization in the early developmental stages. Similarly, samples were frozen rapidly with liquid nitrogen and then stored at −80°C for further utilization.

Diets with different content of HUFAs, including *Artemia nauplii* and egg yolk, were separately used as larval stage feeds to investigate the potential effects of various diets on transcription of *elovl8* in yellow catfish. Meanwhile, approximately 200 yellow catfish larvae were randomly selected and fed with different diets on day 4 after hatching, and three parallel experiments were designed for each group. During the experiment, 25% water changes were carried out daily, the oxygenation pump was kept continuously oxygenated, and the dissolved oxygen in the water was maintained above 6 mg/L. Fishes were fed at 08:00, 12:00, 16:00 and 20:00 to ensure sufficient diet supplement in the experimental tanks. The experiment lasted for 3 days, and five fishes from each tank were collected at 24, 48, and 72 h after feeding. Finally, samples were immediately frozen in liquid nitrogen and stored at −80 °C for further utilization.

Identification of the *elovl8* gene in yellow catfish

Protein similarity BLAST was conducted to identify the genomic and transcriptomic sequences from yellow catfish genome data in NCBI database and transcriptome database using several valid fish Elovl8 protein sequences as queries. Subsequently, potential sequences were verified and confirmed by NCBI-BLAST (https://blast.ncbi.nlm.nih.gov/Blast.cgi). Meanwhile, specific primers used for cloning experiment were designed with the Primer Premier 5.0 software (www.PremierBiosoft.com) (Supplementary Table 1).

PCR was performed to amplify the aimed *elovl8* gene fragment with liver cDNA as template. Then, PCR products were tested by agarose gel electrophoresis and isolated and purified using the TaKaRa gel recovery kit. Finally, PCR products were cloned into the pMD-19T vector (TaKaRa, Dalian, China) and then sequenced at Sangon Co. Ltd. (Guangzhou, China) to ensure the accuracy of the potential *elovl8* gene in yellow catfish.

Bioinformatics analysis

The nucleotide sequence of *elovl8* was obtained from yellow catfish using BLAST in the NCBI database (http://www.ncbi.nlm.nih.gov/BLAST). After validation, the nucleotide sequences were translated into protein sequences using the Primer Premier 5.0 software. Multiple Elovl8 protein sequence alignment was conducted by using Clustal X software as described in our previous studies (Li et al., 2020). Meanwhile, comparative analyses of genetic synteny and gene structure were conducted to determine the evolutionary pattern of *elovl8* genes in teleosts. Additionally, a phylogeny was constructed on the basis of the protein sequences of various teleosts to investigate the evolutionary history of the *elovl8* gene family. Elovl8 protein sequences used for phylogeny were downloaded from the NCBI or Ensembl databases. After calculation, JTT + G was selected as the best model, and the neighbor-joining (NJ) method was chosen to construct the phylogenetic tree. Finally, the robustness of the tree topology was assessed by a nonparametric bootstrap analysis with 1,000 resampling replicates. Details of the selected Elovls family proteins are given in Supplementary Table 2.

RNA extraction and quantitative PCR

Total RNA was extracted with Trizol reagent (Invitrogen, Carlsbad, CA, USA) according to the manufacturer's protocol, and then the concentration and quality of total RNA were confirmed by a spectrophotometer (Nano Drop 2000, Thermo Scientific, USA) as described in our previous studies (Wen et al., 2020; Wen et al., 2021). Subsequently, 1 μg of total RNA was reverse transcribed to cDNA using the QuantiTect® Reverse Transcription kit (Takara Biotech, Dalian, China). Quantitative real-time PCR (qPCR) was conducted to measure the mRNA level of rabbitfish *elovl8* on a Light Cycler Real-Time system with a final volume of 20

μL. Meanwhile, the relative expression level of mRNA was normalized with *β-actin* after assessing the stability of five reference genes. Finally, the relative transcription level of *elovl8* was calculated using the Pfaffl method (Yang et al., 2018; Wen et al., 2019). Sequences of the specific primers used for qPCRs are provided in Supplementary Table 1.

Statistical analysis

SPSS 22.0 (IBM, Armonk, NY, USA) and GraphPad Prism 7.0 (GraphPad, Prism Software Inc., San Diego, California) were used for statistical analysis. All data were shown as mean normalized values ± standard error of the mean (SEM). Significant differences were determined using one-way analysis of variance (ANOVA) followed by Tukey's test, and differences were significant when $p < 0.05$.

Results

Molecular characteristics of the *elovl8* gene in yellow catfish

In the present study, we identified the *elovl8* gene from yellow catfish for the first time. NCBI-Blast revealed that the identified *elovl8* gene is the homolog of *elovl8b* gene in teleost. The open reading frame (ORF) of yellow catfish *elovl8* was 795 bp in length and encoded a protein with 264 amino acids. Multiple Elovl8b protein sequence alignment showed that Elovl8b is highly conserved (protein similarity > 84.4%) in teleosts and that they shared similar structural features, containing six conserved transmembrane α-helix structural domains, four conserved elongase motifs, and three highly conserved cysteine residues (Figure 1).

Phylogenetic analysis

To better understand the evolutionary relationships of the *elovl8* gene family in teleosts, a phylogenetic tree was constructed using the NJ method with MEGA-X software. Results showed that the *elovl8* family was divided into two clades, namely, *elovl8a* and *elovl8b* subfamilies, and the yellow catfish *elovl8* was clustered into the *elovl8b* clade (Figure 2). Notably, red-bellied piranha (*P. nattereri*), chum salmon (*O. keta*), zebrafish (*D. rerio*), Roho labeo (*L. rohita*), fathead minnows (*P. promelas*), grass carp (*C. idella*), cachama (*C. macropomum*), and delta smelt (*H. transpacificus*) contained two *elovl8* paralogs. Differently, north African catfish (*C. gariepinus*), channel catfish (*I. punctatus*), yellow catfish (*P. fulvidraco*), freshwater shark (*P. hypophthalmus*), southern catfish (*S. meridionalis*), Mexican tetra (*A. mexicanus*), the sharp-headed submarginal fish (*X. texanus*), and the common carp (*C. carpio*) only contained the *elovl8b* subtype (Figure 2). Moreover, yellow catfish *elovl8b* shared a close relationship with channel catfish and African catfish *elovl8b* (Figure 2).

Genetic synteny

Comparative genomics were conducted to further explore the exact evolutionary status of *elovl8* genes in eight representative fishes, namely, *L. rohita*, *C. macropomum*, *C. idella*, *A. mexicanus*, *P. hypophthalmus*, *I. punctatus*, *C. gariepinus*, and *P. fulvidraco* (Figure 3). Results showed that three species, namely, *L. rohita*, *C. macropomum*, and *C. idella*, contained the *elovl8a* gene, and a conserved gene cluster *tesk2-toe1-selenop2-elovl8a-zswim5-urod* was identified in these fishes (Figure 3A). Notably, the *elovl8a* gene had been lost in the other five fish species, namely, *P. fulvidraco*, *I. punctatus*, *C. gariepinus*, *P. hypophthalmus*, and *A. mexicanus* (Figure 3A). Moreover, a highly conserved gene cluster *dmap1-guk1b-armh1-mutyh-elovl8b* was identified in all the representative fish genomes (Figure 3B).

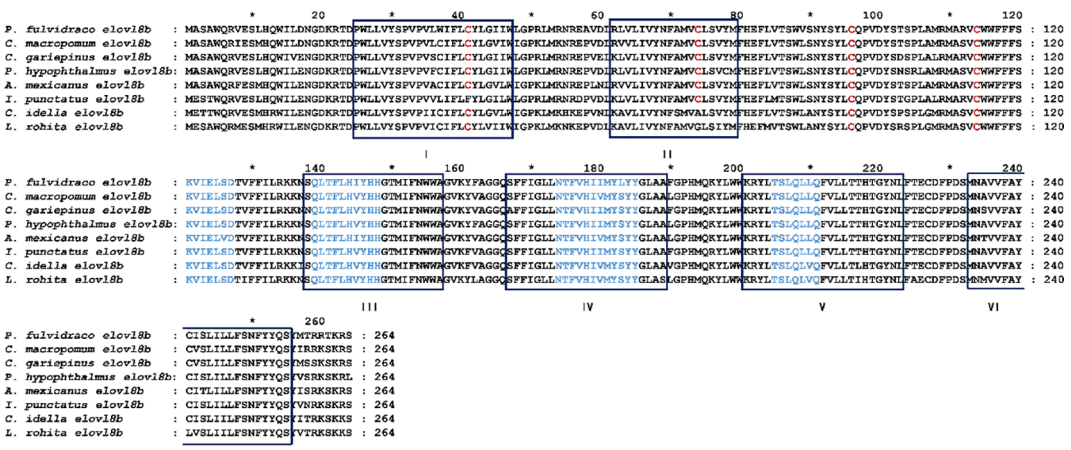

FIGURE 1
Multiple protein sequence alignment of Elovl8b between yellow catfish and other representative teleosts. Six conserved transmembrane α-helix structural domains are labeled with I–VI. The four conserved elongase motifs are labeled in blue font. Cysteines are shown in red. C-terminal ER retrieval signals are marked with dashed boxes. Asterisks (*) indicate the amino acids conserved among all members of the proteins.

10.3389/fmars.2023.1270776

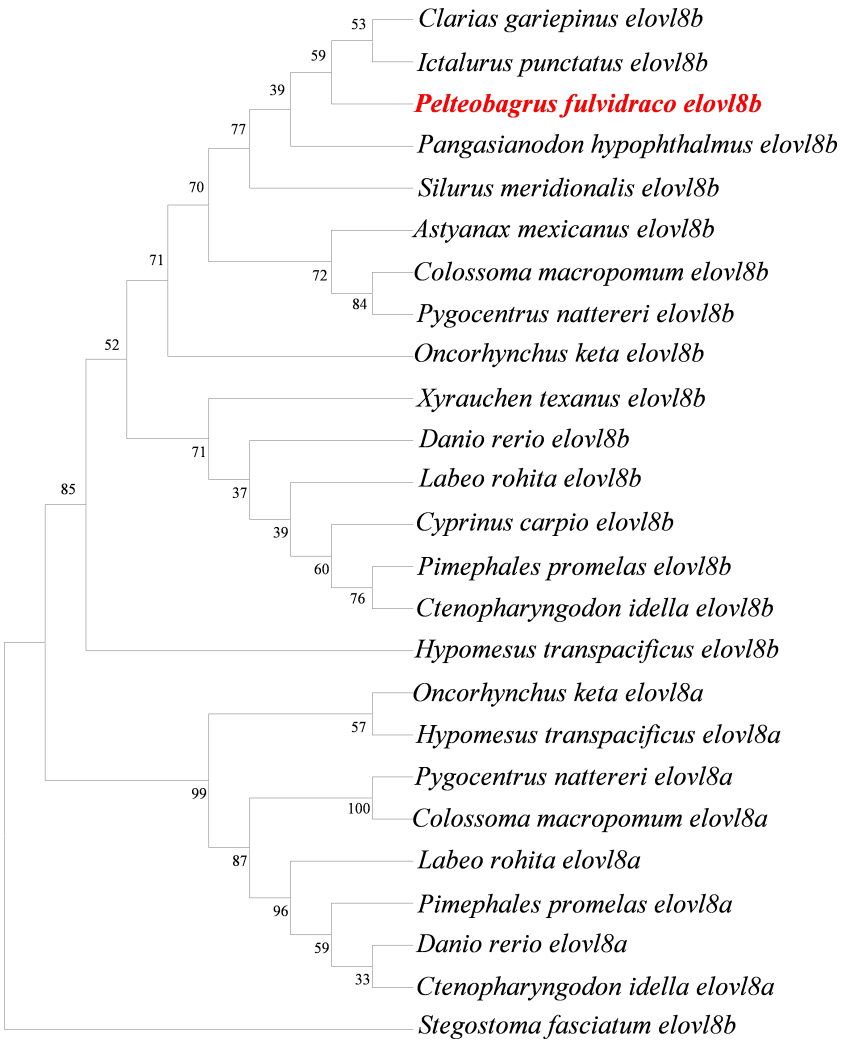

FIGURE 2
Phylogeny reveals the evolutionary history of the *elovl8* gene family in teleosts. Protein sequences were used to construct a phylogenetic tree with the NJ method using MEGA-X software. Numbers up the clades represent the bootstrap percentages from 1,000 replicates and the yellow catfish *elovl8* is labeled in red color. The leopard shark (*Stegostoma fasciatum*) was used as the outgroup.

Gene structure analysis

Gene structure comparison was conducted to reveal the structural and functional differentiation of the *elovl8b* gene in eight representative fish species. Results showed that the *elovl8b* gene of seven selected fish species, namely, *P. fulvidraco*, *A. mexicanus, C. gariepinus, C. idella, C. macropomum, L. rohita*, and *P. hypophthalmus*, had similar gene structures, containing eight exons and seven introns (Figure 4). Differently, the gene structure of *I. punctatus elovl8b* contained nine exons and eight introns, but showed a conserved coding sequence (CDS) region with the seven other fish *elovl8b* genes (Figure 4).

Tissue distribution pattern of *elovl8* in yellow catfish

The distribution pattern of *elovl8* in yellow catfish was determined by real-time quantitative PCR. Results showed that the *elovl8* gene of yellow catfish was widely expressed in most selected tissues including adipose, barbel, brain, gill, gonad, heart, intestine, kidney, liver, muscle, spleen, and stomach, and relative high expression levels were observed in intestine and liver tissues (Figure 5). Differently, no expression was detected in the eyes (Figure 5).

Expression pattern of the *elovl8* gene at early developmental stages in yellow catfish

Quantitative PCR was conducted to detect the expression level of the *elovl8* gene in the early developmental stages of yellow catfish. Results showed that the expression level was not significantly changed at 0, 3, 6, and 12 h, but dramatically decreased at 24, 36, 48, and 72 h, and reached the lowest expression level at 96 h after fertilization (Figure 6).

10.3389/fmars.2023.1270776

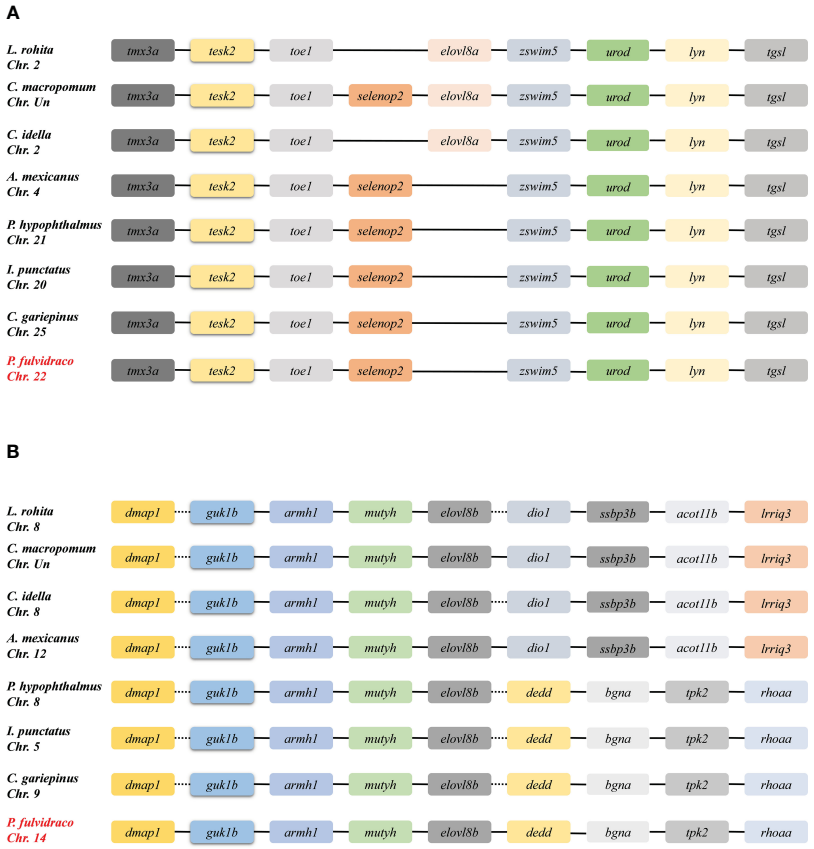

FIGURE 3
Genetic synteny of *elovl8a* **(A)** and *elovl8b* **(B)** in representative fish genomes. The colorful blocks represent different genes. The solid lines represent intergenic regions. The target species in the present study are marked in red front.

Effect of different diets on the expression of the *elovl8* gene in yellow catfish

Transcriptional change patterns of the yellow catfish *elovl8b* gene in response to larval stage diets with different HUFA content were determined (Figure 7). Results showed that the expression level of the *elovl8b* gene was slightly increased but not significantly changed at 1, 2, and 3 days after feeding with *A. nauplii* as in yellow catfish (Figure 7A). Differently, the expression level of the *elovl8b* gene was dramatically increased at 2 days and then significantly decreased at 3 days after feeding with egg yolk in yellow catfish (Figure 7B).

Discussion

Elovls are key rate-limiting enzymes to extend the carbon chain of polyunsaturated fatty acids by catalyzing condensation reaction, which play important roles involved in the biosynthesis of HUFAs in animals (Nugteren, 1965). Thus far, *elovl1–elovl7* are widely studied both in vertebrates and in invertebrates, but less is known about *elovl8*, the newly identified member of the *elovl* family (Ohno et al., 2010; Naganuma et al., 2011; Gregory and James, 2014; Yan et al., 2018). In this study, the *elovl8* gene of the yellow catfish was identified and characterized; it contained a 795- bp-long ORF that encodes a protein of 264 amino acids. Similar results were also

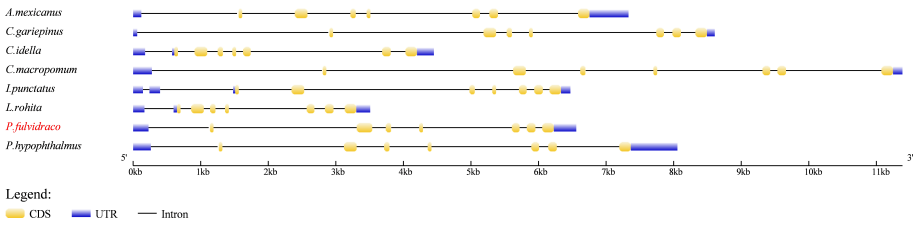

FIGURE 4
Comparison of the gene structure of *elovl8b* in eight representative teleosts. The colorful blocks and solid lines represent the exons and introns, respectively. UTR and CDS are marked with blue and yellow blocks, respectively.

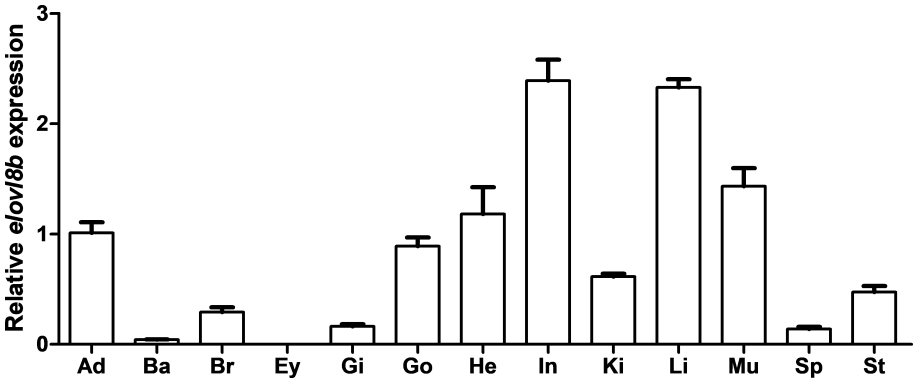

FIGURE 5
Tissue distribution of the *elovl8* gene in yellow catfish. Adipose (Ad); Barbel (Ba); Brain (Br); Eye (Ey); Gill (Gi); Gonad (Go); Heart (He); Intestine (In); Kidney (Ki); Liver (Li); Muscle (Mu); Spleen (Sp); Stomach (St). *β-actin* was selected as the internal reference gene. Data are expressed as mean ± standard error (n = 5).

observed in rabbitfish (*Siganus canaliculatus*) (Li et al., 2020) and hybrid grouper (*Epinephelus fuscoguttatus*♀ × *Epinephelus lanceolatus*♂) (Wu et al., 2022), suggesting that the *elovl8* genes are conserved among different fishes.

Multiple protein sequence comparison showed that yellow catfish Elovl8 possessed all the characteristics of ELOVL protein family members, including four conserved regions (KXXEXXDT, QXXFLHXYHH, NXXXHXXMYXYY, and TXXQXXQ), endoplasmic reticulum (ER)-resident signals, six transmembrane regions, and a histidine cluster (HXXHH) that is involved in fatty acid elongation processes (Jakobsson et al., 2006). The secondary characteristics are similar to that of Elovl8b in the rabbitfish (Li et al., 2020) and hybrid grouper (Wu et al., 2022), implying the evolutionary and functional conservation of the Elovl8b among various teleosts.

Phylogenetic analysis showed that the *elovl8* gene family was clustered into two branches of *elovl8a* and *elovl8b* subfamilies, which was consistent with the findings in previous studies, suggesting that teleost-specific elovl8 family may commonly contain two paralogs in teleost genomes, and this phenomenon may be caused by an additional teleost-specific genome duplication (TSGD) event (Kuraku and Meyer, 2009; Sun et al., 2021). Genetic synteny further supported teleost lineage, which usually contains *elovl8a* and *elovl8b* isoforms, such as fishes that belong to the orders Cyprinodontiformes, Salmoniformes, and Osmeriformes. However, it seemed that the *elovl8a* gene had been lost in Siluriformes teleosts, including *C. gariepinus*, *P. hypophthalmus*, *I. punctatus*, and *P. fulvidraco*, suggesting that *elovl8b* should be more conserved than *elovl8a*, and thus, the former but not the latter may play important roles in HUFA biosynthesis (Li et al., 2020). To our knowledge, the *elovl8a* gene lost in some teleost genomes may be caused by functional redundancy between *elovl8a* and *elovl8b* isoforms in the early period of evolution. In addition, the structure of the *elovl8b* gene commonly contained eight exons and seven introns in teleosts, suggesting that this gene was highly conserved and might play similar functions among various teleosts.

Tissue distribution experiments showed that *elovl8b* was widely expressed in various tissues with high expression levels in liver and intestine, which was different with rabbitfish and hybrid grouper (Li et al., 2020; Wu et al., 2022), indicating that the tissue distribution pattern of *elovl8b* is species-specific and it may play diverse roles in various teleosts. Indeed, this phenomenon may be caused by the different ability to synthesize HUFAs in different fishes (Gong et al., 2014). Notably, the *elovl8b* was highly expressed in liver in most

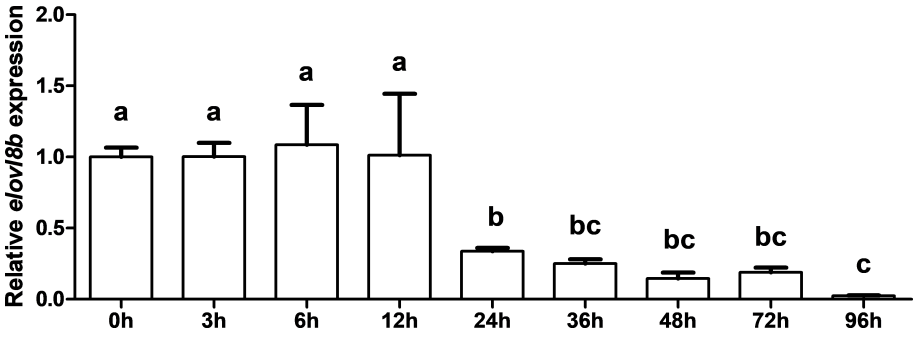

FIGURE 6
Gene expression pattern of the *elovl8b* gene in the early developmental stage of yellow catfish. *β-actin* was selected as the internal reference gene. Data are expressed as mean ± standard error (n = 5). Groups that differ significantly are indicated by different lowercase letters above bars.

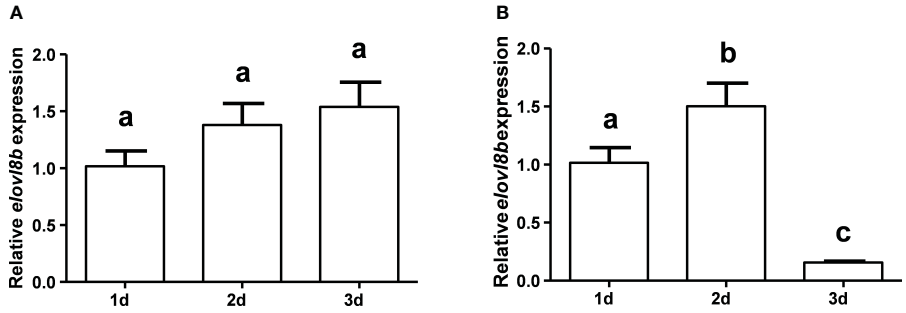

FIGURE 7
Effect of dietary *A nauplii* **(A)** and egg yolk **(B)** on *elovl8* gene expression in yellow catfish larvae. *β-actin* was selected as the internal reference gene. Data are expressed as mean ± standard error (n = 5). Groups that differ significantly are indicated by different lowercase letters above bars.

teleosts, suggesting that this gene may also play similar roles in HUFA biosynthesis because liver is the major organ that is involved in HUFA production.

The gene expression pattern of the *elovl8b* gene during the early development stage of yellow catfish was also determined, and results showed that *elovl8b* was stably expressed within 12 h after fertilization, which was slightly different with other HUFA biosynthesis-related genes in rabbitfish (You et al., 2017), suggesting that HUFA biosynthesis is very important for the early development of embryo despite the fact that the pattern may be different among various species. However, the expression level of yellow catfish *elovl8* was significantly decreased from 24 h to 96 h. It has been shown that during the early stage of embryonic development in yellow catfish, the PUFAs in yolk are involved in metabolism and catabolism to provide energy preparation for embryonic development, with C18:2n-6, C20:4n-3, and DHA dominating (Yao et al., 2009). Interestingly, the *elovl8b* gene was shown to have the ability to prolong C18 (18:2n-6, 18:3n-3, and 18:4n-3) and C20 (20:4n-6 and 20:5n-3) HUFAs to long-chain polyunsaturated fatty acids (LC-HUFAs) in rabbitfish (Li et al., 2020). This expression pattern suggests that yellow catfish *elovl8* is also involved in the synthesis of long-chain polyunsaturated fatty acids and plays an important role in early embryonic development.

Previous studies have shown that diets full of HUFAs could inhibit the transcriptional expression in rabbitfish and hybrid grouper (Li et al., 2020; Wu et al., 2022). In the present study, functional experiments showed that the transcription of *elovl8* was not significantly affected by feeding with *A. salina*, whereas it was inhibited after feeding with egg yolk in yellow catfish. It is shown that the lack of HUFAs in *A. salina* might explain why dietary *A. salina* slightly increased *elovl8* gene expression (Tocher et al., 2003; Garcia et al., 2008). Meanwhile, dietary egg yolk induced but then inhibited *elovl8* expression, which may be caused by the high content of phospholipid in egg yolk. Our findings further supported the idea that a compensatory mechanism also existed in yellow catfish, which was similar to previous reports and could demonstrate a key role for *elovl8b* in LC-PUFA biosynthesis (Cho et al., 1999; Seiliez et al., 2001).

In summary, an *elovl8* gene was identified and characterized from yellow catfish for the first time. Multiple protein sequence alignment, genetic synteny, gene structure comparisons, and phylogeny revealed that *elovl8a* had been lost in Siluriformes, and *elovl8b* was highly conserved among various teleosts. Moreover, spatiotemporal expression analyses suggested that *elovl8* was widely distributed, and it could play important roles in the early development stage in yellow catfish. Finally, functional experiments showed that a diet full of HUFAs may inhibit the transcription of *elovl8* in yellow catfish. Our findings will help us to better understand the evolutionary and functional characteristics of *elovl8* in teleosts, and lay a solid basis for investigating the regulation mechanism of HUFA biosynthesis.

Data availability statement

The datasets presented in this study can be found in online repositories. The names of the repository/repositories and accession number(s) can be found in the article/Supplementary Material.

Ethics statement

The animal study was approved by Neijiang Normal University Animal Care and Use Committee. The study was conducted in accordance with the local legislation and institutional requirements.

Author contributions

W-HZ: Formal Analysis, Investigation, Writing – original draft. X-YW: Writing – original draft, Formal Analysis, Investigation, Software. WQ: Writing – original draft, Investigation. C-JQ: Writing – review & editing. QS: Writing – review & editing. SG: Writing – review & editing, Formal Analysis, Software. PP: Software, Writing – review & editing. SZ: Writing – review & editing, Funding acquisition, Investigation. PF: Writing – review & editing, Formal Analysis, Investigation. WH: Methodology, Supervision, Writing – review & editing. H-WY: Supervision, Writing – review & editing. Z-YW: Funding acquisition, Methodology, Project administration, Supervision, Writing – review & editing.

Funding

This work was financially supported by the Research Fund from Key Laboratory of Sichuan Province for Fishes Conservation and Utilization in the Upper Reaches of the Yangtze River (No. NJTCSC23-3), the Natural Science Fund of Sichuan Province of China (No. 2023NSFSC1221), the Project of Sichuan Provincial Department of Science and Technology (No. 2021YFYZ0015), the Cooperation Fund from Sichuan University (No. 2022H013), and the Important New Varieties Selection Project of Jiangsu Province (No. PZCZ201742).

Conflict of interest

The authors declare that the research was conducted in the absence of any commercial or financial relationships that could be construed as a potential conflict of interest.

Publisher's note

Supplementary material

The Supplementary Material for this article can be found online at: https://www.frontiersin.org/articles/10.3389/fmars.2023.1270776/full#supplementary-material

References

Agbaga, M. P., Brush, R. S., Mandal, M. N., Henry, K., Elliott, M. H., and Anderson, R. E. (2008). Role of Stargardt-3 macular dystrophy protein (ELOVL4) in the biosynthesis of very long chain fatty acids. *Proc. Natl. Acad. Sci. U.S.A.* 105, 12843–12848. doi: 10.1073/pnas.0802607105

Cho, H. P., Nakamura, M., and Clarke, S. D. (1999). Cloning, expression, and fatty acid regulation of the human delta-5 desaturase. *J. Biol. Chem.* 274, 37335–37339. doi: 10.1074/jbc.274.52.37335

Da, F., Wen, Z., Wang, X.-D., and Luo, Y. (2022). Molecular identification, tissue distribution, and effects of fasting and refeeding on the transcription of uncoupling protein 2 in yellow catfish, *Pelteobagrus vachelli*. *Pak J. Zool.* 54, 1539–1547. doi: 10.17582/journal.pjz/20200316080346

De Giuseppe, R., Roggi, C., and Cena, H. (2014). n-3 LC-PUFA supplementation: effects on infant and maternal outcomes. *Eur. J. Nutr.* 53, 1147–1154. doi: 10.1007/s00394-014-0660-9

Du, Z. Y., Clouet, P., Zheng, W. H., Degrace, P., Tian, L. X., and Liu, Y. J. (2006). Biochemical hepatic alterations and body lipid composition in the herbivorous grass carp (*Ctenopharyngodon idella*) fed high-fat diets. *Br. J. Nutr.* 95, 905–915. doi: 10.1079/bjn20061733

Ganga, R., Bell, J. G., Montero, D., Robaina, L., Caballero, M. J., and Izquierdo, M. S. (2005). Effect of dietary lipids on plasma fatty acid profiles and prostaglandin and leptin production in gilthead seabream (*Sparus aurata*). *Comp. Biochem. Physiol. B Biochem. Mol. Biol.* 142, 410–418. doi: 10.1016/j.cbpb.2005.09.010

Garcia, A. S., Parrish, C. C., and Brown, J. A. (2008). Growth and lipid composition of Atlantic cod (*Gadus morhua*) larvae in response to differently enriched *Artemia franciscana*. *Fish. Physiol. Biochem.* 34, 77–94. doi: 10.1007/s10695-007-9149-2

Gong, Y., Wan, X., Jiang, M., Hu, C., Hu, H., and Huang, F. (2014). Metabolic engineering of microorganisms to produce omega-3 very long-chain polyunsaturated fatty acids. *Prog. Lipid Res.* 56, 19–35. doi: 10.1016/j.plipres.2014.07.001

Gregory, M. K., and James, M. J. (2014). Rainbow trout (*Oncorhynchus mykiss*) Elov15 and Elov12 differ in selectivity for elongation of omega-3 docosapentaenoic acid. *Biochim. Biophys. Acta* 1841, 1656–1660. doi: 10.1016/j.bbalip.2014.10.001

Guillou, H., Zadravec, D., Martin, P. G., and Jacobsson, A. (2010). The key roles of elongases and desaturases in mammalian fatty acid metabolism: Insights from transgenic mice. *Prog. Lipid Res.* 49, 186–199. doi: 10.1016/j.plipres.2009.12.002

Guo, S., Zeng, M., Gao, W., Li, F., Wei, X., Shi, Q., et al. (2023). Toll-like receptor 3 in the hybrid yellow catfish (*Pelteobagrus fulvidraco* ♀ × *P. vachelli* ♂): Protein structure, evolution and immune response to exogenous *Aeromonas hydrophila* and Poly (I:C) stimuli. *Animals* 13 (2), 288. doi: 10.3390/ani13020288

Ishak, S. D., Tan, S. H., Khong, H. K., Jaya-Ram, A., Enyu, Y. L., Kuah, M. K., et al. (2008). Upregulated mRNA expression of desaturase and elongase, two enzymes involved in highly unsaturated fatty acids biosynthesis pathways during follicle maturation in zebrafish. *Reprod. Biol. Endocrinol.* 6, 56. doi: 10.1186/1477-7827-6-56

Jakobsson, A., Westerberg, R., and Jacobsson, A. (2006). Fatty acid elongases in mammals: their regulation and roles in metabolism. *Prog. Lipid Res.* 45, 237–249. doi: 10.1016/j.plipres.2006.01.004

Jaya-Ram, A., Ishak, S. D., Enyu, Y. L., Kuah, M. K., Wong, K. L., and Shu-Chien, A. C. (2011). Molecular cloning and ontogenic mRNA expression of fatty acid desaturase in the carnivorous striped snakehead fish (*Channa striata*). *Comp. Biochem. Physiol. A Mol. Integr. Physiol.* 158, 415–422. doi: 10.1016/j.cbpa.2010.11.018

Kuraku, S., and Meyer, A. (2009). The evolution and maintenance of Hox gene clusters in vertebrates and the teleost-specific genome duplication. *Int. J. Dev. Biol.* 53 (5-6), 765–773. doi: 10.1387/ijdb.072533km

Li, Y., Monroig, O., Zhang, L., Wang, S., Zheng, X., Dick, J. R., et al. (2010). Vertebrate fatty acyl desaturase with Δ4 activity. *Proc. Natl. Acad. Sci. U.S.A.* 107, 16840–16845. doi: 10.1073/pnas.1008429107

Li, Y., Wen, Z., You, C., Xie, Z., Tocher, D. R., Zhang, Y., et al. (2020). Genome wide identification and functional characterization of two LC-PUFA biosynthesis elongase (*elovl8*) genes in rabbitfish (*Siganus canaliculatus*). *Aquaculture* 522, 735127. doi: 10.1016/j.aquaculture.2020.735127

Li, S., Yuan, Y., Wang, T., Xu, W., Li, M., Mai, K., et al. (2016). Molecular cloning, functional characterization and nutritional regulation of the putative elongase *elovl5* in the orange-spotted grouper (*Epinephelus coioides*). *PloS One* 11, e0150544. doi: 10.1371/journal.pone.0150544

Naganuma, T., Sato, Y., Sassa, T., Ohno, Y., and Kihara, A. (2011). Biochemical characterization of the very long-chain fatty acid elongase ELOVL7. *FEBS Lett.* 585, 3337–3341. doi: 10.1016/j.febslet.2011.09.024

Nakamura, M. T., and Nara, T. Y. (2004). Structure, function, and dietary regulation of delta6, delta5, and delta9 desaturases. *Annu. Rev. Nutr.* 24, 345–376. doi: 10.1146/annurev.nutr.24.121803.063211

Nugteren, D. H. (1965). The enzymic chain elongation of fatty acids by rat-liver microsomes. *Biochim. Biophys. Acta* 106, 280–290. doi: 10.1016/0005-2760(65)90036-6

Oboh, A., Navarro, J. C., Tocher, D. R., and Monroig, O. (2017). Elongation of very Long-Chain (>C(24)) Fatty Acids in *Clarias gariepinus*: Cloning, Functional Characterization and Tissue Expression of elovl4 Elongases. *Lipids* 52, 837–848. doi: 10.1007/s11745-017-4289-3

Ohno, Y., Suto, S., Yamanaka, M., Mizutani, Y., Mitsutake, S., Igarashi, Y., et al. (2010). ELOVL1 production of C24 acyl-CoAs is linked to C24 sphingolipid synthesis. *Proc. Natl. Acad. Sci. U.S.A.* 107, 18439–18444. doi: 10.1073/pnas.1005572107

Qin, C.-J., Wen, Z.-Y., Yuan, D.-Y., Shao, T., and Gong, Q. (2017). Molecular cloning and expression of fatty acid desaturase and elongase genes in darkbarbel (*Pelteobagrus vachellii*). *J. Oceanol. Limnol.* 48, 884–893.

Ri, K., Lee-Okada, H. C., and Yokomizo, T. (2022). Omega-6 highly unsaturated fatty acids in Leydig cells facilitate male sex hormone production. *Commun. Biol.* 5, 1001. doi: 10.1038/s42003-022-03972-y

Seiliez, I., Panserat, S., Kaushik, S., and Bergot, P. (2001). Cloning, tissue distribution and nutritional regulation of a Delta6-desaturase-like enzyme in rainbow trout. *Comp. Biochem. Physiol. B Biochem. Mol. Biol.* 130, 83–93. doi: 10.1016/s1096-4959(01)00410-9

Song, Y. F., Luo, Z., Pan, Y. X., Zhang, L. H., Chen, Q. L., and Zheng, J. L. (2015). Three unsaturated fatty acid biosynthesis-related genes in yellow catfish *Pelteobagrus fulvidraco*: Molecular characterization, tissue expression and transcriptional regulation by leptin. *Gene* 563 (1), 1–9. doi: 10.1016/j.gene.2014.12.014

Sun, S., Wang, Y., Goh, P. T., Lopes-Marques, M., Castro, L. F. C., Monroig, Ó., et al. (2021). Evolution and functional characteristics of the novel *elovl8* that play pivotal roles in fatty acid biosynthesis. *Genes* 12 (8), 271. doi: 10.3390/genes12081287

Tocher, D. R., Bell, J. G., Dick, J. R., and Crampton, V. O. (2003). Effects of dietary vegetable oil on Atlantic salmon hepatocyte fatty acid desaturation and liver fatty acid compositions. *Lipids* 38 (7), 723–732. doi: 10.1007/s11745-003-1120-y

Wei, X. Y., Wang, J., Guo, S. T., Lv, Y. Y., Li, Y. P., Qin, C. J., et al. (2023). Molecular characterization of a teleost-specific toll-like receptor 22 (tlr22) gene from yellow catfish (*Pelteobagrus fulvidraco*) and its transcriptional change in response to poly I:C and *Aeromonas hydrophila* stimuli. *Fish. Shellfish Immunol.* 134, 108579. doi: 10.1016/j.fsi.2023.108579

Wen, Z. Y., Liu, T., Qin, C. J., Zou, Y. C., Wang, J., Li, R., et al. (2021). MRAP2 interaction with melanocortin-4 receptor in snakehead (*Channa argus*). *Biomolecules* 11 (3), 481. doi: 10.3390/biom11030481

Wen, Z. Y., Qin, C. J., Wang, J., He, Y., Li, H. T., Li, R., et al. (2020). Molecular characterization of two leptin genes and their transcriptional changes in response to fasting and refeeding in Northern snakehead (*Channa argus*). *Gene* 736, 144420. doi: 10.1016/j.gene.2020.144420

Wen, Z. Y., Wang, J., Bian, C., Zhang, X., Li, J., Peng, Y., et al. (2019). Molecular cloning of two kcnk3 genes from the Northern snakehead (*Channa argus*) for quantification of their transcriptions in response to fasting and refeeding. *Gen. Comp. Endocrinol.* 281, 49–57. doi: 10.1016/j.ygcen.2019.05.016

Wu, Q., Zheng, Z., Wang, C., Wang, Y., Sun, Y., and Gao, Y. (2022). Molecular characterization, tissue distribution and differential nutritional regulation of three n-3 LC-PUFA biosynthesis-related genes in hybrid grouper (*Epinephelus fuscoguttatus* ♀ × *Epinephelus lanceolatus* ♂). *Animals* 12 (3), 234. doi: 10.3390/ani12030234

Yan, J., Liang, X., Cui, Y., Cao, X., and Gao, J. (2018). Elovl4 can effectively elongate C18 polyunsaturated fatty acids in loach Misgurnus anguillicaudatus. *Biochem. Biophys. Res. Commun.* 495, 2637–2642. doi: 10.1016/j.bbrc.2017.12.123

Yang, S., Wen, Z. Y., Zou, Y. C., Qin, C. J., Wang, J., Yuan, D. Y., et al. (2018). Molecular cloning, tissue distribution, and effect of fasting and refeeding on the expression of neuropeptide Y in *Channa argus*. *Gen. Comp. Endocrinol.* 259, 147–153. doi: 10.1016/j.ygcen.2017.11.017

Yao, J., Zhao, H. Y., Li, C., He, D., and Hu, C. (2009). Changes in Fatty Acid Composition During Early Embryonic Development of Yellow Catfish *Pelteobagrus f iulvidraco*. *Fish. Sci.* 28, 644–647.

You, C., Miao, S., Lin, S., Wang, S., Waiho, K., and Li, Y. (2017). Expression of long-chain polyunsaturated fatty acids (LC-PUFA) biosynthesis genes and utilization of fatty acids during early development in rabbitfish *Siganus canaliculatus*. *Aquaculture* 479, 774–779. doi: 10.1016/j.aquaculture.2017.07.028

Zárate, R., El Jaber-Vazdekis, N., Tejera, N., Pérez, J. A., and Rodríguez, C. (2017). Significance of long chain polyunsaturated fatty acids in human health. *Clin. Transl. Med.* 6, 25. doi: 10.1186/s40169-017-0153-6

Zhang, T. T., Xu, J., Wang, Y. M., and Xue, C. H. (2019). Health benefits of dietary marine DHA/EPA-enriched glycerophospholipids. *Prog. Lipid Res.* 75, 100997. doi: 10.1016/j.plipres.2019.100997

frontiers | Frontiers in Physiology

TYPE Original Research
PUBLISHED 04 October 2023
DOI 10.3389/fphys.2023.1272267

OPEN ACCESS

EDITED BY
Yiming Li,
Fishery Machinery and Instrument Research Institute, China

REVIEWED BY
Ivan Viegas,
University of Coimbra, Portugal
Jesús M. Míguez,
University of Vigo, Spain

*CORRESPONDENCE
Jaume Pérez-Sánchez,
jaime.perez.sanchez@csic.es

RECEIVED 03 August 2023
ACCEPTED 18 September 2023
PUBLISHED 04 October 2023

CITATION
Holhorea PG, Naya-Català F, Belenguer Á, Calduch-Giner JA and Pérez-Sánchez J (2023), Understanding how high stocking densities and concurrent limited oxygen availability drive social cohesion and adaptive features in regulatory growth, antioxidant defense and lipid metabolism in farmed gilthead sea bream (*Sparus aurata*). *Front. Physiol.* 14:1272267. doi: 10.3389/fphys.2023.1272267

Understanding how high stocking densities and concurrent limited oxygen availability drive social cohesion and adaptive features in regulatory growth, antioxidant defense and lipid metabolism in farmed gilthead sea bream (*Sparus aurata*)

Paul G. Holhorea, Fernando Naya-Català, Álvaro Belenguer, Josep A. Calduch-Giner and Jaume Pérez-Sánchez*

Nutrigenomics and Fish Growth Endocrinology Group, Institute of Aquaculture Torre de la Sal (IATS, Spanish National Research Council (CSIC)), Castellón, Spain

The study combined the use of biometric, behavioral, physiological and external tissue damage scoring systems to better understand how high stocking densities drive schooling behavior and other adaptive features during the finishing growing phase of farmed gilthead sea bream in the Western Mediterranean. Fish were grown at three different final stocking densities (LD, 8.5 kg/m^3; MD, 17 kg/m^3; HD, 25 kg/m^3). Water oxygen concentration varied between 5 and 6 ppm in LD fish to 3–4 ppm in HD fish with the summer rise of water temperature from 19°C to 26°C (May–July). HD fish showed a reduction of feed intake and growth rates, but they also showed a reinforced social cohesion with a well-defined endogenous swimming activity rhythm with feeding time as a main synchronization factor. The monitored decrease of the breathing/swimming activity ratio by means of the AEFishBIT data-logger also indicated a decreased energy partitioning for growth in the HD environment with a limited oxygen availability. Plasma glucose and cortisol levels increased with the rise of stocking density, and the close association of glycaemia with the expression level of antioxidant enzymes (*mn-sod, gpx4, prdx5*) in liver and molecular chaperones (*grp170, grp75*) in skeletal muscle highlighted the involvement of glucose in redox processes via rerouting in the pentose-phosphate-pathway. Other adaptive features included the depletion of oxidative metabolism that favored lipid storage rather than fatty acid oxidation to decrease the oxygen demand as last electron acceptor in the mitochondrial respiratory chain. This was coincident with the metabolic readjustment of the Gh/Igf endocrine-growth cascade that promoted the regulation of muscle growth at the local level rather than a systemic action via the liver Gh/Igf axis. Moreover, correlation analyses within HD fish displayed negative correlations of hepatic transcripts of *igf1* and *igf2* with the data-logger measurements of activity and respiration, whereas the opposite was found for muscle *igf2, ghr1* and *ghr2*. This was indicative of a growth-regulatory transition that supported a proactive instead of a reactive behavior in HD fish, which was considered adaptive to preserve an

active and synchronized feeding behavior with a minimized risk of oxidative stress and epidermal skin damage.

KEYWORDS

gilthead sea bream, stocking density, oxygen availability, welfare indicators, antioxidant defense, lipid metabolism, energy sensing, growth regulation

1 Introduction

Global aquaculture production of aquatic animals increased at an average rate of 2.2% from 1990 to 2020 until reaching a milestone of 88 million tonnes per year (FAO, 2022). This increase of animal aquaculture production mostly supported the augmented human *per capita* consumption of fish from 14 kg (live weigh equivalent) in 1990 to 20.2 kg in 2020. However, the intensification of aquaculture production must deal with inadequate stocking densities that may increase the risk of health issues and welfare impairments due to feed competition and aggressive interactions among other stressful events (Ellis et al., 2002; North et al., 2006; Baldwin, 2011; Jia et al., 2016; Liu et al., 2017; Wu et al., 2018). The legislation limiting stocking density can contribute to support the expansion of a more sustainable and ethical aquaculture production, but a more rational approach might be to define acceptable levels of different welfare indicators for each particular species, life-stage and production system (van de Vis et al., 2020; Saraiva et al., 2022). Certainly, important research efforts have been made over the last decade for finding the golden stocking density of farmed fish, combining criteria of economic profitability with the increasing pressure of consumers in developed countries for an enhanced control and regulation in welfare assurance schemes (Noble et al., 2018). In land-based systems, negative effects on feed utilization and physiological stress markers were found in Atlantic salmon (*Salmo salar*) at stocking densities above 75 kg/m^3, but densities above 25 kg/m^3 reduced feed intake and growth of adult fish kept in sea cages (Calabrese et al., 2017). Signs of external tissue lesions, and impaired growth and feed utilization also occurred above 20–30 kg/m^3 in gilthead sea bream (*Sparus aurata*) and European sea bass (*Dicentrarchus labrax*) (Person-Le Ruyet and Le Bayon, 2009; Carbonara et al., 2019). However, the occurrence of different stress coping styles plays a key role on how rearing density influences welfare-related responses, being generally accepted that fish that respond in a shy and subordinate manner (reactive fish) are more able to cope with higher densities, while individuals that are bold and aggressive (proactive fish) are more able to cope with low densities (Carbonara et al., 2019). In addition, reduced oxygen (O_2) availability exacerbates the negative impact of high stocking density on feed intake and growth in gilthead sea bream, triggering different adaptive responses mediated by changes in the gene expression profile of tissue-specific markers of antioxidant defense, oxidative phosphorylation, protein accretion (muscle growth), and lipid metabolism (Martos-Sitcha et al., 2019a).

In gilthead sea bream, there is also now evidence that groups of proactive and reactive individuals did not exhibit consistent escape behavior responses when fish were subjected to restraining tests, which might be indicative that the social context in which fish are kept has an impact on the manifestation of certain personality traits of individuals (Castanheira et al., 2016). Indeed, animal welfare applies to its positive physical and mental condition (Ashley, 2007), and there is now evidence that both swimming activity and schooling behavior are reinforced by high stocking densities in gilthead sea bream (Carbonara et al., 2019; Arechavala-Lopez et al., 2020). Of note, both behavior and swimming performance are also regulated genetically in this species (Perera et al., 2021; Calduch-Giner et al., 2023). At the same time, swimming performance can be improved by a mild-hypoxia pre-conditioning, which leads to a persistent higher critical speed at exercise exhaustion that shifts towards a higher anaerobic fitness following normoxia restoration (Naya-Català et al., 2021). It must be also taken into account that aquaculture finishing production cycle is often accounted during the summer period with relatively high stocking densities and reduced O_2 availability, and there is still a lack of practical procedures for assessing changes in behavior, physiological traits and welfare indicators in order to fulfill growth performance and welfare status with intensive aquaculture production. Thus, the present study aims to contribute to solve this gap of knowledge, combining the use of AEFishBIT data-loggers for accurate monitoring of swimming activity and breathing rates (Calduch-Giner et al., 2022) with customized PCR-arrays for the simultaneous gene expression profiling of stress-responsive genes (Calduch-Giner et al., 2010; Magnoni et al., 2017; Martos-Sitcha et al., 2019a; Naya-Català et al., 2021), and welfare scores of muscle fat content, blood biochemistry, and external tissue damage (Sánchez-Muros et al., 2013; Seibel et al., 2021; Weirup et al., 2022). The hypothesis of work is that such integrative approach can contribute to better determine the golden stocking density in a given farming condition, encompassing animal welfare and industry interests, with the double aim of mitigating drawback effects but also recognizing the importance of indicators of positive welfare of both physical health and appropriate social interactions (Ashley, 2007; Toni et al., 2019).

2 Materials and methods

2.1 Ethics

All procedures were approved by the Ethics and Animal Welfare Committee of the Institute of Aquaculture Torre de la Sal (IATS), CSIC Ethics Comittee (permission 1295/2022) and Generalitat Valenciana (permission 2022-VSC-PEA-0230). They were carried out in the IATS's registered aquaculture infrastructure facility (code ES120330001055) in accordance with the principles published in the European Animal Directive (2010/63/EU) and Spanish laws (Royal Decree RD53/2013) for the protection of animals used in scientific experiments.

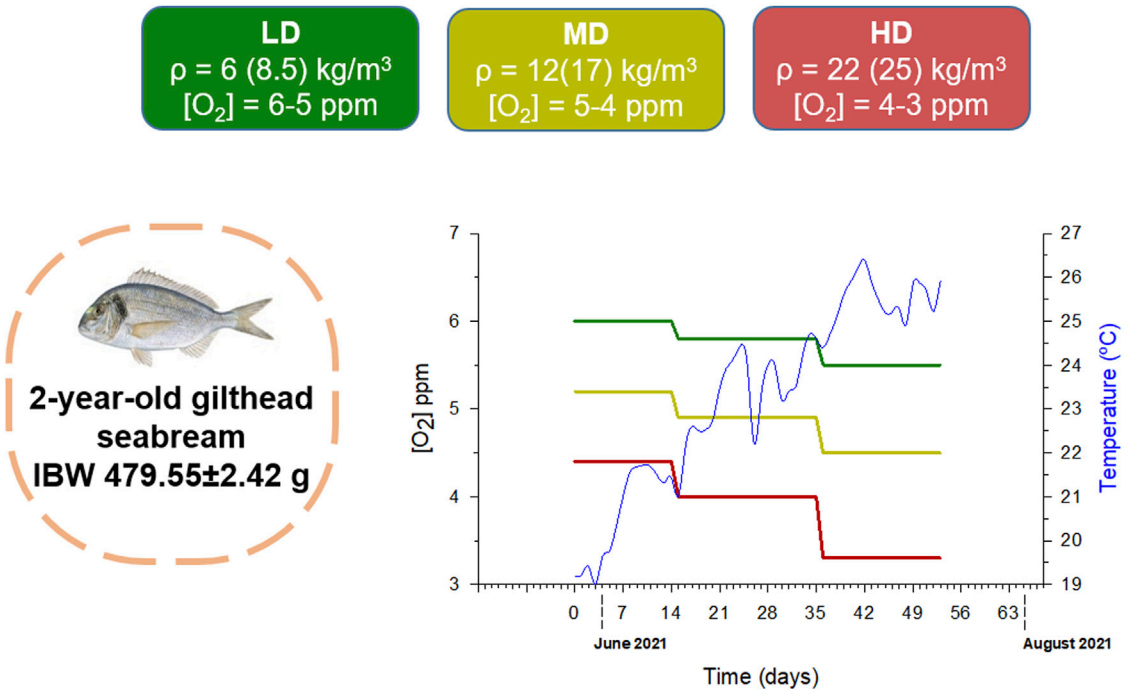

FIGURE 1
Experimental design of gilthead sea bream reared at three different stocking densities (LD—low density, MD—medium density, HD—high density) and dissolved oxygen concentrations during the summer period. Initial stocking density, ρ, and final density (in parenthesis) is shown. Temporal variation (over 53 days experimental period) in dissolved oxygen concentration for each group and temperature are represented. IBW—Initial body weight; FBW—Final body weight.

2.2 Experimental setup

Two year-old gilthead sea bream of Mediterranean origin (Avramar, Burriana, Spain) were grown in 3,000L tanks from January to May (12–16 kg/m^3) in a flow-through system under the natural photoperiod and temperature conditions at the IATS latitude (40° 5′N; 0° 10′E). At the end of May (Figure 1), 462 fish (initial body weight 479.55 ± 2.42 g) were anesthetized with 0.1 g/L MS-222 (Sigma, Saint Louis, MO, United States) and pit-tagged in the dorsal musculature with passive integrated transponders (ID-100A 1.25 Nano Transponder; Trovan, Madrid, Spain). Fish were then re-allocated in experimental tanks (two replicates per condition) at three different stocking densities (low density-LD: 36 fish per tank, 6 kg/m^3; medium density-MD: 72 fish per tank, 12 kg/m^3; high density-HD: 123 fish per tank, 22 kg/m^3), until reaching final stocking densities of 8.5 kg/m^3 (LD), 17 kg/m^3 (MD) and 25 kg/m^3 (HD) after 53 days (mid-July). Body weight and furcal length were recorded at the beginning and at the end of trial, using a FR-200 FishReader W (Trovan, Madrid, Spain). Over the experimental period (May–July, 53 days), fish were fed once daily at a fixed time (12:00 a.m.) with automated feeders near to visual satiety with a standard commercial diet (EFICO 3053, BioMar, Palencia, Spain). Water aeration and flux of inlet water was daily regulated to maintain differentially controlled the water O_2 concentration (LD, 5–6 ppm, 70%–95% saturation; MD, 4–5 ppm, 55%–75% saturation; HD, 3–4 ppm, 45%–60% saturation). Temperature and water O_2 concentration was continuously measured through an online environmental monitoring system. Weekly determinations of unionized ammonia were always below the toxic threshold level (<0.05 mg/L).

2.3 Behavioral monitoring: physical activity and respiratory frequency

At the end of trial, 12 randomly selected fish per experimental condition (n = 6 per replicate tank) were anesthetized with 0.1 g/L MS-222, AEFishBIT devices were externally attached to the operculum for the simultaneous monitoring of physical activity and respiratory frequency, and returned to their original tanks. AEFishBIT is a stand-alone, small, and lightweight motion embedded-microsystem with a tri-axial accelerometer that, by means of attachment to the operculum, monitors physical activity by mapping of the accelerations in X- and Y-axes, while the operculum beats (Z-axis) serve as a measure of respiratory frequency (Calduch-Giner et al., 2022). The devices were programmed for data acquisition of physical activity and respiratory frequency during 2 min every 15 min along two consecutive days, in which fish remained unfed. The sampling frequency of the AEFishBIT device was 100 Hz, and the software pre-processing of raw data was made as described elsewhere (Martos-Sitcha et al., 2019b; Ferrer et al., 2020). At the end of the recording period (48 h post-tagging), all AEFishBIT devices were successfully recovered and pre-processed data were downloaded for tracking the recorded behavioral traits.

10.3389/fphys.2023.1272267

TABLE 1 PCR-array layout for liver (*) and white skeletal muscle (†) gene expression profiling.

Function	Gene	Symbol	GenBank
Gh/Igf SYSTEM	Growth hormone receptor-type 1	*ghr1**†	AF438176
	Growth hormone receptor-type 2	*ghr2**†	AY573601
	Insulin-like growth factor 1	*igf1**†	AY996779
	Insulin-like growth factor 2	*igf2**†	AY996778
	Insulin-like growth factor binding protein 1a	*igfbp1a**	KM522771
	Insulin-like growth factor binding protein 1b	*igfbp1b**	MH577189
	Insulin-like growth factor binding protein 2a	*igfbp2a**	MH577190
	Insulin-like growth factor binding protein 2b	*igfbp2b**	AF377998
	Insulin-like growth factor binding protein 3a	*igfbp3a*†	MH577191
	Insulin-like growth factor binding protein 3b	*igfbp3b*†	MH577192
	Insulin-like growth factor binding protein 4	*igfbp4**	KM658998
	Insulin-like growth factor binding protein 5a	*igfbp5a*†	MH577193
	Insulin-like growth factor binding protein 5b	*igfbp5b*†	MH577194
	Insulin-like growth factor binding protein 6a	*igfbp6a*†	MH577195
	Insulin-like growth factor binding protein 6b	*igfbp6b*†	MH577196
LIPID METABOLISM	Elongation of very long chain fatty acids 1	*elovl1**	JX975700
	Elongation of very long chain fatty acids 4	*elovl4**	JX975701
	Elongation of very long chain fatty acids 5	*elovl5**	AY660879
	Elongation of very long chain fatty acids 6	*elovl6**	JX975702
	Fatty acid desaturase 2	*fads2**	AY055749
	Stearoyl-CoA desaturase 1a	*scd1a**	JQ277703
	Stearoyl-CoA desaturase 1b	*scd1b**	JQ277704
	Hepatic lipase	*hl**	EU254479
	Lipoprotein lipase	*lpl**	AY495672
	Adipose triglyceride lipase	*atgl**	JX975711
	85 kDa calcium-independent phospholipase A2	*pla2g6**	JX975708
	Cholesterol 7-alpha-monooxygenase	*cyp7a1**	KX122017
	Peroxisome proliferator-activated receptor α	*pparα**	AY590299
	Peroxisome proliferator-activated receptor γ	*pparγ**	AY590304
MUSCLE CELL GROWTH	Myoblast determination protein 1	*myod1*†	AF478568
	Myogenic determination protein 2	*myod2*†	AF478569
	Myogenic factor 5	*myf5*†	JN034420
	Myogenic factor 6	*myf6/herculin*†	JN034421
	Myostatin/Growth differentiation factor 8	*mstn/gdf8*†	AF258448
	Myocyte-specific enhancer factor 2a	*mef2a*†	KM522777
	Myocyte-specific enhancer factor 2c	*mef2c*†	KM522778
	Follistatin	*fst*†	AY544167

(Continued on following page)

TABLE 1 (*Continued*) PCR-array layout for liver (*) and white skeletal muscle (†) gene expression profiling.

Function	Gene	Symbol	GenBank
IMMUNE RESPONSE	Interleukin 1β	*il1β*†	AJ419178
	Interleukin 6	*il6*†	EU244588
	Interleukin 8	*il8*†	JX976619
	Interleukin 10	*il10*†	JX976621
	Interleukin 12 subunit β	*il12β*†	JX976624
OXIDATIVE METABOLISM & ENERGY SENSING	Hypoxia inducible factor 1α	*hif1α**†	JQ308830
	Proliferator-activated receptor γ coactivator 1α	*pgc1α**†	JX975264
	Proliferator-activated receptor γ coactivator 1β	*pgc1β*†	JX975265
	Carnitine palmitoyltransferase 1a	*cpt1a**†	JQ308822
	Fatty acid binding protein, heart	*hfabp**	JQ308834
	Citrate synthase	*cs**†	JX975229
	NADH-ubiquinone oxidoreductase chain 2	*nd2**†	KC217558
	NADH-ubiquinone oxidoreductase chain 5	*nd5**†	KC217559
	Cytochrome c oxidase subunit 1	*cox1**†	KC217652
	Cytochrome c oxidase subunit 2	*cox2**†	KC217653
	Uncoupling protein 1	*ucp1**	FJ710211
	Uncoupling protein 3	*ucp3*†	EU555336
	Sirtuin1	*sirt1**†	KF018666
	Sirtuin2	*sirt2**†	KF018667
ANTIOXIDANT DEFENSE	Catalase	*cat*†	JQ308823
	Glutathione peroxidase 1	*gpx1**	DQ524992
	Glutathione peroxidase 4	*gpx4**†	AM977818
	Glutathione reductase	*gr*†	AJ937873
	Peroxiredoxin 3	*prdx3**†	GQ252681
	Peroxiredoxin 5	*prdx5**†	GQ252683
	Superoxide dismutase [Cu-Zn]	*cu-zn-sod/sod1**	JQ308832
	Superoxide dismutase [Mn]	*mn-sod/sod2**†	JQ308833
	Glucose-regulated protein 170 kDa	*grp170**†	JQ308821
	Glucose-regulated protein 94 kDa	*grp94**†	JQ308820
	Glucose-regulated protein 75 kDa	*grp75**†	DQ524993

2.4 Fish sampling for physiological and external tissue damage indicators

After AEFishBIT retrieval, muscle fat content was determined *in situ* with Distell Fish Fat-meter, FM 692 (Distell Ltd., United Kingdom). Fish were then photographed for the evaluation of indicators of external damage (cataracts, exophthalmia, gill status, fin damage and skin lesions) by using a scoring system from 1 to 5 adapted from Hoyle et al. (2007), where 5 indicates maximum damage (Supplementary Figure S1). Such image welfare scoring was completed with 23 additional fish from each experimental condition (35 fish per experimental condition, 105 in total). Additionally, from AEFishBIT recorded fish, blood was taken from caudal vessels with heparinized syringes, and centrifuged at 3,000 g for 20 min at 4°C. The retrieved plasma was aliquoted and stored at −20°C until glucose and cortisol assays. These sampled fish were then killed by cervical section, and portions of liver and dorsal white skeletal muscle (150–200 mg) were excised and collected in RNA later for its storage at −80°C until RNA extraction for gene expression analyses.

2.5 Biochemical and molecular analyses

Plasma glucose was determined using the Invitrogen™ Glucose Colorimetric Detection Kit (Invitrogen, EIAGLUC). Plasma cortisol levels were determined with an enzyme Immunoassay Kit (Arbor Assays, K003-H1W) following the manufacturer's indications. Tissue RNA was extracted using the MagMAX-96 total RNA isolation kit (Life Technologies) after tissue homogenization in TRI reagent following manufacturers' instructions. RNA quantity and purity was determined by Nanodrop (Thermo Scientific) with absorbance ratios at 260 nm/280 nm of 1.9–2.1. Reverse transcription (RT) of 500 ng of total RNA was performed with random decamers using the High-Capacity cDNA Archive Kit (Applied Biosystems). RT reactions were incubated for 10 min at 25°C and 2 h at 37°C. Negative control reactions were run without reverse transcriptase. Real-time quantitative PCR was carried out with an Eppendorf Mastercycler Ep Realplex, using 96-well PCR array layouts designed for the simultaneous profiling of 44 selected genes of liver and white skeletal muscle (Table 1). The genes comprised in the liver array included markers of the Gh/Igf system (9), lipid metabolism (14), oxidative metabolism and energy sensing (11), and antioxidant defense (10). The analyzed transcripts of muscle included markers of the Gh/Igf system (10), muscle cell growth (8), immune response (5), oxidative metabolism and energy sensing (12), and antioxidant defense (9). Specific primer pair sequences for liver and muscle are listed in Supplementary Tables S1, S2, respectively. Controls of general PCR performance were included on each array, and all the pipetting operations were performed by means of an EpMotion 5070 Liquid Handling Robot (Eppendorf). Briefly, reverse transcription reactions were diluted to convenient concentrations and the equivalent of 660 pg of total input RNA was used in a 25 µL volume for each PCR reaction. PCR-wells contained a 2× SYBR Green Master Mix (Bio-Rad) and specific primers at a final concentration of 0.9 µM were used to obtain amplicons of 50–150 bp in length. The PCR amplification program consisted of an initial denaturation step at 95°C for 3 min, followed by 40 cycles of denaturation for 15 s at 95°C and annealing/extension for 60 s at 60 °C. The efficiency of the PCR reactions was consistently higher than 90% and similar among all genes. The specificity of the reactions was verified by melting curve analysis (ramping rates of 0.5°C/10 s over a temperature range of 55–95°C), and linearity of serial dilutions of RT reactions. Gene expression was calculated using the delta-delta Ct method (Livak and Schmittgen, 2001). β-actin was tested for gene expression stability (GeNorm software, M score = 0.21), and it was used as housekeeping gene in the samples normalization procedure. For multigene expression analysis, all values in the liver were referenced to the expression levels of *gpx1* in LD fish with an arbitrary assigned value of 1. In muscle, gene expression values were referenced to those of *gpx4* in LD fish with an arbitrary assigned value of 1.

2.6 Statistical analysis

AEFishBIT data were post-processed using a simple cosinor model, which fitted the achieved measurements to a one-harmonic sinusoidal function (Refinetti et al., 2007). Recorded data from incomplete light and dark phases were excluded to avoid any temporal bias. Statistically significant differences ($p < 0.05$) on cosinor-derived data, external damage, blood biochemistry and tissue gene expression were assessed by one-way ANOVA followed by a Holm-Sidak *post hoc* test, using the SigmaPlot software 14.5 (Systat Software, San Jose, CA, United States). Correlation analysis was also assessed using the SigmaPlot software. Graphical representations of gathered biomarkers networks was made with the Cytoscape v3.9.1 software. Gene expression patterns were further analyzed by partial least-squares discriminant analysis (PLS-DA) using EZinfo v3.0 (Umetrics, Umeå, Sweden). The quality of the PLS-DA model was evaluated by the parameters R2Y (cum) and Q2 (cum), which indicate the fit and prediction ability, respectively. A validation test of the PLS-DA model consisting of 500 random permutations (Ojala and Garriga, 2010) was performed using the Bioconductor R package *ropls* (Thévenot et al., 2015). The list of genes contributing to group separation was determined by the minimum Variable Importance in the Projection (VIP) values. Discriminant genes were considered with a VIP threshold ≥1.0 (Li et al., 2012; Kieffer et al., 2016).

3 Results

3.1 Welfare scores of growth performance, external damage and blood stress markers

As shown in Table 2, the initial body weight (474–484 g) did not differ significantly among the three experimental groups. At the end of trial, the mean body weight of HD fish (598 g) was significantly lower than in MD and LD fish (662 and 669 g, respectively). In parallel, feed intake was significantly higher in LD and MD fish than in HD fish, and specific growth rates (SGR) in HD fish highlighted a 40% reduction (SGR HD, 0.39%; SGR LD-MD, 0.62%–0.66%). Fulton´s body condition factor K (CFK) ranged from 2.95 in LD fish to 2.72 in HD fish. These observations paralleled with a significant increase of feed conversion ratio (FCR) from 1.61–1.66 in LD-MD fish to 1.92 in HD fish. A concurrent decrease of liver weight and hepatosomatic index (HSI) was also found with the increase of stocking density, varying the achieved HSI from 1.17 to 1.14 in LD-MD fish to 0.91 in HD fish. Additionally, a slight (not statistically significant) decrease in muscle fat content was observed in HD fish, pointing out a leaner body shape with a decreased CFK. Regarding blood biochemical parameters, plasma glucose levels were significantly higher in HD fish (108 mg/dL) than in LD fish (89.5 mg/dL), with intermediate values in the MD group that was closer to HD rather than LD fish. Plasma cortisol levels showed the same trend, and the measured values in HD and MD fish (114–106 ng/mL) were significantly higher than in LD fish (64 ng/mL).

Scores of indicators of external damage are represented in the Radar Plot of Figure 2. Epidermal status was progressively impaired with the increase of stocking density and the worst status was clearly achieved in fish held at HD. Dorsal, caudal, pelvic and pectoral fin status were also affected by the stocking density, but in this case HD fish clearly evolved as a differential group in comparison to both LD and MD fish. Signs of cataracts or exophthalmia were absent in all fish groups, and gill status was visually similar and in good condition in all fish.

10.3389/fphys.2023.1272267

TABLE 2 Data on growth performance and basic blood biochemistry of gilthead sea bream reared at three different stocking densities (final density, 8.5–25 kg/m^3) from end of May to mid-July 2021 (53 days). Data on whole body biometrics, feed intake and feed conversion are the mean ± SEM of duplicated tanks. Liver weight, hepatosomatic index, muscle fat content, and plasma cortisol and metabolite levels are the mean ± SEM of 12 fish per experimental condition. Different letters indicate statistically significant differences (Holm-Sidak *post hoc* test, $p < 0.05$).

	LD (8.5)	MD (17)	HD (25)	P^a
Initial body weight (g)	474.7 ± 8.87	474.3 ± 6.55	484.1 ± 4.48	0.379
Initial body length (cm)	25.58 ± 0.16	25.74 ± 0.11	25.86 ± 0.08	0.243
Feed intake (g DM/fish)	313.80 ± 2.55^a	310.51 ± 2.31^a	220.28 ± 2.40^b	<0.001
Final body weight (g)	669.33 ± 11.6^a	661.55 ± 9.41^a	598.39 ± 6.51^b	<0.001
Final body length (cm)	28.33 ± 0.18^{ab}	28.69 ± 0.13^a	28.19 ± 0.09^b	0.008
Final CFK^b	2.95 ± 0.05^a	2.80 ± 0.03^{ab}	2.72 ± 0.06^b	0.041
Liver weight (g)	8.17 ± 0.66^a	7.75 ± 0.52^a	5.89 ± 0.38^b	0.011
HSI (%)^c	1.17 ± 0.09^a	1.14 ± 0.04^a	0.91 ± 0.05^b	0.017
SGR (%)^d	0.66 ± 0.03^a	0.62 ± 0.01^a	0.39 ± 0.01^b	<0.001
FCR^e	1.61 ± 0.06^b	1.66 ± 0.04^b	1.92 ± 0.04^a	0.036
Glucose (mg/dL)	89.48 ± 6.02^b	101.48 ± 7.23^{ab}	107.85 ± 5.60^a	0.036
Cortisol (ng/mL)	64.29 ± 8.69^b	105.79 ± 10.59^a	114.25 ± 11.50^a	0.004
Muscle fat (%)^f	9.88 ± 0.28	10.16 ± 0.38	9.28 ± 0.45	0.257

[a]One-way ANOVA *p-value*.
[b]Fulton's body condition factor, CFK, 100 x (body weight/standard length^c).
[c]Hepatosomatic index, HSI = 100 × (liver weight/fish weight).
[d]Specific growth rate, SGR = 100 × (ln final body weight—ln initial body weight)/days.
[e]Feed conversion ratio, FCR = 100 × (dry feed intake/wet weight gain).
[f]Fatmeter measurements.

3.2 Behavioral synchronization by high stocking density

Visual observations highlighted a more heterogeneous swimming behavior in fish held at low densities than in HD fish. Certainly, the recorded physical activity and respiratory frequency fitted better to the cosinor model in HD fish than in the other two experimental groups, which became especially evident in the case of LD fish (Supplementary Figure S2). This would reflect an improved social cohesion in HD fish, acting the feeding time as a major zeitgeber synchronization factor with the acrophase of physical activity (φ, the time period in which the cycle peaks) clearly surrounding the programmed feeding time in the absence of feed provision (Figure 3). The rhythm of activity in HD fish also disclosed a higher adjusted mean (M, mesor) and a wide range of variation (A, amplitude), which became statistically significant when the comparison was made with the other extreme group (LD fish) (intermediate values were achieved in MD fish). Over the entire diurnal recording period (09:00 to 21:00 h), correlation analyses highlighted a close positive lineal correlation ($p < 0.001$) between physical activity and respiratory frequency for all tracked fish considered as a whole (Figure 4A), which in turn rendered a decreased respiration/activity ratio with the increase of stocking densities (Figure 4B). With independence of this, the respiration tracking rendered a strong negative correlation ($p < 0.001$) with the continuously recorded water O_2 concentration (Figure 4C).

3.3 Tissue-specific gene expression patterns

All the genes in the liver and muscle PCR-arrays were expressed at detectable levels. In liver, up to 10 genes were differentially expressed by One-way ANOVA (Table 3), being 6 downregulated (*igf1*, *igf2*, *cyp7a1*, *pparα*, *cox1*, *cox2*) and 4 upregulated (*igfbp1a*, *scd1a*, *mn-sod/sod2*, *grp94*) in HD fish in comparison to LD fish. The hepatic expression pattern of MD fish was related to HD fish rather than LD fish, and PLS-DA was able to differentiate LD fish and MD-HD fish with 20 genes out of 44 of discriminant value (VIP >1.0) (Figure 5A). Among them, up to 16 were downregulated in HD-MD fish. The fitness and predictability of the PLS-DA model was validated by a 500-random permutation test (Supplementary Figure S3A) ($p < 0.05$), explaining the two first components the 83% and 66% of the observed and predicted variance, respectively.

Gene expression profiling of white skeletal muscle displayed significant differences among experimental groups with 9 upregulated genes (*ghr2*, *igf2*, *igfbp3a*, *il1β*, *sirt1*, *sirt2*, *grp170*, *grp94*, *grp75*) and one downregulated gene (*ghr1*) in HD fish by One-way ANOVA (Table 4). However, in this case, MD fish was related to LD fish rather than HD fish, and PLS-DA was able to differentiate HD fish from MD-LD fish with 13 genes out of 44 of discriminant value (VIP >1.0). Among them, up to 12 were upregulated in HD fish (Figure 5B). The fitness and predictability of the PLS-DA model was validated by a 500-random permutation test (Supplementary Figure S3B) ($p < 0.01$), explaining the two first components the 88% and 67% of the observed and predicted variance, respectively.

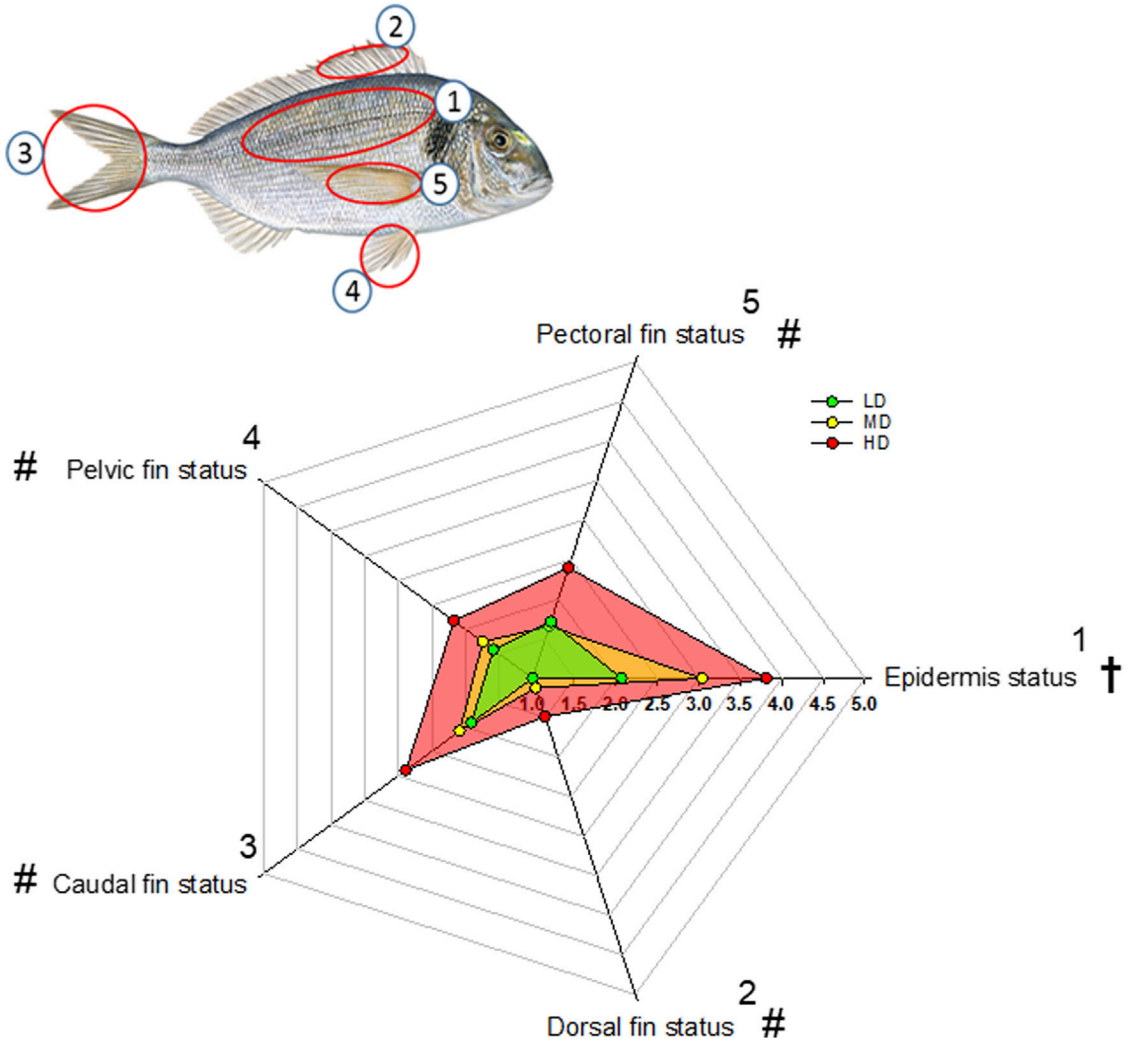

FIGURE 2
Radar plot representing external welfare indicators of gilthead sea bream reared at three different densities (scoring system from 1 to 5 adapted from Hoyle et al. (2007). Numbered fish body parts are indicated for visualization. Colored points are the mean (n = 35) of each welfare indicator. Symbols, † and #, indicate significant differences between the three density groups and between HD and the other two experimental densities, respectively, ($p < 0.05$, ANOVA, Holm-Sidak test).

3.4 Understanding the physiological significance of gathered biomarkers

Based on the differential HD outcomes on growth performance, external damage, behavior, plasma stress markers and tissue gene expression, a biomarker network was built to disclose at a glance the tissue-specific adaptive responses of liver and white skeletal muscle in this group of fish. In the case of liver, a total of 19 significant correlations ($p \leq 0.05$) were established linking hepatic discriminant genes with other welfare indicators (Figure 6A). A direct link between CFK and SGR was presented at the center of the hub, being the rest of markers indirectly connected by different discriminant genes. Hence, SGR and CFK were positively correlated with *igf1* and *igf2*, which were at the same time negatively correlated with physical activity and plasma cortisol, respectively. Moreover, plasma cortisol was negatively correlated with *cyp7a1* and the *igf1/igf2* ratio. The same trend was found between physical activity and the antioxidant defense gene *prdx5*. The CFK was also positively correlated with other defense antioxidant enzymes (*mn-sod, gpx4*) and lipid metabolism-related genes (*cyp7a1*, *pparγ*). Lastly, the *pparγ* was negatively correlated with the respiratory frequency, while plasma glucose was positively correlated with signs of skin damage and with *gpx4* and *mn-sod* genes. There was also a positive correlation between skin damage and *gpx4*. The significance of all the gathered interrelationships with hepatic transcripts can be accessed in Supplementary Table S3.

Regarding the white skeletal muscle, a total of 21 significant correlations ($p < 0.05$) were established among muscle discriminant genes, biometric, behavioral and biochemical blood markers (Figure 7A). As in liver, the SGR-CFK link was indirectly connected to the rest of welfare indicators through discriminant genes. SGR was positively correlated with *hif1α*, *igf1/igf2* ratio and *ghr2*. At the same time, physical activity was indirectly connected to SGR through *ghr2* and *igf1/igf2*, either in a positive or negative

10.3389/fphys.2023.1272267

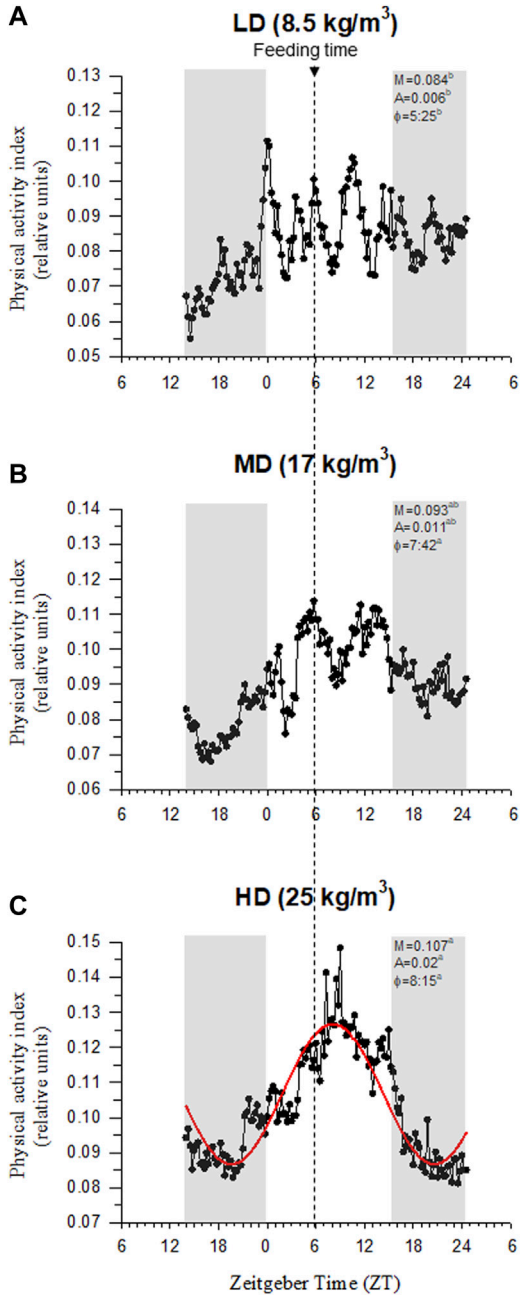

FIGURE 3
Gilthead sea bream physical activity synchronization by feeding at low density **(A)**, medium density **(B)** and high density **(C)**. AEFishBIT data (measures taken every 15 min along 2 consecutive days) of representative individuals (n = 8) is shown as a continuous dotted line in each panel. Best-fit curve (red sinusoidal line) derived from the cosinor analysis of physical activity is only represented in the HD group. Values of mesor (M), amplitude (A), acrophase (φ) and p-value (P) of best-fit curves are shown for each density. Gray shaded areas represent dark phases. Arrow in vertical dotted line indicates the feeding time. Different letters represent significant ($p < 0.05$, ANOVA, Holm-Sidak test) differences between density groups.

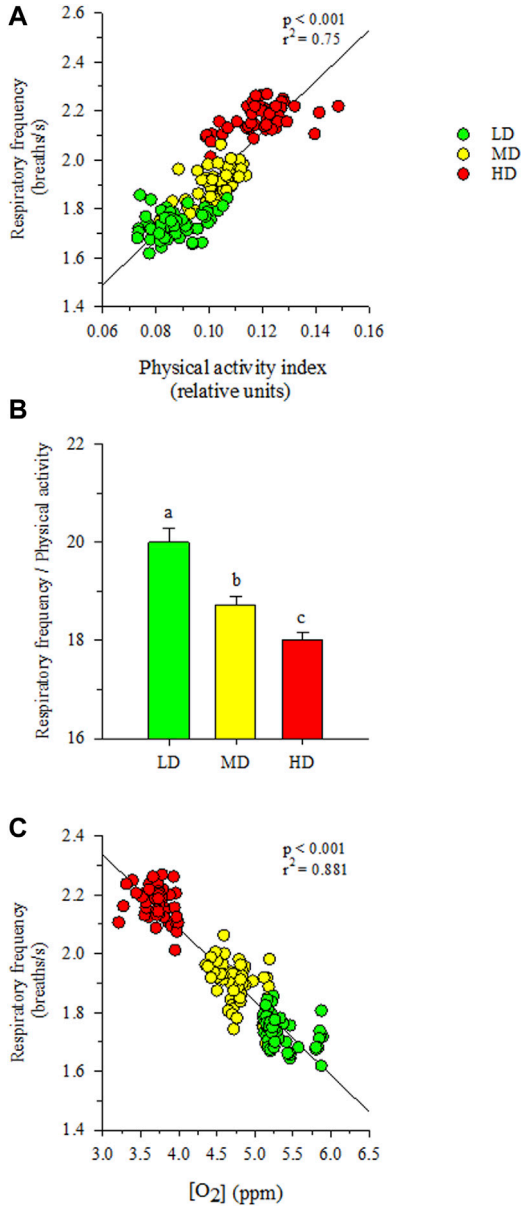

FIGURE 4
(A) Correlation plot of respiratory frequency and physical activity. **(B)** Respiratory frequency/physical activity ratio in each stocking density group. Different letters represent significant ($p < 0.05$, ANOVA, Holm-Sidak test) differences between groups. **(C)** Correlation plot of respiratory frequency and water dissolved oxygen concentration. Values are the mean of physical activity and/or respiratory frequency (n = 8) of each density treatment and dissolved oxygen concentration each 15 min during the diurnal period.

manner, respectively. Physical activity was also positively correlated with a muscle cell growth marker (*myod1*), and the same trend was found between *myod1* and respiratory frequency. Genes related to Gh/Igf system (*igf2* and *ghr1*) were also positively correlated with respiration. On the other side of the SGR-CFK link, *sirt2* was positively correlated with CFK, plasma glucose and skin damage. Plasma glucose was negatively correlated with muscle fat content, and positively correlated with *sirt1*, *gr* and skin damage. In a similar way, skin damage was negatively correlated with muscle fat content, and positively correlated with antioxidant defense genes (*gr*, *grp75*). By last, muscle fat content was negatively correlated with *gr* and *grp170*. The significance of all the gathered interrelationships with muscle transcripts can be accessed in Supplementary Table S4.

TABLE 3 Relative gene expression of liver mRNA transcripts of fish reared at three different stocking densities (final density; 8.5-17-25 kg/m^3). Values are the mean ± SEM of 10–12 fish per experimental condition. All data are in reference to the expression level of *gpx1* in fish from LD group with an arbitrary value of 1. Different letters indicate statistically significant differences (Holm-Sidak *post hoc* test, $p < 0.05$). Differentially expressed genes are in bold.

	LD (8.5)	MD (17)	HD (25)	P^a
ghr1	1.84 ± 0.13	1.78 ± 0.12	1.84 ± 0.14	0.927
ghr2	1.16 ± 0.15	1.14 ± 0.09	1.08 ± 0.11	0.88
igf1	9.92 ± 0.97^a	7.22 ± 0.58^b	6.73 ± 0.55^b	0.008
igf2	3.53 ± 0.63^a	1.85 ± 0.17^b	1.86 ± 0.27^b	0.008
igfbp1a	0.05 ± 0.01^b	0.12 ± 0.03^{ab}	0.22 ± 0.07^a	0.039
igfbp1b	2.44 ± 0.52	2.43 ± 0.78	2.23 ± 0.69	0.969
igfbp2a	0.62 ± 0.07	0.51 ± 0.05	0.46 ± 0.05	0.219
igfbp2b	1.27 ± 0.14	1.30 ± 0.14	1.27 ± 0.10	0.976
igfbp4	0.63 ± 0.06	0.57 ± 0.05	0.50 ± 0.04	0.219
elovl1	5.37 ± 0.48	4.43 ± 0.83	3.82 ± 0.42	0.203
elovl4	0.18 ± 0.01	0.22 ± 0.03	0.21 ± 0.02	0.465
elovl5	0.88 ± 0.18	1.25 ± 0.23	1.14 ± 0.20	0.448
elovl6	1.22 ± 0.15	1.26 ± 0.15	1.07 ± 0.23	0.738
fads2	0.36 ± 0.06	0.42 ± 0.12	0.32 ± 0.05	0.71
scd1a	0.09 ± 0.01^b	0.11 ± 0.01^{ab}	0.16 ± 0.03^a	0.026
scd1b	0.26 ± 0.05	0.41 ± 0.08	0.37 ± 0.17	0.594
hl	4.77 ± 0.41	4.72 ± 0.43	4.58 ± 0.24	0.929
lpl	2.19 ± 0.29	1.94 ± 0.32	2.44 ± 0.30	0.519
atgl	0.29 ± 0.11	0.34 ± 0.10	0.24 ± 0.06	0.753
pla2g6	0.09 ± 0.01	0.10 ± 0.01	0.10 ± 0.01	0.43
cyp7a1	1.40 ± 0.22^a	0.96 ± 0.16^{ab}	0.70 ± 0.11^b	0.02
***ppar*α**	1.83 ± 0.16^a	1.66 ± 0.11^{ab}	1.37 ± 0.09^b	0.048
*ppar*γ	0.28 ± 0.01	0.24 ± 0.01	0.25 ± 0.03	0.321
*hif1*α	0.40 ± 0.02	0.38 ± 0.03	0.41 ± 0.02	0.722
*pgc1*α	0.06 ± 0.01	0.03 ± 0.01	0.05 ± 0.01	0.397
cpt1a	0.45 ± 0.04	0.37 ± 0.07	0.30 ± 0.04	0.133
hfabp	20.83 ± 1.72	20.62 ± 2.62	18.92 ± 1.82	0.779
Cs	0.49 ± 0.03	0.47 ± 0.10	0.38 ± 0.03	0.406
nd2	15.16 ± 2.27	12.90 ± 2.90	10.46 ± 1.51	0.34
nd5	5.56 ± 0.65	4.32 ± 0.38	4.31 ± 0.47	0.157
cox1	58.13 ± 8.60^a	45.31 ± 3.92^{ab}	36.02 ± 3.84^b	0.041
cox2	17.74 ± 2.08^a	13.92 ± 1.38^{ab}	10.66 ± 1.20^b	0.013
ucp1	8.84 ± 1.00	7.05 ± 0.77	8.42 ± 1.13	0.407
sirt1	0.06 ± 0.00	0.05 ± 0.01	0.06 ± 0.00	0.896
sirt2	0.16 ± 0.01	0.16 ± 0.01	0.15 ± 0.01	0.628

(Continued in next column)

TABLE 3 (*Continued*) Relative gene expression of liver mRNA transcripts of fish reared at three different stocking densities (final density; 8.5-17-25 kg/m^3). Values are the mean ± SEM of 10–12 fish per experimental condition. All data are in reference to the expression level of *gpx1* in fish from LD group with an arbitrary value of 1. Different letters indicate statistically significant differences (Holm-Sidak *post hoc* test, $p < 0.05$). Differentially expressed genes are in bold.

	LD (8.5)	MD (17)	HD (25)	P^a
gpx1	1.04 ± 0.08	0.93 ± 0.08	1.11 ± 0.09	0.356
gpx4	4.56 ± 0.31	6.09 ± 0.49	5.71 ± 0.52	0.057
prdx3	0.52 ± 0.04	0.42 ± 0.05	0.49 ± 0.04	0.279
prdx5	0.62 ± 0.05	0.54 ± 0.04	0.52 ± 0.05	0.31
cu-zn-sod/sod1	3.23 ± 0.22	3.13 ± 0.27	2.87 ± 0.22	0.55
mn-sod/sod2	0.56 ± 0.03^b	0.60 ± 0.03^{ab}	0.75 ± 0.07^a	0.031
grp170	0.55 ± 0.06	0.74 ± 0.19	0.80 ± 0.18	0.486
grp94	1.74 ± 0.16^b	3.00 ± 0.31^{ab}	4.09 ± 0.82^a	0.01
grp75	0.39 ± 0.03	0.28 ± 0.02	0.37 ± 0.05	0.079

^{a}One-way ANOVA *p-value*.

4 Discussion

The negative impact of climate change in fisheries and aquaculture has been extensively studied and reviewed at regional and global scales (FAO, 2020; Maulu et al., 2021). Most studies, however, tend to explore the negative effects of climate change, while giving far less attention to the positive ones that are especially critical for the adaptation strategies. Certainly, warmer periods can promote shorter growing periods, helping to the expansion of aquaculture production in both temperate and cold regions, though such positive achievements become outweighed below the Limiting Oxygen Saturation (LOS) level, defined as the threshold level where regulatory mechanism are no longer sufficient to maintain O_2 consumption without compromising any physiological function (Remen et al., 2015; Remen et al., 2016). Thus, in the present study, fish stocked at the highest density (25 kg/m^3, 45%–60% O_2 saturation level) experienced an impaired growth in comparison to fish reared at low (LD, 8.5 kg/m^3) or intermediate (MD, 17 kg/m^3) densities. Similar results were reported by Carbonara et al. (2019) at 15–30 kg/m^3, but negative effects on growth performance were avoided in the range of 5–20 kg/m^3 when the water O_2 concentration remained above 55%–70% saturation level (Araújo-Luna et al., 2018). Moreover, the rearing density can be increased up to 36–44 kg/m^3 without drawback effects in growth performance when the water O_2 level is maintained above the 100% saturation (Parma et al., 2020). Thus, as pointed out by Saraiva et al. (2022), the effects of stocking density on fish welfare are complex and would involve many interacting factors. This notion is supported at the transcriptional level by changes in the tissue-specific expression patterns with a different tissue orchestration of the stress response, according to the nature and intensity of the hypoxic and crowding stress challenge (Martos-Sitcha et al., 2019a). Thus, the liver and heart of gilthead sea bream mostly contributed to cope with a global hypoxic response, involving changes in energy sensing, antioxidant defense and tissue repair. By contrast, the skeletal muscle disclosed

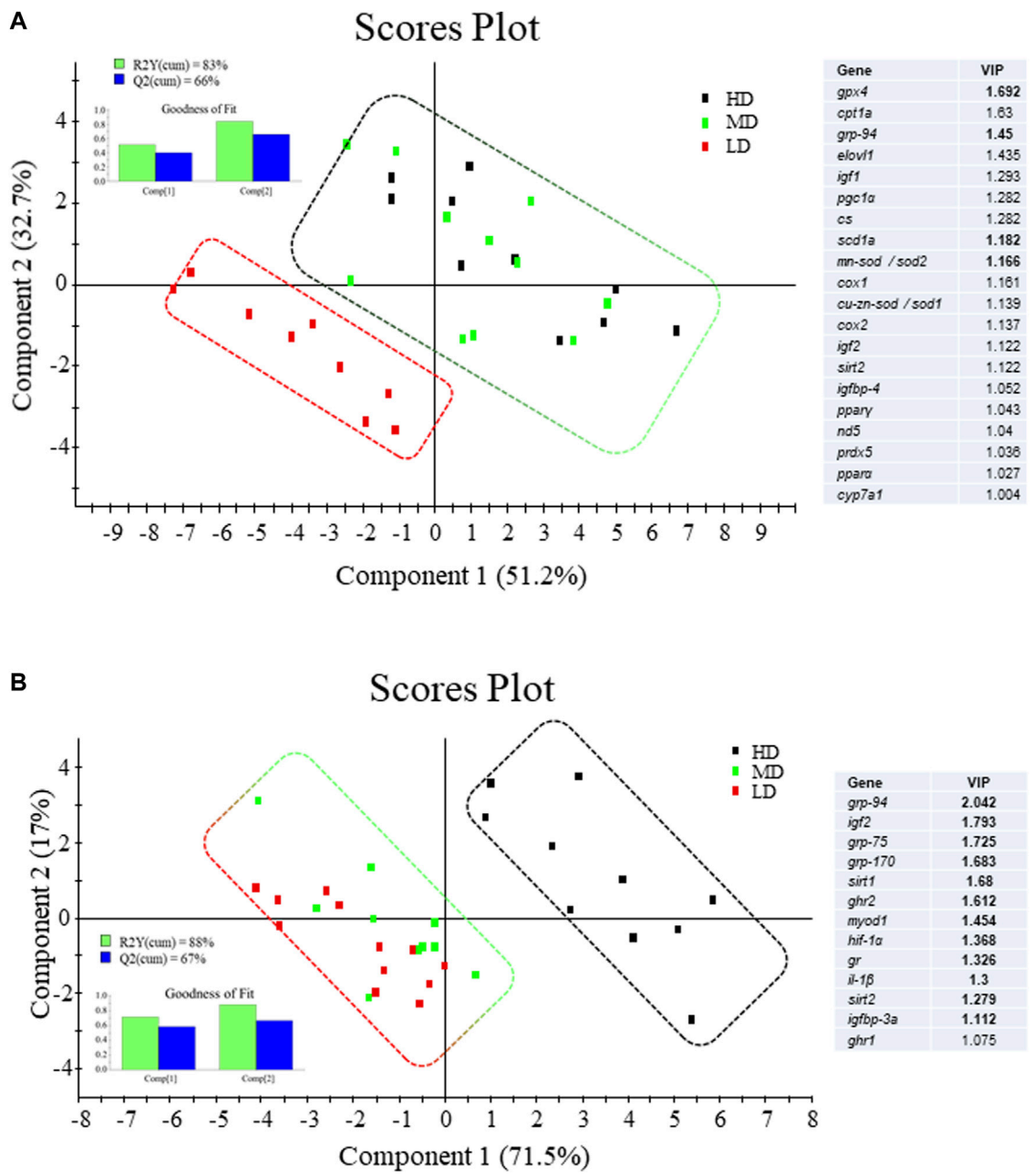

Gene	VIP
gpx4	**1.692**
cpt1a	1.63
grp-94	**1.45**
elovl1	1.435
igf1	1.293
pgc1α	1.282
cs	1.282
sod1a	**1.182**
mn-sod / sod2	**1.166**
cox1	1.161
cu-zn-sod / sod1	1.139
cox2	1.137
igf2	1.122
sirt2	1.122
igfbp-4	1.052
pparγ	1.043
nd5	1.04
prdx5	1.036
pparα	1.027
cyp7a1	1.004

Gene	VIP
grp-94	**2.042**
igf2	**1.793**
grp-75	**1.725**
grp-170	**1.683**
sirt1	**1.68**
ghr2	**1.612**
myod1	**1.454**
hif-1α	**1.368**
gr	**1.326**
il-1β	**1.3**
sirt2	**1.279**
igfbp-3a	**1.112**
ghr1	1.075

FIGURE 5
Two-dimensional PLS-DA score plot of **(A)** liver and **(B)** white skeletal muscle molecular signatures of fish under different stocking densities, representing the distribution of the samples between the first two components in the model. Top left inserted figures represent the cumulative explained [R2Y(cum), green bars] and predicted [Q2(cum), blue bars] variance. Blue tables represent the ordered list of markers by variable importance in the projection (VIP) of the PLS-DA model. Upregulated genes are indicated by VIP values in bold and downregulated genes are shown as VIP values in regular font.

changes in the expression pattern of the components of the Gh/Igf system that appears more related to changes in fish density and behavioral traits rather than water O_2 levels. In any case, wide-transcriptomic analysis in zebrafish (*Danio rerio*), Atlantic salmon and European sea bass did not highlight a conserved transcriptomic signature for a proactive behavior across fish species (Rey et al., 2021), which is perhaps indicative of the complexity and polygenic nature of the behavioral phenotype. Indeed, as discussed below, our gathered biomarker approach was able to connect proactive behavior in HD fish with locally regulated growth, while systemic growth regulation via the liver Gh/Igf system was apparently more related with a reactive coping stress style.

It is worth noting that gilthead sea bream is a schooling fish that displays social hierarchies for the use of space and competition for feed (Goldan et al., 2003; Montero et al., 2009; Arechavala-Lopez et al., 2019; Oikonomidou et al., 2019), which reinforced an enhanced physical activity in HD environments (Carbonara et al., 2019). Similarly, we found herein that measurements of body tail

TABLE 4 Relative gene expression of white skeletal muscle mRNA transcripts of fish reared at three different stocking densities (final density; 8.5-17-25 kg/m3). Values are the mean ± SEM of 10–12 fish per experimental condition. All data are in reference to the expression level of *gpx4* in fish from LD group with an arbitrary value of 1. Different letters indicate statistically significant differences (Holm-Sidak *post hoc* test, $p < 0.05$). Differentially expressed genes are in bold.

	LD (8.5)	MD (17)	HD (25)	P^a
ghr1	3.07 ± 0.24^a	2.54 ± 0.30^{ab}	2.12 ± 0.15^b	0.027
ghr2	0.48 ± 0.06^b	0.44 ± 0.07^b	0.73 ± 0.08^a	0.012
igf1	0.06 ± 0.01	0.06 ± 0.01	0.08 ± 0.01	0.223
igf2	0.53 ± 0.03^b	0.62 ± 0.06^b	0.80 ± 0.06^a	0.003
igfbp3a	1.10 ± 0.13^b	1.26 ± 0.11^{ab}	1.53 ± 0.15^a	0.042
igfbp3b	0.004 ± 0.001	0.004 ± 0.001	0.006 ± 0.002	0.257
igfbp5a	0.26 ± 0.04	0.29 ± 0.05	0.38 ± 0.06	0.241
igfbp5b	2.00 ± 0.22	2.32 ± 0.36	2.56 ± 0.22	0.362
igfbp6a	0.020 ± 0.004	0.018 ± 0.003	0.021 ± 0.002	0.773
igfbp6b	0.09 ± 0.01	0.10 ± 0.02	0.11 ± 0.02	0.849
myod1	4.66 ± 0.33	5.42 ± 0.59	6.10 ± 0.54	0.141
myod2	0.96 ± 0.08	1.13 ± 0.08	0.97 ± 0.09	0.301
myf5	0.15 ± 0.01	0.18 ± 0.01	0.16 ± 0.01	0.222
myf6/herculin	0.19 ± 0.01	0.21 ± 0.02	0.21 ± 0.02	0.52
mstn/gdf8	0.80 ± 0.15	1.03 ± 0.18	1.40 ± 0.42	0.336
mef2a	7.51 ± 0.54	6.60 ± 0.39	7.14 ± 0.44	0.387
mef2c	2.42 ± 0.10	2.21 ± 0.14	2.12 ± 0.16	0.27
fst	0.29 ± 0.03	0.31 ± 0.05	0.30 ± 0.03	0.955
il1β	0.051 ± 0.005^b	0.085 ± 0.011^{ab}	0.106 ± 0.016^a	0.005
il6	0.004 ± 0.001	0.003 ± 0.000	0.004 ± 0.001	0.311
il8	0.012 ± 0.002	0.017 ± 0.002	0.020 ± 0.003	0.115
il10	0.006 ± 0.001	0.008 ± 0.001	0.008 ± 0.001	0.472
il12β	0.012 ± 0.001	0.011 ± 0.001	0.015 ± 0.001	0.151
hif1α	0.70 ± 0.05	0.78 ± 0.07	0.89 ± 0.06	0.086
pgc1α	0.89 ± 0.15	0.60 ± 0.12	0.61 ± 0.17	0.313
pgc1β	0.44 ± 0.04	0.40 ± 0.04	0.38 ± 0.03	0.542
cpt1a	2.22 ± 0.14	2.33 ± 0.19	2.42 ± 0.14	0.656
cs	8.39 ± 0.41	8.00 ± 0.51	8.12 ± 0.44	0.83
nd2	37.93 ± 2.67	37.89 ± 4.35	32.01 ± 3.03	0.383
nd5	12.88 ± 1.03	12.06 ± 0.94	11.16 ± 1.09	0.5
cox1	184.30 ± 14.18	171.38 ± 10.78	176.18 ± 8.87	0.726
cox2	34.06 ± 3.45	35.82 ± 2.48	34.46 ± 2.57	0.903
ucp3	6.68 ± 0.61	5.29 ± 0.56	5.36 ± 0.58	0.175
sirt1	0.21 ± 0.01^b	0.24 ± 0.02^{ab}	0.28 ± 0.01^a	0.009
sirt2	0.46 ± 0.02^b	0.50 ± 0.03^{ab}	0.59 ± 0.04^a	0.016
cat	4.81 ± 0.17	5.02 ± 0.34	5.33 ± 0.29	0.413
gpx4	1.00 ± 0.27	1.02 ± 0.27	1.50 ± 0.37	0.432
gr	0.20 ± 0.01	0.23 ± 0.02	0.25 ± 0.02	0.061
prdx3	1.87 ± 0.13	1.94 ± 0.13	2.16 ± 0.14	0.293
prdx5	6.33 ± 0.36	6.79 ± 0.54	6.13 ± 0.38	0.552
mn-sod/sod2	1.90 ± 0.14	1.96 ± 0.15	2.11 ± 0.17	0.601
grp170	0.25 ± 0.02^b	0.27 ± 0.02^b	0.38 ± 0.03^a	<0.001
grp94	0.72 ± 0.05^b	0.87 ± 0.08^b	1.32 ± 0.11^a	<0.001
grp75	1.17 ± 0.05^b	1.32 ± 0.08^b	1.63 ± 0.10^a	<0.001

^{a}One-way ANOVA *p-value*.

(Continued in next column)

TABLE 4 (*Continued*) Relative gene expression of white skeletal muscle mRNA transcripts of fish reared at three different stocking densities (final density; 8.5-17-25 kg/m3). Values are the mean ± SEM of 10–12 fish per experimental condition. All data are in reference to the expression level of *gpx4* in fish from LD group with an arbitrary value of 1. Different letters indicate statistically significant differences (Holm-Sidak *post hoc* test, $p < 0.05$). Differentially expressed genes are in bold.

jerk accelerations at a high recording frequency clearly highlighted an endogenous swimming activity rhythm with a higher amplitude and adjusted-mean in the group of HD fish (Figure 3). This occurred in parallel with the rise of respiratory frequency (Figure 4A), though this in turn resulted in a slight but progressive decrease of the respiration/activity ratio from LD to HD fish (Figure 4B). Such metabolic feature would be indicative of a decreased energy partitioning for growth in a HD environment with a limited O_2 availability, which makes sense with the observed FCR impairment in this group of fish (Table 2). Certainly, the association of better growth with a lower activity is a well-known selected pattern in livestock production (Rosenfeld et al., 2015; Sibly et al., 2015). According to this, the behavioral monitoring with the AEFishBIT accelerometer have rendered divergent patterns of energy use for growth and activity across representative European farmed fish (gilthead sea bream, European sea bass and Atlantic salmon) (Ferrer et al., 2020; Kolarevic et al., 2021; Rosell-Moll et al., 2021), but also in genetically improved gilthead sea bream for either growth or FCR (Perera et al., 2021; Calduch-Giner et al., 2023). Such genetic progress has an impact in fillet yield (Besson et al., 2022), and perhaps other productive traits affected by the establishment of different social hierarchies and interactions. In that sense, Arechavala-Lopez et al. (2020) pointed out that the time of the first gilthead sea bream response during hypoxia or risk-taking tests is shorter in HD than in LD environments, which might lead to a higher competitiveness for feed if it is not provided in a sufficient quantity and quality. At the same time, however, HD environments can serve to better synchronize the phase of locomotor and metabolic rhythms with the daily feeding time, generating an internal rhythmicity close to 24 h for a better synchronization of the individuals with the environment and their congeners (Mistlberger, 2011; Challet, 2019). This notion was fitted herein by the better cosinor adjustment of the recorded jerk accelerations in the HD fish than in the other two experimental groups (Figure 3). Feeding frequency also operates in a similar manner, and fish fed

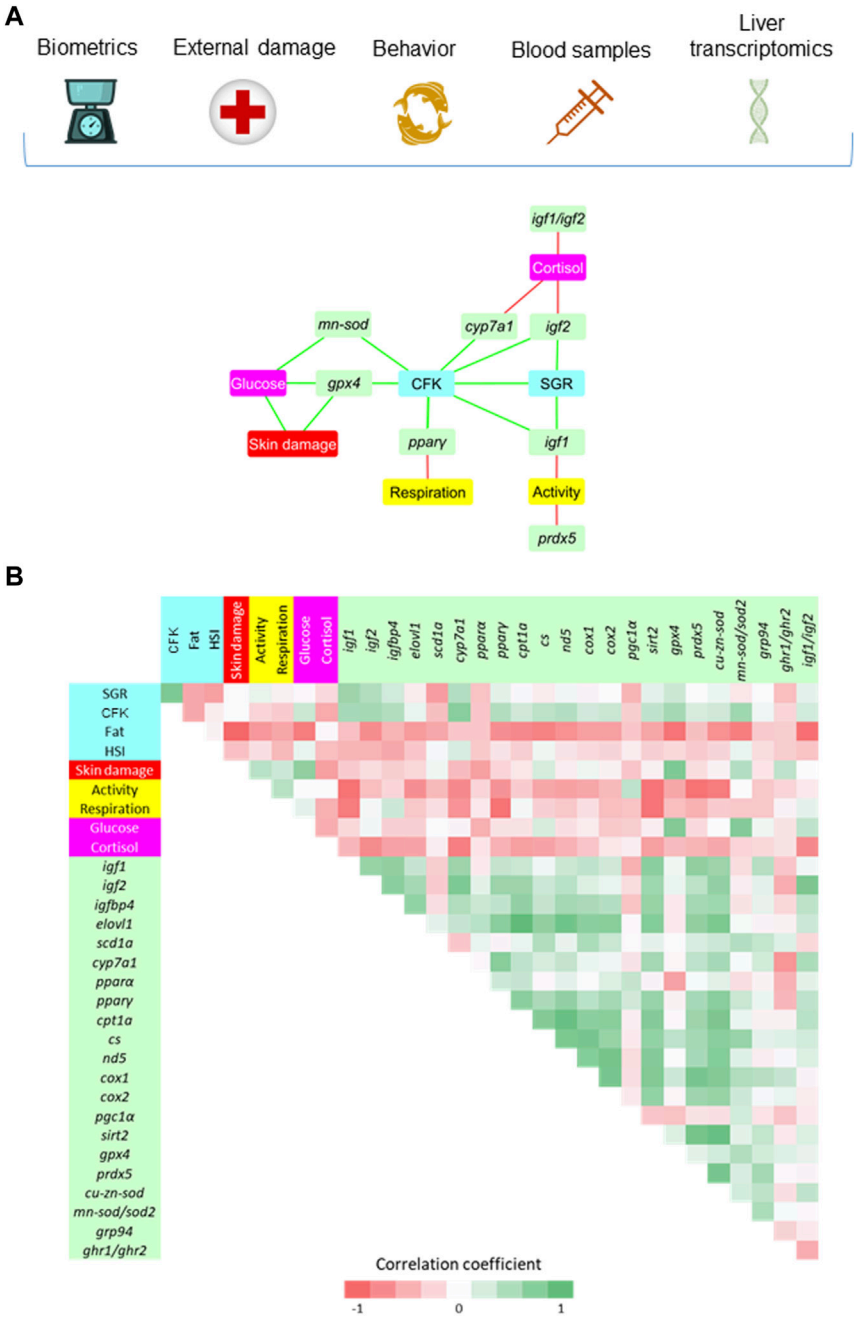

FIGURE 6
(A) Diagram network showing the positive (green) and negative (red) significant ($p < 0.05$) Spearman correlation coefficients (7–12 fish from the HD group) between hepatic genes (VIP > 1), biometric indicators (SGR, CFK, Fat and HSI), external damage (Skin) and behavioral parameters (Activity and Respiration), and blood stress markers (Glucose and Cortisol). **(B)** Correlation matrix showing graphically the entire set of correlation coefficients. The values of Spearman correlation coefficients can be accessed at Supplementary Table S3.

with a single meal per day showed a higher ability to concentrate the self-feeding activity around the programmed meal in comparison to those fed hourly during a 3h-window (Calduch-Giner et al., 2022). Moreover, gilthead sea bream becomes mostly arrhythmic in winter, but the use of feeding schedules with alternate days (maintaining constant the total feed intake, but with an increased supply by the feeding day) restored the typical feeding behavior of the warm season (active feeding period). The pervasiveness of biological rhythms is, thereby, adaptive in nature on a daily and/or seasonal basis, functioning as a timing reference that allows organisms to anticipate and take advantage of the diel fluctuations in their environments (Van der Zee et al., 2008). The bad thing is that the increased contact among individuals in a HD environment might lead to physical injuries (Oppedal et al., 2011; Sveen et al., 2018; Weirup et al., 2021), promoting an aggressive behavior rather than an improved individual social cohesion by the feeding time zeitgeber. In the present study, aggressive interactions among individuals are not specifically monitored, but visual

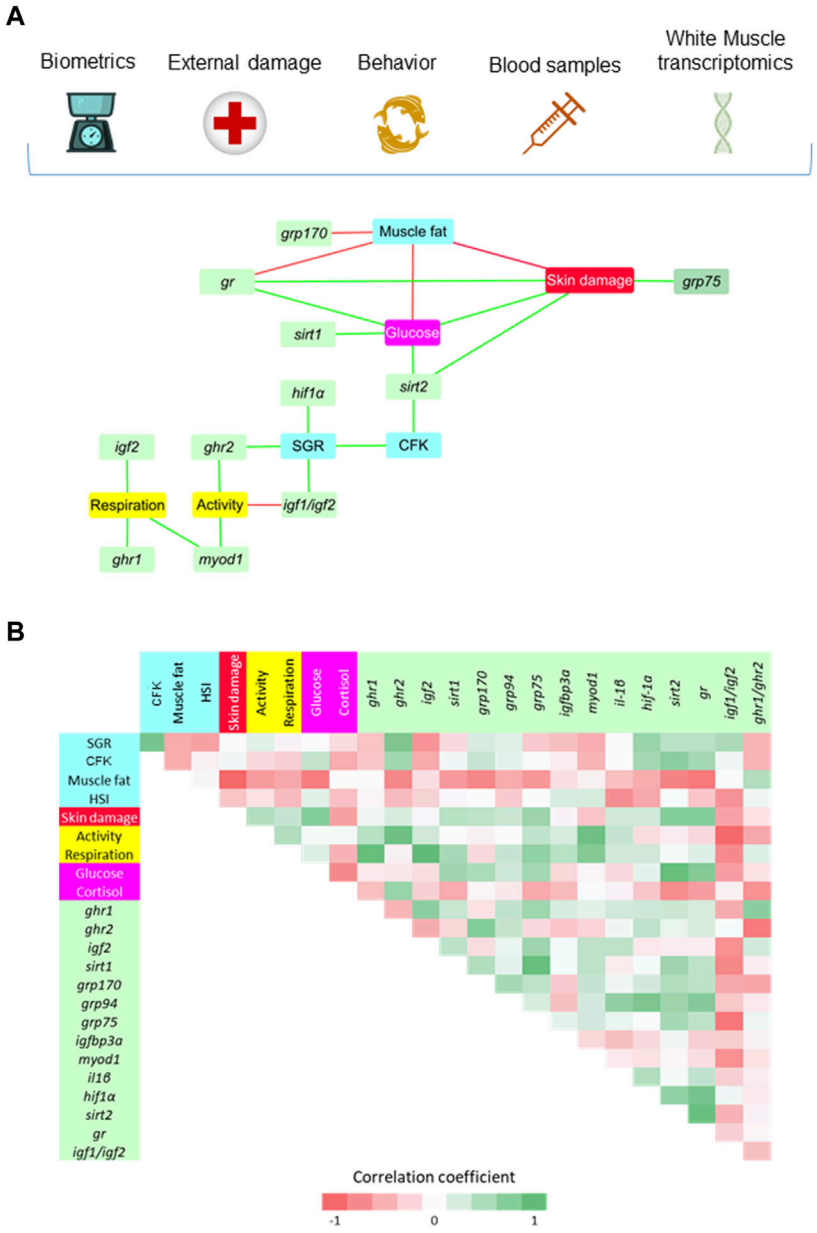

FIGURE 7
(A) Diagram network showing the positive (green) and negative (red) significant ($p < 0.05$) Spearman correlation coefficients (7–12 fish from the HD group) between white skeletal muscle genes (VIP > 1), biometric indicators (SGR, CFK, Fat and HSI), external damage (Skin) and behavioral parameters (Activity and Respiration), and blood stress markers (Glucose and Cortisol). **(B)** Correlation matrix showing graphically the entire set of correlation coefficients. The values of Spearman correlation coefficients can be accessed at Supplementary Table S4.

observations did not reveal biting-chasing activities before-after feeding in any fish group, and more importantly, correlation analysis within the HD group highlighted a positive association between growth and skin erosion and damage (Figure 7). Therefore, it appears likely that the external body signs of welfare impairment in this group of fish (Figure 2) would be primarily due to an active feeding behavior with involuntary collisions during feed dispensation. How this non-desirable effect can be solved by more appropriate feeding schedules and housing environments is becoming an important challenge for the future development of aquaculture in a scenario of a limited space allowance for livestock production.

Plasma/serum cortisol is currently the most widely used stress biomarker in fish (Sadoul and Geffroy, 2019; Noble et al., 2020), though its reliability is limited by a number of drawbacks, including among others: i) exhaustion or adaptive HPI-axis habituation to chronic stress, ii) dramatic increase in circulating cortisol levels by sampling itself, and iii) high biological variability within and among species that hampers a clear conclusion of stress condition. This makes sense because the underlying hypothesis for the fitted low

plasma cortisol levels with the increase of stocking density is that acute stress sampling can become minimized in fish coming from a HD environment (van de Nieuwegiessen et al., 2009; Santos et al., 2010; Othman et al., 2022). Furthermore, it was previously established that the regulation of gilthead sea bream plasma cortisol levels is largely dependent of the type and intensity of stressor (Bermejo-Nogales et al., 2014). It is expected, therefore, that the use of alternative water and fish scales matrix-samples gain more interest in the forthcoming years as a less invasive and reproducible cortisol assessment approach (Fanouraki et al., 2011; Weirup et al., 2021; Vercauteren et al., 2022). In the meantime, cortisol measurements should be supported by other stress indicators for an accurate assessment of fish stress/welfare status. Thus, we considered herein plasma cortisol levels as part of an integrative biomarker procedure in which the measured levels in LD fish were in the lower range of values reported for unstressed gilthead sea bream, while those from MD and HD resulted almost doubled (Table 2). The closeness found between cortisol levels of MD and HD fish can also be indicative of the different discriminant value of the assessed stress/welfare indicators. Indeed, liver and muscle gene expression patterns disclosed a different gene clustering, according to which the expression signature of MD was closer to HD in liver and to LD in muscle (Figure 5). With independence of this, the high plasma cortisol levels in HD fish were associated with a reduced growth through changes in hepatic *igf2* and *cyp7α1* expression (Figure 6), which can be considered adaptive in nature in fish facing a limited O_2 availability that was not able to support the maximum growth of the species.

Cortisol works raising circulating glucose levels across species (Mommsen et al., 1999; Sapolsky et al., 2000), and their concurrent increase would reflect the nature and intensity of stress stimuli as well as the different stress species-specific susceptibility (Fanouraki et al., 2011; Bordin and Freire, 2021). Thus, both glucose and cortisol levels increased at a population level in a HD environment (Table 2), but the gathered biomarker analysis revealed a negative correlation between them in HD fish via the interconnections driven by different hepatic molecular transcripts (Figure 6), which might dictate a negative feedback loop that limits cortisol release promoting the use of blood glucose not only as a fast metabolic fuel, but also as a major antioxidant agent. Certainly, the rerouting of glucose into a pentose-phosphate-pathway (PPP) is a major protective mechanism to counteract acute and severe oxidative stress (Ralser et al., 2007; Stincone et al., 2015) through the production of NADPH that is required for the regeneration of reduced glutathione, a well-known antioxidant that is present in most living cells from bacteria to mammals (Hamilton et al., 2014). At the same time, however, there are several mechanisms contributing to oxidative stress during diabetes and hyperglycemia, which is indicative that exists a delicate balance between the protective and damaging effects of glucose to maintain redox homeostasis through the evolution (Cherkas et al., 2020). In the present study, the protective glucose effects in HD fish were shaped by a positive association of glucose with a number of antioxidant enzymes (*mn-sod, gpx4, prdx5*) in the liver (Figure 6) and glucose responsive proteins (*grp170, grp75*) in skeletal muscle (Figure 7), all of them already identified as highly stress-responsive genes in gilthead sea bream (Bermejo-Nogales et al., 2008; Saera-Vila et al., 2009; Calduch-Giner et al., 2010; Pérez-Sánchez et al., 2013; Malandrakis et al., 2014; Magnoni et al., 2017; Martos-Sitcha et al., 2019a; Naya-Català et al., 2021). Indeed, regardless of glucose-gene correlations, the overall trend in both liver and skeletal muscle was the upregulated expression of *grp* genes (*grp170, grp94 and grp75*) in HD fish. Such genes are normally overexpressed when cells are starved of glucose (Tanaka et al., 1988; Franklin et al., 2022), but the opposite is also true and the *grp75* was consistently upregulated with the increase of glycemia by crowding stress in gilthead sea bream pair-fed fish (Bermejo-Nogales et al., 2008). Likewise, when comparisons are made between gilthead sea bream and common dentex (*Dentex dentex*, a highly sensitive sparid fish to handling stress), this another sparid fish exhibited higher levels of secondary stress markers (glucose, lactate) in combination with an increased expression of pro-inflammatory cytokines and non-enzymatic antioxidant genes, such as *grp75* and metallothionein (*mt*) (Bermejo-Nogales et al., 2007). Most of these stress-responsive genes are primarily located in the mitochondria and endoplasmic reticulum, scavenging the production of reactive oxygen species (ROS) (Rahman et al., 2017; Dhamad et al., 2020). Accordingly, we found herein that the fine adjustments of metabolism in HD fish was also encompassed by the hepatic downregulation of catalytic enzyme subunits of the mitochondrial respiration chain (Complex IV; *cox1, cox2*) and the well-known lipolytic transcription factor *pparα*, which in turn resulted in the upregulated expression of a strong lipogenic marker, the *scd1a* (Table 3). This transcriptional signature is prone to promote a general depletion of oxidative metabolism, redirecting the surplus of metabolic fuels towards lipid storage as reported elsewhere during episodes of heat stress in broilers (Guo et al., 2021; Lan et al., 2022). However, this changing transcriptional signature is part of a more complex and extensive metabolic reprograming of lipid metabolism that also included a strong-down regulation of the hepatic *cyp7α1,* the first rate limiting enzyme of bile acid synthesis from cholesterol (Chiang and Ferrell, 2020). This would adjust the effective dietary fat absorption to O_2 availability, according to the oxystatic theory that assumes that voluntary feed intake is limited by the maximal physiological capacity of O_2 usage (Saravanan et al., 2012). Conversely, the consumption of cholesterol-rich diets can promote the shift of carbohydrate to lipid metabolism, preventing strong hypoglycemic effects following exposure to acute hypoxic stress (Miron and Tirosh, 2019). In any case, most adaptive hypoxia responses appear to be tissue-specific (Martos-Sitcha et al., 2019a), and in the absence of transcriptional changes in markers of oxidative metabolism, the skeletal muscle of HD fish disclosed a pronounced upregulation of *sirt1* and *sirt2* (Table 4). Such metabolic feature is viewed as a higher energy demanding condition that is susceptible to be epigenetically regulated in the case of *sirt1* by changes in the DNA methylation pattern of several CpG positions of a CG island close to the transcription start site (Simó-Mirabet et al., 2020). Indeed, it is well known that fasting upregulated the expression of *sirt1* in the skeletal muscle of gilthead sea bream (Simó-Mirabet et al., 2017). However, the muscle expression of *sirt2* appeared poorly responsive to nutrient deprivation, but it was upregulated in a fast growing fish strain (Simó-Mirabet et al., 2018). If this is also part of an adaptive feature to preserve muscle growth in HD fish warrants further research.

Like the confounding regulation of glucose and redox homeostasis, *Gh*-transgenic fish have a limited capacity to manage hypoxic environments efficiently (McKenzie et al., 2003; Almeida et al.,

2013), though paradoxically studies in mammals indicate that circulating GH can be increased by either the increase in O_2 requirements or the reduction in O_2 availability (VanHelder et al., 1987). In that way, diet and exercise modulate the activity of the *Gh/Igf* axis in gilthead sea bream (Perelló-Amorós et al., 2021), and circulating *Gh* during steady states is becoming a subrogate marker of critical swimming speed (swimming activity that can be maintained theoretically indefinitely without exhaustion) (Martos-Sitcha et al., 2018). However, circulating *Gh* was lowered after acute or chronic confinement in a wide range of species, including tilapia (Aupérin et al., 1997), salmonids (Wilkinson et al., 2006) and gilthead sea bream (Saera-Vila et al., 2009). In the present study, circulating *Gh* was not measured, but the downregulated expression of hepatic *igf1* and *igf2* in HD fish highlighted a lower sensitivity of liver to the anabolic action of *Gh,* probably via post-transcriptional mechanisms because the expression of both *ghr1* and *ghr2* remained almost unaltered among all fish groups (Table 3). However, as reviewed in Pérez-Sánchez et al., 2018, and most recently stated during early development (Naya-Català et al., 2021), a large body of evidence highlighted the tissue-specific regulation of the two Ghr and Igf subtypes by nutrition and season across development in gilthead sea bream. Certainly, in contrast to that found in the liver, the muscle expression of *ghr2* was upregulated in HD fish in comparison to the other two experimental groups (Table 4), which would trigger a compensatory growth response through the enhanced expression of *igf2* as reported elsewhere in fish fed alternative feeds or semi-synthetic diets formulated to be deficient in specific nutrients (Ballester-Lozano et al., 2015; Pérez-Sánchez et al., 2018). Thus, as also pointed out before, the varying contribution of systemic (via liver Gh/Igf axis) and local growth-promoting actions on global growth are indicative of a different welfare condition and metabolic readjustment of the endocrine-growth cascade. This notion was further supported by the expression pattern of the two phylogenetically and functionally divergent clades of Igfbp1/2/4 and Igfbp3/4/6 (see Pérez-Sánchez et al., 2018), which resulted herein in an enhanced expression of hepatic *igfp1a* and muscle *igfbp3a* in HD fish (Tables 3 and 4). A common role of Igfbps among the fish lineage has not been established, but transgenic studies support a main role of Igfbp1 as a negative regulator of fish growth. Thus, *igfbp1* knockdown alleviates the hypoxic growth and development delay in zebrafish, whereas its overexpression caused growth and development retardation under normoxia (Kajimura et al., 2005). By contrast, the enhanced *igfbp3* expression has been related to growth acceleration by *Gh*-transgenesis in coho salmon (*Oncorhynchus kisutch*) (Alzaid et al., 2018). Therefore, it appears likely that all the observed transcriptional changes in the Gh/Igf axis are adaptive attempts to drive a different contribution of systemic and local growth regulatory mechanisms. According to this, our integrative biomarker survey disclosed negative correlations of hepatic Gh/Igf markers (*igf1, igf2*) with behavioral measurements of activity/respiration, whereas the opposite was found for muscle components of the Gh/Igf system (*igf2, ghr1, ghr2*), according to which this growth-regulatory transition was prone to a proactive instead of a reactive behavior. The way in which this differential tissue regulation was driven by a different threshold level of O_2 sensors requires further warrant, though it is noteworthy that the *hif1α,* a master regulator of hypoxia-mediated responses, was apparently more sensitive to the changing crowding and hypoxic condition in muscle ($p < 0.1$) than in liver, being also positively correlated with the individual changes in growth within the HD fish population (Table 4; Figure 7).

In summary, an integrative approach depicting the way in which high stocking densities, accompanied by a decrease in O_2 levels, drive different adaptive features in behavior, growth, antioxidant defense and lipid metabolism has been shown. Of particular relevance are the concomitant changes in behavior, antioxidant defense and growth regulatory mechanisms, which emphasizes on the importance of adaptive stress responses from the cell to the global organism level. The challenge is to translate this new knowledge into effective measures that serve to mitigate the drawback effects of a challenging and poor predictable milieu in a context of global warming, where the fish life history can largely affect the capacity of the farmed livestock to cope with most of the envisaged production threats (see Alfonso et al., 2021). According to the revisited paradigm of epigenetic nutritional/environmental regulation, this assumes the convenience of a precise and adjusted metabolic regulation over time that avoids as much as possible excessive counter-regulatory responses (Belenguer et al., 2023). Meanwhile, the present study has contributed to prescribe new and more appropriate values of welfare indicators for a better definition of a golden stocking density in a challenging environment that mimics the crowding and hypoxic stress condition of most Mediterranean farms during the summer on-growing finishing phase.

Data availability statement

The raw data supporting the conclusion of this article will be made available by the authors, without undue reservation.

Ethics statement

The animal study was approved by the Animal Welfare Committee of the Institute of Aquaculture Torre de la Sal (IATS), CSIC Ethics Comittee (permission 1295/2022) and Generalitat Valenciana (permission 2022-VSC-PEA-0230). The study was conducted in accordance with the local legislation and institutional requirements.

Author contributions

PH: Formal Analysis, Methodology, Writing–original draft, Writing–review and editing. FN-C: Formal Analysis, Methodology, Writing–review and editing. ÁB: Methodology, Writing–review and editing. JC-G: Funding acquisition, Methodology, Writing–review and editing. JP-S: Conceptualization, Formal Analysis, Funding acquisition, Methodology, Writing–original draft, Writing–review and editing.

Funding

The author(s) declare financial support was received for the research, authorship, and/or publication of this article. This work was supported by the EU H2020 Research Innovation Program under grant agreement no. 871108 (AQUAEXCEL3.0). This output reflects only the author's view and the European Union cannot be held responsible for any use that may be made of the information contained therein. Additionally,

this study forms part of the ThinkInAzul program and was supported by MCIN with funding from European Union NextGenerationEU (PRTR-C17.I1) and by Generalitat Valenciana (THINKINAZUL/2021/024).

Acknowledgments

We acknowledge the support of Inmaculada Vicent from the Animalarium Service of IATS for her help during fish rearing and sampling. The authors are grateful to María Angeles González for her assistance on PCR analyses. They also acknowledge the effort of personnel from CSIC (Manuel Lozano, Enric Cabruja) and University of Las Palmas de Gran Canaria (Juan Manuel Afonso, Miguel Àngel Ferrer, Juan Antonio Montiel-Nelson, Javier Sosa) in the previous work of design and validation leading to the invention of the AEFishBIT device.

Conflict of interest

The authors declare that the research was conducted in the absence of any commercial or financial relationships that could be construed as a potential conflict of interest.

Publisher's note

Supplementary material

The Supplementary Material for this article can be found online at: https://www.frontiersin.org/articles/10.3389/fphys.2023.1272267/full#supplementary-material

SUPPLEMENTARY FIGURE S1
Welfare scoring images of **(A)** skin erosion, **(B)** caudal fin status, **(C)** pelvic fin status and **(D)** pectoral fin status. Numbers in parenthesis indicate the assigned welfare score.

SUPPLEMENTARY FIGURE S2
Gilthead sea bream physical activity synchronization by feeding at low density **(A)**, medium density **(B)** and high density **(C)**, and respiratory frequency synchronization by feeding at low density **(D)**, medium density **(E)** and high density **(F)**. AEFishBIT data (measures taken every 15 min along 2 consecutive days) of representative individuals (n = 8) is shown as a continuous dotted line in each panel. Best-fit curves (red sinusoidal line) derived from the cosinor analysis of physical activity and respiratory frequency are represented in the HD group. Values of mesor (M), amplitude (A), acrophase (φ) and p-value (P) of best-fit curves are shown for each density. Gray shaded areas represent dark phases. Arrow in vertical dotted line indicates the feeding time. Different letters represent significant (P < 0.05, ANOVA, Holm-Sidak test) differences between density groups.

SUPPLEMENTARY FIGURE S3
Validation plots of the PLS-DA models in Figures 5A, B **(A,B)** consisting in 500 random permutations each.

SUPPLEMENTARY TABLE S3
Pearson correlation matrix among outcomes on growth performance, skin damage, behavior, plasma stress markers and hepatic gene expression in HD fish. Upper values are the correlation coefficients and lower values are the p-values.

SUPPLEMENTARY TABLE S4
Pearson correlation matrix among outcomes on growth performance, skin damage, behavior, plasma stress markers and muscle gene expression in HD fish. Upper values are the correlation coefficients and lower values are the p-values.

References

Alfonso, S., Gesto, M., and Sadoul, B. (2021). Temperature increase and its effects on fish stress physiology in the context of global warming. *J. Fish Biol.* 98, 1496–1508. doi:10.1111/jfb.14599

Almeida, D. V., Bianchini, A., and Marins, L. F. (2013). Growth hormone overexpression generates an unfavorable phenotype in juvenile transgenic zebrafish under hypoxic conditions. *General Comp. Endocrinol.* 194, 102–109. doi:10.1016/j.ygcen.2013.08.017

Alzaid, A., Kim, J. H., Devlin, R. H., Martin, S. A., and MacQueen, D. J. (2018). Growth hormone transgenesis in coho salmon disrupts muscle immune function impacting cross-talk with growth systems. *J. Exp. Biol.* 221, jeb173146. doi:10.1242/jeb.173146

Araújo-Luna, R., Ribeiro, L., Bergheim, A., and Pousão-Ferreira, P. (2018). The impact of different rearing condition on gilthead seabream welfare: dissolved oxygen levels and stocking densities. *Aquacult. Res.* 49, 3845–3855. doi:10.1111/are.13851

Arechavala-Lopez, P., Diaz-Gil, C., Saraiva, J. L., Moranta, D., Castanheira, M. F., Nuñez-Velázquez, S., et al. (2019). Effects of structural environmental enrichment on welfare of juvenile seabream (*Sparus aurata*). *Aquac. Rep.* 15, 100224. doi:10.1016/j.aqrep.2019.100224

Arechavala-Lopez, P., Nazzaro-Alvarez, J., Jardí-Pons, A., Reig, L., Carella, F., Carrassón, M., et al. (2020). Linking stocking densities and feeding strategies with social and individual stress responses on gilthead seabream (*Sparus aurata*). *Physiol. Behav.* 213, 112723. doi:10.1016/j.physbeh.2019.112723

Ashley, P. J. (2007). Fish welfare: current issues in aquaculture. *Appl. Anim. Behav. Sci.* 104, 199–235. doi:10.1016/j.applanim.2006.09.001

Aupérin, B., Baroiller, J. F., Ricordel, M. J., Fostier, A., and Prunet, P. (1997). Effect of confinement stress on circulating levels of growth hormone and two prolactins in freshwater-adapted tilapia (*Oreochromis niloticus*). *General Comp. Endocrinol.* 108, 35–44. doi:10.1006/gcen.1997.6938

Baldwin, L. (2011). The effects of stocking density on fish welfare. *Plymouth Student Sci.* 4, 372–383.

Ballester-Lozano, G. F., Benedito-Palos, L., Estensoro, I., Sitjà-Bobadilla, A., Kaushik, S., and Pérez-Sánchez, J. (2015). Comprehensive biometric, biochemical and histopathological assessment of nutrient deficiencies in gilthead sea bream fed semi-purified diets. *Br. J. Nutr.* 114, 713–726. doi:10.1017/S0007114515002354

Belenguer, A., Naya-Català, F., Montero, D., Torrecillas, S., Soriano, B., Calduch-Giner, J., et al. (2023). *Genetics drives hepatic transcriptome and DNA methylome of farmed gilthead sea bream after broodstock nutritional programming*. Viena, Austria: Aquaculture Europe 2023 Congress.

Bermejo-Nogales, A., Benedito-Palos, L., Saera-Vila, A., Calduch-Giner, J. A., Sitjà-Bobadilla, A., and Pérez-Sánchez, J. (2008). Confinement exposure induces glucose regulated protein 75 (GRP75/mortalin/mtHsp70/PBP74/HSPA9B) in the hepatic tissue of gilthead sea bream (*Sparus aurata* L.). *Comp. Biochem. Physiology B* 149, 428–438. doi:10.1016/j.cbpb.2007.11.003

Bermejo-Nogales, A., Nederlof, M., Benedito-Palos, L., Ballester-Lozano, G. F., Folkedal, O., Olsen, R. E., et al. (2014). Metabolic and transcriptional responses of gilthead sea bream (*Sparus aurata* L.) to environmental stress: new insights in fish mitochondrial phenotyping. *General Comp. Endocrinol.* 205, 305–315. doi:10.1016/j.ygcen.2014.04.016

Bermejo-Nogales, A., Saera-Vila, A., Calduch-Giner, J. A., Navarro, J. C., Sitjà-Bobadilla, A., and Pérez-Sánchez, J. (2007). Differential metabolic and gene expression profile of juvenile common dentex (*Dentex dentex* L.) and gilthead sea bream (*Sparus aurata* L.) in relation to redox homeostasis. *Aquaculture* 267, 213–224. doi:10.1016/j.aquaculture.2007.01.024

Besson, M., Rombout, N., Salou, G., Vergnet, A., Cariou, S., Bruant, J. S., et al. (2022). Potential for genomic selection on feed efficiency in Gilthead sea bream (*Sparus aurata*), based on individual feed conversion ratio, carcass and lipid traits. *Aquac. Rep.* 24, 101132. doi:10.1016/j.aqrep.2022.101132

Bordin, D., and Freire, C. A. (2021). Remarkable variability in stress responses among subtropical coastal marine teleosts. *Mar. Biol.* 168, 122–217. doi:10.1007/s00227-021-03929-5

Calabrese, S., Nilsen, T. O., Kolarevic, J., EbbessonPedrosa, L. O. E. C., Fivelstad, S., et al. (2017). Stocking density limits for post-smolt Atlantic salmon (*Salmo salar* L.) with emphasis on production performance and welfare. *Aquaculture* 468, 363–370. doi:10.1016/j.aquaculture.2016.10.041

Calduch Giner, J., Rosell-Moll, E., Besson, M., Vergnet, A., Bruan, J.-S., Clota, F., et al. (2023). Changes in transcriptomic and behavioural traits in activity and ventilation rates associated with divergent individual feed efficiency in gilthead sea bream (*Sparus aurata*). *Aquac. Rep.* 29, 101476. doi:10.1016/j.aqrep.2023.101476

Calduch-Giner, J. A., Davey, G., Saera-Vila, A., Houeix, B., Talbot, A., Prunet, P., et al. (2010). Use of microarray technology to assess the time course of liver stress response after confinement exposure in gilthead sea bream (*Sparus aurata* L.). *BMC Genomics* 11, 193. doi:10.1186/1471-2164-11-193

Calduch-Giner, J., Holhorea, P. G., Ferrer, M. Á., Naya-Català, F., Rosell-Moll, E., Vega García, C., et al. (2022). Revising the impact and prospects of activity and ventilation rate bio-loggers for tracking welfare and fish-environment interactions in salmonids and Mediterranean farmed fish. *Front. Mar. Sci.* 9, 854888. doi:10.3389/fmars.2022.854888

Carbonara, P., Alfonso, S., Zupa, W., Manfrin, A., Fiocchi, E., Pretto, T., et al. (2019). Behavioral and physiological responses to stocking density in sea bream (*Sparus aurata*): do coping styles matter? *Physiol. Behav.* 212, 112698. doi:10.1016/j.physbeh.2019.112698

Castanheira, M. F., Cerqueira, M., Millot, S., Gonçalves, R. A., Oliveira, C. C. V., Conceição, L. E. C., et al. (2016). Are personality traits consistent in fish? The influence of social context. *Appl. Anim. Behav. Sci.* 178, 96–101. doi:10.1016/j.applanim.2016.02.004

Challet, E. (2019). The circadian regulation of food intake. *Nat. Rev. Endocrinol.* 15, 393–405. doi:10.1038/s41574-019-0210-x

Cherkas, A., Holota, S., Mdzinarashvili, T., Gabbianelli, R., and Zarkovic, N. (2020). Glucose as a major antioxidant: when, what for, and why it fails? *Antioxidants* 9, 140. doi:10.3390/antiox9020140

Chiang, J. Y., and Ferrell, J. M. (2020). Up to date on cholesterol 7 alpha-hydroxylase (CYP7A1) in bile acid synthesis. *Liver Res.* 4, 47–63. doi:10.1016/j.livres.2020.05.001

Dhamad, A. E., Greene, E., Sales, M., Nguyen, P., Beer, L., Liyanage, R., et al. (2020). 75-kDa glucose-regulated protein (GRP75) is a novel molecular signature for heat stress response in avian species. *Am. J. Physiology-Cell Physiology* 318, C289–C303. doi:10.1152/ajpcell.00334.2019

Ellis, T., North, B., Scott, A. P., Bromage, N. R., Porter, M., and Gadd, D. (2002). The relationships between stocking density and welfare in farmed rainbow trout. *J. Fish. Biol.* 61, 493–531. doi:10.1111/j.1095-8649.2002.tb00893.x

Fanouraki, E., Mylonas, C. C., Papandroulakis, N., and Pavlidis, M. (2011). Species specificity in the magnitude and duration of the acute stress response in Mediterranean marine fish in culture. *General Comp. Endocrinol.* 173, 313–322. doi:10.1016/j.ygcen.2011.06.004

FAO (2020). *The state of world fisheries and aquaculture 2020. Sustainability in action*. Rome: Food and Agriculture Organization of the United Nations.

FAO (2022). *The state of world fisheries and aquaculture 2022. Towards Blue Transformation*. Rome: Food and Agriculture Organization of the United Nations. doi:10.4060/cc0461en

Ferrer, M. A., Calduch-Giner, J. A., Díaz, M., Sosa, J., Rosell-Moll, E., Santana Abril, J., et al. (2020). From operculum and body tail movements to different coupling of physical activity and respiratory frequency in farmed gilthead sea bream and European sea bass. Insights on aquaculture biosensing. *Comput. Electron. Agric.* 175, 105531. doi:10.1016/j.compag.2020.105531

Franklin, J. L., Amsler, M. O., and Messina, J. L. (2022). Regulation of glucose responsive protein (GRP) gene expression by insulin. *Cell Stress Chaperones* 27, 27–35. doi:10.1007/s12192-021-01243-z

Goldan, O., Popper, D., and Karplus, I. (2003). Food competition in small groups of juvenile gilthead seabream (*Sparus aurata*). *Isr. J. Aquac. Bamidgeh* 55, 94–106. doi:10.46989/001c.20340

Guo, Y., Balasubramanian, B., Zhao, Z. H., and Liu, W. C. (2021). Heat stress alters serum lipid metabolism of Chinese indigenous broiler chickens-a lipidomics study. *Environ. Sci. Pollut. Res.* 28, 10707–10717. doi:10.1007/s11356-020-11348-0

Hamilton, C. J., Arbach, M., and Groom, M. (2014). "Beyond glutathione: different low molecular weight thiols as mediators of redox regulation and other metabolic functions in lower organisms," in *Recent advances in redox active plant and microbial products*. Editors C. Jacob, G. Kirsch, A. Slusarenko, P. Winyard, and P. Burkholz (Dordrecht, Netherlands: Springer). doi:10.1007/978-94-017-8953-0_11

Hoyle, I., Oidtmann, B., Ellis, T., Turnbull, J., North, B., Nikolaidis, J., et al. (2007). A validated macroscopic key to assess fin damage in farmed rainbow trout (*Oncorhynchus mykiss*). *Aquaculture* 270, 142–148. doi:10.1016/j.aquaculture.2007.03.037

Jia, R., Liu, B. L., Feng, W. R., Han, C., Huang, B., and Lei, J. L. (2016). Stress and immune responses in skin of turbot (*Scophthalmus maximus*) under different stocking densities. *Fish Shellfish Immunol.* 55, 131–139. doi:10.1016/j.fsi.2016.05.032

Kajimura, S., Aida, K., and Duan, C. (2005). Insulin-like growth factor-binding protein-1 (IGFBP-1) mediates hypoxia-induced embryonic growth and developmental retardation. *Proc. Natl. Acad. Sci.* 102, 1240–1245. doi:10.1073/pnas.0407443102

Kieffer, D. A., Piccolo, B. D., Vaziri, N. D., Liu, S., Lau, W. L., Khazaeli, M., et al. (2016). Resistant starch alters gut microbiome and metabolomic profiles concurrent with amelioration of chronic kidney disease in rats. *Am. J. Physiol. Ren. Physiol.* 310, F857–F871. doi:10.1152/ajprenal.00513.2015

Kolarevic, J., Calduch-Giner, J., Espmark, Å. M., Evensen, T., Sosa, J., and Pérez-Sánchez, J. (2021). A novel miniaturized biosensor for monitoring Atlantic salmon swimming activity and respiratory frequency. *Animals* 11, 2403. doi:10.3390/ani11082403

Lan, R., Wang, Y., Wei, L., Wu, F., and Yin, F. (2022). Heat stress exposure changed liver lipid metabolism and abdominal fat deposition in broilers. *Italian J. Animal Sci.* 21, 1326–1333. doi:10.1080/1828051X.2022.2103461

Li, H., Ma, M.-L., Luo, S., Zhang, R.-M., Han, P., and Hu, W. (2012). Metabolic responses to ethanol in *Saccharomyces cerevisiae* using a gas chromatography tandem mass spectrometry-based metabolomics approach. *Int. J. Biochem. Cell Biol.* 44, 1087–1096. doi:10.1016/j.biocel.2012.03.017

Liu, B., Liu, Y., and Sun, G. (2017). Effects of stocking density on growth performance and welfare-related physiological parameters of Atlantic salmon *Salmo salar* L. recirculating aquaculture system. *Aquac. Res.* 48, 2133–2144. doi:10.1111/are.13050

Livak, K. J., and Schmittgen, T. D. (2001). Analysis of relative gene expression data using real-time quantitative PCR and the 2(-delta delta CT) method. *Methods* 25, 402–408. doi:10.1006/meth.2001.1262

Magnoni, L. J., Martos-Sitcha, J. A., Queiroz, A., Calduch-Giner, J. A., Magalhàes Gonçalves, J. F., Rocha, C. M. R., et al. (2017). Dietary supplementation of heat-treated *Gracillaria* and *Ulva* seaweeds enhanced acute hypoxia tolerance in gilthead seabream (*Sparus aurata*). *Biol. Open* 6, 897–908. doi:10.1242/bio.024299

Malandrakis, E. E., Exadactylos, A., Dadali, O., Golomazou, E., Klaoudatos, S., Panagiotaki, P., et al. (2014). Molecular cloning of four glutathione peroxidase (GPx) homologs and expression analysis during stress exposure of the marine teleost *Sparus aurata*. *Comp. Biochem. Physiology Part B* 168, 53–61. doi:10.1016/j.cbpb.2013.11.005

Martos-Sitcha, J. A., Simó-Mirabet, P., de las Heras, V., Calduch-Giner, J. A., and Pérez-Sánchez, J. (2019a). Tissue-specific orchestration of gilthead sea bream resilience to hypoxia and high stocking density. *Front. Physiology* 10, 840. doi:10.3389/fphys.2019.00840

Martos-Sitcha, J. A., Simó-Mirabet, P., Piazzon, M. C., de las Heras, V., Calduch-Giner, J. A., Puyalto, M., et al. (2018). Dietary sodium heptanoate helps to improve feed efficiency, growth hormone status and swimming performance in gilthead sea bream (*Sparus aurata*). *Aquac. Nutr.* 24, 1638–1651. doi:10.1111/anu.12799

Martos-Sitcha, J. A., Sosa, J., Ramos-Valido, D., Bravo, F. J., Carmona-Duarte, C., Gomes, H. L., et al. (2019b). Ultra-low power sensor devices for monitoring physical activity and respiratory frequency in farmed fish. *Front. Physiology* 10, 667. doi:10.3389/fphys.2019.00667

Maulu, S., Hasimuna, O. J., Haambiya, L. H., Monde, C., Musuka, C. G., Makorwa, T. H., et al. (2021). Climate change effects on aquaculture production: sustainability implications, mitigation, and adaptations. *Front. Sustain. Food Syst.* 5, 609097. doi:10.3389/fsufs.2021.609097

McKenzie, D. J., Martinez, R., Morales, A., Acosta, J., Morales, R., Taylor, E. W., et al. (2003). Effects of growth hormone transgenesis on metabolic rate, exercise performance and hypoxia tolerance in tilapia hybrids. *J. Fish Biol.* 63, 398–409. doi:10.1046/j.1095-8649.2003.00162.x

Miron, N., and Tirosh, O. (2019). Cholesterol prevents hypoxia-induced hypoglycemia by regulation of a metabolic ketogenic shift. *Oxidative Med. Cell. Longev.* 2019, 5829357. doi:10.1155/2019/5829357

Mistlberger, R. E. (2011). Neurobiology of food anticipatory circadian rhythms. *Physiology Behav.* 104, 535–545. doi:10.1016/j.physbeh.2011.04.015

Mommsen, T. P., Vijayan, M. M., and Moon, T. W. (1999). Cortisol in teleosts: dynamics, mechanisms of action, and metabolic regulation. *Rev. Fish Biol. Fish.* 9, 211–268. doi:10.1023/A:1008924418720

Montero, D., Lalumera, G., Izquierdo, M. S., Caballero, M. J., Saroglia, M., and Tort, L. (2009). Establishment of dominance relationships in gilthead sea bream *Sparus aurata* juveniles during feeding: effects on feeding behaviour, feed utilization and fish health. *J. Fish. Biol.* 74, 790–805. doi:10.1111/j.1095-8649.2008.02161.x

Naya-Català, F., Simó-Mirabet, P., Calduch-Giner, J., and Pérez-Sánchez, J. (2021). Transcriptomic profiling of Gh/Igf system reveals a prompted tissue-specific differentiation and novel hypoxia responsive genes in gilthead sea bream. *Sci. Rep.* 11, 16466. doi:10.1038/s41598-021-95408-6

Noble, C., Gismervik, K., Iversen, M. H., Kolarevic, J., Nilsson, J., Stien, L. H., et al. (2018). *Welfare indicators for farmed atlantic salmon: tools for assessing fish welfare*. Tromsø, Norway: Nofima.

Noble, C., Gismervik, K., Iversen, M. H., Kolarevic, J., Nilsson, J., Stien, L. H., et al. (2020). *Welfare indicators for farmed rainbow trout: tools for assessing fish welfare*. Tromsø, Norway: Nofima.

North, B. P., Turnbull, J. F., Ellis, T., Porter, M. J., Migaud, H., Bron, J., et al. (2006). The impact of stocking density on the welfare of rainbow trout (*Oncorhynchus mykiss*). *Aquaculture* 255, 466–479. doi:10.1016/j.aquaculture.2006.01.004

Oikonomidou, E., Batzina, A., and Karakatsouli, N. (2019). Effects of food quantity and distribution on aggressive behaviour of gilthead seabream and European seabass. *Appl. Anim. Behav. Sci.* 213, 124–130. doi:10.1016/j.applanim.2019.02.010

Ojala, M., and Garriga, G. C. (2010). Permutation tests for studying classifier performance. *J. Mach. Learn. Res.* 11, 1833–1863. doi:10.5555/1756006.1859913

Oppedal, F., Vågseth, T., Dempster, T., Juell, J.-E., and Johansson, D. (2011). Fluctuating sea-cage environments modify the effects of stocking densities on production and welfare parameters of Atlantic salmon (*Salmo salar* L.). *Aquaculture* 315, 361–368. doi:10.1016/j.aquaculture.2011.02.037

Othman, R., Wang, H. P., Elabd, H., Xie, D. K., Yao, H., O'Bryant, P., et al. (2022). The effect of density on sex differentiation, sexual dimorphism, stress, and related gene expression in yellow perch. *Plos ONE* 17, e0267904. doi:10.1371/journal.pone.0267904

Parma, L., Pelusio, N. F., Gisbert, E., Esteban, M. A., D'Amico, F., Soverini, M., et al. (2020). Effects of rearing density on growth, digestive conditions, welfare indicators and gut bacterial community of gilthead sea bream (*Sparus aurata*, L. 1758) fed different fishmeal and fish oil dietary levels. *Aquaculture* 518, 734854. doi:10.1016/j.aquaculture.2019.734854

Perelló-Amorós, M., García-Pérez, I., Sánchez-Moya, A., Innamorati, A., Vélez, E. J., Achaerandio, I., et al. (2021). Diet and exercise modulate GH-IGFs axis, proteolytic markers and myogenic regulatory factors in juveniles of gilthead sea bream (*Sparus aurata*). *Animals* 11, 2182. doi:10.3390/ani11082182

Perera, E., Rosell-Moll, E., Martos-Sitcha, J. A., Naya-Català, F., Simó-Mirabet, P., Calduch-Giner, J. A., et al. (2021). Physiological trade-offs associated with fasting weight loss, resistance to exercise and behavioral traits in farmed gilthead sea bream (*Sparus aurata*) selected by growth. *Aquac. Rep.* 20, 100645. doi:10.1016/j.aqrep.2021.100645

Pérez-Sánchez, J., Borrel, M., Bermejo-Nogales, A., Benedito-Palos, L., Saera-Vila, A., Calduch-Giner, J. A., et al. (2013). Dietary oils mediate cortisol kinetics and the hepatic expression profile of stress responsive genes in juveniles of gilthead sea bream (*Sparus aurata*) exposed to crowding stress. *Comp. Biochem. Physiology* 8, 123–130. doi:10.1016/j.cbd.2013.02.001

Pérez-Sánchez, J., Simó-Mirabet, P., Naya-Català, F., Martos-Sitcha, J. A., Perera, E., Bermejo-Nogales, A., et al. (2018). Somatotropic axis regulation unravels the differential effects of nutritional and environmental factors in growth performance of marine farmed fishes. *Front. Endocrinol.* 9, 687. doi:10.3389/fendo.2018.00687

Person-Le Ruyet, J., and Le Bayon, N. (2009). Effects of temperature, stocking density and farming conditions on fin damage in European sea bass (*Dicentrarchus labrax*). *Aquat. Living Resour.* 22, 349–362. doi:10.1051/alr/2009047

Rahman, M. T., Haque, N., Abu Kasim, N. H., and De Ley, M. (2017). Origin, function, and fate of metallothionein in human blood. *Rev. Physiology, Biochem. Pharmacol.* 173, 41–62. doi:10.1007/112_2017_1

Ralser, M., Wamelink, M. M. C., Kowald, A., Gerisch, B., Heeren, G., Struys, E. A., et al. (2007). Dynamic rerouting of the carbohydrate flux is key to counteracting oxidative stress. *J. Biol.* 6, 10. doi:10.1186/jbiol61

Refinetti, R., Cornélissen, G., and Halberg, F. (2007). Procedures for numerical analysis of circadian rhythms. *Biol. Rhythm Res.* 38, 275–325. doi:10.1080/09291010600903692

Remen, M., Nederlof, M. A. J., Folkedal, O., Thorsheim, G., Sitjà-Bobadilla, A., Pérez-Sánchez, J., et al. (2015). Effect of temperature on the metabolism, behavior and oxygen requirements of *Sparus aurata*. *Aquacult. Env. Interac.* 7, 115–123. doi:10.3354/aei00141

Remen, M., Sievers, M., Torgersen, T., and Oppedal, F. (2016). The oxygen threshold for maximal feed intake of Atlantic salmon post-smolts is highly temperature-dependent. *Aquaculture* 464, 582–592. doi:10.1016/j.aquaculture.2016.07.037

Rey, S., Jin, X., Damsgård, B., Bégout, M. L., and Mackenzie, S. (2021). Analysis across diverse fish species highlights no conserved transcriptome signature for proactive behaviour. *BMC Genomics* 22, 33. doi:10.1186/s12864-020-07317-z

Rosell-Moll, E., Piazzon, M. C., Sosa, J., Ferrer, M. A., Cabruja, E., Vega, A., et al. (2021). Use of accelerometer technology for individual tracking of activity patterns, metabolic rates and welfare in farmed gilthead sea bream (*Sparus aurata*) facing a wide range of stressors. *Aquaculture* 539, 736609. doi:10.1016/j.aquaculture.2021.736609

Rosenfeld, J., Van Leeuwen, T., Richards, J., and Allen, D. (2015). Relationship between growth and standard metabolic rate: measurement artefacts and implications for habitat use and life-history adaptation in salmonids. *J. Animal Ecol.* 84, 4–20. doi:10.1111/1365-2656.12260

Sadoul, B., and Geffroy, B. (2019). Measuring cortisol, the major stress hormone in fishes. *J. Fish Biol.* 94, 540–555. doi:10.1111/jfb.13904

Saera-Vila, A., Calduch-Giner, J. A., Prunet, P., and Pérez-Sánchez, J. (2009). Dynamics of liver GH/IGF axis and selected stress markers in juvenile gilthead sea bream (*Sparus aurata*) exposed to acute confinement. Differential stress response of growth hormone receptors. *Comp. Biochem. Physiology, Part A* 154, 197–203. doi:10.1016/j.cbpa.2009.06.004

Sánchez-Muros, M. J., Villacreces, S., Miranda-de la Lama, G., de Haro, C., and García-Barroso, F. (2013). Effects of chemical and handling exposure on fatty acids, oxidative stress and morphological welfare indicators in gilthead sea bream (*Sparus aurata*). *Fish. Physiol. Biochem.* 39, 581–591. doi:10.1007/s10695-012-9721-2

Santos, G. A., Schrama, J. W., Mamauag, R. E. P., Rombout, J. H. W. M., and Verreth, J. A. J. (2010). Chronic stress impairs performance, energy metabolism and welfare indicators in European seabass (*Dicentrarchus labrax*): the combine effects of fish crowding and water quality deterioration. *Aquaculture* 299, 73–80. doi:10.1016/j.aquaculture.2009.11.018

Sapolsky, R. M., Romero, L. M., and Munck, A. U. (2000). How do glucocorticoids influence stress response? Integrative, permissive, suppressive, stimulatory, and preparative actions. *Endocr. Rev.* 21, 55–89. doi:10.1210/edrv.21.1.0389

Saraiva, J. L., Arechavala-Lopez, P., and Sneddon, L. (2022). "Farming fish," in *Routledge handbook of animal welfare*. Editors A. Knight, C. Phillips, and P. Sparks (Abingdon, UK: Routledge), 115–127. doi:10.4324/9781003182351-12

Saravanan, S., Geurden, I., Figueiredo-Silva, A. C., Kaushik, S. J., Haidar, M. N., Verreth, J. A., et al. (2012). Control of voluntary feed intake in fish: a role for dietary oxygen demand in nile tilapia (*Oreochromis niloticus*) fed diets with different macronutrient profiles. *Br. J. Nutr.* 108, 1519–1529. doi:10.1017/S0007114511006842

Seibel, H., Baßmann, B., and Rebl, A. (2021). Blood will tell: what hematological analyses can reveal about fish welfare. *Front. Vet. Sci.* 8, 616955. doi:10.3389/fvets.2021.616955

Sibly, R. M., Baker, J., Grady, J. M., Luna, L. M., Kodric-Vrown, A., Venditti, C., et al. (2015). Fundamental insights into ontogenetic growth from theory and fish. *Proc. Natl. Acad. Sci. U. S. A.* 112, 13934–13939. doi:10.1073/pnas.1518823112

Simó-Mirabet, P., Bermejo-Nogales, A., Calduch-Giner, J. A., and Pérez-Sánchez, J. (2017). Sirtuin energy-sensing at the molecular level. Tissue-specific gene expression and fasting regulation of sirtuin family in gilthead sea bream (*Sparus aurata*). *J. Comp. Physiology* 187, 153–163. doi:10.1007/s00360-016-1014-0

Simó-Mirabet, P., Perera, E., Calduch-Giner, J. A., Afonso, J. M., and Pérez-Sánchez, J. (2018). Co-expression analysis of sirtuins and related metabolic biomarkers in juveniles of gilthead sea bream (*Sparus aurata*) with differences in growth performance. *Front. Physiology* 9, 608. doi:10.3389/fphys.2018.00608

Simó-Mirabet, P., Perera, E., Calduch-Giner, J. A., and Pérez-Sánchez, J. (2020). Local DNA methylation helps to regulate muscle sirtuin 1 gene expression across season and advancing age in gilthead sea bream (*Sparus aurata*). *Front. Zoology* 17, 15. doi:10.1186/s12983-020-00361-1

Stincone, A., Prigione, A., Cramer, T., Wamelink, M. M. C., Campbell, K., Cheung, E., et al. (2015). The return of metabolism: biochemistry and physiology of the pentose phosphate pathway. *Biol. Rev.* 90, 927–963. doi:10.1111/brv.12140

Sveen, L. R., Timmerhaus, G., Krasnov, A., Takle, H., Stefansson, S. O., Handeland, S. O., et al. (2018). High fish density delays wound healing in Atlantic salmon (*Salmo salar*). *Sci. Rep.* 8, 16907. doi:10.1038/s41598-018-35002-5

Tanaka, K., Jay, G., and Isselbacher, K. J. (1988). Expression of heat-shock and glucose-regulated genes: differential effects of glucose starvation and hypertonicity. *Biochim. Biophys. Acta* 950, 138–146. doi:10.1016/0167-4781(88)90006-1

Thévenot, E. A., Roux, A., Xu, Y., Ezan, E., and Junot, C. (2015). Analysis of the human adult urinary metabolome variations with age, body mass index, and gender by implementing a comprehensive workflow for univariate and OPLS statistical analyses. *J. Proteome Res.* 14, 3322–3335. doi:10.1021/acs.jproteome.5b00354

Toni, M., Manciocco, A., Angiulli, E., Alleva, E., Cioni, C., and Malavasi, S. (2019). Review: assessing fish welfare in research and aquaculture, with a focus on European directives. *Animal* 13, 161–170. doi:10.1017/S1751731118000940

van de Nieuwegiessen, P. G., Olwo, J., Khong, S., Verreth, J. A., and Schrama, J. W. (2009). Effects of age and stocking density on the welfare of African catfish, *Clarias gariepinus* Burchell. *Aquaculture* 288, 69–75. doi:10.1016/j.aquaculture.2008.11.009

van de Vis, H., Kolarevic, J., Stien, L. H., Kristiansen, T. S., Gerritzen, M., van de Braak, K., et al. (2020). "Welfare of farmed fish in different production systems and operations," in *The welfare of fish*. Editors T. S. Kristiansen, A. Fernö, M. A. Pavlidis, and H. van de Vis (Cham, Switzerland: Springer), 323–332. doi:10.1007/978-3-030-41675-1_14

Van der Zee, E. A., Havekes, R., Barf, R. P., Hut, R. A., Nijholt, I. M., Jacobs, E. H., et al. (2008). Circadian time-place learning in mice depends on Cry genes. *Curr. Biol.* 18, 844–848. doi:10.1016/j.cub.2008.04.077

VanHelder, W., Casey, K., and Radomski, M. W. (1987). Regulation of growth hormone during exercise by oxygen demand and availability. *Eur. J. Appl. Physiology Occup. Physiology* 56, 628–632. doi:10.1007/BF00424801

Vercauteren, M., Ampe, B., Devriese, L., Moons, C. P. H., Decostere, A., Aerts, J., et al. (2022). Explorative study on scale cortisol accumulation in wild caught common dab (*Limanda limanda*). *BMC Veterinary Res.* 18, 324. doi:10.1186/s12917-022-03385-3

Weirup, L., Schulz, C., Seibel, H., and Aerts, J. (2021). Scale cortisol is positively correlated to fin injuries in rainbow trout (*Oncorhynchus mykiss*) reared in commercial flow through systems. *Aquaculture* 543, 736924. doi:10.1016/j.aquaculture.2021.736924

Weirup, L., Schulz, C., and Seibel, H. (2022). Fish welfare evaluation index (fWEI) based on external morphological damage for rainbow trout (*Oncorhynchus mykiss*) in flow through systems. *Aquaculture* 556, 738270. doi:10.1016/j.aquaculture.2022.738270

Wilkinson, R. J., Porter, M., Woolcott, H., Longland, R., and Carragher, J. F. (2006). Effects of aquaculture related stressors and nutritional restriction on circulating growth factors (GH, IGF-I and IGF-II) in Atlantic salmon and rainbow trout. *Comp. Biochem. Physiology Part A* 145, 214–224. doi:10.1016/j.cbpa.2006.06.010

Wu, F., Wen, H., Tian, J., Jiang, M., Liu, W., Yang, C., et al. (2018). Effect of stocking density on growth performance, serum biochemical parameters, and muscle texture properties of genetically improved farm tilapia, *Oreochromis niloticus*. *Aquac. Int.* 26, 1247–1259. doi:10.1007/s10499-018-0281-z

frontiers | Frontiers in Physiology

TYPE Original Research
PUBLISHED 06 October 2023
DOI 10.3389/fphys.2023.1282900

OPEN ACCESS

EDITED BY
Yiming Li,
Fishery Machinery and Instrument Research Institute, China

REVIEWED BY
Kaida Xu,
Marine Fisheries Research Institute of Zhejiang, China
Kai Liao,
Ningbo University, China

*CORRESPONDENCE
Pengzhi Qi,
qipengzhi@zjou.edu.cn,
qpz2004@vip.sina.com

RECEIVED 25 August 2023
ACCEPTED 25 September 2023
PUBLISHED 06 October 2023

CITATION
Qiu L, Chen X, Zhu L, Yao R and Qi P (2023), ChIP-seq identifies *McSLC35E2* as a novel target gene of *Mc*Nrf2 in *Mytilus coruscus*, highlighting its role in the regulation of oxidative stress response in marine mollusks.
Front. Physiol. 14:1282900.
doi: 10.3389/fphys.2023.1282900

ChIP-seq identifies *McSLC35E2* as a novel target gene of *Mc*Nrf2 in *Mytilus coruscus*, highlighting its role in the regulation of oxidative stress response in marine mollusks

Longmei Qiu, Xinglu Chen, Li Zhu, Ronghui Yao and Pengzhi Qi*

National Engineering Research Center of Marine Facilities Aquaculture, Marine Science and Technology College, Zhejiang Ocean University, Zhoushan, Zhejiang, China

NF-E2-related factor 2 (Nrf2) plays a crucial role in the oxidative regulatory process, which could trigger hundreds of antioxidant elements to confront xenobiotics. In the previous study, we identified Nrf2 from the marine mussel *Mytilus coruscus*, and the findings demonstrated that *Mc*Nrf2 effectively protected the mussels against oxidative stress induced by benzopyrene (Bap). In order to delve deeper into the underlying mechanism, we utilized Chromatin Immunoprecipitation followed by sequencing (ChIP-seq) technology to systematically identify potential novel target genes of *Mc*Nrf2. A total of 3,465 potential target genes were screened, of which 219 owned binding sites located within the promoter region. During subsequent experimental verification, it was found that *Mc*SLC35E2, a candidate target gene of *Mc*Nrf2, exhibited negative regulation by *Mc*Nrf2, as confirmed through dual luciferase and qRT-PCR detection. Further, the enzyme activity tests demonstrated that *Mc*Nrf2 could counteract Bap induced oxidative stress by inhibiting *Mc*SLC35E2. The current study provides valuable insights into the application of ChIP-seq technology in the research of marine mollusks, advancing our understanding of the key role of Nrf2 in antioxidant defense mechanisms, and highlighting the significance of SLC35E2 in the highly sophisticated regulation of oxidative stress response in marine invertebrates.

KEYWORDS

marine mussels, Nrf2, ChIP-seq, SLC35E2, oxidative stress

1 Introduction

In recent years, the thick shell mussel *Mytilus coruscus* has gradually developed into a model organism for studying marine invertebrates responses to environmental changes, including natural influences such as temperature rise and acidification, as well as environmental pollution from organic and inorganic substances (Zhao et al., 2020; Dong et al., 2023; Wang et al., 2023). Our research focuses on the molecular-level responses of *M. coruscus* to polycyclic aromatic hydrocarbons (PAHs) pollution, particularly on its member benzo(a)pyrene (Bap). Bap has been proven to cause severe harm to marine organisms, including immune system disruption, metabolic

inhibition, induction of mutagenic reactions, and tissue damage (Xiu et al., 2014; Kim et al., 2017). To adapt and resist stress, the cellular organisms activate a multi-layered defense system that is closely associated with various cellular processes, with transcription regulation being one of the most crucial components of this integrated system (Hirotsu et al., 2012). NF-E2-related factor 2 (Nrf2), identified as a fundamental leucine zipper nuclear transcription factor, holds a central position in cellular reactions to diverse environmental contaminants (Shaw et al., 2020). The primary function of Nrf2 involves overseeing the expression of numerous antioxidant genes, consequently enabling the activation of the Nrf2 signaling pathway to proficiently govern cellular antioxidant and detoxification reactions (Liu et al., 2021). Nrf2 is also believed to be involved in host defense during the antimicrobial immune response (Wang et al., 2021c). Furthermore, there is increasing evidence suggesting that Nrf2 exerts significant effects on lipid, carbohydrate, and amino acid metabolism (Hayes and Dinkova-Kostova, 2014). These characteristics contributes to its ability to efficiently coordinate different forms of stress responses (Zago et al., 2021). In our previous study, *Mc*Nrf2 was identified from *M. coruscus*, and the experimental results unequivocally demonstrated that *Mc*Nrf2 efficiently plays a pivotal role in protecting the mussels from oxidative stress induced by Bap (Qi and Tang, 2020). Thereafter, the transcriptional regulation mechanism of *Mc*Nrf2 against Bap oxidation is the focus of our next research.

Understanding transcriptional regulation is essential to comprehending the gene regulatory networks behind various cellular pathways and processes. Accurate mapping of transcription factor binding sites (TFBS) on a genome-wide scale can provide invaluable insights into gene regulation. Protein-DNA interactions are key to this mapping process and an extensive genome-wide map of interaction data is necessary to build meaningful models of TFBS (Farnham, 2009). Chromatin immunoprecipitation (ChIP) is a widely used technique to investigate the mechanisms of protein-DNA binding in living cells. This technique uses antibodies to isolate specific proteins or nucleosomes, thereby enriching for DNA fragments bound to them. ChIP is a powerful tool for probing protein-DNA interactions as it allows to accurately pinpoint gene regulatory regions and quantify their respective activities (Solomon et al., 1988). NGS (next-generation sequencing) has rapidly revolutionized the landscape of available genomic assays, transforming them into powerful and versatile tools (Shendure and Ji, 2008). Chromatin immunoprecipitation followed by sequencing (ChIP–seq) was one of the typical applications of NGS. In ChIP-seq, the DNA segments of interest are sequenced directly, rather than hybridized on an array, thus providing greater coverage, higher resolution, and greater dynamic range, ultimately producing better data (Park, 2009). Johnson et al. (2007) demonstrated that ChIP-seq could improves the sensitivity and specificity of genome-wide localization of transcription factor binding sites. Despite the extensive and mature application of ChIP-seq in higher organisms such as human beings, its application in lower eukaryotes is still very rare. Thus far, only a few research groups have made attempts to incorporate this technology into studies involving marine mollusks. Li et al. (2022) employed ChIP-seq to analyse the genes regulated by Heat shock transcription factor 1 (HSF1) in the Pacific oyster *Crassostrea gigas*, and found a number of Heat shock protein (HSP) genes bind to HSF1. This research unveiling the application of ChIP-seq technology in marine mollusks.

In the present study, we employed ChIP-seq assay to comprehensively screen for potential novel target genes of *Mc*Nrf2, followed by subsequent experimental validation. We revealed for the first time that solute carrier family 35 member E2 (SLC35E2) functions as a target gene for *Mc*Nrf2, which is demonstrated by the binding of *Mc*Nrf2 to the promoter region of *Mc*SLC35E2. Subsequent dual-luciferase and qRT-PCR assays further confirmed this fact. Further, the enzyme activity tests determined that *Mc*Nrf2 could target *Mc*SLC35E2 to antagonize Bap induced oxidative stress. The current study provides valuable insights into the application of ChIP-seq technology in the research of marine mollusks. Moreover, the research findings have advanced our understanding of the key role of Nrf2 in antioxidant defense mechanisms and highlights the significance of SLC35E2 in the highly sophisticated regulation of oxidative stress response in marine invertebrates.

2 Materials and methods

2.1 Experimental materials

A total of 200 healthy *M. coruscus* mussels were obtained from Donghe Market, Zhoushan City, Zhejiang Province. These mussels were acclimated in a tank at a temperature of 20°C for 1 week. The seawater used had a salinity of 30% ± 1% and a pH of 8.0 ± 0.3. The seawater was renewed every 2 days, and the mussels were fed with Spirulina powder on a daily basis.

2.2 ChIP sample preparation

The digestive gland cells of mussels were extracted and 20 mL formaldehyde fixative was added to make the final concentration 1%. After incubation at room temperature on a 100 × *g* for 10 min, the cells were added 10 mL of glycine termination solution with a 5 min centrifugation at 300 × *g*, 4°C. The cells were then washed twice with phosphate buffer containing 1 mM PMSF to remove any remaining formaldehyde. After washing, 1 mL of lysis buffer was added, lysed on ice for 30 min, followed by a cells collection by centrifugation at 5,000 × *g*, 4°C for 10 min. Next, 350 μL of pre-warmed digestion buffer was added, and the mixture was incubated at 37°C for 5 min. The cut chromatin was separated, and 10 μL of input DNA was labeled and kept as a control for ChIP samples. The ChIP reaction system was prepared and then incubated overnight at 4°C on a rotating shaker. Subsequently, the magnetic beads were washed, and the chromatin was eluted. Uncross linking and proteinase K treatment were performed afterward. Finally, the resulting DNA was purified, and the detailed steps were described in the Magnetic Chromatin Immunoprecipitation Kit (Active Motif, CA, United States).

2.3 Illumina sequencing

ChIP-seq libraries were generated following the Illumina ChIP-seq library construction protocol. The chip DNA was fragmented into fragments of approximately 200 bp in length. These DNA fragments then underwent end repair and A-tailing processes. Subsequently, adaptor ligation was performed to attach sequencing adaptors to the DNA fragments. To ensure high-quality libraries, the quality assessment of DNA library products was conducted using the Agilent 2200 TapeStation (Agilent Technologies, United States) and Qubit (Thermo Fisher Scientific, United States). Subsequently, the libraries were subjected to pair-end 150 bp sequencing on the Illumina platform (Illumina, NovaSeq 6000, United States) at Ribobio Co., Ltd. (Ribobio, China).

2.4 ChIP-seq data analyses

The raw fastq sequences were processed using Trimmomatic tools (v0.36) with the following options: TRAILING: 20, SLIDINGWINDOW: 4:15, MINLEN: 52. This process was performed to eliminate trailing sequences with a phred quality score below 20 and to obtain uniform sequence lengths for subsequent clustering procedures (Bolger et al., 2014). The genome alignment, based on the UCSC Genome Browser version, was conducted using bowtie2 (version: 2.5.1) to obtain unique mapping reads, aligning them to the *M. coruscus* genome (unpublished) (Langmead and Salzberg, 2012). Subsequently, MACS3 (version 3.0.0a7) was utilized for peak calling, with the corresponding input sample serving as the control for the analysis (Zhang et al., 2008). Then using Hommer (version:4.11.1) to annotate the peaks. The nucleotides in peaks region were used for detection of the consensus m6A motif by DREME (version: 5.5.1) and MEME (version: 5.5.1) (Heinz et al., 2010). Motif central enrichment was performed by CentriMo (version: 5.5.1) (Ma et al., 2014). Kyoto Encyclopedia of Genes and Genomes (KEGG) pathway enrichment analysis was performed using KOBAS3.0/ the "clusterProfiler" package in R Bioconductor. The enriched results were restricted to KEGG pathway terms. The KEGG pathway terms with adjusted $p < 0.05$ were considered to be significant.

2.5 Validation of target genes by a dual luciferase assay

To validate the relationship between *Mc*Nrf2 with a candidate target gene *McSLC35E2*, dual luciferase assays were performed using the Dual-Glo® Luciferase Assay System (Promega, Madison, WI, United States). The experimental procedure followed the instructions provided by the manufacturer. The ChIP-seq data revealed the enrichment of the potential binding site, i.e., the region of the SLC35E2 promoter where Nrf2 is capable of binding. The region approximately 1 kb upstream of the *SLC35E2* gene was cloned into the pGL3-control luciferase reporter plasmid. Additionally, the *Nrf2* fragment was cloned for insertion into the pcDNA3.1 plasmid. After cloning, the recombinant plasmids were transfected into the recipient cells, and subsequent extraction was carried out for sequencing verification. Plasmids that underwent successful sequencing were co-transfected into cells. Then, the activity of the reporter gene was assessed using the Dual-Luciferase Reporter Assay System. The fluorescence signals for both Firefly and Renilla luciferase were captured using the Varioskan Flash Multimode Reader from Thermo Fisher Scientific (Waltham, MA, United States). The recorded fluorescence values for each experimental group were then utilized to evaluate the regulatory effect of Nrf2.

2.6 Determination of expression patterns by qRT-PCR

After 1 week of individual domestication, SFN (Sulforaphane), ML385 (N-[4-[2,3-Dihydro-1-(2-methylbenzoyl)-1H-indol-5-yl]-5-methyl-2-thiazolyl]-1,3-benzodioxole-5-acetamide), and PBS were administered via injection. Digestive gland tissues of *M. coruscus* were collected at 24 h. Three individuals were selected from each group for sampling. Total RNA was extracted using the RNA extraction kit from Solarbio (Beijing, China), followed by a reverse transcription using cDNA synthesis kit (Solarbio, Beijing, China). The housekeeping gene β-actin was employed as a control gene in our study. The qRT-PCR was conducted utilizing the SYBR Green Real-Time PCR Mix (Takara, Nanjing, China) on a ABI 7500 Fast Real-Time PCR System (Applied Biosystems, Foster, CA, United States) and. Data analysis was carried out using the $2^{-\Delta\Delta CT}$ method (Livak and Schmittgen, 2001). The primers were listed in Supplementary Table S1.

2.7 ROS and T-AOC determination

The eukaryotic expression recombinant plasmids of *Mc*Nrf2 and *Mc*SLC35E2, which were prepared in our laboratory, were collected and their final concentration was diluted to 300 ng/μL. *M. coruscus* individuals (Net weight: 19.8 ± 0.3 g) were randomly divided into 5 groups, each consisting of 6 mussels. The adductor muscle of each mussel was injected with either 100 μL *Mc*Nrf2, *Mc*SLC35E2, or 200 μL of both *Mc*Nrf2 and *Mc*SLC35E2. After injection, the individuals were exposed to Bap separately. Subsequently, the reactive oxygen species (ROS) production and total antioxidant capacity (T-AOC) were detected by using kits (Jian cheng, Nanjing, China).

2.8 Statistical analysis

All data were analyzed using SPSS 27.0 software (IBM Corp., Armonk, NY, United States). The results were presented as mean ± SD. Before conducting statistical analysis, normality tests and tests for homogeneity of variances were performed. For comparing two sets of data, the *t*-test was utilized. Data with more than two sets were analyzed using one-way analysis of variance (ANOVA), followed by Tukey's multiple range test for *post hoc* comparisons. Statistical significance was considered for probabilities of $p < 0.05$.

TABLE 1 Statistical summary of ChIP-seq raw data after filtration (average >Q30).

Samples	Raw reads	Raw bases	Clean reads	Clean bases	Clean Q30	Clean rate (%)
Nrf2 chip1	21,213,802	3,182,070,300	20,448,090	2,988,027,409	93.22	93.90
Nrf2 chip2	21,213,802	3,182,070,300	20,448,090	2,973,059,420	90.19	93.43
Nrf2 input1	20,892,596	3,133,889,400	20,056,089	2,883,119,713	93.32	92.00
Nrf2 input2	20,892,596	3,133,889,400	20,056,089	2,866,943,649	89.92	91.48

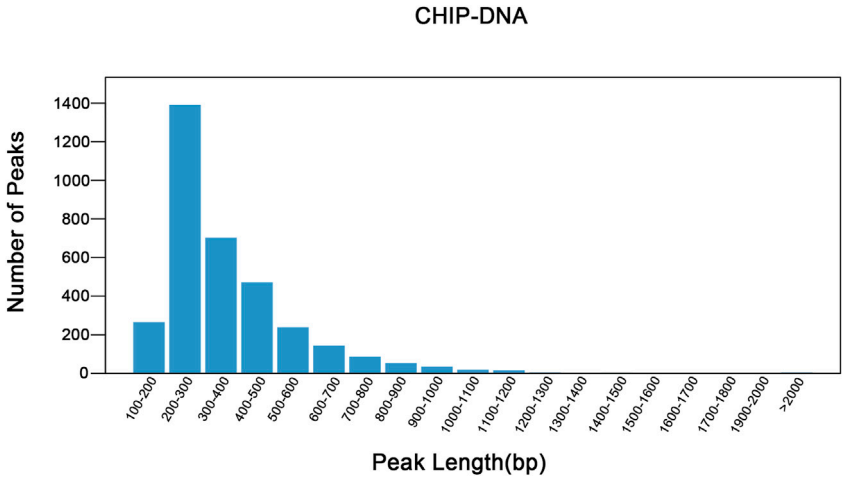

FIGURE 1
Peak length distribution. The abscissa shows the peak length and the ordinate shows the number of the peaks. The plot illustrates the distribution of peak lengths and provides insights into the frequency of peaks with different lengths in the dataset.

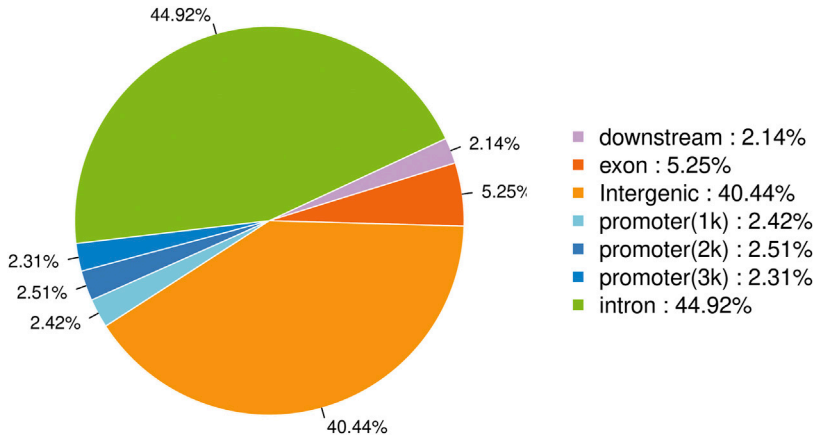

FIGURE 2
Distribution of peaks in genomic regions.

3 Results

3.1 ChIP-seq data analysis

The raw data has been uploaded to the GEO database with the accession number GSE242277. The raw data from the sample (Nrf2 chip) and control (Nrf2 input) groups were 5.96 billion bp and 5.75 billion bp, respectively. After removing low-quality bases or filtering for valid data (Table 1). The quality of the filtered data is high (Q > 30), and the majority of the data surpasses this threshold, indicating that the reads are of high quality. After quality control, 79.44% of the unique reads were localized to *M. coruscus* genome.

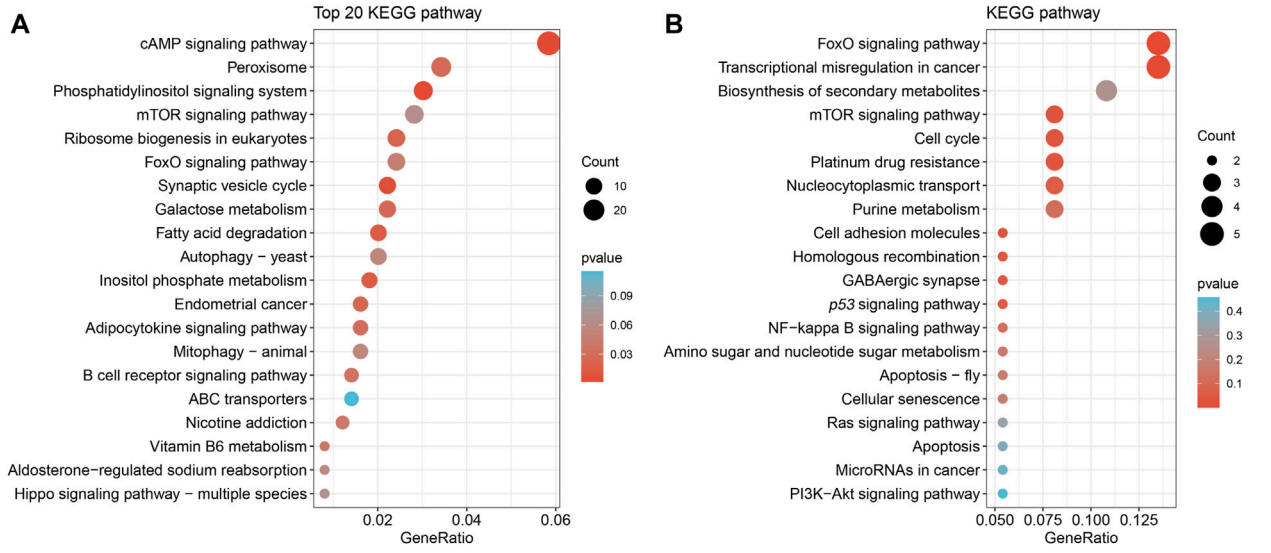

FIGURE 3
Kyoto Encyclopedia of Genes and Genomes (KEGG) pathway enrichment analysis. **(A)** A total of 3,465 peak KEGG enrichment analyses unveiled signaling pathways. **(B)** The analysis of 219 peak KEGG enrichment, situated within the promoter region, unveiled signaling pathways.

The statistical analysis revealed a total of 3,465 peaks, with an average peak length of 383.88 bp and a median peak length of 311 bp. The majority of peak lengths clustered around 200–300 bp (Figure 1). Annotation of 3,465 peaks was conducted to obtain comprehensive information about all the identified peaks in the genome (Supplementary Table S2). Among all the peaks, 7.24% are situated in the promoter transcription start site (TSS) regions (Figure 2). The majority of peaks are located in intergenic regions and introns (Figure 2).

3.2 Annotation of genes identified by Nrf2 ChIP

To obtain a comprehensive set of Nrf2 binding sites, we performed ChIP-seq analysis using the digestive gland of *M. coruscus*. In total, 3,465 peaks were identified as potential binding sites, and among them, 89.24% of the peaks were successfully annotated to the nearest gene. Out of all the peaks, 219 were localized within the promoter zone. Gene functions were established through the utilization of information sourced from diverse databases, notably Swiss-Prot, Interpro, TrEMBL, and KEGG databases. A KEGG enrichment analysis was conducted on a total of 3,465 screened peaks, revealing significant signaling pathways linked to Nrf2 target genes, which included Phosphatidylinositol signaling system (map04070), cAMP signaling pathway (map04024), and Peroxisome (map04146) (Figure 3A). The analysis of enrichment for 219 peaks within the promoter region yielded the subsequent pathways: FoxO signaling pathway (map04068), mTOR signaling pathway (map04150), and p53 signaling pathway (map04115) (Figure 3B). Binding sites located in promoter regions (1K) are likely to be highly regulated by Nrf2. We conducted a screening of our Nrf2 target gene of interest, *SLC35E2*, for which the regulatory relationship with Nrf2 has not been previously mentioned. *SLC35E2* annotated to *M. coruscus* chromosome 13 and there was a clear peak of enrichment for *SLC35E2* compared to the input group (Figure 4).

3.3 Nrf2-specific binding sites

Transcription factors' DNA binding sites often exist as conserved short sequence fragments. Therefore, motif analysis of the ChIP-seq results aids in analyzing the recognition pattern of transcription factors on DNA sequences. Predictions were screened to assess the potential binding of Nrf2 to the identified motif (Table 2).

3.4 Expression patterns and regulatory relationships of target genes

To validate the targeting relationship between SLC35E2 and Nrf2, a dual luciferase assay was employed. The activity of Firefly luciferase was divided by the activity of Renilla luciferase to assess the regulatory effect of SLC35E2 and the role of the transcription factor Nrf2 on SLC35E2. The highest luciferase activity was observed for pcDNA3.1+SLC35E2, whereas Nrf2+SLC35E2 luciferase activity was lower ($p < 0.05$) (Figure 5A). This indicates that the presence of Nrf2 leads to a reduction in the expression of SLC35E2. To explore the regulatory relationship between Nrf2 and SLC35E2, we utilized the Nrf2 agonist SFN and the Nrf2 inhibitor ML385. In comparison to the control group, the expression of *Nrf2* increased following SFN treatment, while the expression of *SLC35E2* decreased significantly ($p < 0.05$) (Figure 5B). In contrast, *Nrf2* expression was reduced, and *SLC35E2* expression significantly increased after ML385 treatment ($p < 0.05$) (Figure 5B).

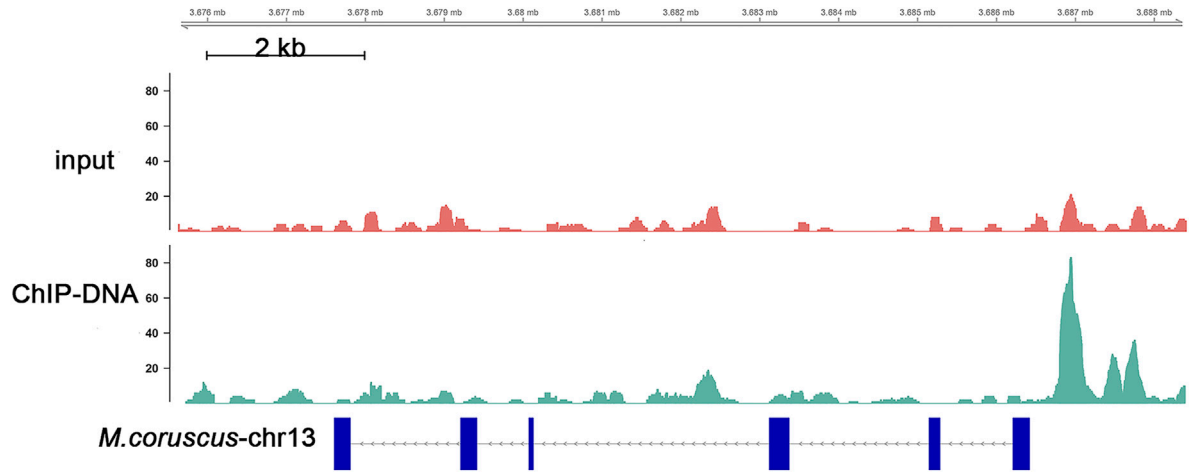

FIGURE 4
Distribution of SLC35E2 in the genome situation. Each data point or peak on the plot represents the localization of SLC35E2 within the genome. The *x*-axis represents the genomic coordinates, and the *y*-axis shows the intensity or frequency of SLC35E2 at each location.

TABLE 2 CentriMo enrichment motif for *de novo* results.

Rank	Motif	E-value
1		9.30E-03
2		4.20E-55
3		3.30E-61

3.5 Nrf2 target genes and oxidative stress regulation

*Mc*Nrf2 and *Mc*SLC35E2 plasmids showed differences in ROS levels after injection and Bap exposure. As depicted in Figure 6A, the level of ROS was higher in the presence of Bap compared to the control group (NC) ($p < 0.05$). However, when Bap was exposed and Nrf2 was overexpressed, the level of ROS was reduced ($p < 0.05$). On the other hand, elevating the level of SLC35E2 was associated with increased ROS levels ($p < 0.05$). Nevertheless, when both Nrf2 and SLC35E2 were overexpressed, the level of ROS was lower than when only SLC35E2 was overexpressed ($p < 0.05$). After injection, there was a notable difference in T-AOC levels in the digestive gland, as depicted in Figure 6B. T-AOC was elevated after exposure to Bap and Nrf2 overexpression in comparison to the NC group ($p < 0.05$). Moreover, T-AOC was decreased in the SLC35E2 overexpression group compared to the Nrf2 overexpression group ($p < 0.05$). However, when both Nrf2 and SLC35E2 were overexpressed, T-AOC levels were elevated compared to SLC35E2 overexpression ($p < 0.05$).

4 Discussion

ChIP-seq is an exceptionally powerful technique for identifying specific transcription factor binding sites (Bansal et al., 2015). Its applications have been expanding rapidly, with recent studies successfully implementing this method in different species. Regrettably, the application of this technology to marine mollusks is still in its infancy. Liu et al. (2020) successfully established the ChIP-seq method in *Crassostrea gigas*. To our knowledge, this is the first application of this technology in marine mollusks. In this study, the researchers employed ChIP-seq technique to scan genes regulated by HSF1. The sequencing yielded a set of unique reads, with a 34.2% match rate to the *C. gigas* genome. Ultimately, a total of 916 peaks corresponding to HSF1 binding sites were identified, of which 6% were located in the TSS region, and a subset of HSP genes displayed a direct binding to HSF1. In the present study, unique reads showed a higher genome matching degree (79.44%), indicating high sequencing quality. Statistical analysis revealed a total of 3,465 peaks corresponding to Nrf2 binding sites, 7.24% of which were located at TSS region, and most of the peaks were located at intergenic regions and introns. Our results aligned with the results of a prior investigation, that Nrf2-ChIP-seq data from A549 cells also revealed an approximately 7% gene binding sites on the TSS promoter (Namani et al., 2019). This consistency between our data and the previous study reinforced the reliability and validity of the present findings.

10.3389/fphys.2023.1282900

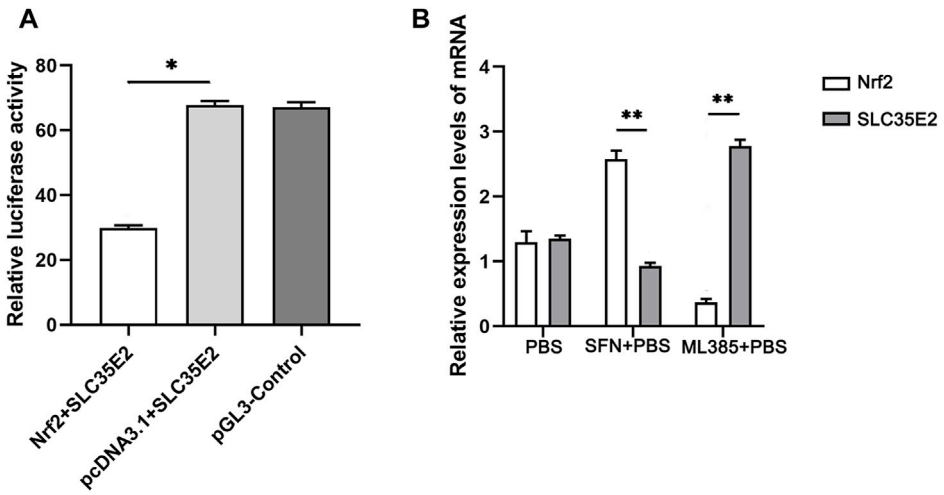

FIGURE 5
Verification of regulatory relationship between Nrf2 and SLC35E2. **(A)** The relative activity of luciferase. The control group was pGL3-control plasmid. The vertical bars represent the mean ± standard deviation (SD) (n = 3); *p < 0.05 **(B)** Expression levels of Nrf2 and SLC35E2 genes after SFN and ML385 treatment. The vertical bars represent the mean ± SD (n = 3). **p < 0.01.

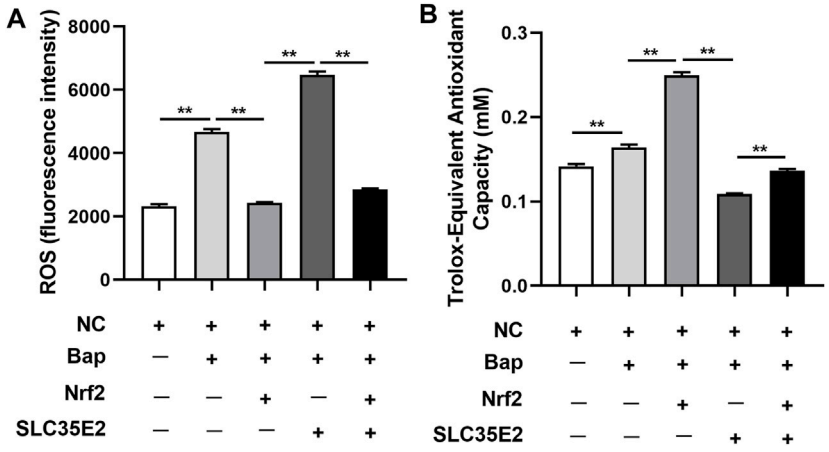

FIGURE 6
Nrf2 targeting SLC35E2 is involved in the antioxidant effect of Bap exposure. **(A)** ROS levels detected. **(B)** T-AOS levels detected. The vertical bars represent the mean ± SD (n = 3). **p < 0.01.

The KEGG analysis of peaks showed a predominant enrichment in the FoxO, mTOR, and p53 signaling pathway. The FoxO signaling pathway has been found to be involved in various aspects, including lifespan regulation, growth and development, as well as resistance to starvation and environmental stressors (Xiao et al., 2018; Wang et al., 2021a; Chen et al., 2023). Considering that Nrf2 acts as a crucial trigger for the body's antioxidant defense mechanisms, the significant association between *Mc*Nrf2 and FoxO implies that when *M. coruscus* mussels face oxidative stress, the activation of the FoxO pathway regulates growth and development, ultimately ensuring the maintenance of normal life activities. In shellfish, the mTOR signaling pathway also acts as a key player, orchestrating crucial processes such as enhanced lysosomal membrane permeability and the initiation of autophagy (Sforzini et al., 2018). This pathway is constantly vigilant and responds to changing environmental conditions, shaping shellfish cell metabolism and growth strategies accordingly. It is widely believed that invertebrates in marine environments encounter various stressors, including pollutants, low oxygen, and pathogens. Studies have shown that the p53 pathway promotes stress response and cell apoptosis in bivalve cells under various stressors (Xie et al., 2022). Nrf2-targeted genes were highly enriched in the mTOR and p53 pathways, indicating that Nrf2 indeed plays an important role in bivalve's physiological responses to stressors, which may be associated with immune response, cell cycle regulation, cell apoptosis, and other processes.

Shin et al. (2013) investigated the functional roles of Nrf2 target genes including glutamate cysteine ligase (*GCLC*), *NAD(P)H*,

quinone oxidoreductase 1 (*NQO-1*), UDP-glucuronosyltransferase (*UGT*), and hemeoxygenase-1 (*HO-1*), in hepatic pathophysiology. They found that these genes play complex and multifaceted roles in liver inflammation, fibrosis, and hepatocarcinogenesis. Nrf2 plays a positive role in the equilibrium state, however, the imbalance of Nrf2 and its target gene expression will inflict severe damage upon the organism. Kong et al. (2021) found that sustained high expression of Nrf2 and its target genes, *NQO1* and B-cell lymphoma-2 (*BCL-2*), induced dysplasia of cell proliferation and apoptosis, and were associated with malignant transformation of human bronchial epithelial cells induced by arsenite. Indeed, the most important role of Nrf2 target genes lies in their contribution to the antioxidant defense system and their ability to mitigate oxidative damage. Nrf2 target genes ensure cell integrity and overall health in the face of oxidative challenges by upregulating antioxidant enzymes and detoxifying proteins (Wang et al., 2021b). Unfortunately, studies of Nrf2 and its target genes have been more extensive in humans and mammals, but there has been very limited reporting in aquatic organisms, especially bivalve mollusks.

In the present study, ChIP-seq scanned a total of 219 candidate target genes of *Mc*Nrf2 with binding sites located within the promoter region, and the enriched peaks corresponding to the putative binding sites of *SLC35E2* and Nrf2 were identified by comparing the sequence reads with and without Nrf2 antibody treatment. Laboratory experiments including the dual luciferase and qRT-PCR assays were employed to verify the *in silico* prediction. Dual luciferase assay showed that compared with *Mc*SLC35E2 alone, the luciferase activity in the Nrf2 supplemental group was lower, indicating that *Mc*Nrf2 could target *Mc*SLC35E2 and was negatively correlated. The qRT-PCR further confirmed this fact, that the transcriptional expression of *McSLC35E2* was activated by Nrf2 inhibitor ML385 while inhibited by Nrf2 agonist SFN. These results suggested that *Mc*Nrf2 may be involved in the regulation of physiological processes in *M. coruscus* mussels by inhibiting *Mc*SLC35E2.

Members of the SLC family play a crucial role in human physiology as transporters that facilitate the transportation of hydrophilic compounds into and out of cells and subcellular organelles. For instance, SLC30 and SLC39 transport zinc, SLC11 and SLC40 transport iron, and SLC19 transport folic acid and thiamine (Lin et al., 2015). In addition, several SLC35 transporter proteins, including the SLC35E2 subfamily, are considered orphan SLC35 transporter proteins due to their unclear physiological functions and substrate specificity (Parker and Newstead, 2019). However, recent studies have revealed that these orphan transporters may not be directly involved in glycosylation processes (Li et al., 2022). Similarly, Sosicka et al. (2019) provided support for the notion that the SLC35 protein family may have diverse roles beyond glycosylation. For example, SLC35D3 enhances the formation of protein complexes associated with autophagy (Meng et al., 2012), while SLC35A4 plays a critical role in subcellular distribution (Sosicka et al., 2017). Additionally, SLC35F2 has been found to promote the progression of papillary thyroid carcinoma (He et al., 2018). As for SLC35E2, the oncogenic effect was confirmed *in vivo* using a mouse tumor model (Li et al., 2022). In addition, the scRNA-seq technique has proved that SLC35E2 mutations are associated with human disease variants (Cuomo et al., 2022). In summary, the SLC family plays a multifunctional role in various physiological activities. Regrettably, limited research has been conducted on SLC35E2. In order to investigate the involvement of *Mc*Nrf2 in Bap-induced antioxidant effects through its targeting of *Mc*SLC35E2, enzyme activities were determined in the digestive glands injected with the recombinant plasmids of *Mc*Nrf2 and *Mc*SLC35E2 under or non-Bap.

Bap, being one of the most toxic types of PAHs, has been extensively characterized toxicologically (Bieser et al., 2011). The detoxification process of PAHs can generate numerous active intermediates and ROS substances, which can interfere with the normal physiological functions of shellfish (Liu et al., 2014). At this stage, the Nrf2 pathway is activated, which further triggers the expression of a series of antioxidant enzyme genes, resulting in the increase of T-AOC in the body. This elevation of T-AOC helps to reduce ROS production and oxidative stress (Ma and He, 2012; Cheng et al., 2022). Consistent with this, ROS production and T-AOC levels in the digestive glands of *M. coruscus* exposed to Bap were significantly increased in the present study compared with the NC group, indicating that the Bap burst caused severe oxidative stress to the mussels. Overexpression of *Mc*Nrf2 leads to a significant reduction in ROS production, on the contrary, a significant increase in T-AOC levels is observed. Similar results were found in zebrafish studies, where Shi and Zhou (2010) demonstrated that zebrafish embryos exposed to POPs exhibited elevated ROS production and increased oxidative stress, whereas ROS levels decreased when Nrf2 was upregulated. It was worth noting that when *Mc*SLC35E2 is overexpressed, ROS production is significantly increased and T-AOC is significantly decreased. This result demonstrated that *Mc*SLC35E2 may exacerbate oxidative damage, leading to increased oxidative stress in mussels. However, when *Mc*Nrf2 and *Mc*SLC35E2 were both overexpressed, the situation is exactly the opposite, suggesting that this two had antagonistic effects on the oxidative stress induced by Bap in mussels.

5 Conclusion

In this study, ChIP-seq technique was employed to identify new target genes of *Mc*Nrf2 in *M. coruscus*. After comprehensive genome-wide survey, 3,465 candidate target genes of *Mc*Nrf2 were scanned, of which 219 owned binding sites located within the promoter region. Following, a typical target gene termed *McSLC35E2* was selected to perform the experimental verification. Specifically, the targeting of *Mc*Nrf2 to *Mc*SLC35E2 was successfully verified using both dual luciferase and qRT-PCR assay. In order to investigate the involvement of *Mc*Nrf2 in Bap-induced antioxidant effects through its targeting of *Mc*SLC35E2, enzyme activities were determined in the digestive glands injected with the recombinant plasmids of *Mc*Nrf2 and *Mc*SLC35E2 under or non-Bap. The results revealed that *Mc*Nrf2 could participate in the anti-Bap oxidative stress process by inhibiting *Mc*SLC35E2. Overall, these findings lay the groundwork for applying ChIP-seq technology in mollusks, opening up new avenues for understanding the function of Nrf2 in the antioxidant defense system of marine mollusks. The study contributes valuable knowledge that may have implications for future research on environmental responses and stress adaptation in mollusks.

Data availability statement

The original contributions presented in the study are included in the article/Supplementary Material, further inquiries can be directed to the corresponding author.

Ethics statement

The manuscript presents research on animals that do not require ethical approval for their study.

Author contributions

LQ: Data curation, Writing–original draft, Writing–review and editing. PQ: Data curation, Methodology, Writing–original draft, Writing–review and editing. XC: Data curation, Methodology, Software, Writing–original draft. LZ: Data curation, Methodology, Software, Writing–original draft. RY: Data curation, Methodology, Software, Writing–original draft.

Funding

The authors declare financial support was received for the research, authorship, and/or publication of this article. This research was supported by the National Natural Science Foundation of China (Grant Numbers: 42176099, 41976111, 42020104009, and 42076119), the Natural Science Foundation for Distinguished Young Scholars of Zhejiang province (Grant Number: LR22D060002).

Conflict of interest

The authors declare that the research was conducted in the absence of any commercial or financial relationships that could be construed as a potential conflict of interest.

Publisher's note

Supplementary material

The Supplementary Material for this article can be found online at: https://www.frontiersin.org/articles/10.3389/fphys.2023.1282900/full#supplementary-material

References

Bansal, M., Mendiratta, G., Anand, S., Kushwaha4, R., Kim, R. H., Kustagi, M., et al. (2015). Direct ChIP-Seq significance analysis improves target prediction. *BMC Genomics* 16 (5), S4–S2164. doi:10.1186/1471-2164-16-S5-S4

Bieser, J., Aulinger, A., Matthias, V., and Quante, M. (2011). Impact of emission reductions between 1980 and 2020 on atmospheric benzo[a]pyrene concentrations over europe. *Water, Air, and Soil Pollut.* 223 (3), 1393–1414. doi:10.1007/s11270-011-0953-z

Bolger, A. M., Lohse, M., and Usadel, B. (2014). Trimmomatic: a flexible trimmer for Illumina sequence data. *Bioinformatics* 30 (15), 2114–2120. doi:10.1093/bioinformatics/btu170

Chen, C., Xie, B., Sun, W., Gu, Z., Huang, J., Qi, P., et al. (2023). Examination of the role of resveratrol in attenuating oxidative damage induced by starvation stress in the marine mussel, *Mytilus coruscus*, through regulation of the sirt1-mediated signaling pathway. *Aquaculture* 564, 739047. doi:10.1016/j.aquaculture.2022.739047

Cheng, C., Ma, H., Liu, G., Fan, S., and Guo, Z. (2022). Mechanism of cadmium exposure induced hepatotoxicity in the mud crab (Scylla paramamosain): activation of oxidative stress and Nrf2 signaling pathway. *Antioxidants (Basel)* 11 (5), 978. doi:10.3390/antiox11050978

Cuomo, A. S. E., Heinen, T., Vagiaki, D., Horta, D., Marioni, J. C., and Stegle, O. (2022). CellRegMap: a statistical framework for mapping context-specific regulatory variants using scRNA-seq. *Mol. Syst. Biol.* 18 (8), e10663. doi:10.15252/msb.202110663

Dong, Z., Li, H., Wang, Y., Lin, S., Guo, F., Zhao, J., et al. (2023). Transcriptome profiling reveals the strategy of thermal tolerance enhancement caused by heat-hardening in *Mytilus coruscus*. *Sci. Total Environ.* 903, 165785. doi:10.1016/j.scitotenv.2023.165785

Farnham, P. J. (2009). Insights from genomic profiling of transcription factors. *Nat. Rev. Genet.* 10 (9), 605–616. doi:10.1038/nrg2636

Hayes, J. D., and Dinkova-Kostova, A. T. (2014). The Nrf2 regulatory network provides an interface between redox and intermediary metabolism. *Trends Biochem. Sci.* 39 (4), 199–218. doi:10.1016/j.tibs.2014.02.002

He, J., Jin, Y., Zhou, M., Li, X., Chen, W., Wang, Y., et al. (2018). Solute carrier family 35 member F2 is indispensable for papillary thyroid carcinoma progression through activation of transforming growth factor-beta type I receptor/apoptosis signal-regulating kinase 1/mitogen-activated protein kinase signaling axis. *Cancer Sci.* 109 (3), 642–655. doi:10.1111/cas.13478

Heinz, S., Benner, C., Spann, N., Bertolino, E., Lin, Y. C., Laslo, P., et al. (2010). Simple combinations of lineage-determining transcription factors prime cis-regulatory elements required for macrophage and B cell identities. *Mol. Cell* 38 (4), 576–589. doi:10.1016/j.molcel.2010.05.004

Hirotsu, Y., Katsuoka, F., Funayama, R., Nagashima, T., Nishida, Y., Nakayama, K., et al. (2012). Nrf2-MafG heterodimers contribute globally to antioxidant and metabolic networks. *Nucleic Acids Res.* 40 (20), 10228–10239. doi:10.1093/nar/gks827

Johnson, D. S., Mortazavi, A., Myers, R. M., and Wold, B. (2007). Genome-wide mapping of *in vivo* protein-DNA interactions. *Science* 316 (5830), 1497–1502. doi:10.1126/science.1141319

Kim, H., Yim, B., Kim, J., Kim, H., and Lee, Y. M. (2017). Molecular characterization of ABC transporters in marine ciliate, euplotes crassus: identification and response to cadmium and benzo[a]pyrene. *Mar. Pollut. Bull.* 124 (2), 725–735. doi:10.1016/j.marpolbul.2017.01.046

Kong, Q., Deng, H., Li, C., Wang, X., Shimoda, Y., Tao, S., et al. (2021). Sustained high expression of NRF2 and its target genes induces dysregulation of cellular proliferation and apoptosis is associated with arsenite-induced malignant transformation of human bronchial epithelial cells. *Sci. Total Environ.* 756, 143840. doi:10.1016/j.scitotenv.2020.143840

Langmead, B., and Salzberg, S. L. (2012). Fast gapped-read alignment with Bowtie 2. *Nat. Methods* 9 (4), 357–359. doi:10.1038/nmeth.1923

Li, Y., Feng, R., Yu, X., Li, L., Liu, Y., Zhang, R., et al. (2022). *SLC35E2* promoter mutation as a prognostic marker of esophageal squamous cell carcinoma. *Life Sci.* 296, 120447. doi:10.1016/j.lfs.2022.120447

Lin, L., Yee, S. W., Kim, R. B., and Giacomini, K. M. (2015). SLC transporters as therapeutic targets: emerging opportunities. *Nat. Rev. Drug Discov.* 14 (8), 543–560. doi:10.1038/nrd4626

Liu, B., Wen, H., Li, X., Yang, J., Li, G., Zhang, M., et al. (2021). Acute hypoxia effects on Keap1/Nrf2 (Mafs)-GST pathway related oxidative metabolism in muscle of Japanese flounder (*Paralichthys olivaceus*). *Sci. Total Environ.* 795, 148646. doi:10.1016/j.scitotenv.2021.148646

Liu, D., Pan, L., Li, Z., Cai, Y., and Miao, J. (2014). Metabolites analysis, metabolic enzyme activities and bioaccumulation in the clam Ruditapes philippinarum exposed to

benzo[a]pyrene. *Ecotoxicol. Environ. Saf.* 107, 251–259. doi:10.1016/j.ecoenv.2014.06.024

Liu, Y., Zhu, Q., Li, L., Wang, W., and Zhang, G. (2020). Identification of HSF1 target genes involved in thermal stress in the *pacific oyster Crassostrea gigas* by ChIP-seq. *Mar. Biotechnol. (NY)* 22 (2), 167–179. doi:10.1007/s10126-019-09942-6

Livak, K. J., and Schmittgen, T. D. (2001). Analysis of relative gene expression data using real-time quantitative PCR and the $2^{-\Delta\Delta}$CT method. *Methods* 25 (4), 402–408. doi:10.1006/meth.2001.1262

Ma, Q., and He, X. (2012). Molecular basis of electrophilic and oxidative defense: promises and perils of Nrf2. *Pharmacol. Rev.* 64 (4), 1055–1081. doi:10.1124/pr.110.004333

Ma, W., Noble, W. S., and Bailey, T. L. (2014). Motif-based analysis of large nucleotide data sets using MEME-ChIP. *Nat. Protoc.* 9 (6), 1428–1450. doi:10.1038/nprot.2014.083

Meng, R., Wang, Y., Yao, Y., Zhang, Z., Harper, D. C., Heijnen, H. F., et al. (2012). SLC35D3 delivery from megakaryocyte early endosomes is required for platelet dense granule biogenesis and is differentially defective in Hermansky-Pudlak syndrome models. *Blood* 120 (2), 404–414. doi:10.1182/blood-2011-11-389551

Namani, A., Liu, K., Wang, S., Zhou, X., Liao, Y., Wang, H., et al. (2019). Genome-wide global identification of NRF2 binding sites in A549 nonsmall cell lung cancer cells by ChIP-Seq reveals NRF2 regulation of genes involved in focal adhesion pathways. *Aging (Albany NY)* 11 (24), 12600–12623. doi:10.18632/aging.102590

Park, P. J. (2009). ChIP–seq: advantages and challenges of a maturing technology. *Nat. Rev. Genet.* 10 (10), 669–680. doi:10.1038/nrg2641

Parker, J. L., and Newstead, S. (2019). Gateway to the golgi: molecular mechanisms of nucleotide sugar transporters. *Curr. Opin. Struct. Biol.* 57, 127–134. doi:10.1016/j.sbi.2019.03.019

Qi, P., and Tang, Z. (2020). The Nrf2 molecule trigger antioxidant defense against acute benzo(a)pyrene exposure in the thick shell mussel *Mytilus coruscus*. *Aquat. Toxicol.* 226, 105554. doi:10.1016/j.aquatox.2020.105554

Sforzini, S., Moore, M. N., Oliveri, C., Volta, A., Jha, A., Banni, M., et al. (2018). Role of mTOR in autophagic and lysosomal reactions to environmental stressors in molluscs. *Aquat. Toxicol.* 195, 114–128. doi:10.1016/j.aquatox.2017.12.014

Shaw, P., Mondal, P., Bandyopadhyay, A., and Chattopadhyay, A. (2020). Environmentally relevant concentration of chromium induces nuclear deformities in erythrocytes and alters the expression of stress-responsive and apoptotic genes in brain of adult zebrafish. *Sci. Total Environ.* 703, 135622. doi:10.1016/j.scitotenv.2019.135622

Shendure, J., and Ji, H. (2008). Next-generation DNA sequencing. *Nat. Biotechnol.* 26 (10), 1135–1145. doi:10.1038/nbt1486

Shi, X., and Zhou, B. (2010). The role of Nrf2 and MAPK pathways in PFOS-induced oxidative stress in zebrafish embryos. *Toxicol. Sci.* 115 (2), 391–400. doi:10.1093/toxsci/kfq066

Shin, S. M., Yang, J. H., and Ki, S. H. (2013). Role of the Nrf2-ARE pathway in liver diseases. *Oxid. Med. Cell Longev.* 2013, 763257. doi:10.1155/2013/763257

Solomon, M. J., Larsen, P. L., and Varshavsky, A. (1988). Mapping proteinDNA interactions *in vivo* with formaldehyde: evidence that histone H4 is retained on a highly transcribed gene. *Cell* 53 (6), 937–947. doi:10.1016/s0092-8674(88)90469-2

Sosicka, P., Bazan, B., Maszczak-Seneczko, D., Shauchuk, Y., Olczak, T., and Olczak, M. (2019). SLC35A5 protein-A golgi complex member with putative nucleotide sugar transport activity. *Int. J. Mol. Sci.* 20 (2), 276. doi:10.3390/ijms20020276

Sosicka, P., Maszczak-Seneczko, D., Bazan, B., Shauchuk, Y., Kaczmarek, B., and Olczak, M. (2017). An insight into the orphan nucleotide sugar transporter SLC35A4. *Biochim. Biophys. Acta Mol. Cell Res.* 1864 (5), 825–838. doi:10.1016/j.bbamcr.2017.02.002

Wang, H., Pan, L., Si, L., Ji, R., and Cao, Y. (2021a). Effects of Nrf2-Keap1 signaling pathway on antioxidant defense system and oxidative damage in the clams *Ruditapes philippinarum* exposure to PAHs. *Environ. Sci. Pollut. Res. Int.* 28, 33060–33071. doi:10.1007/s11356-021-12906-w

Wang, L., Guo, Y., Pan, M., Li, X., Huang, D., Liu, Y., et al. (2021b). Functions of forkhead box O on glucose metabolism in abalone Haliotis discus hannai and its responses to high levels of dietary lipid. *Genes (Basel)* 12 (2), 297. doi:10.3390/genes12020297

Wang, Y.-Q., Liu, Q., Zhou, Y., Chen, L., Yang, Y.-M., Shi, X., et al. (2023). Stage-specific transcriptomes of the mussel *Mytilus coruscus* reveals the developmental program for the planktonic to benthic transition. *Genes* 14 (2), 287. doi:10.3390/genes14020287

Wang, Y., Duan, Y., Huang, J., Wang, J., Zhou, C., Jiang, S., et al. (2021c). Characterization and functional study of nuclear factor erythroid 2-related factor 2 (Nrf2) in black tiger shrimp (*Penaeus monodon*). *Fish. Shellfish Immunol.* 119, 289–299. doi:10.1016/j.fsi.2021.10.016

Xiao, S., Wong, N. K., Li, J., Lin, Y., Zhang, Y., Ma, H., et al. (2018). Analysis of *in situ* transcriptomes reveals divergent adaptive response to hyper- and hypo-salinity in the Hong Kong oyster, Crassostrea hongkongensis. *Front. Physiol.* 9, 1491. doi:10.3389/fphys.2018.01491

Xie, Z., Lu, G., Zhou, R., and Ma, Y. (2022). Thiacloprid-induced hepatotoxicity in zebrafish: activation of the extrinsic and intrinsic apoptosis pathways regulated by p53 signaling pathway. *Aquat. Toxicol.* 246, 106147. doi:10.1016/j.aquatox.2022.106147

Xiu, M., Pan, L., and Jin, Q. (2014). Bioaccumulation and oxidative damage in juvenile scallop Chlamys farreri exposed to benzo[a]pyrene, benzo[b]fluoranthene and chrysene. *Ecotoxicol. Environ. Saf.* 107, 103–110. doi:10.1016/j.ecoenv.2014.05.016

Zago, G., Saavedra, P. H. V., Keshari, K. R., and Perry, J. S. A. (2021). Immunometabolism of tissue-resident macrophages - an appraisal of the current knowledge and cutting-edge methods and Technologies. *Front. Immunol.* 12, 665782. doi:10.3389/fimmu.2021.665782

Zhang, Y., Liu, T., Meyer, C. A., Eeckhoute, J., Johnson, D. S., Bernstein, B. E., et al. (2008). Model-based analysis of ChIP-seq (MACS). *Genome Biol.* 9 (9), R137. doi:10.1186/gb-2008-9-9-r137

Zhao, X., Han, Y., Chen, B., Xia, B., Qu, K., and Liu, G. (2020). CO(2)-driven ocean acidification weakens mussel shell defense capacity and induces global molecular compensatory responses. *Chemosphere* 243, 125415. doi:10.1016/j.chemosphere.2019.125415

frontiers | Frontiers in Physiology

TYPE Original Research
PUBLISHED 25 October 2023
DOI 10.3389/fphys.2023.1280553

OPEN ACCESS

EDITED BY
Yi-Feng Li,
Shanghai Ocean University, China

REVIEWED BY
Chenghua Li,
Ningbo University, China
Enrico D'Aniello,
Zoological Station Anton Dohrn, Italy
Youji Wang,
Shanghai Ocean University, China

*CORRESPONDENCE
Lingling Wang,
wanglingling@dlou.edu.cn
Linsheng Song,
lshsong@dlou.edu.cn

†These authors have contributed equally to this work

RECEIVED 20 August 2023
ACCEPTED 10 October 2023
PUBLISHED 25 October 2023

CITATION
Zhang X, Zhang L, Si Y, Wen X, Wang L and Song L (2023), Unveiling the functional diversity of ionotropic glutamate receptors in the Pacific oyster (*Crassostrea gigas*) by systematic studies. *Front. Physiol.* 14:1280553. doi: 10.3389/fphys.2023.1280553

Unveiling the functional diversity of ionotropic glutamate receptors in the Pacific oyster (*Crassostrea gigas*) by systematic studies

Xueshu Zhang[1,2,3,4†], Linfang Zhang[1,3,4†], Yiran Si[1,3,4], Xue Wen[1,3,4], Lingling Wang[1,2,3,4*] and Linsheng Song[1,2,3,4*]

[1]Liaoning Key Laboratory of Marine Animal Immunology and Disease Control, Dalian Ocean University, Dalian, China, [2]Southern Laboratory of Ocean Science and Engineering, Zhuhai, Guangdong, China, [3]Liaoning Key Laboratory of Marine Animal Immunology, Dalian Ocean University, Dalian, China, [4]Dalian Key Laboratory of Aquatic Animal Disease Prevention and Control, Dalian Ocean University, Dalian, China

Ionotropic glutamate receptors (iGluRs), pivotal in mediating excitatory neurosignals within the central nervous system, are instrumental in environmental stress responses. In this investigation, 12 iGluRs identified in the Pacific oyster are herein designated as *Cgi*GluRs, and further categorized into three distinct subfamilies based on their transmembrane domains. Cross-species evolutionary analysis unveiled a high degree of conservation in the sequence and structural attributes of these *Cgi*GluRs. These receptors are ubiquitously distributed across various tissues, with pronounced expression in the oyster's mantle, labial palps, and gills, underlining their integral role in the oyster's environmental sensing mechanisms. Post the D-shaped larval stage, a marked upward trend in *Cgi*GluRs expression was observed, denoting their critical involvement in oyster development beyond this phase. Exposure to five metals—cadmium (Cd), copper (Cu), zinc (Zn), mercury (Hg), and lead (Pb)—elicited a significant upregulation of *Cg*GRIA4 expression, indicating a robust response to metal stress. A KEGG enrichment analysis on 142 genes, exhibiting parallel expression trends with *Cg*GRIA4 under metal stress, suggests that *Cg*GRIA4 could augment excitatory signal transmission by activating glutamatergic and dopaminergic synapses, thereby contributing to the metal stress response in the oyster. This inquiry not only bolsters our comprehension of the iGluRs gene family in metal stress response but also paves the way for future exploration of its cardinal role in cellular signaling and environmental adaptability.

KEYWORDS

ionotropic glutamate receptors, Crassostrea gigas, metal stress, environmental sensing, physiological adaptation

1 Introduction

Glutamate, the chief excitatory neurotransmitter within the nervous system, directs a plethora of physiological functions, encompassing neural remodeling (Endo et al., 2021), environmental sensing (Wen et al., 2020), and signal transduction (Qiu et al., 2020), via a diverse array of receptors. Pharmacological classifications segregate glutamate receptors into two primary categories: ionotropic (iGluRs) and metabotropic (mGluRs) receptors (Zhu and Gouaux, 2017). A substantial body of research accentuates the superior velocity of iGluRs in information transmission relative to mGluRs, underscoring their capability for rapid

environmental stress responses. iGluRs, functioning as multimeric ion channels, are tasked with the swift excitatory transmission in the nervous system. Upon binding to pre-synaptically released glutamate, iGluRs transduce signals into post-synaptic neuronal excitation within milliseconds. This complex process gives rise to synaptic currents, crucial for neural regulatory functions, and modulates perception and information transmission (Moretto et al., 2018). iGluRs are further classified into N-methyl-D-aspartate (NMDA) receptors, α-amino-3-hydroxy-5-methyl-4-isoxazolepropionic acid (AMPA) receptors, and kainate receptors (Mayer, 2016). According to the Motif structure diagram of model animals (human, mouse, zebrafish), we can see the differences among the three. Compared with NMDA-type receptors, Motif 8 and Motif 9 exist for AMPA-type receptors and KA-type receptors (Supplementary Figure S1). iGluRs subunits, dividing four modular structural domains including amino-terminal domain (ATD), ligand-binding domain (LBD), transmembrane domain (TMD), and C-terminal domain (CTD), coalesce into tetramers within their respective subclasses, forming ligand-gated ion channels (Karakas et al., 2015). The LBD contains two half-domains S1 and S2, which are closed to each other when LBD binds glutamate (Armstrong et al., 1998), and the Lig_Chan domain contains three transmembrane regions M1, M2, M3 and ion channel pore P (Kuner et al., 2003). Despite the extensive investigation of iGluRs in humans, mice, zebrafish, and other vertebrates over past decades (Herbrechter et al., 2021), due to their integral role in neuronal function, research in mollusks, particularly bivalves, is still nascent.

The rapid advancement of industry and agriculture in recent years has triggered a surge in marine pollution (Rahman et al., 2022). The environmental exposure to neurotoxic metals and metalloids, including cadmium, lead, mercury, copper, and zinc, has escalated into a global health concern, affecting millions worldwide (Liu et al., 2023). Research suggests that environmental neurotoxic metal stress can compromise neurotransmitter receptor function, thereby impinging on neural development, behavior, cognition, and precipitating neurodegeneration (Carmona et al., 2021). Existing evidence implicates Cd in directly affecting synaptic transmission mediated by AMPA receptors (Wang et al., 2008). Conversely, neurotoxic Pb exhibits significant selectivity for NMDA receptors, suggesting that the neurotoxicity of this metal is mediated by receptor-type-specific regulation (Marchetti and Gavazzo, 2003). Moreover, copper can bidirectionally modulate hippocampal neuronal synaptic activity: acute copper stimulation can impede signal transmission, but after a 3-h continuous copper stimulation, it amplifies the frequency and amplitude of AMPA currents (Peters et al., 2011). Recent research reveals that Cd downregulates NMDA receptors (GRIN2A and GRIN2B) and inhibits the activity of inhibitory glutamate receptor GluR2, while upregulating the phosphorylation of excitatory glutamate receptor GluR1, inducing functional impairment of glutamate receptors (Yang et al., 2023). Consequently, environmental neurotoxic metals can obstruct various functions of the entire nervous system via iGluRs, thereby disrupting organismal homeostasis (Pochwat et al., 2015). The chosen metals (Zn, Cu, Cd, Hg, and Pb), being prevalent marine pollutants with known iGluR interactions, are pivotal for examining environmental stress responses in Pacific oyster.

In this context, bivalves, such as the Pacific oyster (*Crassostrea gigas*), have emerged as a research focal point due to their unique resilience to metal pollution. Intriguingly, the oysters harbor high concentrations of metals without manifest toxicity, suggesting the evolution of sophisticated metal accumulation regulatory mechanisms (Jonathan et al., 2017). Investigations in vertebrates demonstrate the toxic effects of metals on ionotropic glutamate receptors, which can severely perturb iGluRs signal transmission (Sadiq et al., 2012). Prior research has corroborated the presence of a relatively comprehensive neuroendocrine system in oysters (Liu et al., 2018; Wang, 2022), yet reports on iGluRs and their regulation of metal ions are scant. Elucidating the mechanisms and strategies of bivalve iGluRs in response to metal stimulation holds profound implications for addressing environmental pollution and seafood safety issues.

Against this backdrop, the present study identified and systematically analyzed the iGluRs of *C. gigas*. Subsequently, the spatiotemporal expression spectrum of *Cg*iGluRs genes was scrutinized using the RNA-seq dataset. Furthermore, this study probed the expression level and characteristics of *Cg*iGluRs genes in the gills to decipher the molecular mechanisms underpinning oyster responses to heavy metal stress.

2 Materials and methods

2.1 Identification and characterization of iGluRs genes in *C. gigas*

The BLASTP tool was deployed to decipher the gene sequence of iGluRs in the Pacific oyster. Amino acid sequences of iGluRs from a broad spectrum of invertebrates and vertebrates were leveraged as queries against the NCBI[1] and Uniprot databases[2] (UniProt Consortium, 2018). This exhaustive search spanned species from sea hare to human, inclusive of *Xenopus tropicalis*, *Danio rerio*, and *Homo sapiens*. The oyster transcriptome and whole genome sequences were meticulously examined to identify candidate iGluRs genes. Subsequent analyses involved predicting amino acid sequences using the ORF Finder tool[3], identifying conserved structural domains via the SMART program[4] (Letunic and Bork, 2018), and detecting conserved motifs using the MEME Suite[5] (Nystrom and McKay, 2021), with a maximum motif limit set to 12 (prevent motif overlap and maintain analysis accuracy). All results were visualized using TBtools (Chen et al., 2020). The Compute pI/Mw tool[6] (Wilkins et al., 1999) was utilized to calculate the GRAVY (Grand average of hydropathicity), theoretical isoelectric point (pI), and molecular weight (Mw) of

1 https://www.ncbi.nlm.nih.gov/
2 https://www.uniprot.org/
3 https://www.ncbi.nlm.nih.gov/orffinder/
4 http://smart.embl-heidelberg.de/
5 https://meme-suite.org/meme/tools/meme
6 https://web.expasy.org/compute_pi/

the pore domain, while the secondary structure was predicted using Geneious7.0.6[7] (Kearse et al., 2012).

2.2 Phylogenetic analysis and chromosomal localization of iGluRs in *C. gigas*

For the phylogenetic analysis, iGluRs proteins from *C. gigas* and other selected species, including the invertebrates and vertebrates, were selected. The iGluRs amino acid sequences from selected species were retrieved from the NCBI and Uniprot databases (Supplementary Table S1). Multiple sequence alignment was executed using AliView software (Larsson, 2014), followed by the construction of an evolutionary tree based on the maximum likelihood method via PhyML (v3.0) software[8] (Guindon et al., 2010). The tree was subsequently refined using FigTree (v1.4.4) software[9]. Chromosomal locations and sizes of the iGluRs genes in the oyster were derived from the oyster genome data (cgigas_uk_roslin_v1) (Peñaloza et al., 2021), analyzed through TBtools.

2.3 Spatiotemporal expression profiling of iGluRs in *C. gigas*

Expression analysis was conducted using the RPKM (Reads Per Kilobase Million) values of each iGluRs gene from the publicly available RNA-seq dataset of the oyster. This dataset spans various developmental stages and adult tissues. Expression patterns of these genes across different stages and tissues were visualized using a heatmap generated by TBtools.

2.4 Transcriptional response of iGluRs in *C. gigas* to heavy metal exposures

In investigating the transcriptional dynamics of iGluRs in oysters under heavy metal exposure conditions, we utilized an RNA-Seq dataset (Zhang et al., 2012), encompassing exposure data for Zn, Cu, Cd, Hg, and Pb. Specifically, oysters were exposed to one of the five metals (Zinc 1 mg/L, Cadmium 100 μg/L, Copper 100 μg/L, Lead 500 μg/L, Mercury 20 μg/L), with a control group subjected to seawater treatment. The concentrations of these metals were non-lethal, and no fatalities occurred during the experiment. The sampling time points were at 12 h and 9 days post-exposure. The original RNA-Seq data (Project number: PRJNA146329) were obtained from the NCBI database. Subsequently, these data were aligned to the oyster genome utilizing HISAT2 (v2.0.5) with default parameters. Gene expression levels were then estimated employing the Fragments Per Kilobase Million (FPKM) method. Temporal trends of gene expression under different metal exposures were analyzed and clustered using the Mfuzz R package (Kumar and Futschik, 2007) in R (version 4.2.3). A Venn diagram depicting the common expression trends of *Cg*GRIA4 under five metal exposures was constructed using jvenn[10] (Bardou et al., 2014).

2.5 Pathway enrichment and interaction analysis of iGluRs in *C. gigas*

Following the Venn diagram analysis, KEGG enrichment analysis was performed on all intersecting treatments using the R package clusterProfiler (Yu et al., 2012). The enrichKEGG function was used to identify enriched KEGG pathways among the genes listed in the Venn diagram, with a p-value <0.05 set as the threshold for significance. To further elucidate the response mechanism of *Cg*GRIA4 to heavy metals, significantly enriched pathways ($p < 0.05$) involving the *Cg*GRIA4 gene were screened. A network diagram of these pathways was constructed using the KEGG network tool of OmicShare Tools[11]. Enrichment pathways and gene information are detailed in Supplementary Table S2. Collectively, through KEGG enrichment analysis and pathway network diagramming, we aim to gain a deeper understanding of the expression pattern of *Cg*GRIA4 under different metal exposures and its role in biological processes.

3 Result

3.1 Identification and characterization of iGluRs genes in *C. gigas*

To elucidate the genomic landscape of the oyster, a comprehensive analysis of the transcriptome and genome databases was undertaken, leading to the discovery of 12 iGluRs genes. These genes, detailed in Table 2, were classified into three distinct subfamilies based on sequence homology and domain architecture: AMPA receptors, NMDA receptors, and kainate receptors (Table 1). The open reading frames (ORFs) of *Cgi*GluRs spanned from 2,385 to 3,675, encoding between 794 and 1,224 amino acids. GRIA2 was found to be the most complex, comprising 19 exons and 18 introns (Supplementary Figure S2; Table 2). The predicted molecular weights of *Cgi*GluRs ranged from 89.49 to 138.79 kDa, with predicted isoelectric points (pI) between 5.78 and 8.81. The secondary structure of the proteins encoded by iGluRs suggested a composition of 29–53 alpha helices, 44 to 74 beta strands, 58 to 93 coils, and 52 to 99 turns (Table 2). The amino acid consistency between *Cgi*GluRs and iGluRs of other invertebrates ranged from 27.25% to 90.46%, and it ranged from 23.96% to 50.76% with vertebrate iGluRs (Table 3).

A phylogenetic tree was constructed for *Cgi*GluRs, and subsequent analysis of domain information and gene base sequence was conducted (Figure 1). All *Cgi*GluRs were found to possess a Pfam Lig_Chan domain centrally, which belongs to the TMD module. (Figure 1C). The N-terminus of the *Cg*NMDA

7 https://www.geneious.com/

8 http://www.atgc-montpellier.fr/

9 http://tree.bio.ed.ac.uk/software/Figtree/

10 https://jvenn.toulouse.inrae.fr/app/example.html

11 https://www.genedenovo.com/

TABLE 1 Statistical table of gene members of iGluRs subfamily in different species.

Species	NMDAR	AMPAR	KAR	Total
Homo sapiens	7	4	5	16
Mus musculus	7	4	5	16
Gallus gallus	6	4	4	14
Larimichthys crocea	7	4	5	16
Xenopus tropicalis	7	4	5	16
Danio rerio	8	4	5	17
Octopus bimaculoides	3	0	1	4
Aplysia californica	1	1	3	5
Lingula anatina	2	0	1	3
Strongylocentrotus purpuratus	0	1	1	2
Ciona intestinalis	1	3	1	5
Crassostrea virginica	3	0	2	5

subfamily was found to feature a PBP_type1 superfamily domain, which belongs to the LBD module. Certain *Cgi*GluRs also contained specific structural regions, such as the Cam_bdg_C0 domain at the C-terminus of *Cg*GRIN1, which is the key with NMDA-type receptors that allow calcium ions to pass through (Figure 1C). Twelve conserved motifs were identified in *Cgi*GluRs, with *Cgi*GluRs sharing eight common motifs (1–3, 5–9; Figure 1B). *Cg*GRIN contained a unique motif, motif 11. All proteins, except for *Cg*GRIN3A and *Cg*GRIN1, possess motif 4 (Figure 1B). *Cg*GRIN2B and *Cg*GRIK3 lack motifs 10 and 12, *Cg*GRIN2A and *Cg*GRIN3A lack motif 10, and *Cg*GRIK1 lacks motif 12 (Figure 1B).

3.2 Phylogenetic relationship and Chromosomal Localization of *Cgi*GluRs

A chromosome map of *Cgi*GluRs was constructed based on the oyster genome sequence (Figure 2A). All 12 identified *Cgi*GluRs were found to be located on the oyster chromosomes, primarily on chromosomes 1, 5, 7, and 10. Chr 7 hosts the majority (5 *Cgi*GluRs) of *Cgi*GluRs genes, while Chr 5 contains only two. Most *Cgi*GluRs genes are found on Chr7 and Chr10 (9 out of 12, 75%), suggesting that the number of *Cgi*GluRs genes is not related to chromosome size (Figure 2A).

In this study, a phylogenetic tree was constructed by comparing the full-length amino acid sequences of *Cgi*GluRs and those from other species (Figure 2B; Table 4). The results reveal that the *Cgi*GluRs family can be divided into two main branches: NMDA and non-NMDA receptors, which are further subdivided into three subfamilies, namely, GRIA, GRIK, and GRIN (Figure 2B). The classification of each subfamily is based on genetic similarity. Within each subfamily, the iGluRs members of vertebrates and invertebrates form independent branches. Notably, the genes of the American oyster and the oyster share the closest evolutionary relationship within the same iGluRs subfamily (Figure 2B). In the specific construction of the phylogenetic tree, the red branch represents the GRIA subfamily. Among them, *Cg*GRIA1, *Cg*GRIA1-like, and A.CA GRIA2 form a branch. *Cg*GRIA2 and A.CA GRIK4 form a branch. *Cg*GRIA4, O.BI GRIK2, and *Cg*GRIK5 form a branch, and then form a branch with *Cg*GRIK3, C.VI GRIK2, and C.VI GRIK3 forms a branch. The green branch represents the GRIK subfamily. In this subfamily, *Cg*GRIK1 forms a branch with the A.CA GRIK5, while *Cg*GRIK2-like forms a branch with A.CA GRIK2, L. AN GRIK2. The blue branch represents the GRIN subfamily, which contains four *Cg*GRIN genes. It is worth noting that the number of three subfamilies including GRIA, GRIK, and GRIN has significantly increased in vertebrates, indicating that these iGluRs subfamilies have been continuously expanded during evolution (Figure 2B).

3.3 Spatiotemporal Expression Patterns of *Cgi*GluRs

RNA-seq datasets from different developmental stages and adult tissues of the oyster were used to detect the spatiotemporal expression spectrum of *Cgi*GluRs (Figure 3). The expression patterns of *Cgi*GluRs can be divided into two groups across different developmental stages (Figure 3A). The first group consists of 9 *Cgi*GluRs that are highly expressed after D-shaped larvae, and these *Cgi*GluRs have higher expression levels during the Pediveliger period than during the Later umbo larva period and Spat period. The second group consists of 3 *Cgi*GluRs that are highly expressed before D-shaped larvae, and these *Cgi*GluRs have different expression patterns throughout the development of the oyster.

In adult oyster tissues, *Cgi*GluRs expression patterns are categorized into four distinct groups as illustrated in Figure 3B. GRIN3A, GRIA4, and GRIK5 from the first group predominantly exhibit expression in the mantle and its edge. The second group, which includes *Cg*GRIK3, *Cg*GRIN1, *Cg*GRIA1, and *Cg*GRIA1-like, primarily shows expression in the inner edge of the mantle. The labial palps are the main expression site for the third group, containing *Cg*GRIK1, *Cg*GRIN2B, and *Cg*GRIA2. The adductor muscle expresses the fourth group, represented by *Cg*GRIK2-like and *Cg*GRIN2A. Additionally, peak expressions of *Cgi*GluRs in adult oysters are found in neural tissues associated with environmental perception, encompassing areas like the labial palps, adductor muscle, and mantle edges.

3.4 *Cgi*GluRs expression under metal exposures

To detect the expression pattern of *Cgi*GluRs in response to heavy metal stress, the RNA-seq dataset of oyster gills under the stress of five heavy metals Zn, Cu, Cd, Hg, Pb were analyzed (Figure 4). The expression levels of GRIA1 and GRIA1-like mRNA decreased after short-term exposure to the five heavy metals, but under long-term exposure to Cu, the expression of these two *Cgi*GluRs returned to normal level (Figures 4A–E). In addition, long-term exposure to Cu and Cd inhibited the expression of *Cg*GRIA2 (Figures 4A, B). Under short-term exposure to Cu, Cd, Hg, and Pb, the expression of *Cg*GRIA4 and *Cg*GRIK5 was

TABLE 2 Sequence characteristics of iGluRs gene family of *C. gigas*.

Gene name	Gene ID	cDNA length (bp)	ORF length (bp)	Exons no.	Introns no.	Amino acid no.	Molecular weight (kDa)	Theoretical PI	AlpHa no.	Beta no.	Colins no.	Turn no.	GRAVY of PD
GRIN3A	LOC105318495	4,665	3,675	9	8	1224	138789.05	7.04	53	74	93	99	−0.271
GRIK3	LOC105323215	3,257	2,595	3	2	864	97918.54	6.37	44	44	58	52	−0.206
GRIA2	LOC105336269	3,751	2,907	19	18	968	110793.88	8.35	38	54	68	68	−0.235
GRIK2-like	LOC105332320	4,499	2,751	15	14	916	104746.63	5.78	45	56	68	74	−0.226
GRIN2B	LOC105347230	5,380	3,357	17	16	1,118	129258.96	8.69	50	64	83	89	−0.280
GRIK1	LOC105348088	3,070	2,403	13	12	800	89486.81	6.15	36	47	60	55	0.025
GRIA4	LOC105327395	2,970	2,463	14	13	820	94127.40	6.68	37	48	59	59	−0.152
GRIK5	LOC105327397	4,422	2,385	12	11	794	90691.87	6.29	29	52	66	62	−0.116
GRIA1	LOC105326127	3,359	2,691	17	16	864	98015.03	8.81	42	57	68	71	−0.175
GRIA1-like	LOC105326132	3,141	2,640	17	16	879	100006.41	6.41	34	57	70	65	−0.204
GRIN2A	LOC105322565	3,407	2,529	14	13	842	95416.69	6.17	38	47	65	67	−0.339
GRIN1	LOC105333721	4,314	2,667	18	17	888	99428.99	6.13	52	51	65	59	−0.200

10.3389/fphys.2023.1280553

TABLE 3 Percentage of Identity(I) of *C.gigas* iGluRs with selected iGluRs proteins in other species.

Gene	*H. sapiens* (%)	*M. musculus* (%)	*G gallus*	*X tropicalis* (%)	*D. rerio* (%)	*L crocea* (%)	*C intestinalis*	*O bimaculoides*	*A californica*	*L anatina*	*D melanogaste*	*C. virginica*
GRIN3A	27.79	27.56	30.05%	28.16	26.28	29.34	—	43.72%	—	—	—	75.55%
GRIK3	28.79	28.92	28.69%	27.43	32.61	28.59	—	—	—	—	—	76.85%
GRIA2	42.64	42.52	44.19%	41.06	40.94	44.66	27.90%		39.74%	—	—	—
GRIK2-like	40.26	40.26	41.49%	40.60	40.76	40.52	27.25%	27.25%	45.16%	39.52%	32.39%	28.81%
GRIN2B	30.32	30.55	30.89%	30.89	30.48	34.72	—	—	—	39.64%	—	42.62%
GRIK1	24.00	24.05	24.65%	24.94	23.96	24.59	—	—	—	—	—	—
GRIA4	32.26	31.86	32.13%	31.77	31.51	37.88	—	—	—	—	—	—
GRIK5	31.08	31.58	—	34.65	33.07	30.33	—	—	23.79%	—	—	—
GRIA1	39.88	40.02	40.27%	40.62	39.21	38.86	—	—	—	—	39.42%	—
GRIA1-like	41.60	41.53	42.10%	42.54	40.54	38.98	—	—	—	—	42.76%	—
GRIN2A	33.14	33.14	33.90%	33.48	33.24	31.93	35.67%	53.42%	—	—	—	—
GRIN1	48.98	48.75	50.76%	48.29	47.07	47.65	34.97%	58.58%	—	58.24%	51.70%	90.46%

10.3389/fphys.2023.1280553

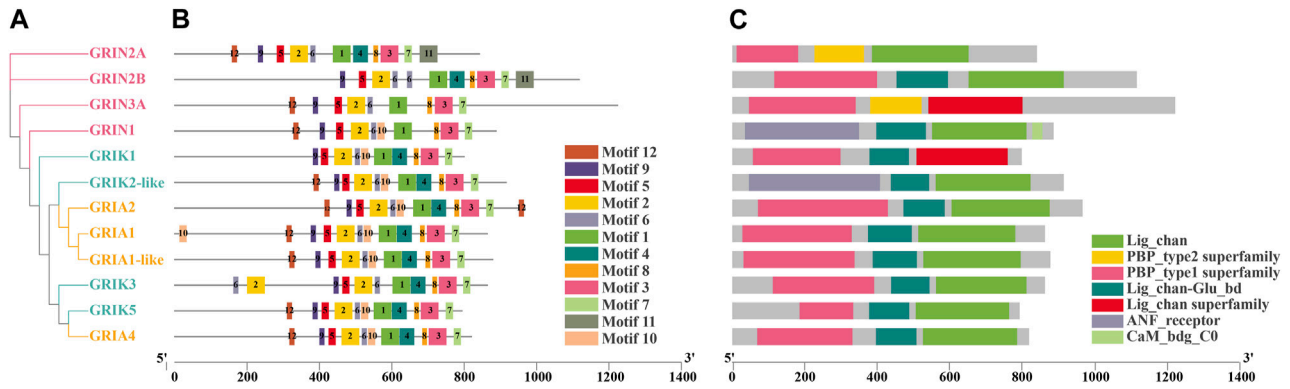

FIGURE 1
Phylogenetic relationships, protein motifs, and gene structures of 12 *Cgi*GluRs genes. **(A)** Phylogenetic tree of *Cgi*GluRs. Protein sequences were aligned using AliView, and the phylogenetic tree was constructed applying the maximum likelihood method. **(B)** Protein motifs of *Cgi*GluRs. Conserved motifs (1–12) are depicted by different colored boxes, with non-conserved sequences represented by black lines. Motifs were visualized using Tbtools. **(C)** Gene structures: Lig_Chan domains, PBP_type1 superfamily domains, Lig_chan superfamily domains, ANF_receptor domains, and PBP_Type_2 superfamily domains are represented by green, yellow, pink, blue, and red boxes respectively.

upregulated (Figures 4A–D). The expression levels of *Cg*GRIA4 and *Cg*GRIK5 were upregulated under long-term exposure to Zn (Figure 4E). Collectively, the results highlight the pronounced responsiveness of *Cg*GRIA4 and *Cg*GRIK5 to heavy metal perturbations.

3.5 Mechanism of *Cg*GRIA4 in response to metal stress

The analysis prioritized CgGRIA4 over GRIK5 due to the established association of AMPA-type receptors, to which GRIA4 belongs, with calcium ion permeation critical in metal stress response. To better understand GRIA4's role in metal exposure, a detailed analysis following exposure to five metals identified 142 genes with similar expression trends (Supplementary Figure S3; Figure 4F). Through KEGG enrichment analysis of these genes, we found that pathways related to neural signal transmission, such as Glutamatergic synapse (ko04724), Dopaminergic synapse (ko04728), and Neuroactive ligand-receptor interaction (ko04080), were significantly enriched (Figure 5A). In addition, some antioxidant-related metabolic pathways, such as Vitamin B6 metabolism (ko00750), Vitamin digestion and absorption (ko04977), and Selenocompound metabolism (ko00450), were also significantly enriched (Figure 5A). To reveal the mechanism of *Cg*GRIA4 in metal stress response more deeply, we drew a KEGG network map of the genes in the 142 genes that share the same pathway with *Cg*GRIA4 (Figure 5B). In the KEGG network map, *Cg*GRIA4 mainly participates in the activation of Glutamatergic synapse and Dopaminergic synapse, and *Cg*GRIA4 mainly affects two neurodegenerative disease-related pathways, Spinocerebellar ataxia (ko05017), and Huntington disease (ko05016), and the activation of these two pathways is closely related to calcium ion homeostasis imbalance (Figure 5) (Begum et al., 2018; Zhou et al., 2018).

4 Discussion

Ionotropic Glutamate Receptors (iGluRs) are a key type of ion channel widely distributed across the animal kingdom. Upon activation, they transmit signals of sodium, potassium, or calcium ions, participating in various sensory processes (Manookin et al., 2008; Sánchez-Alcañiz et al., 2018) and playing a crucial role in physiological processes such as neuroplasticity (Budreck et al., 2013), learning and memory, cell life cycle, and immune defense. In this study, a complete set of iGluRs family genes was identified in the genome of the oyster *C. gigas*, and their protein structure, phylogenetic relationships, expression patterns during developmental stages and in the adult tissues under heavy metal stress were analyzed. The results provide a new perspective for a deeper understanding of the molecular evolution and functional diversity of the iGluRs channel family.

Our comprehensive genomic screening revealed the presence of 12 *Cgi*GluRs family genes in oysters. These genes are widely distributed across the three iGluRs subfamilies: NMDA receptors (NMDAR), AMPA receptors (AMPAR), and kainate receptors (KAR). By contrast, the iGluRs family gene combination in vertebrates, such as humans (Hansen et al., 2021), is more diverse, encompassing 7 NMDARs, 4 AMPARs, and 5 KARs. In vertebrate evolution, the expansion of KAR and AMPAR genes is notably more significant than in mollusks, as evidenced by the pronounced difference in the neural system. This expansion is likely an adaptation to the more complex requirements of neural signal transmission. In the *Cg*NMDAR subfamily of oysters, a singular *Cg*GRIN1 with the CaM_bdg_C0 domain has been discerned. Contrarily, zebrafish exhibit an array of GRIN copies, each embedded with the CaM_bdg_C0 domain, pivotal for the regulation of Ca^{2+} influx (Cox et al., 2005). Such distinctions underscore the potential evolutionary adaptation of calcium ion mediation in tandem with the intricacies of the neural system. In summary, the genomic variations in iGluRs family genes between oysters and vertebrates underscore the evolutionary intricacies and

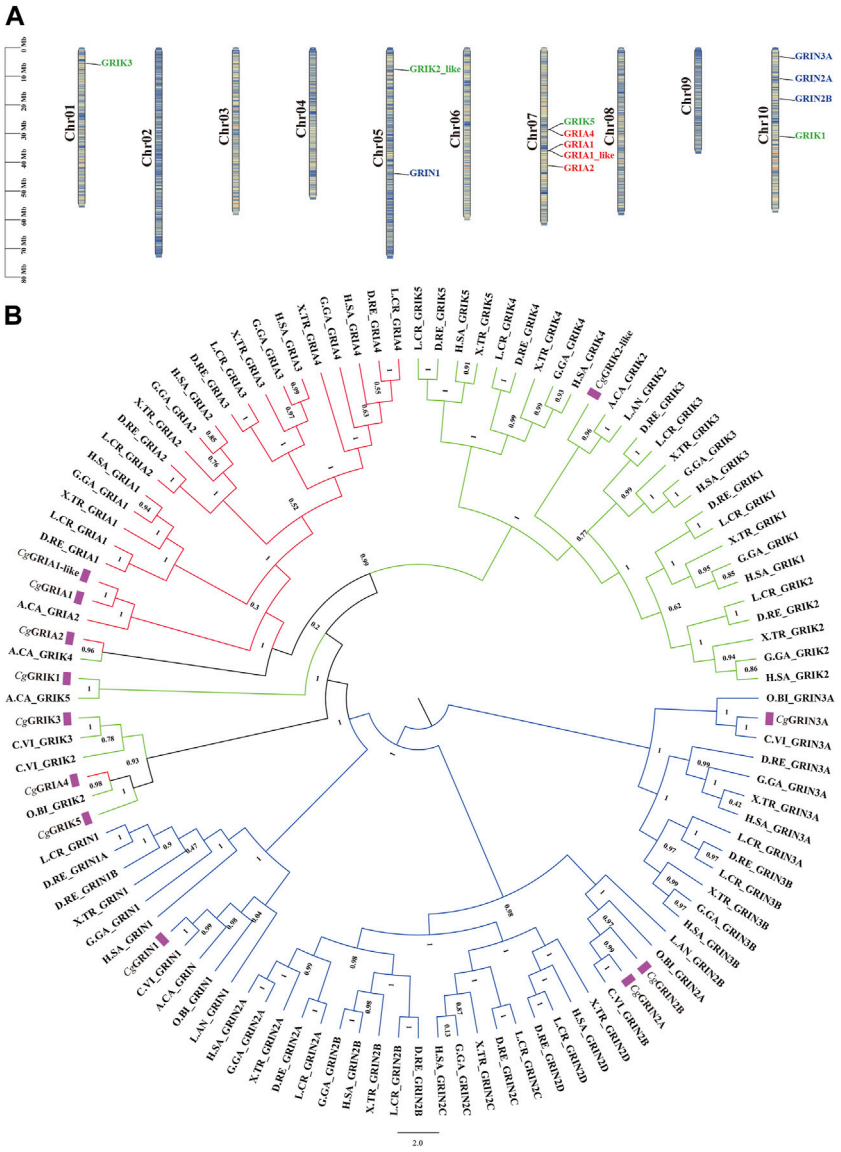

FIGURE 2
Phylogenetic Analysis and Chromosomal Localization of *Cg*iGluRs. **(A)** Chromosomal distribution of the 12 *Cg*iGluRs genes, along with the dispersion of duplicate gene pairs. Each gene is positioned on a chromosome according to its physical location, with the chromosome number (Chr01-Chr10) indicated on the left. **(B)** A multispecies phylogenetic tree, derived from the protein sequences of iGluRs from *C. gigas* and other selected species, was constructed using the maximum likelihood method and supported by 1,000 bootstrapped pseudoreplicates. *Cg*iGluRs are marked in purple. Branches representing different subfamilies are highlighted in distinct colors (*Cg*NMDAR: blue, *Cg*AMPAR: red, *Cg*KAR: green). Species abbreviations are as follows: Cg, *Crassostrea gigas*; H.SA, *Homo sapiens*; G.GA, *Gallus gallus*; X. TR, *Xenopus tropicalis*; D.RE, *Danio rerio*; O.BI, *Octopus bimaculoides*; A.CA, *Aplysia californica*; L. AN, *Lingula anatine*; L. CR, *Larimichthys crocea*; C.VI, *Crassostrea virginica*.

adaptive nature of neural systems, especially in calcium ion mediation, to environmental complexity.

In both vertebrate and invertebrate species, proteins of the iGluRs class, including those in the *Cg*iGluRs family, consistently exhibit four distinct transmembrane structural domains. Intriguingly, comparative analyses reveal no significant divergence in these domains across the various iGluRs subfamilies. Within vertebrates, these subfamilies are systematically designated based on their specific affinities for synthetic agonists, namely, AMPA, NMDA, and kainate (Hansen et al., 2021). In *Cg*GRIN1, the NMDA receptor GRIN1 subunit calmodulin binding domain C0 domain (CaM_bdg_C0) was found. This is a necessary subunit that allows Ca^{2+} to pass through, constant with the role of GRIN1 as an essential subunit of the NMDA receptor and its mediating function of Ca^{2+} channels (Ganor and Levite, 2014). There was an ANF_receptor domain identified in *Cg*GRIN2A and *Cg*GRIK2-like. The rest of the *Cg*iGluRs possess the PBP_Type_2 superfamily domain. These domains form the structural basis for the C-terminal structural domain (CTD) of *Cg*iGluRs to recognize extracellular signals. In *Cg*iGluRs, the CTD length varies between different iGluRs subfamilies. Compared with *Cg*AMPAR and *Cg*KAR, *Cg*NMDA receptors, excluding GRIN1, have a longer CTD. Studies have shown that the CTD of GluN2 is the longest (Dravid et al., 2010). This diversity

TABLE 4 Comparison table of scientific name of species.

Abbreviation	Scientific name
H.SA	*Homo sapiens*
G.GA	*Gallus gallus*
X.TR	*Xenopus tropicalis*
D.RE	*Danio rerio*
O.BI	*Octopus bimaculoides*
A.CA	*Aplysia californica*
L.AN	*Lingula anatina*
L.CR	*Larimichthys crocea*
C.VI	*Crassostrea virginica*
Cg	*Crassostrea gigas*

of subunits in the CTD is thought to play specialized and complex roles in neurons. The above results indicate that *Cg*iGluRs share similar domain structure with their homologues from other species, and the structural differences between members of the *Cg*iGluRs family may directly reflect their functional diversity.

Phylogenetic analysis showcases a primary bifurcation of the *Cg*iGluRs family into NMDA-type and non-NMDA-type receptors, aligning with prior research (Stroebel and Paoletti, 2021). *Cg*GRIA4, *Cg*GRIK3, and *Cg*GRIK5 cluster with other invertebrate iGluRs proteins like the GRIK2 and GRIK3 of the Portuguese oyster, and the GRIK2 of the California double sheath, highlighting a close phylogenetic relationship. This relationship is likely fostered by structural similarities between AMPA-type and KA-type receptors, and is further supported by the molecular secretion complexity of glutamatergic synapses, illustrating an intricate evolutionary interplay. A comparative study reveals a significant phylogenetic link between the iGluRs families of the Pacific oyster and the California Sea Hare (*Aplysia californica*), with bootstrap analyses supporting this relationship. This underlines the conservation of the iGluRs family across species and its key role in environmental adaptability. NMDAR subfamily members are found from bacteria to mammals, suggesting it as the most ancestral lineage, followed by KAR and AMPAR (Chen et al., 1999). The iGluRs family attains functional diversity via subunit combinations and RNA editing, vital for environmental adaptation. The divergence into NMDA and non-NMDA types might reflect environmental pressures, with each type potentially offering different adaptive advantages in response to varying environmental conditions such as temperature and salinity changes (Busnardo et al., 2016; Stroebel and Paoletti, 2021). This insight offers a refined perspective on the role of iGluRs in neural signal transmission and environmental adaptability.

Prior research underscores the crucial role of iGluRs in embryonic development, with AMPA (3, 4) and Kainate (3, 4, 5) receptor abnormalities affecting mouse blastocyst development (Spirkova et al., 2022). While in vertebrates like mice, iGluRs function primarily as excitatory neurotransmitters, in bivalves, they serve different functional roles, illuminating the functional divergence across phylogenetically distant taxa. This study reveals an increase in iGluRs expression correlating with oyster larvae development (egg average RPKM = 1.5, juvenile average RPKM = 137.9), indicating *Cg*iGluRs' involvement in this process. Notably, iGluRs expression escalates during the pediveliger period (average RPKM = 133.7), a critical stage where the eyespot and the foot develop. Recent findings suggest the eyespot has photoreceptive abilities, and the foot engages in sensory perception and locomotion (Vogeler et al., 2016; Zhang et al., 2021). Vertebrate iGluRs are pivotal in signal transduction for environmental cue perception (Levitz et al., 2016; van Giesen and Garrity, 2017). The pronounced iGluRs expression during the

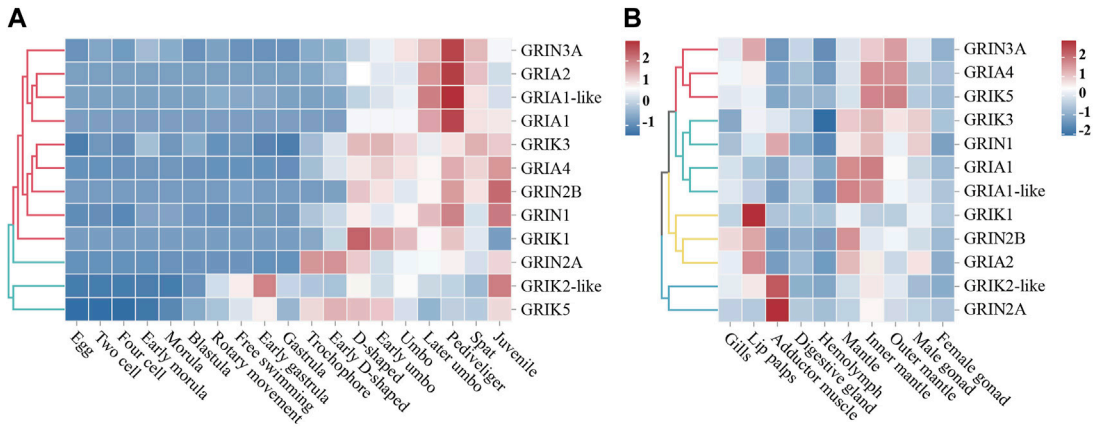

FIGURE 3
Spatiotemporal Expression Patterns of *Cg*iGluRs. **(A)** A heat map depicting the expression profiles of *Cg*iGluRs genes across various developmental stages, quantified by Log_{10}RPKM. The stages included are egg, two-cell, four-cell, early morula, morula, blastula, rotary movement, free swimming, early gastrula, gastrula, trochophore, early D-shaped, D-shaped, early umbo, umbo, later umbo, pediveliger, spat, and juvenile. Based on the expression patterns of *Cg*iGluRs, two primary clusters are delineated, represented in red and blue colors. **(B)** A heat map presenting the tissue-specific expression profiles of *Cg*iGluRs genes in adult oysters, quantified by Log_{10}RPKM. The tissues represented include gills, lip palps, adductor muscle, digestive gland, hemolymph, mantle, inner margin of mantle, outer margin of mantle, female gonad, and male gonad. Based on the expression patterns of *Cg*iGluRs are grouped into four clusters, denoted by red, cyan, yellow, and blue.

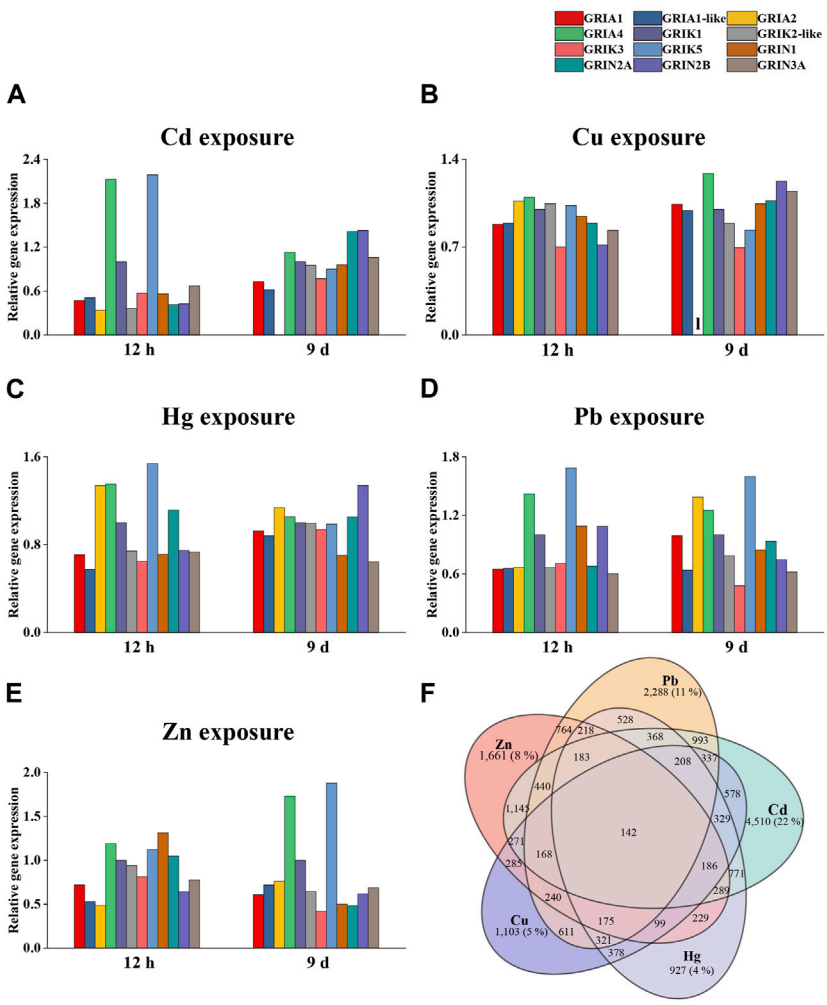

FIGURE 4
Expression of *Cgi*GluRs in Response to Metal Exposure. **(A)** Changes in relative gene expression (expressed as fold change relative to control) in oysters exposed to cadmium (Cd). **(B)** Relative gene expression alterations (expressed as fold change relative to control) in oysters in response to copper (Cu) exposure. **(C)** Modulations in relative gene expression (expressed as fold change relative to control) in oysters following Mercury (Hg) exposure. **(D)** Adjustments in relative gene expression (expressed as fold change relative to control) in oysters subjected to lead (Pb) exposure. **(E)** Changes in relative gene expression (expressed as fold change relative to control) in oysters upon zinc (Zn) exposure. **(F)** A Venn diagram presenting the genes demonstrating similar expression trends to GRIA4 under the stimulation of the five metals.

pediveliger stage highlights their essential role in pediveligers' environmental perception. Particularly, *Cg*GRIA4 expression peaks in this phase (RPKM = 416), aligning with its AMPA-type counterparts. The functional assembly of AMPA-type receptors as either homomeric or heteromeric tetramers (Hanada, 2020) suggests the dominance of CgGRIA4 in steering the perceptual processes of pediveligers.

iGluRs are central to neural systems, mediating complex cerebral functions including neural transmission and memory (Sachser et al., 2017; Shahin et al., 2018; Hayashi, 2021). Our data from adult oysters show receptor-specific expression profiles. Elevated expression of *Cg*GRIA4 in the mantle suggests its role in sensory and environmental perception, aligning with GRIA4's known role in vertebrate synaptic transmission (Sagata et al., 2010). Enhanced *Cg*GRIK1 expression in the labial palps hints at its potential role in alimentary or environmental detection, mirroring the sensory function of GRIK1 (Englund et al., 2021). Notably, pronounced *Cg*GRIN2A expression in the adductor muscle indicates possible implications in shell dynamics, resonating with Zhao et al. (2023) identification of GRIN2A as a neural excitability modulator. Our findings highlight the critical roles of *Cgi*GluRs in oyster physiology, emphasizing their evolutionary conservation and parallels with vertebrate neural systems. Additionally, we propose that oyster iGluRs might detect metal concentration changes, with certain metal ions potentially interacting with specific iGluRs domains, thus altering channel dynamics, and influencing neural or other physiological responses to environmental stress.

iGluRs are instrumental in mitigating the neurotoxic effects of heavy metals (Slotkin and Seidler, 2009). Our analyses delineate the nuanced responses of *Cgi*GluRs to specific metal challenges. Intriguingly, *Cg*GRIA1 expression is reduced under acute exposure to five metals (Zn, Cu, Cd, Hg, and Pb), yet

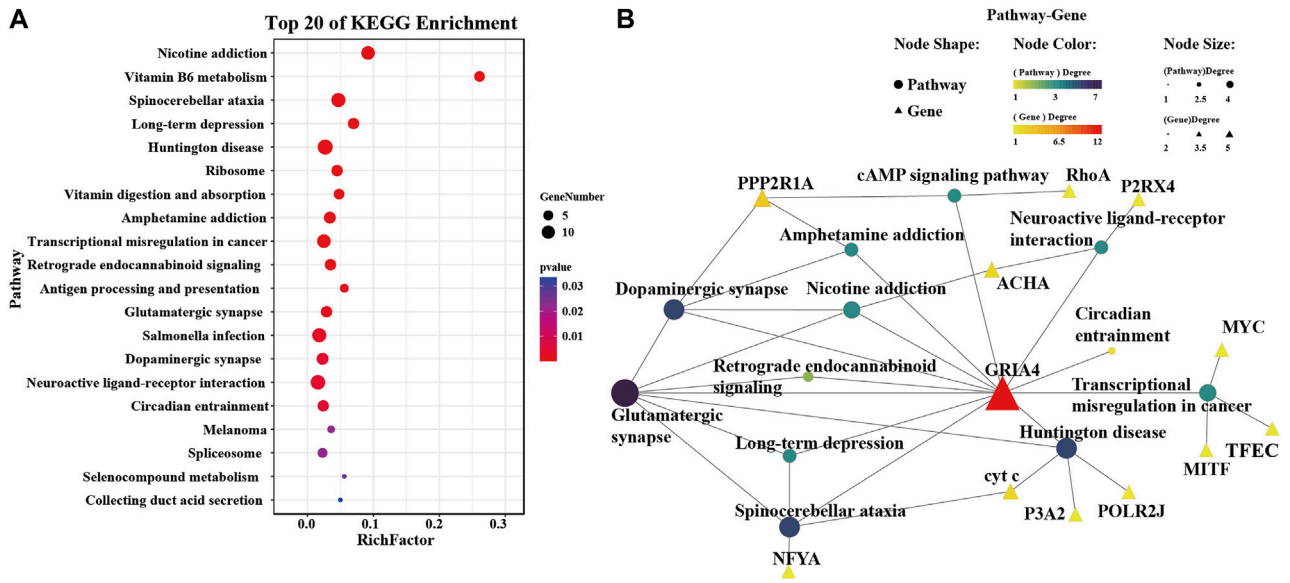

FIGURE 5
KEGG enrichment analysis of genes expressing similarly to *Cg*GRIA4. **(A)** The top 20 enriched KEGG terms identified among the 142 genes depicted in Figure 4F. **(B)** A network interaction model constructed from the KEGG enrichment analysis performed on the 142 intersecting genes presented in Figure 4F. This analysis enabled the identification of KEGG pathways significantly engaged by *Cg*GRIA4, and these pathways are depicted in the model to demonstrate their interconnections.

demonstrates resilience during extended Cu and Pb challenges. This pattern suggests that *Cg*GRIA1 might bolster cellular robustness by dynamically modulating its expression in response to metal-induced stress. Studies in vertebrates emphasize the neuroprotective advantages of GRIA1 downregulation. Furthermore, shifts in the GRIA1 to GRIA2 ratio are postulated to modulate the calcium permeability of CP-AMPAR (Li et al., 2023). In our dataset, *Cg*GRIA2 shows a contrasting expression pattern under copper and lead exposure. Given GRIA2's pivotal role in dictating AMPAR calcium permeability, it is plausible that *Cg*AMPAR receptors adapt to metal stress by fine-tuning calcium homeostasis. We observed a marked upregulation of *Cg*GRIA4 under metal stress. As a subtype of the AMPA receptor, GRIA4 is integral to rapid synaptic signaling (Song and Huganir, 2002). The pronounced expression of *Cg*GRIA4 intimates an adaptive strategy in oysters, potentially fortifying cellular defenses against metal-induced stress. However, while the majority of AMPA receptors typically have low calcium permeability, certain stressors, such as metals, might amplify this characteristic, risking neuronal integrity. The enhanced expression of *Cg*GRIA4, albeit potentially beneficial, could also precipitate calcium dysregulation and subsequent neurotoxicity if unchecked (Kim and von Gersdorff, 2016; Yang et al., 2023).

Within the neural framework, iGluRs play an indispensable role in preserving neuronal health and orchestrating functional dynamics. Our research highlights the sensitivity of *Cg*GRIA4 to heavy metal stress. We observed genes with expression patterns that mirror *Cg*GRIA4, primarily associated with Glutamatergic and Dopaminergic synapses. GRIA4, recognized for its prompt responsiveness to glutamate, is pivotal in facilitating efficient neurotransmission (Tritsch and Sabatini, 2012). Parallelly, dopaminergic modulation has been documented to sculpt the functional dynamics and membrane transport of AMPA receptors. This interplay suggests that *Cg*GRIA4 might channel neurotransmission via the Glutamatergic pathway, with its signal intensity potentially under the regulatory purview of the Dopaminergic signaling axis. Additionally, our data suggest a potential role for *Cg*GRIA4 in pathways related to neurodegenerative conditions. The activation of these pathways appears to be intertwined with perturbations in calcium homeostasis (Wakazono et al., 2023), underscoring the prospective role of *Cg*GRIA4 in bolstering cellular defenses against heavy metal stress through judicious calcium regulation. Additionally, our analysis reveals a pronounced enrichment in antioxidant metabolic pathways, notably those pivoting around Vitamin B6 and selenium derivatives (Binte Hossain et al., 2018; Ko et al., 2022). This enrichment suggests a strategic role for *Cg*GRIA4 in mitigating oxidative duress stemming from heavy metal exposure, echoing seminal research that underscores the neuroprotective virtues of Vitamin B6 and selenium compounds in countering oxidative stress. This suggests a strategic role for *Cg*GRIA4 in mitigating oxidative stress from heavy metal exposure, possibly aiding in oysters' environmental adaptability to varying conditions like different water temperatures, salinity levels, or pollution levels.

5 Conclusion

This research illuminates the pervasive distribution of iGluRs in oysters, emphasizing their central importance in physiological functions. A comprehensive set of iGluRs family genes has been identified within the genome, with these genes demonstrating varied expression patterns across developmental stages, within adult

tissues, and under the duress of heavy metal stress. Importantly, our findings indicate that *Cg*GRIA4 can actively respond to heavy metal stress, potentially aiding cells in resisting such stress by engaging in neural signal transmission and antioxidant stress response. However, the specific modulation of these signaling pathways by *Cg*GRIA4, and the question of whether its upregulation might precipitate calcium overload and neurotoxicity, still necessitates further exploration. These findings provide a fresh vantage point for a more profound understanding of the mechanisms of neurotoxicity.

Data availability statement

The original contributions presented in the study are publicly available. This data can be found here: https://www.ncbi.nlm.nih.gov/bioproject/PRJNA146329.

Ethics statement

The animal study was approved by the Laboratory Animal Ethics Committee of Dalian Ocean University. The study was conducted in accordance with the local legislation and institutional requirements.

Author contributions

XZ: Conceptualization, Data curation, Formal Analysis, Investigation, Methodology, Project administration, Software, Supervision, Validation, Visualization, Writing–original draft, Writing–review and editing. LZ: Data curation, Formal Analysis, Investigation, Software, Visualization, Writing–original draft. YS: Visualization, Writing–original draft, Data curation, Investigation, Methodology, Software. XW: Visualization, Writing–original draft, Formal Analysis. LW: Data curation, Funding acquisition, Methodology, Project administration, Resources, Writing–review and editing. LS: Data curation, Funding acquisition, Methodology, Project administration, Resources, Writing–review and editing.

Funding

The authors declare financial support was received for the research, authorship, and/or publication of this article. This research was supported by grants from National Natural Science Foundation of China (41961124009), National key R&D Program of China (2018YFD0900606), earmarked fund (CARS-49) from Modern Agro-industry Technology Research System, the fund for Outstanding Talents and Innovative Team of Agricultural Scientific Research in MARA, Distinguished Professor in Liaoning (to LW, XLYC1902012), the innovation team of Aquaculture Environment Safety from Liaoning Province (LT202009), and Dalian High Level Talent Innovation Support Program (2022RG14), and Talented Scholars in Dalian Ocean University.

Conflict of interest

The authors declare that the research was conducted in the absence of any commercial or financial relationships that could be construed as a potential conflict of interest.

The authors declared that they were an editorial board member of Frontiers, at the time of submission. This had no impact on the peer review process and the final decision

Publisher's note

Supplementary material

The Supplementary Material for this article can be found online at: https://www.frontiersin.org/articles/10.3389/fphys.2023.1280553/full#supplementary-material

SUPPLEMENTARY TABLE S1
Statistical information on the amino acid sequences of the iGluRs of the selected species (search databases: NCBI, Uniprot).

SUPPLEMENTARY TABLE S2
Statistical table of KEGG-enriched gene and pathway information.

SUPPLEMENTARY FIGURE S1
Phylogenetic relationships and protein motifs of vertebrates iGluRs genes (*Homo sapiens*, *Mus musculus*, *Danio rerio*). (A) Phylogenetic tree of vertebrates iGluRs (*Homo sapiens*, *Mus musculus*, *Danio rerio*). Protein sequences were aligned using AliView, and the phylogenetic tree was constructed applying the maximum likelihood method. (B) Protein motifs of vertebrates iGluRs (*Homo sapiens*, *Mus musculus*, *Danio rerio*). Conserved motifs (1–12) are depicted by different colored boxes, with non-conserved sequences represented by black lines. Motifs were visualized using Tbtools.

SUPPLEMENTARY FIGURE S2
Phylogenetic tree and gene structure of *Cgi*GluRs. (A) Phylogenetic tree of *Cgi*GluRs. (B) Black lines, green and yellow boxes indicate the structure of the untranslated region (UTR), Intervening region, and expressed region.

SUPPLEMENTARY FIGURE S3
Temporal trend and clustering of gene expression under different metal stimulation were analyzed using the Mfuzz package. A to E correspond to different time patterns of protein expression under the stimulation of five metals (Cd, Cu, Hg, Pb, and Zn). The x axis represents three stimulation duration, while the y axis represents log2-transformed, normalized intensity ratios in each stage.

References

Armstrong, N., Sun, Y., Chen, G.-Q., and Gouaux, E. (1998). Structure of a glutamate-receptor ligand-binding core in complex with kainate. *Nature* 395, 913–917. doi:10.1038/27692

Bardou, P., Mariette, J., Escudié, F., Djemiel, C., and Klopp, C. (2014). jvenn: an interactive Venn diagram viewer. *BMC Bioinforma.* 15, 293. doi:10.1186/1471-2105-15-293

Begum, G., Otsu, M., Ahmed, U., Ahmed, Z., Stevens, A., and Fulton, D. (2018). NF-Y-dependent regulation of glutamate receptor 4 expression and cell survival in cells of the oligodendrocyte lineage. *Glia* 66, 1896–1914. doi:10.1002/glia.23446

Binte Hossain, K. F., Rahman, Md. M., Sikder, Md. T., Saito, T., Hosokawa, T., and Kurasaki, M. (2018). Inhibitory effects of selenium on cadmium-induced cytotoxicity in PC12 cells via regulating oxidative stress and apoptosis. *Food Chem. Toxicol.* 114, 180–189. doi:10.1016/j.fct.2018.02.034

Budreck, E. C., Kwon, O.-B., Jung, J. H., Baudouin, S., Thommen, A., Kim, H.-S., et al. (2013). Neuroligin-1 controls synaptic abundance of NMDA-type glutamate receptors through extracellular coupling. *Proc. Natl. Acad. Sci.* 110, 725–730. doi:10.1073/pnas.1214718110

Busnardo, C., Crestani, C. C., Fassini, A., Resstel, L. B. M., and Corrêa, F. M. A. (2016). NMDA and non-NMDA glutamate receptors in the paraventricular nucleus of the hypothalamus modulate different stages of hemorrhage-evoked cardiovascular responses in rats. *Neuroscience* 320, 149–159. doi:10.1016/j.neuroscience.2016.02.003

Carmona, A., Roudeau, S., and Ortega, R. (2021). Molecular mechanisms of environmental metal neurotoxicity: a focus on the interactions of metals with synapse structure and function. *Toxics* 9, 198. doi:10.3390/toxics9090198

Chen, G.-Q., Cui, C., Mayer, M. L., and Gouaux, E. (1999). Functional characterization of a potassium-selective prokaryotic glutamate receptor. *Nature* 402, 817–821. doi:10.1038/45568

Chen, C., Chen, H., Zhang, Y., Thomas, H. R., Frank, M. H., He, Y., et al. (2020). TBtools: an integrative toolkit developed for interactive analyses of big biological data. *Mol. Plant* 13, 1194–1202. doi:10.1016/j.molp.2020.06.009

Cox, J. A., Kucenas, S., and Voigt, M. M. (2005). Molecular characterization and embryonic expression of the family of N-methyl-D-aspartate receptor subunit genes in the zebrafish. *Dev. Dyn.* 234, 756–766. doi:10.1002/dvdy.20532

Dravid, S. M., Burger, P. B., Prakash, A., Geballe, M. T., Yadav, R., Le, P., et al. (2010). Structural determinants of d-cycloserine efficacy at the NR1/NR2C NMDA receptors. *J. Neurosci.* 30, 2741–2754. doi:10.1523/JNEUROSCI.5390-09.2010

Endo, Y., Zhang, Y., Olumi, S., Karvar, M., Argawal, S., Neppl, R. L., et al. (2021). Exercise-induced gene expression changes in skeletal muscle of old mice. *Genomics* 113, 2965–2976. doi:10.1016/j.ygeno.2021.06.035

Englund, J., Haikonen, J., Shteinikov, V., Amarilla, S. P., Atanasova, T., Shintyapina, A., et al. (2021). Downregulation of kainate receptors regulating GABAergic transmission in amygdala after early life stress is associated with anxiety-like behavior in rodents. *Transl. Psychiatry* 11, 538. doi:10.1038/s41398-021-01654-7

Ganor, Y., and Levite, M. (2014). The neurotransmitter glutamate and human T cells: glutamate receptors and glutamate-induced direct and potent effects on normal human T cells, cancerous human leukemia and lymphoma T cells, and autoimmune human T cells. *J. Neural Transm.* 121, 983–1006. doi:10.1007/s00702-014-1167-5

Guindon, S., Dufayard, J.-F., Lefort, V., Anisimova, M., Hordijk, W., and Gascuel, O. (2010). New algorithms and methods to estimate maximum-likelihood phylogenies: assessing the performance of PhyML 3.0. *Syst. Biol.* 59, 307–321. doi:10.1093/sysbio/syq010

Hanada, T. (2020). Ionotropic glutamate receptors in epilepsy: a review focusing on AMPA and NMDA receptors. *Biomolecules* 10, 464. doi:10.3390/biom10030464

Hansen, K. B., Wollmuth, L. P., Bowie, D., Furukawa, H., Menniti, F. S., Sobolevsky, A. I., et al. (2021). Structure, function, and pharmacology of glutamate receptor ion channels. *Pharmacol. Rev.* 73, 1469–1658. doi:10.1124/pharmrev.120.000131

Hayashi, T. (2021). Post-translational palmitoylation of ionotropic glutamate receptors in excitatory synaptic functions. *Br. J. Pharmacol.* 178, 784–797. doi:10.1111/bph.15050

Herbrechter, R., Hube, N., Buchholz, R., and Reiner, A. (2021). Splicing and editing of ionotropic glutamate receptors: a comprehensive analysis based on human RNA-Seq data. *Cell. Mol. Life Sci.* 78, 5605–5630. doi:10.1007/s00018-021-03865-z

Jonathan, M. P., Muñoz-Sevilla, N. P., Góngora-Gómez, A. M., Luna Varela, R. G., Sujitha, S. B., Escobedo-Urías, D. C., et al. (2017). Bioaccumulation of trace metals in farmed pacific oysters *Crassostrea gigas* from SW Gulf of California coast, Mexico. *Chemosphere* 187, 311–319. doi:10.1016/j.chemosphere.2017.08.098

Karakas, E., Regan, M. C., and Furukawa, H. (2015). Emerging structural insights into the function of ionotropic glutamate receptors. *Trends Biochem. Sci.* 40, 328–337. doi:10.1016/j.tibs.2015.04.002

Kearse, M., Moir, R., Wilson, A., Stones-Havas, S., Cheung, M., Sturrock, S., et al. (2012). Geneious Basic: an integrated and extendable desktop software platform for the organization and analysis of sequence data. *Bioinformatics* 28, 1647–1649. doi:10.1093/bioinformatics/bts199

Kim, M.-H., and von Gersdorff, H. (2016). Postsynaptic plasticity triggered by Ca^{2+}-permeable AMPA receptor activation in retinal amacrine cells. *Neuron* 89, 507–520. doi:10.1016/j.neuron.2015.12.028

Ko, J. W., Jeon, S., and Kwon, Y. H. (2022). Dietary vitamin B6 restriction aggravates neurodegeneration in mice fed a high-fat diet. *Life Sci.* 309, 121041. doi:10.1016/j.lfs.2022.121041

Kumar, L., and Futschik, M. E. (2007). Mfuzz: a software package for soft clustering of microarray data. *Bioinformation* 2, 5–7. doi:10.6026/97320630002005

Kuner, T., Seeburg, P. H., and Robert Guy, H. (2003). A common architecture for K^+ channels and ionotropic glutamate receptors? *Trends Neurosci.* 26, 27–32. doi:10.1016/S0166-2236(02)00010-3

Larsson, A. (2014). AliView: a fast and lightweight alignment viewer and editor for large datasets. *Bioinformatics* 30, 3276–3278. doi:10.1093/bioinformatics/btu531

Letunic, I., and Bork, P. (2018). 20 years of the SMART protein domain annotation resource. *Nucleic Acids Res.* 46, D493–D496. doi:10.1093/nar/gkx922

Levitz, J., Popescu, A. T., Reiner, A., and Isacoff, E. Y. (2016). A toolkit for orthogonal and *in vivo* optical manipulation of ionotropic glutamate receptors. *Front. Mol. Neurosci.*, 9. doi:10.3389/fnmol.2016.00002

Li, Y., Liang, Z., Lei, S., Wu, X., Yuan, T., Ma, K., et al. (2023). Sevoflurane preconditioning downregulates GRIA1 expression to attenuate cerebral ischemia-reperfusion-induced neuronal injury. *Neurotox. Res.* 41, 29–40. doi:10.1007/s12640-022-00620-5

Liu, Z., Li, M., Yi, Q., Wang, L., and Song, L. (2018). The neuroendocrine-immune regulation in response to environmental stress in marine bivalves. *Front. Physiol.* 9. doi:10.3389/fphys.2018.01456

Liu, D., Shi, Q., Liu, C., Sun, Q., and Zeng, X. (2023). Effects of endocrine-disrupting heavy metals on human health. *Toxics* 11, 322. doi:10.3390/toxics11040322

Manookin, M. B., Beaudoin, D. L., Ernst, Z. R., Flagel, L. J., and Demb, J. B. (2008). Disinhibition combines with excitation to extend the operating range of the OFF visual pathway in daylight. *J. Neurosci.* 28, 4136–4150. doi:10.1523/JNEUROSCI.4274-07.2008

Marchetti, C., and Gavazzo, P. (2003). Subunit-dependent effects of nickel on NMDA receptor channels. *Mol. Brain Res.* 117, 139–144. doi:10.1016/S0169-328X(03)00293-6

Mayer, M. L. (2016). Structural biology of glutamate receptor ion channel complexes. *Curr. Opin. Struct. Biol.* 41, 119–127. doi:10.1016/j.sbi.2016.07.002

Moretto, E., Murru, L., Martano, G., Sassone, J., and Passafaro, M. (2018). Glutamatergic synapses in neurodevelopmental disorders. *Prog. Neuropsychopharmacol. Biol. Psychiatry* 84, 328–342. doi:10.1016/j.pnpbp.2017.09.014

Nystrom, S. L., and McKay, D. J. (2021). Memes: a motif analysis environment in R using tools from the MEME Suite. *PLoS Comput. Biol.* 17, e1008991. doi:10.1371/journal.pcbi.1008991

Peñaloza, C., Gutierrez, A. P., Eöry, L., Wang, S., Guo, X., Archibald, A. L., et al. (2021). A chromosome-level genome assembly for the Pacific oyster *Crassostrea gigas*. *Gigascience* 10. doi:10.1093/gigascience/giab020

Peters, C., Muñoz, B., Sepúlveda, F. J., Urrutia, J., Quiroz, M., Luza, S., et al. (2011). Biphasic effects of copper on neurotransmission in rat hippocampal neurons. *J. Neurochem.* 119, 78–88. doi:10.1111/j.1471-4159.2011.07417.x

Pochwat, B., Nowak, G., and Szewczyk, B. (2015). Relationship between zinc (Zn^{2+}) and glutamate receptors in the processes underlying neurodegeneration. *Neural Plast.* 2015, 1–9. doi:10.1155/2015/591563

Qiu, X. M., Sun, Y. Y., Ye, X. Y., and Li, Z. G. (2020). Signaling role of glutamate in plants. *Front. Plant Sci.* 10. doi:10.3389/fpls.2019.01743

Rahman, M. M., Hossain, M. K. F. B., Afrin, S., Saito, T., and Kurasaki, M. (2022). "Effects of metals on human health and ecosystem," in *The handbook of environmental chemistry* (Berlin, Heidelberg: Springer), 81–119. doi:10.1007/698_2021_825

Sachser, R. M., Haubrich, J., Lunardi, P. S., and de Oliveira Alvares, L. (2017). Forgetting of what was once learned: exploring the role of postsynaptic ionotropic glutamate receptors on memory formation, maintenance, and decay. *Neuropharmacology* 112, 94–103. doi:10.1016/j.neuropharm.2016.07.015

Sadiq, S., Ghazala, Z., Chowdhury, A., and Büsselberg, D. (2012). Metal toxicity at the synapse: presynaptic, postsynaptic, and long-term effects. *J. Toxicol.* 2012, 1–42. doi:10.1155/2012/132671

Sagata, N., Iwaki, A., Aramaki, T., Takao, K., Kura, S., Tsuzuki, T., et al. (2010). Comprehensive behavioural study of GluR4 knockout mice: implication in cognitive function. *Genes. Brain Behav.* 9, 899–909. doi:10.1111/j.1601-183X.2010.00629.x

Sánchez-Alcañiz, J. A., Silbering, A. F., Croset, V., Zappia, G., Sivasubramaniam, A. K., Abuin, L., et al. (2018). An expression atlas of variant ionotropic glutamate receptors identifies a molecular basis of carbonation sensing. *Nat. Commun.* 9, 4252. doi:10.1038/s41467-018-06453-1

Shahin, S., Banerjee, S., Swarup, V., Singh, S. P., and Chaturvedi, C. M. (2018). From the cover: 2.45-GHz microwave radiation impairs hippocampal learning and spatial memory: involvement of local stress mechanism-induced suppression of iGluR/ERK/CREB signaling. *Toxicol. Sci.* 161, 349–374. doi:10.1093/toxsci/kfx221

Slotkin, T. A., and Seidler, F. J. (2009). Oxidative and excitatory mechanisms of developmental neurotoxicity: Transcriptional profiles for chlorpyrifos, diazinon,

dieldrin, and divalent nickel in PC12 cells. *Environ. Health Perspect.* 117 (4), 587–596. doi:10.1289/ehp.0800251

Song, I., and Huganir, R. L. (2002). Regulation of AMPA receptors during synaptic plasticity. *Trends Neurosci.* 25, 578–588. doi:10.1016/S0166-2236(02)02270-1

Spirkova, A., Kovaříková, V., Šefčíková, Z., Pisko, J., Kšiňanová, M., Koppel, J., et al. (2022). Glutamate can act as a signaling molecule in mouse preimplantation embryos. *Biol. Reprod.* doi:10.1093/biolre/ioac126

Stroebel, D., and Paoletti, P. (2021). Architecture and function of NMDA receptors: an evolutionary perspective. *J. Physiol.* 599, 2615–2638. doi:10.1113/JP279028

Tritsch, N. X., and Sabatini, B. L. (2012). Dopaminergic modulation of synaptic transmission in cortex and striatum. *Neuron* 76, 33–50. doi:10.1016/j.neuron.2012.09.023

UniProt Consortium, T. (2018). UniProt: the universal protein knowledgebase. *Nucleic Acids Res.* 46, 2699. doi:10.1093/nar/gky092

van Giesen, L., and Garrity, P. A. (2017). More than meets the IR: The expanding roles of variant Ionotropic Glutamate Receptors in sensing odor, taste, temperature and moisture. *F1000Research* 6, 1753. doi:10.12688/f1000research.12013.1

Vogeler, S., Bean, T. P., Lyons, B. P., and Galloway, T. S. (2016). Dynamics of nuclear receptor gene expression during Pacific oyster development. *BMC Dev. Biol.* 16, 33. doi:10.1186/s12861-016-0129-6

Wakazono, Y., Midorikawa, R., and Takamiya, K. (2023). Temporal and quantitative analysis of the functional expression of Ca^{2+}-permeable AMPA receptors during LTP. *Neurosci. Res.* doi:10.1016/j.neures.2023.07.002

Wang, S., Hu, P., Wang, H., Wang, M., Chen, J., Tang, J., et al. (2008). Effects of Cd^{2+} on AMPA receptor-mediated synaptic transmission in rat hippocampal CA1 area. *Toxicol. Lett.* 176, 215–222. doi:10.1016/j.toxlet.2007.11.008

Wang, L. (2022). Regulatory mechanism of neuroendocrine system on immune response in molluscs:a review. *J. Dalian Ocean Univ.* 37, 363–375. doi:10.16535/j.cnki.dlhyxb.2022-140

Wen, X., Chen, Y.-H., Li, R., Ge, M.-H., Yin, S.-W., Wu, J.-J., et al. (2020). Signal decoding for glutamate modulating egg laying oppositely in *Caenorhabditis elegans* under varied environmental conditions. *iScience* 23, 101588. doi:10.1016/j.isci.2020.101588

Wilkins, M. R., Gasteiger, E., Bairoch, A., Sanchez, J. C., Williams, K. L., Appel, R. D., et al. (1999). "Protein identification and analysis tools in the ExPASy server," in *2-D proteome analysis protocols* (New Jersey: Humana Press), 531–552. doi:10.1385/1-59259-584-7:531

Yang, J. Y., Wang, J., Hu, Y., Shen, D. Y., Xiao, G. L., Qin, X. Y., et al. (2023). Paeoniflorin improves cognitive dysfunction, restores glutamate receptors, attenuates gliosis and maintains synaptic plasticity in cadmium-intoxicated mice. *Arabian J. Chem.* 16, 104406. doi:10.1016/j.arabjc.2022.104406

Yu, G., Wang, L. G., Han, Y., and He, Q.-Y. (2012). clusterProfiler: an R Package for comparing biological themes among gene clusters. *OMICS* 16, 284–287. doi:10.1089/omi.2011.0118

Zhang, G., Fang, X., Guo, X., Li, L., Luo, R., Xu, F., et al. (2012). The oyster genome reveals stress adaptation and complexity of shell formation. *Nature* 490, 49–54. doi:10.1038/nature11413

Zhang, X., Fan, C., Zhang, X., Li, Q., Li, Y., and Wang, Z. (2021). Effects of light intensity and wavelength on the phototaxis of the *Crassostrea gigas* (♂) and *Crassostrea sikamea* (♀) hybrid larvae. *Front. Mar. Sci.* 8. doi:10.3389/fmars.2021.698874

Zhao, T., Zhong, R., Zhang, X., Li, G., Zhou, C., Fang, S., et al. (2023). Efavirenz restored NMDA receptor dysfunction and inhibited epileptic seizures in GluN2A/Grin2a mutant mice. *Front. Neurosci.* 17. doi:10.3389/fnins.2023.1086462

Zhou, H., Cheng, Z., Bass, N., Krystal, J. H., Farrer, L. A., Kranzler, H. R., et al. (2018). Genome-wide association study identifies glutamate ionotropic receptor GRIA4 as a risk gene for comorbid nicotine dependence and major depression. *Transl. Psychiatry* 8, 208. doi:10.1038/s41398-018-0258-8

Zhu, S., and Gouaux, E. (2017). Structure and symmetry inform gating principles of ionotropic glutamate receptors. *Neuropharmacology* 112, 11–15. doi:10.1016/j.neuropharm.2016.08.034

frontiers | Frontiers in Physiology

TYPE Original Research
PUBLISHED 08 November 2023
DOI 10.3389/fphys.2023.1294729

OPEN ACCESS

EDITED BY
Yiming Li,
Fishery Machinery and Instrument Research Institute, China

REVIEWED BY
Yijiang Hong,
Nanchang University, China
Kai Liao,
Ningbo University, China

*CORRESPONDENCE
Qigen Liu,
qgliu@shou.edu.cn
Jiamin Sun,
jmsun@shou.edu.cn

†These authors have contributed equally to this work and share first authorship

RECEIVED 15 September 2023
ACCEPTED 17 October 2023
PUBLISHED 08 November 2023

CITATION
Cheng X, Li F, Kumilamba G, Liao J, Cao J, Sun J and Liu Q (2023), Transcriptome analysis in hepatopancreases reveals the response of domesticated common carp to a high-temperature environment in the agricultural heritage rice–fish system. *Front. Physiol.* 14:1294729. doi: 10.3389/fphys.2023.1294729

Transcriptome analysis in hepatopancreases reveals the response of domesticated common carp to a high-temperature environment in the agricultural heritage rice–fish system

Xiangbing Cheng[1,2,3†], Fangcheng Li[1,2,3†], Gilbert Kumilamba[1,2,3], Jiayi Liao[1,2,3], Jiangwei Cao[1,2,3], Jiamin Sun[1,2,3*] and Qigen Liu[1,2,3*]

[1]Centre for Research on Environmental Ecology and Fish Nutrition of the Ministry of Agriculture, Shanghai Ocean University, Shanghai, China, [2]Key Laboratory of Integrated Rice-fish Farming, Ministry of Agriculture and Rural Affairs, Shanghai Ocean University, Shanghai, China, [3]Key Laboratory of Freshwater Aquatic Genetic Resources, Ministry of Agriculture and Rural Affairs, Shanghai Ocean University, Shanghai, China

Qingtian paddy field carp (PF-carp) is a local carp cultivated in the paddy field of Qingtian, Zhejiang. This rice–fish co-culture system has been recognized as one of the Globally Important Agriculture Heritage Systems (GIAHS). PF-carp has been acclimatized to the high-temperature environment of shallow paddy fields after several centuries of domestication. To reveal the physiological and molecular regulatory mechanisms of PF-carp, we chose to use 28°C as the control group and 34°C as the treatment group. We measured biochemical parameters in their serum and hepatopancreases and also performed transcriptome sequencing analysis. Compared with the control group, the serum levels of malondialdehyde (MDA), glucose (GLU), glutathione peroxidase (GSH-Px), catalase (CAT), alanine aminotransferase (ALT), and aspartate aminotransferase (AST) show no significant change. In addition, superoxide dismutase (SOD), GSH-Px, and CAT also show no significant change in hepatopancreases. We identified 1,253 differentially expressed genes (DEGs), and their pathway analysis revealed that heat stress affected AMPK signaling pathway, protein export, and other biological processes. It is worth noting that protein processing in the endoplasmic reticulum (ER) was the most significantly enriched pathway identified by the Kyoto Encyclopedia of Genes and Genomes (KEGG) and gene set enrichment analysis (GSEA). Significantly higher levels of HSP40, HSP70, HSP90, and other ubiquitin ligase-related genes were upregulated. In summary, heat stress did not lead to tissue damage, inflammation, oxidative stress, and ER stress in the hepatopancreases of PF-carp. This study provides valuable insights into the adaptation mechanism of this species to the high-temperature environment of paddy fields.

KEYWORDS

Qingtian paddy field carp, domestication, heat stress, RNA-seq, hepatopancreases

1 Introduction

Modern human civilization has developed based on the successful domestication of various plants and animals (Diamond, 2002). The earliest truly domesticated fish is the common carp (*Cyprinus carpio*) (Balon, 2004). Influenced by geographic, cultural, and other factors, the common carp has been domesticated into a variety of local varieties that are widely distributed in different farming systems (ponds or paddy fields). Due to the disparity in altitude and the few plains in Qingtian, Zhejiang, humans have domesticated the most successful paddy-farmed fish in this region and have been named Qingtian paddy field carp (PF-carp). In Qingtian, a system of rice–fish symbiosis has been created by the integration of PF-carp and rice farming. As one of the first Globally Important Agricultural Heritage Systems (GIAHS), this system was acknowledged by the Food and Agriculture Organization (FAO) in 2005 (Lu and Li, 2006).

From rivers and lakes to paddy fields, the environment in which common carp live has changed dramatically. Common carp is a natural demersal fish inhabiting in the lower layer of rivers and lakes, where the temperature is more stable and less susceptible to external environmental influences. However, paddy fields have a small water body and are shallow (5–25 cm) compared to rivers and lakes (Chen, X. et al., 2021). The shallow paddy water environment is often hot in the summer afternoons due to the intense sunlight. According to our monitoring, the summer temperature of the paddy field where PF-carp lives is approximately 34°C. Yet, PF-carp has been domesticated

TABLE 1 Effects of the oxidative index of the enzymatic type in the serum of PF-carp during heat stress.

Group	SOD activity (U/mL)	MDA content (nmol/mL)	GSH-Px activity (U/mL)	CAT activity (U/mL)
G	291.27 ± 16.74^{c}	6.91 ± 0.31	187.95 ± 8.08^{abc}	1.03 ± 0.18^{cd}
G0	304.12 ± 21.81^{bc}	7.99 ± 0.50	185.65 ± 18.87^{abc}	1.26 ± 0.25^{c}
G2	309.29 ± 23.43^{bc}	7.97 ± 0.29	191.72 ± 17.04^{abc}	1.42 ± 0.01^{abc}
G6	341.51 ± 4.49^{ab}	7.90 ± 0.22	170.50 ± 12.54^{bcd}	0.63 ± 0.08^{d}
G12	357.85 ± 7.95^{a}	8.18 ± 0.33	183.77 ± 9.79^{abc}	0.65 ± 0.03^{d}
G24	313.66 ± 13.91^{bc}	8.10 ± 0.24	182.05 ± 10.00^{abc}	0.64 ± 0.19^{d}

The values presented are the sum of the means and standard deviations (mean ± SD) of three replicates. Values in the same column with different lowercase letters indicate significant differences ($p < 0.05$). G, G0, G2, G6, G12, and G24 represent the control group and heat stress at 0, 2, 6, 12, and 24 h, respectively.

TABLE 2 Effects of metabolism and hepatopancreatic injury in the serum of PF-carp during heat stress.

Group	GLU content (mmol/L)	TG content (mmol/L)	ALT activity (U/L)	AST activity (U/L)
G	6.08 ± 0.50	2.57 ± 0.34^{c}	1.30 ± 0.29^{bcde}	7.78 ± 1.18^{ab}
G0	9.93 ± 1.65	2.96 ± 0.17^{bc}	1.58 ± 0.43^{abcd}	9.04 ± 0.54^{ab}
G2	9.73 ± 1.24	2.81 ± 0.35^{bc}	1.83 ± 0.40^{abc}	8.46 ± 1.45^{ab}
G6	7.21 ± 1.13	3.15 ± 0.42^{bc}	1.91 ± 0.35^{ab}	10.65 ± 0.65^{a}
G12	6.91 ± 0.59	3.62 ± 0.35^{ab}	1.79 ± 0.09^{abc}	9.28 ± 1.48^{ab}
G24	7.66 ± 0.60	3.70 ± 0.55^{ab}	1.72 ± 0.35^{abcd}	9.89 ± 0.95^{ab}

The values presented are the sum of means and standard deviations (mean ± SD) of three replicates. Values in the same column with different lowercase letters indicate significant differences ($p < 0.05$). G, G0, G2, G6, G12, and G24 represent the control group and heat stress at 0, 2, 6, 12, and 24 h, respectively.

TABLE 3 Effects of the oxidative index of the enzymatic type in the hepatopancreas of PF-carp during heat stress.

Group	SOD activity (U/mgprot)	MDA content (nmol/mgprot)	GSH-Px activity (U/mgprot)	CAT activity (U/mgprot)
G	535.64 ± 22.04^{abcd}	0.69 ± 0.11^{b}	252.32 ± 28.49	19.06 ± 2.79^{a}
G0	576.52 ± 60.53^{abc}	0.88 ± 0.09^{ab}	222.95 ± 15.90	19.45 ± 2.76^{a}
G2	587.90 ± 26.17^{ab}	0.97 ± 0.11^{ab}	228.94 ± 15.77	19.86 ± 1.65^{a}
G6	520.76 ± 3.72^{bcd}	0.81 ± 0.04^{ab}	225.89 ± 29.99	14.98 ± 2.30^{ab}
G12	520.76 ± 35.25^{bcd}	0.88 ± 0.09^{ab}	263.16 ± 27.71	15.71 ± 2.45^{ab}
G24	568.41 ± 21.71^{abc}	1.21 ± 0.11^{a}	269.97 ± 24.70	19.83 ± 3.27^{a}

The values presented are the sum of means and standard deviations (mean ± SD) of three replicates. Values in the same column with different lowercase letters indicate significant differences ($p < 0.05$). G, G0, G2, G6, G12, and G24 represent the control group and heat stress at 0, 2, 6, 12, and 24 h, respectively.

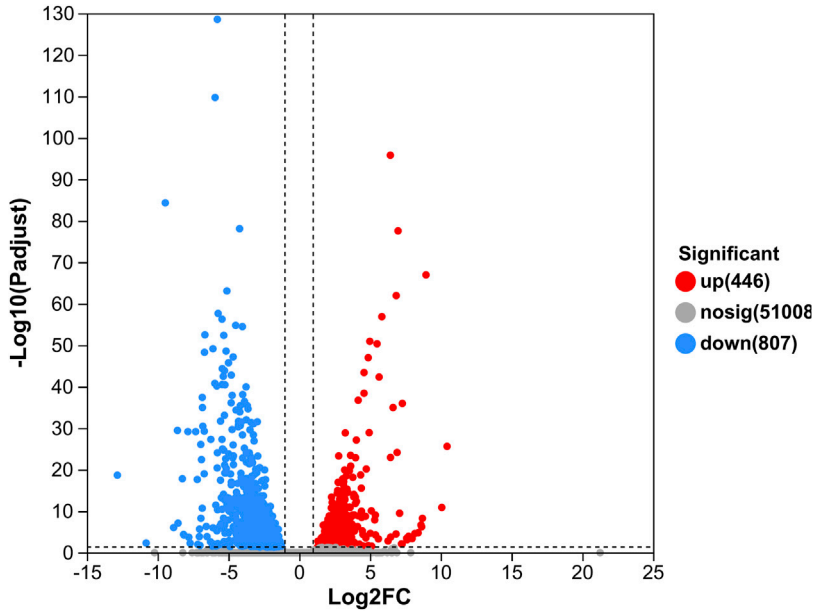

FIGURE 1
Volcano plot of DEGs in GM vs. GC groups. Each dot represents one gene, red color indicates significantly upregulated genes, blue color indicates significantly downregulated genes, and gray color indicates non-significantly differentially expressed genes.

in this environment for more than 12 centuries (Xie et al., 2011). Therefore, we hypothesize that they have been domesticated with special physiological and molecular regulatory mechanisms to adapt to the high-temperature environment of shallow paddy fields in Qingtian.

In order to investigate the adaptation mechanism of this species to the high-temperature environment of shallow paddy fields, we measured its biochemical parameters and performed RNA-seq analyses. The main objectives of our study were to characterize 1) the physiological changes in PF-carp in response to the high-temperature environment of shallow paddy fields and 2) the major signaling pathways and genes involved in the adaptation of PF-carp to the high-temperature environment of shallow paddy fields.

2 Materials and methods

2.1 Ethical statement

The experiments were conducted in accordance with the Guidelines for the Care and Use of Laboratory Animals in China. The animals used in this study were cultured and euthanized following the terms approved by the Institutional Animal Care and Use Committee at Shanghai Ocean University (Shanghai, China) with approval number: SHOU-DW-2018-026.

2.2 Animals

Fifty-four healthy PF-carp juveniles (weighing 104.69 ± 3.08 g and measuring 14.65 ± 0.46 cm in length) used in this experiment were procured from Yugong Ecological Agricultural Technology Co., Ltd (Qingtian, Lishui, Zhejiang, China). They were then transported to the PF-Carp Research Center (Qingtian, Lishui, Zhejiang, China) for a 7-day acclimation period. They were randomly divided into three circular tanks (18 fish per tank). Furthermore, they were acclimatized in laboratory settings with the aerating water maintained at 28°C ± 0.5°C and dissolved oxygen levels of approximately 7 mg/L. The water was changed daily, and the fish were given artificial food twice daily.

2.3 Experimental design and sample collection

We randomly selected nine individuals in three tanks after 7°days of acclimatization to serve as the control group. Then, the other experimental fish were elevated from 28°C to 34°C at a rate of 1°C per hour and maintained at 34°C for 24 h.

After maintaining the experimental temperature for 0, 2, 6, 12, and 24 h, samples were collected at each time point. Three PF-carp were randomly selected from each of the three tanks and anesthetized with MS-222 (300 mg/L) prior to sampling. A syringe was used to draw blood from the caudal vessel. Then, the fish were immediately dissected, and their hepatopancreases were collected for examination. The obtained samples were immediately frozen in liquid nitrogen and stored at −80 C until subsequent use. The same sampling procedure was applied to the control group.

2.4 Biochemical parameter determination

The changes in superoxide dismutase (SOD), malondialdehyde (MDA), glutathione peroxidase (GSH-Px), catalase (CAT), glucose

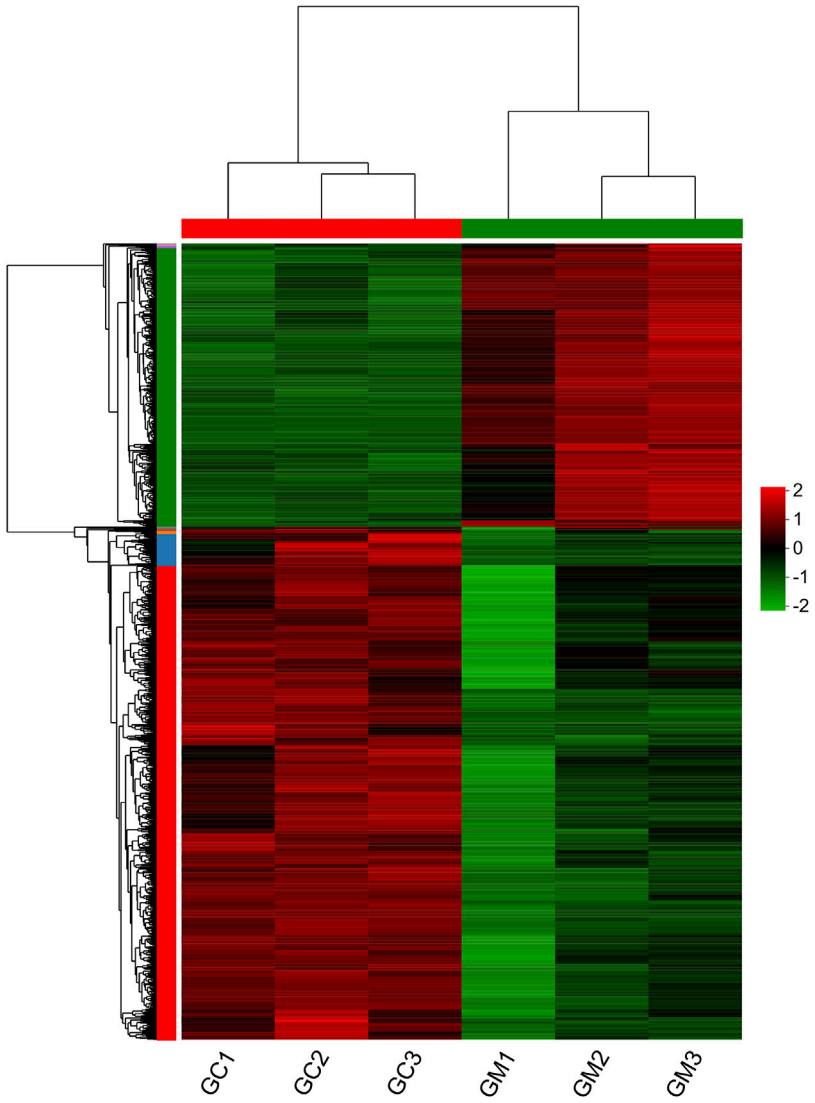

FIGURE 2
Heatmap of DEGs in GM vs. GC groups. Each row represents one gene. Colors ranging from green to red indicate gene expression from low to high.

(GLU), triglyceride (TG), alanine aminotransferase (ALT), and aspartate aminotransferase (AST) levels in the serum were determined. The supernatants of hepatopancreatic tissue homogenate were used for oxidative stress analysis, including SOD, MDA, GSH-Px, and CAT. According to the standard protocols, all the biochemical parameters were determined using reagent kits (Jiancheng Institute of Biotechnology, Nanjing, China).

2.5 Transcriptome sequencing

In this study, we selected hepatopancreatic tissues subjected to 6 h of heat stress for RNA-seq as the GM group. The TRIzol reagent (Invitrogen, Carlsbad, CA, United States) was used to isolate RNA of hepatopancreases (n = 3 per group); genomic RNA was removed using RNase I (Takara, Shanghai, China). Bioanalyzer 2100 (Agilent Technologies, United States) was used to determine RNA quality, and then ND-2000 (NanoDrop Technologies, United States) was used to quantify RNA. OD 260/280 ≥ 1.8 and OD 260/230 ≥ 1 were used for sequencing libraries.

These RNAs were reversed into cDNAs after a quality control process, and sequencing was carried out by Major Bioinformatics Technology Co., Ltd. (Shanghai, China) on Illumina NovaSeq 6000 (Illumina, United States). All transcriptome datasets can be found in the Sequence Read Archive (SRA) of the National Center for Biotechnology Information (NCBI). The accession number of the GM group was PRJNA1002641. RNA-seq results from a concurrent experiment were used as a control group (GC group), and its accession number was PRJNA971384.

2.6 Transcriptome analysis

SeqPrep and Sickle software programs were used to eliminate low-quality raw reads, and then the clean reads were mapped to the genome of common carp (accession number: ERS541549) (Xu et al., 2014) using

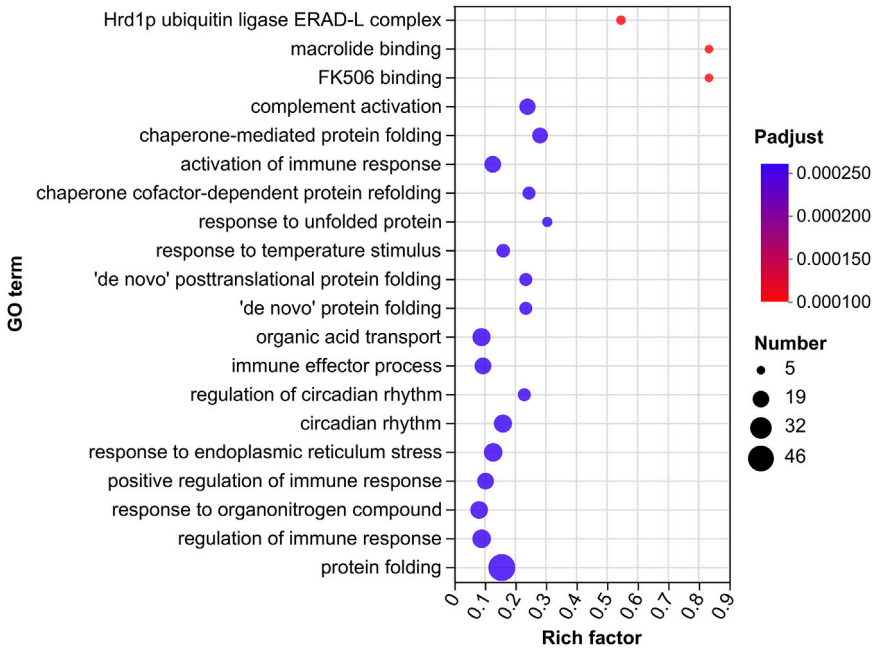

FIGURE 3
GO enrichment analysis of DEGs in GM vs. GC groups. Colors ranging from blue to red indicate GO term significance from low to high. The size of the dot represents the number of genes enriched from more to less.

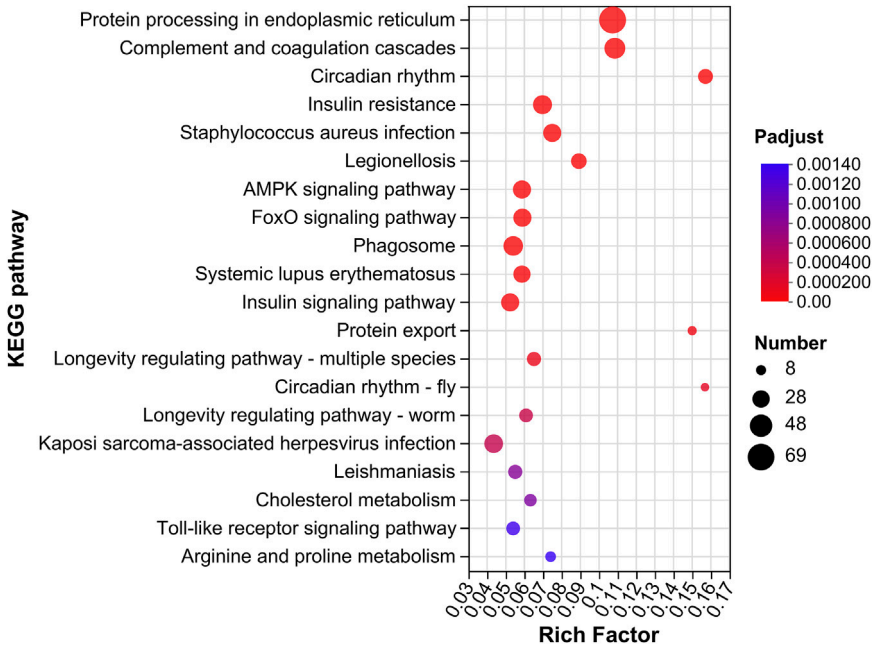

FIGURE 4
KEGG enrichment analysis of DEGs in GM vs. GC groups. Colors ranging from blue to red indicate the KEGG pathway significance from low to high. The size of the dot represents the number of genes enriched from more to less.

HISAT 2 software and then aligned using StringTie. The levels of gene expression were estimated using transcripts per million reads (FPKM) in the present study. Genes with $|\log_2\text{FoldChange}| \geq 2$ and p-adjust <0.05 were regarded as differentially expressed genes (DEGs) using DESeq2. Furthermore, GOATOOLS software and R package were used to perform GO and KEGG enrichment analyses, respectively. The gene sets of the KEGG pathway were used to perform further GSEA using GSEA 3.0 software.

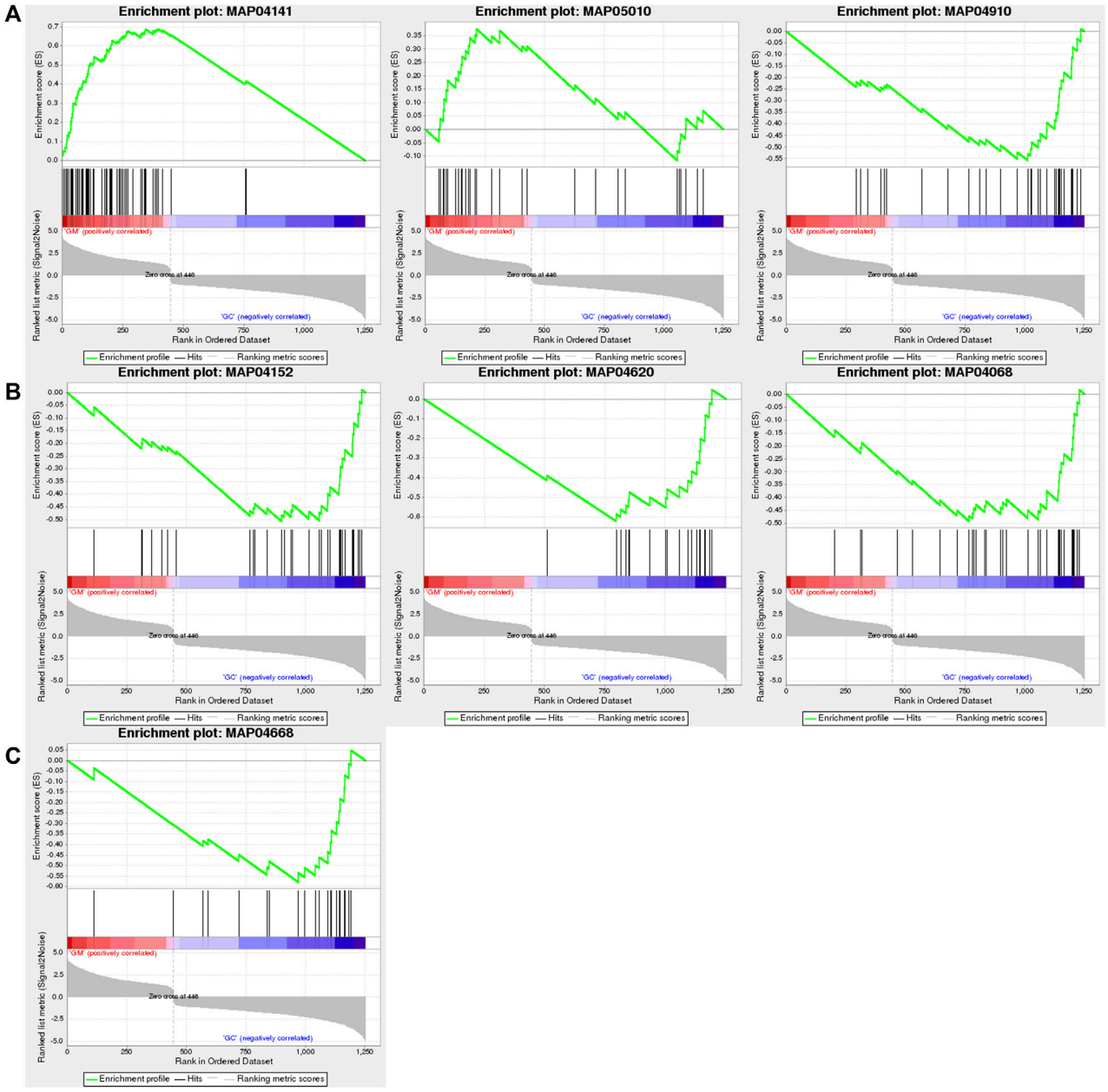

FIGURE 5
GSEA of DEGs in GM vs. GC groups. **(A)** "Protein processing in endoplasmic reticulum," "Alzheimer's disease," and "insulin signaling pathway" are shown from left to right. **(B)** "AMPK signaling pathway," "Toll-like receptor signaling pathway," and "FoxO signaling pathway" are shown from left to right. **(C)** "TNF signaling pathway."

2.7 Real-time quantitative PCR validation

We randomly chose nine DEGs for real-time quantitative PCR (RT-qPCR) verification to assess the accuracy of the transcriptome sequencing results. Primer Premier v.6.0 was used to design primers for DEGs (Supplementary Table S1). RT-qPCR was performed using the ChamQ SYBR Color qPCR Master Mix (2X) (Novozymes Bio, Nanjing, China) on a real-time fluorescence quantitative PCR instrument (ABI 7300, United States). The PCR conditions were as follows: 95°C for 5 min, followed by 40 cycles of 95°C for 5 s, 55°C for 30 s, and 72°C for 40 s. Gene expression levels were standardized relative to *β-actin* and calculated using Ct values ($2^{-\Delta\Delta CT}$).

2.8 Statistical analysis

All statistical analyses were carried out using SPSS 19.0. All results were analyzed using one-way ANOVA. Values are presented as mean ± standard deviation (mean ± SD). $p < 0.05$ was considered significant. In addition, GraphPad Prism 9 was used to display the results.

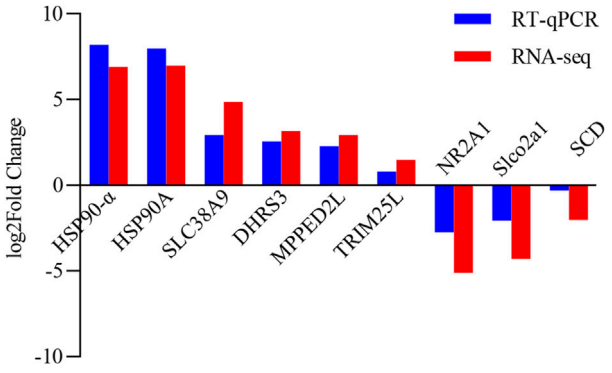

FIGURE 6
Comparison of gene expression between RT-qPCR and RNA-seq, with gene names on the *X*-axis and $\log_2$ value of relative gene expression on the *Y*-axis.

3 Results

3.1 Changes in biochemical indicators after heat stress

When PF-carp was maintained at 34°C, significant differences in the activity of SOD in serum ($p < 0.05$)were observed between the control and treatment groups at 6 h and 12 h. For the TG content in serum, significant changes were also observed to be higher in the treatment group than the control group at 12 h and 24 h ($p < 0.05$). However, there were no significant changes in the contents of MDA and GLU and the activities of GSH-Px, CAT, ALT, and AST in serum ($p > 0.05$) (Tables 1, 2).

The MDA content in hepatopancreases of the treatment group was significantly higher than that of the control group at 24 h ($p < 0.05$). In contrast, the activities of SOD, GSH-Px, and CAT were not significantly changed ($p > 0.05$) (Table 3).

3.2 Overview of RNA-seq

We used six samples for transcriptome sequencing with three replicates for the hepatopancreatic tissue in the two distinct groups. After filtering low-quality reads, 272,933,850 clean reads were obtained. Parameter statistics of clean reads among two groups were Q20: 97.84%–98.21%; Q30: 93.88%–94.62%; GC content: 48.4%–50.43%; and error rate: 0.0246%–0.0254%. The mapping of clean reads to the reference genome was also carried out, and the total mapped ratio was in the range of 78.07%–79.87% (Table 4).

3.3 Identification of DEGs

In our study, 1,253 DEGs were identified, including 446 upregulated genes and 807 downregulated genes (Figure 1). Clustering analysis indicated that the GC and GM groups were clustered separately, with quite different expression patterns in each group (Figure 2).

3.4 Enrichment analysis

Gene Ontology (GO) terms are classified into three basic categories: biological processes (BPs), cellular components (CCs), and molecular functions (MFs). There were 255 GO terms significantly enriched in the GM vs. GC groups ($p < 0.05$), which contain 144 BPs, 73 MFs and 38 CCs (Figure 3; Supplementary Table S2).

In the GM vs. GC groups, we found 57 KEGG pathways that were significantly enriched ($p < 0.05$). Within these pathways, "protein processing in endoplasmic reticulum, map04141" was the most significantly enriched pathway. Other pathways such as "AMPK signaling pathway, map04152," "FoxO signaling pathway, map04068," and "protein export, map03060" were also significantly enriched (Figure 4; Supplementary Table S3).

Through GSEA, we also found that only "protein processing in endoplasmic reticulum (NES = 4.52)" and "Alzheimer's disease (NES = 1.93)" were positively enriched, while "insulin signaling pathway (NES = −2.62)," "AMPK signaling pathway (NES = −2.43)," "Toll-like receptor signaling pathway (NES = −2.42)," "TNF signaling pathway (NES = −2.37)," and "FoxO signaling pathway (NES = −2.29)" were negatively enriched (Figure 5; Supplementary Table S4).

3.5 Verification of RNA-seq using RT-qPCR

In order to determine the accuracy and reliability of RNA-seq, nine genes were randomly chosen for RT-qPCR validation. In both RNA-seq and RT-qPCR, the chosen genes had consistent expression patterns (Figure 6).

4 Discussion

Domestication is a widely known example of artificial selection and has helped understand some of the most extreme within-species phenotypic variations over the years (Hoglund et al., 2020). PF-carp has been domesticated by humans for more than 1,200 years in paddy fields, developing phenotypic traits and genetic structure to adapt to the environment of the paddy fields (Ren et al., 2018; Qi et al., 2020). The liver of fish plays a crucial role in metabolic and immunological processes (Nakamura and Nishina, 2009). Many studies have reported the effect of heat stress on the structure and function of the liver (Li B et al., 2019; Dettleff et al., 2022; Yang et al., 2022). However, underlying physiological and molecular regulatory mechanisms of hepatopancreases in PF-carp responses to the high-temperature environment of shallow paddy fields remain elusive. Therefore, to better understand the adaptation mechanism of PF-carp to the paddy field environment after extensive domestication, we assessed the pertinent physiological parameters and performed RNA-seq on PF-carp that were under heat stress.

In our current study, only SOD activity and TG content showed significant changes in serum, and MDA content in the hepatopancreas also showed significant changes after undergoing 24 h of high-temperature stress at 34°C, whereas the rest of the various enzyme activity indexes measured in serum and hepatopancreas did not show any significant changes. Fish have been reported to produce large amounts of ROS at high temperatures (Messina et al., 2023). In fish, SOD is the most important system that is used as the first line of defense

10.3389/fphys.2023.1294729

TABLE 4 RNA-seq library sequencing data statistics.

Sample	Raw reads	Clean reads	Q20 (%)	Q30 (%)	GC content (%)	Error rate (%)	Total mapped rate (%)
Control group (28°C)							
GC1	55,559,072	49,347,690	97.84	94.01	48.84	0.0254	79.57
GC2	45,756,400	44,193,878	98.03	94.11	48.8	0.0251	79.71
GC3	43,748,700	42,303,354	98.15	94.48	49.07	0.0247	79.87
Experimental group (34°C)							
GM1	47,388,262	45,363,630	98.21	94.62	50.43	0.0246	78.07
GM2	46,657,000	45,108,462	97.92	93.88	48.95	0.0253	78.64
GM3	48,723,702	46,616,836	97.95	93.97	48.4	0.0252	79.05

GC1–GC3 are the three parallel experimental group samples of the control group. GM1–GM3 are the three parallel experimental group samples of the heat stress group.

against oxidative stress to remove the ROS that is released as a response to heat stress (Wang et al., 2019). Free radicals attack unsaturated fatty acids in the cell membrane to produce MDA (Papadimitriou and Loumbourdis, 2002). However, only SOD activity in the serum antioxidant defense system showed significantly changes, and MDA content in the hepatopancreas was significantly upregulated after 24 h of heat stress, suggesting that the body of PF-carp does not undergo stress when experiencing heat stress in rice paddy fields. In contrast, the antioxidant systems of *Acipenser baerii* (*A. baerii*) (Yang et al., 2021), rainbow trout (*Oncorhynchus mykiss*) (Li et al., 2022), and pikeperch (*Sander lucioperca*) (Li, C. et al., 2019) are significantly activated after thermal stress to maintain homeostasis in their internal environment.

TG is the main form of intracellular fat in fish and is critical for the storage and supply of energy (Komprda et al., 2014). GLU is the primary source of energy in fish that is produced by the digestion and absorption of glucose from meals and the breakdown of glycogen in the liver (Mommsen et al., 1999). TG levels increased significantly during heat stress in PF-carp, while the GLU content did not significantly change, indicating that PF-carp does not need to consume energy during heat stress. Certain particular enzymes may be released into the blood by damaged tissues or organs (Islam et al., 2021). It is reported that cytolysis and enzyme leakage into the bloodstream could lead to an increase in ALT and AST levels, which suggests liver damage (Bacchetta et al., 2014). In our findings, serum levels of ALT and AST in PF-carp during heat stress showed no significant changes, suggesting that heat stress did not affect the dysfunction of the hepatopancreas. In addition, Japanese flounder (*Paralichthys olivaceus*) (Han et al., 2023), pikeperch (*Sander lucioperca*) (Chen, Y. et al., 2021), and largemouth bass (*Micropterus salmoides*) (Zhao et al., 2022) often show damage to their tissues after experiencing heat stress.

RNA-seq has been well established and used to study the impact of high temperatures on fish, such as channel catfish (*Ictalurus punctatus*) (Tan et al., 2019), turbot (*Scophthalmus maximus*) (Huang, Z. et al., 2022), and blunt snout bream (*Megalobrama amblycephala*) (Li, B. et al., 2019). In this novel study, RNA-seq was used to determine the molecular changes in hepatopancreases of PF-carp. Through GO enrichment analysis, we reported that protein processing was significantly enriched. Furthermore, protein processing in the endoplasmic reticulum was the most significantly enriched pathway identified via KEGG enrichment analysis. According to the GSEA results, it was demonstrated that protein processing in the endoplasmic reticulum was the most significantly enriched and upregulated gene set. The endoplasmic reticulum is essential for intracellular calcium homeostasis, modification, and transport, as well as protein synthesis and folding (Kang and Jeon, 2021). The change in temperature could cause ER stress and protein misfolding (Tang et al., 2023). Heat shock proteins (HSPs) aid the folding and function of many proteins and could prevent protein misfolding (Lanneau et al., 2010). In addition, misfolded proteins through endoplasmic reticulum-associated protein degradation (ERAD) can be promoted by the coordination between the HSPs and ubiquitin ligase (Bozaykut et al., 2014; Kang and Jeon, 2021). In our study, HSP40, HSP70, HSP90, and various genes related to ubiquitin ligase were significantly upregulated. Therefore, we hypothesized that PF-carp removes abnormal proteins from the body mainly through protein processing in the endoplasmic reticulum during acclimatization to the high-temperature environment of shallow paddy fields. This is consistent with the way in which Atlantic salmon (*Salmo salar*)

(Shi et al., 2019), rainbow trout (*Oncorhynchus mykiss*) (Li et al., 2017), and largemouth bass (*Micropterus salmoides*) (Zhao et al., 2022) maintain cellular homeostasis during heat stress.

Furthermore, GSEA revealed that the insulin, AMPK, FoxO , Toll-like receptor, and TNF signaling pathways were downregulated and insulin, AMPK, and FoxO signaling pathways could regulate body energy metabolism (Glauser and Schlegel, 2007; Wang et al., 2015; Schell et al., 2021). The insulin signaling pathways could be activated and take part in regulating glucose production in the liver. Additionally, it plays a role in the absorption of glucose into fat and muscle cells, helping maintain the body's glucose balance. (Suren Garg et al., 2023). A variety of physiological stimuli could activate the AMPK signaling pathway, such as glucose deprivation and oxidative stress, which may lead to a reduction in the cellular energy level and an increase in the AMP/ATP ratio (Schultze et al., 2012). Many genes in the FoxO signaling pathway are involved in the production of fat and glucose, and their upregulated expression can stimulate the production of these substances (Gross et al., 2009). It is reported that when fish are subjected to stress, the organism spends a large amount of energy to protect itself from external stresses (Petitjean et al., 2019). For example, gilthead sea bream (*Sparus aurata L.*) will improve mitochondrial metabolism when it faces stress (Bermejo-Nogales et al., 2014). However, these signaling pathways associated with metabolism were downregulated in our results, suggesting that PF-carp does not need to consume a lot of energy to adapt to the high-temperature environment of shallow paddy fields, which is also consistent with the results of our physiological parameters. Therefore, we believe that it is well adapted to paddy fields.

When the organism is exposed to heat stress, it activates a variety of immunomodulatory pathways, such as the Toll-like receptor and TNF signaling pathways. The activation of these immune pathways mediates the inflammatory response and reduces the damage caused by heat stress (Basu et al., 2015; Huang, T. et al., 2022). However, these immune pathways were downregulated when PF-carp was subjected to heat stress, suggesting that the organism did not initiate immune regulation. Pikeperch (*Sander lucioperca*) (Liu et al., 2022), rainbow trout (*Oncorhynchus mykiss*) (Guo et al., 2023), and grass carp (*Ctenopharyngodon idella*) (Zhang et al., 2022) activate these immune pathways to fight against damage when exposed to heat stress.

In a word, to maintain cellular homeostasis in PF-carp, protein processing in the endoplasmic reticulum plays a key role when it is subjected to high temperature stress in shallow paddy fields. In addition, the organism does not produce a stress response, nor does it consume a large amount of energy and trigger an inflammatory response to withstand any harm caused by heat stress. Instead, it adapts well to the high-temperature environment of the paddy field.

Data availability statement

The datasets presented in this study can be found in online repositories. The names of the repository/repositories and accession number(s) can be found in the article/Supplementary Material.

Ethics statement

The animal study was approved by the Institutional Animal Care and Use Committee at Shanghai Ocean University (Shanghai, China). The study was conducted in accordance with the local legislation and institutional requirements.

Author contributions

XC: writing–Original draft, formal analysis, investigation, data curation. FL: writing–Original draft, formal analysis, investigation, data curation. GK: visualization. JL: visualization. JC: investigation. JS: methodology, writing–review & editing, supervision. QL: methodology, writing–review & editing, supervision.

Funding

The author(s) declare that financial support was received for the research, authorship, and/or publication of this article. This research was funded by the National Natural Science Foundation of China (No. 32172995), Shanghai Committee of Science and Technology (No. 22010502100), and Shanghai Pujiang Program (No. 22PJ1404500).

Acknowledgments

The authors thank Minfang Wu and others for their support in all the field work.

Conflict of interest

The authors declare that the research was conducted in the absence of any commercial or financial relationships that could be construed as a potential conflict of interest.

Publisher's note

Supplementary material

The Supplementary Material for this article can be found online at: https://www.frontiersin.org/articles/10.3389/fphys.2023.1294729/full#supplementary-material

References

Bacchetta, C., Rossi, A., Ale, A., Campana, M., Julieta Parma, M., and Cazenave, J. (2014). Combined toxicological effects of pesticides: a fish multi-biomarker approach. *Ecol. Indic.* 36, 532–538. doi:10.1016/j.ecolind.2013.09.016

Balon, E. K. (2004). About the oldest domesticates among fishes. *J. Fish Biol.* 65 (1), 1–27. doi:10.1111/j.0022-1112.2004.00563.x

Basu, M., Paichha, M., Swain, B., Lenka, S. S., Singh, S., Chakrabarti, R., et al. (2015). Modulation of TLR2, TLR4, TLR5, NOD1 and NOD2 receptor gene expressions and their downstream signaling molecules following thermal stress in the Indian major carp catla (Catla catla). *3 Biotech.* 5 (6), 1021–1030. doi:10.1007/s13205-015-0306-5

Bermejo-Nogales, A., Nederlof, M., Benedito-Palos, L., Ballester-Lozano, G. F., Folkedal, O., Olsen, R. E., et al. (2014). Metabolic and transcriptional responses of gilthead sea bream (*Sparus aurata* L.) to environmental stress: new insights in fish mitochondrial phenotyping. *Gen. Comp. Endocrinol.* 205, 305–315. doi:10.1016/j.ygcen.2014.04.016

Bozaykut, P., Ozer, N. K., and Karademir, B. (2014). Regulation of protein turnover by heat shock proteins. *Free Radic. Biol. Med.* 77, 195–209. doi:10.1016/j.freeradbiomed.2014.08.012

Chen X, X., Tang, J., Hu, L., Wu, M., and Ren, W. (2021). *Rice-fish system in qingtian: Ecology, conservation & utilization*. The science press of China.

Chen Y, Y., Liu, E., Li, C., Pan, C., Zhao, X., Wang, Y., et al. (2021). Effects of heat stress on histopathology, antioxidant enzymes, and transcriptomic profiles in gills of pikeperch *Sander lucioperca*. *Aquaculture* 534. doi:10.1016/j.aquaculture.2020.736277

Dettleff, P., Zuloaga, R., Fuentes, M., Gonzalez, P., Aedo, J., Manuel Estrada, J., et al. (2022). High-temperature stress effect on the red cusk-eel (geypterus chilensis) liver: transcriptional modulation and oxidative stress damage. *Biology-Basel* 11 (7), 990. doi:10.3390/biology11070990

Diamond, J. (2002). Evolution, consequences and future of plant and animal domestication. *Nature* 418 (6898), 700–707. doi:10.1038/nature01019

Glauser, D. A., and Schlegel, W. (2007). The emerging role of FOXO transcription factors in pancreatic beta cells. *J. Endocrinol.* 193 (2), 195–207. doi:10.1677/JOE-06-0191

Gross, D. N., Wan, M., and Birnbaum, M. J. (2009). The role of FOXO in the regulation of metabolism. *Curr. Diabetes Rep.* 9 (3), 208–214. doi:10.1007/s11892-009-0034-5

Guo, H., Whitehouse, L., Danzmann, R., and Dixon, B. (2023). Effects of juvenile thermal preconditioning on the heat-shock, immune, and stress responses of rainbow trout upon a secondary thermal challenge. *Comp. Biochem. Physiol. A Mol. Integr. Physiol.* 280, 111413. doi:10.1016/j.cbpa.2023.111413

Han, P., Qiao, Y., He, J., and Wang, X. (2023). Stress responses to warming in Japanese flounder (*Paralichthys olivaceus*) from different environmental scenarios. *Sci. Total Environ.* 897, 165341. doi:10.1016/j.scitotenv.2023.165341

Hoglund, A., Henriksen, R., Fogelholm, J., Churcher, A. M., Guerrero-Bosagna, C. M., Martinez-Barrio, A., et al. (2020). The methylation landscape and its role in domestication and gene regulation in the chicken. *Nat. Ecol. Evol.* 4 (12), 1713–1724. doi:10.1038/s41559-020-01310-1

Huang T, T., Gu, W., Liu, E., Wang, B., Wang, G., Dong, F., et al. (2022). miR-301b-5p and its target gene nfatc2ip regulate inflammatory responses in the liver of rainbow trout (*Oncorhynchus mykiss*) under high temperature stress. *Ecotoxicol. Environ. Saf.* 242, 113915. doi:10.1016/j.ecoenv.2022.113915

Huang Z, Z., Guo, X., Wang, Q., Ma, A., Zhao, T., Qiao, X., et al. (2022). Digital RNA-seq analysis of the cardiac transcriptome response to thermal stress in turbot *Scophthalmus maximus*. *J. Therm. Biol.* 104, 103141. doi:10.1016/j.jtherbio.2021.103141

Islam, M. J., Kunzmann, A., and Slater, M. J. (2021). Extreme winter cold-induced osmoregulatory, metabolic, and physiological responses in European seabass (*Dicentrarchus labrax*) acclimatized at different salinities. *Sci. Total Environ.* 771, 145202. doi:10.1016/j.scitotenv.2021.145202

Kang, J. A., and Jeon, Y. J. (2021). How is the fidelity of proteins ensured in terms of both quality and quantity at the endoplasmic reticulum? Mechanistic insights into E3 ubiquitin ligases. *Int. J. Mol. Sci.* 22 (4), 2078. doi:10.3390/ijms22042078

Komprda, T., Zornikova, G., Knoll, A., Vykoukalova, Z., Rozikova, V., Skultety, O., et al. (2014). Effect of dietary eicosapentaenoic and docosahexaenoic acid on expression of rat liver genes controlling cholesterol homeostasis and on plasma cholesterol level. *Czech J. Animal Sci.* 59 (9), 391–398. doi:10.17221/7650-cjas

Lanneau, D., Wettstein, G., Bonniaud, P., and Garrido, C. (2010). Heat shock proteins: cell protection through protein triage. *Thescientificworldjournal* 10, 1543–1552. doi:10.1100/tsw.2010.152

Li B, B., Sun, S., Zhu, J., Yanli, S., Wuxiao, Z., and Ge, X. (2019). Transcriptome profiling and histology changes in juvenile blunt snout bream (*Megalobrama amblycephala*) liver tissue in response to acute thermal stress. *Genomics* 111 (3), 242–250. doi:10.1016/j.ygeno.2018.11.011

Li C, C., Wang, Y., Wang, G., Chen, Y., Guo, J., Pan, C., et al. (2019). Physicochemical changes in liver and Hsc70 expression in pikeperch *Sander lucioperca* under heat stress. *Ecotoxicol. Environ. Saf.* 181, 130–137. doi:10.1016/j.ecoenv.2019.05.083

Li, Y. J., Huang, J. Q., Liu, Z., Zhou, Y. J., Xia, B. P., Wang, Y. J., et al. (2017). Transcriptome analysis provides insights into hepatic responses to moderate heat stress in the rainbow trout (*Oncorhynchus mykiss*). *Gene* 619, 1–9. doi:10.1016/j.gene.2017.03.041

Li, S., Liu, Y., Li, B., Ding, L., Wei, X., Wang, P., et al. (2022). Physiological responses to heat stress in the liver of rainbow trout (*Oncorhynchus mykiss*) revealed by UPLC-QTOF-MS metabolomics and biochemical assays. *Ecotoxicol. Environ. Saf.* 242, 113949. doi:10.1016/j.ecoenv.2022.113949

Liu, E., Zhao, X., Li, C., Wang, Y., Li, L., Zhu, H., et al. (2022). Effects of acute heat stress on liver damage, apoptosis and inflammation of pikeperch (*Sander lucioperca*). *J. Therm. Biol.* 106, 103251. doi:10.1016/j.jtherbio.2022.103251

Lu, J., and Li, X. (2006). Review of rice-fish-farming systems in China - one of the globally important ingenious agricultural heritage systems (GIAHS). *Aquaculture* 260 (1-4), 106–113. doi:10.1016/j.aquaculture.2006.05.059

Messina, S., Costantini, D., and Eens, M. (2023). Impacts of rising temperatures and water acidification on the oxidative status and immune system of aquatic ectothermic vertebrates: a meta-analysis. *Sci. Total Environ.* 868, 161580. doi:10.1016/j.scitotenv.2023.161580

Mommsen, T. P., Vijayan, M. M., and Moon, T. W. (1999). Cortisol in teleosts: dynamics, mechanisms of action, and metabolic regulation. *Rev. Fish Biol. Fish.* 9 (3), 211–268. doi:10.1023/a:1008924418720

Nakamura, T., and Nishina, H. (2009). Liver development: lessons from knockout mice and mutant fish. *Hepatology Res.* 39 (7), 633–644. doi:10.1111/j.1872-034X.2009.00522.x

Papadimitriou, E., and Loumbourdis, N. S. (2002). Exposure of the frog *Rana ridibunda* to copper: impact on two biomarkers, lipid peroxidation, and glutathione. *Bull. Environ. Contam. Toxicol.* 69 (6), 885–891. doi:10.1007/s00128-002-0142-2

Petitjean, Q., Jean, S., Gandar, A., Cote, J., Laffaille, P., and Jacquin, L. (2019). Stress responses in fish: from molecular to evolutionary processes. *Sci. Total Environ.* 684, 371–380. doi:10.1016/j.scitotenv.2019.05.357

Qi, M., Wu, Q., Liu, T., Hou, Y., Miao, Y., Hu, M., et al. (2020). Hepatopancreas transcriptome profiling analysis reveals physiological responses to acute hypoxia and reoxygenation in juvenile qingtian paddy field carp *Cyprinus carpio* var qingtianensis. *Front. Physiol.* 11, 1110. doi:10.3389/fphys.2020.01110

Ren, W., Hu, L., Guo, L., Zhang, J., Tang, L., Zhang, E., et al. (2018). Preservation of the genetic diversity of a local common carp in the agricultural heritage rice-fish system. *Proc. Natl. Acad. Sci. U. S. A.* 115 (3), E546–E554. doi:10.1073/pnas.1709582115

Schell, M., Wardelmann, K., and Kleinridders, A. (2021). Untangling the effect of insulin action on brain mitochondria and metabolism. *J. Neuroendocrinol.* 33 (4), e12932. doi:10.1111/jne.12932

Schultze, S. M., Hemmings, B. A., Niessen, M., and Tschopp, O. (2012). PI3K/AKT, MAPK and AMPK signalling: protein kinases in glucose homeostasis. *Expert Rev. Mol. Med.* 14, e1. doi:10.1017/S1462399411002109

Shi, K. P., Dong, S. L., Zhou, Y. G., Li, Y., Gao, Q. F., and Sun, D. J. (2019). RNA-seq reveals temporal differences in the transcriptome response to acute heat stress in the Atlantic salmon (*Salmo salar*). *Comp. Biochem. Physiology D-Genomics Proteomics* 30, 169–178. doi:10.1016/j.cbd.2018.12.011

Suren Garg, S., Kushwaha, K., Dubey, R., and Gupta, J. (2023). Association between obesity, inflammation and insulin resistance: insights into signaling pathways and therapeutic interventions. *Diabetes Res. Clin. Pract.* 200, 110691. doi:10.1016/j.diabres.2023.110691

Tan, S., Wang, W., Tian, C., Niu, D., Zhou, T., Jin, Y., et al. (2019). Heat stress induced alternative splicing in catfish as determined by transcriptome analysis. *Comp. Biochem. Physiol. Part D. Genomics Proteomics* 29, 166–172. doi:10.1016/j.cbd.2018.11.008

Tang, Z., Yang, Y., Wu, Z., and Ji, Y. (2023). Heat stress-induced intestinal barrier impairment: current insights into the aspects of oxidative stress and endoplasmic reticulum stress. *J. Agric. Food Chem.* 71 (14), 5438–5449. doi:10.1021/acs.jafc.3c00798

Wang, B., Liu, Y., Feng, L., Jiang, W. D., Kuang, S. Y., Jiang, J., et al. (2015). Effects of dietary arginine supplementation on growth performance, flesh quality, muscle antioxidant capacity and antioxidant-related signalling molecule expression in young grass carp (Ctenopharyngodon idella). *Food Chem.* 167, 91–99. doi:10.1016/j.foodchem.2014.06.091

Wang, Y., Li, C., Pan, C., Liu, E., Zhao, X., and Ling, Q. (2019). Alterations to transcriptomic profile, histopathology, and oxidative stress in liver of pikeperch (*Sander lucioperca*) under heat stress. *Fish Shellfish Immunol.* 95, 659–669. doi:10.1016/j.fsi.2019.11.014

Xie, J., Hu, L., Tang, J., Wu, X., Li, N., Yuan, Y., et al. (2011). Ecological mechanisms underlying the sustainability of the agricultural heritage rice-fish coculture system. *Proc. Natl. Acad. Sci. U. S. A.* 108 (50), E1381–E1387. doi:10.1073/pnas.1111043108

Xu, P., Zhang, X., Wang, X., Li, J., Liu, G., Kuang, Y., et al. (2014). Genome sequence and genetic diversity of the common carp, *Cyprinus carpio*. *Nat. Genet.* 46 (11), 1212–1219. doi:10.1038/ng.3098

Yang, S., Yang, X., Li, Y., Li, D., Gong, Q., Huang, X., et al. (2021). The multilevel responses of *Acipenser baerii* and its hybrids (*A. baerii* ♀ × A. schrenckii ♂) to chronic heat stress. *Aquaculture* 541, 736773. doi:10.1016/j.aquaculture.2021.736773

Yang, C., Dong, J., Sun, C., Li, W., Tian, Y., Liu, Z., et al. (2022). Exposure to heat stress causes downregulation of immune response genes and weakens the disease resistance of *Micropterus salmoides*. *Comp. Biochem. Physiology D-Genomics Proteomics* 43, 101011. doi:10.1016/j.cbd.2022.101011

Zhang, W., Xu, X., Li, J., and Shen, Y. (2022). Transcriptomic analysis of the liver and brain in grass carp (Ctenopharyngodon idella) under heat stress. *Mar. Biotechnol. (NY)* 24 (5), 856–870. doi:10.1007/s10126-022-10148-6

Zhao, X., Li, L., Li, C., Liu, E., Zhu, H., and Ling, Q. (2022). Heat stress-induced endoplasmic reticulum stress promotes liver apoptosis in largemouth bass (*Micropterus salmoides*). *Aquaculture* 546, 737401. doi:10.1016/j.aquaculture.2021.737401

frontiers | Frontiers in Marine Science

TYPE Original Research
PUBLISHED 23 November 2023
DOI 10.3389/fmars.2023.1285427

OPEN ACCESS

EDITED BY
Yi-Feng Li,
Shanghai Ocean University, China

REVIEWED BY
Yao Zheng,
Chinese Academy of Fishery Sciences (CAFS), China
Adnan H. Gora,
Central Marine Fisheries Research Institute (ICAR), India
Hong Li,
Nanjing Normal University, China

*CORRESPONDENCE
Qichen Jiang
qichenjiang@live.cn
Weiwei Lv
wwlv1986@sina.com

†These authors share first authorship

RECEIVED 30 August 2023
ACCEPTED 16 October 2023
PUBLISHED 23 November 2023

CITATION
Liu H, Zhou W, Zhou Z, Yu C, Tye GJ, Lv W and Jiang Q (2023) Effects of polystyrene nanoplastic exposure on energy metabolism, lipid metabolism, and amino acid changes in *Monopterus albus*. *Front. Mar. Sci.* 10:1285427. doi: 10.3389/fmars.2023.1285427

Effects of polystyrene nanoplastic exposure on energy metabolism, lipid metabolism, and amino acid changes in *Monopterus albus*

Huaqiang Liu[2†], Wenzong Zhou[1†], Zihan Zhou[3], Cigang Yu[4], Gee Jun Tye[2], Weiwei Lv[1*] and Qichen Jiang[3*]

[1]Eco-environmental Protection Research Institute, Shanghai Academy of Agricultural Sciences, Shanghai, China, [2]Institute for Research in Molecular Medicine, Universiti Sains Malaysia, Penang, China, [3]Freshwater Fisheries Research Institute of Jiangsu Province, Nanjing, China, [4]Nanjing Institute of Environmental Sciences, Ministry of Ecology and Environment, Nanjing, China

Nanoplastics (NPs) have emerged as contaminants in recent years and have attracted widespread attention because of their ecotoxicological effects. This study aimed to document the effects of different concentrations of NPs on the *Monopterus albus*. *M. albus*. *M. albus* were orally administered three different concentrations of 100 nm polystyrene NPs (0.05%, 0.5%, and 1% of the feed) for 35 days. The effects of different NPs concentrations on energy metabolism, enzyme biomarker responses, gene expression responses, and amino acid changes were investigated in *M. albus* after exposure. The results revealed that the gene expression of phosphoenolpyruvate carboxykinase and glucose-6-phosphatase was up-regulated after the ingestion of high concentrations of NPs. The gluconeogenic pathway was inhibited, lactic acid (LA) content was increased, anaerobic glycolysis was used to produce LA to power the organism, and the accumulation of NPs led to a decrease in total cholesterol and triglyceride levels in liver tissues. There were increases in the relative liver content of glutamine, glycine, and methionine, which may be due to antioxidation in the liver. The stress may caused by NPs leads to the formation of some glutamylated amino acids, which are converted into glutathione to play an antioxidant role. NPs also induced lipotoxicity of the liver organoid by increasing lipid accumulation, these include methyl tetradecanoate (myristate), pentadecanoic acid, eicosanoic acid (arachidic acid), heptadecanoic acid (margaric acid), 5,8,11,14-eicosatetraenoic acid, and doconexent (Docosahexaenoic acid). Interestingly, some immune-related metabolites, such as 9-octadecenoic acid (oleic acid) and 9,12-octadecadienoic acid (linoleic acid), were significantly reduced, and these changes were probably caused by disturbances in hepatic lipid metabolism following NPs exposure.

KEYWORDS

NPS, *M. albus*, energy metabolism, gene expression, antioxidant

1 Introduction

The accumulation of plastic waste in the aquatic environment is one of the common and persistent ecological problems on Earth, with significant impacts on ecosystems, food safety, and human health. At present, microplastics (MPs) are accumulating in the global marine and freshwater ecosystems, and the environmental problem of pollution has become the focus of global attention (Lamichhane et al., 2023). MP particles (<5 mm diameter) are found ubiquitous, from the Arctic to the Antarctic, from thin air layers to deep dense seawater, and from remote land to the middle of the ocean (Rochman, 2018). Over time, the plastic disintegrates into MPs and nanoplastics (NP <0.1 μm diameter) (Smith et al., 2018). When NPs are ingested and accumulate in different tissues of aquatic organisms, they can affect their biological systems. NPs are bioaccumulated in fish liver and muscle and cause DNA damage after a chronic exposure (Issac and Kandasubramanian, 2021; Brandts et al., 2022) and may clog the digestive system (Van Dyck et al., 2016). NPs can also adhere and enter to the gills, transfer to various tissues (Li et al., 2022b).

Currently, studies on the effects of NPs on aquatic organisms have been conducted mainly in populations and individuals (Gong et al., 2023). Exposure of aquatic organisms to NPs can affect enzyme activity, as well as cholesterol, glucose, and fat levels (Brandts et al., 2018). NPs have been reported in bivalves, copepods, and fish to raise the levels of reactive oxygen species (ROS), cause the buildup of cellular oxidative damage, and affect the levels, activity, or expression of antioxidant biomolecules (Trevisan et al., 2022). Teng et al. found that the accumulation of NPs in the zebrafish gut caused intestinal inflammation and inhibited zebrafish growth and development (Teng et al., 2022). When mammals consume aquatic organisms containing NPs, they accumulate in the liver, kidneys, and intestines of the organism, causing energy and lipid metabolism disorders, as well as oxidative stress (Trevisan et al., 2022). However, few researches have been done on the effect of NPs on energy metabolism and amino acid changes in freshwater fish.

M. albus is a fish that lives in the coastal areas of China, Japan, and the Korean Peninsula (Shafland et al., 2009). In recent years, with the increasing use of various agricultural chemicals and the discharge of industrial pollutants, the habitat of wild *M. albus* has deteriorated. The number of *M. albus* is also greatly reduced due to overfishing, and MPs in the water of artificially raised *M. albus* and the wastewater of rice fields has increased significantly (Nuryadin et al., 2020; Zhu et al., 2023). MPs and NPs are associated with ecological risks in aquaculture, however there is very little research on their toxic effects on *M. albus*. As shown in Figure 1, we investigated the effects of adding different concentrations of NPs to feed on liver energy metabolism, as well as changes in amino acids and fatty acids. The results of this study provide valuable ecotoxicological data for better evaluating the impact of NPs on artificially cultured *M. albus*.

2 Materials and methods

2.1 Culture of *M. albus*

The experimental *M. albus* were obtained from the Shanghai Academy of Agricultural Sciences. All the *M. albus* were healthy individuals with an average weight of 22.7 ± 0.4 g and were bred from the same parent. During the temporary culture period, they were all raised in an 8 m × 6 m × 6 m cement pool, with water aerated continuously at a temperature of 28 ± 0.9°C and pH of 7.8 ± 0.3. The *M. albus* were fed with commercial feed (Hubei Zhaoliang Biotechnology Co., Ltd.) at 4 pm every day. The main ingredients of the feed were fish meal, fish oil, soybean meal, flour, yeast powder, multivitamins, and minerals. Approximately one-third of the total volume of water was replaced before feeding.

2.2 Polystyrene NPs

Polystyrene NPs were purchased from BaseLine Chromtech Research Centre in Tianjin, China. These NPs were monodisperse polystyrene microspheres with a diameter of 100 nm and a concentration of 10 mg/mL (5.32×10^{12} particles/mL). In this study, fish meal, soybean meal, and soybean protein concentrate were used as protein sources, α-starch was used as a binder and a source of carbohydrates, and fish oil was used as a lipid source. Additionally, all components were crushed into a fine powder and sieved through a 320 μm mesh for A, B, and C groups, where the NPs were 0.5, 5, and 10 g/kg, respectively. The materials for the experimental meals were completely blended with fish oil using a mixer, then stored in sample bags at −20°C until use.

2.3 Toxicity test

After temporary cultivation, the *M. albus* were divided into four groups, namely A, B, C, and CK (E). Each group consists of three repeated water tanks, with four *M. albus* fed in a 10 L water tank. The CK (E) group of *M. albus* received normal feed without NPs, while the A, B, and C groups received 1%, 0.5%, and 0.05% concentrations of polystyrene NPs in the feed. The water in each water tank was changed every 24 hours and the same weight (3 g) of feed was added every day. After 35 days of NPs exposure, the liver of *M. albus* was removed and stored in liquid nitrogen to prepare for the subsequent enzyme activity and transcriptome experiments.

2.4 Analysis of biomarkers

Nine *M. albus* were collected from each group, and their livers were used to prepare tissue homogenate. The method was as follows: the livers were homogenized in phosphate buffer (50 mM

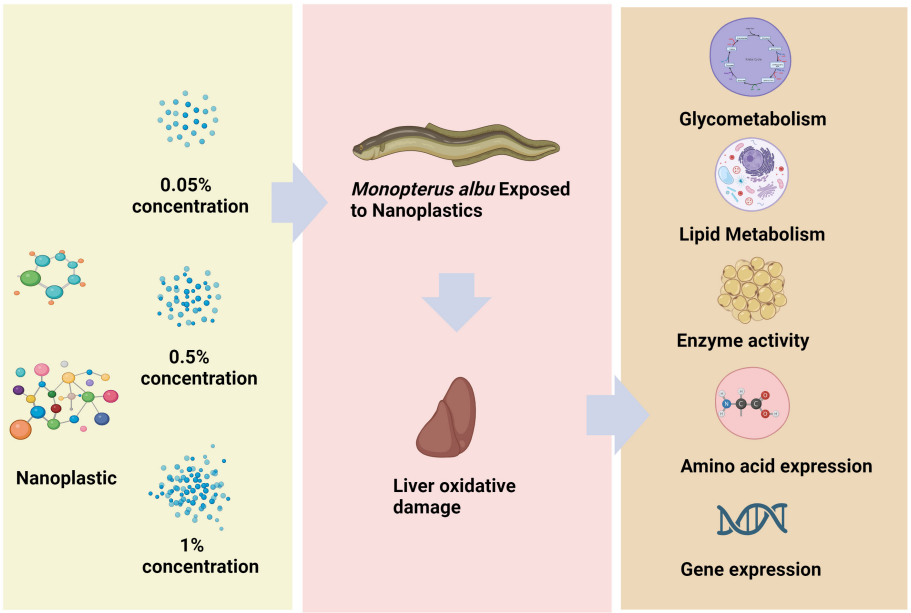

FIGURE 1
Summary figure.

monopotassium phosphate; 50 mM monopotassium phosphate dibasic; 1 mM EDTA; pH 7.0) with an IKA homogenizer (Ultra Turrax IKA T10 basic), and then centrifuged at 10000 g for 20 minutes at 4°C to obtain the supernatant. Commercial kits (Nanjing Jiancheng Bioengineering Institute) were used to determine the levels of energy metabolism-related biochemical substances, total cholesterol (T-CHO), and CoA carboxylase (ACC) according to the manufacturer's instructions. Levels of triglyceride (TG) were analyzed by the Bucolo et al. method (Bucolo and David, 1973), and fatty acid synthase (FAS) activity was analyzed by the procedure described by Tian et al. (Tian et al., 1985). All these parameters were measured using an enzyme plate spectrophotometer (BioTek Instruments).

2.5 Gene expression

Primer 5 software was used to design primers for energy metabolism-related genes, hexokinase (HK), protein kinases (PK), phosphoenolpyruvate carboxykinase (PCK), phosphofructokinase (PFK), maltase-glucoamylase (MGAM), glucose-6-phosphatase (G6PC), and citrate (Si)-synthase (SI). The primers used for qRT-PCR were synthesized by the Anhui General Biology Company. β-Actin was used as an internal reference gene. Total RNA extraction, RNA integrity analysis, cDNA synthesis, and qRT PCR were performed as previously described (Limbu et al., 2019). Detailed information is shown in Table 1.

TABLE 1 Primers used for the real-time PCR analysis of *Monopterus albus* genes.

Gene	Forward primer (5'->3')	Reverse primer (5'->3')	Annealing temperature (°C)	Size (bp)
HK1	CAGAGAGAACCGAGGAGTGG	CAGAGAGAACCGAGGAGTGG	60	178
PFK (pfkA)	CTGGTCTTCCACCCTGTTGT	TGGCAACTGAAGCATCTGAC	60	199
PK (pkmb)	TGTCTGCTGGACATCGACTC	GCCTCACGGACATTCTTGAT	60	191
PCK	TCCCTTCAGTATGGGTCCTG	CAGCGAACAAACTCCTCTCC	60	153
G6PC	CCTTTGGCCAGCTTGTTTAG	GTCAAGGAACTGCAGCAACA	60	171
MGAM	CCATCCAGAGGAGAATCCAA	CACGGAGTGTGTCAATGTCC	60	224
SI	ACTGCGATCCTCCAGAGAAA	CTTGGTCAATCCGCCTGTAT	60	212
Beta -actin	CTGCGGAATCCACGAAAC	GTCAGCAATGCCAGGGTA	60	121

2.6 Proximate composition analysis

The proximate composition of the samples in different groups was determined according to methods described previously (Taşbozan et al., 2016). The data were examined by Nanjing Innovation Biotechnology.

2.7 Amino acid analysis

The powdered sample (0.2 g) was added to 0.1 mol/L hydrochloric acid (1.0 mL) in a 10 mL centrifuge tube, shaken, and placed in ice water. The centrifuge tube containing the sample, ice water, and a rack were placed together into an ultrasonic instrument. The sample was extracted for 40 minutes and shaken three times halfway through the process. The sample was then centrifuged at 4°C for 10 minutes at high speed. The supernatant was retrieved and 1 ml of 0.1 mol/L hydrochloric acid was added. The sample was extracted once according to the above steps, and the supernatant was merged twice. The supernatant was placed into a 10 mL centrifuge tube and 750 μl of 0.1 mol/L PITC acetonitrile solution and 750 μl of 1 moL/L triethylamine acetonitrile solution were added, then vortexed for 1 minute. The sample was then placed in a water bath at 25°C for 40 minutes. Then, 6 mL of n-hexane was added, vortexed for 1–2 min, and let stand for 5 min. The sample was then subjected to high-speed centrifugation for 5 minutes and extracted twice. A syringe was used to absorb the lower layer of liquid, which was passed through a 0.22 μm filter membrane and transferred to a chromatographic flask to perform liquid phase analysis. The data was tested by Nanjing Innovation Biotechnology.

2.8 Related fatty acids analysis

A uniform sample was weighed and 500 mg was transferred into a 10 mL test tube with a stopper. Petroleum ether (2 ml) was added and 1 mL of potassium hydroxide methanol solution was added to the ether mixture as a methylating reagent. The mixture was subjected to vortex oscillation and then left stationary for 1 hour. Then vortexed again, 2 mL of deionized water was added and the mixture was left to stand for 30 minutes until layers formed. It was then centrifuged at 4500 g for 2 minutes and the supernatant was removed to be analyzed using gas chromatography-mass spectrometry. The data was tested by Nanjing Innovation Biotechnology.

2.9 Statistics

The mean and standard error (Mean ± SE) of all data from this experiment were calculated using SPSS. One-way ANOVA, followed by Tukey's multiple comparisons, were used to analyze group differences. Differences with a $p < 0.05$ (*), $p < 0.01$ (**) were considered significant, whereas those with a $p < 0.001$ (***), $p < 0.0001$ (****) were considered highly significant. Graphs were generated using the R package and GraphPad Prism 10 program.

3 Results

3.1 Effects of NPs on the energy metabolism of *M. albus*

Figure 2 shows the effect of different NPs concentrations on energy metabolism in the liver of *M. albus* after 35 days of treatment with NPs. In the 1% concentration group the expression levels of PK, HK genes in liver tissue decreases ($p < 0.05$). At the same time, it was observed that the expression levels of the SI, PCK, MGAM, and G6PC genes increased ($p < 0.05$), especially in the 1% high-concentration group, where the expression levels were the highest.

To evaluate the changes in energy reserve substances in liver tissue caused by exposure to NPs, as shown in Figure 3, the levels of T-CHO and TG in liver tissue were detected. Changes occurred in T-CHO and TG liver content, especially in the 1% high-concentration group, where the content of T-CHO and TG was the lowest. At the same time, in the 1% and 0.5% concentration group, it was observed that the activity of FAS and ACC enzymes increased ($p < 0.05$), especially in the 1% high-concentration group, where ACC had the highest activity.

3.2 Effects of NPs on lipid metabolism in the liver of *M. albus*

Significant changes in lipid metabolism in *M. albus* liver induced by NPs exposure were evident in Table 2. Eighteen fatty acids were found to accumulate in the liver. The levels of methyl tetradecanoate, pentadecanoic acid, eicosanoic acid, heptadecanoic acid, 5,8,11,14-eicosatetraenoic acid, and doconexent were significantly increased, and the levels of 9-octadecenoic acid and 9,12-octadecadienoic acid were significantly decreased in the A group than that in the CK(E) group ($p \leq 0.05$). These data demonstrate that exposure to NPs induces the accumulation of fatty acids in the liver of *M. albus* and affects its immune function.

3.3 Effects of NPs on the liver proximate composition and amino acids of *M. albus*

The content of water, crude protein, crude fat and ash in the liver of *M. albus* is shown in Table 3. NPs significantly increased the crude fat content, and the ash content also in the A group were significantly higher than that in the CK(E) group ($p \leq 0.05$). In addition, NPs did not significantly affect the water and crude protein content of the liver and pancreas of *M. albus*($p > 0.05$).

Eighteen amino acids in the liver of *M. albus* were analyzed and evaluated: Glutamate, asparagine, serine, glutamine, glycine, histidine, arginine, threonine, alanine, proline, tyrosine, valine, methionine, isoleucine, leucine, phenylalanine, and lysine. The effect of different concentrations of NPs on the amino acid content in the liver of *M. albus* is shown in Table 4. The levels of glutamine, glycine, and methionine increased significantly in the A group than that in the CK(E) group ($p \leq 0.05$).

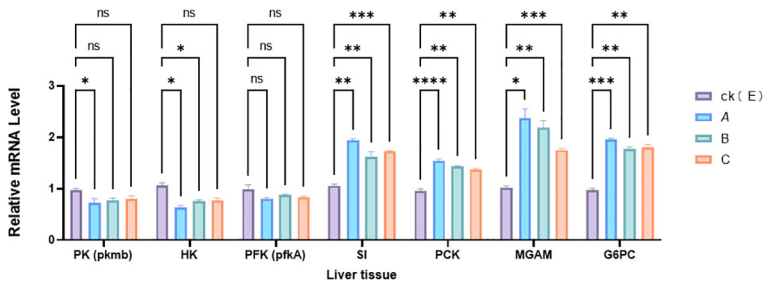

FIGURE 2
Effect of NPs on the expression of genes related to liver metabolism in *M. albus*. CK(E) indicates control samples A, B, and C groups received 1%, 0.5%, and 0.05% concentrations of polystyrene NPs in the feed. The data represents the average standard error (N=3 replicates). $p < 0.001$ (***), $p < 0.01$ (**), and $p < 0.05$ (*) are considered statistically significant differences, ns is no significance. Different asterisks indicate statistical differences between treatments.

4 Discussion

This study investigated how oral exposure to different concentrations of 100 nm plastic particles affected the liver of *M. albus*. Our results confirm that after 35 days of NPs ingestion, there are changes in the expression of energy metabolism enzyme biomarkers and related genes in the liver. *M. albus* may use increased glycolysis to provide energy to adapt to the oxidative damage of the liver after exposure to NPs. At the same time, NPs also changed the amino acid content in the liver. The experiment found that the concentration of NPs is closely related to disordered energy metabolism in the liver.

The glycolytic pathway is crucial for the metabolism of carbohydrates and glucose. When aerobic metabolism produces ATP, anaerobic glycolysis is used to produce lactic acid and provide energy for the organism (Li et al., 2022a). Previous studies have found that NPs may alter the energy related enzymes of *Dicentrarchus labrax*, reducing their energy reserves and

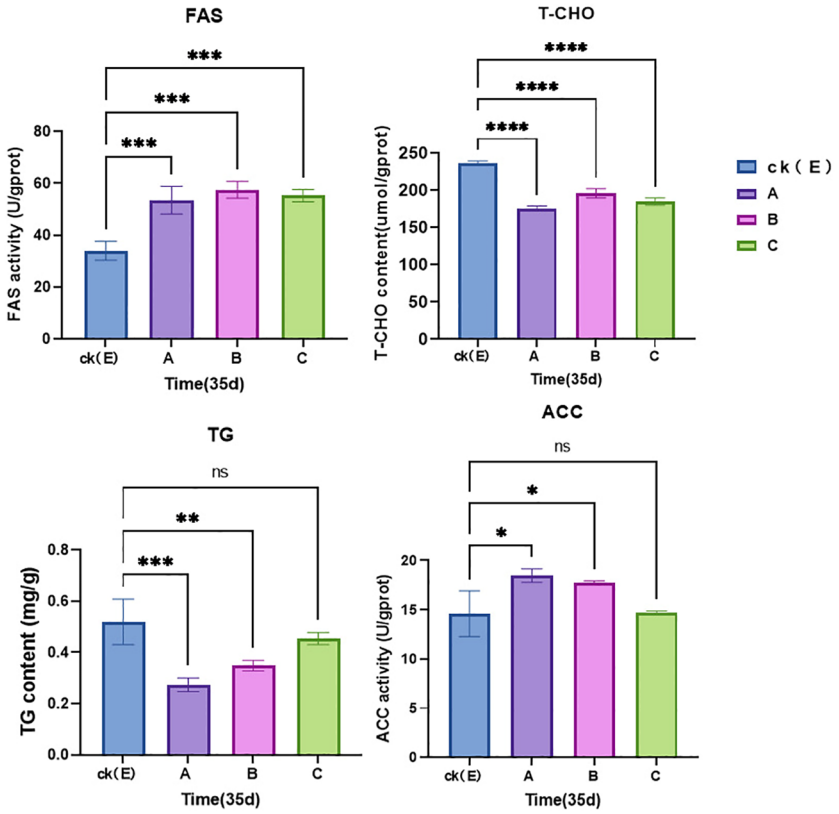

FIGURE 3
Relative levels of enzyme activities in the liver tissue of *M. albus*. CK(E) indicates control samples. A, B and C groups received 1%, 0.5%, and 0.05% concentrations of polystyrene NPs in the feed. Data represent the mean and standard errors (N = 3 replicate treatments). $p < 0.0001$ (****), $p < 0.001$ (***), $p < 0.01$ (**), and $p < 0.05$ (*) were considered statistically significant differences, ns is no significance. Different asterisks indicate statistical differences between groups.

TABLE 2 Effects of different concentrations of NPs on fatty acid content in the liver and pancreas of *M. albus* (mg/kg dry matter).

Fatty acid	A	B	C	CK(E)
Methyl tetradecanoate	25.92 ± 6.61^{b}	15.52 ± 3.07^{a}	15.36 ± 2.83^{a}	10.10 ± 2.24^{a}
Pentadecanoic acid, methyl ester	8.07 ± 1.77^{c}	7.23 ± 1.83^{bc}	4.56 ± 1.66^{ab}	3.37 ± 0.70^{a}
Pentadecanoic acid, 14-methyl-, methyl ester	380.40 ± 178.18^{a}	471.72 ± 231.36^{a}	615.58 ± 295.52^{a}	474.89 ± 220.90^{a}
7-Hexadecenoic acid, methyl ester, (Z)-	14.86 ± 6.74^{a}	17.24 ± 15.45^{a}	32.02 ± 35.44^{a}	9.00 ± 5.53^{a}
9-Hexadecenoic acid, methyl ester, (Z)-	95.28 ± 24.81^{a}	92.29 ± 53.14^{a}	153.89 ± 81.88^{a}	121.67 ± 73.41^{a}
Heptadecanoic acid, methyl ester	13.33 ± 2.89^{c}	10.21 ± 1.82^{bc}	6.99 ± 1.84^{b}	2.57 ± 1.93^{a}
Methyl stearate	432.61 ± 99.71^{a}	412.81 ± 111.79^{a}	474.81 ± 133.70^{a}	556.53 ± 121.25^{a}
9-Octadecenoic acid (Z)-, methyl ester	142.60 ± 24.58^{a}	183.18 ± 31.77^{ab}	268.03 ± 51.70^{b}	425.03 ± 100.24^{c}
9,12-Octadecadienoic acid, methyl ester	793.22 ± 218.99^{a}	1234.94 ± 323.35^{b}	1212.59 ± 178.28^{ab}	1505.91 ± 128.15^{b}
9,12,15-Octadecatrienoic acid, methyl ester, (Z,Z,Z)-	28.61 ± 12.69^{a}	18.19 ± 2.70^{a}	24.18 ± 3.93^{a}	27.17 ± 8.17^{a}
Nonadecanoic acid, methyl ester	21.15 ± 13.25^{a}	18.35 ± 4.52^{a}	16.54 ± 3.01^{a}	18.97 ± 3.50^{a}
Eicosanoic acid, methyl ester	10.52 ± 0.85^{b}	9.25 ± 2.05^{b}	4.90 ± 1.89^{a}	3.67 ± 1.61^{a}
cis-11-Eicosenoic acid, methyl ester	43.16 ± 21.44^{a}	32.92 ± 16.90^{a}	38.50 ± 3.88^{a}	48.64 ± 18.74^{a}
cis-11,14-Eicosadienoic acid, methyl ester	148.27 ± 65.81^{a}	132.13 ± 46.88^{a}	140.06 ± 12.82^{a}	167.39 ± 59.25^{a}
5,8,11,14-Eicosatetraenoic acid, methyl ester, (all-Z)-	110.70 ± 10.65^{b}	107.29 ± 24.75^{b}	62.41 ± 5.59^{a}	52.32 ± 13.22^{a}
11,14,17-Eicosatrienoic acid methyl ester	26.60 ± 7.41^{a}	20.96 ± 4.28^{a}	22.50 ± 2.05^{a}	23.99 ± 3.50^{a}
cis-13,16-Docasadienoic acid, methyl ester	42.72 ± 18.48^{a}	34.56 ± 8.94^{a}	39.72 ± 6.50^{a}	39.73 ± 9.29^{a}
Methyl 7,10,13,16-docosatetraenoate	59.91 ± 2.44^{b}	70.88 ± 19.55^{b}	29.55 ± 3.05^{a}	56.74 ± 8.65^{b}
Doconexent	56.88 ± 5.09^{b}	34.47 ± 15.10^{a}	28.16 ± 1.24^{a}	24.26 ± 2.78^{a}

Values are means ± SEM of four replications the same letters on the columns in the figure indicate non-significant differences ($p > 0.05$), and different letters indicate significant differences ($p \leq 0.05$).

nutritional quality (Barboza et al., 2018). As a limiting enzyme of glycolysis, PK catalyzes the conversion of phosphate groups from phosphoenolpyruvic acid to adenosine diphosphate (ADP), producing pyruvic acid and adenosine triphosphate (ATP) (Israelsen and Vander Heiden, 2015). HK promotes the phosphorylation of glucose to produce glucose 6-phosphate, which is the first step of the glycolysis pathway. PK and HK are important enzymes that control the direction and rate of glucose metabolism, and their levels can reflect the vitality of the body. By measuring the activities of energy metabolism related enzymes HK and PK, the effect of exposure to NPs on sugar metabolism in *M. albus* was studied. The results showed that with the increase of NPs concentration, the PK and HK activities in *M. albus* liver tissue generally decreased. Therefore, with the increase of NPs concentration, the glycolysis pathway is restricted, and the occurrence of anaerobic glucose metabolism increases. These results are consistent with a previous study conducted by Teng et al. (Teng et al., 2021). NPs may cause changes in metabolites and disrupt some mechanisms, including oxidative stress, immune regulation, and Trojan horse effects, and even energy metabolism (Li et al., 2021). A relevant research shows that zebrafish exposed to NPs increase glucose consumption, and have a shortage of energy supplies (Chen et al., 2020). Therefore, our results indicate that exposure to NPs can have a negative impact on glucose metabolism in *M. albus* significantly inhibits the glycolytic pathway and leads to a shift from aerobic metabolism to anaerobic metabolism.

Gluconeogenesis is the process by which fresh glucose is created in animals from common metabolites such as amino acids, glycerol, lactate, pyruvate, and intermediate tricarboxylic acid cycle metabolites (TeSlaa et al., 2021). Of these metabolites, only amino acids and glycerol lead to net glucose production. Lactate, the main gluconeogenic substrate, is synthesized from glucose but can be

TABLE 3 Effects of different concentrations of NPs on liver proximate composition of *M. albus*.

Parameters	A	B	C	CK(E)
Crude fat(%)	36.99 ± 1.65^{c}	24.86 ± 6.21^{b}	18.20 ± 2.07^{a}	15.25 ± 0.81^{a}
Ash(%)	5.87 ± 1.35^{b}	5.43 ± 1.06^{b}	3.49 ± 0.30^{a}	2.69 ± 0.26^{a}
Crude protein g/kg	176.12 ± 12.67^{a}	161.47 ± 12.49^{a}	172.02 ± 11.14^{a}	161.21 ± 30.08^{a}
Water content(%)	65.00 ± 1.55^{a}	68.07 ± 3.41^{a}	68.44 ± 0.69^{a}	67.81 ± 3.22^{a}

Values are means ± SEM of four replications the same letters on the columns in the figure indicate non-significant differences ($p > 0.05$), and different letters indicate significant differences ($p \leq 0.05$).

TABLE 4 Effect of different concentrations of NPs on amino acid content in the liver of *M. albus* (mg/kg dry matter).

Amino acid	A	B	C	CK(E)
Glutamate	157.43 ± 93.52[a]	210.84 ± 88.85[a]	163.27 ± 57.26[a]	166.50 ± 96.94[a]
Asparagine	223.47 ± 142.48[a]	189.90 ± 84.61[a]	205.22 ± 55.86[a]	185.03 ± 114.57[a]
Serine	165.24 ± 109.66[a]	165.19 ± 123.21[a]	127.30 ± 45.05[a]	144.25 ± 118.54[a]
Glutamine	2331.48 ± 332.42[b]	1454.35 ± 385.64[a]	1101.34 ± 457.11[a]	710.23 ± 364.12[a]
Glycine	286.85 ± 68.84[b]	158.67 ± 49.63[a]	191.36 ± 75.75[ab]	80.83 ± 27.92[a]
Histidine	122.15 ± 33.87[a]	360.84 ± 252.88[a]	231.75 ± 10.81[a]	132.24 ± 11.69[a]
Arginine	156.68 ± 53.81[a]	118.25 ± 54.79[a]	137.26 ± 52.33[a]	129.78 ± 78.76[a]
Threonine	77.61 ± 20.37[a]	97.67 ± 70.35[a]	98.48 ± 50.97[a]	73.49 ± 6.36[a]
Alanine	164.32 ± 65.54[a]	195.65 ± 53.04[a]	198.94 ± 27.73[a]	137.93 ± 54.79[a]
Proline	36.51 ± 16.24[a]	328.60 ± 442.16[a]	57.31 ± 14.51[a]	66.30 ± 18.16[a]
Tyrosine	34.89 ± 11.04[a]	27.28 ± 12.04[a]	34.07 ± 18.61[a]	33.57 ± 14.36[a]
Valine	54.20 ± 36.09[a]	63.01 ± 43.89[a]	42.45 ± 15.03[a]	53.11 ± 5.16[a]
Methionine	44.61 ± 5.94[b]	32.63 ± 4.91[ab]	21.55 ± 9.02[a]	20.46 ± 5.39[a]
Isoleucine	44.10 ± 24.10[a]	30.57 ± 13.74[a]	33.00 ± 16.35[a]	36.04 ± 14.46[a]
Leucine	77.37 ± 43.41[a]	55.79 ± 27.65[a]	59.79 ± 24.34[a]	63.80 ± 22.58[a]
Phenylalanine	42.38 ± 14.93[a]	25.62 ± 3.73[a]	40.00 ± 21.63[a]	45.90 ± 18.51[a]
Lysine	325.05 ± 168.77[a]	149.14 ± 58.92[a]	304.27 ± 145.01[a]	348.67 ± 134.11[a]

Values are means ± SEM of four replications the same letters on the columns in the figure indicate non-significant differences ($p > 0.05$), and different letters indicate significant differences ($p \leq 0.05$).

converted back to glucose using fuels made from fat (TeSlaa et al., 2021). So, during the process of energy metabolism, glucose content is in a steady state. This is also true of alanine, another important glycolysis byproduct. It is used to return amino groups from other organs to the liver. Glutamine, as an amino shuttle from other organs to the kidneys, can once again be quantitatively converted into glucose using energy from fat sources (Nuttall et al., 2008). PCK and G6PC are the limiting enzymes of the gluconeogenesis pathway (Tang et al., 2018). In this study, we found that when *M. albus* was exposed to NPs, the expression levels of PCK and G6PC genes were up-regulated, whereas the glucose production pathway was inhibited. The double enzyme (sucrase/maltase) system completes carbohydrate digestion. The digestion of carbohydrates such as sucrose and starch in aquatic organisms is believed to be widespread. In aquatic organisms, SI and MGAM can not only hydrolyze maltose but also starch (Diaz-Sotomayor et al., 2013). MGAM seems to have a higher activity to oligosaccharides with higher residue number, MGAM has higher activity to oligosaccharides with higher residue number than SI and has higher specificity to maltose (Lee et al., 2016). Therefore, the combined effect of SI and MGAM is crucial for digesting food sources of α-maltose. When *M. albus* was exposed to NPs for a short time, the expression of SI and MGAM genes increased, which helped to hydrolyze maltose and starch obtained from feed.

Fish must strictly regulate lipid storage and mobilization in order to adapt to their living environment and meet their energy needs for physiological activities. The lipids in feed are absorbed and transported to storage sites, usually in the form of TG combined with proteins to form chyle particles (Van de Pol et al., 2017). During lipid metabolism, stored TG is hydrolyzed in a stepwise manner into free fatty acids and glycerol. The hydrolysis reaction is catalyzed by different lipases (Althaher, 2022). Fish lipid metabolism is a very complex process, and the influencing factors are also diverse. Therefore, how to improve fish's stress resistance and nutrient utilization efficiency through lipids, as well as the impact of certain fatty acids on exposure to NPs, is one of the future research directions that needs to be studied. Lipids are energy-rich compounds and are generally considered indicators to evaluate the nutritional status and health of aquatic animals (Filimonova et al., 2016). Lipids are an important source of energy reserve in crustaceans (Glover, 2019). In addition, lipid metabolism is the main pathway for providing energy in organisms and plays an important role in the response of crustaceans to environmental pressure (Teng et al., 2021). Various studies have shown that partial pressure of carbon dioxide, food quality, hunger, salinity, and chemical exposure can affect lipid metabolism in aquatic invertebrates (Yoon et al., 2022). As the main components of

lipids, TG and T-CHO play key roles in the metabolism of organisms. Our research shows that NPs cause a decrease in T-CHO and TG levels in the liver of *M. albus*, which is probably due to lipid metabolism disorders caused by exposure to NPs. Similarly, lipid metabolism disorders were also observed in other fish exposed to NPs (Von Moos et al., 2012; Wan et al., 2019; Ye et al., 2021).

FAS and ACC activities can be used to evaluate the digestive and metabolic abilities of animals (Yue-qiang et al., 2010). The increase in ACC and FAS activity in *M. albus* exposed to NPs reflects an increase in the amount of fatty acids synthesized by the organism (Lv et al., 2023), this may be an important cause of liver lipid accumulation. TG can be hydrolyzed into glycerol and fatty acids, which can be oxidized to generate energy (Chen et al., 2020). In addition, fatty acids derived from TG hydrolysis play an important role as a source of phospholipids, especially in repairing oxidative damage to lipid membranes (Chan and Wang, 2018). In our study, the TG content in the liver of *M. albus* decreased significantly, possibly due to the pressure of the external NP environment promoting lipid accumulation, leading to an increase in the energy reserve of *M. albus*.

Currently, a research has shown that NPs can reduce the immune function of fish (Limbu et al., 2019). Some immune-related metabolites, 9-octadecenoic acid, 9,12-octadecadienoic acid, and arachidonic acid, were affected by NPs in our study. Linoleic acid and arachidonic acid belong to the linoleic acid family (Bieber and Fiol, 1986). Studies have confirmed that 9-octadecenoic acid, 9,12-octadecadienoic acid, and arachidonic acid can improve the immunity of fish (Calder, 2011). In our results, we found that the liver content of 9-octadecenoic acid and 9,12-octadecadienoic acid in *M. albus* decreased significantly in the A group than that in the CK(E) group (Table 2). Therefore, we speculate that this will lead to further interference of the immune system by NPs. After exposure to NPs, the level of 2-mono palmitic acid glyceride in the liver of *Oryzias melastigma* significantly increased, the synthesis of triglycerides increased, and the degradation of triglycerides decreased. In addition, methyl esters and ethyl esters also accumulate in the liver of *Oryzias melastigma*, which confirms the lipid disorder induced by NPs exposure in the liver (Ye et al., 2021). Our results showed that the liver content of methyl tetradecanoate, pentadecanoic acid, eicosanoic acid, heptadecanoic acid, 5,8,11,14-eicosatetraenoic acid, and doconexent significantly increased when *M. albus* were received 1% concentrations of polystyrene NPs in the feed, which caused the accumulation of fatty acids in the liver.

The liver plays a central role in the metabolism of amino acids in humans and other animals, This organ synthesizes many amino acids (including glutamic acid, glutamine, alanine, aspartic acid, asparagine, glycine, serine, and homoarginine), glucose, and glutathione (a major antioxidant) (Hou et al., 2020). In addition to the hydrolysis of arginine and glutamine, the oxidation of proline, and the gluconeogenesis of amino acids, the liver of fish also has a high rate of glutamate and glutamine oxidation to produce ATP, which controls the metabolic stability of glutamine (Vadlakonda et al., 2020). Under the action of NPs, on the one hand, glutamine catabolism is transformed into glutamic acid through glutaminase (GLS) in mitochondria, and the metabolism of GLS eventually leads to the increase of reduction potential, thus increasing levels of NADPH (Sun et al., 2023). However, on the other hand, some glutamylated amino acids are formed and converted into glutathione to exert antioxidant effects (Cruzat et al., 2018). Functional amino acids (such as methionine, cysteine, and glycine) can reduce or prevent oxidative stress and injury in fish liver. Methionine is an aliphatic sulfur-containing essential amino acid and is the precursor of succinyl-CoA, homocysteine, cysteine, creatine, and carnitine (Martínez et al., 2017). Recent studies have shown that methionine can regulate the metabolic process, innate immune system, and digestive function of mammals. It also interferes with lipid metabolism, activation of endogenous antioxidant enzymes, and biosynthesis of glutathione to counteract oxidative stress. In addition, methionine restriction can prevent changes in methionine/transmethylation metabolism, thereby reducing DNA damage and carcinogenic processes, and potentially preventing arterial, neuropsychiatric, and neurodegenerative diseases (Hou et al., 2020). Our results have similar findings. After exposure to NPs, the levels of functional amino acids such as glutamine, glycine, and methionine in the liver of *M. albus* significantly increase, which plays an active role in preventing oxidative damage to the liver caused by exposure to NPs. These findings provide basic data for assessing the ecological risks of NPs pollution to wild or artificially bred *M. albus* in the real environment.

5 Conclusion

Our results show that the NPs may interfere with the metabolism of amino acids and lipids in the liver of *M. albus* and provide a possible mechanism (Figure 4). After the intake of NPs, the activities of enzymes related to sugar metabolism (PK, HK, and PFK) are inhibited, this can explain that the intake of NPs lead to a decrease in *M. albus* energy reserves, possibly failed to maintain liver energy metabolism and provide ATP for other stress responses. The dihydroxyacetone phosphate produced by glycolysis is reduced to form glycerol, and the oxidative decarboxylation of pyruvic acid forms acetylCoA, which is the raw material for fatty acid synthesis, The increased activity of ACC and FAS on exposure to NPs simultaneously reflects an increase in the amount of fatty acids synthesized by the organism, which may play a positive role in the accumulation of fatty acids in the liver of *M. albus*. In addition, we also found that the down-regulation of some immune-related metabolites, such as 9-octadecenoic acid and 9,12-octadecadienoic acid, and the up-regulation of functional amino acids, such as methionine, cysteine, and glycine, may be the result of a defensive strategy by

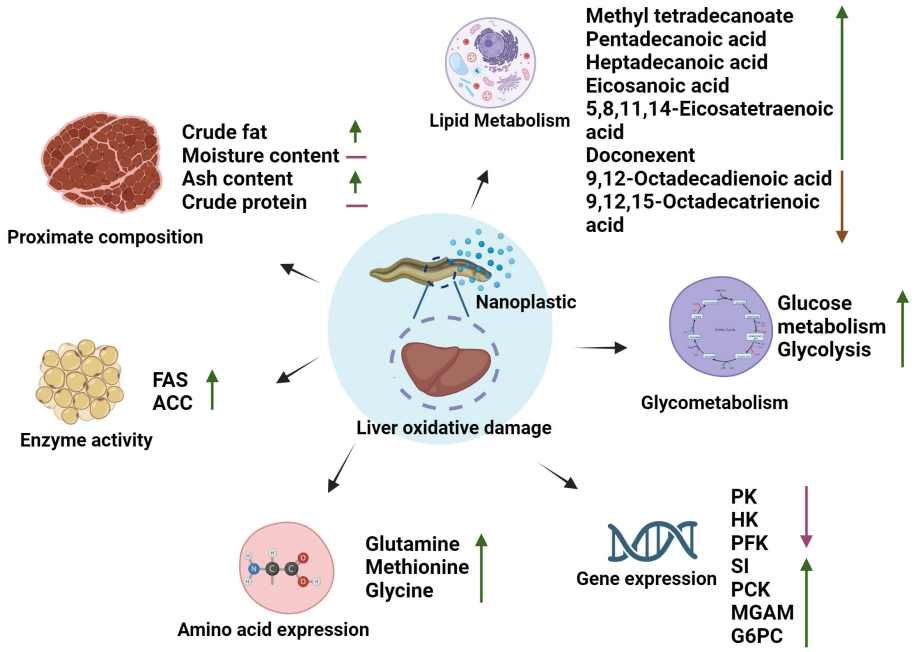

FIGURE 4
The potential mechanism of NPs interference with energy metabolism, amino acid, and lipid metabolism in the liver of *M. albus*.

M. albus to combat oxidative damage to the liver and pancreas caused by NPs. The results of this research provide valuable ecotoxicological data for better evaluating the impact of NPs on artificially cultured *M. albus*.

Data availability statement

The raw data supporting the conclusion of this article will be made available by the authors, without undue reservation.

Ethics statement

The animal study was approved by Freshwater Fisheries Research Institute of Jiangsu Province. The study was conducted in accordance with the local legislation and institutional requirements.

Author contributions

HL: Data curation, Formal Analysis, Investigation, Methodology, Software, Writing – original draft. WZ: Methodology, Writing – original draft. ZZ: Data curation, Software, Writing – original draft. CY: Investigation, Writing – original draft. GT: Software, Writing – original draft. WL: Formal Analysis, Funding acquisition, Project administration, Resources, Supervision, Writing – review & editing. QJ: Formal Analysis, Funding acquisition, Project administration, Resources, Supervision, Visualization, Writing – review & editing.

Funding

The author(s) declare financial support was received for the research, authorship, and/or publication of this article. This work was funded by projects grants by the National Natural Science Foundation of China (42277273); Shanghai Municipal Science and Technology Commission (23N61900500); and the China Agriculture Research System of MOF and MARA (grant number CARS-46); and the Demonstration of RiceLoach-Eel Green Co-cultivation in Northern Jiangsu province [CX (20) 2031].

Conflict of interest

The authors declare that the research was conducted in the absence of any commercial or financial relationships that could be construed as a potential conflict of interest.

Publisher's note

References

Althaher, A. R. (2022). An overview of hormone-sensitive lipase (HSL). *Sci. World J.* 2022, 1964684. doi: 10.1155/2022/1964684

Barboza, L. G. A., Vieira, L. R., Branco, V., Figueiredo, N., Carvalho, F., Carvalho, C., et al. (2018). Microplastics cause neurotoxicity, oxidative damage and energy-related changes and interact with the bioaccumulation of mercury in the European seabass, Dicentrarchus labrax (Linnaeus 1758). *Aquat. Toxicol.* 195, 49–57. doi: 10.1016/j.aquatox.2017.12.008

Bieber, L., and Fiol, C. (1986). "[29] Purification and assay of carnitine acyltransferases." in *Methods enzymology*. (Elsevier). 123, 276–284. doi: 10.1016/S0076-6879(86)23031-1

Brandts, I., Cánovas, M., Tvarijonaviciute, A., Llorca, M., Vega, A., Farré, M., et al. (2022). Nanoplastics are bioaccumulated in fish liver and muscle and cause DNA damage after a chronic exposure. *Environ. Res.* 212, 113433. doi: 10.1016/j.envres.2022.113433

Brandts, I., Teles, M., Tvarijonaviciute, A., Pereira, M., Martins, M., Tort, L., et al. (2018). Effects of polymethylmethacrylate nanoplastics on Dicentrarchus labrax. *Genomics* 110 (6), 435–441. doi: 10.1016/j.ygeno.2018.10.006

Bucolo, G., and David, H. (1973). Quantitative determination of serum triglycerides by the use of enzymes. *Clin. Chem.* 19 (5), 476–482. doi: 10.1093/clinchem/19.5.476

Calder, P. C. (2011). Fatty acids and inflammation: the cutting edge between food and pharma. *Eur. J. Pharmacol.* 668, S50–S58. doi: 10.1016/j.ejphar.2011.05.085

Chan, C. Y., and Wang, W.-X. (2018). A lipidomic approach to understand copper resilience in oyster Crassostrea hongkongensis. *Aquat. Toxicol.* 204, 160–170. doi: 10.1016/j.aquatox.2018.09.011

Chen, Q., Lackmann, C., Wang, W., Seiler, T.-B., Hollert, H., and Shi, H. (2020). Microplastics lead to hyperactive swimming behaviour in adult zebrafish. *Aquat. Toxicol.* 224, 105521. doi: 10.1016/j.aquatox.2020.105521

Cruzat, V., Macedo Rogero, M., Noel Keane, K., Curi, R., and Newsholme, P. (2018). Glutamine: metabolism and immune function, supplementation and clinical translation. *Nutrients* 10 (11), 1564. doi: 10.3390/nu10111564

Diaz-Sotomayor, M., Quezada-Calvillo, R., Avery, S. E., Chacko, S. K., Yan, L.-Y., Lin, A. H.-M., et al. (2013). Maltase-glucoamylase modulates gluconeogenesis and sucrase-isomaltase dominates starch digestion glucogenesis. *J. Pediatr. Gastroenterol. Nutr.* 57 (6), 704–712. doi: 10.1097/MPG.0b013e3182a27438

Filimonova, V., Goncalves, F., Marques, J. C., De Troch, M., and Goncalves, A. M. (2016). Biochemical and toxicological effects of organic (herbicide Primextra® Gold TZ) and inorganic (copper) compounds on zooplankton and phytoplankton species. *Aquat. Toxicol.* 177, 33–43. doi: 10.1016/j.aquatox.2016.05.008

Glover, C. N. (2019). Cellular and molecular approaches to the investigation of piscine osmoregulation: current and future perspectives. *Fish Osmoregulation* 177–234. doi: 10.1201/9780429063909-7

Gong, H., Li, R., Li, F., Guo, X., Xu, L., Gan, L., et al. (2023). Toxicity of nanoplastics to aquatic organisms: Genotoxicity, cytotoxicity, individual level and beyond individual level. *J. Hazardous Materials* 443, 130266. doi: 10.1016/j.jhazmat.2022.130266

Hou, Y., Hu, S., Li, X., He, W., and Wu, G. (2020). Amino acid metabolism in the liver: nutritional and physiological significance. *Amino Acids Nutr. Health: Amino Acids Syst. Funct. Health* 21–37. doi: 10.1007/978-3-030-45328-2_2

Israelsen, W. J., and Vander Heiden, M. G. (2015). "Pyruvate kinase: Function, regulation and role in cancer." in: *Semin. Cell Dev. Biol.* (Elsevier), 43–51. doi: 10.1016/j.semcdb.2015.08.004

Issac, M. N., and Kandasubramanian, B. (2021). Effect of microplastics in water and aquatic systems. *Environ. Sci. pollut. Res.* 28, 19544–19562. doi: 10.1007/s11356-021-13184-2

Lamichhane, G., Acharya, A., Marahatha, R., Modi, B., Paudel, R., Adhikari, A., et al. (2023). Microplastics in environment: global concern, challenges, and controlling measures. *Int. J. Environ. Sci. Technol.* 20 (4), 4673–4694. doi: 10.1007/s13762-022-04261-1

Lee, B.-H., Rose, D. R., Lin, A. H.-M., Quezada-Calvillo, R., Nichols, B. L., and Hamaker, B. R. (2016). Contribution of the individual small intestinal α-glucosidases to digestion of unusual α-linked glycemic disaccharides. *J. Agric. Food Chem.* 64 (33), 6487–6494. doi: 10.1021/acs.jafc.6b01816

Li, L., Wang, M., Ma, Q., Ye, J., and Sun, G. (2022a). Role of glycolysis in the development of atherosclerosis. *Am. J. Physiology-Cell Physiol.* 323 (2), C617–C629. doi: 10.1152/ajpcell.00218.2022

Li, Y., Liu, Z., Jiang, Q., Ye, Y., and Zhao, Y. (2022b). Effects of nanoplastic on cell apoptosis and ion regulation in the gills of Macrobrachium nipponense. *Environ. pollut.* 300, 118989. doi: 10.1016/j.envpol.2022.118989

Li, Y., Liu, Z., Yang, Y., Jiang, Q., Wu, D., Huang, Y., et al. (2021). Effects of nanoplastics on energy metabolism in the oriental river prawn (Macrobrachium nipponense). *Environ. pollut.* 268, 115890. doi: 10.1016/j.envpol.2020.115890

Limbu, S. M., Ma, Q., Zhang, M.-L., and Du, Z.-Y. (2019). High fat diet worsens the adverse effects of antibiotic on intestinal health in juvenile Nile tilapia (Oreochromis niloticus). *Sci. Total Environ.* 680, 169–180. doi: 10.1016/j.scitotenv.2019.05.067

Lv, W., Gu, H., He, D., Liu, Z., Yao, C., Huang, W., et al. (2023). Polystyrene nanospheres-induced hepatotoxicity in swamp eel (Monopterus albus): From biochemical, pathological and transcriptomic perspectives. *Sci. Total Environ.* 893, 164844. doi: 10.1016/j.scitotenv.2023.164844

Martínez, Y., Li, X., Liu, G., Bin, P., Yan, W., Más, D., et al. (2017). The role of methionine on metabolism, oxidative stress, and diseases. *Amino Acids* 49, 2091–2098. doi: 10.1007/s00726-017-2494-2

Nuryadin, K., Rahim, A. R., and Aminin, A. (2020). ANALISIS PENGGUNAAN LIMBAH ORGANIK YANG BERBEDA TERHADAP PERTUMBUHAN DAN KELANGSUNGAN HIDUP BELUT SAWAH (Monopterus albus). *Jurnal Perikanan Pantura (JPP)* 3 (1), 9–15. doi: 10.30587/jpp.v3i1.1396

Nuttall, F. Q., Ngo, A., and Gannon, M. C. (2008). Regulation of hepatic glucose production and the role of gluconeogenesis in humans: is the rate of gluconeogenesis constant? *Diabetes/metabolism Res. Rev.* 24 (6), 438–458. doi: 10.1002/dmrr.863

Rochman, C. M. (2018). Microplastics research—from sink to source. *Science* 360 (6384), 28–29. doi: 10.1126/science.aar7734

Shafland, P. L., Gestring, K. B., and Stanford, M. S. (2009). An assessment of the Asian swamp eel (Monopterus albus) in Florida. *Rev. Fisheries Sci.* 18 (1), 25–39. doi: 10.1080/10641260903225542

Smith, M., Love, D. C., Rochman, C. M., and Neff, R. A. (2018). Microplastics in seafood and the implications for human health. *Curr. Environ. Health Rep.* 5, 375–386. doi: 10.1007/s40572-018-0206-z

Sun, Z., Wen, Y., Zhang, F., Fu, Z., Yuan, Y., Kuang, H., et al. (2023). Exposure to nanoplastics induces mitochondrial impairment and cytomembrane destruction in Leydig cells. *Ecotoxicology Environ. Saf.* 255, 114796. doi: 10.1016/j.ecoenv.2023.114796

Tang, Y., Zhang, Y., Wang, C., Sun, Z., Li, L., Cheng, S., et al. (2018). Overexpression of PCK1 gene antagonizes hepatocellular carcinoma through the activation of gluconeogenesis and suppression of glycolysis pathways. *Cell. Physiol. Biochem.* 47 (1), 344–355. doi: 10.1159/000489811

Taşbozan, O., Gökçe, M. A., and Erbaş, C. (2016). The effect of different growing conditions to proximate composition and fatty acid profiles of rainbow trouts (Oncorhynchus mykiss). *J. Appl. Anim. Res.* 44 (1), 442–445. doi: 10.1080/09712119.2015.1091323

Teng, J., Zhao, J., Zhu, X., Shan, E., Zhang, C., Zhang, W., et al. (2021). Toxic effects of exposure to microplastics with environmentally relevant shapes and concentrations: Accumulation, energy metabolism and tissue damage in oyster Crassostrea gigas. *Environ. Pollut.* 269, 116169. doi: 10.1016/j.envpol.2020.116169

Teng, M., Zhao, X., Wang, C., Wang, C., White, J. C., Zhao, W., et al. (2022). Polystyrene nanoplastics toxicity to zebrafish: dysregulation of the brain–intestine–microbiota axis. *ACS nano* 16 (5), 8190–8204. doi: 10.1021/acsnano.2c01872

TeSlaa, T., Bartman, C. R., Jankowski, C. S., Zhang, Z., Xu, X., Xing, X., et al. (2021). The source of glycolytic intermediates in mammalian tissues. *Cell Metab.* 33 (2), 367–378.e365. doi: 10.1016/j.cmet.2020.12.020

Tian, W. X., Hsu, R., and Wang, Y. S. (1985). Studies on the reactivity of the essential sulfhydryl groups as a conformational probe for the fatty acid synthetase of chicken liver. Inactivation by 5, 5'-dithiobis-(2-nitrobenzoic acid) and intersubunit cross-linking of the inactivated enzyme. *J. Biol. Chem.* 260 (20), 11375–11387. doi: 10.1016/S0021-9258(17)39189-5

Trevisan, R., Ranasinghe, P., Jayasundara, N., and Di Giulio, R. T. (2022). Nanoplastics in aquatic environments: impacts on aquatic species and interactions with environmental factors and pollutants. *Toxics* 10 (6), 326. doi: 10.3390/toxics10060326

Vadlakonda, L., Indracanti, M., Kalangi, S. K., Gayatri, B. M., Naidu, N. G., and Reddy, A. B. (2020). The role of pi, glutamine and the essential amino acids in modulating the metabolism in diabetes and cancer. *J. Diabetes Metab. Disord.* 19, 1731–1775. doi: 10.1007/s40200-020-00566-5

Van de Pol, I., Flik, G., and Gorissen, M. (2017). Comparative physiology of energy metabolism: fishing for endocrine signals in the early vertebrate pool. *Front. Endocrinol.* 8, 36. doi: 10.3389/fendo.2017.00036

Van Dyck, I. P., Nunoo, F. K., and Lawson, E. T. (2016). An empirical assessment of marine debris, seawater quality and littering in Ghana. *J. Geosci. Environ. Prot.* 4 (5), 21–36. doi: 10.4236/gep.2016.45003

Von Moos, N., Burkhardt-Holm, P., and Köhler, A. (2012). Uptake and effects of microplastics on cells and tissue of the blue mussel Mytilus edulis L. after an experimental exposure. *Environ. Sci. Technol.* 46 (20), 11327–11335. doi: 10.1021/es302332w

Wan, Z., Wang, C., Zhou, J., Shen, M., Wang, X., Fu, Z., et al. (2019). Effects of polystyrene microplastics on the composition of the microbiome and metabolism in larval zebrafish. *Chemosphere* 217, 646–658. doi: 10.1016/j.chemosphere.2018.11.070

Ye, G., Zhang, X., Liu, X., Liao, X., Zhang, H., Yan, C., et al. (2021). Polystyrene microplastics induce metabolic disturbances in marine medaka (Oryzias melastigmas) liver. *Sci. Total Environ.* 782, 146885. doi: 10.1016/j.scitotenv.2021.146885

Yoon, D.-S., Byeon, E., Kim, D.-H., Lee, M.-C., Shin, K.-H., Hagiwara, A., et al. (2022). Effects of temperature and combinational exposures on lipid metabolism in aquatic invertebrates. *Comp. Biochem. Physiol. Part C: Toxicol. Pharmacol.* 262, 109449. doi: 10.1016/j.cbpc.2022.109449

Yue-qiang, G., Li, L., Hui-chun, W., and Zhi-li, W. (2010). Effects of hypoxia on respiratory metabolism and antioxidant capability of Macrobrachium nipponense. *J. Hebei Univ. (Natural Sci. Edition)* 30 (3), 301–306. doi: 10.3969/j.issn.1000-1565.2010.03.017

Zhu, C., Zhou, W., Han, M., Yang, Y., Li, Y., Jiang, Q., et al. (2023). Dietary polystyrene nanoplastics exposure alters hepatic glycolipid metabolism, triggering inflammatory responses and apoptosis in Monopterus albus. *Sci. Total Environ.* 891, 164460. doi: 10.1016/j.scitotenv.2023.164460

frontiers | Frontiers in Marine Science

TYPE Original Research
PUBLISHED 30 November 2023
DOI 10.3389/fmars.2023.1310415

OPEN ACCESS

EDITED BY
Yiming Li,
Fishery Machinery and Instrument Research Institute, China

REVIEWED BY
Yulong Gong,
Chinese Academy of Sciences (CAS), China
Xiufei Cao,
Nanjing Agricultural University, China

*CORRESPONDENCE
Mengqing Liang
liangmq@ysfri.ac.cn

RECEIVED 09 October 2023
ACCEPTED 16 November 2023
PUBLISHED 30 November 2023

CITATION
Ma Q, Xu H, Limbu SM, Wei Y and Liang M (2023) Comparative analysis of glucose and fructose tolerance in two marine fishes: effects on insulin secretion and acute hypoxia tolerance.
Front. Mar. Sci. 10:1310415.
doi: 10.3389/fmars.2023.1310415

Comparative analysis of glucose and fructose tolerance in two marine fishes: effects on insulin secretion and acute hypoxia tolerance

Qiang Ma[1], Houguo Xu[1], Samwel Mchele Limbu[2], Yuliang Wei[1] and Mengqing Liang[1]*

[1]Yellow Sea Fisheries Research Institute, Chinese Academy of Fishery Sciences, Qingdao, China, [2]School of Aquatic Sciences and Fisheries Technology, University of Dar es Salaam, Dar es Salaam, Tanzania

Carbohydrates are a common and economical energy source in animal feeds. However, most fish show a persistent postprandial hyperglycemia after intake of a high-carbohydrate diet. Unfortunately, the mechanism of glucose metabolism in fish is still unclear. In the present study, tiger puffer (*Takifugu rubripes*) and turbot (*Scophthalmus maximus*) were intraperitoneally injected or orally administered with glucose or fructose (500 mg/kg body weight) to evaluate the ability of fish to utilize carbohydrates. Afterwards, serum glucose, fructose, pyruvate, insulin levels, and acute hypoxia tolerance were measured. Our results showed increased serum glucose level and then decreased post intraperitoneal injection with glucose, and reached a peak after 0.5 hours in turbot and 1 hour in tiger puffer. Tiger puffer had significantly lower liver glycogen, serum glucose, fructose, pyruvate, and insulin contents than turbot. Glucose and fructose only induced insulin secretion in turbot, but did not change serum insulin level in tiger puffer. Glucose was a stronger stimulator of insulin than fructose in the two marine species. Both intraperitoneal injection and oral fructose intake increased serum glucose level, while intraperitoneal or oral glucose also increased serum fructose level. Intraperitoneal injection of glucose promoted absorption and utilization of glucose in the blood more effectively than oral glucose intake. In addition, turbot and tiger puffer were intolerant to acute hypoxia, whereas supplementation with glucose or fructose improved hypoxia tolerance in the two marine fishes by activating anaerobic glycolysis. Taken together, our results provide important scientific information for understanding the mechanism for glucose and fructose utilization and improving hypoxia tolerance in fish.

KEYWORDS

glucose tolerance test, fructose tolerance test, carbohydrate utilization, insulin secretion, hypoxia tolerance

1 Introduction

Carbohydrates, such as starch and glucose, are a common and digestible energy source in food for mammals. Appropriate levels of carbohydrates in animal feeds promote growth and reduce the use of fat and protein ingredients (Ren et al., 2011; Kamalam et al., 2017; Zhang et al., 2019). However, many fish species show persistent postprandial hyperglycemia after a glucose tolerance test (GTT) or intake of high-carbohydrate feed, generally considered as glucose intolerance (Moon, 2001; Stone, 2003). GTT, including intraperitoneal glucose tolerance test (IPGTT) and oral glucose tolerance test (OGTT), are accepted methods used to evaluate glucose utilization capacity in humans and animals (Hemre and Hansen, 1998; Tuomilehto et al., 2001). However, carbohydrates utilization and GTT in fish are affected by various factors including insulin secretion, insulin receptor content, perception and transporter ability of glucose, glycolysis and gluconeogenesis-related enzymes activities, intestinal digestive enzymes activities, dietary carbohydrate sources, fish size, water temperature and hypoxia stress (Panserat et al., 2000; Blasco et al., 2001; Moon, 2001; Hemre et al., 2002; Alexander et al., 2011; Caruso and Sheridan, 2011). Accordingly, IPGTT and OGTT have been used in various cultured fish species to evaluate carbohydrate utilization.

Previous studies on IPGTT and OGTT revealed different peaks in measured parameters for various fish species. In carnivorous fish, such as Japanese flounder (*Paralichthys olivaceus*), serum glucose content reached the peak after 5 hours and returned to normal level until 48 hours post intraperitoneal glucose injection at 1000 mg glucose/kg body weight (Liu et al., 2018). However, serum insulin content decreased to the lowest level at 3 hours and returned to normal level until 48 hours after IPGTT (Liu et al., 2018). In largemouth bass (*Micropterus salmoides*), intraperitoneal glucose injection at 500 mg glucose/kg body weight increased serum glucose level that reached the peak after 3 hours and returned to normal level after 12 hours following IPGTT, but IPGTT did not affect the gene expression of insulin receptors (Li et al., 2021). In omnivorous fish, such as zebrafish (*Danio rerio*) GTT at 1000 mg glucose/kg body weight caused a peak serum glucose level after 0.5 hour and returned to normal level after 6 hour post injection (Eames et al., 2010). In Nile tilapia (*Oreochromis niloticus*), another omnivorous fish species GTT at 1000 mg glucose/kg body weight caused a glucose level peak in the plasma after 1 hour, which returned to normal level after 3 hour post injection (Chen et al., 2020). These results suggest that omnivorous fish have a greater ability to utilize glucose than carnivorous fish. Currently, the mechanism for glucose metabolism and carbohydrate utilization in fish are still unclear.

Fructose is an isomer of glucose, both with the molecular formula of $C_6H_{12}O_6$. The two are the most common monosaccharides in most foods. In mammals, fructose is metabolized mainly in the liver and intestine by the fructose-1-phosphate pathway and the fructose-6-phosphate pathway, where solute carrier family 2 member 5 (SLC2A5/GLUT5) and ketohexokinase (KHK) enzymes play important roles (Havel, 2005; Tolan, 2007). Dietary excessive fructose cause nonalcoholic fatty liver, diabetes, insulin resistance, hyperuricemia, dyslipidemia, and obesity (Tesz and Bence, 2020). However, few studies exist on fructose metabolism in fish. In the fruit-eating fish *Piaractus mesopotamicus*, oral fructose at 2000 mg/kg body weight caused lower blood glucose levels than oral glucose and starch treatments (Takahashi et al., 2018). Moreover, feeding diets containing 22% and 15% fructose decreased growth performance and hepatic health in Amur sturgeon (*Acipenser schrenckii*) and Nile tilapia (Jiang et al., 2014; Zhou et al., 2022). The existence of limited studies, calls for more research to explain the effects of fructose on cultured fish species.

Ocean warming, eutrophication, diurnal alternation, extreme weather in nature and high-density culture, long-distance transportation, and power interruption in aquaculture all cause water environment hypoxia, which affect the growth performance and health of aquatic animals (Wu et al., 2003; Ma et al., 2023a). Acute hypoxia cause mass death of cultured fishes within a short time resulting in severe economic losses (Landman et al., 2005). Therefore, it is crucial to improve the tolerance of fish to acute hypoxia for sustainable aquaculture production. In mammals and fish, acute hypoxia activates hypoxia-inducible factor (HIF) and anaerobic glycolysis pathway and promotes the breakdown of glycogen into glucose and the production of lactic acid (Koukourakis et al., 2001; Li et al., 2018a). Accordingly, a naked mole-rat (*Heterocephalus glaber*) survived for 18 minutes in a zero oxygen environment without significant damage because it utilizes only fructose for anaerobic glycolysis and produces lactic acid in hypoxia condition (Park et al., 2017). This study indicated that not only glucose but also fructose improved hypoxia tolerance in animals. However, the effects of glucose and fructose on acute hypoxia tolerance and metabolism in fish have not been evaluated.

Marine fish farming is an important part of world aquaculture due to the rapid development of deep-sea net pens, large-scale aquaculture vessels, and land-based factory recirculating aquaculture. Tiger puffer (*Takifugu rubripes*) and turbot (*Scophthalmus maximus*) are important farmed marine fish species in northern China with annual outputs of around 16,000 tons and 50,000 tons, respectively, which are famous for their tasty meat and high economic value (Ma et al., 2023b). However, the effects of glucose and fructose on insulin secretion and hypoxia tolerance of the two marine fishes have not been studied. Therefore, tiger puffer and turbot were intraperitoneally injected or orally administered with glucose or fructose solution at 500 mg/kg body weight. Afterward, glucose, fructose, pyruvate, and insulin levels in the serum and the survival rate of eight fish species under acute hypoxia were measured. Our study compares the ability of tiger puffer and turbot to utilize glucose and fructose and assesses the effects of glucose and fructose on acute hypoxia tolerance in the two-marine fish species.

2 Materials and methods

2.1 Ethics approval

All experimental procedures and animal care were conducted under a protocol approved by experimental animal care, ethics, and

safety inspection from the Yellow Sea Fisheries Research Institute, Chinese Academy of Fishery Sciences.

2.2 Experimental animals

Juvenile tiger puffer (*Takifugu rubripes*), turbot (*Scophthalmus maximus*), half-smooth tongue sole (*Cynoglossus semilaevis*), goby (*Acanthogobius ommaturus*), Japanese sea bass (*Lateolabrax japonicas*), grey mullet (*Mugil cephalus Linnaeus*), yunlong grouper (*Epinephelus moara*♀ × *Epinephelus lanceolatus*♂), and pearl gentian grouper (*Epinephelus fuscoguttatus*♀ × *Epinephelus lanceolatus*♂) were provided by Huanghai Aquaculture Co. Ltd. (Yantai, China). The initial weights of the fish species ranged from 30 to 125 g. All fish were acclimatized in a flow-through seawater system and fed with the same commercial marine fish feed (protein 46%, lipid 10%, ash 11%, moisture 10%, Shengsuo fishery culture feed research center, Shangdong, China) for two weeks. Salinity, water temperature, dissolved oxygen (DO), pH, and total ammonia nitrogen were kept at 26 to 30‰, 20 to 23°C, 6 to 7 mg/L, 7 to 8, and < 0.02 mg/L, respectively.

2.3 Intraperitoneal injection or oral administration of glucose or fructose

One hundred and eight tiger puffer (113.5 ± 10.9 g) and the same number of turbot (105.2 ± 15.6 g) were randomly distributed into 36 tanks (6 fish of each species per tank, 200 L). Before intraperitoneal injection or oral gavage, tiger puffer and turbot were fasted for 12 h to empty residual food in the digestive tract. Glucose and fructose powder (purity ≥ 99%) were purchased from China National Pharmaceutical Group Corporation (Sinopharm). Glucose and fructose were weighed and dissolved in normal saline solution (NS) to obtain glucose and fructose solutions at concentrations of 100 mg/mL. The injection or oral doses were all 5 μL/g body weight (500 mg/kg body weight).

Six tiger puffer or turbot were anaesthetized with MS-222 (10 mg/L) and injected with normal saline solution as a zero hour treatment. Forty-eight tiger puffer and the same number of turbot were injected with glucose or fructose solution. Blood was collected from six fish per tank (n = 6) after 0.5, 1, 3, and 7 hours post intraperitoneal glucose or fructose injection. In the same way, six tiger puffer or turbot were fed with normal saline solution orally as a zero hour treatment. Forty-eight tiger puffer and the same number of turbot were fed with glucose or fructose solution orally. Afterward, blood was collected from six fish per tank (n = 6) after 0.5, 1, 3, and 7 hours post oral glucose or fructose. The blood was placed at 4°C for two hours, centrifuged at 3000 rpm for 10 minutes, and then serum was collected. The design and sampling of the experiment are shown in Figure 1.

2.4 Acute hypoxia tolerance test

After two weeks of acclimatization, eight marine fish species (n = 20, two replicates per species, 10 fish per species per tank) were fasted for 12 h and transferred to customized hypoxic equipment (patent number: ZL202020482406.9) to evaluate the tolerance to acute hypoxia. The initial DO was 7.0 mg/L, the aquarium air pump was turned off, and then DO was decreased continuously to 0.1 mg/L with the prolonging of hypoxic time. The fish mortality was recorded every 0.5 hours. A fish was regarded dead when the gill stopped breathing. All the fish died after 12 h acute hypoxia. The survival rate was calculated by using the following formula: Survival rate (%) = alive fish number/initial fish number × 100.

Moreover, one hundred tiger puffer or turbot were randomly distributed into five treatments: normal saline (NS), intraperitoneal glucose (IG), intraperitoneal fructose (IF), oral glucose (OG), and oral fructose (OF), respectively. Each treatment had 20 tiger puffer

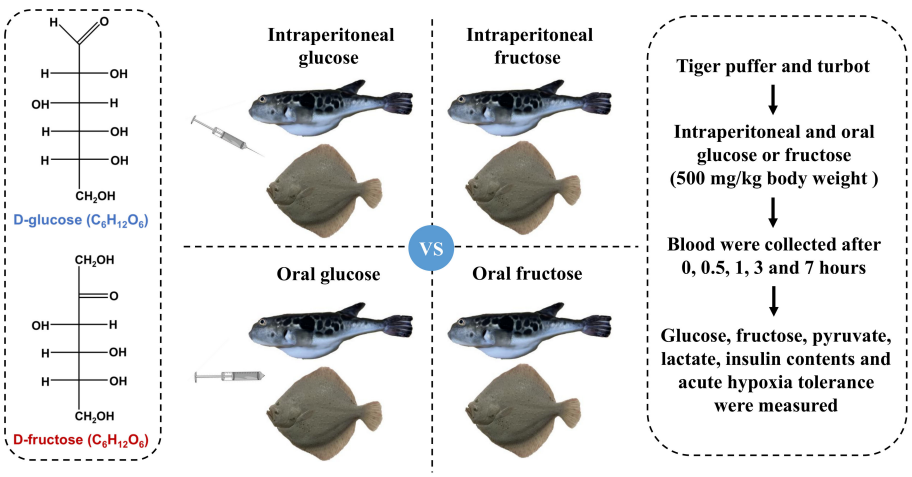

FIGURE 1
Design and sampling of the experiment. Tiger puffer and turbot were fasted for 12 h and then given 500 mg/kg body weight glucose solution or fructose solution via intraperitoneal injection or oral gavage, respectively. Serum biochemical indicators and survival rate during acute hypoxia were measured.

or turbot (two replicates, 10 fish for each species per tank). Then, the tiger puffer or turbot were intraperitoneal injected or orally fed with glucose or fructose solution and studied for acute hypoxia stress. The fish died after the DO level in the water decreased. After 2 hours of hypoxia stress, the number of dead fish was counted and the survival rate after hypoxia was calculated. Afterward, the fish that survived were anesthetized with MS-222, and blood was collected for further analysis.

2.5 Biochemical parameters assays

The concentrations of glucose (F006-1-1), fructose (A085-1-1), lactate (A019-2-1), and pyruvate (A081-1-1) in the serum were measured by using specific commercial kits (Nanjing Jiancheng Bioengineering Institute, China). Insulin content was determined by using a fish insulin enzyme-linked immune sorbent assay (ELISA) kit (HB407-QT, Shanghai Hengyuan Biological Technology Co., LTD, China). All the results were read by using a microplate reader (Tecan Infinite M200, Switzerland).

2.6 Statistical analyses

All data were tested for normality and homogeneity of variances by using Shapiro-Wilk and Levene's tests, respectively. One-way analysis of variance (ANOVA, Duncan) was performed to evaluate significant differences among different sampling times (0, 0.5, 1, 3, and 7 hours). An independent-sample *t*-test was applied to determine the significant difference between tiger puffer and turbot, glucose and fructose, or between intraperitoneal injection and oral gavage. Significant differences were set at $P < 0.05$ and graphs were made by GraphPad Prism 8.0 software. All data were analyzed by using the SPSS Statistics 21.0 software (IBM company, USA). The results are reported as means ± standard error of means (SEM).

3 Results

3.1 The differences in glucose or fructose utilization between tiger puffer and turbot

The fish intraperitoneal injected with glucose increased in serum glucose level and then decreased with the extension of sampling time compared with zero hour treatment (normal saline injection). The serum glucose level reached a peak after 0.5 hours in turbot and at 1 hour in tiger puffer (Figure 2A). The serum fructose and pyruvate levels also showed a similar trend in turbot (Figures 2B) and tiger puffer (Figures 2C) after glucose intraperitoneal injection. As the sampling time was extended, the serum insulin level showed an increasing trend in the turbot, but there was no significant effect on insulin level in the tiger puffer (Figure 2D). In oral glucose treatments, the two marine fishes showed a continuously increasing trend in serum glucose level, but the increase of glucose level in tiger puffer was more rapid than that in turbot (Figure 2E). The serum fructose level increased and then decreased with the extension of sampling time, and reached a peak after 1 hour in both turbot and tiger puffer (Figure 2F). The serum pyruvate and insulin levels separately showed a decreasing and an increasing trend in turbot as the sampling time was extended (Figure 2G), but the trend was reversed in the tiger puffer (Figure 2H). These data illustrate that intraperitoneal injection and oral glucose increased serum glucose and fructose contents in both tiger puffer and turbot, but only increased serum insulin content in the turbot.

Both turbot and tiger puffer intraperitoneal injected with fructose increased the serum glucose and pyruvate levels compared to the zero hour treatments and the significances were found in the tiger puffer (Figures 2I, K). Meanwhile, the fructose and insulin contents also showed an increasing trend in turbot (Figure 2J), but showed an increasing and then decreasing trend in tiger puffer (Figure 2L). In oral fructose treatments, the serum glucose level increased first and then decreased in tiger puffer with the extension of sampling time and reached the peak at 3 hours (Figure 2M). The turbot orally treated with fructose had a significant difference in serum glucose level after 7 hours (Figure 2M). The serum fructose and pyruvate levels showed an increasing and decreasing trend in the both turbot and tiger puffer after oral administration of fructose (Figure 2N). The fructose content reached a peak after 3 hours, and pyruvate content reached a peak after 0.5 hours (Figures 2N, O). Oral fructose did not affect the serum insulin content in turbot, but decreased the serum insulin content in tiger puffer (Figure 2P). In particular, the serum glucose level of tiger puffer was higher than that of turbot after 1 and 3 hours of oral administration of glucose or fructose. These data demonstrate that both intraperitoneal injection and oral fructose increased serum fructose and pyruvate contents in both tiger puffer and turbot, but only significantly increased serum glucose content in the tiger puffer. In general, the serum glucose, fructose, pyruvate, and insulin contents in turbot fish were all significantly higher than those in tiger puffer fish.

3.2 The differences between glucose and fructose utilization in fish

The intraperitoneal glucose treatments had significantly higher glucose content in the serum from 0.5 to 3 hours compared with the intraperitoneal fructose treatments (Figures 3A, I). However, both turbot and tiger puffer had lower fructose content in the serum (Figures 3B, J). In tiger puffer, the fish intraperitoneal injected with fructose had higher pyruvate levels than the fish intraperitoneal injected with glucose (Figure 3C). However, there was no significant effect on serum insulin content between fructose and glucose injections (Figure 3D). In turbot, the fish intraperitoneal injected with glucose had higher pyruvate and insulin levels in the serum than those injected intraperitoneal with fructose, and the significance was found in insulin content at 1 and 3 hours (Figures 3K, L).

In both tiger puffer and turbot, the oral glucose treatments had lower glucose content in the serum from 0.5 to 3 hours, but had significantly higher glucose content than the oral fructose after 7 hours (Figures 3E, M). In tiger puffer, the fish treated with oral fructose had significantly higher fructose content in the serum after 3

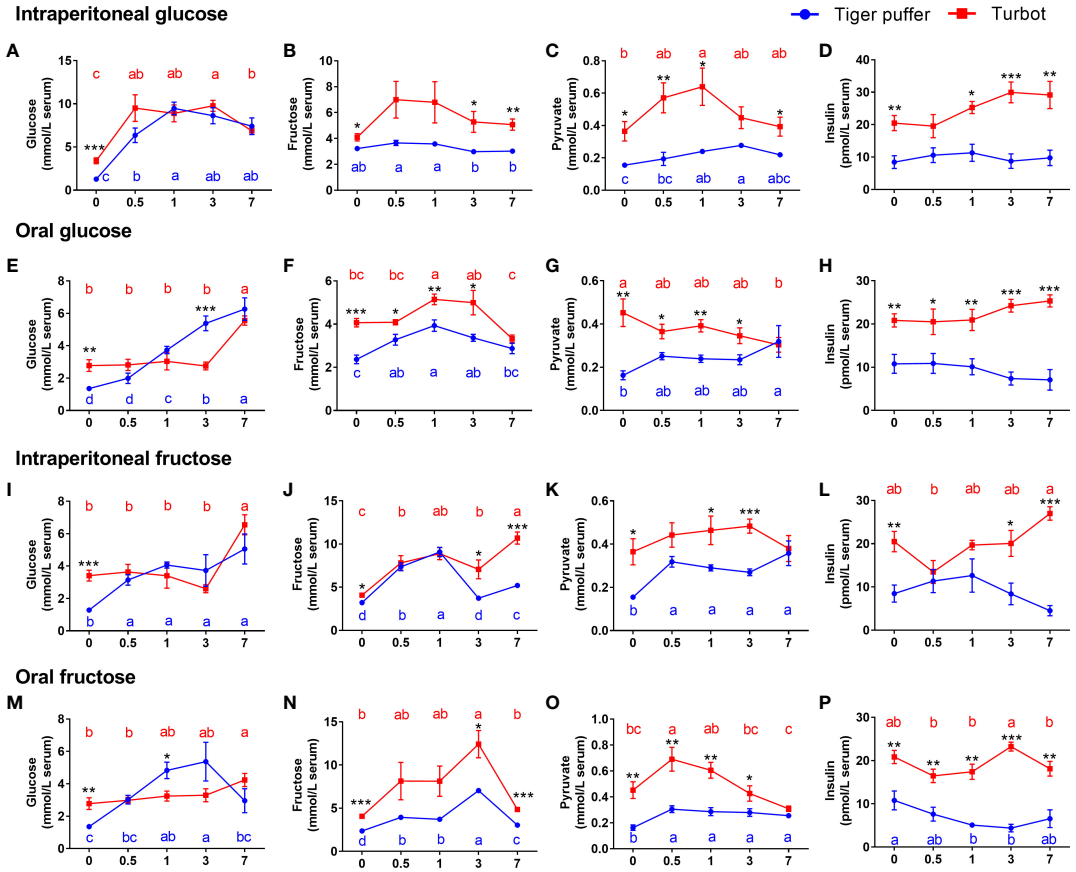

FIGURE 2
Comparison of differences in glucose or fructose utilization between tiger puffer and turbot. **(A, E, I, M)** glucose content. **(B, F, J, N)** fructose content. **(C, G, K, O)** pyruvate content. **(D, H, L, P)** insulin content. All values are means ± SEM (n=6). Different letters **(A–C)** with the same color indicate significant differences in the same fish species with different sampling times. *($p < 0.05$), **($p < 0.01$), and ***($p < 0.001$) indicate significant differences at the same sampling time among different fish species.

hours than the oral glucose treatment (Figure 3F). However, there was no significant effect on pyruvate levels between oral fructose and glucose treatments (Figure 3G). In turbot, the oral fructose treatment had significantly higher fructose and pyruvate contents in the serum than those treated with oral glucose treatment (Figures 3N, O). The oral glucose treatments had higher serum insulin content in both tiger puffer and turbot compared with oral fructose treatments (Figures 3H, P). All these results indicate that glucose and fructose may be converted to each other in fish. Glucose is a stronger stimulator of insulin secretion than fructose in the two marine fishes.

3.3 Effects of intraperitoneal injection and oral gavage on glucose or fructose utilization

The intraperitoneal glucose treatments had significantly higher serum glucose content from 0.5 to 3 hours in the both tiger puffer and turbot compared with oral glucose treatments (Figures 4A, I). In turbot, intraperitoneal glucose treatment had higher fructose, pyruvate, and insulin contents in the serum than that in the oral glucose treatment (Figures 4J–L). However, these indicators did not change between intraperitoneal glucose and oral glucose treatments in tiger puffer (Figures 4B–D). In tiger puffer, the intraperitoneal fructose treatment had significantly higher serum fructose content at 0, 0.5, 1, and 7 hours (Figure 4F). Moreover, the intraperitoneal fructose treatment had higher insulin levels after 0.5, 1, and 3 hours than the oral fructose treatment (Figure 4H). However, the two administration methods did not affect glucose and pyruvate levels in the serum (Figures 4E, G). In turbot, the intraperitoneal fructose treatment had significantly higher serum glucose, fructose, and insulin contents only after 7 hours than the oral fructose treatment (Figures 4M, N, P). However, the intraperitoneal fructose treatment had a significantly lower fructose level after 3 hours and pyruvate level after 0.5 hour than the oral fructose treatment in the serum (Figures 4N, O). These data prove that intraperitoneal injection can promote the absorption and utilization of glucose compared with oral administration.

3.4 Effects of glucose and fructose utilization on acute hypoxia tolerance

The hypoxic survival rate of the eight fish species is shown in Figure 5. Turbot (*Scophthalmus maximus*) was the most intolerant

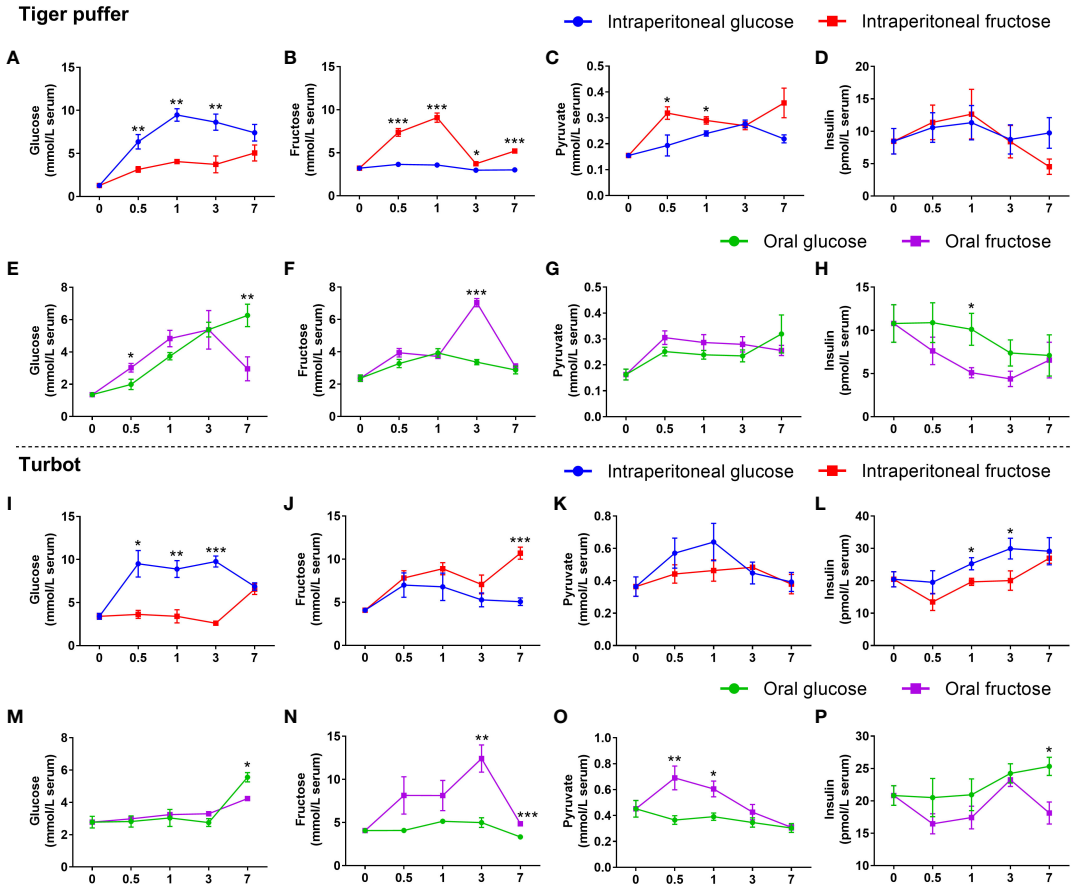

FIGURE 3
The differences between glucose and fructose utilization in fish. **(A, E, I, M)** glucose content. **(B, F, J, N)** fructose content. **(C, G, K, O)** pyruvate content. **(D, H, L, P)** insulin content. All values are means ± SEM (n=6). *($p < 0.05$), **($p < 0.01$), and ***($p < 0.001$) indicate significant differences between glucose and fructose at the same sampling time (compared to the same data in Figure 2 in different ways).

to hypoxia, while pearl gentian grouper (*Epinephelus fuscoguttatus*♀ × *Epinephelus lanceolatus*♂) was the most tolerant to hypoxia (Figures 5A). The hypoxia tolerance ability of the eight species was in the order: turbot (*Scophthalmus maximus*) < tiger puffer (*Takifugu rubripes*) < half-smooth tongue sole (*Cynoglossus semilaevis*) < goby (*Acanthogobius ommaturus*) < Japanese sea bass (*Lateolabrax japonicas*) < grey mullet (*Mugil cephalus Linnaeus*) < yunlong grouper (*Epinephelus moara* ♀× *Epinephelus lanceolatus*♂) < pearl gentian grouper (*Epinephelus fuscoguttatus*♀ × *Epinephelus lanceolatus*♂). Both turbot and tiger puffer were intolerant to hypoxia. However, there were distinct physiological differences between the two fish species. Tiger puffer had a significantly higher liver fat level than turbot (Figure 5B). However, liver glycogen content was significantly lower in tiger puffer than turbot (Figure 5C). Intraperitoneal glucose (IG), intraperitoneal fructose (IF), oral glucose (OG), and oral fructose (OF) treatments all increased hypoxic survival rate compared with the normal saline (NS) treatment, and the significances were found in the OG treatment in tiger puffer and in the IG and IF treatments in turbot (Figures 5D, F). Meanwhile, the fish treated with OG, IG, OF, and IF all had significantly higher serum lactate levels than the NS treatment both in turbot and tiger puffer (Figures 5E, G). These data suggest that supplementation with glucose or fructose can improve hypoxia tolerance in the two fish species.

4 Discussion

Fish especially carnivorous fish, have a limited ability to utilize carbohydrates in their diet and commonly show postprandial hyperglycemia for extended periods. GTT is an important tool to evaluate the ability of fish to utilize glucose, which can be performed orally or intraperitoneally (Enes et al., 2009; Liu et al., 2018). In omnivorous fishes such as hybrid Amazon catfish (*Pseudoplatystoma fasciatum* × *Leiarius marmoratus*) and traíra (*Hoplias malabaricus*), the serum glucose content rose to the highest point from 2 to 4 hours and declined to baseline after 16 hours post-IPGTT at 1000 mg glucose/kg body weight (De Souza et al., 2021). However, intraperitoneal fructose injection did not affect serum glucose level (De Souza et al., 2021). In omnivorous fishes such as Nile tilapia and piau (*Leporinus elongatus*), serum glucose content rose to the highest point from 0.5 to 1 hour and declined to baseline at 8 hours post-IPGTT at 1000 mg glucose/kg body weight (De Souza et al., 2021). In grass carp

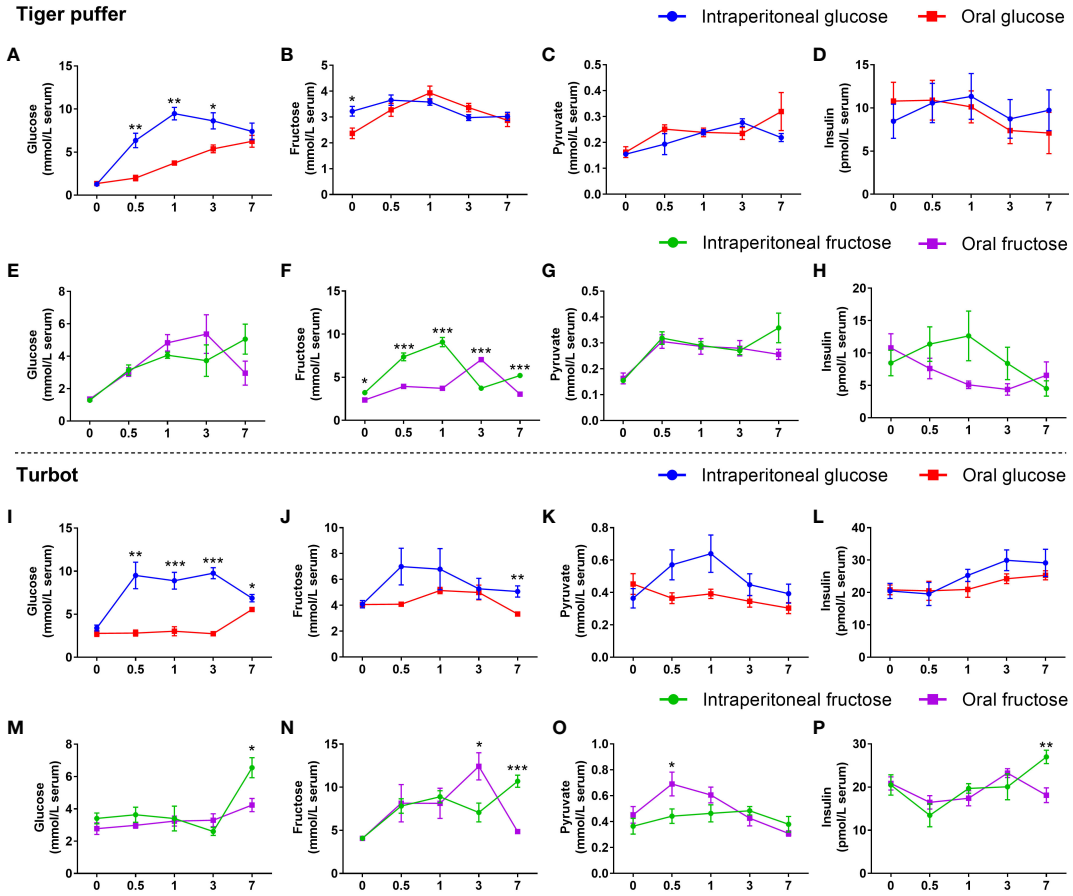

FIGURE 4
Effects of intraperitoneal injection and oral gavage on glucose or fructose utilization. **(A, E, I, M)** glucose content. **(B, F, J, N)** fructose content. **(C, G, K, O)** pyruvate content. **(D, H, L, P)** insulin content. All values are means ± SEM (n=6). *($p < 0.05$), **($p < 0.01$), and ***($p < 0.001$) indicate significant differences between intraperitoneal injection and oral gavage at the same sampling time (compared to the same data of Figure 2 in different ways).

(*Ctenopharyngodon idellus*), serum glucose content peaked after 1 hour and returned to normal level after 12 hours post intraperitoneal glucose at 300 mg glucose/kg body weight (Li et al., 2018b). In the fruit-eating fish *Piaractus mesopotamicus*, oral admission with three types of carbohydrates (glucose, fructose, and starch at 2000 mg/kg body weight) all resulted in raised blood glucose content (Takahashi et al., 2018). The highest blood glucose content was reached after 2 hours post oral fructose and 4 hours post oral glucose or starch, respectively, and glucose content recovered to baseline level within 12 hours after carbohydrates gavage (Takahashi et al., 2018). In grass carp, the high-carbohydrate treatment (60% corn starch) had increased glucose tolerance, glycogen content, and glucokinase (Gk, key enzyme of glycolysis) activity in the liver compared to the low-carbohydrate treatment (20% corn starch). However, the liver had lower phosphoenolpyruvate carboxykinase (Pepck, key enzyme of gluconeogenesis) activity than the low-carbohydrate treatment (Li et al., 2018b). In Nile tilapia, a high-carbohydrate diet (32.3% corn starch) lowered weight gain and condition factor versus the low-carbohydrate treatment (13.1% corn starch) (Chen et al., 2020). However, increased hepatosomatic index, intraperitoneal fat ratio, glucose and triglyceride contents in the serum, glycogen content, phosphofructokinase (Pfk) activity, and mRNA expression of glucose transporter (glut2/4) and pfk in the liver and white muscle (Chen et al., 2020). These results confirm that omnivorous fish have the ability to clear glucose more quickly than carnivorous fish. In the present study, we found that intraperitoneal glucose injected fish first increased and then decreased the serum glucose level with the extension of sampling time, and reached the peak after 0.5 hours in turbot and after 1 hour in tiger puffer, which proved that, the two marine fishes had the ability to clear excessive glucose. However, the time for blood glucose to return to normal level was slower than in some omnivorous freshwater fishes.

In mammals, insulin is one of the key anabolic hormones for maintaining glucose homeostasis by stimulating postprandial glucose uptake in peripheral tissues, promoting glycogen and lipid synthesis, and inhibiting gluconeogenesis in the liver (Saltiel and Kahn, 2001). Intraperitoneal glucose at 1000 mg glucose/kg body weight increased serum glucose concentration that reached the peak after 2 to 6 hours and returned to normal level after 12 hours post-IPGTT (Conde-Sieira et al., 2015). However, it did not change the serum insulin content in European sea bass (*Dicentrarchus labrax*) (Conde-Sieira et al., 2015). In white sea bream (*Diplodus sargus*), serum glucose and insulin contents were increased and reached the peak after 2 hours and returned to

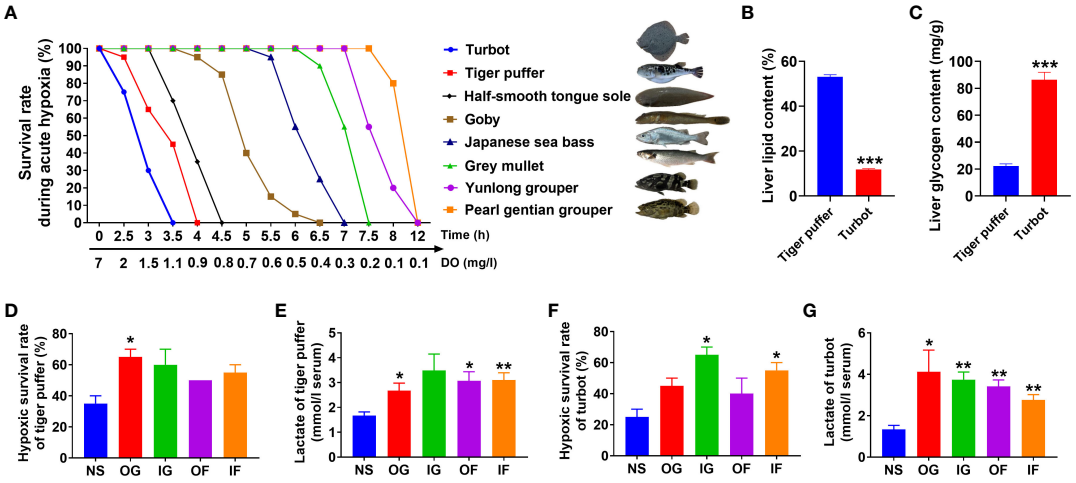

FIGURE 5
Effects of glucose and fructose utilization on acute hypoxia tolerance. **(A)** The survival rates of 8 marine fish species under acute hypoxia (values are means of two replications, n=20). **(B)** Liver lipid content in the tiger puffer and turbot. **(C)** Liver glycogen content in the tiger puffer and turbot. **(D)** Survival rate of tiger puffer with intraperitoneal and oral glucose or fructose after 2 h acute hypoxia stress. **(E)** Serum lactate content of tiger puffer after 2 h acute hypoxia. **(F)** Survival rate of turbot with intraperitoneal and oral glucose or fructose after 2 h acute hypoxia stress. **(G)** Serum lactate content of turbot after 2 h acute hypoxia (values are means ± SEM, n=4). *($p < 0.05$) and **($p < 0.01$) indicate significant differences between OG (oral glucose), IG (intraperitoneal glucose), OF (oral fructose), IF (intraperitoneal fructose) group, and NS (normal saline) group. ***($p < 0.001$) indicates significant differences between tiger puffer and turbot.

normal levels after 9 hours post intraperitoneal glucose at 1000 mg glucose/kg body weight (Enes et al., 2012). On the contrary, IPGTT reduced the insulin content of serum in Japanese flounder (Liu et al., 2018). In the present study, we found that intraperitoneal glucose, oral glucose, and intraperitoneal fructose all increased the serum insulin content in turbot, but did not change the serum insulin level in the tiger puffer, while oral fructose even decreased the serum insulin content in the tiger puffer. The above data suggest that glucose and fructose only induce insulin secretion in turbot, but not in tiger puffer. The decrease of serum glucose after GTT in tiger puffer may not be insulin-dependent. Meanwhile, intraperitoneal or oral glucose treatments had higher serum insulin content than the intraperitoneal or oral fructose treatments, which indicated that glucose is a stronger stimulator of insulin than fructose in fish. In rainbow trout (*Oncorhynchus mykiss*), dietary glucose increased *gk* gene expression in the liver, but dietary fructose did not affect the expression of the *gk* gene (Panserat et al., 2001). In omnivorous fish species, intraperitoneal fructose at 1000 mg glucose/kg body weight did not affect serum glucose level in Nile tilapia and piau, but increased serum glucose level in tambaqui (*Colossoma macropomum*) (De Souza et al., 2021). In the present study, we found that intraperitoneal or oral fructose all increased serum glucose levels, and intraperitoneal or oral glucose also increased serum fructose levels. These results indicate that glucose and fructose may be converted to each other in fish. However, the mechanism of the interconversion of the two monosaccharides is still unclear. In addition, the serum glucose, fructose, pyruvate, and insulin contents in turbot were all higher than those in the tiger puffer. Tiger puffer is a fish that stores fat mainly in the liver, and has significantly higher liver fat content than turbot. However, turbot has significantly higher liver glycogen content than tiger puffer. These physiological differences suggest that turbot may have better glucose utilization than tiger puffer. In Senegalese sole (*Solea senegalensis*) intraperitoneal glucose at 600 mg glucose/kg body weight, increased first and then decreased serum glucose level with the extension of sampling time, and reached a peak after 4 hours and returned to normal level after 24 hours post IPGTT. However, oral glucose feeding at 1000 mg glucose/kg body weight increased serum glucose level that reached a peak after 1 hour and returned to normal level after 10 hours post OGTT (Conde-Sieira et al., 2015). In the present study, we found that in oral glucose treatments, the serum glucose level showed a continuously increasing trend in the two marine fishes. Indeed, the glucose absorption and metabolism rates in intraperitoneal glucose treatments were faster than in oral glucose treatments. These data prove that compared with oral administration (into the intestine), intraperitoneal injection can promote the absorption and utilization of glucose, which indicates slow intestinal digestion and absorption of carbohydrates may be responsible for persistent postprandial hyperglycemia in marine carnivorous fish.

With the rapid development of marine fish farming, acute hypoxia stress has been a common and harmful stress in aquaculture. In Norway and Chile, the high-density culture mode of salmon requires high dissolved oxygen levels, and uncontrollable ocean currents, which cause acute hypoxia, resulting in massive mortality and serious economic losses (Martínez et al., 2020). However, few studies have been conducted to improve hypoxia tolerance in marine fish. In the present study, we selected eight marine fish species to perform acute hypoxia stress simultaneously. We found that the hypoxia tolerance ability of the eight species was in the order: turbot < tiger puffer < half-smooth tongue sole < goby < Japanese sea bass < grey mullet < yunlong grouper < pearl gentian grouper, which proved that both turbot and tiger puffer are very intolerant to acute hypoxia. In a hypoxia environment, the naked mole-rat increased fructose concentration in the liver, kidney, and blood, while fructose but not glucose entered anaerobic glycolysis to

produce energy and lactate by activating GLUT5 and KHK (Park et al., 2017). In zebrafish, feeding a high-carbohydrate diet increased the survival rate during acute hypoxia stress by activating the anaerobic glycolysis pathway (Ma et al., 2020). Crucian carp (*Carassius auratus*) are the most hypoxia-tolerant vertebrates and can survive for months in water without any oxygen. In hypoxia, glucose from the liver glycogen produces energy and lactate via an anaerobic glycolysis pathway, and lactate can be converted to ethanol that is excreted into water from the gills to avoid acidosis (Shoubridge Eric and Hochachka, 1980). In our study, intraperitoneal or oral glucose or fructose both increased survival rate and serum lactate level after acute hypoxia than the normal saline treatment in turbot and tiger puffer. Our study proved that supplementation with glucose or fructose improves hypoxia tolerance in the two marine fishes.

5 Conclusion

Turbot and tiger puffer are able to clear excessive glucose after GTT, but the time for serum glucose to return to normal level was slower than some omnivorous fishes. Tiger puffer has lower liver glycogen, serum glucose, fructose, pyruvate, and insulin contents than turbot. Glucose and fructose only induce insulin secretion in turbot, but did not change serum insulin level in tiger puffer. Glucose is a stronger stimulator of insulin than fructose, and glucose and fructose may be converted to each other in the two fish species. Intraperitoneal glucose promotes the absorption and utilization of glucose more than oral glucose. Turbot and tiger puffer are intolerant to acute hypoxia. However, supplementation with glucose or fructose improves hypoxia tolerance in the two marine fishes by activating anaerobic glycolysis. Our results help to understand the mechanism glucose and fructose utilization in fish and provide guidance to improve fish tolerance to acute hypoxia.

Data availability statement

The original contributions presented in the study are included in the article/supplementary material. Further inquiries can be directed to the corresponding author.

Ethics statement

The animal study was approved by Yellow Sea Fisheries Research Institute, Chinese Academy of Fishery Sciences. The study was conducted in accordance with the local legislation and institutional requirements.

Author contributions

QM: Conceptualization, Data curation, Formal Analysis, Funding acquisition, Investigation, Methodology, Writing – original draft, Writing – review & editing. HX: Data curation, Formal Analysis, Methodology, Writing – review & editing. SML: Formal Analysis, Writing – review & editing. YW: Methodology, Writing – review & editing, Data curation, Formal Analysis. ML: Formal Analysis, Writing – review & editing, Data curation, Methodology.

Funding

The author(s) declare financial support was received for the research, authorship, and/or publication of this article. This work was supported by the National Natural Science Foundation of China (32202950), the China Postdoctoral Science Foundation (2022M713471), the Central Public-interest Scientific Institution Basal Research Fund, CAFS (2023TD52), and the earmarked fund for China Agriculture Research System (CARS47-G15).

Acknowledgments

We thank Dr. Zhang-Bin Liao for technical assistance in the study.

Conflict of interest

The authors declare that the research was conducted in the absence of any commercial or financial relationships that could be construed as a potential conflict of interest.

Publisher's note

References

Alexander, C., Sahu, N. P., Pal, A. K., Akhtar, M. S., Saravanan, S., Xavier, B., et al. (2011). Higher water temperature enhances dietary carbohydrate utilization and growth performance in *Labeo rohita* (Hamilton) fingerlings. *J. Anim. Physiol. An. N.* 95, 642–652. doi: 10.1111/j.1439-0396.2010.01095.x

Blasco, J., Marimon, I., Viaplana, I., and Fernandez-Borras, J. (2001). Fate of plasma glucose in tissues of brown trout in *vivo*: effects of fasting and glucose loading. *Fish Physiol. Biochem.* 24, 247–258. doi: 10.1023/A:1014084313207

Caruso, M. A., and Sheridan, M. A. (2011). New insights into the signaling system and function of insulin in fish. *Gen. Comp. Endocr.* 173, 227–247. doi: 10.1016/j.ygcen.2011.06.014

Chen, J. X., Feng, J. Y., Zhu, J., Luo, L., Lin, S. M., Wang, D. S., et al. (2020). Starch to protein ratios in practical diets for genetically improved farmed Nile tilapia *Oreochromis niloticus*: Effects on growth, body composition, peripheral glucose metabolism and glucose tolerance. *Aquaculture* 515, 734538. doi: 10.1016/j.aquaculture.2019.734538

Conde-Sieira, M., Soengas, J. L., and Valente, L. M. P. (2015). Potential capacity of Senegalese sole (*Solea Senegalensis*) to use carbohydrates: Metabolic responses to hypo- and hyper-glycaemia. *Aquaculture* 438, 59–67. doi: 10.1016/j.aquaculture.2014.12.042

De Souza, A. M., Copatti, C. E., Campeche, D. F. B., De Melo, F. V. S. T., and Melo, J. F. B. (2021). Glucose tolerance in six fish species reared in Brazil: Differences between carnivorous and omnivorous. *An. Acad. Bras. Cienc.* 93, e20201541. doi: 10.1590/0001-3765202120201541

Eames, S. C., Philipson, L. H., Prince, V. E., and Kinkel, M. D. (2010). Blood sugar measurement in zebrafish reveals dynamics of glucose homeostasis. *Zebrafish* 7, 205–213. doi: 10.1089/zeb.2009.0640

Enes, P., Panserat, S., Kaushik, S., and Oliva-Teles, A. (2009). Nutritional regulation of hepatic glucose metabolism in fish. *Fish Physiol. Biochem.* 35, 519–539. doi: 10.1007/s10695-008-9259-5

Enes, P., Peres, H., Pousao-Ferreira, P., Sanchez-Gurmaches, J., Navarro, I., Gutierrez, J., et al. (2012). Glycemic and insulin responses in white sea bream *Diplodus sargus*, after intraperitoneal administration of glucose. *Fish Physiol. Biochem.* 38, 645–652. doi: 10.1007/s10695-011-9546-4

Havel, P. J. (2005). Dietary fructose: Implications for dysregulation of energy homeostasis and lipid/carbohydrate metabolism. *Nutr. Rev.* 63, 133–157. doi: 10.1301/nr.2005.may.133-157

Hemre, G. I., and Hansen, T. (1998). Utilisation of different dietary starch sources and tolerance to glucose loading in Atlantic salmon (*Salmo salar*), during parr-smolt transformation. *Aquaculture* 161, 145–157. doi: 10.1016/S0044-8486(97)00266-4

Hemre, G. I., Mommsen, T. P., and Krogdahl, A. (2002). Carbohydrates in fish nutrition: effects on growth, glucose metabolism and hepatic enzymes. *Aquacult. Nutr.* 8, 175–194. doi: 10.1046/j.1365-2095.2002.00200.x

Jiang, M., Liu, W., Wen, H., Huang, F., Wu, F., Tian, J., et al. (2014). Effect of dietary carbohydrate sources on the growth performance, feed utilization, muscle composition, postprandial glycemic and glycogen response of Amur sturgeon, *Acipenser schrenckii* Brand. *J. Appl. Ichthyol.* 30, 1613–1619. doi: 10.1111/jai.12600

Kamalam, B. S., Medale, F., and Panserat, S. (2017). Utilisation of dietary carbohydrates in farmed fishes: New insights on influencing factors, biological limitations and future strategies. *Aquaculture* 467, 3–27. doi: 10.1016/j.aquaculture.2016.02.007

Koukourakis, M. I., Giatromanolaki, A., Skarlatos, J., Corti, L., Blandamura, S., Piazza, M., et al. (2001). Hypoxia inducible factor (HIF-1a and HIF-2a) expression in early esophageal cancer and response to photodynamic therapy and radiotherapy. *Cancer Res.* 61, 1830–1832. doi: 10.1046/j.1523-5394.2001.009002104.x

Landman, M. J., Van Den Heuvel, M. R., and Ling, N. (2005). Relative sensitivities of common freshwater fish and invertebrates to acute hypoxia. *New. Zeal. J. Mar. Fresh.* 39, 1061–1067. doi: 10.1080/00288330.2005.9517375

Li, M., Wang, X., Qi, C., Li, E., Du, Z., Qin, J. G., et al. (2018a). Metabolic response of Nile tilapia (*Oreochromis niloticus*) to acute and chronic hypoxia stress. *Aquaculture* 495, 187–195. doi: 10.1016/j.aquaculture.2018.05.031

Li, R. X., Liu, H. Y., Chen, Q., Tan, B. P., Dong, X. H., Chi, S. Y., et al. (2018b). Glucose tolerance of grass carp *Ctenopharyngodon idellus* after a long-term adaptation to carbohydrate-to-lipid ratio diets. *Aquac. Res.* 49, 3881–3888. doi: 10.1111/are.13856

Li, S., Wang, A., Wei, Z., Liu, R., Wang, D., and Chen, N. (2021). Insulin receptors in largemouth bass (*Micropterus salmoides*): Cloning, characterization, tissue expression profile and transcriptional response to glucose tolerance test. *Aquac. Res.* 52, 625–634. doi: 10.1111/are.14919

Liu, D., Guo, B., Han, D., Deng, K., Gu, Z., Yang, M., et al. (2018). Comparatively study on the insulin-regulated glucose homeostasis through brain-gut peptides in Japanese flounder *Paralichthys olivaceus* after intraperitoneal and oral administration of glucose. *Gen. Comp. Endocr.* 266, 9–20. doi: 10.1016/j.ygcen.2018.02.013

Ma, Q., Hu, C. T., Yue, J., Luo, Y., Qiao, F., Chen, L. Q., et al. (2020). High-carbohydrate diet promotes the adaptation to acute hypoxia in zebrafish. *Fish Physiol. Biochem.* 46, 665–679. doi: 10.1007/s10695-019-00742-2

Ma, Q., Luo, Y., Zhong, J., Limbu, S. M., Li, L. Y., Chen, L. Q., et al. (2023a). Hypoxia tolerance in fish depends on catabolic preference between lipids and carbohydrates. *Zool. Res.* 44, 954–966. doi: 10.24272/j.issn.2095-8137.2023.098

Ma, Q., Xu, H., Wei, Y., and Liang, M. (2023b). Effects of acute hypoxia on nutrient metabolism and physiological function in turbot, *Scophthalmus maximus*. *Fish Physiol. Biochem*. doi: 10.1007/s10695-022-01154-5

Martínez, D., De Lázaro, O., Cortés, P., Oyarzún-Salazar, R., Paschke, K., and Vargas-Chacoff, L. (2020). Hypoxia modulates the transcriptional immunological response in *Oncorhynchus kisutch*. *Fish Shellfish. Immun.* 106, 1042–1051. doi: 10.1016/j.fsi.2020.09.025

Moon, T. W. (2001). Glucose intolerance in teleost fish: fact or fiction? *Comp. Biochem. Phys. B.* 129, 243–249. doi: 10.1016/S1096-4959(01)00316-5

Panserat, S., Capilla, E., Gutierrez, J., Vachot, C., Plagnes-Juan, E., Aguirre, P., et al. (2001). Dietary fructose does not specifically induce hepatic glucokinase expression in rainbow trout. *J. Fish Biol.* 59, 455–458. doi: 10.1111/j.1095-8649.2001.tb00144.x

Panserat, S., Medale, F., Blin, C., Breque, J., Vachot, C., Plagnes-Juan, E., et al. (2000). Hepatic glucokinase is induced by dietary carbohydrates in rainbow trout, gilthead seabream, and common carp. *Am. J. Physiol-Reg. I.* 278, R1164–R1170. doi: 10.1152/ajpregu.2000.278.5.R1164

Park, T. J., Reznick, J., Peterson, B. L., Blass, G., Omerbasic, D., Bennett, N. C., et al. (2017). Fructose-driven glycolysis supports anoxia resistance in the naked mole-rat. *Science* 356, 305–308. doi: 10.1126/science.aab3896

Ren, M., Ai, Q., Mai, K., Ma, H., and Wang, X. (2011). Effect of dietary carbohydrate level on growth performance, body composition, apparent digestibility coefficient and digestive enzyme activities of juvenile cobia. *Rachycentron canadum L. Aquac. Res.* 42, 1467–1475. doi: 10.1111/j.1365-2109.2010.02739.x

Saltiel, A. R., and Kahn, C. R. (2001). Insulin signalling and the regulation of glucose and lipid metabolism. *Nature* 414, 799–806. doi: 10.1038/414799a

Shoubridge Eric, A., and Hochachka, P. W. (1980). Ethanol: novel end product of vertebrate anaerobic metabolism. *Science* 209, 308–309. doi: 10.1126/science.7384807

Stone, D. A. J. (2003). Dietary carbohydrate utilization by fish. *Rev. Fish Sci.* 11, 337–369. doi: 10.1080/10641260390260884

Takahashi, L. S., Ha, N., Pereira, M. M., Biller-Takahashi, J. D., and Urbinati, E. C. (2018). Carbohydrate tolerance in the fruit-eating fish *Piaractus mesopotamicus* (Holmber). *Aquac. Res.* 49, 1182–1188. doi: 10.1111/are.13571

Tesz, G. J., and Bence, K. K. (2020). Finding the sweet spot: parsing tissue-specific contributions of fructose metabolism. *Cell Metab.* 32, 6–8. doi: 10.1016/j.cmet.2020.06.009

Tolan, D. R. (2007). Fructose metabolism in the cerebellum. *Cerebellum* 6, 130–140. doi: 10.1080/14734220601064759

Tuomilehto, J., Lindstrom, J., Eriksson, J. G., Valle, T. T., Hamalainen, H., Ilanne-Parikka, P., et al. (2001). Prevention of type 2 diabetes mellitus by changes in lifestyle among subjects with impaired glucose tolerance. *New Engl. J. Med.* 344, 1343–1350. doi: 10.1056/NEJM200105033441801

Wu, R. S. S., Zhou, B. S., Randall, D. J., Woo, N. Y. S., and Lam, P. K. S. (2003). Aquatic hypoxia is an endocrine disruptor and impairs fish reproduction. *Environ. Sci. Technol.* 37, 1137–1141. doi: 10.1021/es0258327

Zhang, Y., Wei, Z., Liu, G., Deng, K., Yang, M., Pan, M., et al. (2019). Synergistic effects of dietary carbohydrate and taurine on growth performance, digestive enzyme activities and glucose metabolism in juvenile turbot. *Scophthalmus maximus L. Aquaculture* 499, 32–41. doi: 10.1016/j.aquaculture.2018.08.082

Zhou, W. H., Wu, C. C., Limbu, S. M., Li, R. X., Chen, L. Q., Qiao, F., et al. (2022). More simple more worse: Simple carbohydrate diets cause alterations in glucose and lipid metabolism in Nile tilapia (*Oreochromis niloticus*). *Aquaculture* 550, 737857. doi: 10.1016/j.aquaculture.2021.737857

frontiers | Frontiers in Physiology

TYPE Original Research
PUBLISHED 08 February 2024
DOI 10.3389/fphys.2024.1289903

OPEN ACCESS

EDITED BY
Yiming Li,
Fishery Machinery and Instrument Research Institute, China

REVIEWED BY
Sébastien Alfonso,
Université de Nice Sophia Antipolis, France
Prunet Patrick,
Institut National de recherche pour l'agriculture, l'alimentation et l'environnement (INRAE), France

*CORRESPONDENCE
Lluís Tort,
lluis.tort@uab.cat

†These authors have contributed equally to this work and share first authorship

RECEIVED 06 September 2023
ACCEPTED 09 January 2024
PUBLISHED 08 February 2024

CITATION
Ruiz N, García-Meilán I, Khansari AR, Teles M, Pastor J and Tort L (2024), Repeated hypoxic episodes allow hematological and physiological habituation in rainbow trout. *Front. Physiol.* 15:1289903.
doi: 10.3389/fphys.2024.1289903

Repeated hypoxic episodes allow hematological and physiological habituation in rainbow trout

Nuria Ruiz[1†], Irene García-Meilán[2†], Ali Reza Khansari[1], Mariana Teles[1], Josep Pastor[3] and Lluís Tort[1*]

[1]Department of Cell Biology, Physiology and Immunology, Universitat Autònoma de Barcelona, Barcelona, Spain, [2]Department of Cell Biology, Physiology and Immunology, Universitat de Barcelona, Barcelona, Spain, [3]Departament of Animal Medicine and Surgery, Universitat Autònoma de Barcelona, Barcelona, Spain

Introduction: Under climate change, the increase in temperature in aquatic environments may induce oxygen depletion. In extreme cases, low oxygen may become a limiting factor for fish, thus generating stress. In addition, consecutive hypoxic episodes may complicate the recovery of individuals and hinder their ability to modulate physiological and biochemical responses to maintain homeostasis. Thus, the aim of this study was to determine the hematological and physiological responses of rainbow trout under a condition of repeated hypoxic and manipulation stresses at three different time points.

Methods: Every hypoxic episode consisted of exposing the fish to low dissolved oxygen concentrations (2 mgO_2/L for 1 h). Following the exposure, the fish were allowed to recover for 1 h, after which they were sampled to investigate hematological and physiological parameters.

Results and discussion: The results showed a pattern of habituation reflected by values of hematocrit, hemoglobin, and mean corpuscular volume, indicating a certain ability of rainbow trout to resist this type of repeated hypoxic events, provided that the fish can have some recovery time between the exposures.

KEYWORDS

repeated stress, hematology, fish, rainbow trout, hypoxia, dissolved oxygen concentration, cortisol

1 Introduction

The current context of climate change is expected to strongly affect fish because of its consequences on water temperature and other tightly linked quality parameters. The expected changes are related to biotic (primary production, pathogens, and food availability) and abiotic (temperature, salinity, pH, and, particularly, hypoxia) factors, affecting aquatic organisms in their distribution, growth, size, and overall health (Action, 2020). As wild populations may be exposed to more than one of these environmental stressors, much uncertainty is generated about the consequences of these stressors and their potential synergy (e.g., hypoxia and temperature rise) (Petitjean et al., 2019). As fish are aerobic organisms, the concentration of dissolved oxygen (DO) is a limiting factor both in the environment and in production systems, and its availability depends on its amount and solubility. Episodes of repeated hypoxia may become more common in the future. For instance, diel cycling hypoxia, a worldwide phenomenon affecting freshwater and coastal systems due to an

increase in partial pressure during daylight hours associated with photosynthetic activity and a subsequent diminution overnight as a consequence of biological demand, is particularly common during spring and summer months (Williams et al., 2019). In natural environments, it can be a result of eutrophication and increasing temperatures. Furthermore, hypoxic phenomena may be amplified in aquaculture settings because of overstocking or overfeeding (Bera et al., 2017).

Hypoxia occurs when oxygen concentrations drop low enough to cause negative physiological, immune, and behavioral effects on fish, affecting their growth and overall performance (Abdel-Tawwab et al., 2019). This can affect acutely or chronically, depending on the duration and recurrence of the impact of temperature change, seasonality, water flow, and/or chemical composition (Xiao, 2015). Most species have a high ability to habituate to fluctuating oxygen levels, modifying O_2 uptake, delivery, and metabolism to prevent hypoxemia and energy exhaustion (Boutilier, 2001). However, if fluctuations are recurrent, they can compromise the overall health and lead to increased mortality. Nevertheless, preconditioning exposure to hypoxia demonstrated the existence of physiological plasticity in fish (Borowiec et al., 2015), even in rainbow trout, which is considered a species particularly sensitive to this stressor (Gamperl et al., 2001). Therefore, to maintain optimal fish performance, growth, and feeding, oxygen levels should be kept near saturation. Ideally, DO levels in aquaculture settings should be above 5 mgO_2/L, which is the accepted baseline for most species (Abdel-Tawwab et al., 2019). Although under aquaculture conditions, DO levels are generally monitored and controlled, some factors, such as overcrowding or abnormal increases in temperature, may lead to suboptimal rearing conditions, and if the fish are unable to adapt, they may develop a stress response and maladaptation (Magnoni et al., 2019).

The stress response is a very primitive and highly conserved response in extant species since it preserves the organism's homeostasis (Barton, 2002). By activating primary, secondary, and tertiary responses (Schreck and Tort, 2016), it has been shown that animals are able to adapt to different stressors, including hypoxia, by reducing their physiological costs and modifying behavioral responses (Conde-Sieira et al., 2018; Alfonso et al., 2020). However, the capacity for habituation will depend on several factors, namely, the species itself, as well as the type and intensity of stress (Nilsson et al., 2012; Koakoski et al., 2013). Moreover, as the importance of animal welfare and its public awareness in production systems is increasing, the maintenance of suitable conditions for fish husbandry should consider the consequences of these stress episodes.

In the present work, we monitored the hematological and physiological parameters as they can be suitable indicators of the process of oxygen uptake and distribution to tissues (Fazio, 2019). The number of red blood cells (RBCs), hemoglobin concentration (HGB), hematocrit (HCT), mean corpuscular volume (MCV) of red blood cells, and mean hemoglobin concentration (MHC) are most commonly used to evaluate the hematological status in fish (Pavlidis et al., 2007). However, other less-investigated factors, such as the widening of the distribution of red blood cells (RDW), a parameter related to the pathway of ionic erythropoiesis to measure the size and volume of erythrocytes, have been monitored as additional indicators of health status, as shown in humans (Fish et al., 2019). In addition, the determination of the number of white blood cells (WBCs) provides information on the animal's immune status, as well as the proportion of heterophilic cells (neutrophils, basophils, and eosinophils) and mononuclear cells (lymphocytes and monocytes). Finally, the number of platelets (PLTs) was also assessed (Fazio, 2019). Altogether, the correlation between hematological parameters, as indicators of oxygen uptake and distribution (Abdel-Tawwab et al., 2019), and physiological stress markers, such as cortisol, glucose, and lactate in plasma (Groff and Zinkl, 1999), provides valuable insights on the specific physiological compartments of functional allostasis, thus becoming markers of a range of physiological variations and useful tools to detect, identify, and calibrate specific stressors.

Many studies have addressed the hypoxia effects on fish (Pollock et al., 2007; Xiao, 2015), particularly in rainbow trout (*Oncorhynchus mykiss*) (see, for instance, the work of Pilgaard et al. (1994), Sappal et al. (2016), and Zhang et al. (2018)). The present study focuses on two aspects that have been discussed in previously published work. First, studies on hypoxia have dealt with fish that have been taken out of the water, so, effectively, subjected to anoxia. Furthermore, these fish are simultaneously subjected to the consequent handling stress associated with catching and restricting the fish out of the water. However, these two stressors are difficult to separate. Second, studies on repeated hypoxia are scarce, and the ability of fish to respond repeatedly to this stressor is, therefore, less understood. Since hypoxic episodes may become more frequent in the context of climate change, the aim of the present research was to determine the effects of repeated hypoxia and manipulation by subjecting the animals to one, two, or three acute hypoxic shocks and to determine whether there is a cumulative effect, a certain adaptive capacity or, on the contrary, a constant response. In addition, the stress recovery phases, specifically at 1, 6, and 24 h after hypoxia and manipulation, were also investigated.

2 Materials and methods

2.1 Fish and rearing conditions

A total of 135 rainbow trout (*Oncorhynchus mykiss*) with a mean weight of 62.89 ± 11.10 g, a mean length of 17.58 ± 1.09 cm, and a condition factor of 1.2 ± 0.1 were obtained from a local fish farm (Molinou, Rialb, Spain) and acclimated to a recirculating aquaculture system (RAS) in the facilities of the Autonomous University of Barcelona (AQUAB) for 2 weeks. The RAS is equipped with water pumps, a recirculating cooling system, a sand filter, a biofilter, and an aeration system for the tanks, allowing for the DO concentrations to be maintained between 7.20–8.10 mgO_2/L. The photoperiod was held at 12 L: 12 D, and an average temperature of 14.6°C ± 0.3°C was maintained. Throughout the acclimation and experimental periods, the density was 6.80 ± 0.1 Kg/m^3. All experimental procedures involving fish were submitted and authorized by the Ethics and Animal Care Committee of the

"Universitat Autònoma de Barcelona" (permit numbers OH4218 4219 and DAMM 11251), in accordance with the international Guiding Principles for Biomedical Research Involving Animals (EU2010/63).

2.2 Experimental design

Five experimental groups were established, divided into two control groups and three treatment groups, each undergoing a different number of manipulation and hypoxic shocks. Each group had 9 fish per sampling time, with a total of 27 rainbow trout per group. The first group was the absolute control (AC) group, being the only group that was sampled without prior manipulation. Since it is known that the manipulation of individuals is an additional stressor to hypoxia, a manipulated control (MC) group was considered with the aim of determining how manipulation by itself can alter the evaluated parameters without decreasing the DO concentration. The remaining three groups were subjected to hypoxic shocks, all handled in the same manner as the MC group and subsequently exposed to a decreased concentration of oxygen. The H1 group was exposed to hypoxic conditions once, whereas fish in the H2 group were challenged with two hypoxic shocks, and the H3 group was subjected to low levels of DO for a total of three hypoxic shocks. Thus, the H2 and H3 groups suffered repeated acute hypoxia stress, with 48 h between hypoxia shocks. The MC group is only comparable to the H1 group, as H2 and H3 had more manipulations than the MC group. Since H2 and H3 were only compared with the AC group, we cannot exclude the effect of hypoxia and manipulation in these groups. In the groups where several hypoxic shocks were performed, the fish were returned to the acclimation tank under normal oxygen and water physicochemical levels until the next shock. Once the fish experienced the last shock, they were transferred to the recovery tank until sampling. As the number of fish in the tank decreased after each sampling, the water volume was accordingly decreased with the aim to maintain the density at 6.80 ± 0.1 Kg/m^3.

2.3 Hypoxic shock and the sampling procedure

Hypoxic levels were reached by decreasing the DO concentration by adding nitrogen gas (N_2) into the water (i.e., 5 min to reach hypoxic condition), as in the work of Schurmann and Steffensen (1992), and not removing the fish from the water. Three tanks were used to replicate the treatment procedure by maintaining a density of 6.80 ± 0.1 Kg/m^3. After the procedure, all fish were placed in the same recovery tank to avoid any tank effect. The shock included catching the fish from the experimental tanks and putting them into the hypoxia tanks, where the DO concentration was decreased from 7.5 ± 0.5 to 2.2 ± 0.5 mgO_2/L by adding nitrogen gas. The fish were introduced once the oxygen level had reached the desired values and remained there for 1 h. It should be added that during the shock, the DO concentration was continuously monitored to check that the levels were within the study range and to avoid a decrease below 1.5 mgO_2/L, which would prove lethal to this species. Throughout the experiment, the density was constantly maintained at 6.80 ± 0.1 Kg/m^3 (Figure 1). Following the hypoxia shock, the fish were transferred to a recovery tank with 7.2—8.1 mgO_2/L, which was isolated from the system to avoid any possible circulating cortisol levels affecting the other fish, as a chemical detection by peripheral cortisol receptors that may affect fish response has been previously suggested (Kolosov and Kelly, 2019). After the last hypoxia shock, the fish were transferred to a recovery tank where sampling took place. As the number of fish per tank changed, the water volume was adjusted to maintain the same density throughout the experiment. By the time the sampling of the experimental group was finished, the oxygen and water turnover levels were returned to optimal levels. For sampling, a total of 27 fish per group, with 9 fish per time point of the hypoxia and treatment groups (AC, MC, H1, H2, and H3), were anesthetized with sublethal doses of tricaine methanesulfonate (MS-222) buffered with sodium bicarbonate. All fish were weighed and measured, and blood samples were collected within 3 min. After that, fish were sacrificed by sectioning the spinal cord.

2.4 Hematological analysis

Blood collection was performed using a heparinized syringe through caudal puncture. The first 500 μL aliquot of blood was added to Eppendorf tubes containing heparin (1:40) for the determination of hematological parameters. A second aliquot was centrifuged at 1500 *g* for 10 min to collect the plasma, which was subsequently frozen at −20°C until the physiological analysis. Hematological analyses were performed within 2–12 h after blood sampling using the automated flow cytometer blood cell analyzer Sysmex XN-1000V for veterinary use (Sysmex Corporation, Kobe, Japan). Internal quality control (QC) was performed daily using three levels of commercially available QC material (Sysmex XN Check level 1 or low range, level 2 or normal range, and level 3 or abnormal high range; Sysmex Corporation, Kobe, Japan).

2.5 Physiological analysis

For cortisol analysis, the plasma was first diluted in the analysis buffer, and the aliquots were frozen at -20°C for at least 24 h until analysis with an ELISA test using a commercial EIA kit (Cortisol ELISA Kit; Neogen® Corporation, Ayr, United Kingdom) following the manufacturer's instructions. This kit has been previously validated for this species and used in past experiments (Carbajal et al., 2019).

Glucose and lactate analyses were performed using colorimetric test kits (LO-POD glucose and LO-POD lactate, SPINREACT, Spain) following the manufacturer's recommendations.

2.6 Statistical analysis

The obtained data were analyzed with a generalized linear model (GzLM) using the Gaussian family for all the variables using RStudio (R Core Team 2022. R: a language and environment for statistical computing, R Foundation for Statistical Computing, Vienna, Austria, URL https://www.R-project.org/). Data normality

10.3389/fphys.2024.1289903

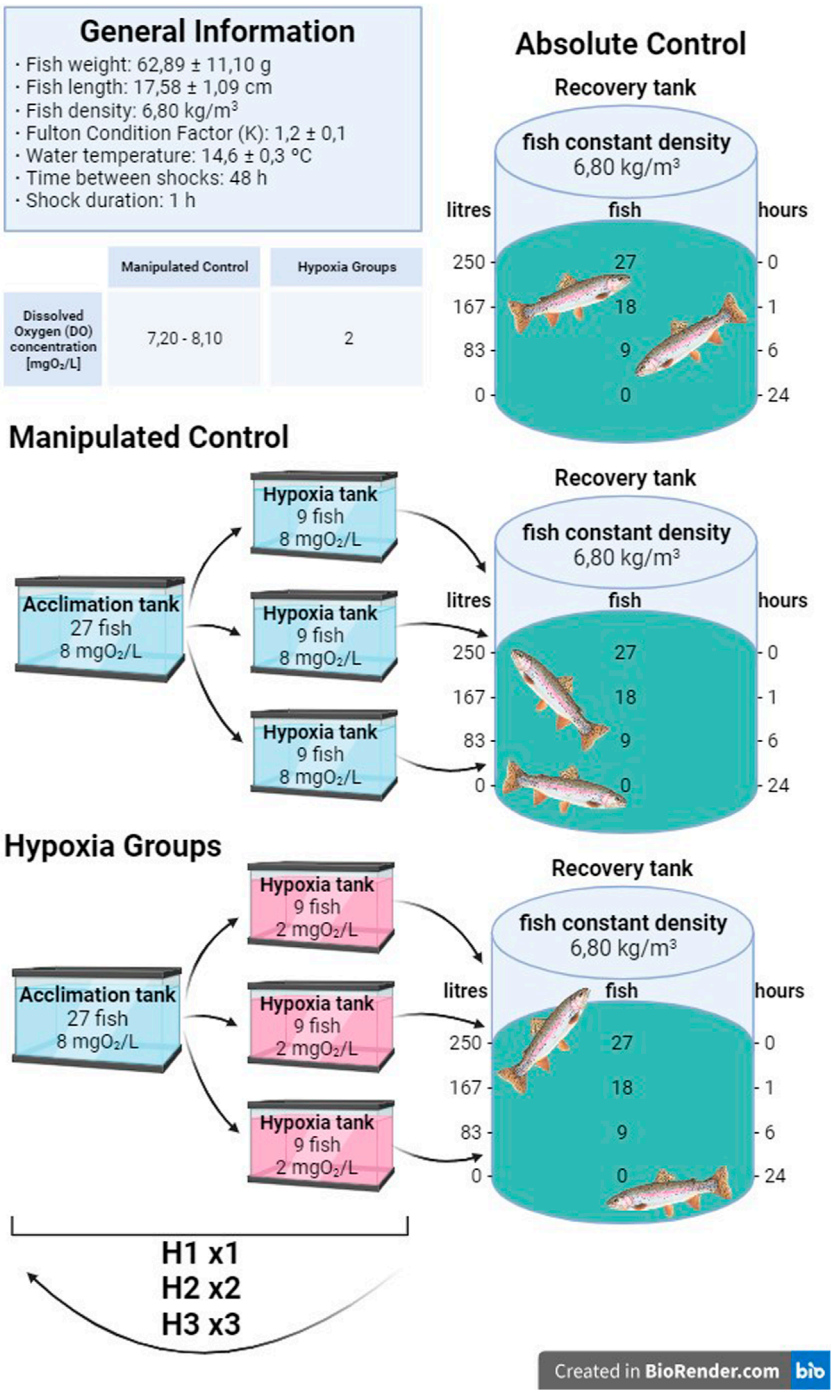

FIGURE 1
Graphical abstract of the design of the experiments.

and residual distribution of the model were checked through Shapiro–Wilk tests. The factors analyzed were hypoxia treatments, time, and the interaction between them. If significant differences (p-value < 0.05) were found, pairwise comparisons by Tukey's correction were applied. Therefore, variables where only the effect of treatment is found are presented first, followed by those with only time effect significance, and finally, all the parameters that had interaction between the two factors. For the pairwise comparisons, the effects of manipulation and hypoxia were differentiated and, therefore, AC, MC, and H1 were compared on one side and AC, H1, H2, and H3 on the other. Regarding treatment and time effect, it has to be added that only when one factor was significant, all the data were gathered by treatment or time, depending on the case.

10.3389/fphys.2024.1289903

TABLE 1 RBC number, HGB, PLT number, MHC, and heterophil cells in percentage in rainbow trout. Data are represented as mean ± SEM (n = 27 fish per treatment). Significant differences between treatments are marked with different letters (p-value < 0.05). AC, absolute control; MC, manipulated control; H1, one hypoxic shock; H2, two hypoxic shocks; and H3, three hypoxic shocks.

Group	RBC (10^3/μL)	HGB (g/dL)	PLT (10^3/μL)	MHC (pg)	Heterophils (%)
AC	0.961 ± 0.0224 ^{b}	5.57 ± 0.108 ^{ab}	2.34 ± 0.140	50.8 ± 0.770 ^{ab}	17.5 ± 1.37 ^{b}
MC	1.058 ± 0.0229 ^{a}	5.78 ± 0.110 ^{a}	2.34 ± 0.162	48.3 ± 0.770 ^{bc}	20.1 ± 1.40^{b}
H1	0.939 ± 0.0224 ^{b}	5.61 ± 0.108 ^{ab}	2.38 ± 0.149	52.8 ± 0.770 ^{a}	22.0 ± 1.49 ^{ab}
H2	1.031 ± 0.0229 ^{a}	5.77 ± 0.123 ^{ab}	2.28 ± 0.154	49.5 ± 0.846 ^{bc}	27.3 ± 1.46 ^{a}
H3	0.975 ± 0.0224 ^{ab}	5.35 ± 0.108 ^{b}	2.61 ± 0.154	47.6 ± 0.770 ^{c}	19.3 ± 1.43 ^{b}

3 Results

In this section, the results are presented according to the significant effect of each factor and the significant interaction between them in the order mentioned above. As can be observed in the figures, the significance is shown for the differences among the factors. For instance, a parameter included only in the treatment effect indicates that significant differences can be found between treatments but not between times or with interacting factors.

3.1 Treatment effects

The number of RBCs, the amount of HGB and PLTs, and MHC were affected by treatment (Table 1) but not by time or interaction between them. An increase in RBC and HGB levels, likely due to handling stress, was observed in the MC compared to the AC group, whereas one hypoxic shock tended to decrease these values since the values of H1 are lower than MC and, in theory, it had to be higher due to manipulation. In addition, significantly higher RBC values were measured in H2 compared to H1, with H3 displaying intermediate values, similar to those found in AC.

PLT count displayed a decreasing trend with an increase in the number of hypoxic shocks and manipulations, although above the threshold for statistical significance ($p < 0.07$; Table 1), except for H3, which showed increased PLT values. Finally, the results indicated an increase in MHC in H1 compared to MC, with a return to AC in H2, and a significant reduction in MHC in H3 compared to AC (Table 1). Furthermore, the results suggest that both hypoxia plus manipulation and time independently alter the proportion of heterophilic and mononuclear cells, although no interactive effect of these factors was found. It should be noted that H2 is the treatment group that showed the highest levels of heterophils compared to the AC and H1 groups, regardless of the time after hypoxia exposure and manipulation (Table 1).

3.2 Time effects

A time effect was observed in both hematocrit values (Figure 2) and the percentage of heterophilic and mononuclear cells (Figure 3). Interestingly, in both parameters, a significant increase was observed at 1 h regardless of the experimental treatment.

3.3 Interaction effects

A significant interaction between manipulation and exposure to hypoxia and time was found in MCV, RDW, WBC, glucose, lactate, and cortisol (Figure 4). In H1 and MC groups, a gradual reduction of the MCV can be observed over time t = 1 h vs. 24 h. In addition, H1 also presented higher MCV levels at 1 and 6 h compared to both AC and MC and the other groups that underwent manipulations and hypoxic shocks (H2 and H3) (Figure 4A). RDW showed differences between AC, MC, and H1 in all the sampling times and AC with all the groups that underwent manipulation and hypoxic exposures only at the sampling point t = 6 h. On one side, looking at t = 6 h, it can be observed that H1 and MC are the groups with the highest values, and AC is the group with the lowest values. On the other side, at t = 6 h, comparing the groups that underwent manipulations and hypoxia, H1 is the group with the highest values. In addition, the more the manipulations and hypoxias, the less the RDW values. Thus, H3 shows similar values as AC. The most relevant difference regarding time occurs in MC and H1 groups, showing lower RDW values at 1 h and 24 h after treatment than at 6 h. This trend was also found when comparing all experimental groups versus AC, being higher in H1 and, therefore, suggesting a greater anisocytosis 6 h after treatment (Figure 4B). Regarding immune cells, the lowest WBC levels occurred 6 h after either manipulation or hypoxic exposure when compared with AC. In MC, these differences are maintained even after 24 h; however, this is not observed in the groups subjected to repeated hypoxia and manipulations (H2 and H3) (Figure 4C). In terms of physiological response, plasma glucose levels significantly increased 6 h after treatment in H1 compared with AC and all the groups that suffer manipulation and hypoxia. In contrast, glucose values were reduced at 24 h, except in the MC and H1 groups (Figure 4D). Lactate levels clearly increased 1 h after exposure and then decreased until recovering basal levels, except for the H2 group, which presented higher levels at 24 h than AC. It should be highlighted that lactate did not peak at 1 h in the H3 group, as observed in H1 and H2 (Figure 4E). Finally, a significant rise in plasma cortisol levels at 1 h post-exposure was observed in rainbow trout that underwent hypoxic shock and manipulation (H1, H2, and H3) compared with the AC group. Similarly, the MC group also had elevated cortisol levels when compared to the AC group. The cortisol levels dropped at 6 h and then interestingly rose again at 24 h (Figure 4F). Significant differences were maintained at 24 h post-shock between AC and both MC and H1, but not H2 nor H3, both groups showing intermediate values.

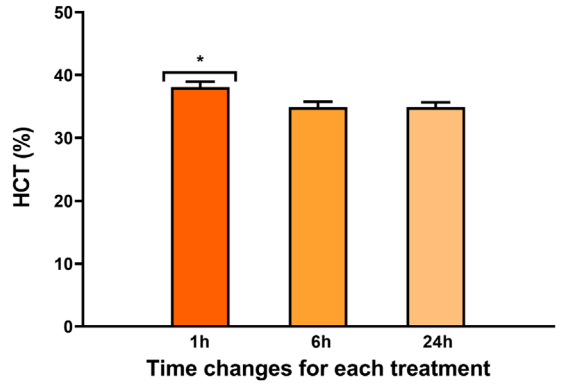

FIGURE 2
Percentage of hematocrit in rainbow trout blood 1, 6, and 24 h after treatment. Data are represented as mean ± SEM (n = 45 per sampling time). The significant differences in sampling time are indicated by an asterisk (p-value < 0.05).

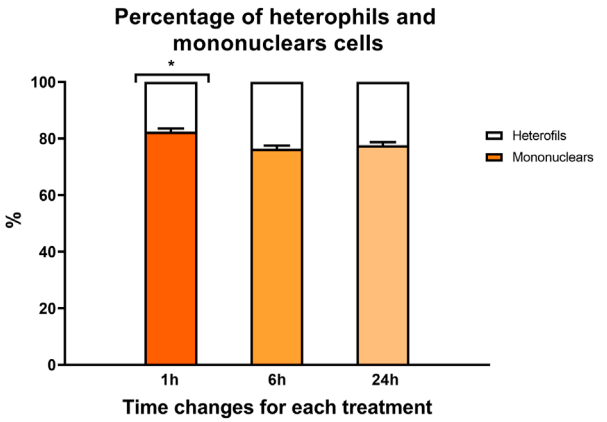

FIGURE 3
Percentage of mononuclear cells (color bars) and heterophils (white bars) in rainbow trout blood 1, 6, and 24 h after treatment. Data are represented as mean ± SEM (n = 45 per sampling time). The significant differences in sampling time are indicated by an asterisk (p-value < 0.05).

4 Discussion

In this work, the results are presented in two sets of groups, the first including the control with the manipulated control and one hypoxia exposure groups and the second including the groups experiencing repeated manipulations and hypoxias. In the first set, AC represents the basal levels that are expected to represent the basal resting values. The MC group allows to differentiate between the basal and manipulated fish, and finally, hypoxia 1 (H1) allows to differentiate the effects between the manipulated and one hypoxia groups. In the second set, we compare the effect of repeated manipulations and hypoxia exposures related to AC as the basal levels of our animals. Since there is no MC group with two and three manipulations, we excluded the MC group from the analysis of this second set of groups as they are not directly comparable.

The overall results suggest that rainbow trout are able to cope with repeated manipulation and acute hypoxia (1 h with DO levels down to 2 mgO_2/L) and recover from the shock 24 h after the stressor and that subjecting the fish again to the same stressor leads to a certain level of habituation. Among the hematological variables, red blood cells and hemoglobin showed an increase in the MC group, presumably due to the handling of the animals, as observed in the work of Acerete et al. (2004). On the contrary, as observed in H1, hypoxia generates a decrease in RBC, probably due to an excessive alteration of the oxygen delivery system, resulting in an reduction in the overall metabolism and activity (Pichavant et al., 2002). After the second manipulation and shock (H2), the RBC level increased, suggesting a recovery in oxygen content and an improvement in blood transport (Aboagye and Allen, 2018), and recovered control values in H3. A similar trend was observed in HCT, which tended to diminish as exposures and manipulations increased. Moreover, the increase of HCT 1 h after manipulation and/or treatment could be associated with balancing out the additional requirements for oxygen under hypoxia (Muusze et al., 1998). All these data suggest an adaptation of the animals, resulting in a lower use of oxygen in habituated fish (Petersen and Gamperl, 2011; Remen et al., 2012).

Significant differences in MCV were observed both between groups and sampling points. The highest MCV was observed in H1, which indicates that the erythrocyte volume increased. This could be explained by two mechanisms that have been previously described. On one hand, the osmoregulatory changes that occur over time in an attempt to increase the efficiency of oxygen transfer through the cell membrane (Aboagye and Allen, 2018). On the other hand, the increase in HCT and MCV values, without much change in RBC, may suggest the swelling of erythrocytes (Aboagye and Allen, 2018). The swelling of the erythrocytes has been observed as a result of catecholamine release after stress, trying to compensate for the efficiency of cell oxygen uptake due to the increased demand of oxygen, in this case caused by the hypoxic stress and manipulations (Caldwell and Hinshaw, 1994). Interestingly, both HCT and MCV displayed a correlation with MHC. In this case, the groups with higher levels of HCT and MCV presented higher MHC. This could be explained by cellular hemolysis, which may occur during the first hour after the manipulation and hypoxic shock, as previously demonstrated (Caldwell and Hinshaw, 1994; Muusze et al., 1998). Furthermore, this effect is reduced over time, suggesting recovery. This idea of hemolysis was initially proposed by Swift and Lloyd (1974), describing how HCT and MCV values increase because of cell swelling, which causes hemolysis. Afterward, differences were also observed between treatments, and as in the rest of the erythrocyte-related parameters, a certain degree of habituation can be observed in the groups subjected to hypoxia. Therefore, the more the hypoxia shocks accumulate, the lower the response, as previously seen during chronic hypoxia exposure (Caldwell and Hinshaw, 1994).

It has been previously demonstrated that stressors, such as infections by trematode metacercaria, entail a significant decrease in the distribution by the size and volume of the cell (i.e., RDW) (Khan et al., 2017). In other studies associated with nutritional stress, an inverse relationship between RDW and other hematological parameters, such as MCV or HGB, was observed (Goran et al., 2017). In the present study, RDW resulted higher 6 h

10.3389/fphys.2024.1289903

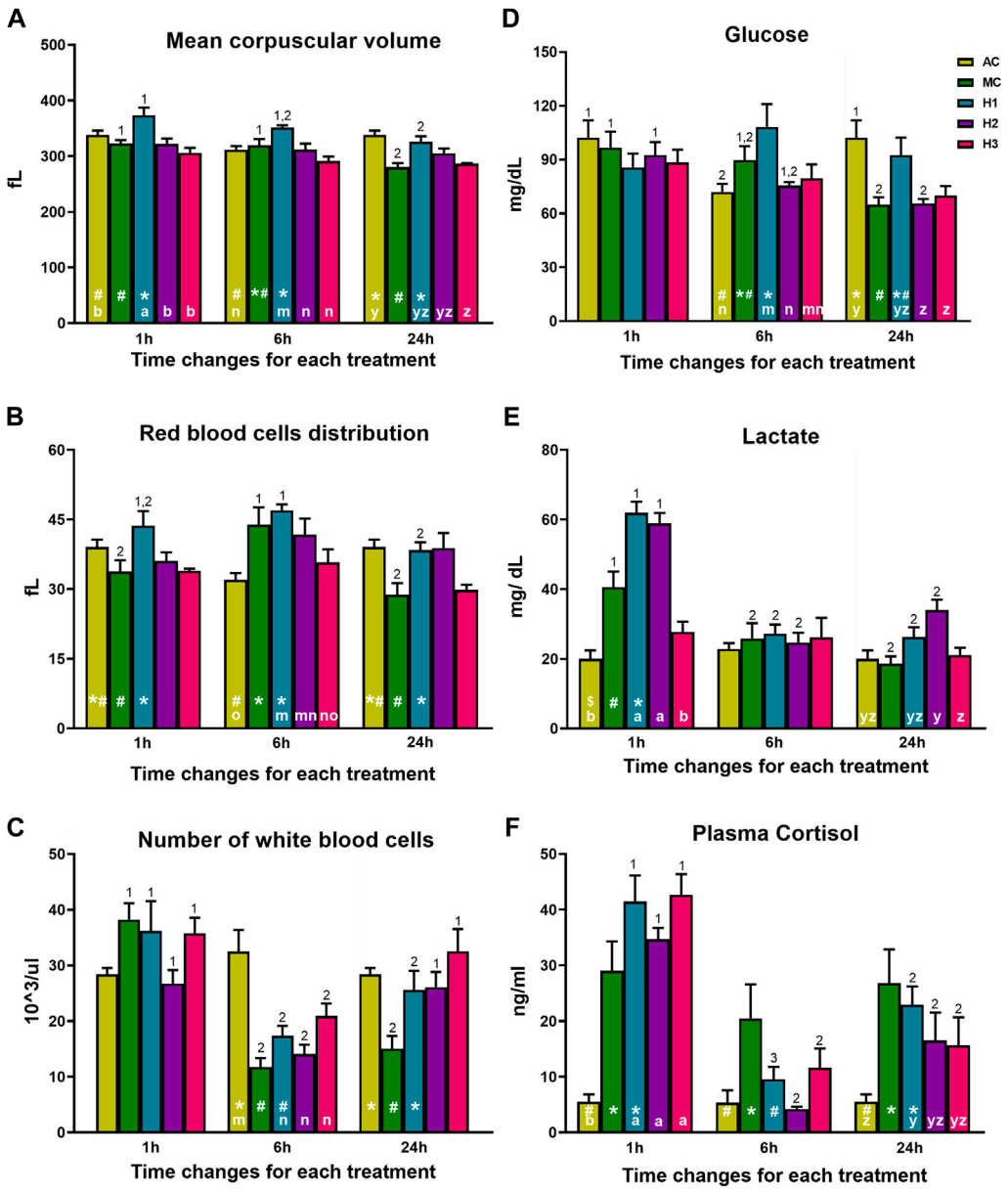

FIGURE 4
(A) Mean corpuscular volume, **(B)** erythrocyte distribution width (RDW-SD), **(C)** number of white blood cells, **(D)** plasma glucose, **(E)** plasma lactate, and **(F)** plasma cortisol in rainbow trout blood 1, 6, and 24 h after treatment. Data are represented as mean ± SEM (n = 9 per sampling time). Significant differences ($p < 0.05$) between treatments at the same sampling time are shown with different letters (a/b at 1 h, m/n at 6 h, and y/z at 24 h after treatment). Significant differences in sampling time among the same treatment are shown by numbers (p-value < 0.05). Differences between AC, MC, and H1 are shown by * and #.

post-shock, suggesting greater heterogeneity and, therefore, greater anisocytosis, since some cells are recovering while others are not, thus increasing the heterogeneity levels at this time point. After 24 h, homogeneity is restored, but since the cells are smaller because no swelling is produced, the values at 24 h are lower than those at 1 h. It should be added that this parameter has been little studied in fish; however, in humans, a decrease in RDW levels may reflect anemia, implying that erythrocytes do not have the capacity to efficiently transport oxygen (Maiolo et al., 1991). As it has been seen with the rest of the parameters, in the case of H3, RDW returns to the levels of the AC at 1 and 24 h, suggesting, once again, habituation.

For white blood cells, all treatments showed a decrease at 6 h with respect to the absolute control group, especially fish subjected to two hypoxic shocks that also presented a significant decrease at 1 h after treatment. These results agree with those found by Sheng et al. (2019) in the face of repeated stress (hypoxia and manipulation) and may be related to cell damage detection, one of the functions of WBCs (Sheng et al., 2019; Missinhoun et al., 2021). Moreover, H3 rainbow trout showed an ability to recover WBC levels, further suggesting habituation.

Among white blood cells, two different cell types can be distinguished depending on their nuclear morphology: heterophils

and mononuclear cells. Heterophils can be further classified into neutrophils, eosinophils, and basophils. The majority of heterophils are neutrophils, which do not show relevant changes when there is circulating cortisol, as described by McLeay (1973). On the other hand, in the face of a stressful situation, eosinophils have been shown to decrease, whereas no changes have been observed in the basophil populations. In this sense, the depletion of eosinophils would match with the peak of plasma cortisol (Wojtaszek et al., 2002). Similarly, mononuclear cells can be subdivided into monocytes and lymphocytes. These authors demonstrated a lack of changes in monocyte levels when facing a stressful situation, whereas lymphocytes displayed a significant reduction in their abundance. The decrease in monocytes observed in the present study could be explained by the combination of the reduction of lymphocytes and the small proportion of eosinophils among this group of cells. Further studies are needed to ascertain the less-known consequences of hypoxia and manipulation on white blood cells.

The main function of PLTs is related to clotting, and since no lesions were observed at any point of the experiment, no differences were expected in levels of these particular cells after hypoxia and manipulation. In addition, it has been reported that cortisol levels do not alter thrombocyte levels (Wojtaszek et al., 2002). Although a trend of decrease by repeated hypoxia and manipulation is suggested, differences were not significant.

The variation observed in cortisol levels between treated groups and control ones is commonly found in stress studies and is particularly associated with handling procedures (Acerete et al., 2004; Sadoul and Geffroy, 2019). This may also be the case in our results under hypoxia exposure since, as observed in the work of O'Connor et al. (2011), neither acute nor chronic exposure to hypoxia caused significant differences with respect to the control groups. On the other hand, handling is a stressor to which the fish responds with increased cortisol levels, although the potential for habituation has been suggested (Pagès et al., 1995), so manipulation and hypoxia can raise the levels of cortisol, as observed in this study. In addition, it can be observed that the WBC levels seem to mimic the rise in cortisol levels and, therefore, the activated response of the hypothalamic–pituitary–interrenal axis (Pottinger and Carrick, 1999), as cortisol and WBC levels show a high correlation (Figures 4C, F). Similar results have been observed in other studies, such as in the work of Carbajal et al. (2019), where WBCs were higher in a polluted environment under suboptimal conditions inducing neutrophilia and/or lymphopenia in fish. Furthermore, the increase in WBCs is related to the migration of these cells from the spleen to the blood (Barcellos et al., 2004). Moreover, regarding cortisol measurements, two different types of response patterns can be observed. On one hand, the groups that were not subjected to hypoxia did not display any significant differences between sampling points, although statistically significant differences arise when comparing the AC and MC groups, as expected. On the other hand, there is a significant reduction in cortisol levels in all groups exposed to hypoxic conditions at t = 6h, with a subsequent significant increase at t = 24 h. This could be partly due to circadian rhythms inherent to the species, as described by Naderi et al. (2018), although the lack of differences within the AC and MC groups suggests there are other factors at play. Therefore, it can be hypothesized that the decrease observed at t = 6 h reflects the start of the recovery period but that the fish have developed, to some extent, a predictable behavior to this specific stressor, as both shocks occurred at the exact same time 1 day apart. This would explain the significant increase in cortisol levels at t = 24 h in the treatment groups. Nonetheless, further research is needed to investigate this possible adaptive behavior in *O. mykiss*. This hypothesis is supported by the fact that the predictability in fish was demonstrated after a positive stress stimulus (i.e., feeding) or a negative one (i.e., crowding) by changes in plasma cortisol levels (Galhardo and Oliveira, 2009; Galhardo et al., 2011), and the anticipatory responses are not unusual in animals. This fact allows self-preparation for the upcoming event, giving to the fish a certain control capacity on the stressor response, thus optimizing the efficacy of the response (Galhardo et al., 2011). In our work, plasma cortisol levels 24 h after the hypoxic shock were higher in hypoxic groups versus the AC group, suggesting that there is no lower response as expected. This difference should be attributed to the type of the stressor, which, in this case, is hypoxia in water instead of anoxia, like in most of the studies. We must consider that the predictability response depends on the stressor properties (nature, intensity, and frequency), the signaling cascade, and the time elapsed between the signal and the onset of the negative event, as it is currently observed in stress studies (Galhardo and Oliveira, 2009).

At this point, it is interesting to emphasize that, in the present work, hypoxia was achieved by reducing the oxygen concentration in water, which is rather different than the hypoxia caused by air exposure. The latter involves a concurrent stressor, such as significant manipulation plus the maintenance of fish out of its aquatic environment. As observed in the study by Franco-Martinez et al. (2022), where an aerial exposure experiment on trout was performed, cortisol levels were much higher in percentage than in the present case, in which hypoxia was achieved by reducing the levels of oxygen from the water by displacement with nitrogen. It should be noted that the physiological stress response is effectively and quickly detected as plasma cortisol increases as early as 3 min post-stress, although the maximum peak is detected after approximately 1 h post-stress (Gesto et al., 2013; Gesto et al., 2015). Fish that have suffered different types of stress (manipulation and hypoxia shocks) show a progressive decrease in glucose levels since it is used as a substrate for glycolytic activity, leading to the release of cell energy (Dunn and Hochachka, 1986). In the present work, this is observed neither in the case of the AC group, which displays a return to initial levels 24 h, nor in H1, which did not display any significant variations in glucose levels throughout the sampling points. Furthermore, in most cases, acute stress induces an increase in plasma glucose, in part because of the energetic needs derived from the stress situation and the mediating effects of cortisol and catecholamines (Abdel-Tawwab et al., 2019). In addition, the absence of significant differences between the different groups at 1 h indicates that the animals have the capacity to replenish their reserves during the 48 h recovery period between different shocks. Moreover, lactate, the product generated by the glycolytic activity (Dunn and Hochachka, 1986), displays significant increases when facing a situation of hypoxia to help maintain cellular energy balance (Dunn and Hochachka, 1986; Richards, 2011), as observed in the present study. This happens because oxygen-independent energetic mechanisms are needed since oxygen-dependent mechanisms are

15 times lower under hypoxic conditions (Richards, 2011). In this sense, the group subjected to one hypoxia is the one with the highest lactate values, so it would be the group that activated anaerobic metabolism the most. It is important to highlight the fact that the group subjected to three exposures and manipulations did not display significant increases in lactate levels, which, again, suggests habituation in the same way as occurs in the case of hematological parameters. This habituation may be facilitated by the mildness of the stressor, which was applied only for short periods of time (Tort et al., 2001).

5 Conclusion

The overall results show tolerance and a capacity for a certain degree of habituation in an oxygen-sensitive species such as *O. mykiss* as a response to repeated manipulation and hypoxia. Initial differences are observed in hematological parameters between treated groups and the control, although these differences are overall minimized after three shocks. This return to absolute control levels suggests habituation of some sort, regarding both the correct functioning of red blood cells in transporting and supplying oxygen and white blood cells in host immunity and cell repair. Although cortisol measurements did not return to absolute control levels, they did display a decreasing trend, indicating that, in the long term, fish might be able to recover basal levels, provided that the stressors hypoxia and manipulation maintain the same characteristics. The hypothesis of habituation is further supported by the trends observed in glucose and lactate levels, which display significant alterations associated with changes in aerobic and anaerobic metabolism but return to absolute control levels after the third shock and manipulation. As a general conclusion, it can be stated that rainbow trout are capable of habituating to both these temporary hypoxia episodes and manipulation events without having significant negative consequences at the functional level. However, to firmly affirm this, it would be necessary to analyze how gene and protein expression are modulated since it may help to understand basic molecular and cellular changes associated with the tolerance of hypoxia and manipulation.

Data availability statement

The raw data supporting the conclusion of this article will be made available by the authors, without undue reservation.

Ethics statement

The animal study was approved by the Ethics and Animal Care Committee of the "Universitat Autonoma de Barcelona" (permit numbers OH42184219 and DAMM 11251). The study was conducted in accordance with the local legislation and institutional requirements.

Author contributions

NR: conceptualization, formal analysis, methodology, and writing–original draft. IG-M: conceptualization, data curation, formal analysis, methodology, visualization, and writing–review and editing. AK: methodology and writing–review and editing. MT: methodology, and writing–review and editing. JP: methodology and writing–review and editing. LT: conceptualization, funding acquisition, investigation, methodology, project administration, resources, supervision, and writing–review and editing.

Funding

The authors declare that financial support was received for the research, authorship, and/or publication of this article. This research was funded by MICIN/ AEI/10.13039/501100011033/ "FEDER Una manera de hacer Europa," grant number PID-2020-117557RB-C21."

Acknowledgments

The authors thank Pilar Tudela, Chanuka Fernando, and Pinky Debnath for their technical help.

Conflict of interest

The authors declare that the research was conducted in the absence of any commercial or financial relationships that could be construed as a potential conflict of interest.

The authors declare that they were editorial board members of Frontiers, at the time of submission. This had no impact on the peer review process and the final decision.

Publisher's note

All claims expressed in this article are solely those of the authors and do not necessarily represent those of their affiliated organizations, or those of the publisher, the editors, and the reviewers. Any product that may be evaluated in this article, or claim that may be made by its manufacturer, is not guaranteed or endorsed by the publisher.

References

Abdel-Tawwab, M., Monier, M. N., Hoseinifar, S. H., and Faggio, C. (2019). Fish response to hypoxia stress: growth, physiological, and immunological biomarkers. *Fish physiology Biochem.* 45, 997–1013. doi:10.1007/s10695-019-00614-9

Aboagye, D. L., and Allen, P. J. (2018). Effects of acute and chronic hypoxia on acid–base regulation, hematology, ion, and osmoregulation of juvenile american paddlefish. *J. Comp. Physiology B* 188, 77–88. doi:10.1007/s00360-017-1104-7

Acerete, L., Balasch, J., Espinosa, E., Josa, A., and Tort, L. (2004). Physiological responses in eurasian perch (perca fluviatilis, l.) subjected to stress by transport and handling. *Aquaculture* 237, 167–178. doi:10.1016/j.aquaculture.2004.03.018

Action, S. I. (2020). *World fisheries and aquaculture*. Rome, Italy: Food and Agriculture Organization, 1–244.

Alfonso, S., Sadoul, B., Cousin, X., and Begout, M.-L. (2020). Spatial distribution and activity patterns as welfare indicators in response to water quality changes in european sea bass, dicentrarchus labrax. *Appl. Animal Behav. Sci.* 226, 104974. doi:10.1016/j.applanim.2020.104974

Barcellos, L. J. G., Kreutz, L. C., de Souza, C., Rodrigues, L. B., Fioreze, I., Quevedo, R. M., et al. (2004). Hematological changes in jundiá (rhamdia quelen quoy and gaimard pimelodidae) after acute and chronic stress caused by usual aquacultural management, with emphasis on immunosuppressive effects. *Aquaculture* 237, 229–236. doi:10.1016/j.aquaculture.2004.03.026

Barton, B. A. (2002). Stress in fishes: a diversity of responses with particular reference to changes in circulating corticosteroids. *Integr. Comp. Biol.* 42, 517–525. doi:10.1093/icb/42.3.517

Bera, A., Sawant, P. B., Dasgupta, S., Chadha, N., Sawant, B. T., and Pal, A. K. (2017). Diel cyclic hypoxia alters plasma lipid dynamics and impairs reproduction in goldfish (carassius auratus). *Fish physiology Biochem.* 43, 1677–1688. doi:10.1007/s10695-017-0401-0

Borowiec, B. G., Darcy, K. L., Gillette, D. M., and Scott, G. R. (2015). Distinct physiological strategies are used to cope with constant hypoxia and intermittent hypoxia in killifish (fundulus heteroclitus). *J. Exp. Biol.* 218, 1198–1211. doi:10.1242/jeb.114579

Boutilier, R. G. (2001). Mechanisms of cell survival in hypoxia and hypothermia. *J. Exp. Biol.* 204, 3171–3181. doi:10.1242/jeb.204.18.3171

Caldwell, C. A., and Hinshaw, J. (1994). Physiological and haematological responses in rainbow trout subjected to supplemental dissolved oxygen in fish culture. *Aquaculture* 126, 183–193. doi:10.1016/0044-8486(94)90259-3

Carbajal, A., Soler, P., Tallo-Parra, O., Isasa, M., Echevarria, C., Lopez-Bejar, M., et al. (2019). Towards non-invasive methods in measuring fish welfare: the measurement of cortisol concentrations in fish skin mucus as a biomarker of habitat quality. *Animals* 9, 939. doi:10.3390/ani9110939

Conde-Sieira, M., Valente, L. M., Hernandez-Perez, J., Soengas, J. L., Míguez, J. M., and Gesto, M. (2018). Short-term exposure to repeated chasing stress does not induce habituation in senegalese sole, solea senegalensis. *Aquaculture* 487, 32–40. doi:10.1016/j.aquaculture.2018.01.003

Dunn, J., and Hochachka, P. (1986). Metabolic responses of trout (salmo gairdneri) to acute environmental hypoxia. *J. Exp. Biol.* 123, 229–242. doi:10.1242/jeb.123.1.229

Fazio, F. (2019). Fish hematology analysis as an important tool of aquaculture: a review. *Aquaculture* 500, 237–242. doi:10.1016/j.aquaculture.2018.10.030

Fish, E. J., Hansen, S. C., Spangler, E. A., Gaillard, P. R., Fan, S., and Bacek, L. M. (2019). Retrospective evaluation of serum/plasma iron, red blood cell distribution width, and nucleated red blood cells in dogs with acute trauma (2009–2015): 129 cases. *J. Veterinary Emerg. Crit. Care* 29, 521–527. doi:10.1111/vec.12886

Franco-Martinez, L., Brandts, I., Reyes-López, F., Tort, L., Tvarijonaviciute, A., and Teles, M. (2022). Skin mucus as a relevant low-invasive biological matrix for the measurement of an acute stress response in rainbow trout (oncorhynchus mykiss). *Water* 14, 1754. doi:10.3390/w14111754

Galhardo, L., and Oliveira, R. F. (2009). Psychological stress and welfare in fish. *Annu. Rev. Biomed. Sci.* 1–20. doi:10.5016/1806-8774.2009v11p1

Galhardo, L., Vital, J., and Oliveira, R. F. (2011). The role of predictability in the stress response of a cichlid fish. *Physiology Behav.* 102, 367–372. doi:10.1016/j.physbeh.2010.11.035

Gamperl, A., Todgham, A., Parkhouse, W., Dill, R., and Farrell, A. (2001). Recovery of trout myocardial function following anoxia: preconditioning in a non-mammalian model. *Am. J. Physiology-Regulatory, Integr. Comp. Physiology* 281, R1755–R1763. doi:10.1152/ajpregu.2001.281.6.R1755

Gesto, M., López-Patiño, M., Hernández, J., Soengas, J., and Míguez, J. (2015). Gradation of the stress response in rainbow trout exposed to stressors of different severity: the role of brain serotonergic and dopaminergic systems. *J. Neuroendocrinol.* 27, 131–141. doi:10.1111/jne.12248

Gesto, M., López-Patiño, M. A., Hernández, J., Soengas, J. L., and Míguez, J. M. (2013). The response of brain serotonergic and dopaminergic systems to an acute stressor in rainbow trout: a time course study. *J. Exp. Biol.* 216, 4435–4442. doi:10.1242/jeb.091751

Goran, S. M. A., Omar, S. S., and Anwer, A. Y. (2017). Assessment of yeast as a dietary additive on haematology and water quality of common carp in a recirculating aquaculture system. *AIP Conf. Proc.* 1888, 020023. doi:10.1063/1.5004300

Groff, J. M., and Zinkl, J. G. (1999). Hematology and clinical chemistry of cyprinid fish: common carp and goldfish. *Veterinary Clin. N. Am Exot. Animal Pract.* 2, 741–776. doi:10.1016/s1094-9194(17)30120-2

Khan, S., Ahmed, S., and Saifullah, M. (2017). Haematological studies on trichogaster fasciatus fish infected with clinostomum complanatum metacercariae. *J. Biol. Sci. Med.* 3, 35–39.

Koakoski, G., Kreutz, L. C., Fagundes, M., Oliveira, T. A., Ferreira, D., Rosa, J. G. S. d., et al. (2013). Repeated stressors do not provoke habituation or accumulation of the stress response in the catfish rhamdia quelen. *Neotropical Ichthyol.* 11, 453–457. doi:10.1590/s1679-62252013005000010

Kolosov, D., and Kelly, S. P. (2019). The mineralocorticoid receptor contributes to barrier function of a model fish gill epithelium. *J. Exp. Biol.* 222, jeb192096. doi:10.1242/jeb.192096

Magnoni, L. J., Novais, S. C., Eding, E., Leguen, I., Lemos, M. F., Ozório, R. O., et al. (2019). Acute stress and an electrolyte-imbalanced diet, but not chronic hypoxia, increase oxidative stress and hamper innate immune status in a rainbow trout (oncorhynchus mykiss) isogenic line. *Front. Physiology* 10, 453. doi:10.3389/fphys.2019.00453

Maiolo, A. T., Gidiuli, R., Damilano, I., Massaro, P., and Polli, E. E. (1991). Relevance of red cell distribution width (rdw) in the differential diagnosis of microcytic anaemias. *Clin. Laboratory Haematol.* 13, 141–151. doi:10.1111/j.1365-2257.1991.tb00263.x

McLeay, D. (1973). Effects of cortisol and dexamethasone on the pituitary-interrenal axis and abundance of white blood cell types in juvenile coho salmon, oncorhynchus kisutch. *General Comp. Endocrinol.* 21, 441–450. doi:10.1016/0016-6480(73)90103-2

Missinhoun, D., Qiang, J., Jin-Wen, B., Yi-Fan, T., Hao-Jun, Z., Mutebi, T. E., et al. (2021). Effects of acute hypoxia stress on hemato-biochemical parameters, oxidative resistance ability, and immune responses of hybrid yellow catfish (pelteobagrus fulvidraco× p. vachelli) juveniles. *Aquac. Int.* 29, 2181–2196. doi:10.1007/s10499-021-00742-1

Muusze, B., Marcon, J., van den Thillart, G., and Almeida-Val, V. (1998). Hypoxia tolerance of amazon fish: respirometry and energy metabolism of the cichlid astronotus ocellatus. *Comp. Biochem. Physiology Part A Mol. Integr. Physiology* 120, 151–156. doi:10.1016/s1095-6433(98)10023-5

Naderi, F., Hernández-Pérez, J., Chivite, M., Soengas, J. L., Míguez, J. M., and López-Patiño, M. A. (2018). Involvement of cortisol and sirtuin1 during the response to stress of hypothalamic circadian system and food intake-related peptides in rainbow trout, oncorhynchus mykiss. *Chronobiology Int.* 35, 1122–1141. doi:10.1080/07420528.2018.1461110

Nilsson, J., Stien, L. H., Fosseidengen, J. E., Olsen, R. E., and Kristiansen, T. S. (2012). From fright to anticipation: reward conditioning versus habituation to a moving dip net in farmed atlantic cod (gadus morhua). *Appl. Animal Behav. Sci.* 138, 118–124. doi:10.1016/j.applanim.2012.02.014

O'Connor, E., Pottinger, T., and Sneddon, L. (2011). The effects of acute and chronic hypoxia on cortisol, glucose and lactate concentrations in different populations of three-spined stickleback. *Fish physiology Biochem.* 37, 461–469. doi:10.1007/s10695-010-9447-y

Pagès, T., Gomez, E., Suner, O., Viscor, G., and Tort, L. (1995). Effects of daily management stress on haematology and blood rheology of the gilthead seabream. *J. fish Biol.* 46, 775–786. doi:10.1006/jfbi.1995.0071

Pavlidis, M., Futter, W., Katharios, P., and Divanach, P. (2007). Blood cell profile of six mediterranean mariculture fish species. *J. Appl. Ichthyology* 23, 70–73. doi:10.1111/j.1439-0426.2006.00771.x

Petersen, L., and Gamperl, A. K. (2011). Cod (gadus morhua) cardiorespiratory physiology and hypoxia tolerance following acclimation to low-oxygen conditions. *Physiological Biochem. Zoology* 84, 18–31. doi:10.1086/657286

Petitjean, Q., Jean, S., Gandar, A., Côte, J., Laffaille, P., and Jacquin, L. (2019). Stress responses in fish: from molecular to evolutionary processes. *Sci. Total Environ.* 684, 371–380. doi:10.1016/j.scitotenv.2019.05.357

Pichavant, K., Maxime, V., Thebault, M., Ollivier, H., Garnier, J., Bousquet, B., et al. (2002). Effects of hypoxia and subsequent recovery on turbot scophthalmus maximus: hormonal changes and anaerobic metabolism. *Mar. Ecol. Prog. Ser.* 225, 275–285. doi:10.3354/meps225275

Pilgaard, L., Malte, H., and Jensen, F. B. (1994). Physiological effects and tissue accumulation of copper in freshwater rainbow trout (oncorhynchus mykiss) under normoxic and hypoxic conditions. *Aquat. Toxicol.* 29, 197–212. doi:10.1016/0166-445x(94)90068-x

Pollock, M., Clarke, L., and Dubé, M. (2007). The effects of hypoxia on fishes: from ecological relevance to physiological effects. *Environ. Rev.* 15, 1–14. doi:10.1139/a06-006

Pottinger, T., and Carrick, T. (1999). Modification of the plasma cortisol response to stress in rainbow trout by selective breeding. *General Comp. Endocrinol.* 116, 122–132. doi:10.1006/gcen.1999.7355

Remen, M., Oppedal, F., Torgersen, T., Imsland, A. K., and Olsen, R. E. (2012). Effects of cyclic environmental hypoxia on physiology and feed intake of post-smolt atlantic salmon: initial responses and acclimation. *Aquaculture* 326, 148–155. doi:10.1016/j.aquaculture.2011.11.036

Richards, J. G. (2011). Physiological, behavioral and biochemical adaptations of intertidal fishes to hypoxia. *J. Exp. Biol.* 214, 191–199. doi:10.1242/jeb.047951

Sadoul, B., and Geffroy, B. (2019). Measuring cortisol, the major stress hormone in fishes. *J. Fish Biol.* 94, 540–555. doi:10.1111/jfb.13904

Sappal, R., Fast, M., Purcell, S., MacDonald, N., Stevens, D., Kibenge, F., et al. (2016). Copper and hypoxia modulate transcriptional and mitochondrial functional-biochemical responses in warm acclimated rainbow trout (oncorhynchus mykiss). *Environ. Pollut.* 211, 291–306. doi:10.1016/j.envpol.2015.11.050

Schreck, C. B., and Tort, L. (2016). The concept of stress in fish. *Fish. Physiol.* 35, 1–34. doi:10.1016/B978-0-12-802728-8.00001-1

Schurmann, H., and Steffensen, J. (1992). Lethal oxygen levels at different temperatures and the preferred temperature during hypoxia of the atlantic cod, gadus morhua l. *J. Fish Biol.* 41, 927–934. doi:10.1111/j.1095-8649.1992.tb02720.x

Sheng, Y., Hua, Z. Y., Yang, Z., Wei, X. L., Sheng, Y. J., Jia, H. L., et al. (2019). Effects of acute hypoxic stress on biochemical parameters, immune regulation and metabolic capacity of the blood in genetically improved farmed tilapia (gift, oreochromis niloticus). *J. Appl. Ichthyology* 35, 978–986. doi:10.1111/jai.13930

Swift, D., and Lloyd, R. (1974). Changes in urine flow rate and haematocrit value of rainbow trout salmo gairdneri (richardson) exposed to hypoxia. *J. Fish Biol.* 6, 379–387. doi:10.1111/j.1095-8649.1974.tb04555.x

Tort, L., Montero, D., Robaina, L., Fernández-Palacios, H., and Izquierdo, M. (2001). Consistency of stress response to repeated handling in the gilthead sea bream sparus aurata linnaeus, 1758. *Aquac. Res.* 32, 593–598. doi:10.1046/j.1365-2109.2001.00607.x

Williams, K. J., Cassidy, A. A., Verhille, C. E., Lamarre, S. G., and MacCormack, T. J. (2019). Diel cycling hypoxia enhances hypoxia tolerance in rainbow trout (oncorhynchus mykiss): evidence of physiological and metabolic plasticity. *J. Exp. Biol.* 222, jeb206045. doi:10.1242/jeb.206045

Wojtaszek, J., Dziewulska-Szwajkowska, D., Łozińska-Gabska, M., Adamowicz, A., and Dżugaj, A. (2002). Hematological effects of high dose of cortisol on the carp (cyprinus carpio l.): cortisol effect on the carp blood. *General Comp. Endocrinol.* 125, 176–183. doi:10.1006/gcen.2001.7725

Xiao, W. (2015). The hypoxia signaling pathway and hypoxic adaptation in fishes. *Sci. China Life Sci.* 58, 148–155. doi:10.1007/s11427-015-4801-z

Zhang, Y., Healy, T., Vandersteen, W., Schulte, P., and Farrell, A. (2018). A rainbow trout oncorhynchus mykiss strain with higher aerobic scope in normoxia also has superior tolerance of hypoxia. *J. Fish Biol.* 92, 487–503. doi:10.1111/jfb.13530

Frontiers in Physiology

Understanding how an organism's components work together to maintain a healthy state

The second most-cited physiology journal, promoting a multidisciplinary approach to the physiology of living systems - from the subcellular and molecular domains to the intact organism and its interaction with the environment.

Discover the latest Research Topics

See more →

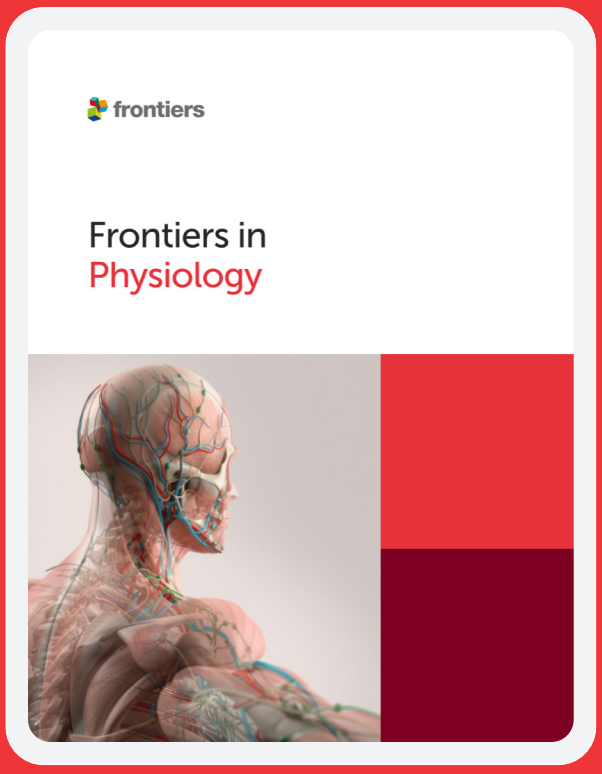

Frontiers

Avenue du Tribunal-Fédéral 34
1005 Lausanne, Switzerland
frontiersin.org

Contact us

+41 (0)21 510 17 00
frontiersin.org/about/contact